

UNIVERSIDADE DE BRASÍLIA  
FACULDADE DE MEDICINA  
PROGRAMA DE PÓS-GRADUAÇÃO EM PATOLOGIA MOLECULAR

Tese de Doutorado

Lucas Silva de Oliveira

Enriquecimento de proteínas parceiras de  
KAHRP e mapeamento de proteínas organelares  
de *Plasmodium falciparum* utilizando CRISPR-Cas9,  
APEX2 e proteômica

Supervisão:

Dr. Sébastien Olivier Charneau  
Universidade de Brasília (UnB)  
Departamento de Biologia Celular (CEL)

Co-Supervisão:

Dr. Marcos Rodrigo Alborghetti  
Centro Nacional de Pesquisa em Energia e Materiais (CNPEM)  
Laboratório Nacional de Biociências (LNBio)

BRASÍLIA - DF  
Setembro  
2021



**Universidade de Brasília  
Faculdade de Medicina  
Programa de Pós-Graduação em Patologia Molecular**

**TESE DE DOUTORADO**

**Lucas Silva de Oliveira**

**“Enriquecimento de proteínas parceiras de KAHRP e mapeamento de proteínas organelares de *Plasmodium falciparum* utilizando CRISPR-Cas9, APEX2 e proteômica”**

Tese de doutorado apresentado ao Programa de Pós-Graduação em Patologia Molecular, associado à Faculdade de Medicina da Universidade de Brasília, como requisito parcial para a obtenção do título de Doutor em Patologia Molecular, na área de concentração de Bioquímica e Biologia Molecular.

**Supervisão:** Dr. Sébastien Olivier Charneau  
**Co-supervisão:** Dr. Marcos Rodrigo Alborghetti

**Brasília – DF  
Setembro  
2021**

Ficha catalográfica elaborada automaticamente,  
com os dados fornecidos pelo(a) autor(a)

SO48e Silva de Oliveira, Lucas  
Enriquecimento de proteínas parceiras de KAHRP e mapeamento de proteínas organelares de Plasmodium falciparum utilizando CRISPR-Cas9, APEX2 e proteômica / Lucas Silva de Oliveira; orientador Sébastien Olivier Charneau; co orientador Marcos Rodrigo Alborghetti. -- Brasília, 2021.  
204 p.

Tese (Doutorado - Doutorado em Patologia Molecular) -- Universidade de Brasília, 2021.

1. P. falciparum. 2. KAHRP. 3. CRISPR-Cas9. 4. APEX2. 5. mapeamento de organelas. I. Olivier Charneau, Sébastien, orient. II. Rodrigo Alborghetti, Marcos, co-orient. III. Título.

**Este trabalho está sendo realizado em parceria com as seguintes instituições:**

Laboratório de Bioquímica e Química de Proteínas (LBQP)  
Universidade de Brasília, Departamento de Biologia Celular, Bloco J  
Campus Darcy Ribeiro, Asa Norte, Brasília, Distrito Federal, Brasil.

Wellcome Trust Sanger Institute, Malaria Programme  
Cambridge, Inglaterra, Reino Unido.

Muséum National d'Histoire Naturelle  
Molécules de Communication et Adaptation des Micro-organismes (MCAM), UMR  
7245, Paris, França.

Institut Curie, PSL Research University, Centre de Recherche, Laboratoire de  
Spectrométrie de Masse Protéomique, Paris, França.

## **BANCA EXAMINADORA**

**Presidente: Prof. Dr. Sébastien Olivier Charneau (supervisor)**  
Universidade de Brasília, Departamento de Biologia Celular

**Membro 1: Prof. Dr. Bergmann Morais Ribeiro (*memorian*)**  
Universidade de Brasília, Departamento de Biologia Celular

**Membro 2: Prof. Dr. Giuseppe Palmisano**  
Universidade de São Paulo, Departamento de Parasitologia

**Membro 3: Prof. Dr. Philippe Grellier**  
Muséum National d'Histoire Naturelle, UMR 7245, CNRS, Molécules de  
Communication et Adaptation des Micro-organismes (MCAM)

**Suplente: Prof<sup>a</sup>. Dr<sup>a</sup>. Izabela Marques Dourado Bastos Charneau**  
Universidade de Brasília, Departamento de Biologia Celular

**Local: Ambiente virtual**

**Data: 03/09/2021**

**Horário: 9h00min**

***Dedico este trabalho à verdade científica, à ciência brasileira e aos cientistas brasileiros.***

## AGRADECIMENTOS

À minha família, por todo o apoio e suporte na minha vida acadêmica. Muitos obstáculos apareceram, porém, com o apoio de vocês, foram todos superados. Um agradecimento muito carinhoso aos meus pais, Cleide e Jorge, pela perseverança em me apoiar mesmo nas muitas adversidades.

Ao meu supervisor de doutorado, Prof. Dr. Sébastien Olivier Charneau, pela generosidade científica, respeito e apoio em muitos momentos de dificuldade. Não consigo achar palavras, para expressar o tamanho da admiração e respeito que tenho por você. Sou muito grato à você por todas as oportunidades dadas, dentre elas, em realizar o meu sonho de estudar no exterior. *Vraiment, mon grand merci!*

Ao querido co-supervisor de doutorado, Dr. Marcos Rodrigo Alborghetti, pela parceria, carinho e generosidade científica, durante o tempo em que esteve conosco aqui no laboratório. Sou muito grato à você por todos os momentos e palavras de apoio. Desejo toda felicidade e sucesso na sua jornada!

Aos membros da banca, Prof. Dr. Bergmann Morais Ribeiro, Prof. Dr. Giuseppe Palmisano, Prof. Dr. Philippe Grellier e Prof<sup>a</sup>. Dr<sup>a</sup>. Izabela Marques Dourado Bastos-Charneau, por terem aceitado o convite para compor a banca examinadora.

Ao Prof. Dr. Philippe Grellier pela acolhida mais que especial no “*Muséum National d’Histoire Naturelle (MNHN)*”, onde realizei parte do meu doutorado. Agradeço imensamente à sua disponibilidade, preocupação e parceria em proporcionar as melhores condições para a realização de uma parte significativa deste trabalho.

Ao Prof. Dr. Jaime Martins de Santana pelo compromisso e seriedade. Embora estejamos vivenciando um momento de crise e descredibilização da ciência, você sempre nos mantém otimistas quanto a um futuro melhor, e seus esforços para a internacionalização da UnB tornou realidade o meu sonho de estudar no exterior. Espero que os tempos melhorem, para que você possa ser instrumento da realização de outros sonhos! Muito obrigado!

Aos professores do Laboratório de Bioquímica e Química de Proteínas (LBQP): Prof. Dr. Marcelo Valle de Sousa, Prof. Dr. Carlos André Ornelas Ricart, Prof. Dr. Wagner Fontes, Prof<sup>a</sup>. Dr<sup>a</sup>. Mariana de Souza Castro, Prof<sup>a</sup>. Dr<sup>a</sup>. Consuelo Medeiros Rodrigues de Lima, Prof<sup>a</sup>. Dr<sup>a</sup>. Ana Flávia Alves Parente e Prof<sup>a</sup>. Dr<sup>a</sup>. Fabiane Hiratsuka Veiga de Souza. Agradeço à todos, pelos os momentos de descontração e discussão científica compartilhados. Certamente, me sinto em casa quando estou no laboratório compartilhando estes momentos com vocês.

Aos professores do Laboratório da Interação Patógeno-Hospedeiro (LIPH). De modo especial: à Prof<sup>a</sup>. Dr<sup>a</sup>. Izabela Marques Dourado Bastos-Charneau, à Prof<sup>a</sup>. Dr<sup>a</sup>. Carla Nunes de Araújo e à Prof<sup>a</sup>. Dr<sup>a</sup>. Flávia Nader Motta. Agradeço a disponibilidade e a parceria.

Aos colegas e amigos do laboratório que, durante este tempo de doutoramento fizeram parte do meu cotidiano: Bruna Gomes (Bruninha), Raphaela Menezes (gatona), Reynaldo Magalhães (Doctor Rey), Natália Guimarães (Naty crossfiteira),

Débora Alves (Symone), Hylane Damascena, Adriano Rios, Isabelle Luz (Isa), Katyelle Botelho (Katy), Philippe Braga, Gabriel Freitas, Gislene Baptista (Gi), Joyce Santos e muitos outros que porventura estou esquecendo... Meu muito obrigado!

Aos colegas e amigos do grupo de pesquisa “Malária Molecular”: Farah Murthada (Farahhhhhhh), Renata Carneiro (Rê), José Miguel Quintero (Señor Quintero), Anna Fernanda Vasconcelos (gatona), Lorena Silveira (Lorens), Jhordan Placides, Camila Hime (Camis), Leonardo Jordão, Flávia Cabral, Thiago Alburquerque, Renan Nascimento e Carlos Paternina. Agradeço à todos pelo companheirismo e pelo espírito de equipe. Um abraço fraterno e carinhoso à todos vocês. Desejo todo o sucesso do mundo à todos! Juntos somos mais fortes!

Aos colegas do Laboratório da Interação Patógeno-Hospedeiro (LIPH). De modo especial, à Clênia Azevedo e à Milene Andrade, pela disponibilidade, compromisso e seriedade científica.

Ao querido, Dr. Samuel Coelho Mandacaru, agradeço imensamente os momentos compartilhados quando estivemos no nosso período de trabalho em Paris. Certamente, a minha admiração por você só aumentou! Desejo todo o sucesso do mundo na sua carreira!

À todos os colegas e amigos do MNHN da equipe PPL (do francês, *Parasites et Protistes Libres*): Amélie BOUISSOU, Jana ALLAZAZ, Soraya CHAOUCH, Véronique-Gail BONRAISIN, Amandine LABAT, Elisabeth MOURAY, Estelle REMION e Lisy RAVEENDRAN. Agradeço à todos pela receptividade e disponibilidade para me auxiliar em realizar todas as atividades que, apesar da pandemia do COVID-19, foi uma experiência única para mim. Agradeço também, de modo especial, a disponibilidade da Amélie e da Jana por terem tido a paciência em tirar as minhas dúvidas acerca da língua francesa: “*Je vous remercie beaucoup pour toute la assistance à propos de mes doutes en français!*”

Aos demais professores, mestres de conferência e encarregados de pesquisa do MNHN: Dr<sup>a</sup>. Isabelle FLORENT, Dr<sup>a</sup>. Coralie MARTIN, Dr<sup>a</sup>. Delphine DEPOIX, Dr<sup>a</sup>. Linda KOHL, Dr<sup>a</sup>. Christiane DEREGNAUCOURT e Dr<sup>a</sup>. Linda DUVAL. Agradeço pela disponibilidade em dialogar e trocar experiências científicas.

À Dr<sup>a</sup>. Thuany de Moura Cordeiro e à Juliana Penteado, da Fundação Hemocentro de Brasília (FHB), pelo provisionamento de hemocompetentes para a realização das nossas atividades de pesquisa.

À Joyce Sucupira, da Hemoclínica – Clínica de Hematologia e Hemoterapia Ltda., pela parceria instituída, disponibilidade e presteza em realizar o provisionamento complementar de hemocompetentes para a realização das nossas atividades de pesquisa.

Às agências de fomento, sem às quais, não teríamos a possibilidade de realizar as atividades de pesquisa: CAPES-COFECUB (Coordenação de Aperfeiçoamento de Pessoal de Nível Superior – *Comité Français d’Evaluation de la Coopération universitaire et scientifique avec le Brésil*), CNPq (Conselho Nacional de Desenvolvimento Científico e Tecnológico), FAPDF (Fundação de Amparo à Pesquisa do Distrito Federal) e FINEP (Financiadora de Estudos e Projetos).



Aos fornecedores dos insumos utilizados para as nossas atividades de pesquisa, agradeço a presteza e seriedade.

À todos àqueles que, porventura eu me esqueci, deixo aqui o meu muito obrigado.

Lucas Oliveira

## REMERCIEMENTS

Evidemment, j'étais obligé de faire des remerciements particuliers dans la langue de Molière.

D'abord, je voulais remercier la France (ce merveilleux pays) pour l'accueil et le privilège d'étudier au Muséum National d'Histoire Naturelle.

Ensuite, je voudrais profiter de ce moment et remercier quelques personnes qui m'ont aidé pendant ces 4 ans de doctorat et qui ont ensoleillé le temps durant lequel suis resté avec eux.

À mon directeur de recherche, Pr. Sébastien Olivier CHARNEAU pour toute la générosité scientifique et l'engagement pour nous fournir les meilleures conditions de travail possibles. Je sais que ce n'est parfois pas facile de travailler avec moi, mais je voulais que tu saches que toutes les situations et discussions, parfois un peu énergiques, que nous avons eu n'étaient que pour honorer cette opportunité et l'encadrement d'un postulant de doctorat comme tu le mérites. Comme je te l'ai déjà dit autrefois, je te remercie vraiment pour tout !

Au Pr. Philippe GRELLIER pour tout ton soutien dans les moments absolument cruciaux pour analyser les échantillons de protéomique et de spectrométrie de masse. Grâce à toi, nous avons réussi à traiter tous les données et on a pu écrire le brouillon d'article présenté ici. Malgré la situation pandémique que nous avons tous appréhendé au fur et à mesure, ton aide et ta préoccupation de notre bien-être ont été véritablement fondamentales pour profiter notre séjour à Paris malgré la situation. Vraiment, un grand merci !

Au Pr. Jaime SANTANA pour ton engagement dans l'internationalisation de l'Université de Brasília. C'était depuis longtemps mon rêve d'étudier à l'étranger, mais grâce à ton engagement pour les étudiants de l'École de doctorat et de ton incroyable optimisme face à la situation un peu chaotique chez nous au Brésil, tu as fait de mon rêve une réalité. J'espère que la situation au Brésil deviendra plus agréable dans un futur proche et que tu pourra être l'instrument de réalisation de nombreux autres rêves.

À toutes les personnes du Muséum National d'Histoire Naturelle pour tous les bons moments et le partage culturel. Particulièrement à Mlle. Amélie BOUISSOU et Mme. Jana ALAZZAZ qui m'ont surtout donné un coup de main avec la langue et la culture française (incluant ce discours qu'Amélie a relu), je vous remercie beaucoup par tous les moments d'apprentissage.

À Mme. Delphine DEPOIX pour tous les moments d'apprentissage et le soutien dans plusieurs moments où j'étais un peu troublé et préoccupé. À Mme. Elisabeth MOURAY, pour tous les moments de soutien sur les équipements au MNHN. À Mme. Lisy RAVEENDRAN pour sa disponibilité pour préparer les milieux des cultures dès que nécessaire. Bref, à tous et toutes qu'éventuellement je n'ai pas mentionné, un grand merci !

À toutes les personnes de la Fondation suisse, logement dans lequel j'étais accueilli comme résident pendant mon séjour à Paris. C'était tout à fait incroyable de partager

des moments avec vous tous. Je me souviendrai de vous avec une grande affection pour toute ma vie et je vous souhaite toute la réussite dans vos métiers.

À directrice de la Fondation suisse, Mme. Monica CORRADO, le personnel de l'assistance de direction Mmes. Lien NGUYEN et Miriam ROMERO ; et, M. João LOPES pour toute l'aide et la patience lors de mes premiers jours à Paris. Je me suis senti vraiment bien accueilli là-bas. Un grand merci à vous tous !

C'était pour moi vraiment, un grand plaisir et un privilège de travailler ou de vivre avec vous tous ! À la prochaine !

Lucas Oliveira

*“The aim and final end of all music should be none other than the glory of God and the refreshment of the soul”.*

**Johann Sebastian Bach**

*« En sciences, nous devons nous intéresser aux choses, pas aux personnes ».*

**Marie Curie**

*“O que vale na vida não é o ponto de partida e sim a caminhada. Caminhando e semeando, no fim terás o que colher”.*

**Cora Coralina**

## RESUMO

A malária é uma doença tropical, causada por espécies do gênero *Plasmodium* spp. O *Plasmodium falciparum* é a espécie mais virulenta, pois é a única capaz de produzir o quadro clínico mais grave da doença: a malária cerebral. De acordo com as últimas estimativas, cerca de 229 milhões de pessoas são acometidas pela malária, e, estudos que possam viabilizar a descoberta de novos alvos terapêuticos se tornam altamente necessários, haja vista aos crescentes casos de resistência aos antimaláricos disponíveis. Neste sentido, a fim de poder explorar melhor os parceiros de interação com a proteína KAHRP (do inglês, *knob-associated histidine rich protein*), uma proteína relacionada à citoaderência ao endotélio do hospedeiro humano facilitando a formação de “rosetas” em *P. falciparum*, foi implementado o uso de CRISPR-Cas9 juntamente com a abordagem de marcação por proximidade mediada por ascorbato-peroxidase modificada (APEX2), a fim de criar uma proteína quimérica da KAHRP fusionada a APEX2 por *knock-in*, utilizando o sistema CRISPR-Cas9, com a finalidade de promover a biotinição de proteínas vizinhas parceiras. Para avaliar a funcionalidade da proteína quimérica KAHRP-Flag-APEX2, ensaios de validação por Western-blot, estreptavidina-blot e imunofluorescência foram realizados. As análises de proteômica e de bioinformática revelaram que dentre as 208 proteínas do parasita biotiniladas vizinhas da KAHRP-Flag-APEX2, algumas delas são preditas por serem exportadas pelo translocon PTEX presente na membrana do vacúolo parasitóforo, e, outras preditas por serem exportadas por mecanismos não clássicos. Dentre as proteínas observadas, encontramos: GBP130, PTP2, membros do grupo PHISTb, UIS2, Pf332, RESA, as proteínas que compõe o complexo RhopH/CLAG (RhopH1/CLAG3.1, RhopH2 e RhopH3) e do complexo PTEX: PTEX88 e 150. Adicionalmente, seguindo o princípio da acurácia e proximidade proporcionada pelo uso da APEX2, construções similares foram realizadas, a fim de endereçar a HA-APEX2 para algumas organelas de *P. falciparum*. Pelo fato do parasita apresentar organelas especializadas, tais como o apicoplasto e as roptrias, o conhecimento do arsenal de proteínas presentes nestas estruturas, podem fornecer evidências para que futuras estratégias para a erradicação da doença, baseado no desenvolvimento de quimioterápicos e/ou vacinas sejam realizadas. O uso da APEX2 tem se mostrado altamente eficiente nesse quesito, pois permite uma descrição altamente precisa acerca das proteínas presentes em uma organela de interesse, baseando-se na sua resolução temporal e espacial. Assim, construções episomais foram adicionalmente obtidas, endereçando a HA-APEX2 para o apicoplasto (pCC1-SP<sub>(ACP)</sub>-HA-APEX2), a mitocôndria (pCC1-SP<sub>(TIR)</sub>-HA-APEX2) e as roptrias (pCC1-SP<sub>(RAP1)</sub>-HA-APEX2). O controle citosólico também foi obtido (pCC1-HA<sub>(cito)</sub>-APEX2). Com a mudança da metodologia de transfecção com o uso da plataforma Amaxa II Nucleofector II AAD-1001N (Lonza) e a determinação da ineficácia da droga anti-folato WR99210 proveniente da Sigma-Aldrich para selecionar os parasitas mutantes por [<sup>3</sup>H] hipoxantina, a obtenção dos parasitas transfectados foi possível após 3-4 semanas de seleção. Os ensaios de validação da expressão e da marcação por biotinição propiciada pela APEX2 por Western-blot e estreptavidina-blot dos respectivos compartimentos estão em andamento.

**Palavras-chave:** *P. falciparum*, KAHRP, CRISPR-Cas9, APEX2 e mapeamento de organelas.

**Suporte financeiro:** CAPES-COFECUB, CNPq, FAPDF e FINEP.

## ABSTRACT

Malaria is a tropical disease caused by *Plasmodium* species. *P. falciparum* is the most virulent specie from this genus, because is the only one capable to produce the most life-threatening clinical state of the illness: cerebral malaria. In agreement with the last estimative, about 229 million people are diagnosed with malaria worldwide, and studies that might shed light into novel therapeutic strategies turn-out very required, especially when an increasing of the numbers of resistance cases have been reported. Therefore, in order to explore neighboring interacting proteins of KAHRP (knob-associated histidine rich protein), a widely known protein involved with cytoadherence properties onto host endothelium facilitating rosetting in *P. falciparum*, it was implemented the use of CRISPR-Cas9 system together with proximity-tagging based on the use of ascorbate-peroxidase modified (APEX2), in order to produce a chimeric protein of KAHRP fused to APEX2 by knock-in, allowing biotinylation of neighboring proteins of KAHRP-Flag-APEX2. To assess the activity of this chimeric protein, validation assays were performed, such as Western-blot, streptavidin-blot and immunofluorescence. From our proteomic and bioinformatic analyses, a total of 208 parasite-derived neighboring proteins of KAHRP-Flag-APEX2 were identified. Some of them are predicted to be exported through translocon PTEX at parasitophorous vacuole membrane, and others are predicted to be exported through non-classical mechanisms. Among these proteins, we have found in our subproteomic dataset: GBP130, PTP2, PHISTb members, UIS2, Pf332, RESA, proteins from RhopH/CLAG complex (RhopH1/CLAG3.1, RhopH2 and RhopH3) and PTEX complex: PTEX88 and 150. In addition, taking advantage of the accuracy and proximity labeling allowed by APEX2 technology, similar vector constructions were made, in order to address HA-APEX2 to some *P. falciparum* compartments. As some compartments of this parasite are unique, such as apicoplast and rhoptries, the knowledge of the proteomic arsenal from these organelles, might provide novel insights for the disease eradication through rational drug design pipelines and/or vaccine development. The use of APEX2 has been shown very insightful in this state-of-the-art, because it allows an accurate description of the protein content of a given compartment, merely based on temporal and spatial resolution of the technology. Thus, episome-based constructions were additionally obtained addressing HA-APEX2 to apicoplast (pCC1-SP<sub>(ACP)</sub>-HA-APEX2), mitochondrion (pCC1-SP<sub>(TrxR)</sub>-HA-APEX2) and rhoptries (pCC1-SP<sub>(RAP1)</sub>-HA-APEX2). A cytosolic episome-based expressing APEX2 was also obtained (pCC1-HA<sub>(cito)</sub>-APEX2). After changing our transfection platform to Amaxa II Nucleofector II AAD-1001N (Lonza) and with determination of the WR99210 inefficacy purchased from Sigma-Aldrich to select mutant parasites through [<sup>3</sup>H] hypoxanthine, we were able to obtain the first transfected parasites after 3-4 weeks under drug pressure. Validation assays regarding protein expression and biotinylation proximity tagging into the compartments provided by APEX2 through Western-blot and streptavidin-blot are under progress.

**Key words:** *P. falciparum*, KAHRP, CRISPR-Cas9, APEX2 and organelle mapping.

**Financial support:** CAPES-COFECUB, CNPq, FAPDF and FINEP.

## SUMÁRIO

LISTA DE ABREVIATURAS .....	xviii
LISTA DE FIGURAS.....	xxvi
LISTA DE TABELAS .....	xxxii
i. INTRODUÇÃO / REFERENCIAL TEÓRICO .....	32
CAPÍTULO 1 – UMA VISÃO GERAL SOBRE A MALÁRIA .....	32
1.1. A malária no mundo e seus impactos.....	32
1.2. Quimioterapia e resistência aos antimaláricos .....	36
1.3. O vetor do gênero <i>Anopheles</i> spp. e os desafios do controle vetorial.....	38
1.4. A malária no Brasil .....	40
1.5. O gênero <i>Plasmodium</i> spp. e o ciclo biológico.....	42
CAPÍTULO 2 – O EXPORTOMA DE <i>P. falciparum</i> .....	46
As proteínas exportadas em <i>P. falciparum</i> e o papel da KAHRP .....	46
CAPÍTULO 3 – O ESTUDO DE ORGANELAS NO <i>P. falciparum</i> : O APICOPLASTO, A MITOCÔNDRIA E AS ROPTRIAS .....	54
3.1. A inter-relação entre o apicoplasto e a mitocôndria.....	54
3.2. As roptrias e a invasão em <i>P. falciparum</i> .....	58
CAPÍTULO 4 – A TÉCNICA CRISPR-Cas9 E SUAS APLICAÇÕES.....	64
4.1. O sistema de edição genômica CRISPR-Cas9 .....	64
4.2. As aplicações de CRISPR-Cas9 .....	66
CAPÍTULO 5 – INTERAÇÃO PROTEÍNA-PROTEÍNA (IPP).....	70
Estudo da interação proteína-proteína por ensaios de proximidade: APEX2 e BioID.....	70
ii. JUSTIFICATIVA.....	76
iii. OBJETIVOS E ETAPAS METODOLÓGICAS .....	77
Objetivo Geral .....	77
Etapas metodológicas concluídas .....	77
Etapas metodológicas em andamento .....	78
iv. MATERIAL E MÉTODOS.....	79
Cultura de <i>P. falciparum</i> e comitê de ética .....	79
Construção dos plasmídeos de expressão episomal .....	79
Ensaio de [ <sup>3</sup> H] hipoxantina .....	81
Transfecção em <i>P. falciparum</i> .....	82
Expressão heteróloga da proteína APEX2 em <i>Escherichia coli</i> .....	84
Produção de soros policlonais anti-APEX2 e validação por Western-blot.....	84

Ensaio de biotilação e confirmação da expressão dos mutantes epissomais (pCC1-SP <sub>(cito, acp, rap1, trxr)</sub> -HA-APEX2) por Western-blot .....	85
Enriquecimento das proteínas biotiniladas por APEX2 .....	86
Ensaio de imunofluorescência (IFA).....	86
Preparação das amostras para espectrometria de massas .....	87
Análise por espectrometria de massas.....	88
CAPÍTULO 6 – MANUSCRITO: “APEX2-based proteomic analysis depicts candidate protein partners of KAHRP in <i>Plasmodium falciparum</i> ” .....	90
ABSTRACT .....	90
INTRODUCTION .....	91
EXPERIMENTAL PROCEDURES.....	93
Culture conditions.....	93
Vector constructions for CRISPR-Cas9.....	93
Plasmid preparation and transfection procedure .....	95
Biotinylation assay.....	96
Protein extraction and pull-down of biotinylated proteins.....	96
NuPAGE™, Western-blot and streptavidin-blot.....	97
Immunofluorescence assays .....	97
Proteomic analysis .....	98
Bioinformatic analysis.....	100
RESULTS .....	100
Construction and validation of KAHRP-Flag-APEX2 expressing parasites for <i>in vivo</i> biotinylation assay.....	100
Imaging analysis by confocal immunofluorescence.....	101
Proteomic and <i>in silico</i> analysis.....	102
DISCUSSION .....	108
Proximity tagging approaches as feasible tools to decipher organelle proteomes and to unveil novel neighboring proteins of a target of interest .....	108
KAHRP and its neighboring candidate proteins.....	110
CONCLUSIONS AND PERSPECTIVES .....	114
REFERENCES .....	118
CAPÍTULO 7 - Mapeamento de proteínas organelares de <i>P. falciparum</i> utilizando APEX2: resultados preliminares .....	147
7.1. Construção dos vetores de expressão epissomal da proteína HA-APEX2 direcionada à diferentes organelas .....	147
7.2. Confirmação da orientação dos insertos e da sequência dos plasmídeos .....	148
7.3. Viabilidade de diferentes linhagens de <i>P. falciparum</i> na presença da WR99210 por ensaio de [ <sup>3</sup> H] hipoxantina .....	151



7.4. Expressão heteróloga e purificação da proteína recombinante APEX2 ....	153
7.5. Validação dos soros anti-APEX2 por Western-blot .....	153
7.6. Obtenção dos mutantes de <i>P. falciparum</i> expressando pCC1-SP <sub>(cito, acp, rap1, trxr)</sub> -HA-APEX2.....	155
v. CONCLUSÕES E PERSPECTIVAS .....	156
vi. REFERÊNCIAS BIBLIOGRÁFICAS.....	162
vii. ANEXOS .....	191

## LISTA DE ABREVIATURAS

- [<sup>3</sup>H]: tritiada
- μCi: microcurie
- μg: micrograma
- μL: microlitro
- μM: micromolar
- 3' UTR: do inglês, *3' untranslated region*
- 5' UTR: do inglês, *5' untranslated region*
- AAV: do inglês, *adeno-associated viral*
- ABCF1: do inglês, *ABCF-family protein*
- ACP: do inglês, *acyl-carrier protein*
- ACTs: do inglês, *artemisin combination therapies*
- AflI: enzima de restrição
- AGC: do inglês, *auto gain control*
- AL: artemether-lumefantrina
- ALA: δ-aminolevulanato
- ALAD: δ-aminolevulanato desidratase
- ALAS: δ-aminolevulanato sintase
- AMA-1: do inglês, *apical membrane antigen*
- APEX2: ascorbato peroxidase modificada
- APEX-RIP: metodologia baseada no uso da APEX2 que realiza o *crosslink* entre ribonucleoproteínas-RNAs
- AS-AQ: artesunato-amodiaquina
- ATP: do inglês, *adenosine triphosphate*
- ATQ: atovaquona
- AVIDITY: do inglês, *streptavidin binding capacity assay*
- B2AR: do inglês, *beta-2 adrenergic receptor* ou receptor beta-2 adrenérgico
- BioID: do inglês, *proximity-dependent Biotin-IDentification*
- BioSITE: do inglês, *biotinylation site identification technology*

BirA\*: biotina-ligase modificada de *E. coli*

BMAL1: do inglês, gene do *brain and muscle ARNT-like 1*

BP: do inglês, *biotin-phenol*

BSA: do inglês, *bovine serum albumin*

C7ORF55: Complexo V da cadeia respiratória, ATP-sintetase

CaCl<sub>2</sub>: cloreto de cálcio

CEP/UnB: Comitê de Ética em pesquisa da Faculdade de Ciências da Saúde da Universidade de Brasília

CMI: Complexo de Membrana Interno

CO<sub>2</sub>: dióxido de carbono

CPIII: coproporfirinogênio III

CPO: coproporfirinogênio oxidase

CQ: cloroquina

CRISPR: do inglês, *clustered regularly interspaced short palindromic repeats*

crRNAs: do inglês, *CRISPR associated RNAs*

CYC: cicloguanil

CYP6M2: um gene pertencente à família das P450 mono-oxigenases

CYTb: subunidade *b* da citocromo

D.O.<sub>600nm</sub>: densidade óptica medida no comprimento de onda a 600 nanômetros

DAPI: do inglês, *4',6-diamidino-2-phenylindole dihydrochloride*

DDT: diclodifeniltricloroetano

DHA-PPQ: diidroartemisinina-piperaquina

DHFR: diidrofolato redutase

DHPS: diidropteroato sintase

DiDBiT: do inglês, *direct detection of biotin-containing tags*

DiQ-BioID: do inglês, *dimerization-induced quantification BioID*

DNA: do inglês, *deoxyribonucleic acid* ou ácido desoxirribonucleico

DSB: do inglês, *double-strand break* ou clivagem da dupla fita do DNA

DTT: do inglês, *dithiothreitol*

E-64: inibidor de protease (do inglês, *trans-Epoxy succinyl-L-leucylamido(4-guanidino)butane, L-trans-3-Carboxyoxiran-2-carbonyl-L-leucylagmatine, N-(trans-Epoxy succinyl)-L-leucine 4-guanidinobutylamide*)

EBA-175: do inglês, *erythrocyte binding antigen-175*

EC<sub>50</sub>: do inglês, *half maximal effective concentration* ou metade da concentração efetiva máxima

*EcoRI*: enzima de restrição

EDTA: do inglês, *ethylenediamine tetraacetic acid*

EGTA: do inglês, *ethylene glycol-bis(β-aminoethyl ether)-N,N,N',N'-tetraacetic acid*

EM: do inglês, *electron microscopy* ou microscopia eletrônica

EPIC: *exported protein-interacting complex*

ER: do inglês, *endoplasmic reticulum*

ERD2: do inglês, *cis-Golgi / endoplasmic reticulum retention-defective protein*

EROs: espécies reativas de oxigênio

EVs: do inglês, *exosome-like vesicles* ou vesículas exosoma-*like*

EXP3: do inglês, *exported protein-3*:

FASII: do inglês *fatty acid synthase type II* ou via de biossíntese de ácidos graxos do tipo II

FASTKD1: Serina/treonina quinase-*like* ativado por Fas

FDR: do inglês, *false discovery rate*

FEPECS/SES-DF: Fundação de Ensino e Pesquisa em Ciências da Saúde do Distrito Federal

Flag-APEX2-NES: APEX2 marcado com o tag FLAG com peptídeo de endereçamento nuclear

FRET: do inglês, *Förster resonance energy transfer*

G6PD: glicose-6-fosfato desidrogenase

GBP130: do inglês, *glycophorin binding protein 130*

gDNA: do inglês, *genomic DNA* ou DNA genômico

GFP: do inglês, *green fluorescent protein*

GO: do inglês, *gene ontology*

GPCR: do inglês, *G-protein-coupled receptors* ou receptor acoplado a proteína G

gRNA: do inglês, *guide RNA* ou RNA-guia

GSTE2: um gene pertencente à família das glutationa-S-transferases

H<sub>2</sub>O<sub>2</sub>: peróxido de hidrogênio

HAT: do inglês, *histone acetyltransferase*

HBC: do inglês, *hepatites C virus*

HbS: hemoglobina com traço falciforme

HBsAg: antígeno de superfície do vírus hepatite B

HBV: do inglês, *hepatites B virus*

HCD: do inglês, *high energy collision dissociation*

HCl: ácido clorídrico

HDAC: do inglês, *histone deacetylase*

HDR: do inglês, *homology-directed repair*

HEPES: do inglês, *4-(2-hydroxyethyl)-1-piperazineethanesulfonic acid*

HindIII: enzima de restrição

hiPSCs: do inglês, *human induced pluripotent stem cells*

HIV: do inglês, *human immunodeficiency virus*

HR1: do inglês, *homology region 1*

HR2: do inglês, *homology region 2*

HRP: do inglês, *horseradish peroxidase*

HSP40: do inglês, *heat shock protein 40*

HSP70: do inglês, *heat shock protein 70*

HSP70-x: do inglês, *heat shock protein 70-x*

IPTG: isopropil- $\beta$ -D-1-tiogalactopiranosideo

iRBCs: do inglês, *infected-red blood cells*

IRS: do inglês, *indoor residual spraying* ou IRS ou pulverização residual interna

ISP3: do inglês, *IMC Subcompartment Protein 3*

ITN: do inglês *insecticide-treated mosquito net* ou mosquiteiro tratado com inseticida

ITTs: infecções transmitidas por transfusão

J-dots: pequenas estruturas que transportam chaperonas

K<sub>2</sub>HPO<sub>4</sub>: fosfato de potássio dibásico

KAHRP: do inglês, *knob-associated histidine rich protein*

KAHRP-Flag-APEX2: proteína quimérica expressando KAHRP e APEX2

kb: do inglês, *kilobase*

KCl: cloreto de potássio

KH<sub>2</sub>PO<sub>4</sub>: fosfato de potássio monobásico

L: litro

lncRNAs: do inglês, *long non-coding RNAs*

log<sub>10</sub>: escala logarítmica na base 10

M: molar

MAHRP1: do inglês, *membrane-associated histidine rich protein 1*

mCi/mmol: milicurie por milimolar

MCs: *Maurer's clefts*

MEP/ DOXP: 2-C-metil-D-eritritol-4-fosfato/1-deoxi-D-xilulose-5-fosfato

MFQ: mefloquina

mg: miligrama  
MgCl<sub>2</sub>: cloreto de magnésio  
mL: mililitro  
mM: milimolar  
mRNA: RNA mensageiro  
mtDNA: DNA mitocondrial  
MVP: membrana do vacúolo parasitóforo  
N<sub>2</sub>: gás nitrogênio  
N-Ac: N-acetilação  
NaCl: cloreto de sódio  
NADH: do inglês, *nicotinamide adenine dinucleotide*  
NADPH: do inglês, *nicotinamide adenine dinucleotide phosphate hydrogen*  
NaHCO<sub>3</sub>: bicarbonato de sódio  
NCE: do inglês, *normalized collision energy*  
Ncol: enzima de restrição  
ND3: uma subunidade do Complexo I da cadeia respiratória, NADH desidrogenase  
N-DRC: do inglês, *nexin-dynein regulatory complex*  
NDUFS6: Complexo I da cadeia respiratória, NADH desidrogenase  
NHEJ: do inglês, *non-homologous end-joining*  
nM: nanomolar  
NPPs: do inglês, *new permeability pathways* ou novas vias de permeabilidade  
NTM5: do inglês, *normal trabecular meshwork 5*  
O<sub>2</sub>: gás oxigênio  
OMS: Organização Mundial da Saúde  
ORF: do inglês, *open reading frame*  
PAM: do inglês, *protospacer adjacent motif*  
PBGD/UROGEN III: porfobilinogênio deaminase/uroporfirinogênio III sintase  
PBO: piperonil-butóxido  
PBS: do inglês, *phosphate buffer saline*  
pCC1: vetor de expressão utilizado neste estudo  
pCC1-HA<sub>(cito)</sub>-APEX2: construção epissomal endereçando a APEX ao citosol  
pCC1-SP<sub>(ACP)</sub>-HA-APEX2: construção epissomal endereçando a APEX ao apicoplasto  
pCC1-SP<sub>(RAP1)</sub>-HA-APEX2: construção epissomal endereçando a APEX às roptrias

pCC1-SP<sub>(TrxR)</sub>-HA-APEX2: construção episomal endereçando a APEX à mitocôndria

PCR: do inglês, *polymerase chain reaction*

PD: piruvato-desidrogenase

pDC2: vetor de expressão para Cas9 e gRNA

PEMS: do inglês, *parasitophorous-enclosed merozoite structures*

PEP: do inglês, *phosphoenolpyruvate* ou fosfoenolpiruvato

PET: do inglês, *position-emission computed tomography*

PEXEL: do inglês, *Protein EXport ELement*

Pf332: *P. falciparum* antigen 332

PfATP4: do inglês, *P. falciparum* ATPase 4

*pfcr1*: do inglês, gene do *chloroquine resistance transporter*

PfEMP1: do inglês, *P. falciparum* erythrocyte membrane protein 1

PfITPT: do inglês, *P. falciparum* innermost triose phosphate translocator

PfKelch13: do inglês, *kelch propeller domain* ou *K13-propeller*

*pfmdr1*: do inglês, gene do *multidrug resistance transporter 1*

PfoTPT: do inglês, *P. falciparum* outermost triose phosphate translocator

pH: potencial hidrogeniônico

PHISTb: do inglês, *Plasmodium helical interspaced subtelomeric family*

PI(3)P: fosfatidilinositol-3-fosfato

PMV: plasmepsina V

PNEPs: do inglês, *PEXEL-negative exported proteins*

pPK: *plastidial pyruvate kinase* ou piruvato-quinase plastidial

ppm: do inglês, *parts per million*

PPO: protoporfirinogênio oxidase

pPTs: do inglês, *plastidic phosphate translocators*)

PQ: primaquina

PSAC: do inglês, *plasmodial surface anion channel*

PTEX: do inglês, *Plasmodium translocon of exported proteins*

PTM: do inglês, *post-translational modification*

PTP1-6: do inglês, *PfEMP1-trafficking proteins 1-6*

PV1 and 2: do inglês, *parasitophorous vacuolar protein-1 and 2*

PVM: do inglês, *parasitophorous vacuole membrane*

PYR: pirimetamina

R21/Matrix-M: Protótipo de uma vacina baseada na RTS,S

RAP 1-3: do inglês, *hoptry-associated proteins 1-3*  
rAPEX2: APEX2 recombinante  
RBCs: do inglês, *red blood cells*  
RE: retículo endoplasmático  
RESA: do inglês, *ring-infected erythrocyte surface antigen*  
REX1-3: do inglês, *ring-exported proteins 1-3*  
Rh: do inglês, *reticulocyte-binding homologs*  
RhopH/CLAG: do inglês, *high molecular weight hoptry proteins* ou *cytoadherence linked asexual proteins*  
RNA: do inglês, *ribonucleic acid* ou ácido ribonucleico  
RONs 2, 4 e 5: do inglês, *hoptry neck proteins*  
ROPs: do inglês, *hoptry bulb proteins*  
rPSCs: do inglês, *rat pluripotent stem cells*  
rRNA: RNA ribossomal  
RTS,S: Protótipo de uma vacina baseada na proteína circumsporozóito  
SacI: enzima de restrição  
Sall: enzima de restrição  
SBD: do inglês, *substrate binding domain*  
SBP1: do inglês, *skeleton-binding protein 1*  
SDS: do inglês, *sodium dodecyl sulfate*  
SDX: sulfadoxina  
shRNAs: do inglês, *short hairpin RNAs*  
SP: sulfadoxina/pirimetamina  
TE: Tris-EDTA  
TEAB: do inglês, *triethylammonium bicarbonate buffer*  
TJ/MJ: do inglês, *tight/moving junction*  
TLR9: do inglês *toll-like receptors 9* ou receptores *toll-like 9*  
TNF: do inglês, *tumor necrosis factor* ou fator de necrose tumoral  
tracrRNA: do inglês, *trans-activating crRNAs*  
tRNA: RNA transportador  
TrxR: do inglês, *thioredoxin reductase*  
TurbOLD: metodologia baseada no uso da BirA\* modificada de: BirA\*-R118G para BirA\*-R118S  
v/v: volume/volume



VGSC: do inglês, *voltage gated sodium channel* ou canal de sódio controlado por voltagem

VTS: do inglês, *vacuolar transport signal*

w/v: do inglês, *weight/volume*

WR99210: droga anti-folato para selecionar parasitas de *P. falciparum*

WT: do inglês, *wild type*

*Xho*I: enzima de restrição

yDHODH: do inglês, *yeast dihydroorotate dehydrogenase*

## LISTA DE FIGURAS

**Figura 1. Distribuição geográfica dos países acometidos pela malária.** As estimativas são provenientes do acompanhamento do período de 2000-2019. Os países em vermelho são aqueles que apresentam maior incidência e prevalência de malária. Os países em azul são aqueles que não apresentaram nenhum caso, nas estimativas dos últimos 3 anos, enquanto que, os países em verde são aqueles que foram diagnosticados como livres da malária desde 2000. Os países em branco são aqueles que não são endêmicos da doença. **(Extraído de: World Health Organization (2020). World Malaria Report)**.....pg. 32

**Figura 2. Mecanismo de ação e resistência dos principais antimaláricos.** Frequentemente, as vias biológicas que são alvos para os antimaláricos atuais são: (i) detoxificação do grupo heme no vacúolo digestivo; (ii) folato e biossíntese de pirimidinas no citosol; e, (iii) a cadeia transportadora de elétrons na mitocôndria. As 4-aminoquinolinas, incluindo CQ e AQ, bem como PPQ possuem ação no vacúolo digestivo, ligando-se ao grupo heme reativo e interferindo na sua detoxificação através da formação da hemozoína. O íon heme ferroso ( $Fe^{2+}$ ) liberado da degradação da hemoglobina (Hb), pode clivar e ativar os derivados de ART (símbolo de estrela). As mutações nos transportadores PfCRT e PfMDR1 (círculos lilás) são determinantes importantes relacionados com a resistência à 4-aminoquinolinas. As formas variantes do marcador molecular kelch-13 (quadros vermelhos), conferem resistência à ART. As mutações em duas enzimas-chave na via de biossíntese do folato, diidropteroato sintase (DHPS) e diidrofolato redutase (DHFR), conferem resistência aos antifolatos: sulfadoxina (SDX), pirimetamina (PYR) e cicloguanil (CYC). ATQ inibe a cadeia transportadora de elétrons mitocondrial, devido à uma mutação pontual na subunidade *b* da citocromo (CYTb). **(Extraído de: Blasco et al. (2017). Nat. Med., 23(8), pp. 917-928)**.....pg. 38

**Figura 3. O ciclo biológico de *P. falciparum* e *P. vivax*.** **(A)** Durante o repasto sanguíneo, o vetor invertebrado do gênero *Anopheles*, transmite **(B)** os esporozoítos na corrente sanguínea do hospedeiro vertebrado humano, onde o mesmo irá migrar para os hepatócitos, multiplicando-se em esquizontes hepáticos. Com a ruptura do merossoma, **(C)** os merozoítos invadirão as hemácias, seguindo para o ciclo eritrocitário assexuado, transitando das formas de anel, trofozoíto e esquizonte. Possivelmente, devido à parasitemia elevada e mecanismos de comunicação celular, alguns parasitas se diferenciam em gametócitos **(D)**, que são posteriormente ingeridos pelo vetor invertebrado em um novo repasto sanguíneo **(E)**, com a fecundação dos gametócitos, e a formação de novos esporozítos e migração para as glândulas salivares **(F)**. **(Extraído de: Cowman et al. (2016). Cell, 167(20), pp. 610-624)**.....pg. 44

**Figura 4. Esquema do processamento das proteínas com a sequência consenso PEXEL.** Após o processamento por proteases (PMV, peptidases do peptídeo sinal e N-acetil-transferases), as proteínas acetiladas são marcadas para serem exportadas para o citosol da célula hospedeira.....pg. 47

**Figura 5. Mecanismo de exportação de proteínas PEXEL e PNEPs.** As proteínas contendo o motivo PEXEL são liberadas a partir do retículo endoplasmático (ER), pela plasmepsina V (PM5) e encaminhadas para uma via de secreção clássica até o

vacúolo parasitóforo (VP). Por outro lado, as proteínas contendo apenas o peptídeo sinal N-terminal não clássico (ou PNEPs), se ligam na membrana do lúmen do ER, pelo domínio transmembrana (TM). Uma vez no VP, as proteínas contendo o motivo PEXEL, são exportadas pelo translocon PTEX presente na membrana do vacúolo parasitóforo (MVP), podendo ser liberadas dentro das vesículas organelares, denominadas por *Maurer's Clefts*, até a superfície da membrana da célula hospedeira, ou ainda se associarem à outras cargas vesiculares, tais como os "*J-dots*". (**Extraído de:** Spillman et al., (2015). Annu. Rev. Biochem. 84, pp. 14.1-14.29).....pg.48

**Figura 6. Micrografia eletrônica de transmissão da interação célula-célula entre as hemácias infectadas por *P. falciparum* (P) e o endotélio (En).** (A) Uma hemácia infectada com *P. falciparum* (P) com a presença normal dos knobs ( $K^+$ ) está aderindo à superfície das células endoteliais (En). Barra de 1  $\mu$ m. (B) Detalhe da interface entre a interface de  $K^+$  e uma célula endotelial mostrando as faixas de conexão entre as células (setas). Note a presença das Maurer's clefts (M). Barra de 100 nm. (C) Detalhe da interface entre uma hemácia infectada com *P. falciparum* com a redução dos knobs ( $K^-$ ), mostra um material denso entre o endotélio e as hemácias (setas), sem uma adesão evidente ao endotélio. Barra de 100 nm. (Extraído de: Horrocks et al., (2005). J. Cell Sci., 118(11), pp. 2507-2518).....pg. 50

**Figura 7. Localização sub-celular das proteínas exportadas por *P. falciparum*.** A adesina PfEMP1 está disposta na superfície dos eritrócitos infectados por *P. falciparum*, onde aparecem os knobs, tendo a ancoragem da KAHRP. A proteína RESA, MESA, PHISTb, PfEMP3 e possivelmente outras proteínas (STEVORs, RIFINs e SURFINs), se associam ao citoesqueleto da célula hospedeira para facilitar a citoaderência às células endoteliais. As *Maurer's clefts* e "*J-dots*" constituem as "cargas" vesiculares que transportam muitas das proteínas que exercerão seu papel na superfície da hemácia infectada. Possivelmente, a liberação dos exosomas seja um mecanismo adicional que o parasita possui, para comunicar-se com o meio extracelular e favorecer a sua sobrevivência. (**Extraído de:** Spillman et al., (2015). Annu. Rev. Biochem. 84, pp. 14.1-14.29).....pg. 51

**Figura 8. Modelo de exportação da PfEMP1 pelo complexo EPIC.** É proposto que a PfEMP1 é translocada até o RE por um mecanismo mediado pelo complexo Sec61-62-63 e trafega através de uma via de secreção com o suporte de chaperonas residentes no RE. Mediante a secreção até o VP, é proposto que a PfEMP1 é reconhecida pelo complexo EPIC e transportado até o translocon PTEX, para ser exportado até as hemácias. O complexo EPIC pode também ser responsável pela marcação das vias alternativas do tráfego de "cargas" vesiculares. (**Extraído de:** Batinovic et al., (2017). Nat. Commun., 8(16044), pp. 1-14).....pg. 53

**Figura 9. Esquema da inter-relação metabólica entre o apicoplasto e a mitocôndria em *P. falciparum*.** As fontes de carbono fornecidas por intermediários da via glicolítica (trioses-fostato e fosfoenolpiruvato), atravessam os transportadores PfoTPT e PfiTPT, e são utilizados para produzir substratos para a biossíntese de ácidos graxos (p. ex. Acetil-CoA) e isoprenoides (pela via MEP/DOXP). Por outro lado, a biossíntese do grupo heme ocorre com a produção de  $\delta$ - aminolevulanato (ALA) pela  $\delta$ - aminolevulanato sintase (ALAS) pela mitocôndria, que atravessa as membranas do apicoplasto por transportadores desconhecidos, produzindo o CPiII, que por sua vez, retorna para a mitocôndria, para ser finalizado. (**Extraído de:** Lim & McFadden (2010). Phil. Trans. R. Soc. B. 365, pp. 749-763).....pg. 55

**Figura 10. *P. falciparum* expressando uma proteína GFP marcada para o apicoplasto; e, marcação da mitocôndria por MitoTracker® Red. (Extraído de: Waller et al., (2000), EMBO J. 19(8), pp. 1794-1802 e reproduzido por Ralph et al., (2004). Nat. Rev., (2), pp. 203-216).....pg. 57**

**Figura 11. As roptrias e o processo de adesão e invasão em *P. falciparum*. Os merozoítos ao invadirem uma nova hemácia, estabelecem o contato inicial com proteínas com âncora GPI da membrana da célula hospedeira. Possivelmente com o auxílio de adesinas apicais, interagindo com receptores da membrana das hemácias (p. ex. interação Rh5-basigina), o parasita se reorienta, com a formação das “tight junctions” (TJs), seguida da liberação do conteúdo proteico das roptrias (RONs e ROPs), e formação do vacúolo parasitóforo. (Extraído de: Harvey et al. (2012). Int. J. Parasitol., 42(6), pp. 567-573).....pg. 58**

**Figura 12. Microscopia eletrônica de transmissão das etapas de invasão dos merozoítos na célula hospedeira. (1) Reconhecimento da célula hospedeira. (2) Reorientação do merozoíto e início do estabelecimento da invasão. (3) Formação do TJ/MJ com a interação entre o complexo RON-AMA1, e, possivelmente, liberação do conteúdo das roptrias e outras organelas secretórias. (4) Início da invasão. (5-7) Invasão do merozoíto com a formação do vacúolo parasitóforo. (8 e 9) Finalização da invasão com a selagem da membrana da hemácia. (Extraído de: Riglar et al., (2011), Cell Host Microbe, 9, pp.9-20).....pg. 60**

**Figura 13. Esquema da translocação do complexo RhopH/CLAG até a membrana da célula hospedeira. (1) Possivelmente, o complexo RhopH/CLAG seja introduzido na membrana do vacúolo parasitóforo (MVP) durante a invasão pelos merozoítos. (2) Logo após a invasão, o translocon PTEX, inicia a exportação de proteínas produzidas pelo parasita para o ambiente citosólico da célula hospedeira. Algumas dessas proteínas (tais como, PHISTb, MESA, LyMP, GBP130 e SEMP1), trafegam até o citoesqueleto das hemácias. O complexo RhopH/CLAG (3) liga-se a essas proteínas exportadas na membrana dos eritrócitos ou (4 e 5) se agrega com essas proteínas *en route* até a superfície. (6) Uma vez na superfície, o complexo RhopH/CLAG juntamente com as proteínas que formam NPPs, criam seus próprios poros que atravessam a membrana ou “abrem” um poro eritrocitário. A função das NPPs é permitir a entrada de nutrientes e possivelmente eliminar produtos residuais do parasita. (Extraído de: Counihan et al., (2017), eLIFE, 2(6), pp.1-31).....pg. 62**

**Figura 14. O sistema CRISPR-Cas na imunidade adquirida em procarionotes. (A) O DNA proveniente de fagos/vírus invasores é reconhecido pelas proteínas Cas, que os fragmentam e os incorporam nas sequências *spacers*, adjacente ao operon dos genes *cas*. (B) Em uma eventual re-invasão, o locus CRISPR é ativado, com a transcrição dos crRNAs (provenientes do DNA exógeno invasor) que é associado com a Cas9, no qual, este complexo CRISPR-Cas9 realiza a degradação do DNA invasor. (Extraído de: Ishino et al. (2018). J. Bacteriol., 200(7), pp.1-17).....pg. 64**

**Figura 15. O mecanismo de clivagem da dupla fita do DNA por CRISPR-Cas9. (A) O complexo CRISPR-Cas9, (B) reconhece o motivo PAM (NGG), presente no DNA genômico (gDNA), que (C) com o pareamento do RNA guia (gRNA), ocorre a abertura da dupla fita do DNA, seguida da (D) clivagem do DNA através dos domínios RuvC-**

*like* e HNH da Cas9. (**Extraído de:** Doudna & Charpentier (2014), *Science*, 346(6213), pp. 1258096.1-1258096.9).....pg. 65

**Figura 16. Mecanismo de biotilação de proteínas por APEX2.** Neste esquema, a APEX2 é fusionada ao peptídeo sinal da mitocôndria (mito) que a conduz para a matriz mitocondrial, onde com o uso do substrato biotina-fenol e o agente oxidante/catalisador H<sub>2</sub>O<sub>2</sub> (peróxido de hidrogênio), em uma reação de aproximadamente 1 min, as proteínas mitocondriais são biotiniladas nos resíduos de Tyr (principalmente), Trp, His e Cys por um radical fenólico, que serão posteriormente enriquecidas em colunas de estreptavidina e submetidas à análise por espectrometria de massas. (**Extraído de:** Rhee et al (2013), *Science* (80- )339, pp. 1328–1331).....pg. 71

**Figura 17. Mecanismo do *crosslinking* entre ribonucleoproteínas e RNA com o uso da abordagem APEX-RIP.** Neste esquema, a APEX2 é fusionada ao peptídeo sinal da mitocôndria (mito) que a conduz para a matriz mitocondrial, onde com o uso do substrato biotina-fenol e o agente catalisador H<sub>2</sub>O<sub>2</sub> (peróxido de hidrogênio), em uma reação de aproximadamente 1min, seguida de uma incubação com 0.1% de formaldeído, por cerca de 10min, promoverá o *crosslinking* entre ribonucleoproteínas e RNAs, que é posteriormente enriquecido em coluna de estreptavidina, sendo os RNAs analisados por RNA-seq. (**Extraído de:** Kaewsapsak et al (2017). *eLife*, 6, pp. 1–31).....pg. 72

**Figura 18. Confirmação das construções episomais dos plasmídeos pCC1-HA<sub>(cito)</sub>-APEX2, pCC1-SP<sub>(ACP)</sub>-HA-APEX2, pCC1-SP<sub>(RAP1)</sub>-HA-APEX2 e pCC1-SP<sub>(TrxR)</sub>-HA-APEX2. (A)** Esquema do vetor pCC1 com os insertos da HA-APEX2 com seus respectivos peptídeos sinais de endereçamento ao apicoplasto (ACP), roptrias (RAP1) e mitocôndria (TrxR). **(B)** Padrão das digestões usando *XhoI* e *Sall*, após as sub-clonagens em pCC1, analisado por gel de agarose 1%. Painel à esquerda: (M) corresponde ao marcador 1kb Plus (Thermo Scientific); (1) corresponde ao vetor pCC1 vazio linearizado por *XhoI* e *Sall*; (2) inserto, correspondendo ao tamanho aproximado esperado das sequências SP-HA-APEX2. Somente os clones do poço 4 (referente à construção HA-APEX2), poço 13 (referente à construção RAP-HA-APEX2) e, os poços 15 e 17 (referentes à construção TrxR-HA-APEX2), apresentaram uma ligação eficiente do inserto ao vetor pCC1 (representados em verde). **(C)** Devido ao fato de que a ligação da construção ACP-HA-APEX2 não ter ocorrido em (B), foi realizada uma nova ligação, com a obtenção dos clones nos poços 4 e 8, referentes à ligação eficiente da construção ACP-HA-APEX2. Todos os clones positivos foram utilizados para o procedimento de transfecção.....pg. 147/148

**Figura 19. Confirmação da orientação do inserto e sequenciamento dos plasmídeos. (A)** Gel de agarose mostrando os fragmentos obtidos com a digestão dos plasmídeos pCC1-SP<sub>(cito, acp, rap1, trxr)</sub>-HA-APEX2 utilizando *HindIII*: (M) marcador 1kb Plus (Thermo Scientific); (2) digestão da construção HA-APEX2, com liberação de dois fragmentos com tamanhos de 3,2 kb e 3,9 kb; (3 e 4) digestão da construção ACP-HA-APEX2, com liberação de dois fragmentos com tamanhos de 3,4 kb e 3,9 kb; (5) digestão da construção RAP-HA-APEX2, com liberação de dois fragmentos com tamanhos de 3,35 kb e 3,9 kb; e, (6 e 7) digestão da construção TrxR-HA-APEX2, com liberação de dois fragmentos com tamanhos de 3,4 kb e 3,9 kb. **(B)** Histograma ilustrativo do sequenciamento das construções transientes HA<sub>(cito)</sub>-APEX2, SP<sub>(ACP)</sub>-HA-APEX2, SP<sub>(RAP1)</sub>-HA-APEX2 e SP<sub>(TrxR)</sub>-HA-APEX2. Note que no quadro vermelho

e verde, constam o sítio de restrição *Xho*I e o *start* códon (ATG), respectivamente, sugerindo que todas as construções estão em *frame*.....pg. 149

**Figura 20. Alinhamento do gene *hDHFR* comparando os vetores pCC1-SP<sub>(cito, acp, rap1, trxr)</sub>-HA-APEX2 e vetor pCC1-empty.** Trata-se do sequenciamento do gene de resistência *hDHFR* (*human dihydrofolate reductase*). Somente o códon 9 da sequência possui uma mutação silenciosa (destacado em vermelho), portanto, possivelmente não compromete a sua função.....pg. 150

**Figura 21. Curvas-resposta de IC<sub>50</sub> em diferentes linhagens de *P. falciparum* na presença da WR99210 das marcas Jacobus Pharmaceuticals Inc.\* e Sigma-Aldrich.** (A) Curva de IC<sub>50</sub> para *P. falciparum* linhagem 3D7. (B) Curva de IC<sub>50</sub> para *P. falciparum* linhagem FcB1. (C) Curva de IC<sub>50</sub> para *P. falciparum* linhagem NF54. As curvas de IC<sub>50</sub> foram realizadas pelo método de [<sup>3</sup>H] hipoxantina. Uma diluição seriada da droga anti-folato WR99210 (em escala nM: 250; 125; 62,5; 31,25; 15,63; 7,81; 3,90; 1,95; 0,98; 0,49; 0,24 e 0,12) das marcas Jacobus Pharmaceuticals Inc.\* (●) e Sigma-Aldrich (■) foi realizada para cada linhagem de *P. falciparum*. O controle negativo contendo apenas DMSO, para cada linhagem também foi realizado.....pg. 152

**Figura 22. Expressão e purificação da proteína recombinante APEX2.** O vetor pET100/D-TOPO®, contendo a sequência da 6xHis-APEX2 modificada foi transformado em bactérias competentes *E. coli* linhagem Rosetta™(DE3)pLyS. A lise se deu por BugBuster (Merck-Millipore) e sonicação. O extrato total foi aplicado como *input*, seguida das frações de eluição com imidazol (5-500mM). Como controle positivo do SDS-PAGE, um gradiente de BSA (variando entre 20 µg- 200 µg) também foi aplicado, bem como, o extrato não-ligado (*flowthrough*). As frações de 20mM de imidazol foram utilizadas para a produção de anticorpos policlonais anti-APEX2.....pg. 153

**Figura 23. Validação do soro anti-APEX2 por Western-blot.** Os camundongos da linhagem BALB/c foram imunizados conforme descrito. Os soros dos animais 3974, 3975 e 3976 foram obtidos após 60 dias da primeira imunização. Uma titulação de 1:200, 1:1.000 e 1:5.000 foi realizada para o soro de cada animal contra a proteína APEX2 recombinante. O controle pré-imune também seguiu a mesma titulação. O anticorpo secundário acoplado a fosfatase alcalina foi utilizado na titulação 1:10.000. O Western-blot foi revelado com o uso do substrato BCIP/NBT.....pg. 154

**Figura 24. Micrografia das linhagens de *P. falciparum* transfectadas obtidas até o momento.** (A) pCC1-HA<sub>(cito)</sub>-APEX2 (parasitas expressando APEX2 citosólica). (B) pCC1- SP<sub>(RAP1)</sub>-HA-APEX2 (parasitas expressando APEX2 endereçada às roptrias). (C) pCC1-SP<sub>(TRXR)</sub>-HA-APEX2 (parasitas expressando APEX2 endereçada à mitocôndria). As formas de anel (painéis à esquerda), trofozoíto (painéis do meio) e esquizonte (painéis à direita) também são mostrados.....pg. 155

## LISTA DE TABELAS

**Tabela 1. Lista dos oligonucleotídeos utilizados para o sequenciamento dos plasmídeos de transfecção em *P. falciparum*.....pg. 80/81**

**Tabela 2. Mutações detectadas por sequenciamento dos plasmídeos pCC1.....pg. 151**

A circular inset showing a microscopic view of numerous red blood cells (erythrocytes) against a dark background. The cells are biconcave and appear as reddish-orange spheres. The text is overlaid on this circular area.

I - INTRODUÇÃO /  
REFERENCIAL TEÓRICO





## **CAPÍTULO 1**

# **“UMA VISÃO GERAL SOBRE A MALÁRIA”**

## i. INTRODUÇÃO / REFERENCIAL TEÓRICO

### CAPÍTULO 1 – UMA VISÃO GERAL SOBRE A MALÁRIA

#### 1.1. A malária no mundo e seus impactos

A malária é uma doença tropical amplamente distribuída em todo o mundo e acomete diretamente milhões de pessoas por anos, sendo uma das mais sérias doenças infecciosas capazes de levar os acometidos à morte (Phillips et al., 2017; Moxon et al., 2020). A estimativa é que, em 2019, cerca de 229 milhões de casos de malária causado por *Plasmodium falciparum* e *Plasmodium vivax* ocorreram no mundo, comparado com cerca de 238 milhões de casos registrados em 2000. A estimativa é que até 2019, um total de 409.000 mortes foram decorrentes da malária. De 87 países acometidos pela doença, a região africana ainda apresenta a maior prevalência reportada, com cerca de 94% dos casos e óbitos estimados globalmente (cerca de 215 milhões de casos e 384.000 mortes). As regiões do sudeste da Ásia e do Mediterrâneo também são regiões endêmicas da doença, entretanto, uma considerável redução do número de casos, e, conseqüentemente, da mortalidade tem sido observados (Global Malaria Programme: WHO Global, 2020) (**Figura 1**).

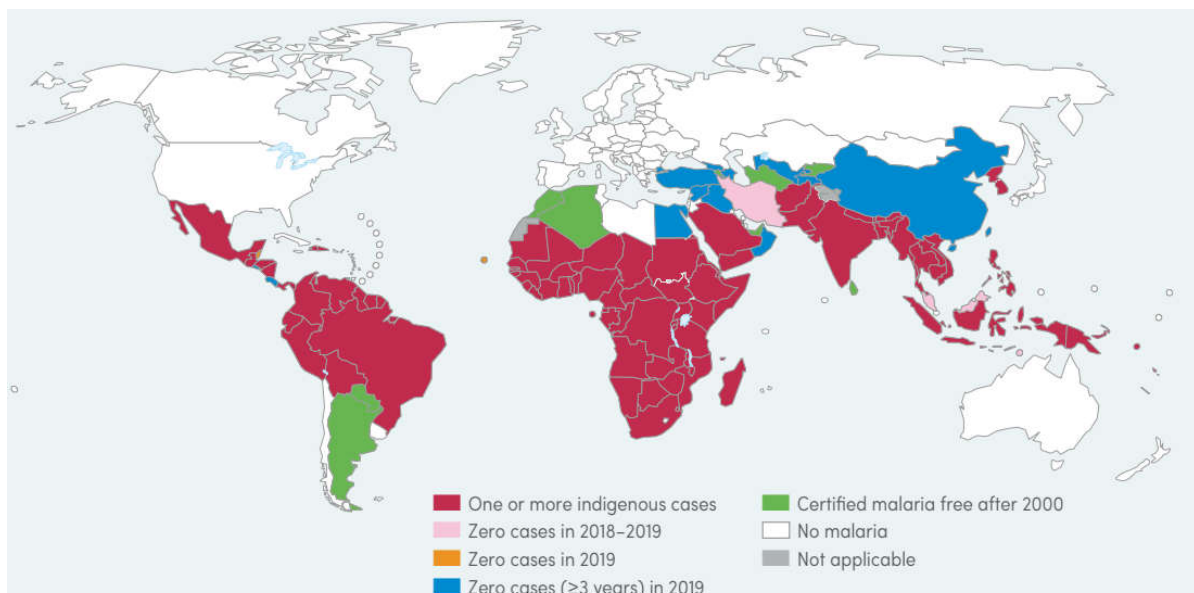


**Figura 1. Distribuição geográfica dos países acometidos pela malária.** As estimativas são provenientes do acompanhamento do período de 2000-2019. Os países em vermelho são aqueles que apresentam maior incidência e prevalência de malária. Os países em azul são aqueles que não apresentaram nenhum caso, nas estimativas dos últimos 3 anos, enquanto que, os países em verde são aqueles que foram diagnosticados como livres da malária desde 2000. Os países em branco são aqueles que não são endêmicos da doença. (**Extraído de:** World Health Organization (2020). *World Malaria Report*).

Apesar da redução do número de novos casos, a malária ainda causa inúmeras mortes anualmente, principalmente em crianças abaixo de 5 anos de idade. Estima-se que a porcentagem total de mortes causadas em crianças nesta faixa etária era de 84% em 2000, comparando-se com 67% em 2019. Além disso, o número de mortes causadas por malária, no contexto geral, também segue essa tendência de redução linear, à qual entre 2000-2019, foram estimados um decréscimo de 736.000 mortes em 2000 para 409.000 em 2019. Os riscos inerentes da malária aplicam-se também, de forma substancial às mulheres grávidas. As acometidas podem desenvolver anemia, podendo agravar o quadro clínico da doença com risco de morte antes ou depois do parto, além de ser fator de risco também para natimortos e nascimentos prematuros (Global Malaria Programme: WHO Global, 2020).

Em algumas regiões endêmicas, onde múltiplas espécies do gênero *Plasmodium* existem, é comum haver co-infecção por diferentes espécies. Já foi relatado através de estudos de vigilância hospitalar que, uma parcela dos pacientes admitidos apresentavam co-infecção de *P. falciparum* e *P. vivax*. Curiosamente, os quadros de anemia severa eram geralmente associados às crianças com idade entre 1-5 anos, sendo estes mais propensos à admissão hospitalar (Douglas et al., 2013). Ainda, em muitos casos, o uso de primaquina, um antimalárico amplamente utilizado para combater a forma dormente recidiva de *P. vivax*, o hipnozoíto, ou, gametócitos de *P. falciparum*, pode ocasionar a um quadro hemolítico perigosamente elevado, em pacientes com deficiência de glicose-6-fosfato desidrogenase (G6PD). A prevalência da deficiência de G6PD, geralmente está associada a pessoas em áreas endêmicas da malária (Howes et al., 2012).

De forma geral, a malária é classificada como assintomática, não-complicada (sintomatologia não evidente) e severa (danos teciduais e de órgãos). Os sintomas são típicos, tais como: febre, calafrios e dores musculares. A presença da sudorese e exaustão se dá pela hemólise das hemácias infectadas com *Plasmodium* spp. (Phillips et al., 2017). O quadro clínico severo da malária frequentemente leva ao óbito, pois o acometido muitas vezes apresenta anemia, comprometimento de vários órgãos devido a obstrução da microcirculação, incluindo o cérebro, podendo culminar na malária cerebral, sendo esta a forma mais grave da doença (Wassmer & Grau, 2017; Moxon et al., 2020). Nessas áreas de alta transmissibilidade de malária, praticamente todas as crianças com idade entre 1-5 anos e adultos tem uma concentração reduzida de hemoglobina em decorrência da doença. Desse modo, em muitos casos de anemia decorrentes da doença requer transfusão de sangue (White, 2018).

Neste cenário, outras complicações podem surgir, tais como a contaminação pelo vírus do HIV (Vermeulen et al., 2019). Outros tipos de infecções transmitidas por transfusão são adicionalmente relatadas, tais como pelos vírus da hepatite B e C (HBV e HCV, respectivamente), sífilis e malária (Ahmadpour et al., 2019; Mremi et al., 2021). A maior parte dessas infecções transmitidas por transfusões (ITTs) ocorrem na região africana. Possivelmente, o fato desses doadores serem assintomáticos para essas doenças seja um fator que pode contribuir para que essas contaminações acidentais ocorram, somado à, talvez, uma limitação técnica e financeira na emissão de laudos com métodos moleculares mais acurados, como PCR (do inglês, *polymerase chain reaction*) (Ahmadpour et al., 2019).

No caso das mulheres grávidas, o cenário é ainda mais delicado, pois a malária está associada com um aumento da prevalência de anemia durante a gravidez, sobretudo na região da África Subsaariana, onde existe o risco de co-infecção por malária-HIV (Ssentongo et al., 2020). Algumas das complicações adicionais decorrentes incluem, baixo peso do recém-nascido, altas taxas de mortalidade neonatal, infecção por malária através da placenta, transferência reduzida dos anticorpos maternos e risco aumentado da transmissão de mãe para filho pelo HIV (Briand et al., 2009; Brickley et al., 2016; Fried & Duffy, 2017; Rogerson et al., 2018). Além disso, nessa região, a baixa concentração de hemoglobina também é causada por deficiência nutricional de ferro (Peña-Rosas et al., 2015), vitamina B12 e folato (Accrombessi et al., 2015; Kupka, 2015); hemoglobinopatias, tais como o traço falciforme (HbS, hemoglobina S) (Elguero et al., 2015; Pule et al., 2017); infecções parasitárias causadas por ancilostomíase (Smith & Brooker, 2010) e esquistossomose (King et al., 2005).

Um dos grandes desafios no controle da malária – de modo especial, na região africana – é o financiamento para subsidiar a compra e distribuição dos antimaláricos para os acometidos pela doença; e investimento em pesquisa científica. A estimativa de financiamento global para estes fins para o período de 2020-2022 é de US\$ 4,8 bilhões. Desse valor, cerca de US\$ 2,1 bilhões foram alocados para 11 países: Burkina Faso, Camarões, República Democrática do Congo, Gana, Índia, Mali, Moçambique, Nigéria, República do Níger, Uganda e Tanzânia. Juntos, estes países representam cerca de 70% dos casos e mortes causadas por malária. Entre o período de 2010-2019, o investimento internacional que compõe 70% do fundo para o controle da malária foi liderado por EUA, Reino Unido e França (Global Malaria Programme: WHO Global, 2020).

Além disso, entre os anos 2007-2018, cerca de US\$ 7,3 bilhões foram investidos na pesquisa básica e aplicada relacionadas à malária. Grande parte deste valor foi distribuído da seguinte forma: (i) US\$ 2,6 bilhões na pesquisa baseada no desenvolvimento de novas drogas antimaláricas; (ii) US\$ 1,9 bilhão na pesquisa básica; e, (iii) US\$ 1,8 bilhão na pesquisa baseada no desenvolvimento de vacinas. Os investimentos relacionados ao controle vetorial e diagnóstico, ainda representaram US\$ 453 milhões e US\$ 185 milhões, respectivamente (Global Malaria Programme: WHO Global, 2020). Dentro deste contexto, pode-se dizer que todos os esforços econômicos tem resultado em boas perspectivas quanto a novas estratégias no controle da doença. O protótipo de uma vacina contra a malária de fase III, conhecida como RTS,S, obteve resultados promissores iniciais, entretanto, devido à sua baixa proteção à longo prazo (Partnership, 2015), com a possibilidade de rebote anos mais tarde (Olotu et al., 2016), não se torna uma candidata viável para aprovação pelas agências reguladoras competentes.

Ainda assim, com os últimos resultados de fase IIb, o protótipo de vacina baseado na RTS,S, conhecida como R21/Matrix-M, pode ser a candidata mais promissora no combate à malária, pois nenhum efeito adverso grave foi atribuído à vacinação, com apenas alguns casos de febre leve registrados. A formulação desta vacina é baseada na utilização da proteína circumsporozoíto (CSP), encontrada nos parasitas de fase pré-eritrocitária, ou hepática, os esporozoítos (Dattoo et al., 2021). Assim como foi feito para a formulação da vacina RTS,S (Partnership, 2015), parte da CSP (repetições centrais) são fusionadas e co-expressas com um antígeno de superfície do vírus da hepatite B (HBsAg). No entanto, o que difere essa formulação da RTS,S é o uso de apenas porções das proteínas de fusão, juntamente com um potente adjuvante (Matrix-M). De forma geral, a sua eficácia permaneceu entre 74-77% nos grupos estudados, após 2-6 meses da última imunização, permanecendo nessa mesma faixa de eficácia ao completar 1 ano (Dattoo et al., 2021).

Além de ser a doença tropical mais letal do mundo, a malária está totalmente relacionada ao *status* socioeconômico, sobretudo entre os países da África Subsaariana (Tusting et al., 2013; Carrasco-Escobar et al., 2021). A possibilidade de uma melhor moradia, educação, empregabilidade e distribuição de renda podem ajudar a reduzir os níveis de desigualdade, e, conseqüentemente, diminuir os casos de malária (Tusting et al., 2013, 2016; Degarege et al., 2019). Dentro deste contexto, uma melhor educação, por exemplo, poderia ser um atributo que facilitaria a prevenção da malária, além de propiciar uma chance melhor de moradia, instrução e

nutrição (Tusting et al., 2016; Degarege et al., 2019). Diante disso, a preocupação com essa doença ainda permanece, pois o parasita e o vetor anofelino são altamente adaptados ao hospedeiro humano, tornando a erradicação da doença um desafio para a saúde pública mundial, diante dos inúmeros obstáculos enfrentados em relação à biologia do agente etiológico e do vetor, bem como as dificuldades financeiras enfrentadas pelas regiões acometidas pela doença.

## 1.2. Quimioterapia e resistência aos antimaláricos

A eficácia no tratamento é um componente crítico para o controle e eliminação da malária. Atualmente, a terapia baseada na combinação de artemisinina (ART) (do inglês, *artemisin combination therapies* ou ACTs) é recomendada como linha de frente para todos os países endêmicos da malária (Cowman et al., 2016; Phillips et al., 2017; Global Malaria Programme: WHO Global, 2020). Na região africana, os tratamentos da linha de frente contra *P. falciparum*, incluem: (i) artemether-lumefantrina (AL), apresentando 98% de eficácia; (ii) artesunato-amodiaquina (AS-AQ) apresentando 98,4% de eficácia; e, (iii) diidroartemisinina-piperaquina (DHA-PPQ) apresentando 99,4% de eficácia, reportados entre 2010-2019. Essas estratégias de tratamento, seguem o mesmo padrão em outras regiões do mundo, tratando-se do *P. falciparum* (Global Malaria Programme: WHO Global, 2020). No entanto, a prevalência e expansão clonal das mutações da *PfKelch13* (do inglês, *kelch propeller domain* ou *K13-propeller*), um marcador molecular associado ao fenótipo de resistência à artemisinina, tem levantado sérias preocupações tanto em relação à eficácia dos antimaláricos quanto da possibilidade do surgimento de novos fenótipos de resistência (Ariey et al., 2014; Straimer et al., 2015; Tilley et al., 2016; Suresh & Haldar, 2018; Global Malaria Programme: WHO Global, 2020).

Apesar de ser considerada como tratamento de linha de frente para casos de malária não-complicada e severa (Adebayo et al., 2020; Global Malaria Programme: WHO Global, 2020), fenótipos resistentes à artemisinina no Camboja (Noedl et al., 2008, 2010; Ariey et al., 2014; Straimer et al., 2015), Myanmar (Nyunt et al., 2017; He et al., 2019) e Vietnã (Thanh et al., 2017; Bui et al., 2020) já foram relatados. Além disso, na tentativa de reverter a prospecção da malária nas regiões endêmicas, o uso de terapias combinadas com artemisinina, ou ACTs, tem funcionado como uma estratégia eficaz para combater fenótipos resistentes à artemisinina. Entretanto, um sutil, porém crescente, aumento do fenótipo de resistência das drogas parceiras

utilizadas em conjunto com ART (Blasco et al., 2017; Adebayo et al., 2020; Ippolito et al., 2021) tem levantado bastante preocupação, já que nenhuma alternativa totalmente eficaz para substituir ACTs está disponível (Bhagavathula et al., 2016; Mavoko et al., 2017), podendo colapsar a saúde pública mundial.

A resistência à outras classes de antimaláricos vem sendo um problema que tem sido observado com grande afinco nas últimas décadas. Os derivados de 4-aminoquinolinas, tais como cloroquina (CQ) e amodiaquina (AQ), talvez tenham sido a primeira classe de antimaláricos modernos a apresentar resistência. Essa classe de antimaláricos atua no vacúolo digestivo do parasita, ligando-se aos cristais de hemozoína, impedindo a detoxificação e incorporação do grupo heme (Payne, 1987; Ridley, 2002). Os polimorfismos dos genes *pfcr1* (do inglês, *chloroquine resistance transporter*) e *pfmdr1* (do inglês, *multidrug resistance transporter 1*), estão associados com o fenótipo de resistência à cloroquina e amodiaquina em *P. falciparum*, respectivamente (Ehlgen et al., 2012; Venkatesan et al., 2014; Otienoburu et al., 2016; Lee et al., 2018).

Diante disso, a CQ foi gradualmente substituída pela administração conjunta de sulfadoxina/pirimetamina (SP), entretanto, a resistência apareceu rapidamente logo após a sua introdução (Rønn et al., 1996; Roper et al., 2004). Outras alternativas foram introduzidas, tais como mefloquina (MFQ), piperquina (PPQ) e atovaquona (ATQ), entretanto, parasitas resistentes logo emergiram (Price et al., 2004; Eastman et al., 2011; Staines et al., 2018). Além disso, o aumento no número de cópias do gene *pfmdr1* foi associado com o aumento da resistência *in vitro* e *in vivo* à MFQ (Price et al., 2004), enquanto que, um novo polimorfismo no gene *pfcr1* foi associado com a resistência à PPQ (Eastman et al., 2011) (**Figura 2**). Estas observações sugerem que os genes do parasita que codificam proteínas transportadoras envolvidas no efluxo de drogas, podem causar o fenótipo de resistência à mais de uma classe de antimalárico, tornando-se ainda mais necessários os estudos que possam viabilizar a identificação de novos alvos terapêuticos.

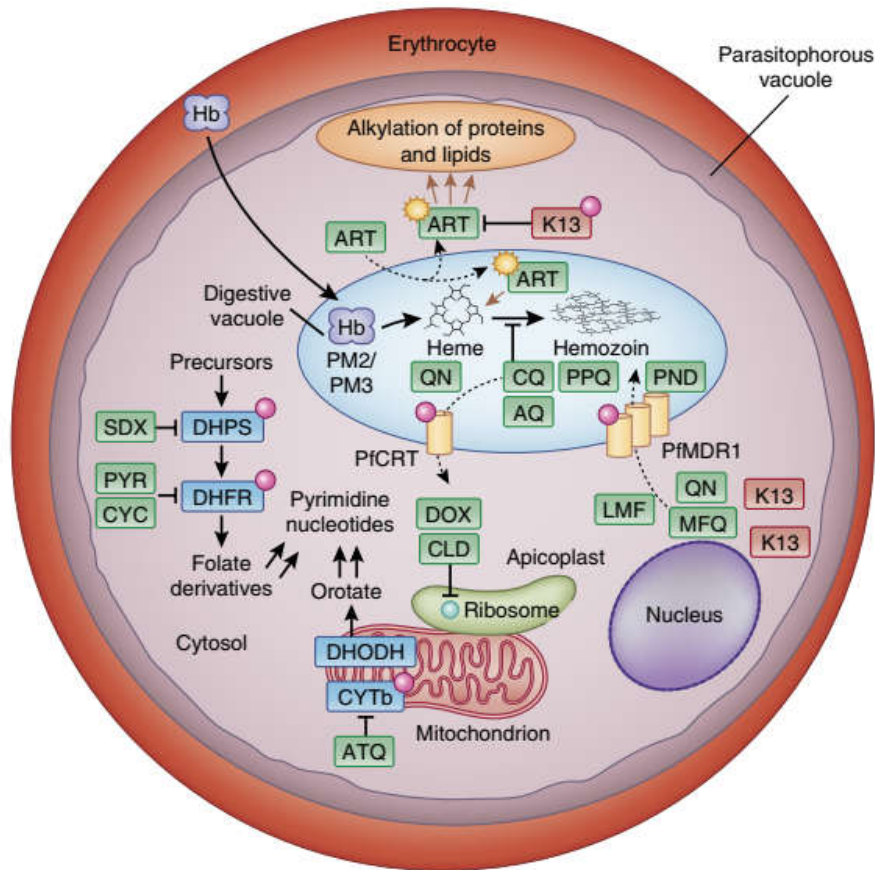


**Figura 2. Mecanismo de ação e resistência dos principais antimaláricos.** Frequentemente, as vias biológicas que são alvos para os antimaláricos atuais são: (i) detoxificação do grupo heme no vacúolo digestivo; (ii) folato e biossíntese de pirimidinas no citosol; e, (iii) a cadeia transportadora de elétrons na mitocôndria. As 4-aminoquinolinas, incluindo CQ e AQ, bem como PPQ possuem ação no vacúolo digestivo, ligando-se ao grupo heme reativo e interferindo na sua detoxificação através da formação da hemozoina. O íon heme ferroso ( $Fe^{2+}$ ) liberado da degradação da hemoglobina (Hb), pode clivar e ativar os derivados de ART (símbolo de estrela). As mutações nos transportadores PfCRT e PfMDR1 (círculos lilás) são determinantes importantes relacionados com a resistência à 4-aminoquinolinas. As formas variantes do marcador molecular kelch-13 (quadros vermelhos), conferem resistência à ART. As mutações em duas enzimas-chave na via de biossíntese do folato, diidropteroato sintase (DHPS) e diidrofolato redutase (DHFR), conferem resistência aos antifolatos: sulfadoxina (SDX), pirimetamina (PYR) e cicloguanil (CYC). ATQ inibe a cadeia transportadora de elétrons mitocondrial, devido à uma mutação pontual na subunidade *b* da citocromo (CYTb). (Extraído de: Blasco et al. (2017). Nat. Med., 23(8), pp. 917-928).

### 1.3. O vetor do gênero *Anopheles* spp. e os desafios do controle vetorial

Cerca de 70 espécies de mosquitos pertencentes do gênero *Anopheles* spp. são conhecidas por ter a capacidade de transmitir a malária aos humanos (Sinka et al., 2012; Molina-Cruz et al., 2016). Apenas na Indonésia, por exemplo, é relatado que cerca de 29 espécies do gênero possam atuar como vetor da doença (Elyazar et al., 2013). Em um contexto mundial, cerca de 41 espécies de vetores são dominantes, distribuídas entre as Américas, Europa, Oriente Médio, África e Ásia (Sinka et al.,



2012). Dentre as espécies com maior representatividade na região africana, estão: *Anopheles arabiensis*, *Anopheles gambiae* e *Anopheles funestus* (Sinka et al., 2012; Molina-Cruz et al., 2016).

O uso de mosquiteiro tratado com inseticida (do inglês *insecticide-treated mosquito net* ou ITN) e a pulverização residual interna (do inglês, *indoor residual spraying* ou IRS) com uso de inseticidas baseados em piretroides, organofosfatos, carbamatos e, mais raramente, o organoclorino diclodifeniltricloroetano (DDT) são as estratégias geralmente recomendadas, para o controle vetorial (Global Malaria Programme: WHO Global, 2020). Uma crescente preocupação tem surgido em relação a um aumento da resistência aos inseticidas atualmente utilizados (Killeen et al., 2013). Um total de 82 países reportaram resistência aos inseticidas para o monitoramento de dados da Organização Mundial da Saúde (OMS), dentre eles, 73 confirmaram a resistência para pelo menos um inseticida em uma espécie do vetor causador da malária entre 2010-2019 (Global Malaria Programme: WHO Global, 2020).

Além disso, o número de países que relataram resistência às quatro principais classes de inseticidas utilizados, aumentou de 26 (entre 2010-2018) para 28 (entre 2010-2019). Dentre as classes de inseticidas com resistência relatadas por estes países, 86,4% é atribuída à piretroides, 80,6% é atribuída à organoclorinos (DDT), 68,8% é atribuída à carbamatos e 58,8% é atribuída à organofosfatos (Global Malaria Programme: WHO Global, 2020). Apesar de ser utilizado mais raramente, pelo fato de ser um poluente orgânico persistente que pode comprometer o meio ambiente e a saúde humana, o uso do DDT tem sido usado com modéstia em muitos países endêmicos da malária (van den Berg et al., 2017). Além disso, a resistência ao DDT pelas espécies, *An. gambiae* e *An. funestus* já foi reportada, respectivamente (Djègbè et al., 2014; Tchigossou et al., 2018).

Neste sentido, evidências moleculares discutem ainda que, alguns marcadores genéticos poderiam ajudar a explicar a resistência dos vetores aos inseticidas. Por exemplo, dois genes de marcadores metabólicos: (i) *GSTE2*, um gene pertencente à família das glutathione-S-transferases; e, (ii) *CYP6M2*, um gene pertencente à família das P450 mono-oxigenases são associados com a resistências aos inseticidas DDT e piretroide nas espécies *An. gambiae* e *An. funestus* (Djègbè et al., 2014; Tchigossou et al., 2018). No entanto, os polimorfismos L1014F, L1014S e N1575Y, para um outro marcador molecular, um canal de sódio controlado por voltagem (do inglês, *voltage gated sodium channel* ou VGSC) parecem estar associados ao fenótipo de resistência

à diferentes tipos de inseticidas, com padrões polimórficos distintos entre as espécies, *An. gambiae*, *An. funestus* e *Anopheles coluzzii* (Djègbè et al., 2014; Irving & Wondji, 2017; Tchigossou et al., 2018; Muhammad et al., 2021).

Em contrapartida, o uso dos inseticidas baseado no uso de (i) piperonil-butóxido (PBO) juntamente com piretróides; e, (ii) neonicotinoides, tem revelado uma interessante perspectiva quanto à eficácia destes, contra os vetores da malária, pelo fato de possuírem uma longa eficácia residual ao serem utilizados nos mosquiteiros, e, alta taxa de mortalidade dos vetores (Ngufor et al., 2017; Oxborough et al., 2019; Gleave et al., 2021). Além disso, outras estratégias para o controle vetorial através da esterilização química, com uso do hormônio piriproxifeno (Jaffer et al., 2015; Koama et al., 2015) ou esterilização genética com uso de CRISPR-Cas9 (Pham et al., 2019), especialmente em regiões com casos reportados de mosquitos resistentes à piretróides, tem sido vislumbradas.

#### **1.4. A malária no Brasil**

Entre os anos de 1990-2017, um total de 11.327.462 casos de malária foram confirmados no Brasil. Destes, 73,5% foram causados por *P. vivax*, 25,5% causados por *P. falciparum*, e, 1% por outras espécies (Bezerra et al., 2020). Essas estimativas estão em consonância com o que é estimado pela OMS. Estima-se que cerca de 72,3% dos casos de malária na região das Américas é causado por *P. vivax*, correspondendo a 3% das estimativas globais de casos registrados de malária, causados por esta espécie. Na América do Sul, o Brasil, Colômbia e Venezuela somam 86% dos casos relatados. Apesar disso, uma redução de cerca de 40% da incidência e mortalidade causadas pela malária foram registradas nessa região, condizente com a linearidade de redução reportada em outras regiões (Global Malaria Programme: WHO Global, 2020). No Brasil, os casos registrados tem caído anualmente, com 267.047 casos em 2011, 242.756 casos em 2012 (uma redução de 9,1%), e, 178.613 casos em 2013 (uma redução de 26,4%) (Pina-Costa et al., 2014).

No território brasileiro, a região mais acometida pela malária é a amazônica. Grande parte disso se dá pelo fato que, a partir da metade nos anos 60, um crescente e desorganizado processo de antropização da região, devido ao aumento progressivo da migração, desmatamento para exploração madeireira, pecuária, agricultura, bem como assentamentos improvisados, contribuem para o aumento da transmissão da doença (Oliveira-Ferreira et al., 2010; Souza et al., 2019). Portanto, as dificuldades

econômicas e os riscos sociais fazem com seja quase impossível eliminar a malária nesta região. Geralmente, as infecções causadas por *P. vivax* são caracterizadas como uma doença “benigna” pois, apesar de ocasionar febre, a sua taxa de mortalidade é considerada baixa. De acordo com as estatísticas oficiais, entre 1998-2008, apenas 234 mortes foram relatadas decorrentes da malária causada por *P. vivax* na Amazônia brasileira (Oliveira-Ferreira et al., 2010).

Além disso, um padrão de complicações clínicas atípicas tem sido associados à malária *vivax*, tais como o diagnóstico de infecção por *P. vivax* em pacientes com anemia falciforme (Cabral et al., 2006). Uma parte dos pacientes diagnosticados com malária severa causada por *P. vivax* que falecem, apresentam outras co-morbidades que poderiam ter contribuído para a morte, tais como doenças no fígado e no coração, bem como deficiência de G6PD (Oliveira-Ferreira et al., 2010). É importante ressaltar que a forma dormente do *P. vivax*, os hipnozoítos, são tratados com primaquina, a única droga hipnozoítica atualmente aprovada para uso clínico (Howes et al., 2012). Desse modo, o uso dessa droga, pode ocasionar quadros de anemia em pacientes com deficiência de G6PD, que são estimados em cerca de 3% nos homens de Manaus, por exemplo (Santana et al., 2009).

Os antimaláricos de linha de frente para o tratamento da malária causada por *P. falciparum* no Brasil são artemether-lumefantrina (AL) e artesunato-amodiaquina (AS-AQ), enquanto que, a cloroquina (CQ), ou a combinação de CQ e primaquina (PQ) são as estratégias recomendadas para o tratamento da malária causada por *P. vivax* (Ferreira & Castro, 2016; Global Malaria Programme: WHO Global, 2020). Ainda, um fator que dificulta muito o diagnóstico correto e, eventualmente, a administração do tratamento é a falta de uma sintomatologia clara, pois frequentemente as infecções causadas por *P. vivax* são assintomáticas, podendo apresentar uma prevalência de até 4-5 vezes maior do que àquela apresentada em infecções sintomáticas (Alves et al., 2002; Carlos et al., 2019). Por exemplo, em um estudo realizado com a população dos assentamentos da área de Remansinho, na Amazônia brasileira, foi observado que cerca de 17% dos pacientes assintomáticos, só apresentaram sintomas após 6 semanas de infecção (Barbosa et al., 2014).

Outro fator agravante é o sutil aumento da resistência aos antimaláricos utilizados no tratamento contra *P. vivax*. O tratamento contra a malária *vivax* mudou pouco nos últimos 60 anos. O uso da CQ ou a combinação da CQ-PQ ainda continua sendo a linha de frente contra a malária causada por *P. vivax*, entretanto, este tratamento vem sendo ameaçado com o surgimento de linhagens de *P. vivax*

resistentes à CQ, em todo o mundo (Price et al., 2014). No Brasil, o primeiro caso de *P. vivax* resistente à CQ relatado se deu em 1992 (Garavelli & Corti, 1992) e, desde então, esta temática tem recebido uma maior atenção (Santana-Filho et al., 2007; Chehuan et al., 2013; Marques et al., 2014). Embora essas linhagens resistentes representem uma pequena parcela dos isolados, elas tem sido associadas à complicações secundárias, tais como a anemia (Chehuan et al., 2013; Marques et al., 2014).

Ainda que o principal vetor da doença no Brasil, *Anopheles darlingi*, esteja presente em cerca de 80% do país, a incidência da malária no Brasil é quase exclusivamente restrita à região amazônica (cerca de 99,8% dos casos) (Oliveira-Ferreira et al., 2010). No entanto, outras espécies já foram relatadas na região nordeste do Brasil, tais como *Anopheles aquasalis*, *Anopheles minor* e *Anopheles albitarsis* (Gomes et al., 2020). Desse modo, uma vigilância efetiva quanto a estratégias que possam melhor combater a propagação do vetor devem ser pensadas, pois alguns fatores, tais como hábitos variáveis de picada pelo vetor, movimento humano, efeitos ambientais e climáticos, podem afetar a variabilidade das taxas de transmissão (Ferreira & Castro, 2016).

### 1.5. O gênero *Plasmodium* spp. e o ciclo biológico

Até o momento, um total de sete espécies de parasitas do gênero *Plasmodium* spp., são capazes de infectar os humanos: (i) *P. falciparum* e *P. vivax*, ambas espécies conhecidas por infectar apenas humanos; e, (ii) *P. ovale*, *P. malariae*, *P. knowlesi*, *P. cynomolgi* e *P. brasilianum*, conhecidas por serem espécies zoonóticas, com potencial de infectar humanos. Conforme já exposto, *P. falciparum* está distribuída nas regiões tropicais, de modo especial na região africana, e, *P. vivax*, está distribuída nas regiões de clima temperado e tropicais, de modo especial a região das Américas, sobretudo a América do Sul e Central (Phillips et al., 2017; Global Malaria Programme: WHO Global, 2020). Como já abordado, a maioria dos casos fatais da doença que acometem crianças abaixo de 5 anos de idade, e, mulheres grávidas são associadas à espécie *P. falciparum* (Phillips et al., 2017; Moxon et al., 2020). Estima-se ainda que, cerca de 1.200 crianças abaixo de 5 anos na região africana são mortas pela malária por dia (Maitland, 2016).

As infecções causadas por *P. ovale* e *P. malariae* são menos frequentes, e, raramente causam a forma severa da doença (Cowman et al., 2016; Phillips et al.,

2017; Moxon et al., 2020). A espécie *P. knowlesi*, foi inicialmente considerada por acometer apenas primatas não-humanos, entretanto, casos de malária severa, ou ainda, fatais, já foram reportados, associados à esta espécie em humanos (Singh et al., 2004; Cox-Singh et al., 2008; Singh & Daneshvar, 2013). As razões para a emergência de infecções por *P. knowlesi* em humanos, ainda não são bem compreendidas, entretanto, é possível que esteja ligada ao manejo da terra, colocando os humanos em proximidade com os hospedeiros primatas e vetores infectados com *P. knowlesi* (Brock et al., 2016). Pouco se sabe acerca da capacidade infectiva das espécies *P. cynomolgi* e *P. brasilianum*, entretanto, casos em humanos de ambas as espécies já foram relatados, inclusive episódios assintomáticos (Lalremruata et al., 2015; Imwong et al., 2019).

De modo geral, as espécies com maior representatividade clínica, *P. falciparum* e *P. vivax*, apresentam o mesmo ciclo biológico. O ciclo de vida do parasita é dixênico, alterando entre as formas infectivas entre o hospedeiro invertebrado do gênero *Anopheles* spp. e o hospedeiro vertebrado humano (**Figura 3**). O vetor invertebrado, do gênero *Anopheles* spp., durante o repasto sanguíneo, transmite a forma esporozoítio do *Plasmodium* spp. para o hospedeiro vertebrado humano. Dentro dos primeiros 30-60 minutos, os esporozoítios inoculados pelo vetor invadem os hepatócitos através das células de Kupffer ou células endoteliais, formando o vacúolo parasitóforo, aonde eles multiplicam-se e dividem-se para formar os merozoítios, por um processo denominado esquizogonia (**Figura 3, Painel A e B**) (Cowman et al., 2016; Phillips et al., 2017).

Com a ruptura do merossoma, os merozoítios liberados das células hepáticas, entram na corrente sanguínea, iniciando o estágio extra-hepático, constituindo assim, o ciclo intra-eritrocitário ou a fase assexuada do ciclo biológico. Aproximadamente, a cada 48h do ciclo, o parasita transita pelas formas de anel, trofozoítio e esquizonte (estrutura segmentada contendo as formas infectivas, chamadas de merozoítios), sendo que, este último propicia o rompimento das hemácias infectadas (**Figura 3, Painel C**), onde a hemozoína, proveniente do metabolismo do ferro da hemoglobina, associada ao DNA do parasita, ativará os receptores *toll-like 9* (TLR9), um receptor sensível ao DNA de patógenos (Parroche et al., 2007), levando a um aumento da produção do fator de necrose tumoral (TNF), contribuindo para a sintomatologia da fase aguda da doença (Karunaweera et al., 1992; Wijesekera et al., 1996; Vijaykumar et al., 2001). Nesta fase do desenvolvimento do parasita, o paciente acometido

começa a apresentar os sintomas clássicos da infecção: febre e sudorese (Phillips et al., 2017).

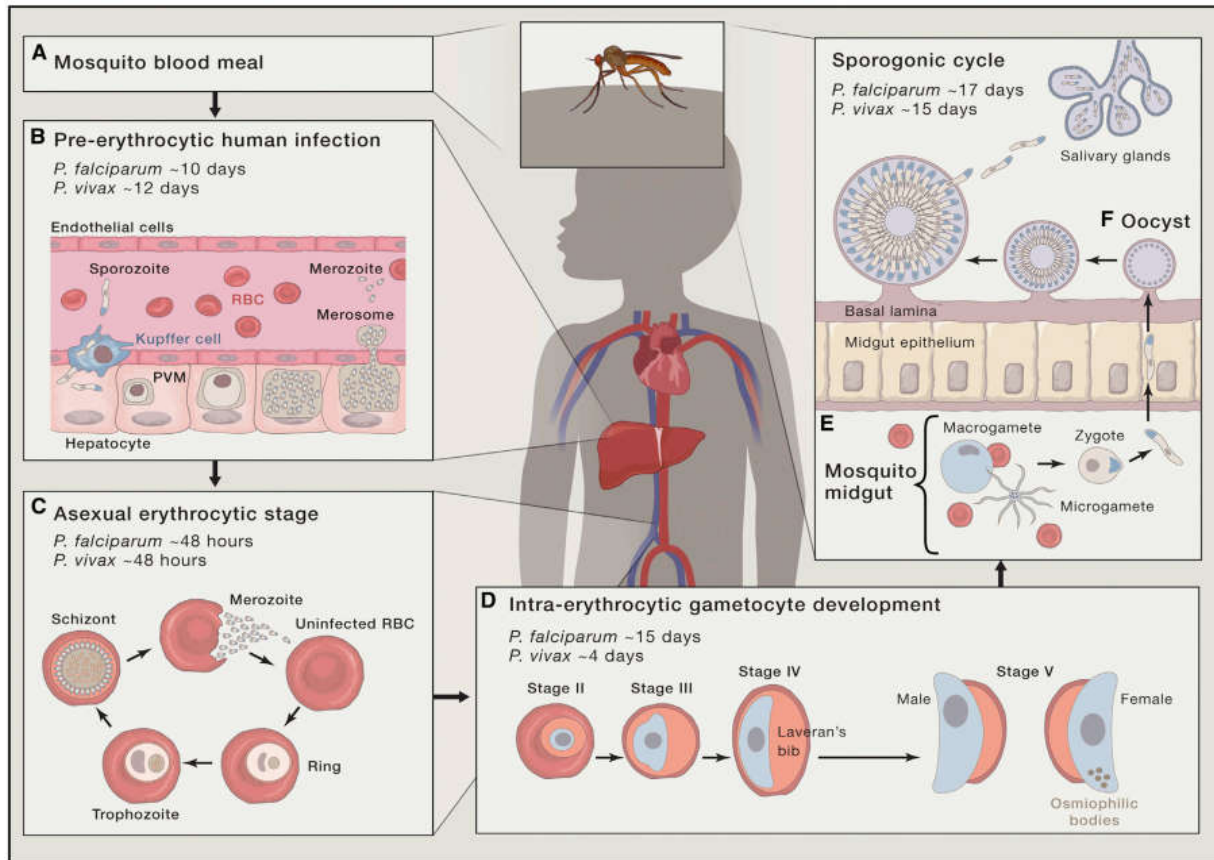


**Figura 3. O ciclo biológico de *P. falciparum* e *P. vivax*.** (A) Durante o repasto sanguíneo, o vetor invertebrado do gênero *Anopheles*, transmite (B) os esporozoítos na corrente sanguínea do hospedeiro vertebrado humano, onde o mesmo irá migrar para os hepatócitos, multiplicando-se em esquizontes hepáticos. Com a ruptura do merossoma, (C) os merozoítos invadirão as hemácias, seguindo para o ciclo eritrocitário assexual, transitando das formas de anel, trofozoíto e esquizonte. Possivelmente, devido à parasitemia elevada e mecanismos de comunicação celular, alguns parasitas se diferenciam em gametócitos (D), que são posteriormente ingeridos pelo vetor invertebrado em um novo repasto sanguíneo (E), com a fecundação dos gametócitos, e a formação de novos esporozoítos e migração para as glândulas salivares (F). (Extraído de: Cowman et al. (2016). Cell, 167(20), pp. 610-624).

À partir de alguns merozoítos liberados, ditos como “sexualmente comprometidos” e, possivelmente, através de estímulos ambientais, tais como uma alta parasitemia e exposição à agentes farmacológicos, a “decisão” para a produção de gametócitos é tomada (Figura 3, Painel D) (Baker, 2010; Cowman et al., 2016). Além disso, tem sido proposto que vesículas contendo proteínas e DNA facilitam a comunicação celular dos parasitas, favorecendo a produção de gametócitos (Mantel et al., 2013; Regev-Rudzki et al., 2013). Estes, migram para os capilares da pele, e, quando o vetor invertebrado, o mosquito do gênero *Anopheles* spp., realiza um repasto sanguíneo, dentro do intestino do vetor, alguns destes sofrem mitose, produzindo oito microgametócitos (gametócito masculino) e, alguns maturam para macrogametócito (gametócito feminino) (Cowman et al., 2016; Phillips et al., 2017).

Como o microgametócito é flagelado, o mesmo irá fecundar o macrogametócito, dando origem a um zigoto, que cerca de 24h mais tarde, transitará para um oocineto e, por ser móvel, esta forma do parasita consegue migrar através do epitélio do intestino do vetor, convertendo-se em um oocisto (**Figura 3, Painei E**). Ali, o oocisto irá passar pela replicação assexual esporogônica, dando origem a novos esporozoítos, que se movem do abdômen do vetor, para as glândulas salivares, onde em um eventual repasto sanguíneo, o mosquito do gênero *Anopheles* spp., se tornará capaz de re-infectar um novo hospedeiro vertebrado com novos esporozoítos, em um eventual repasto sanguíneo, completando assim, o ciclo biológico do parasita (Cowman et al., 2016; Phillips et al., 2017).



## CAPÍTULO 2

### “O EXPORTOMA DE *P. falciparum*”



## CAPÍTULO 2 – O EXPORTOMA DE *P. falciparum*

### As proteínas exportadas em *P. falciparum* e o papel da KAHRP

Devido ao fato das hemácias não possuírem alguns mecanismos celulares, tais como a secreção de moléculas, tráfego de vesículas e síntese de proteínas, o parasita *P. falciparum* ao invadi-las necessita impor algumas modificações estruturais, a fim de permitir a sua sobrevivência. Dentre as modificações propiciadas pelo parasita, estão as propriedades de permeabilidade, rigidez e citoaderência da célula hospedeira, sendo que, todo esse remodelamento, permite a exportação de proteínas para o citosol e para a membrana das hemácias, que são essenciais na virulência do *P. falciparum* (Spillman et al., 2015). Para que as proteínas exportadas atinjam a membrana da célula hospedeira, é necessário que uma organela secretória denominada como *Maurer's clefts* (MCs), amplamente reconhecida por carregar fatores de virulência, seja utilizada (Bhattacharjee et al., 2008).

As modificações exercidas na célula hospedeira são predominantemente realizadas por proteínas que são exportadas a partir do parasita, estimando-se que ~5-8% de seu genoma (200-400 proteínas) seja exportado para o citosol da hemácia (Hiller et al., 2004; Marti et al., 2004). Muitas dessas proteínas apresentam um peptídeo sinal N-terminal e uma sequência consenso que fica após ~35 resíduos do peptídeo sinal. Essa região é denominada PEXEL (do inglês, *Protein EXport ELEMENT*) ou VTS (do inglês, *vacuolar transport signal*), que é constituída por uma sequência pentamérica RxLxE/Q/D (Hiller et al., 2004; Marti et al., 2004), clivada por uma protease do retículo endoplasmático, denominada plasmepsina V (PMV), na região C-terminal da leucina (L) (Boddey et al., 2010; Russo et al., 2010). Após a clivagem, a proteína receberá no retículo endoplasmático (RE) uma N-acetilação (N-Ac), onde a proteína processada pelas proteases, com o domínio de exportação PEXEL (Ac-xE/Q/D) será conduzida até a célula hospedeira (Chang et al., 2008) (**Figura 4**).

Além disso, inicialmente havia sido proposto que o suposto reconhecimento do PEXEL pela fosfatidilinositol-3-fosfato (PI(3)P), seria essencial para que este processamento ocorresse de forma eficiente no RE, inclusive de forma independente da PMV. Ainda, foi sugerido que sequências divergentes da sequência consenso

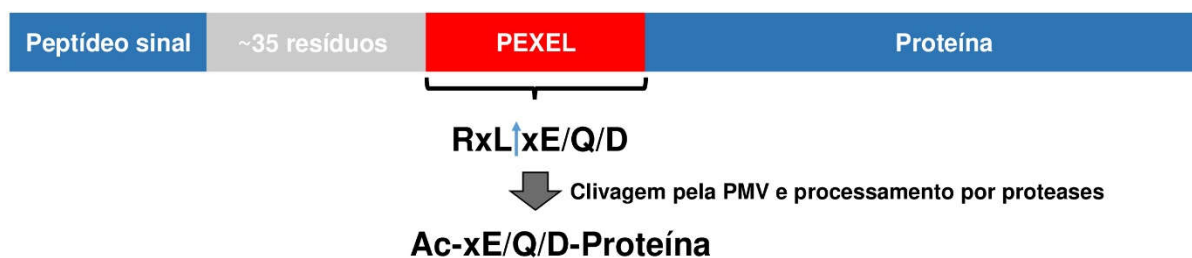


**Figura 4. Esquema do processamento das proteínas com a sequência consenso PEXEL.** Após o processamento por proteases (PMV, peptidases do peptídeo sinal e N-acetil-transferases), as proteínas acetiladas são marcadas para serem exportadas para o citosol da célula hospedeira.

PEXEL, poderiam promover a exportação das proteínas por este mecanismo (Bhattacharjee et al., 2012). Mais recentemente, esta proposta foi totalmente refutada. As proteínas que possuem o domínio PEXEL não só, não tem nenhuma ligação com PI(3)P, como também este lipídeo não se localiza no ER, e, sim nas membranas do vacúolo digestivo e apicoplasto de *P. falciparum*. Além disso, o domínio PEXEL é funcionalmente imutável, permitindo assim o processamento co-traducional das proteínas exportadas pela protease PMV. Portanto, a interação entre PI(3)P e PEXEL no RE não é um mecanismo seletivo para exportar proteínas para o ambiente citosólico da célula hospedeira infectada por *P. falciparum* (Boddey et al., 2016).

Apesar disso, algumas proteínas não são exportadas por esse mecanismo. Por exemplo, a PfEMP1 (do inglês, *P. falciparum erythrocyte membrane protein 1*), que é uma adesina amplamente descrita como um dos fatores de virulência mais importantes em *P. falciparum*, e, pertencente a uma família com 60 genes variáveis (família *var*) (Scherf et al., 2008), é exportada por um mecanismo alternativo PEXEL-independente, denominado PNEPs (do inglês, *PEXEL-negative exported proteins*). Neste mecanismo, as proteínas podem apresentar regiões hidrofóbicas que podem representar um peptídeo sinal N-terminal não-clássico ou um domínio transmembrana, e não necessitam da sequência consenso PEXEL para serem exportadas até a célula hospedeira. Ao invés disso, é proposto que essas proteínas sejam exportadas através de “cargas” vesiculares até a superfície da membrana da célula hospedeira (Spielmann & Gilberger, 2010; Heiber et al., 2013).

Para as proteínas que possuem a sequência consenso PEXEL, como é o caso da KAHRP (do inglês, *knob-associated histidine rich protein*) (Marti et al., 2004), após o processamento pela PMV, a mesma será encaminhada para o translocon PTEX (do inglês, *Plasmodium translocon of exported proteins*), presente na membrana do

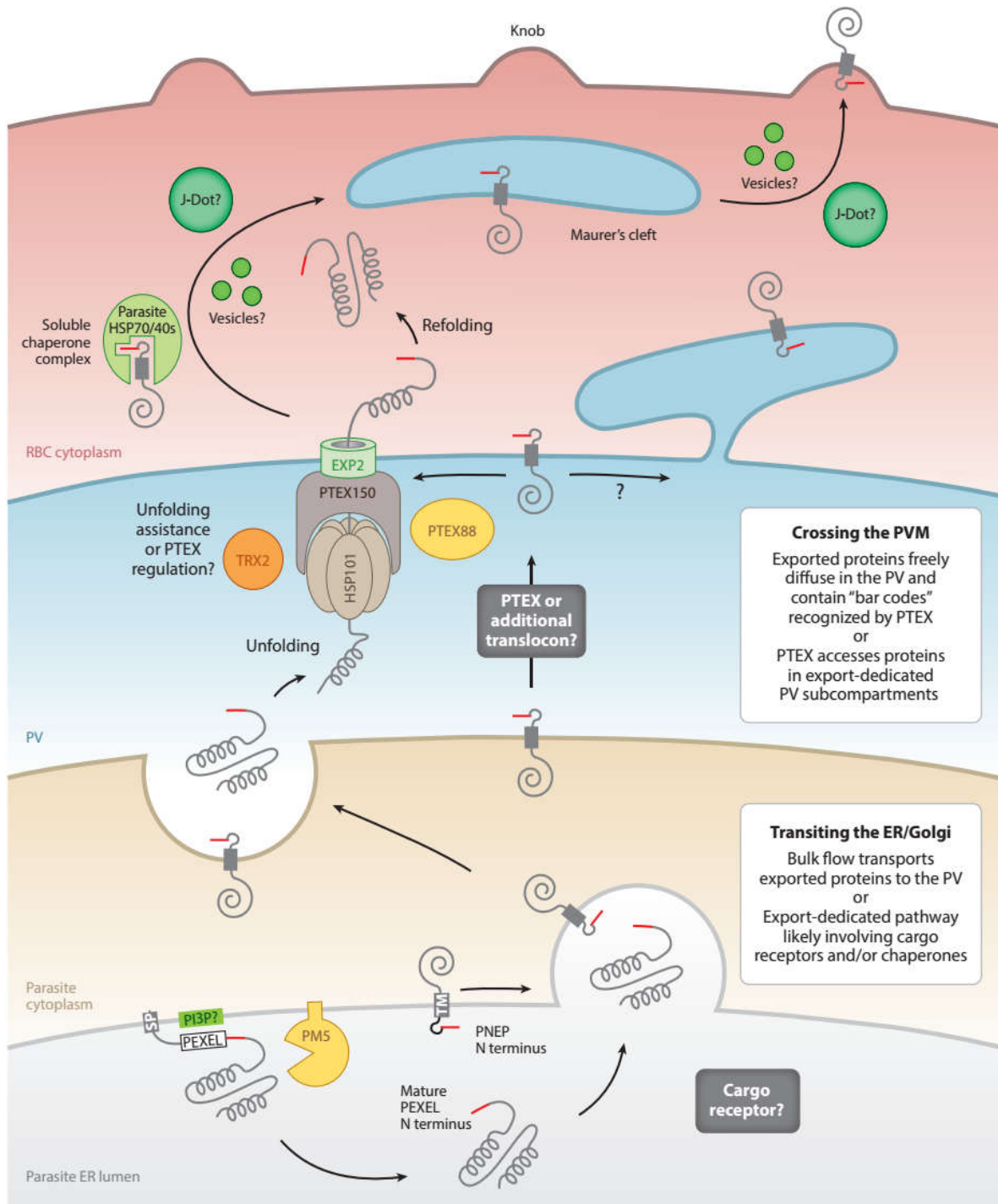


**Figura 5. Mecanismo de exportação de proteínas PEXEL e PNEPs.** As proteínas contendo o motivo PEXEL são liberadas a partir do retículo endoplasmático (ER), pela plasmepsina V (PM5) e encaminhadas para uma via de secreção clássica até o vacúolo parasitário (VP). Por outro lado, as proteínas contendo apenas o peptídeo sinal N-terminal não clássico (ou PNEPs), se ligam na membrana do lúmen do ER, pelo domínio transmembrana (TM). Uma vez no VP, as proteínas contendo o motivo PEXEL, são exportadas pelo translocon PTEX presente na membrana do vacúolo parasitário (MVP), podendo ser liberadas dentro das vesículas organelares, denominadas por *Maurer's Clefts*, até a superfície da membrana da célula hospedeira, ou ainda se associarem à outras cargas vesiculares, tais como os “*J-dots*”. (Extraído de: Spillman et al., (2015). Annu. Rev. Biochem. 84, pp. 14.1-14.29).

vacúolo parasitário (MVP), que é constituído pelo conjunto das proteínas: PTEX150 e PTEX88, que formam o arcabouço do translocon, a estrutura hexamérica da HSP101, que pertence à família ClpA AAA+ ATPase de chaperonas, que favorece o

desnovelamento das proteínas exportadas, tendo o aporte da TRX2, que possivelmente atua na redução das pontes dissulfeto dos resíduos de cisteína, e encaminhando a proteína a ser exportada para o poro EXP2 (Koning-Ward et al., 2009) (**Figura 5**).

As *Maurer's clefts* (MCs) representam uma dessas “cargas” vesiculares que desempenham um papel essencial na exportação de proteínas até a célula hospedeira (Lanzer et al., 2006). Após o processamento via PTEX, a KAHRP será exportada para a superfície da hemácia através destas estruturas vesiculares que brotam a partir da MVP e alcançarão a membrana plasmática da célula hospedeira, onde a KAHRP juntamente com *PfEMP1* formarão diversas estruturas denominadas de “*knobs*” (protrusões), que facilitarão os processos de citoaderência e formação de Rosettas (um aglomerado de hemácias infectadas e não-infectadas); e, rigidez da membrana plasmática do eritrócito, podendo culminar em obstrução da microcirculação (Crabb et al., 1997; Wickham et al., 2001; Wickert et al., 2003; Spycher et al., 2008).

Sabe-se que a KAHRP e a *PfEMP1* são proteínas importantes na formação dos *knobs* (Oh et al., 2000; Waller et al., 2002), onde é sugerido que o domínio ATS (do inglês, *acidic terminal sequence*) da *PfEMP1* interage especialmente com o domínio 5' rico em histidina da KAHRP (Waller et al., 2002). Ainda, foi observado que em linhagens mutantes para diversas porções da região C-terminal do gene *kahrp*, não impossibilitou a exportação da *PfEMP1* para a superfície da hemácia, porém afetou a formação funcional dos *knobs*, especialmente para as linhagens expressando menores versões da KAHRP, apresentando ainda uma citoaderência diminuída (Rug et al., 2006). Possivelmente, essa citoaderência reduzida esteja ligada a expressão reduzida de *PfEMP1* na superfície das hemácias infectadas por *P. falciparum*, resultando em hemácias com uma distribuição reduzida dos *knobs* (Horrocks et al., 2005) (**Figura 6**).

Dentro deste contexto, muitas proteínas tem sido estudadas em relação à qual tipo de transporte elas utilizam, para atingir o ambiente da célula hospedeira (Marti et al., 2004; Maier et al., 2008). Mesmo a KAHRP não sendo essencial no transporte da *PfEMP1* para a membrana da hemácia infectada (Subramani et al., 2015), estima-se que algumas proteínas exportadas via PEXEL ou PNEPs, sejam importantes neste transporte. Dentre as proteínas PNEPs, a MAHRP (do inglês, *membrane associated histidine rich protein*) e a SBP1 (do inglês, *skeleton-binding protein 1*) são designadas

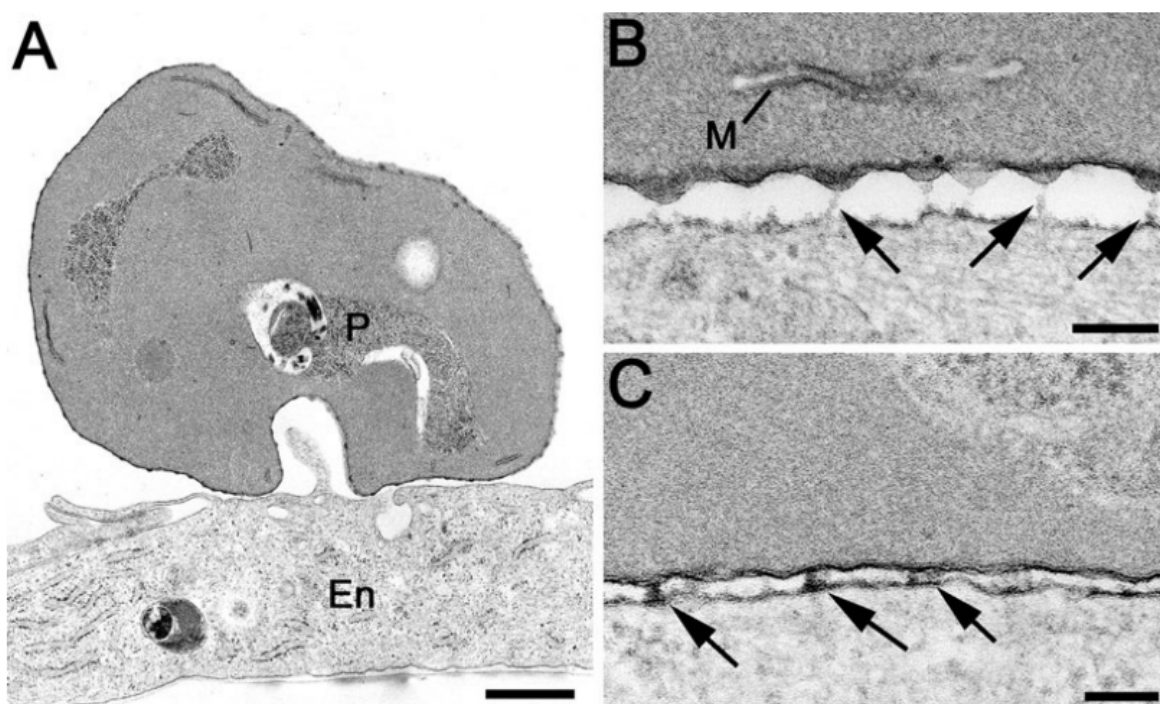


**Figura 6. Micrografia eletrônica de transmissão da interação célula-célula entre as hemácias infectadas por *P. falciparum* (P) e o endotélio (En).** (A) Uma hemácia infectada com *P. falciparum* (P) com a presença normal dos *knobs* (K<sup>+</sup>) está aderindo à superfície das células endoteliais (En). Barra de 1 um. (B) Detalhe da interface entre a interface de K<sup>+</sup> e uma célula endotelial mostrando as faixas de conexão entre as células (setas). Note a presença das *Maurer's clefts* (M). Barra de 100 nm. (C) Detalhe da interface entre uma hemácia infectada com *P. falciparum* com a redução dos *knobs* (K<sup>-</sup>), mostra um material denso entre o endotélio e as hemácias (setas), sem uma adesão evidente ao endotélio. Barra de 100 nm. (Extraído de: Horrocks et al., (2005). J. Cell Sci., 118(11), pp. 2507-2518).

como proteínas pertencentes das MCs, sendo essenciais na transferência da *PfEMP1* para esta estrutura. Os mutantes nocauteados para os genes *sbp1* e *mahrp1* não inviabilizam a formação das MCs, entretanto, não apresentam a *PfEMP1* na superfície da hemácia, reforçando a hipótese de que elas são essenciais no transporte dessa proteína (Cooke et al., 2006; Spycher et al., 2008).

Outras PNEPs exportadas à partir do *P. falciparum* possuem relevante papel na integridade do tráfego vesicular, ancoragem da *PfEMP1* e citoaderência. Por exemplo, a proteína REX1 (do inglês, *ring-exported protein 1*) está associada com a organização estrutural das MCs. Na sua ausência, o número de MCs é reduzido, ainda apresentando uma morfologia aberrante. Em linhagens mutantes com deficiência funcional da REX1, a *PfEMP1* apresenta uma redução da sua exposição na superfície da membrana da célula hospedeira com uma considerável redução da ligação ao receptor endotelial CD36 (McHugh et al., 2015). Além disso, dois genes do cluster “*ring-stage specific genes*”, codificantes para: (i) REX2 (do inglês, *ring-exported*

*protein 2*), uma proteína integral associada às MCs (Spielmann et al., 2006; Haase et al., 2009); e, (ii) REX3 (do inglês, *ring-exported protein 3*), uma proteína solúvel exportada (Spielmann et al., 2006), estão dispostos no cromossomo 9, ligados a uma região de genes associados à citoaderência (Hawthorne et al., 2004) (**Figura 7**).

Em contrapartida, as proteínas com motivo PEXEL, denominadas PTP1-6 (do inglês, *PfEMP1-trafficking proteins 1-6*), são propostas como essenciais no transporte da *PfEMP1* para a superfície das hemácias (Maier et al., 2008). Além disso, a proteína GBP130 (do inglês, *glycophorin binding protein 130*) (Maier et al., 2008; Boddey et al., 2016), PHISTb (do inglês, *Plasmodium helical interspaced subtelomeric family*) (Marti

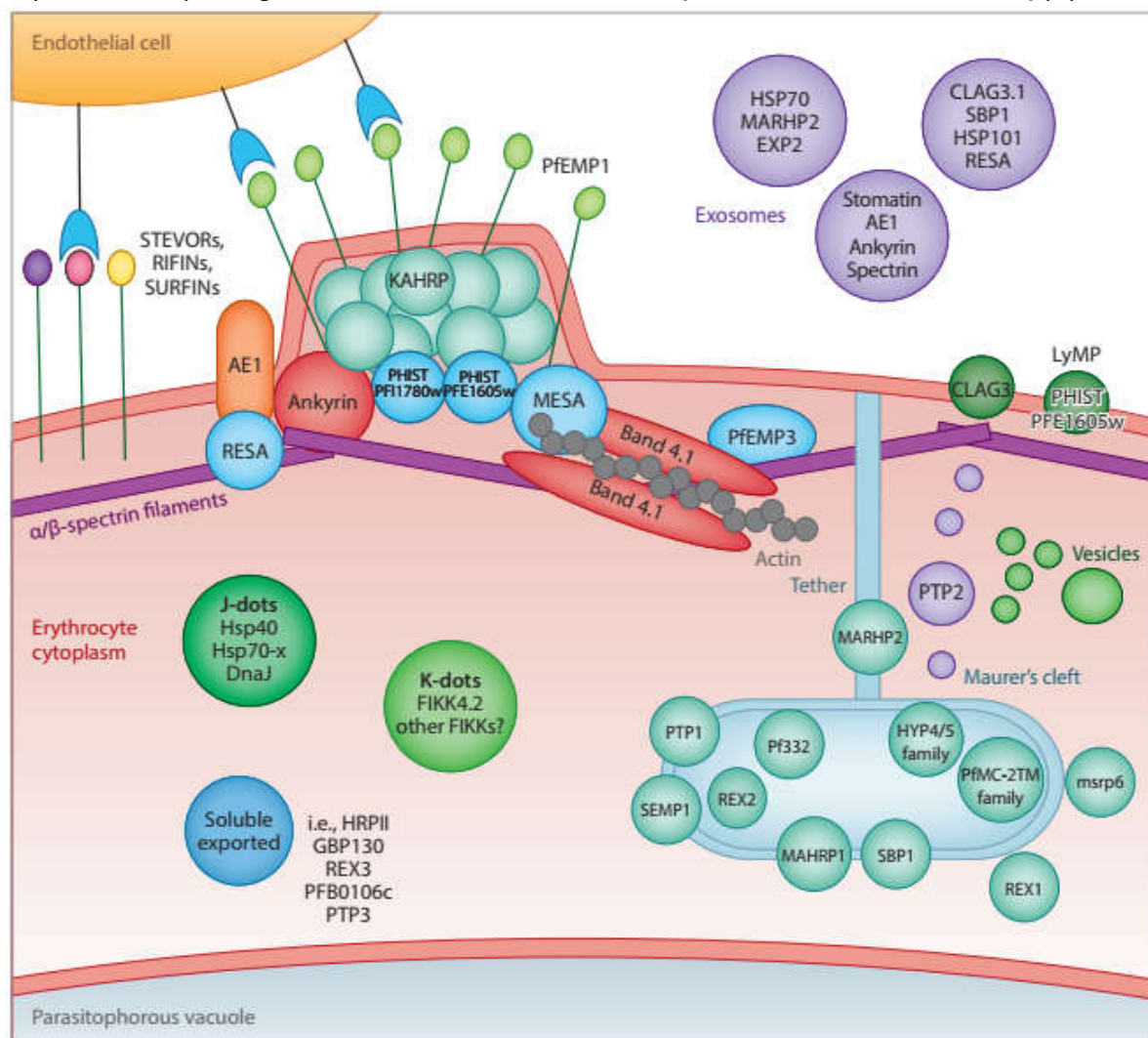


**Figura 7. Localização sub-celular das proteínas exportadas por *P. falciparum*.** A adesina PfEMP1 está disposta na superfície dos eritrócitos infectados por *P. falciparum*, onde aparecem os knobs, tendo a ancoragem da KAHRP. A proteína RESA, MESA, PHISTb, PfEMP3 e possivelmente outras proteínas (STEVORs, RIFINs e SURFINs), se associam ao citoesqueleto da célula hospedeira para facilitar a citoaderência às células endoteliais. As *Maurer's clefts* e “*J-dots*” constituem as “cargas” vesiculares que transportam muitas das proteínas que exercerão seu papel na superfície da hemácia infectada. Possivelmente, a liberação dos exosomas seja um mecanismo adicional que o parasita possui, para comunicar-se com o meio extracelular e favorecer a sua sobrevivência. (**Extraído de:** Spillman et al., (2015). *Annu. Rev. Biochem.* 84, pp. 14.1-14.29).

et al., 2004; Jonsdottir et al., 2021) e RESA (do inglês, *ring-infected erythrocyte surface antigen*) (Mills et al., 2007; Pei et al., 2007; Jonsdottir et al., 2021), são proteínas propostas por serem exportadas via PEXEL, sendo que elas desempenham algum papel associado à rigidez da membrana da hemácia infectada, devido à sua associação com o citoesqueleto, ou ainda, na captação de nutrientes, nas chamadas “novas vias de permeabilidade” (do inglês, *new permeability pathways* ou NPPs).

Muitas evidências ainda tem apontado que, outras formas de exportar as suas proteínas até a superfície da membrana da hemácia infectada ou para o ambiente extracelular são utilizadas por *P. falciparum*. Por exemplo, as vesículas exosoma-like liberadas no sobrenadante das culturas são sugeridas por participar da comunicação celular, com a participação crucial da PfPTP2, antes conhecida por ser apenas associada às MCs (Maier et al., 2008), sugerindo que vesículas derivadas das MCs participam desse processo de comunicação célula-célula (Regev-Rudzki et al., 2013). Além disso, a composição proteômica dessas vesículas liberadas são de proteínas antigênicas de membrana e aquelas envolvidas na invasão derivadas do *P. falciparum*, tais como proteínas do complexo RhopH/CLAG (do inglês, *cytoadherence linked asexual proteins* ou *high molecular weight rhoptry proteins*), EBA-175 (do inglês, *erythrocyte binding antigen-175*), SBP1 e RESA, potencialmente envolvidas na modulação da resposta imune inata (Mantel et al., 2013; Sampaio et al., 2018) (**Figura 7**).

Mais recentemente, evidências adicionais apontam que os “J-dots” atuam no transporte de chaperonas e co-chaperonas que possivelmente são necessárias no enovelamento das proteínas exportadas (Külzer et al., 2010). Dentre elas, HSP40, HSP70 e a espécie específica, HSP70-x, estão presentes nessas estruturas. Possivelmente, o domínio flexível de Gly/Phe (domínio GF) e o domínio de ligação ao substrato (do inglês, *substrate binding domain* ou SBD) sejam necessários para que estes substratos sejam transportados dessa maneira (Petersen et al., 2016). Alternativamente, um mecanismo denominado “complexo de interação das proteínas exportadas” (do inglês, *exported protein-interacting complex* ou EPIC) encontrado na MVP foi desvendado, onde é proposto que a PfEMP1 além de interagir com o EPIC, interage também com todos os componentes do translocon PTEX e com proteínas das MCs. Além da proteína PV1 (do inglês, *parasitophorous vacuolar protein-1*), duas novas proteínas do vacúolo parasitóforo (VP), denominadas PV2 (do inglês, *parasitophorous vacuolar protein-2*) e EXP3 (do inglês, *exported protein-3*), foram identificadas interagindo com PfEMP1, sendo estas propostas por fazerem parte do

complexo EPIC. Destas proteínas, PV1 interage com HSP70 e HSP70-x, sugerindo ainda uma inter-relação entre EPIC e “*J-dots*”. Estes resultados, fortemente sugerem que uma mesma proteína pode ser transportada por diversas maneiras nas hemácias infectadas por *P. falciparum* (Batinovic et al., 2017) (Figura 8).

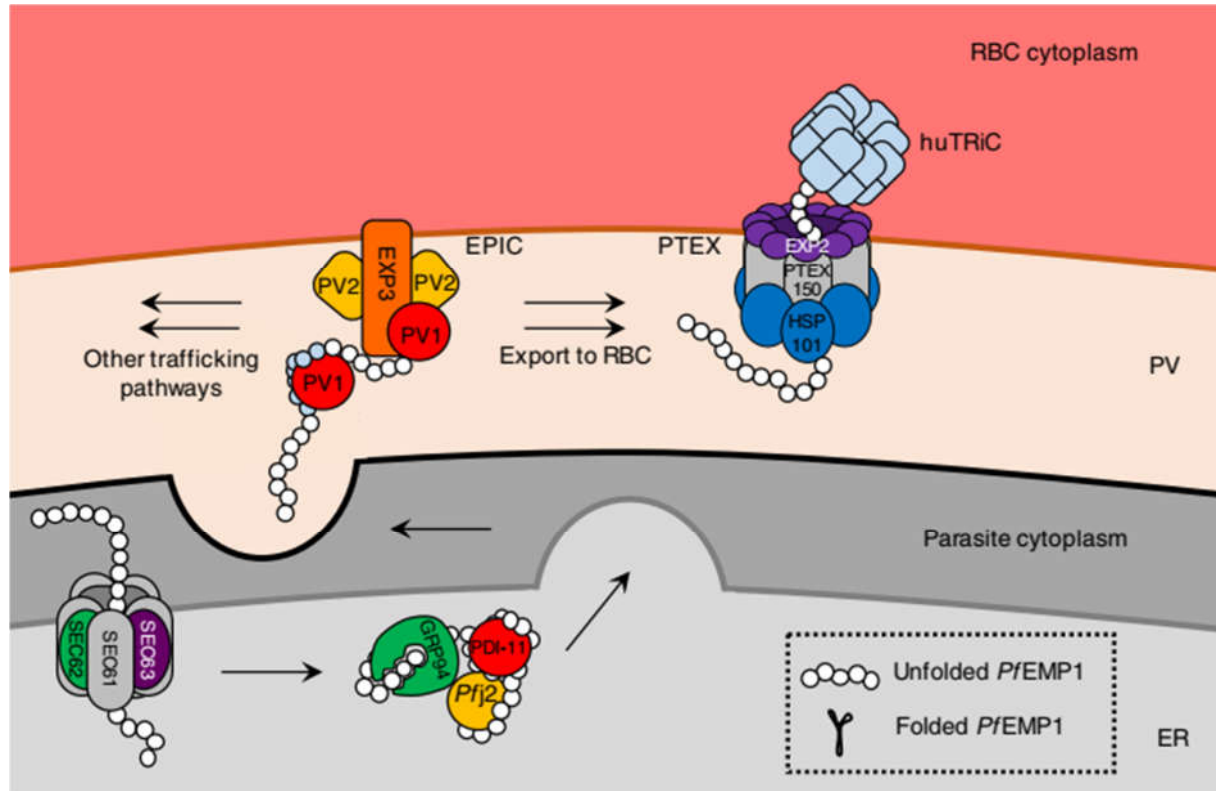


**Figura 8. Modelo de exportação da PfEMP1 pelo complexo EPIC.** É proposto que a PfEMP1 é translocada até o RE por um mecanismo mediado pelo complexo Sec61-62-63 e trafega através de uma via de secreção com o suporte de chaperonas residentes no RE. Mediante a secreção até o VP, é proposto que a PfEMP1 é reconhecida pelo complexo EPIC e transportado até o translocon PTEX, para ser exportado até as hemácias. O complexo EPIC pode também ser responsável pela marcação das vias alternativas do tráfego de “cargas” vesiculares. (Extraído de: Batinovic et al., (2017). Nat. Commun., 8(16044), pp. 1-14).





## **CAPÍTULO 3**

**“O ESTUDO DE ORGANELAS  
NO *P. falciparum*: O  
APICOPLASTO, A  
MITOCÔNDRIA E AS  
ROPTRIAS”**

## CAPÍTULO 3 – O ESTUDO DE ORGANELAS NO *P. falciparum*: O APICOPLASTO, A MITOCÔNDRIA E AS ROPTRIAS

### 3.1. A inter-relação entre o apicoplasto e a mitocôndria

Estudos moleculares que buscam compreender melhor a biologia do parasita se tornam essenciais, pois a descoberta de novos alvos terapêuticos se baseia, sobretudo, nas proteínas (Chen et al., 2018). Por princípio, um bom alvo terapêutico, deve estar presente nas espécies com maior representatividade clínica: *P. falciparum* e *P. vivax*, pois tratamentos emergentes devem ser igualmente eficazes para ambas as espécies (Ludin et al., 2012). Diante disso, o estudo das organelas neste parasita, tais como o apicoplasto e mitocôndria, se tornam altamente pertinentes, considerando que estas organelas desempenham papéis cruciais na sobrevivência do parasita. Desse modo, devido à ancestralidade comum de ambas estruturas, e, diante da evidente inter-relação entre essas organelas plastidiais em *P. falciparum*, um campo com diversas possibilidades para o desenvolvimento de novas estratégias terapêuticas podem ser exploradas (Ralph et al., 2001; van Dooren et al., 2006; Dahl & Rosenthal, 2008).

Sabe-se que o apicoplasto é uma organela vestigial oriunda de algas (possivelmente, uma cianobactéria-like e uma alga vermelha endossimbiontes) em parasitas do filo Apicomplexa, tais como *Plasmodium* spp. e *Toxoplasma gondii*, que devido a sua ancestralidade, tem características “plant-like” tornando-a um alvo interessante para intervenções terapêuticas (Ralph et al., 2001; Dahl & Rosenthal, 2008). Diante das evidências experimentais, é proposto que o apicoplasto esteja diretamente envolvido com: (i) a biossíntese de ácidos graxos do tipo II possivelmente devido à sua ancestralidade (Waller et al., 1998, 2003; Ralph et al., 2004); (ii) biossíntese de isoprenoides, que segue uma via de biossíntese alternativa comparada com a que é encontrada em eucariotos superiores, tendo a 2-C-metil-D-eritritol-4-fosfato (MEP)/1-deoxi-D-xilulose-5-fosfato (DOXP), como intermediários, ao invés do mevalonato (Jomaa et al., 1999; Ralph et al., 2004), além do fato, de que a via MEP/DOXP pode produzir precursores para a síntese de ubiquinonas, utilizadas na cadeia transportadora de elétrons da mitocôndria (Ralph et al., 2004); e, (iii) grupo heme, que é um grupo prostético de muitas proteínas, como os citocromos, que são altamente necessários na fosforilação oxidativa. Além disso, é sugerido que a

mitocôndria e o apicoplasto, neste caso, possam compartilhar intermediários para a síntese de heme (Ralph et al., 2004; van Dooren et al., 2006) (**Figura 9**).

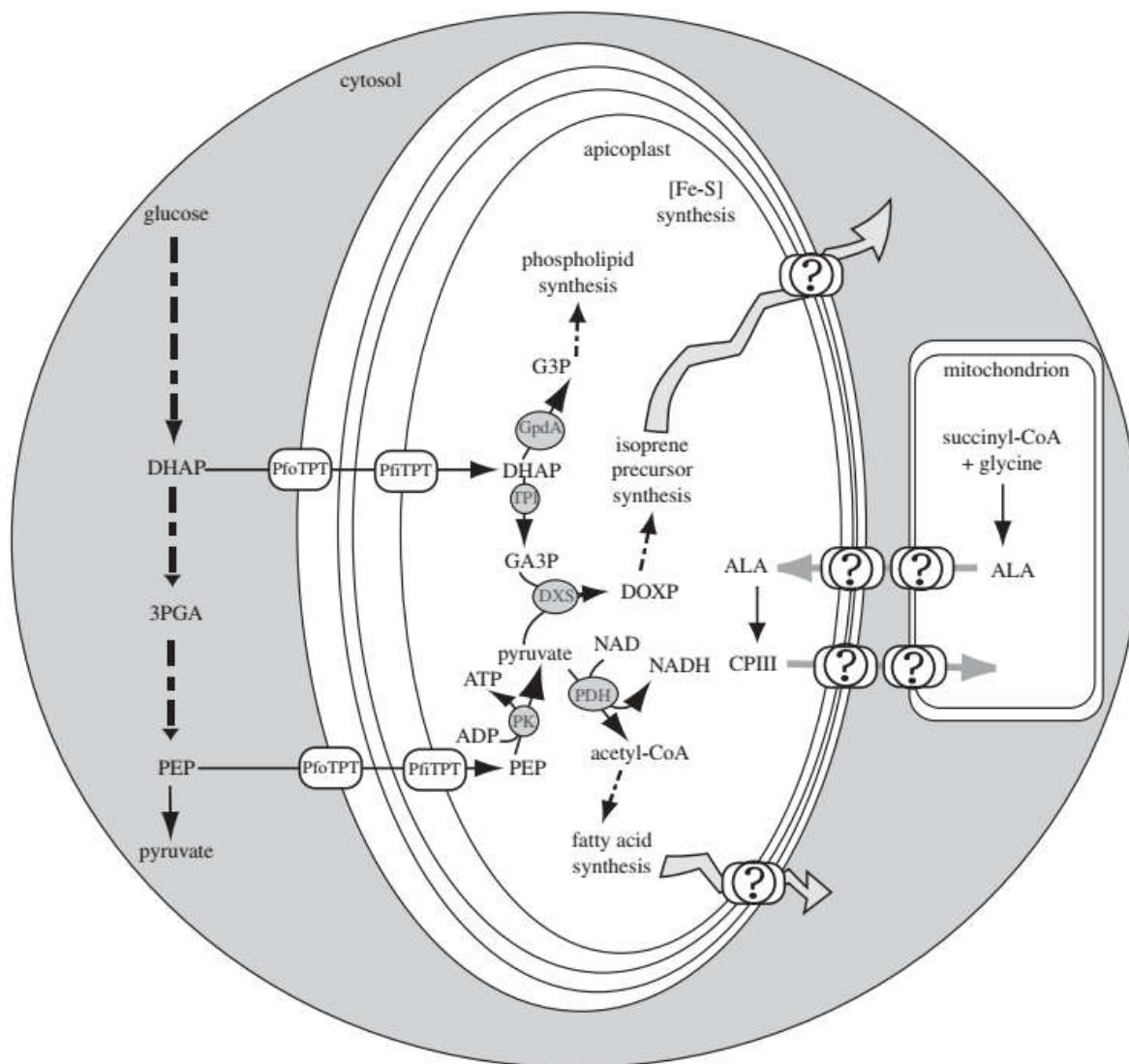


**Figura 9. Esquema da inter-relação metabólica entre o apicoplasto e a mitocôndria em *P. falciparum*.** As fontes de carbono fornecidas por intermediários da via glicolítica (trioses-fostato e fosfoenolpiruvato), atravessam os transportadores PfoTPT e PfiTPT, e são utilizados para produzir substratos para a biossíntese de ácidos graxos (p. ex. acetil-CoA) e isoprenoides (pela via MEP/DOXP). Por outro lado, a biossíntese do grupo heme ocorre com a produção de  $\delta$ -aminolevulanato (ALA) pela  $\delta$ -aminolevulanato sintase (ALAS) pela mitocôndria, que atravessa as membranas do apicoplasto por transportadores desconhecidos, produzindo o CPIII, que por sua vez, retorna para a mitocôndria, para ser finalizado. (**Extraído de:** Lim & McFadden (2010). *Phil. Trans. R. Soc. B.* 365, pp. 749-763.)

No caso da biossíntese do grupo heme, a  $\delta$ -aminolevulanato sintase (ALAS), que é uma enzima encontrada na mitocôndria, forma o  $\delta$ -aminolevulanato (ALA) (Varadharajan et al., 2002), que por sua vez, atravessa as membranas do apicoplasto

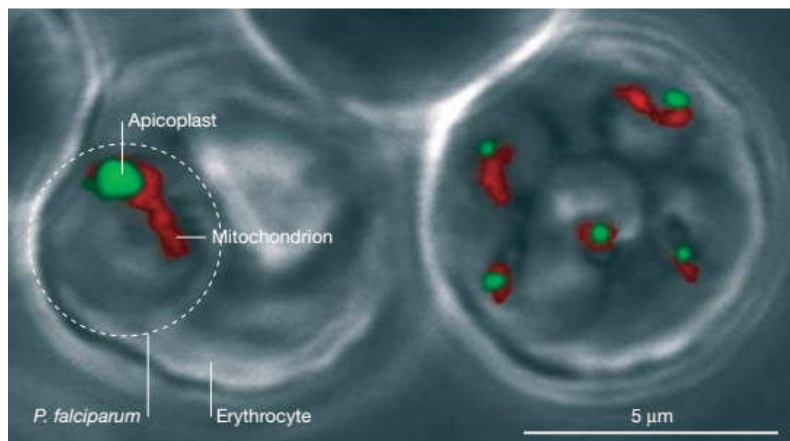
e interage com outras enzimas envolvidas na biossíntese do grupo heme, tais como a  $\delta$ -aminolevulanato desidratase (ALAD) (Sato & Wilson 2002), a porfobilinogênio deaminase (PBGD)/uroporfinogênio III sintase (UROGEN III) (Nagaraj et al., 2008) e uroporfirinogênio III descarboxilase (UROD) (Sato et al., 2004). Apesar disso, algumas enzimas envolvidas nesse processo ainda não foram observadas neste compartimento, tais como: coproporfirinogênio oxidase (CPO) e protoporfirinogênio oxidase (PPO), tornando essenciais estudos que visam à descrição detalhada do conteúdo proteico dessa organela, a fim de elucidar como a coproporfirinogênio III (CPH) e outros metabólitos poderiam atravessar as membranas do apicoplasto, sendo esta, uma questão que ainda permanece elusiva (Lim & McFadden 2010).

Com o auxílio de transportadores do tipo pPTs (do inglês, *plastidic phosphate translocators*), os dois homólogos: (i) PfiTPT (do inglês, *P. falciparum innermost triose phosphate translocator*), e; (ii) PfoTPT (do inglês, *P. falciparum outermost triose phosphate translocator*) (Ralph et al. 2004; Mullin et al. 2006; Lim & McFadden 2010), alguns intermediários da via glicolítica (trioses-fosfato e fosfoenolpiruvato) são utilizados como fonte de carbono para a biossíntese de lipídeos, atravessando as quatro membranas do apicoplasto, utilizando estes transportadores (Ralph et al., 2004; Lim & McFadden, 2010). Neste sentido, sugere-se ainda que, a troca reversa da 3-fosfoglicerato (uma triose-fosfato) do apicoplasto, por outras trioses-fosfato do citosol poderia ser uma fonte alternativa de ATP e NADPH para o apicoplasto (Ralph et al., 2004; Fleige et al., 2007). Alternativamente, o fosfoenolpiruvato (PEP) é convertido em piruvato por uma piruvato-quinase plastidial (pPK) residente do apicoplasto, que é filogeneticamente distinta da piruvato-quinase citosólica (Saito et al., 2008; Maeda et al., 2009). Este piruvato é direcionado para as vias de biossíntese FASII e MEP/DOXP, podendo ser a única fonte de ATP do apicoplasto (Ralph et al., 2004).

Em *P. falciparum*, sugere-se ainda que o acetil-CoA seja produzido no apicoplasto pela piruvato-desidrogenase (PD) podendo ser exportado para a mitocôndria, pois esta não possui PD para produzir acetil-CoA, utilizado em seu atípico ciclo do ácido cítrico (Foth et al., 2005). A importação de PEP, conversão para piruvato seguida da produção de acetil-CoA, poderia ainda fornecer os meios necessários para suprir os déficits de ATP e NADH no apicoplasto, bem como o suposto déficit de acetil-CoA da mitocôndria (Lim & McFadden, 2010). Propõe-se ainda que, a biossíntese de ácidos graxos em plastídios possa utilizar acetato como fonte de carbono, sendo este hidrolisado pela acetil-CoA mitocondrial (Neuhaus & Emes, 2000; Rawsthorne, 2002).

Embora essas suposições ainda sejam especulativas, todas reforçam a ideia da inter-relação entre o apicoplasto e a mitocôndria. Neste sentido, evidências experimentais fomentam a discussão acerca da relação entre o apicoplasto e a mitocôndria, propondo-se ainda que essas duas organelas são fisicamente ligadas uma a outra em *P. falciparum* (Ralph et al., 2004; Kobayashi et al., 2007) (**Figura 10**).

**Figura 10.** *P. falciparum* expressando uma proteína GFP marcada para o apicoplasto; e, marcação da mitocôndria por MitoTracker® Red. (Extraído de: Waller et al., (2000), EMBO J. 19(8), pp. 1794-1802 e reproduzido por Ralph et al., (2004). Nat. Rev., (2), pp. 203-216.)



Diversas proteínas presentes no apicoplasto que estão associadas a funções exclusivas desta organela por sua ancestralidade molecular, já tem sido alvos para intervenções terapêuticas (Ralph et al., 2001; Dahl & Rosenthal, 2008). Desse modo, o uso de antibióticos amplamente conhecidos por intervirem nos processos de replicação do DNA, transcrição em RNAs e tradução em polipeptídeos em bactérias, tem sido descritos com atividade antimalárica (Botté et al., 2012), interferindo no funcionamento do apicoplasto (Dahl & Rosenthal, 2007, 2008; Pradel & Schlitzer, 2010; Yeh & DeRisi, 2011) e potencialmente da mitocôndria (Goodman et al., 2007, 2016).

Por exemplo, a ciprofloxacina, que é um antibiótico sintético da classe das quinolonas, atua na DNA-girase do apicoplasto, inibindo a replicação do DNA, levando-o a morfologias aberrantes com a morte tardia dos parasitas (Fichera & Roos 1997; Dahl & Rosenthal 2007), sobretudo em linhagens de *P. falciparum* resistentes à cloroquina (Winter et al., 2008). Outro exemplo é o caso do uso da doxiciclina, um antibiótico semi-sintético pertencente da família das tetraciclina, que atua nas unidades ribossomais da mitocôndria e do apicoplasto, dificultando a síntese proteica (Dahl et al., 2006; Goodman et al., 2007), apesar do mecanismo de ação detalhado não ser bem esclarecido. Muitas outras moléculas com potencial antimalárico estão sendo estudadas, sobretudo com efeito nas vias metabólicas na biossíntese de ácidos graxos (FASII) e isoprenóides (via MEP/DOXP, que auxilia na produção de âncoras

GPI, ubiquinona mitocondrial e dolicol), que regem essa inter-relação do apicoplasto e a mitocôndria (Botté et al., 2012).

### 3.2. As roptrias e a invasão em *P. falciparum*

*P. falciparum* dispõe de organelas apicais secretórias que facilitam a sua adesão e invasão nas hemácias: as roptrias, os micronemas e os grânulos densos. Após a ancoragem com a célula hospedeira e formação da junção de adesão/movimento (ou do inglês, *tight/moving junction* ou TJ/MJ), o parasita se reorienta para invadir a hemácia, utilizando o motor actina-miosina, criando o vacúolo parasitóforo (VP), separando o parasita do citoplasma da hemácia. Uma das estruturas com grande participação neste processo são as roptrias, que estão envolvidas na adesão e invasão. Estas estruturas possuem duas regiões distintas: um ducto apical, denominada como “pescoço” (ou do inglês, *neck*) da roptria, e, uma região rica em lipídeos, denominada como “bulbo” (ou do inglês, *bulb*) da roptria, sendo que cada uma dessas regiões possuem diferentes proteínas que estão associadas com a adesão à célula hospedeira antes, durante ou após a invasão (Proellocks et al., 2010; Besteiro et al., 2011; Counihan et al., 2013) (**Figura 11**).

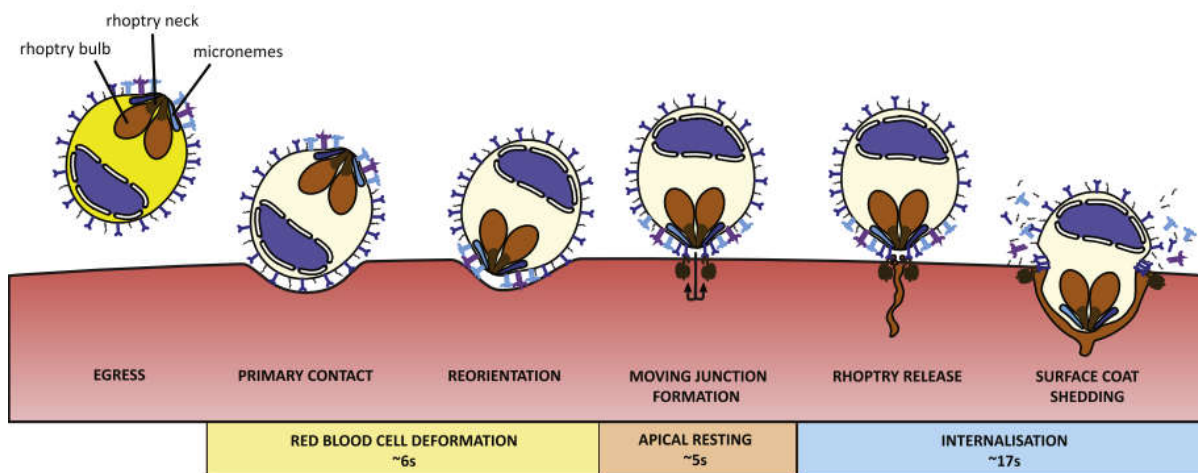


**Figura 11. As roptrias e o processo de adesão e invasão em *P. falciparum*.** Os merozoítos ao invadirem uma nova hemácia, estabelecem o contato inicial com proteínas com âncora GPI da membrana da célula hospedeira. Possivelmente com o auxílio de adesinas apicais, interagindo com receptores da membrana das hemácias (p. ex. interação Rh5-basigina), o parasita se reorienta, com a formação das “*tight junctions*” (TJs), seguida da liberação do conteúdo proteico das roptrias (RONs e ROPs), e formação do vacúolo parasitóforo. (**Extraído de:** Harvey et al. (2012). *Int. J. Parasitol.*, 42(6), pp. 567-573).

Dentre as proteínas que são descritas por serem características desta organela, estão: (i) as adesinas da classe Rh (ou do inglês, *reticulocyte-binding homologs*) e do

complexo RON-AMA1, que estão envolvidas no estabelecimento da adesão e invasão dos merozoítos às hemácias (Counihan et al., 2013; Wright & Rayner, 2014); (ii) o complexo RAP (ou do inglês, *roptry-associated proteins*), também associadas com a invasão dos parasitas às células hospedeiras (Baldi et al., 2000, 2002); e, (iii) o complexo RhopH/CLAG, que tem sido associado a processos pós-invasivos, tais como a citoaderência das hemácias infectadas (iRBCs) (Trenholme et al., 2000; Proellocks et al., 2010) e permeabilidade a nutrientes (Nguitrageol et al., 2011; Gupta et al., 2015; Counihan et al., 2017; Ahmad et al., 2020).

De forma geral, as proteínas que pertencem ao pescoço das roptrias são classificadas como RONS (do inglês, *roptry neck proteins*), e as proteínas que pertencem ao bulbo das roptrias são classificadas como ROPs (do inglês, *roptry bulb proteins*) (Proellocks et al., 2010; Counihan et al., 2013). Dentre as proteínas características do pescoço das roptrias, ou RONS, está a família das adesinas da família Rh em *Plasmodium* spp., que é constituída por cinco membros: Rh1, Rh2a, Rh2b, Rh4 e Rh5, que estão intimamente relacionadas com a adesão e invasão dos merozoítos às células hospedeiras. Apesar disso, pouco se conhece acerca dessa classe de proteínas e a sua função no processo de adesão e invasão, pois ainda se conhece pouco sobre os seus receptores nas células hospedeiras (Harvey et al., 2012). Contudo, foi descrito por Crosnier et al. (2011), que a proteína Rh5, em *P. falciparum*, tem como receptor nos eritrócitos, a basigina, que anteriormente havia sido descrita por Baum et al. (2009) como uma adesina essencial no processo de invasão do parasita.

As proteínas do complexo RON (RON2, RON4 e RON5), constituem outro grupo importante de proteínas do pescoço das roptrias. Esse complexo é conhecido por se interagir com o domínio hidrofóbico extracelular da proteína AMA-1 (do inglês, *apical membrane antigen*), pertencente dos micronemas (Richard et al., 2010; Besteiro et al., 2011; Riglar et al., 2011; Harvey et al., 2012; Wright & Rayner, 2014), que constitui outra importante organela secretória em *P. falciparum*. As proteínas RON são translocadas até a membrana da hemácia, onde o complexo RON é formado, reorientando o merozoíto para o processo de invasão e permitindo a formação do TJ/MJ, com a liberação do conteúdo do bulbo das roptrias, no vacúolo parasitóforo em formação, ou seja, o parasita fornece o seu próprio receptor para a célula hospedeira (complexo RON), e o seu respectivo ligante (AMA-1), a fim de favorecer o processo de invasão (Richard et al., 2010; Riglar et al., 2011) (**Figura 12**).

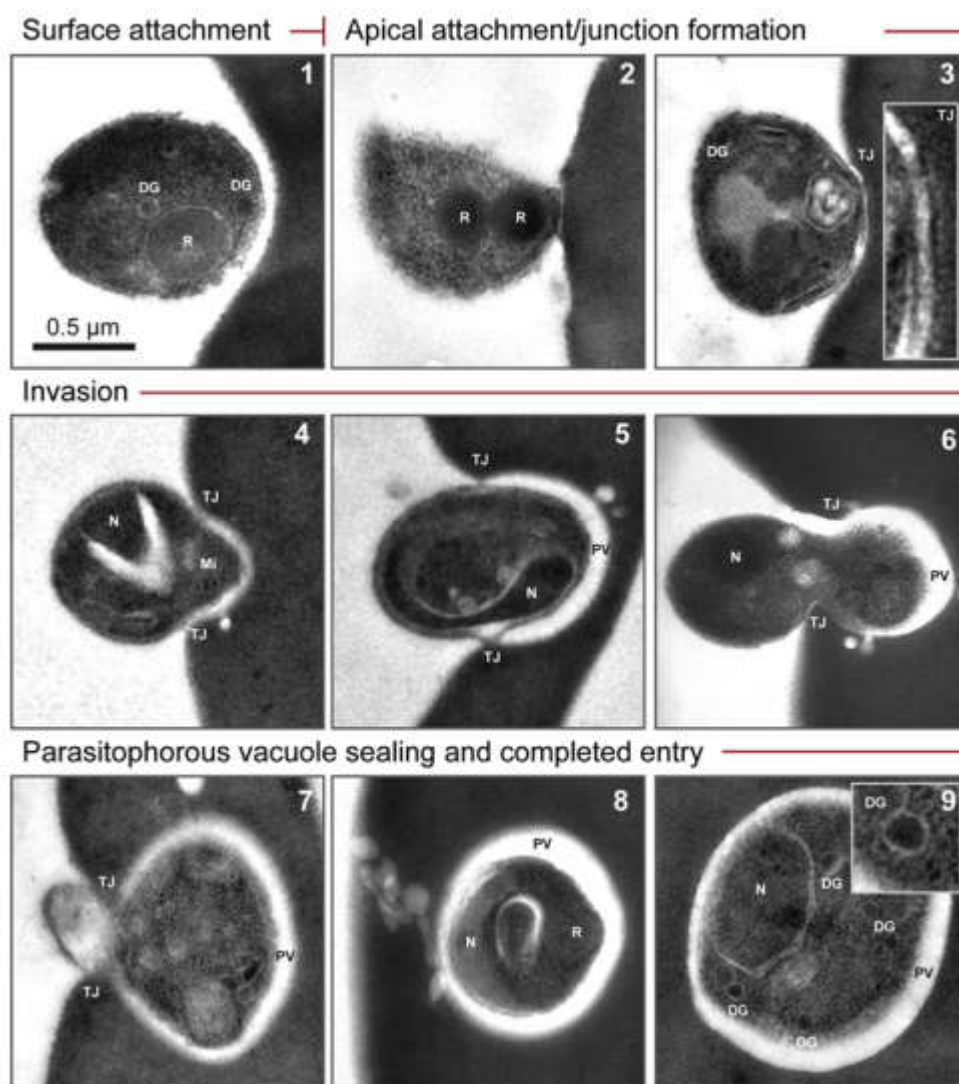


**Figura 12. Microscopia eletrônica de transmissão das etapas de invasão dos merozoítos na célula hospedeira.** (1) Reconhecimento da célula hospedeira. (2) Reorientação do merozoíto e início do estabelecimento da invasão. (3) Formação do TJ/MJ com a interação entre o complexo RON-AMA1, e, possivelmente, liberação do conteúdo das roptrias e outras organelas secretórias. (4) Início da invasão. (5-7) Invasão do merozoíto com a formação do vacúolo parasitóforo. (8 e 9) Finalização da invasão com a selagem da membrana da hemácia. (**Extraído de:** Riglar et al., (2011), *Cell Host Microbe*, 9, pp.9-20).

Após a formação do vacúolo parasitóforo, o bulbo das roptrias libera algumas proteínas características, tais como as proteínas do complexo RAP (RAP1, RAP2 e RAP3) e complexo RhopH/CLAG (RhopH1/CLAG3, RhopH2 e RhopH3), que são proteínas classificadas como ROPs (Baldi et al., 2002; Kats et al., 2006; Counihan et al., 2013), sendo ainda conhecidos como complexos de baixa e alta massa molecular, respectivamente. A proteína recombinante RAP2, pertencente do complexo RAP, pode induzir uma resposta imune *in vivo*. O potencial antigênico desta proteína já foi avaliado, demonstrando resultados promissores em macacos do gênero *Saimiri* spp. (Collins et al., 2000). Ainda, é proposto que a RAP1 seja essencial na localização correta da RAP2, pois em mutantes  $\Delta rap1$ , a proteína RAP2, fica retida no retículo endoplasmático (Baldi et al., 2000), sendo que, mais tarde, Richard et al. (2009),



ratificou a importância de uma via secretória no tráfego correto das proteínas endereçado as roptrias, incluindo a participação da proteína RAMA (do inglês, *rhoptry associated membrane antigen*), que é uma proteína com âncora GPI, com o papel de “escolta” nesse processo. Mais recentemente, ainda foi observado que RAMA pode interagir com uma proteína pouco caracterizada do bulbo da roptria, RON3, entretanto, a função biológica desta interação necessita ainda ser investigada (Ito et al., 2021).

Por sua vez, é proposto que as proteínas que constituem o complexo RhopH/CLAG sejam lançadas no citoplasma das células hospedeiras, ou ainda, possivelmente associadas às *Maurer’s clefts* (MCs), sugerindo a síntese *de novo* das proteínas pertencentes do complexo e exportação até a membrana das hemácias (Vincensini et al., 2008). Essa possibilidade da síntese *de novo* do complexo RhopH/CLAG, foi recentemente reforçada por um estudo proteômico que revelou a associação deste complexo ao vacúolo parasitóforo, “*J-dots*” e às MCs, associando-se ainda à proteínas notoriamente importantes no remodelamento da célula hospedeira (Jonsdottir et al., 2021). No contexto geral, esse grupo de proteínas tem sido associado com a citoaderência e a captação de nutrientes.

O membro do complexo RhopH1/CLAG ou apenas RhopH1, é proposto por integrar uma família de múltiplos genes: *clag2*, *clag3.1*, *clag3.2*, *clag8* e *clag9* (Kaneko et al., 2001, 2005; Gupta et al., 2015). Curiosamente, estes genes estão localizados em diferentes cromossomos: (i) *clag3.1* e *clag3.2*, no cromossomo 3 (Kaneko et al., 2001); (ii) *clag2*, no cromossomo 2 (Kaneko et al., 2001); (iii) *clag8*, no cromossomo 8 (Kaneko et al., 2005); e, (iv) *clag9*, no cromossomo 9 (Kaneko et al., 2001; Gardiner et al., 2004). Todos os membros do complexo RhopH1/CLAG tem o seu ápice de expressão na fase de esquizonte (42-46h) (Kaneko et al., 2005).

Sugere-se ainda que, a proteína CLAG9 (do inglês, *cytoadherence linked asexual gene 9*), integre o complexo RhopH1/CLAG, presente nas roptrias (Kaneko et al., 2005), podendo esta, estar associada a RhopH2 (Gardiner et al., 2004; Ling et al., 2004) e RhopH3 (Gardiner et al., 2004). Por sua vez, os genes *clag9*, *rhoph2* e *rhoph3* são localizados no cromossomo 9 (Hall et al., 2002; Ling et al., 2003; Gardiner et al., 2004). Este cromossomo tem sido amplamente relacionado à genes associados com a citoaderência (Hawthorne et al., 2004; Spielmann et al., 2006). Neste sentido, CLAG9 tem sido associada à citoaderência (Trenholme et al., 2000), possivelmente auxiliando no tráfego da PfEMP1 (Goel et al., 2010), apesar que, este papel ainda seja controverso (Nacer et al., 2011).

O remodelamento da célula hospedeira propiciado pelo parasita impõe uma necessidade de aumentar a permeabilidade, favorecendo o seu desenvolvimento. Através dos canais iônicos de superfície de plasmódios (ou do inglês, *plasmodial surface anion channel* ou PSAC), o complexo RhopH/CLAG facilita a captação de nutrientes, pelas denominadas “novas vias de permeabilidade” (ou do inglês, *new permeability pathways* ou NPPs) (Nguitragool et al., 2011; Gupta et al., 2015; Counihan et al., 2017; Ahmad et al., 2020). As evidências iniciais sugerem que após a invasão e liberação das proteínas pelas organelas secretórias, tais como as roptrias, as proteínas RhopH1/CLAG3, RhopH2 e RhopH3 sejam translocadas até a membrana da célula hospedeira, a fim de formar o complexo RhopH/CLAG (Sam-Yellowe et al., 1991) (Figura 13).

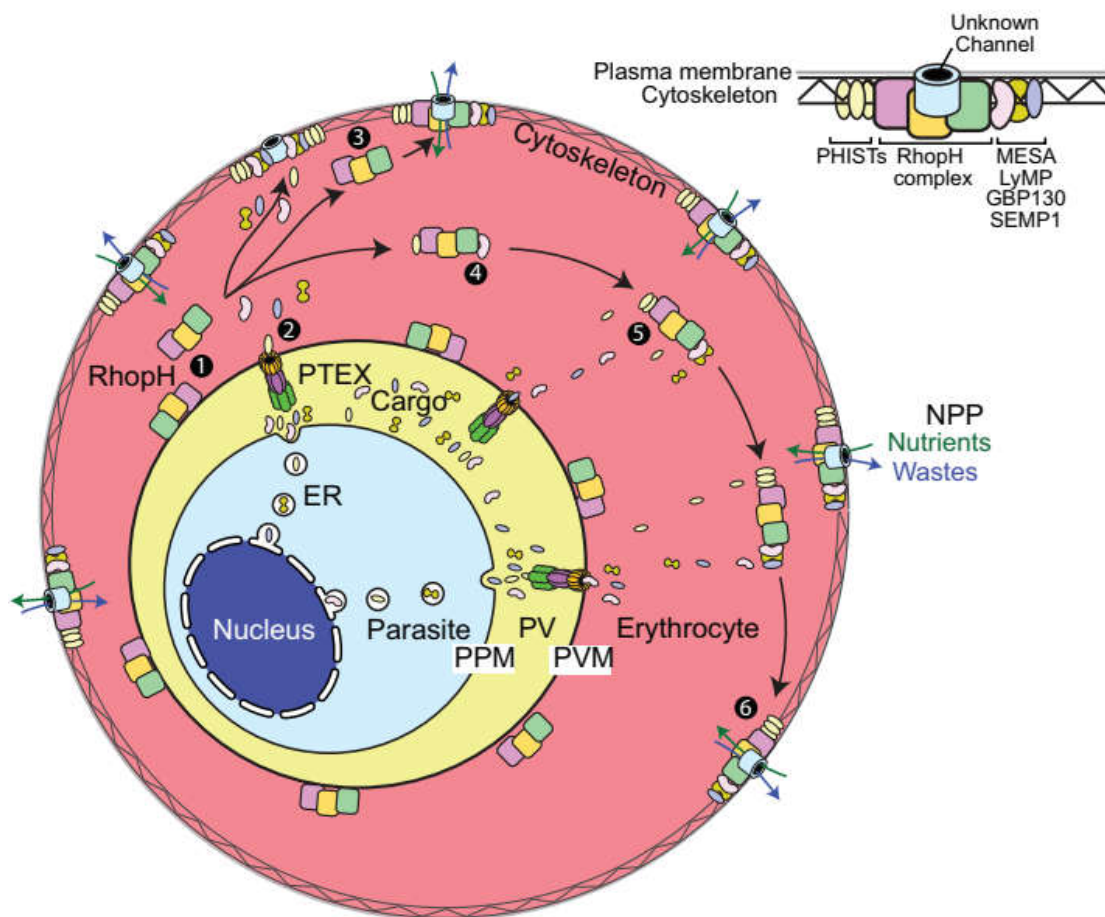


**Figura 13. Esquema da translocação do complexo RhopH/CLAG até a membrana da célula hospedeira.** (1) Possivelmente, o complexo RhopH/CLAG seja introduzido na membrana do vacúolo parasitóforo (MVP) durante a invasão pelos merozoítos. (2) Logo após a invasão, o translocon PTEX, inicia a exportação de proteínas produzidas pelo parasita para o ambiente citosólico da célula hospedeira. Algumas dessas proteínas (tais como, PHISTb, MESA, LyMP, GBP130 e SEMP1), trafegam até o citoesqueleto das hemácias. O complexo RhopH/CLAG (3) liga-se a essas proteínas exportadas na membrana dos eritrócitos ou (4 e 5) se agrega com essas proteínas *en route* até a superfície. (6) Uma vez na superfície, o complexo RhopH/CLAG juntamente com as proteínas que formam NPPs, criam seus próprios poros que atravessam a membrana ou “abrem” um poro eritrocitário. A função das NPPs é permitir a entrada de nutrientes e possivelmente eliminar produtos residuais do parasita. (Extraído de: Counihan et al., (2017), eLIFE, 2(6), pp.1-31).

Sugere-se ainda que, algumas proteínas deste complexo começam a interagir entre si, mesmo antes de atingir a membrana célula hospedeira. Através da análise de imagens utilizando FRET (do inglês, *Förster resonance energy transfer*), foi observado que RhopH1/CLAG3 e RhopH2 permanecem totalmente associadas durante a exportação até a membrana das hemácias (Ahmad et al., 2020). Além disso, diversos estudos ratificam ainda a interação entre as proteínas que compõem o complexo RhopH/CLAG (Counihan et al., 2017; Sherling et al., 2017; Jonsdottir et al., 2021). Relata-se ainda que, a diminuição da expressão da RhopH2 leva a uma diminuição da captação de vitaminas essenciais e co-fatores, implicando na diminuição da síntese *de novo* de pirimidinas e da capacidade invasiva em *P. falciparum* (Counihan et al., 2017). No caso da RhopH3, o truncamento condicional do gene *rhop3*, leva a uma localização incorreta das outras proteínas constituintes do complexo RhopH/CLAG (RhopH2 e RhopH3), reduzindo consideravelmente também a capacidade invasiva e de sobrevivência em uma eventual re-invasão (Sherling et al., 2017). Em conjunto, estes dados fortemente sugerem que as proteínas secretadas pelas roptrias, possuem papéis absolutamente importantes para a sobrevivência e virulência de *P. falciparum*.



## **CAPÍTULO 4**



# **“A TÉCNICA DE CRISPR-Cas9 E SUAS APLICAÇÕES”**

## CAPÍTULO 4 – A TÉCNICA CRISPR-Cas9 E SUAS APLICAÇÕES

### 4.1. O sistema de edição genômica CRISPR-Cas9

Em 1987, Ishino e colaboradores, descreveram uma série de sequências pequenas, interespaçadas e repetidas no genoma de *E. coli*, ao qual se denominou como CRISPR (do inglês, *clustered regularly interspaced short palindromic repeats*) (Ishino et al., 1987). Posteriormente, estas sequências espaçadas foram associadas ao DNA exógeno proveniente de plasmídeos e infecções virais (Bolotin et al., 2005; Mojica et al., 2005; Pourcel et al., 2005), sendo que o *locus* CRISPR seria “rearranjado” de acordo com estas infecções, produzindo sequências *spacers*. Novas evidências surgiram, acerca da transcrição do *loci* CRISPR, com a produção de proteínas associadas à CRISPR (Cas), que possuem domínios de nuclease (Jansen et al., 2002; Bolotin et al., 2005; Haft et al., 2005; Pourcel et al., 2005), que possivelmente estariam vinculadas a um “sistema imune adaptativo” natural mediado por CRISPR-Cas em procariotos, propiciando a degradação de novos invasores virais ou DNA exógenos (Barrangou et al., 2007). Após alguns estudos terem apontado a associação entre os CRISPR RNAs (crRNAs) maduros e as proteínas Cas, sendo que o crRNA funcionaria como um “guia” para a Cas, e a evidente interferência na proliferação de vírus em *E. coli* (Brouns et al., 2008), uma ferramenta com alto potencial biotecnológico havia sido descoberta (**Figura 14**).

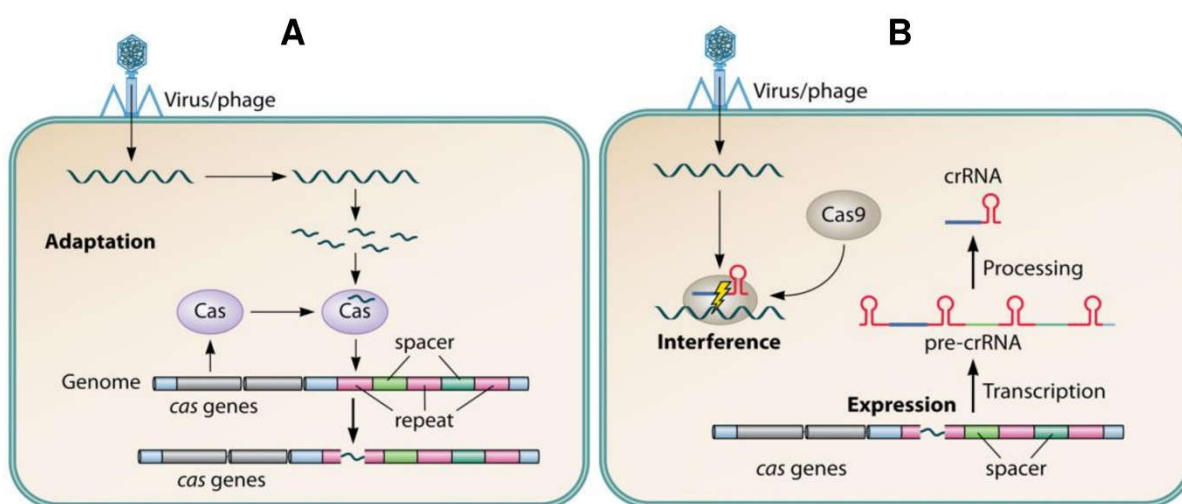


**Figura 14. O sistema CRISPR-Cas na imunidade adquirida em procariotos. (A)** O DNA proveniente de fagos/vírus invasores é reconhecido pelas proteínas Cas, que os fragmentam e os incorporam nas sequências *spacers*, adjacente ao operon dos genes *cas*. **(B)** Em uma eventual re-invasão, o locus CRISPR é ativado, com a transcrição dos crRNAs (provenientes do DNA exógeno invasor) que é associado com a Cas9, no qual, este complexo CRISPR-Cas9 realiza a degradação do DNA invasor. (Extraído de: Ishino et al. (2018). *J. Bacteriol.*, 200(7), pp.1-17).

O sistema CRISPR-Cas é subdividido nas classes I e II. Dentro da classe II, encontra-se a Cas9, que dentro da mais recente classificação, ela é ainda enquadrada dentro do complexo tipo II de enzimas Cas, pois é a mais atrativa para eventuais manipulações genéticas, pois requer apenas uma proteína para funcionar: a Cas9 (Gasiunas et al., 2012; Ishino et al., 2018). Em 2012, Jinek e colaboradores, demonstraram que o sistema CRISPR-Cas9 possibilitava a clivagem dupla da fita do DNA, guiada pelo complexo tracrRNA:crRNA em *Streptococcus pyogenes* (Jinek et al., 2012). Essa clivagem é permitida devido ao reconhecimento da sequência de 20 nucleotídeos do RNA guia (gRNA, o complexo tracrRNA:crRNA), que por sua vez, se tornou programável, com o sítio complementar no DNA genômico e reconhecimento do motivo PAM (do inglês, *protospacer adjacent motif*), NGG, que graças aos domínios de nuclease HNH e RuvC-like da Cas9, viabilizou e facilitou a manipulação genética de qualquer região do DNA (Gasiunas et al., 2012; Jinek et al., 2012).

Após a clivagem da dupla fita do DNA (ou do inglês, *double-strand break* ou DSB) no *loci* genômico, a maquinaria de reparo do DNA, NHEJ (do inglês, *non-homologous end-joining*), pode religar as extremidades do DNA, podendo ocasionar mutações pontuais, com a inserção ou deleção de nucleotídeos (*indel*), ou, ainda promover o reparo por HDR (do inglês, *homology-directed repair*), no qual, ambas as situações podem resultar na mudança de uma determinada ORF (do inglês, *open reading frame*), produzindo proteínas defeituosas. No caso do reparo HDR, é possível ainda, promover *knock-outs*, *knock-ins*, mutagênese sítio-dirigida e correções do DNA genômico (Doudna & Charpentier 2014; Wang et al. 2016) (**Figura 15**).

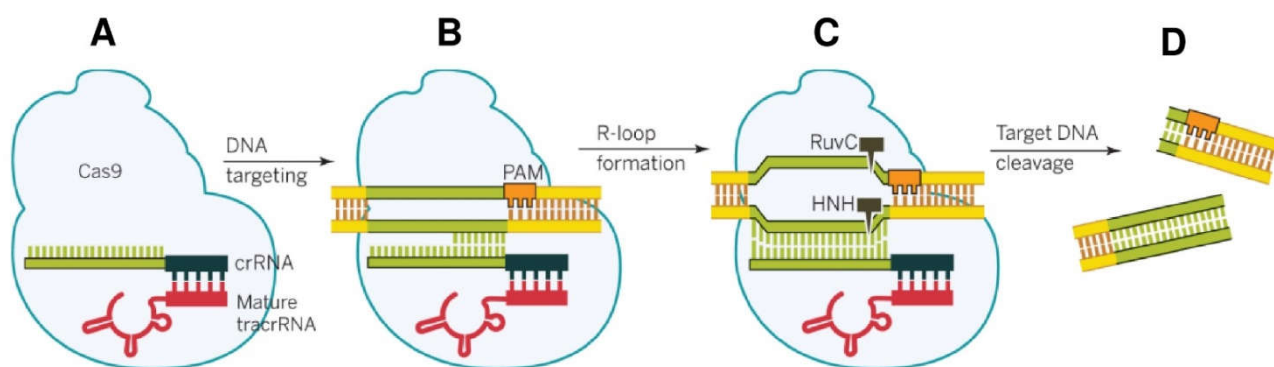


**Figura 15. O mecanismo de clivagem da dupla fita do DNA por CRISPR-Cas9.** (A) O complexo CRISPR-Cas9, (B) reconhece o motivo PAM (NGG), presente no DNA genômico (gDNA), que (C) com o pareamento do RNA guia (gRNA), ocorre a abertura da dupla fita do DNA, seguida da (D) clivagem do DNA através dos domínios RuvC-like e HNH da Cas9. (Extraído de: Doudna & Charpentier (2014), Science, 346(6213), pp. 1258096.1-1258096.9).

## 4.2. As aplicações de CRISPR-Cas9

Diversos estudos direcionaram os seus esforços no estudo de doenças genéticas, utilizando a abordagem de CRISPR-Cas9, como uma possível ferramenta na reversão de diversos fenótipos, como por exemplo, na distrofia muscular de Duchenne (Young et al., 2016; Bengtsson et al., 2017). Young et al. (2016), utilizaram linhagens reprogramadas (ou do inglês, *human induced pluripotent stem cells* ou hiPSCs) de fibroblastos oriundos de pacientes humanos distróficos, no qual, através da correção do DNA realizado por CRISPR-Cas9, foi possível observar um reestabelecimento da funcionalidade da distrofina rearranjada de 60% em cardiomiócitos e células da musculatura esquelética, com a excisão de um fragmento de 725kb do DNA genômico, pertencente do gene da distrofina disfuncional. Em outra ocasião, Bengtsson et al. (2017), em uma abordagem similar, utilizou o sistema CRISPR-Cas9 através de vetores virais (AAV, *adeno-associated viral*), onde observaram que o fenótipo distrófico de camundongos *mdx<sup>4cv</sup>*, era potencialmente revertido com a correção da ORF, e aparente retomada da função do sarcolema.

O uso da tecnologia CRISPR-Cas9 utilizando animais modelo tem sido implementada, a fim de proporcionar novas perspectivas das doenças que acometem os humanos (Wu et al., 2013, 2017; Niu et al., 2014; Bengtsson et al., 2017; Jain et al., 2017). Como exemplo da implementação dessa abordagem, pode-se citar o estudo de Jain et al. (2017), que através do uso de CRISPR-Cas9, foi possível corrigir o *loci* do gene da miocilina defeituosa (*MYOC<sup>Y437H</sup>*) em células NTM5 (do inglês, *normal trabecular meshwork 5*), bem como o mesmo *loci* em camundongos com glaucoma (*Tg-MYOC<sup>Y437H</sup>*), revertendo significativamente o fenótipo da doença em relação a pressão intraocular e o acúmulo exagerado da miocilina na malha trabecular.

Outro exemplo bem-sucedido, reportado no estudo de Wu et al. (2013), conseguiu corrigir o *loci* do gene *Crygc* em zigotos de camundongos com o fenótipo da catarata, que produz a proteína  $\gamma$ C-cristalina. Quando este gene possui uma deleção de 1 bp, no éxon 3, a proteína é truncada no resíduo do aminoácido 76, levando-a a disfuncionalidade. Ainda, em outro estudo mais audacioso, Wu et al. (2017), conseguiram produzir camundongos quimeras, utilizando células pluripotentes de ratos (ou do inglês, *rat pluripotent stem cells* ou rPSCs). Com o nocauteamento duplo por CRISPR-Cas9 dos genes: (i) *Pdx1<sup>-/-</sup>*, responsável pelo desenvolvimento do pâncreas; (ii) *Nkx2.5<sup>-/-</sup>*, envolvido na cardiogênese; e, (iii) *Pax6<sup>-/-</sup>*, que é um gene codificante para um fator de transcrição envolvido no desenvolvimento dos olhos, nariz

e cérebro, em zigotos de camundongos, foi possível observar a compensação funcional das células oriundas do rato (rPSCs), na formação dos respectivos órgãos, fornecendo novas perspectivas quanto ao xenotransplante.

Por outro lado, tem sido usado animais primatas, não-humanos, ao se estudar doenças que acometem os seres humanos, constituindo um bom modelo experimental. Diante disso, recentemente, alguns estudos concentraram os seus esforços no estudo de doenças psiquiátricas, com o uso de CRISPR-Cas9, para entender melhor os mecanismos que permeiam este tipo de doença. É o caso do estudo realizado por Tu et al. (2019), que investigou o papel do gene *SHANK3*, codificante para uma proteína pós-sináptica, no fenótipo de autismo-*like* em macacos. Com a ruptura dos éxons 6 e 12 no *loci* do gene *SHANK3*, foi possível observar anormalidades comportamentais, incluindo uma diminuição da interação social e da atividade cerebral, observada por PET (do inglês, *position-emission computed tomography*), sendo que todos esses sintomas melhoravam com a administração de fluoxetina, um antidepressivo amplamente utilizado.

Em outro trabalho, foi utilizado CRISPR-Cas9 para entender melhor o papel do gene *BMAL1* (do inglês, *brain and muscle ARNT-like 1*), um componente do complexo do fator de transcrição CLOCK-BMAL1, em macacos, no distúrbio do ciclo circadiano e os riscos fisiológicos inerentes dessa perturbação. Com a ruptura do gene *BMAL*, foi possível observar a aparente disfunção do sono e uma alteração hormonal, bem como, comportamentos similares aos encontrados em humanos, tais como ansiedade e depressão (Qiu et al., 2019). O uso de animais geneticamente modificados, para estudar doenças que acometem os humanos, é uma forma de permitir novos *insights* acerca de uma determinada doença e, possivelmente, ao melhoramento no tratamento e desenvolvimento de estratégias para possivelmente curá-las.

Em paralelo, muitos estudos tem utilizado a edição genômica mediada pelo sistema CRISPR-Cas9 para entender melhor os mecanismos moleculares que favorecem a sobrevivência e virulência de agentes etiológicos causadores de doenças tropicais, tais como *Leishmania donovani* (Zhang & Matlashewski 2015), *Toxoplasma gondii* (Zheng et al., 2015), *Trypanosoma cruzi* (Lander et al., 2016) e *Plasmodium falciparum* (Ghorbal et al., 2014; Wagner et al., 2014; Lu et al., 2016; Mogollon et al., 2016; Crawford et al., 2017; Xiao et al., 2019). Em *P. falciparum*, os primeiros estudos neste sentido foram realizados por Ghorbal et al. (2014) e Wagner et al. (2014), que se arriscaram a realizar a edição genômica neste parasita, considerando seu genoma altamente abundante em conteúdo A+T (Gardner et al., 2002). Neste caso, tendo



como gene alvo, a *kahrp* (do inglês, *knob-associated histidine rich protein*), foi possível truncá-la sem maiores dificuldades, substituindo-a pelo gene *hdhfr* (do inglês, *human dihydrofolate reductase*), conferindo resistência à droga anti-folato WR99210 (Ghorbal et al., 2014; Wagner et al., 2014).

Apesar disso, outros estudos foram realizados buscando alternativas mais eficientes na obtenção de mutantes de *P. falciparum*, considerando que as marcas de seleção utilizadas para este fim, são escassas e potencialmente tóxicas (Ghorbal et al., 2014). Diante disso, Lu et al. (2016) e Mogollon et al. (2016), conseguiram aperfeiçoar a edição genômica por CRISPR-Cas9 em *P. falciparum*, com o uso de genes repórteres (p. ex. GFP, do inglês, *green fluorescent protein*), que evitariam o uso contínuo das drogas utilizadas na seleção dos parasitas, tais como: WR99210 (seleção positiva da transfecção) e 5-fluorocitosina (seleção positiva da integração do gDNA).

Crawford et al. (2017), conseguiram produzir duas mutações pontuais (SNPs), no gene da *PfATP4* (do inglês, *P. falciparum ATPase 4*), um canal de efluxo de sódio, que tem sido estudado como um possível alvo para o composto SJ733, um potencial antimalárico, com o uso de CRISPR-Cas9 livre de plasmídeos ou recombinação homóloga. Neste estudo, foi possível caracterizar os polimorfismos relacionados com a resistência à droga SJ733, associada às mutações L350H e P412T. Através de ensaios da metade da concentração efetiva máxima (ou do inglês, *half maximal effective concentration* ou EC<sub>50</sub>), foi possível estabelecer que o uso de aproximadamente 100 vezes a mais de SJ733, em parasitas apresentando estes polimorfismos seria necessário para inibir o crescimento dos parasitas (Crawford et al., 2017).

Ainda, no intuito de se observar os mecanismos epigenéticos relacionados com a regulação transcricional mediada pela acetilação de histonas, Xiao et al. (2019), através do uso de CRISPR-dCas9, onde, neste caso, a Cas9 está na forma "d" para desativada, por duas mutações, D10A e H840A, foi possível regular a transcrição de genes relacionados com a invasão: (i) *rh4* (do inglês, *reticulocyte binding protein homolog 4*) e *eba-175* (do inglês, *erythrocyte binding protein 175*), utilizando o domínio enzimático da histona acetilase (HAT), *PfGCN5*, para ativar o gene *rh4*, e, o domínio enzimático da histona desacetilase (HDAC), *PfSir2a*, para desativar o gene *eba-175*. Observou-se ainda, (i) um aumento de pelo menos 113 vezes nos níveis transcricionais de *rh4*, possivelmente devido ao aumento da acetilação da histona 3

(H3) pela *PfGCN5*, e; (ii) uma hipoacetilação da H3 e baixa expressão da EBA-175 pela *PfSir2a*.

Certamente, o uso de CRISPR-Cas9 em *P. falciparum* pode ser eficientemente utilizado para diferentes aplicações. Uma dificuldade inerente da própria biologia do parasita, é o fato do genoma de *P. falciparum* possuir cerca de ~80% de conteúdo A+T (Gardner et al., 2002), tornando a manipulação genética, um grande desafio neste organismo. A escolha do gRNA e o tamanho das regiões de homologia aparentemente são muito importantes para se obter linhagens mutantes nesta espécie por CRISPR-Cas9 (Ghorbal et al., 2014; Wagner et al., 2014; Xiao et al., 2019). A aplicação desta metodologia acoplada à ferramentas de marcação por proximidade, tais como as APEX2 e BioID, certamente poderão trazer informações valiosas quanto à biologia do parasita.



## **CAPÍTULO 5**

# **“INTERAÇÃO PROTEÍNA- PROTEÍNA (IPP)”**

## CAPÍTULO 5 – INTERAÇÃO PROTEÍNA-PROTEÍNA (IPP)

### Estudo da interação proteína-proteína por ensaios de proximidade: APEX2 e BioID

Em 2013, Rhee e colaboradores, empregaram uma nova abordagem, onde acoplaram o uso da enzima ascorbato peroxidase modificada (APEX2), seguida de uma reação de biotinylação, utilizando como substrato a biotina-fenol e como agente oxidante/catalisador, o peróxido de hidrogênio ( $H_2O_2$ ), que permite a marcação de proteínas totais de um determinado compartimento celular, ou de proteínas-parceiras (quando a proteína de interesse é fusionada a APEX2), através da biotinylação dessas proteínas, que em seguida são analisadas por espectrometria de massas *shotgun label-free* (Rhee et al., 2013). Inicialmente, esta metodologia foi empregada para análises de microscopia eletrônica (EM), devido às dificuldades de se realizar as marcações em alguns compartimentos celulares com os *tags* já utilizados e pela própria natureza da amostra, pois a espessura e fixação do material pode ser um empecilho para a EM (Martell et al., 2012).

De forma geral, a abordagem de biotinylação de proteínas por APEX2 seguida por análise proteômica, combina o poder da alta resolução da espectrometria de massas e a característica funcional da própria enzima utilizada para se obter a biotinylação da(s) proteína(s) de interesse, oferecendo um panorama temporal e espacial de um determinado cenário molecular, enquanto o organismo permanece vivo, preservando suas estruturas celulares e seus parceiros proteicos (Rhee et al., 2013). Isso é possível graças às características moleculares da APEX2, que realiza a biotinylação das proteínas por proximidade (um raio de <20nm), com o uso do substrato, biotina-fenol, catalisado pela  $H_2O_2$ , em uma reação que dura cerca de 1 min (minuto), com a modificação de resíduos de Tyr (principalmente), Trp, His e Cys, pelo radical fenoxil, onde, após a marcação, as proteínas modificadas são enriquecidas com *beads* magnéticas acopladas a estreptavidina (Rhee et al., 2013) (**Figura 16**).

Rhee et al. (2013), realizaram através desta abordagem o enriquecimento de proteínas da matriz mitocondrial (e membrana mitocondrial interna), utilizando como modelo as células HEK293 expressando uma construção transiente mito-APEX2. Foram identificadas 495 proteínas, sendo que destas, 31 proteínas não haviam sido

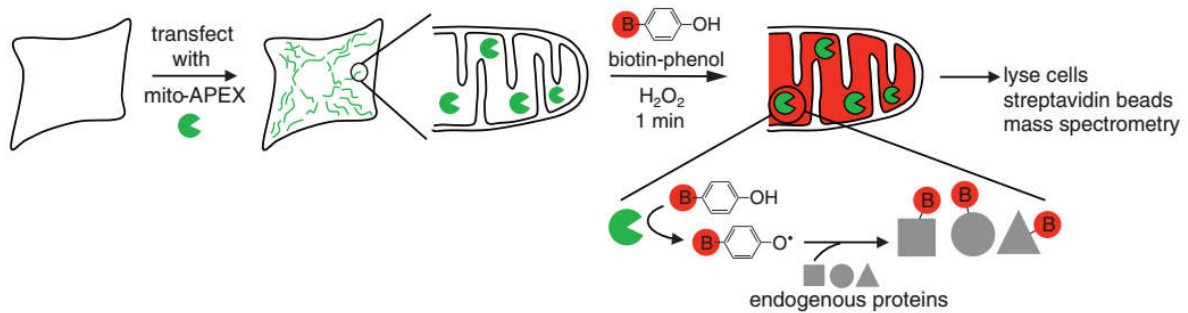


**Figura 16. Mecanismo de biotilação de proteínas por APEX2.** Neste esquema, a APEX2 é fusionada ao peptídeo sinal da mitocôndria (mito) que a conduz para a matriz mitocondrial, onde com o uso do substrato biotina-fenol e o agente oxidante/catalisador H<sub>2</sub>O<sub>2</sub> (peróxido de hidrogênio), em uma reação de aproximadamente 1 min, as proteínas mitocondriais são biotiladas nos resíduos de Tyr (principalmente), Trp, His e Cys por um radical fenólico, que serão posteriormente enriquecidas em colunas de estreptavidina e submetidas à análise por espectrometria de massas. (**Extraído de:** Rhee et al (2013), Science (80- )339, pp. 1328–1331).

descritas por fazerem parte do conjunto de proteínas mitocondriais em humanos. Esse resultado reforça o princípio da técnica, bem como fornece uma ferramenta para realizar estudos em outros organismos, permitindo a descrição de novas proteínas que podem desempenhar um papel significativo e que ainda não foram descritas em um determinado compartimento celular.

Após a descrição desta nova metodologia de enriquecimento de proteínas, diversos outros trabalhos têm sido publicados recentemente, buscando desvendar novas proteínas de uma determinada organela ou mesmo, descrever novas proteínas parceiras de um alvo de interesse. É o caso do trabalho de Lee et al. (2016), que faz um mapeamento topológico de proteínas do retículo endoplasmático (RE), utilizando as linhagens de células HEK293, HeLa e U2OS, em uma proposta onde cada uma das construções epissomais expressavam versões de proteínas quiméricas destinadas para diferentes porções do RE, mitocôndria (membrana interna e externa), núcleo e citosol. Neste trabalho, demonstrou-se que as proteínas que expressavam a APEX2, geram um *barcode* molecular específico e, assim, um padrão distinguível de proteínas biotiladas, fornecendo informações mais acuradas.

Além disso, a partir dessa metodologia, outras abordagens baseadas no uso da APEX2 para realizar a análise do transcriptoma com o enriquecimento do *crosslink* entre ribonucleoproteínas-RNAs (APEX-RIP) a partir de compartimentos celulares (Kaewsapsak et al., 2017), o enriquecimento de proteínas relacionadas com o mtDNA (Han et al., 2017), e, realizar uma deconvolução espacial e temporal de proteínas de

um determinado cenário molecular (Lobingier et al., 2017) foram implementadas. No primeiro caso, Kaewsapsak et al. (2017), adaptou a abordagem utilizada por Rhee et al. (2013), para capturar as ribonucleoproteínas e, a partir do enriquecimento em *beads* magnéticas com estreptavidina, realizar o sequenciamento dos RNAs “capturados” por RNA-seq (**Figura 17**). Através dessa técnica, foi possível detectar com acurácia todos os 13 mRNA, 2 rRNAs e 22 tRNAs codificados pelo genoma mitocondrial, além de detectar milhares de RNAs nucleares e citosólicos com altíssima definição analítica, dentre eles os lncRNAs, separando-os em grupos bem distintos, mesmo comparando a abordagem com outros métodos de fracionamento.

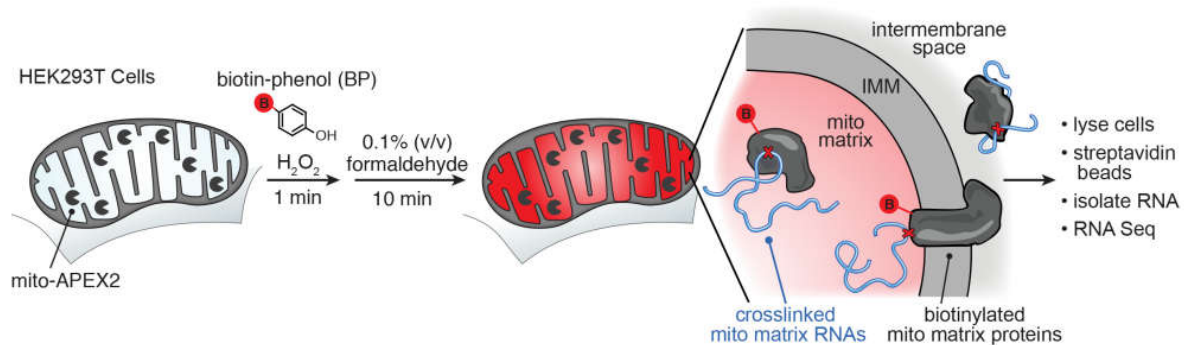


**Figura 17. Mecanismo do *crosslinking* entre ribonucleoproteínas e RNA com o uso da abordagem APEX-RIP.** Neste esquema, a APEX2 é fusionada ao peptídeo sinal da mitocôndria (mito) que a conduz para a matriz mitocondrial, onde com o uso do substrato biotina-fenol e o agente catalisador H<sub>2</sub>O<sub>2</sub> (peróxido de hidrogênio), em uma reação de aproximadamente 1min, seguida de uma incubação com 0.1% de formaldeído, por cerca de 10min, promoverá o *crosslinking* entre ribonucleoproteínas e RNAs, que é posteriormente enriquecido em coluna de estreptavidina, sendo os RNAs analisados por RNA-seq. (**Extraído de:** Kaewsapsak et al (2017). eLife, 6, pp. 1–31).

Em relação às proteínas que possuem associação com o mtDNA, o estudo de Han et al. (2017) proporcionou a descrição de sete proteínas que nunca haviam sido associadas ao nucleóide mitocondrial, dentre elas a NDUF56 (Complexo I da cadeia respiratória, NADH desidrogenase), C7ORF55 (Complexo V da cadeia respiratória, ATP-sintetase) e FASTKD1 (Serina/treonina quinase-*like* ativado por Fas). Essas proteínas órfãs foram avaliadas quanto a sua especificidade de ligação ao mtDNA em relação às proteínas encontradas na matriz mitocondrial, por uma triagem analítica dos dados e confirmação por *Western-blot*, sugerindo que essas proteínas podem participar de um mecanismo celular capaz de mitigar os danos causados por espécies reativas de oxigênio (EROs) ao DNA. Inclusive, ainda foi demonstrado que a atenuação do gene FASTKD1, por *knockdown* utilizando shRNA, pode aumentar a

expressão de mRNAs de ND3 (uma subunidade do Complexo I da cadeia respiratória, NADH desidrogenase) e, conseqüentemente, interferir positivamente nos níveis dessa proteína.

Apesar da APEX2 ter uma alta resolução temporal para determinar proteomas organelares, o quesito espacial pode ser um desafio, levando em consideração todas as proteínas que fazem parte de um determinado contexto molecular. A fim de resolver esse gargalo, Lobingier et al. (2017), aperfeiçoaram o uso da APEX2, para realizar uma deconvolução espacial-temporal de forma quantitativa de proteínas, utilizando o receptor beta-2 adrenérgico (ou do inglês, *beta-2 adrenergic receptor* ou B2AR), que é um receptor acoplado a proteína G (ou do inglês, *G-protein-coupled receptors* ou GPCR), característico dos endossomos, para definir em uma resolução espaço-tempo as suas proteínas parceiras. Com o uso de agonistas, para ativar a cascata de sinalização, foi possível quantificar, em uma janela temporal, a presença das proteínas arrestina-3, clatrina e o complexo retrômero (subunidade VPS35), que interagem em diferentes momentos com a B2AR, sugerindo que o uso da abordagem APEX2 para desvendar proteínas de baixa afinidade/transientes com o GPCR em um determinado espaço-tempo de um cenário molecular é altamente eficiente.

Em contrapartida, outras abordagens para estudar a interação entre proteínas têm emergido. Uma metodologia alternativa que tem sido utilizada é baseada no uso da enzima biotina-ligase modificada (BirA\*-R118G) de *E. coli*, denominada como BioID (do inglês, *proximity-dependent Biotin-IDentification*), que de forma bastante similar a APEX2, promove a biotinilação de proteínas parceiras, em um raio de ~10 nm, quando a BirA\* é utilizada como *tag* da proteína de interesse (N- ou C-terminal), resultando na modificação covalente dos resíduos de Lys (K), sendo posteriormente capturadas em coluna de estreptavidina e analisadas por espectrometria de massas. O único fator limitante que torna o uso da técnica menos atraente, é o fato de haver a necessidade de entre 18-24h de incubação com a biotina para marcar as proteínas parceiras (Rees et al. 2015; Varnaité & MacNeill 2016; Li et al. 2017).

Vários estudos tem sido publicados utilizando a metodologia de BioID em organismos unicelulares, de modo especial os protozoários. Em *Trypanosoma brucei*, agente etiológico da “doença do sono”, o uso dessa abordagem propiciou a descrição de novos parceiros das proteínas TbMORN1 (Morriswood et al., 2013), SAS-4 (Hu et al., 2015) e TbPLK (McAllaster et al., 2015), que estão envolvidas na motilidade e morfogênese do parasita. Em *Toxoplasma gondii*, o uso dessa metodologia permitiu a descrição de 19 novas proteínas parceiras de ISP3 (do inglês, *IMC Subcompartment*

*Protein 3*) associadas ao citoesqueleto e a região apical, sendo que a ISP3 é uma proteína característica do Complexo de Membrana Interno (CMI), que está associado a motilidade, invasão e replicação destes parasitas (Chen et al., 2015). Em outra ocasião, Long et al. (2017), partindo dessa mesma estratégia, conseguiram observar que as proteínas *CaM-like 1, 2 e 3* estão associadas a MyoH de *T. gondii*, que é uma classe de miosina especializada envolvida no processo de invasão, possibilitando ainda a identificação de proteínas típicas da região apical do parasita, reforçando a hipótese da co-localização destas proteínas.

No gênero *Plasmodium* spp., apenas alguns estudos foram publicados dentro deste contexto. Boucher et al. (2018) utilizaram a BirA\* fusionada a uma sequência líder ACP (do inglês, *acyl-carrier protein*), para realizar o mapeamento proteômico organelar do apicoplasto, onde através de uma análise robusta de bioinformática, foi possível compilar o proteoma desta organela em 346 proteínas em *P. falciparum*. Dentre elas, novas proteínas foram descritas, inclusive a essencialidade do transportador de membrana ABCF1 (do inglês, *ABCF-family protein*), podendo este, ser considerado um alvo terapêutico de grande interesse.

Em outro estudo, foi possível realizar a descrição de 61 proteínas pertencentes da membrana do vacúolo parasitóforo (MVP) do *Plasmodium berghei*, que interagiram com a proteína quimérica EXP1-BirA\*-V5 (sendo a EXP1, uma proteína característica deste compartimento), com a detecção de 3 novas proteínas desta estrutura: uma proteína serina/treonina fosfatase UIS2 e duas proteínas não-caracterizadas (PBANKA\_0519300 e PBANKA\_0509000) (Schnider et al., 2018). Neste mesmo ano, Khosh-Naucke et al. (2018), fizeram a descrição das proteínas do vacúolo parasitóforo (VP) de *P. falciparum*, utilizando uma construção portando um peptídeo sinal (SP) fusionado à GFP-BirA\* transiente com a identificação de 77 proteínas, onde é observado que a proteína ortóloga UIS2, antes observada por Schnider et al. (2018) em *P. berghei*, é essencial na sobrevivência do parasita, pois a obtenção de mutantes nocauteados não foi possível em *P. falciparum*.

Apesar da abordagem BioID ser eficiente, ela demanda uma incubação muito longa, conforme já mencionado. Diante disso, Branon et al. (2018) aperfeiçoaram o uso da BirA\*, em uma plataforma denominada como TurboID, onde foi realizado uma modificação no resíduo 118 da arginina (R), para um resíduo de serina (S), ao invés de um resíduo de glicina (G) utilizado na abordagem BioID convencional (BioID: BirA\*-R118G / TurboID: BirA\*-R118S). Com essa modificação, foi possível observar uma eficiência de 3-6 vezes de diferença no sinal de biotinylation (em uma incubação de



apenas 30 min), do que a BioID nos pontos iniciais, e 15-23 vezes de intensidade na biotilação nos pontos tardios (em uma incubação de apenas 3h). Apesar disso, em apenas ~10 min de reação com o substrato biotina-fenol, foi possível detectar níveis equivalentes de biotilação àquela produzida pela BioID em 18h de reação.

O estudo da interação proteína-proteína de um determinado cenário molecular pode fornecer inúmeras pistas acerca do papel biológico que uma proteína, até então desconhecida, pode desempenhar. Desde o advento do uso da técnica do duplo-híbrido, que possibilitou a descrição de diversas interações entre proteínas, em diferentes organismos (Formstecher et al., 2005; Marchadier et al., 2011; Yu et al., 2011), fornecendo subsídio experimental para o aprofundamento do conhecimento acerca deste tema, outras abordagens que tem o mesmo objetivo surgiram, como é o caso da APEX2 e BioID (Rees et al. 2015; Varnaité & MacNeill 2016; Li et al. 2017). Devido ao curto tempo de reação, talvez, a abordagem por APEX2 ainda seja a mais atrativa, mesmo que o aperfeiçoamento da BioID para TurboID (Branon et al. 2018) tenha diminuído o tempo de reação. Apesar de alguns trabalhos terem sido publicados em *Plasmodium* spp., com o uso de BioID (Khosh-Naucke et al., 2018; Schnider et al., 2018), até o momento, nenhum vislumbrou o uso da APEX2, o que torna ainda mais instigante, o que podemos obter com essa metodologia.

A circular inset showing a microscopic view of numerous red blood cells (erythrocytes) against a dark background. The cells are biconcave and appear as reddish-orange discs. The text "II - JUSTIFICATIVA" is overlaid on the right side of the circle.

## II - JUSTIFICATIVA

## ii. JUSTIFICATIVA

O tráfego de proteínas em *P. falciparum* é certamente um processo complexo, pois, necessita que diferentes estruturas participem do mecanismo de exportação/translocação para o ambiente citosólico da célula hospedeira (Boddey & Cowman 2013; Spillman et al. 2015). Apesar de ser um processo relativamente bem descrito, sobretudo levando em consideração a importância das proteínas KAHRP e PfEMP1 na citoaderência ao endotélio da microcirculação do hospedeiro, constituindo um dos principais mecanismos de virulência em *P. falciparum*, é importante que o uso de metodologias que propiciem uma descrição mais detalhada acerca dos parceiros moleculares de um determinado alvo sejam implementadas, a fim de se conhecer melhor os processos biológicos que permeiam a sobrevivência do parasita. Além disso, o uso da edição genômica mediada por CRISPR-Cas9 tem sido implementada, em estudos funcionais utilizando *P. falciparum* (Mogollon et al. 2016; Crawford et al. 2017; Xiao et al. 2019). O uso de abordagens de marcação por proximidade utilizando BioID, por exemplo, tem trazido novas informações acerca do apicoplasto e vacúolo parasitóforo em espécies de *Plasmodium* spp. (Boucher et al., 2018; Khosh-Naucke et al., 2018; Schnider et al., 2018).

Até o momento, nenhum estudo utilizou a tecnologia APEX2 em espécies de *Plasmodium* spp. Em outras espécies de parasitas, tais como *T. gondii* (Seidi et al., 2018; Pan et al., 2019) e *T. brucei* (Vélez-Ramírez et al., 2021), o uso da APEX2 já é realidade, mostrando sua eficiência e precisão para estudar as proteínas parceiras de um determinado alvo, ou ainda, um compartimento celular. Devido à facilidade do uso da técnica, sobretudo, por sua rapidez e alto rendimento na biotinylation das proteínas, este trabalho é o pioneiro, tratando-se do uso da tecnologia APEX2 para marcar um gene endógeno de *P. falciparum* e realizar a descrição das proteínas vizinhas parceiras deste alvo. Desse modo, diante da dificuldade em se obter um enriquecimento organelar sem contaminação proveniente de outras estruturas, o uso da abordagem APEX2, traz uma nova perspectiva quanto ao estudo de organelas, até então, pouco caracterizadas em *P. falciparum*. Além disso, está em andamento um projeto com resultados preliminares que, visa realizar o mapeamento de proteínas presentes no apicoplasto, mitocôndria e roptrias de *P. falciparum*, podendo trazer instigantes resultados acerca da sua biologia, podendo trazer à tona mecanismos até então desconhecidos, que possam contribuir na sua invasão e sobrevivência, podendo ainda constituir possíveis alvos terapêuticos em futuros estudos funcionais.

A circular inset showing a microscopic view of numerous red blood cells (erythrocytes) against a dark background. The cells are biconcave and appear as reddish-orange discs. The text is overlaid on this circular area.

### III - OBJETIVOS E ETAPAS METODOLÓGICAS

### iii. OBJETIVOS E ETAPAS METODOLÓGICAS

#### Objetivo Geral

Descrever as proteínas vizinhas parceiras da proteína KAHRP e mapear as proteínas organelares do apicoplasto, mitocôndria e roptrias durante o processo de esquizogonia de *P. falciparum* utilizando CRISPR-Cas9, APEX2 e proteômica.

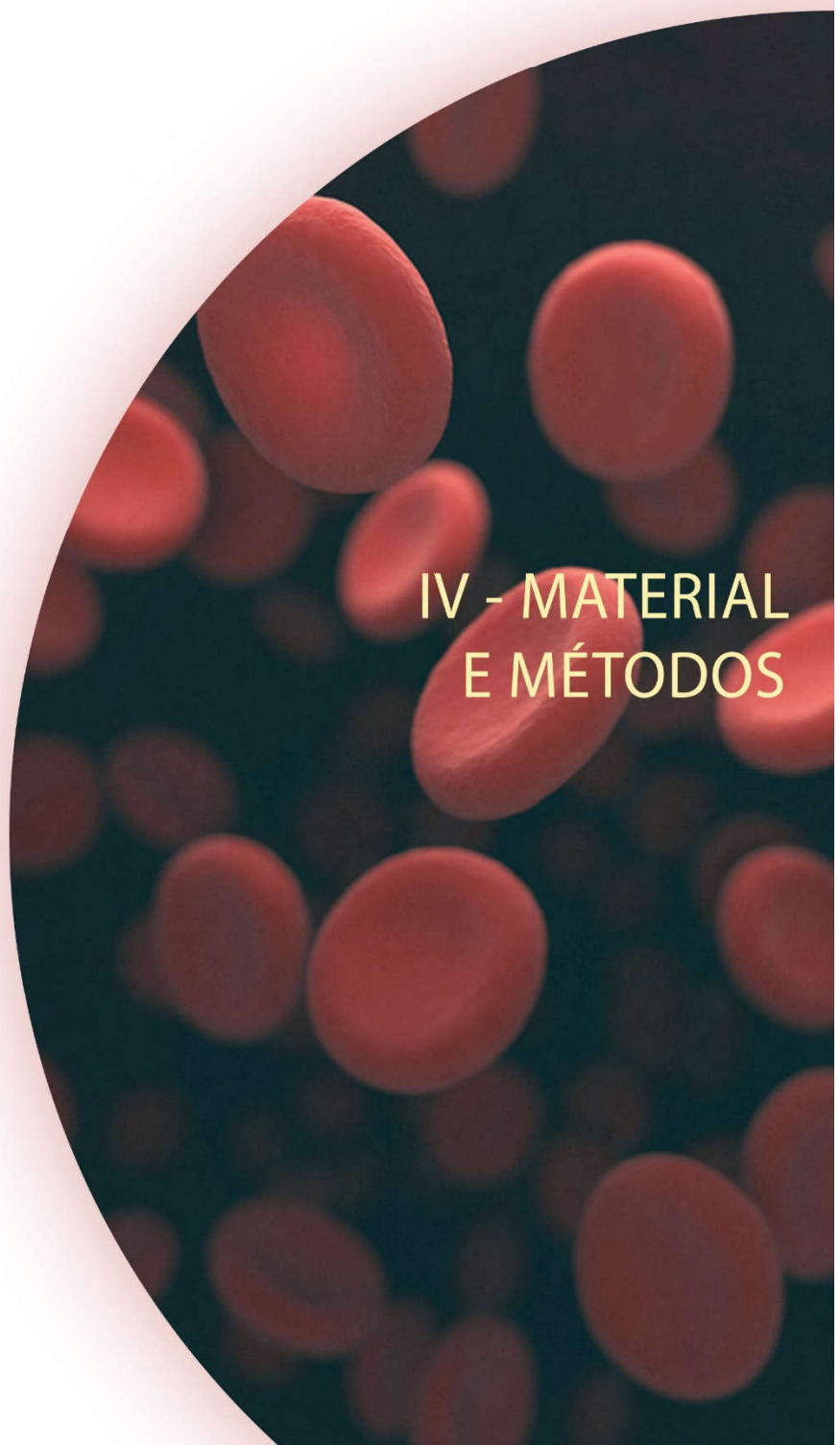
#### Etapas metodológicas concluídas

- (i) Produção de mutantes *knock-in* para o gene *kahrp* e validação da integração do cassete ao gDNA por PCR;
- (ii) Confirmação da expressão da proteína quimérica KAHRP-Flag-APEX2 por Western-blot;
- (iii) Realizar o ensaio de biotinylação das proteínas potencialmente parceiras de KAHRP-Flag-APEX2 e analisar por Western-blot;
- (iv) Avaliar a biotinylação das proteínas por microscopia de fluorescência;
- (v) Enriquecimento das proteínas biotiniladas por KAHRP-Flag-APEX2 com *beads* magnéticas de estreptavidina;
- (vi) Preparar as proteínas biotiniladas para análise por espectrometria de massas;
- (vii) Redação do manuscrito: **“APEX2-based proteomic analysis depicts candidate protein partners of KAHRP in *Plasmodium falciparum*”**.
- (viii) Construção dos plasmídeos que endereçam a APEX2 ao citosol, apicoplasto, mitocôndria e roptrias (pCC1-HA<sub>(cito)</sub>-APEX2, pCC1-SP<sub>(ACP)</sub>-HA-APEX2, pCC1-SP<sub>(RAP1)</sub>-HA-APEX2 e pCC1-SP<sub>(TRXR)</sub>-HA-APEX2);
- (ix) Determinar as curvas-reposta de IC<sub>50</sub> através do ensaio de [<sup>3</sup>H] hipoxantina com uso da droga WR99210 (Sigma-Aldrich e Jacobus Pharmaceuticals Inc.\*) utilizando diferentes linhagens de *P. falciparum*;
- (x) Produção da proteína APEX2 recombinante (rAPEX2) por um sistema heterólogo utilizando *Escherichia coli*;
- (xi) Produção dos soros policlonais à partir da rAPEX2 e validá-los por Western-blot;
- (xii) Confirmação da orientação dos insertos das construções por ensaio de digestão com enzima de restrição *HindIII* e sequenciamento;

- (xiii) Padronização da obtenção de parasitas mutantes de expressão episomal por transfecção com uso da plataforma Amaxa II Nucleofector II AAD-1001N (Lonza), com a obtenção dos parasitas transfectados com os vetores pCC1-HA<sub>(cito)</sub>-APEX2 (APEX2 de expressão citosólica), pCC1-SP<sub>(RAP1)</sub>-HA-APEX2 (APEX2 endereçada às roptrias) e pCC1-SP<sub>(TRXR)</sub>-HA-APEX2 (APEX2 endereçada à mitocôndria);

### **Etapas metodológicas em andamento**

- (xiv) Obtenção dos parasitas transfectados com o vetor pCC1-SP<sub>(ACP)</sub>-HA-APEX2 (APEX2 endereçada ao apicoplasto);
- (xv) Validação da expressão da HA-APEX2 à partir dos parasitas mutantes com uso de anti-HA e/ou anti-APEX2;
- (xvi) Validação da biotilação das proteínas organelares com o uso de estreptavidina-HRP;
- (xvii) Avaliar a biotilação das proteínas organelares por microscopia de fluorescência;
- (xviii) Enriquecimento das proteínas organelares biotiniladas por HA-APEX2 com *beads* magnéticas de estreptavidina;
- (xix) Preparar as proteínas biotiniladas para análise por espectrometria de massas;
- (xx) Análise dos dados proteômicos com o uso das ferramentas de bioinformática (DAVID, BlastKOALA, KEGG, MoMo, MEME, PlasmoDB, GO term, PATS, PlasmoAP, ApicoAP, SignalP, SecretomeP, TMHMM, Phobius, etc.);
- (xxi) Participação de eventos nacionais e/ou internacionais de divulgação científica;
- (xxii) Redação de artigos científicos.

A circular inset showing a microscopic view of numerous red blood cells (erythrocytes) against a dark background. The cells are biconcave and appear as reddish-orange spheres. The text 'IV - MATERIAL E MÉTODOS' is overlaid on the right side of the inset.

## IV - MATERIAL E MÉTODOS

#### iv. MATERIAL E MÉTODOS

##### **Cultura de *P. falciparum* e comitê de ética**

A linhagem 3D7 de *P. falciparum* foi cultivada em eritrócitos humanos tipo A<sup>+</sup> ou O<sup>+</sup> em meio RPMI 1640 (Gibco™) suplementado com 10% de soro humano inativado ou 0,5% de AlbuMAX II Lipid Rich BSA (Thermo Scientific), 4 g/L de glicose, 2 g/L de bicarbonato de sódio (NaHCO<sub>3</sub>), 25 mM de HEPES, 25 mg/L de gentamicina e 50 mg/L hipoxantina (Trager & Jensen, 1976). Para a seleção de mutantes, o uso de 1,25 nM da droga WR99210 (Jacobus Pharmaceuticals Inc.\*) foi utilizada. As culturas foram condicionadas em estufas a 37°C com saturação de 5% de CO<sub>2</sub>. Quando necessário, as culturas eram condicionadas a 37°C com saturação de mistura de gases: 6% de CO<sub>2</sub>, 5% de O<sub>2</sub> e 89% de N<sub>2</sub>.

O uso de eritrócitos e plasma de doadores humanos para a cultura parasitária foi aprovado pelo Comitê de Ética em pesquisa da Faculdade de Ciências da Saúde da Universidade de Brasília (CEP/UnB): parecer número 4.562.740 de 26 de fevereiro de 2021 e pela Fundação de Ensino e Pesquisa em Ciências da Saúde do Distrito Federal (FEPECS/SES-DF): parecer número 4.659.331 de 19 de abril de 2021. As retiradas das bolsas de concentrado de hemácias e plasma dos doadores humanos são retiradas periodicamente nas instituições parceiras: Fundação Hemocentro de Brasília e Hemoclínica.

##### **Construção dos plasmídeos de expressão epissomal**

As construções foram baseadas no uso dos peptídeos sinais para as organelas: apicoplasto (peptídeo sinal: ACP, *acyl-carrier protein*) (Waller et al., 2000), mitocôndria (peptídeo sinal: TrxR, *thioredoxin reductase*) (Kehr et al., 2010), e, roptrias (peptídeo sinal: RAP, *roptry-associated protein*) (Richard et al., 2009). Os peptídeos sinais foram fusionados *upstream* a sequência da APEX2, sendo que para cada construção foi adicionado um *tag* de HA na região N-terminal, após a sequência do peptídeo sinal. As sub-clonagens foram realizadas com o uso do vetor pCC1. Todos os plasmídeos possuem a marca de seleção *hDHFR* (do inglês, *human dihydrofolate reductase*), que confere resistência a droga anti-folato WR99210 (Jacobus Pharmaceuticals Inc.\*).

Os insertos foram sintetizados (GeneArt, Thermo Scientific), e clonados em vetores comerciais pMAT, flanqueados por *XhoI* e *Sall*. Para o procedimento de sub-clonagem, as enzimas de restrição *XhoI* (Promega) e *Sall* (Promega) foram utilizadas,



conforme instruções do fabricante. Após a digestão dos vetores, os insertos foram analisados em gel de agarose 1%, com a excisão manual dos mesmos. Após a excisão, as bandas do gel contendo os insertos foram extraídos com o uso do kit de purificação PureLink™ PCR Purification (Invitrogen™). Para o procedimento de ligação dos insertos HA<sub>(cito)</sub>-APEX2 (APEX2 de expressão citosólica), SP<sub>(ACP)</sub>-HA-APEX2 (APEX2 endereçada ao apicoplasto), SP<sub>(RAP1)</sub>-HA-APEX2 (APEX2 endereçada às roptrias) e SP<sub>(TrxR)</sub>-HA-APEX2 (APEX2 endereçada a mitocôndria), no vetor de expressão pCC1, foi necessário realizar uma digestão prévia do vetor pCC1-*empty*, para retirar o gene da citosina deaminase permitindo a linearização do vetor.

A ligação dos insertos ao vetor pCC1 foi realizada com o uso da enzima T4 DNA ligase (Promega), conforme instruções do fabricante. Após a ligação, os vetores contendo os insertos: pCC1-HA<sub>(cito)</sub>-APEX2, pCC1-SP<sub>(ACP)</sub>-HA-APEX2, pCC1-SP<sub>(RAP1)</sub>-HA-APEX2 e pCC1-SP<sub>(TrxR)</sub>-HA-APEX2, foram inseridos em células competentes de *Escherichia coli* TOP10 (Invitrogen™), através do método de transformação por choque térmico, e plaqueadas em meio LB sólido contendo 100 µg/mL de ampicilina. Após a incubação, em estufa bacteriológica, a 37°C, as colônias referentes aos clones positivos da transformação, foram cultivados em meio LB líquido contendo 100 µg/mL de ampicilina, e submetidos ao protocolo de Miniprep (Sambrook & Russell 2001), com posterior digestão com as enzimas de restrição *Xho*I e *Sal*I, para averiguar se a ligação foi eficiente.

Após a confirmação da ligação, os clones positivos foram submetidos a um ensaio de digestão com uso da enzima de restrição *Hind*III (Promega), para averiguar se o inserto se ligou ao vetor pCC1 na orientação correta (5' → 3'). Os oligonucleotídeos foram desenhados para analisar a sequência da APEX2, o gene *hDHFR*, as regiões promotoras 5' UTR (5' *CAM* e 5' *hsp86*) e terminadoras 3' UTR (3' UTR *PbDT* e 3' UTR *hrp2*) (Tabela 1). Todos os oligonucleotídeos foram checados nas plataformas: OligoCalc (<http://biotools.nubic.northwestern.edu/OligoCalc.html>) ou GeneRunner (<http://www.generunner.net/>).

**Tabela 1. Lista dos oligonucleotídeos utilizados para o sequenciamento dos plasmídeos de transfecção em *P. falciparum*.**

Região	Posição	Sequência
3' UTR_ <i>hrp2</i>	FW: 5' → 3'	CACGTTTTTTCCAGAAATTGATTTGG
	RV: 5' → 3'	GTACTGAGAGTGCACCATATGC
3' UTR_ <i>PbDT</i>	FW: 5' → 3'	GTATGTTGTGTGGAATTGTGAGC

<b>5' CAM</b>	RV: 5' → 3'	CCTGTATTCCGCCCTCTCG
	FW: 5' → 3'	CCAATGGCCCCTTTCCGCG
<b>5' hsp86</b>	RV: 5' → 3'	GAAATATCTAAATTCGTTCTGAGC
	FW: 5' → 3'	GGAGCGCATCTCTTCTCAGC
<b>APEX2</b>	RV: 5' → 3'	TTTATTATTAGAAATAGATATTTTTATAATAAACC
	FW: 5' → 3'	AGTTGGCTGGCGTTGTTGCC
<b>hDHFR</b>	RV: 5' → 3'	CCAAACACATCTCTCAAATGGTC
	FW: 5' → 3'	TATGTATATTTTAAACTAGAAAAGGAATAAC
	RV: 5' → 3'	ATAAGGAAGATTACAAAAAAAAAATTCATATG

---

As plataformas ClustalW (<https://www.genome.jp/tools-bin/clustalw>) ou Clustal Omega (<https://www.ebi.ac.uk/Tools/msa/clustalo/>) foram utilizados para realizar o alinhamento das sequências obtidas de todos os plasmídeos. A plataforma ExpASY ([https://www.bioinformatics.org/sms/rev\\_comp.html](https://www.bioinformatics.org/sms/rev_comp.html)) foi utilizada para obter as sequências reversas-complementares para o alinhamento dos *contigs* obtidos dos oligonucleotídeos anti-sense.

### Ensaio de [<sup>3</sup>H] hipoxantina

As culturas assincronizadas de *P. falciparum* das linhagens 3D7, NF54 e FcB1 foram utilizadas para este ensaio. O ensaio foi realizado em placas de leitura de fundo achatado de 96 poços. Para cada poço foi utilizado 200 µL de meio de cultura RPMI completo contendo apenas 5 µM de hipoxantina, contendo 1% de hematócrito e uma parasitemia aproximada de 1%. As alíquotas de WR99210 (Sigma-Aldrich e Jacobus Pharmaceuticals Inc.\*) foram dissolvidas em DMSO para a concentração estoque de 20 mM. Uma solução intermediária de 20 µM de WR99210 foi preparada de ambas as marcas. Para todas as linhagens de *P. falciparum*, uma diluição seriada foi aplicada para determinar a eficácia da WR99210 de ambas as marcas, partindo de uma quantidade de 250 nM até uma quantidade de 0,12 nM. Em seguida, foi adicionado às culturas 0,5 µCi de uma solução estoque de [<sup>3</sup>H] hipoxantina (11,1 mCi/mmol; Perkin-Elmer, France) em meio RPMI, e incubado por 24 h adicionais em estufa a 37°C e 5% CO<sub>2</sub>. Após este período de incubação, as placas foram congeladas a -20 °C e descongeladas em seguida para a lise das hemácias infectadas. As amostras foram coletadas em filtros de fibra de vidro e analisados por um espectrofotômetro de cintilação em líquido (Microbeta, Wallac, Perkin-Elmer) (Arnold et al., 2016; Cózar et

al., 2016). Os dados foram computados em Microsoft Office Excel e as curvas de IC<sub>50</sub> geradas pelo software GraphPad Prism (GraphPad Software, CA). Os valores das quantidades de WR99210 utilizadas foram normalizadas para a escala de log<sub>10</sub>. Os resultados foram expressos com as médias ± erro padrão das leituras em escala normalizada CCPM dos experimentos, de forma independente.

### **Transfecção em *P. falciparum***

Apenas as culturas de *P. falciparum* da linhagem 3D7 foram utilizadas para os ensaios de transfecção. O ensaio de transfecção foi padronizado para ser realizado com o uso de parasitas na fase de esquizonte segmentado (42-44 h), denominado por PEMS (do inglês, *parasitophorous-enclosed merozoite structures*) (Fang et al., 2018; Hoeijmakers et al., 2019; Jonscher et al., 2019; Wilde et al., 2019; Birnbaum et al., 2020). Para tal, as culturas foram previamente sincronizadas com 5% (w/v) de sorbitol (Sigma-Aldrich) (Lambros & Vanderberg, 1979). Após atingir uma parasitemia de aproximadamente ≥10% de esquizontes, foi realizado a separação dos esquizontes com uso de um gradiente de 63% (v/v) de Percoll® (GE Healthcare) (Kramer et al., 1982). Os esquizontes recuperados, foram transferidos para um frasco T75 contendo 2% (v/v) de hematócrito, para o ensaio de re-invasão em uma janela de 2-3 h. Após este período, as culturas foram novamente sincronizadas com 5% (w/v) de sorbitol (Sigma-Aldrich). Desse modo, as culturas poderão seguir uma janela síncrona de desenvolvimento, permitindo uma melhor obtenção de PEMS para o ensaio de transfecção.

Todos os plasmídeos purificados (pCC1-HA<sub>(cito)</sub>-APEX2, pCC1-SP<sub>(ACP)</sub>-HA-APEX2, pCC1-SP<sub>(RAP1)</sub>-HA-APEX2 e pCC1-SP<sub>(TRXR)</sub>-HA-APEX2), foram obtidos em colunas de Maxiprep, conforme as instruções do fabricante (QIAGEN). Para esterilizar os plasmídeos utilizados para a transfecção, os mesmos foram precipitados com o uso de 3 volumes (v/v) de etanol e 10% do volume correspondente à 100 µg de DNA plasmidial com 3 M de acetato de sódio (C<sub>2</sub>H<sub>3</sub>NaO<sub>2</sub>) pH 5,2 (Green & Sambrook, 2017). Após a precipitação, os pellets de DNA foram lavados com etanol 70% gelado. Após a secagem dos pellets em fluxo laminar, os mesmos foram ressuspensos com cerca de 15-20 µL de tampão TE (Tris-EDTA) pH 7,5 e estocados a -20°C até o dia do uso.

Após 3-4 ciclos de desenvolvimento dos parasitas previamente sincronizadas, e com a obtenção de uma parasitemia de 10-15% de esquizontes, um novo gradiente

de 63% (v/v) de Percoll® (GE Healthcare) foi realizado para recuperar estes parasitas dentro da janela de 2-3 h. Os esquizontes recuperados, foram ainda submetidos a um tratamento com o uso de 10 µM do inibidor de protease E-64 (Sigma-Aldrich) por mais 4-6 h, a fim de obter os PEMS. Uma parasitemia elevada é necessária, pois para este protocolo, utiliza-se cerca de 15-20 µL de hemácias infectadas por *P. falciparum* (ou do inglês, *infected-red blood cells* ou iRBCs). Este volume deve corresponder a aproximadamente  $1 \times 10^6 - 5 \times 10^7$  de iRBCs. A contagem foi realizada com uso da câmara de Malassez e microscópio óptico.

Em paralelo, uma preparação da solução Nucleofector™ Kit 2 (Lonza, catalog number: VMI-1021), contendo 85 µL da solução *basic nucleofector solution 2* e 15 µL da solução *supplement 3* foi realizada. Foi adicionado esta preparação da solução Nucleofector™ para cada DNA previamente preparado em tampão TE, incubando-o por 30 min em temperatura ambiente. Após o período de incubação com E-64, os parasitas PEMS foram recuperados com uma centrifugação a 900 x g, por 5 min (freio baixo), e todo o sobrenadante foi removido. Os pellets de PEMS foram gentilmente ressuspendidos com a preparação da solução Nucleofector™. O volume total (PEMS, solução Nucleofector™ com o DNA plasmidial) foi imediatamente transferido para uma cubeta de eletroporação. O uso do programa U-033 do equipamento Amaxa II Nucleofector II AAD-1001N (Lonza) foi utilizado para realizar a eletroporação.

Após o choque elétrico, os parasitas foram imediatamente transferidos para tubos de 1,5 mL contendo 500 µL de meio RPMI 1640 (Gibco™) suplementado com 0,5% de AlbuMAX II (Thermo Scientific) e 300 µL de hemácias frescas previamente aquecidas a 37°C em um thermomixer, e submetidos a uma agitação de 1100 rpm por 20 min. Este processo facilitará a liberação dos merozoítos transfectados, aumentando a taxa de re-invasão (Boyle et al., 2010). Após o período de incubação, transferiu-se imediatamente este volume para um frasco T25 contendo 200 µL de hemácias frescas e 10 mL meio RPMI 1640 (Gibco™) suplementado com 0,5% de AlbuMAX II (Thermo Scientific) (5% (v/v) de hematócrito final) previamente preparada e condicionada a 37°C. As garrafas foram gaseificadas com uma mistura de gases (6% de CO<sub>2</sub>, 5% de O<sub>2</sub> e 89% de N<sub>2</sub>), e condicionadas em estufas a 37°C durante todo o período de seleção dos parasitas. Após 24 h, a pressão seletiva com a droga WR99210 (Jacobus Pharmaceuticals Inc.\*) foi iniciada. Durante os 10 primeiros dias, os meios de cultura foram trocados diariamente. A cada 7 dias, hemácias frescas eram adicionadas. Os esfregaços sanguíneos eram realizados rotineiramente, até que 3-4 semanas pós-transfecção os primeiros parasitas foram observados.

## **Expressão heteróloga da proteína APEX2 em *Escherichia coli***

A expressão heteróloga da proteína APEX2 modificada foi realizada conforme já descrito (Oliveira et al., 2018). A sequência do gene *apex2* foi sintetizado e clonado no plasmídeo pET100/D-TOPO® com uma cauda 6xHis na extremidade N-terminal. As bactérias *E. coli* linhagem Rosetta(DE3)pLyS, foram utilizadas para a transformação por choque térmico e selecionadas com meio LB sólido contendo 100 µg/mL de ampicilina (Sigma-Aldrich). A indução da proteína recombinante ocorreu com o uso de 1 mM de isopropil-β-D-1-tiogalactopiranosídeo (IPTG), por durante 3h sob agitação a 200 rpm, condicionado a 37 °C. Após o crescimento e averiguação da D.O.<sub>600nm</sub> entre 0,4 - 0,6 por espectrofotometria, as células foram colhidas e centrifugadas a 5.000 x g, durante 15 min, condicionado a 4°C.

Para a lise das células foi utilizado BugBuster (Merck-Millipore) durante 7 min, sob leve agitação. A fim de obter um alto rendimento da extração, as células foram ainda sonicadas por 2 min, com o uso do equipamento Ultrasonic Liquid Processors (Qsonica Sonicators), seguindo a programação: 12 ciclos de 10 s, com intervalos de 30 s no gelo. Após o período de incubação, o *pellet* foi centrifugado a 12.000 x g, durante 15 min, condicionado a 4°C. As frações solúveis e insolúveis foram obtidas, entretanto somente a fração solúvel foi utilizada para o processo de purificação. Para o processo de purificação, foi utilizado a resina de níquel His-Select HF Nickel (Sigma-Aldrich), usando um gradiente de imidazol (Sigma-Aldrich) variando entre 5 mM até 500 mM. Para averiguar a eficiência do procedimento um gel SDS-PAGE foi feito, utilizando todas as frações de eluição e utilizando BSA como controle positivo da aplicação.

## **Produção de soros policlonais anti-APEX2 e validação por Western-blot**

A produção de soros policlonais contra a proteína purificada APEX2 modificada foi realizado conforme já descrito (Oliveira et al., 2018). Um total de 3 (três) camundongos da linhagem BALB/c foram utilizados para a imunização intraperitoneal. Uma punção ocular foi realizada para obter os soros pré-imune. Um total de 200 µg de proteína purificada foi utilizada para realizar a imunização em cada animal. Na primeira imunização, foi utilizado a proporção (v/v) de proteína purificada e coadjuvante de Freund completo (Sigma-Aldrich). Três reforços com adjuvante de

Freund incompleto (Sigma-Aldrich) foram realizados com intervalos de 15 dias entre as imunizações. Após as imunizações os animais foram eutanasiados em câmara de CO<sub>2</sub> e o sangue total foi coletado com a seguida obtenção do soro anti-APEX2. Para averiguar a eficiência dos anticorpos anti-APEX2 de cada animal, um gel preparativo foi feito, seguido da realização de Western-blot utilizando cerca de 10 µg da proteína purificada. Após a transferência, a membrana foi corada com 0,1% (w/v) Ponceau S (Sigma-Aldrich) em 5% (v/v) de ácido acético (Sigma-Aldrich), e as tiras foram cortadas manualmente. Uma titulação de 1:200, 1:1.000 e 1:5.000 foi utilizada para cada soro anti-APEX2 e a revelação foi realizada com BCIP/NBT.

### **Ensaio de biotinição e confirmação da expressão dos mutantes epissomais (pCC1-SP<sub>(cito, acp, rap1, trxr)</sub>-HA-APEX2) por Western-blot**

As culturas dos parasitas mutantes serão submetidas ao ensaio de biotinição com o uso do substrato da APEX2, 500 µM de biotina-fenol (Adipogen, CDX-B0270, *biotinyl-tyramide*), incubado por 30 min a 37°C em uma estufa com saturação de 5% de CO<sub>2</sub>, seguido do uso do agente oxidante/catalisador, 1 mM de H<sub>2</sub>O<sub>2</sub>, incubado por apenas 1 min para realizar a biotinição das proteínas organelares. Para interromper a reação de biotinição, as células serão lavadas 3 vezes, com uma solução *quencher* (10 mM de azida de sódio, 10 mM de ascorbato de sódio e 5 mM de Trolox) em PBS (Rhee et al., 2013; Lee et al., 2016; Lobingier et al., 2017). Diversas condições serão utilizadas para analisar a expressão da HA-APEX2 e a potencial biotinição dos compartimentos celulares: (i) ausência de biotina-fenol/ausência de H<sub>2</sub>O<sub>2</sub> (BP-/H<sub>2</sub>O<sub>2</sub>-); (ii) ausência de biotina-fenol/presença de H<sub>2</sub>O<sub>2</sub> (BP-/H<sub>2</sub>O<sub>2</sub>+); (iii) presença de biotina-fenol/ausência de H<sub>2</sub>O<sub>2</sub> (BP+/H<sub>2</sub>O<sub>2</sub>-); e, (iv) presença de biotina-fenol/presença de H<sub>2</sub>O<sub>2</sub> (BP+/H<sub>2</sub>O<sub>2</sub>+).

Após a reação de biotinição, os parasitas mutantes serão extraídos no estágio de esquizonte com 0,15% (w/v) de saponina (Sigma-Aldrich) em PBS, sendo posteriormente solubilizados em tampão de lise RIPA contendo 50 mM de Tris-HCl pH 7,0 (Invitrogen™), 150 mM de NaCl (Sigma-Aldrich), 0,1% (w/v) de SDS (Invitrogen™), 0,5% (w/v) de deoxicolato de sódio (Sigma-Aldrich), 1% (v/v) de Triton X-100 (Sigma-Aldrich), 1 pastilha de inibidor de protease (cOmplete™, EDTA-free protease inhibitor cocktail, Roche), 10 mM de azida de sódio (Sigma-Aldrich), 10 mM de ascorbato de sódio (Sigma-Aldrich) e 5 mM de Trolox (Sigma-Aldrich). Os extratos proteicos serão analisados por SDS-PAGE, transferidos para membranas de

nitrocelulose e corados com 0,1% (w/v) Ponceau S (Sigma-Aldrich) em 5% (v/v) de ácido acético (Sigma-Aldrich).

Após a transferência, as membranas de nitrocelulose serão lavadas 3 vezes com tampão TBS-T (137 mM de NaCl; 2,7 mM de KCl; 24,8 mM de Tris e 0,1% (v/v) de Tween-20). O bloqueio e a incubação das membranas com o anticorpo primário *mouse* anti-HA (Sigma-Aldrich, diluição 1:10.000) e secundário *goat* anti-*mouse* IgG conjugado com a HRP (*horseradish peroxidase*) (Invitrogen™, diluição 1:20.000) serão realizadas em tampão M-TBS-T (tampão TBS-T contendo 5% (w/v) de leite em pó desnatado). Para as proteínas biotiniladas por HA-APEX2 nas organelas será utilizado a estreptavidina-HRP (Invitrogen™, diluição 1:10.000). Após as devidas incubações, todas as membranas de nitrocelulose serão expostas no filtro de quimioluminescência do fotodocumentador Fusion Solo 6X Basic (Vilber), para a obtenção das imagens.

## Enriquecimento das proteínas biotiniladas por APEX2

O uso das *beads* magnéticas revestidas de estreptavidina (Pierce™, Thermo Scientific) será proporcional às quantidades dos extratos proteicos dos parasitas mutantes expressando a proteína HA-APEX2 e o controle, a linhagem selvagem de *P. falciparum* 3D7 (cerca de 50µL por 0,5 mg de proteína). As *beads* serão lavadas duas vezes com tampão RIPA e separadas do sobrenadante com o uso de *MagJET separation rack* (Thermo Scientific). Todos os extratos proteicos das condições em análise, serão incubadas sob agitação suave por 1 h, a 4°C. Após o período de incubação, as *beads* serão lavadas e separadas da fração não-ligada com o uso da raque magnética, da seguinte forma: (i) lavagem com tampão RIPA 2 vezes; (ii) uma lavagem com tampão RIPA contendo 1 M de ureia, e; (iii) lavagem com tampão RIPA 2 vezes. A eluição será realizada por desnaturação com uso de um tampão contendo 20 mM de DTT (GE Healthcare), 2 mM de biotina (Sigma-Aldrich) e tampão Laemmli, aquecido a 95°C, durante 5 min (Rhee et al., 2013; Lee et al., 2016; Lobingier et al., 2017).

## Ensaio de imunofluorescência (IFA)

Após a validação dos parasitas mutantes quanto a expressão da HA-APEX2 e biotinilação das proteínas organelares, os parasitas serão submetidos a uma

análise por microscopia de fluorescência e/ou confocal à laser. Os parasitas serão sincronizados com 5% (w/v) de sorbitol (Sigma-Aldrich), com um enriquecimento dos parasitas no estágio de anel (4-20 h). Após 20-22 h do procedimento de sincronização, será adicionado 10  $\mu$ M de E-64 (Sigma-Aldrich), um inibidor de protease que inibe o rompimento do esquizonte, permitindo o enriquecimento dos parasitas nessa fase do desenvolvimento (40-42 h). As culturas serão mantidas nestas condições por um período de 4-6 h antes do procedimento de enriquecimento dos esquizontes/merozoítos por centrifugação através de um gradiente de 63% (v/v) de Percoll® (GE Healthcare). Os esquizontes/merozoítos oriundos desse processo serão ressuspensos em um pequeno volume de RPMI morno e depositados em lâminas de vidro. Os ensaios de imunofluorescência serão realizados como descrito anteriormente (Charneau et al., 2007).

O uso de anticorpos primários específicos quanto aos compartimentos celulares, tais como anti-EXP2 ( $\alpha$ -EXP2, marcação do vacúolo parasitóforo), anti-ERD2 ( $\alpha$ -ERD2, marcação do *cis*-Golgi / retículo endoplasmático), anti-MAHRP1 ( $\alpha$ -ERD2, marcação das *Maurer's clefts*), ou ainda, pelo soro anti-APEX2 (marcação da APEX2 nativa nos compartimentos), serão utilizados para fornecer um contraste de imagem dos compartimentos devidamente marcados do *P. falciparum*. Para marcar a mitocôndria será utilizado o MitoTracker™ Red FM (Invitrogen™). Os anticorpos secundários serão acoplados com AlexaFluor-488 (AF-488, Invitrogen™) ou AlexaFluor-594 (AF-594, Invitrogen™). Para as proteínas biotinizadas, será utilizado estreptavidina-AF488 (Invitrogen™). O uso de DAPI (do inglês, *4',6-diamidino-2-phenylindole*) ou Hoescht 33342 serão utilizados para marcação nuclear. O uso de *anti-fading* também será empregado. As análises das fluorescências serão realizadas com uso do microscópio de fluorescência Nikon Eclipse Ti2 (NIKON) ou confocal à laser TCS SP8 CSU (Leica).

### **Preparação das amostras para espectrometria de massas**

As frações enriquecidas contendo as proteínas biotinizadas serão precipitadas *overnight* com 4 volumes de acetona gelada e 100 mM de NaCl, adicionados ao volume das amostras (proporção 80:20), condicionadas a -20°C. Após o período de incubação, as amostras serão centrifugadas a 16.000 x *g*, por 10 min, a 4°C (Crowell et al., 2013). Após a secagem do pellet, será adicionado à ele, 25 mM de tampão TEAB (do inglês, *triethylammonium bicarbonate buffer*) (Sigma-Aldrich), seguida da



redução das pontes dissulfeto com 5 mM de DTT (GE Healthcare) durante 30 min, a 55°C; e, alquilação das pontes dissulfeto com 14 mM de iodoacetamida (Sigma-Aldrich), durante 40 min, ao abrigo da luz, em temperatura ambiente. Em seguida, as amostras serão submetidas à digestão triptica com uso da Tripsina Gold (Promega) na proporção de 1:50 (1 µg de enzimas para 50 µg de substrato), incubadas a 37°C, durante aproximadamente 18 h.

Após a digestão triptica, as amostras serão dessalinizadas com um sistema preparado manualmente, utilizando as colunas de C18 (3M™ Empore™) e Poros OligoR3 (Applied Biosystems™) empacotadas em ponteiras P-200 (Axygen®). O *pipeline* para ativação, carregamento dos peptídeos e lavagens serão empregadas da seguinte forma: (i) 100 µL 0,5% (v/v) de metanol; (ii) 2 x 100 µL de 80% (v/v) de acetonitrila / 0,5% (v/v) de ácido acético; (iii) 2 x 100 µL de 0,5% (v/v) de ácido acético; (iv) carregamento dos peptídeos nas colunas; (v) 2 x 100 µL de 0,5% (v/v) de ácido acético; (vi) eluição com uso de um gradiente de: 1 x 20 µL de 25% (v/v) de acetonitrila / 0,5% (v/v) de ácido acético; 1 x 20 µL de 50% (v/v) de acetonitrila / 0,5% (v/v) de ácido acético; 1 x 20 µL de 80% (v/v) de acetonitrila / 0,5% (v/v) de ácido acético; e, 1 x 20 µL de acetonitrila (Rappsilber et al., 2007). Os peptídeos eluídos serão secos em uma centrífuga SpeedVac (Eppendorf™) com uso de tubos LoBind® (Eppendorf™) e estocados a -20°C, até o dia das análises por espectrometria de massas.

## **Análise por espectrometria de massas**

Os digestos serão analisados pelo sistema de cromatografia líquida de alto desempenho 3000 (HPLC) (Dionex; Thermo Fisher Scientific), acoplado a um espectrômetro de massas LTQ-Orbitrap Elite™ (Thermo Fisher Scientific) por meio de uma fonte de ionização *nanoelectrospray* (Proxeon; Thermo Fisher Scientific). Os dados brutos *.raw* serão vistos em Xcalibur v.2.1 (Thermo Scientific Waltham, EUA) e os dados de processamento serão obtidos por meio do PEAKS 7.0 Studio Software (Thermo Scientific™). Os espectros obtidos serão comparados com o banco de dados de proteínas de *P. falciparum* da linhagem 3D7 (proteoma UP000001450), à partir do Uniprot (<https://www.uniprot.org/>). As proteínas contaminantes (p. ex. queratina, BSA e tripsina), incluindo as proteínas provenientes das hemácias humanas (à partir do proteoma UP000005640), serão manualmente adicionados ao banco de dados, e, posteriormente removidas das análises.

As buscas serão realizadas com os seguintes parâmetros: precisão do MS1 de 10 ppm, precisão de MS2 de 0.05 Da e dois sítios de clivagem perdidas permitidos. Somente as modificações variáveis (i) oxidação de metionina (+15.99); (ii) acetilação da extremidade N-terminal (+42.01); e, (iii) biotilação dos resíduos de Tyr (Y, +363.16) serão permitidas nas buscas. Somente a carbamidometilação da cisteína (+57.02) será ajustada como modificação fixa. O número de proteínas, grupos de proteínas e número de peptídeos serão filtrados por FDR (do inglês, *false discovery rate*) inferior ou igual a 0.01. Será apenas considerado uma identificação válida aquelas proteínas que apresentarem ao menos 1 peptídeo único e um mínimo de 2 peptídeos por proteína.

As análises de bioinformática serão realizadas nas seguintes plataformas: (i) DAVID (<https://david.ncifcrf.gov/>) para a classificação funcional das proteínas; (ii) BlastKOALA (<https://www.kegg.jp/blastkoala/>) e Pathview (<https://pathview.uncc.edu/>) para a análise do enriquecimento das vias metabólicas; (iii) PlasmoDB (<https://plasmodb.org/plasmo/app>) para as análises específicas relacionadas ao *P. falciparum*, tais como: análise de *GO terms* e predição de proteínas do apicoplasto e/ou mitocondriais (p. ex. PATS, PlasmoAP e ApicoAP); (iv) SignalP (<http://www.cbs.dtu.dk/services/SignalP/>) e SecretomeP (<http://www.cbs.dtu.dk/services/SecretomeP/>) para as proteínas potencialmente secretadas pelas próprias.



## **CAPÍTULO 6**

# **MANUSCRITO**

**“APEX2-based proteomic analysis depicts candidate protein partners of KAHRP in *Plasmodium falciparum*”**

**Formatado para ser submetido na “*Journal of Proteome Research*”**

1 **CAPÍTULO 6 – MANUSCRITO: “APEX2-based proteomic analysis**  
2 **depicts candidate protein partners of KAHRP in *Plasmodium***  
3 ***falciparum*”**

4  
5 **Proposed first authors:** Sébastien Charneau and Lucas Silva de Oliveira (**from**  
6 Laboratory of Biochemistry and Protein Chemistry, Department of Cell Biology,  
7 Institute of Biology, University of Brasília, Distrito Federal, Brazil).

8  
9 **In collaboration with:** Zenon Zenonos, Christine Hopp and Julian C. Rayner  
10 (**from** Malaria Programme, Wellcome Trust Sanger Institute, Cambridge,  
11 England); Damarys Loew and Bérangère Lombard (**from** Institut Curie, PSL  
12 Research University, Centre de Recherche, Laboratoire de Spectrométrie de  
13 Masse Protéomique, 26 rue d’Ulm, Paris 75248 Cedex 05, France); Izabela M.  
14 D. Bastos (**from** Laboratory of Host Pathogen Interaction, Department of Cell  
15 Biology, Institute of Biology, University of Brasília, Distrito Federal, Brazil); and,  
16 Philippe Grellier (**from** Unité Molécules de Communication et Adaptation des  
17 Microorganismes (MCAM), UMR 7245, CNRS Muséum National d’Histoire  
18 Naturelle, Paris Cedex 05, France).

19  
20 **ABSTRACT**

21  
22 Malaria still being a public health burden worldwide, mostly because no protective  
23 long-term vaccine is available and most of the main treatments employed today  
24 are facing resistant-phenotype parasites strains. Therefore, novel targets are a  
25 prerequisite to develop novel therapeutic strategies to eradicate malaria. In this  
26 context, it is highly demanded that molecular studies point towards new structures  
27 that might be used as potential target for antimalarial interventions. Thus,  
28 exported parasite proteins have a crucial role in the host cell remodeling, playing  
29 an important function on the host cell cytoadherence and invasion. Two players  
30 involved in these functions are KAHRP and *PfEMP1*, allowing the formation of  
31 protrusions on the host cell surface, called “knobs”. Most of our understanding of  
32 cellular and molecular processes are based on the protein-protein interaction  
33 (PPI) network, therefore, a wider comprehension about KAHRP neighboring

34 partners, may shed light into novel exported proteins or related processes that  
35 are still unknown. In this work, we have implemented a set of approaches to  
36 decipher potential candidate neighboring proteins of KAHRP in *P. falciparum*, by  
37 using CRISPR-Cas9, APEX2 and mass-spectrometry label-free based  
38 proteomics. By using a chimeric KAHRP-Flag-APEX2, a total of 208 parasite-  
39 neighboring proteins were identified as potential candidates of interaction with  
40 KAHRP. Among them, GBP130, PTP2, Pf332, PHISTb members, RhopH/CLAG  
41 complex members and RESA. To the best of our knowledge, this work is the first  
42 one, which implemented the use of APEX2 technology in *P. falciparum*.

43

44 **Key words:** KAHRP, protein-protein interaction, APEX2, cytoadherence,  
45 exported proteins.

46

47 **Financial support:** CAPES-COFECUB, CNPq, FAPDF, FINEP and Fondation  
48 pour la Recherche Médicale.

49

## 50 INTRODUCTION

51

52 Malaria has been the most life-threatening tropical disease in the world  
53 capable to lead the patients to death in severe cases. In 2019, it was estimated  
54 229 million malaria cases with a mark of 409.000 deaths worldwide, mainly  
55 caused by *Plasmodium falciparum*<sup>1</sup>. In the last decades, many efforts to develop  
56 a vaccine against malaria have been employed, such as RTS,S<sup>2</sup>. Unfortunately,  
57 RTS,S showed an unsatisfactory lifelong protection<sup>2</sup>, with risk of rebound<sup>3</sup>.  
58 Possibly, the promising R21/Matrix-M vaccine candidate<sup>4</sup>, may be a feasible  
59 alternative to protect in a long-term manner, but this remain to be assessed in a  
60 near future. For this reason, treatment of malaria continues to be based on  
61 chemotherapies<sup>1,5</sup>. However, the rapid spread of drug-resistant strains of  
62 *Plasmodium* species over the years, turned-out malaria a public health issue  
63 worldwide<sup>1</sup>.

64

65 *P. falciparum* is the only specie capable to lead into the most dangerous  
66 state of malaria disease, the cerebral malaria<sup>6,7</sup>. This state is mainly caused  
67 because of parasite expressed ligands on the surface of infected red blood cells  
(iRBCs), by which triggers the formation of aggregates with iRBCs and/or

68 uninfected red blood cells (RBCs), known as rosettes <sup>7</sup>, avoiding spleen  
69 clearance mechanisms, causing the microvasculature endothelium obstruction  
70 <sup>6,8</sup>. To promote this host cell remodeling, many proteins are exported by *P.*  
71 *falciparum* <sup>9,10</sup>, usually through tubulovesicular network vesicles, named as  
72 Maurer's clefts (MC's) <sup>8,11</sup>.

73 Among these proteins, two *P. falciparum* ligands play fundamental roles:  
74 (i) the PfEMP1 multigene family (*P. falciparum* erythrocyte membrane protein 1)  
75 is widely recognized as having a central role in the cytoadherence process,  
76 especially on the avidity to the host receptors <sup>12</sup>; and, (ii) another well-known  
77 protein, named KAHRP (*knob-associated histidine rich protein*), that anchors  
78 PfEMP1 as a backbone structure to the molecular small protrusions of iRBC  
79 surface, called “knobs”, facilitating the “rosetting” process <sup>13–15</sup>. Both PfEMP1 and  
80 KAHRP are transiently located in MC's in the erythrocyte cytosol reaching the  
81 knobs <sup>16</sup>.

82 Beyond its role for the progression to the malaria disease, KAHRP is a  
83 non-essential gene, and some reports have been using successfully CRISPR-  
84 Cas9 genome editing system <sup>17</sup> for *P. falciparum kahrp* gene disruption <sup>18,19</sup>. This  
85 technology has changed the paradigm of the functional genomic manipulation in  
86 *Plasmodium* species, especially considering its genome highly A+T rich content  
87 <sup>20</sup>. Since a comprehensive study of protein-protein interaction (PPI) networks is  
88 very useful for protein functional characterization, in the same period, a proximity-  
89 dependent biotin identification approach, named as BioID, coupled to the mass-  
90 spectrometry based proteomics were developed allowing neighbouring and  
91 potentially interacting proteins in a native environment to be identified <sup>21</sup>. This  
92 technology has been showing its usefulness in the study of Apicomplexan  
93 parasite models, such as *P. falciparum* <sup>22–24</sup>, *Plasmodium berghei* <sup>25</sup> and  
94 *Toxoplasma gondii* <sup>26,27</sup>.

95 Alternatively, a similar approach based on the use of ascorbate-  
96 peroxidase modified (APEX2), emerged as a faster and equally sensible  
97 methodology to solve accurately complex PPI networks <sup>28–30</sup>. The two goals of  
98 this study were: (i) the implementation of CRISPR-Cas9 and APEX2 proximity  
99 tagging followed by label-free mass-spectrometry based proteomics, allowing  
100 identification of protein-partners from *P. falciparum*, targeting the endogenous  
101 *kahrp* gene as model, and; (ii) to determine the subset of candidate parasite

102 proteins interacting with KAHRP. Herein, we have identified 208 neighbouring  
103 and potentially interacting protein partners of KAHRP in the parasite. Some of  
104 these proteins are known to be interacting with KAHRP. *In silico* analysis,  
105 additionally suggest that some of these protein species may be exported to the  
106 host cell environment through translocon PTEX, as expected. Overall, we  
107 demonstrated for the first time, the feasibility to use APEX2 proximity tagging in  
108 *P. falciparum*.

109

## 110 **EXPERIMENTAL PROCEDURES**

111

### 112 **Culture conditions**

113

114 The parasites of *P. falciparum* strain 3D7 obtained from Malaria Research  
115 and Reference Reagent Resource Centre (available at: [www.mr4.org](http://www.mr4.org)) were  
116 continuously maintained in O<sup>+</sup> human erythrocytes, RPMI 1640 medium without  
117 phenol red (Gibco™) supplemented with 0.5% AlbuMAX™ II (Gibco™), 2 mM L-  
118 glutamine, 25 mg/L of gentamycin and 50 mg/L of hypoxanthine<sup>31</sup>. Cultures were  
119 kept in incubators at 37 °C, with a pre-mixed gas combination of 1% O<sub>2</sub>, 3% CO<sub>2</sub>  
120 and 96% N<sub>2</sub>. The parasite growth was observed by optic microscopy through  
121 Giemsa staining and diluted or synchronized by treatment with 5% (w/v) sorbitol  
122 (Sigma-Aldrich) when required. The use of erythrocytes from human donors for  
123 parasite culture was approved by the Ethics Committee of NHS Cambridgeshire  
124 4 Research and all donors supplied written informed consent.

125

### 126 **Vector constructions for CRISPR-Cas9**

127

128 The constructions were done by using SeqBuilder software (DNASTAR)  
129 for both plasmids: pCC1 (targeting vector) and pDC2 (expression vector). Sanger  
130 sequencing confirmed all insert sequences in both directions. *P. falciparum* 3D7  
131 genomic DNA was extracted and purified from 500 µL of high parasitaemia  
132 culture (QIAamp DNA blood mini kit (QIAGEN)). To edit *kahrp* gene by  
133 CRISPR/Cas9 approach, we modified pDC2-cam-Cas9-U6-sgRNA-hDHFR  
134 construct containing a *Pfcam* promoter<sup>32</sup> into pDC2-cam-Cas9-U6-sgRNA-  
135 yDHODH (yeast dihydroorotate dehydrogenase)<sup>33</sup> to target specifically *kahrp*

136 gene. The gRNA oligonucleotides FWsgRNA-KAHRP  
137 ([Phos]attgCGTATTTAAGCATAAATATA) and RVsgRNA-KAHRP  
138 ([Phos]aaacTATATTTATGCTTAAATACG) were annealed and ligated into *BbsI*  
139 digested pDC2-cam-Cas9-U6-sgRNA-yDHODH plasmid. The gRNA target site  
140 was chosen using CHOPCHOP (<https://chopchop.cbu.uib.no>) at first rank and  
141 confirmed by sgRNA Designer  
142 (<http://www.broadinstitute.org/rnai/public/analysis-tools/sgrna-design>), localised  
143 after the stop codon.

144 The 813 bp sequence of Flag-APEX2-NES gene was amplified from  
145 pcDNA3APEX2-NES (Addgene plasmid # 49386)<sup>34</sup> with primers (GibsonPcc1-  
146 Apex-FW: 5'-agtccgaagatctgtcttaagATGGACTACAAGGATGACGAC-3' and  
147 Gibson-RV-APEX2-HSP86: 5'-ttaattttttacaaaatgcTTAGTCCAGGGTCAGGCG-  
148 3'), which contained a sequence overlapping *AflII*-digested pCC1-hDHFR  
149 transfection vector and hsp86 3'UTR, respectively. The 835bp of the hsp86  
150 3'UTR sequence was amplified from pINT<sup>34</sup> with primers (Gibson-FW-APEX2-  
151 HSP86: 5'-ctggactaaGTCGAGTTATATAATATATTTATGTACTCAC-3' and  
152 Gibson-RV-HSP86-pCC1: 5'-  
153 ttaattttttacaaaatgcTATTTGATGAATTAACACTTAAAATAATAC-3'), which  
154 contained sequence overlap to the Flag-APEX2-NES gene and *AflII*-digested  
155 pCC1-hDHFR transfection vector, respectively. The final assembled vector  
156 pCC1-Flag-APEX2-HSP86-3'UTR was performed in a single Gibson assembly  
157 reaction. HR1 is upstream the stop codon of the *kahrp* gene and the HR2 is  
158 downstream the gRNA cleavage site in the 3' UTR.

159 The sequence of *kahrp* gene (PF3D7\_0202000, knob-associated histidine  
160 rich protein) was obtained from PlasmoDB databank  
161 (<https://plasmodb.org/plasmo/app>). The homology regions 1 and 2 (HR1 and  
162 HR2) were amplified from 3D7 genomic DNA by PCR using primers flanking the  
163 regions with restriction enzymes *SacI* and *AflII* for HR1 (primers, FW-KAHRP-  
164 HR1-*SacII*: 5'-ccgcggAGCATGAAGGAAATGACGGTGAAGGAG-3' and RV-  
165 KAHRP-HR1-*AflIII*: 5'-cttaagACCACAGCATCCTCTTTTCTTCTTTTCTTTCC-  
166 3'), and *EcoRI* and *NcoI* for HR2 (primers, FW-KAHRP-HR2-*EcoRI*: 5'-  
167 gaattcTTTAATTTGACGTTTATACAGAAAAGAGTTATTCTG-3' and RV-KAHRP-  
168 HR2-*NcoI*: 5'-ccatggCCCTTTCTAAATATTATACGGATTTTCTTAATTC-3').  
169 The PCR products were cloned into pCR®2.1-TOPO (Thermo Scientific).



170 *SacI* and *AflIII* digested HR1 and *EcoRI* and *NcoI* digested HR2 were  
171 subcloned into multiple cloning site 1 and 2, respectively, of pCC1-FlagAPEX2-  
172 HSP86-3'UTR. The resulting vector contained the donor DNA cassette Flag-  
173 APEX2-NES with *hsp86* 3' UTR, following by the drug-selectable marker *hdhfr*  
174 (human dihydrofolate reductase), which confers resistance to the antifolate drug  
175 WR99210<sup>35</sup>, under the control of calmodulin promoter and the 3' UTR of *hrp2*  
176 gene, all flanked by HR1 and HR2 of *kahrp* gene.

177

## 178 **Plasmid preparation and transfection procedure**

179

180 All plasmids suitable for the transfection protocol were obtained from  
181 transformed *E. coli* TOP10 cells containing pCC1-FlagAPEX2-HSP86-3'UTR-  
182 KAHRP-HR1-HR2 or pDC2-cam-Cas9-U6-sgRNA<sub>*kahrp*</sub>-yDHODH and purified  
183 using Maxiprep kit (QIAGEN) accordingly manufacturer's instructions. The  
184 plasmids were precipitated using 3 volumes (v/v) of ethanol and 10% of the initial  
185 volume of DNA solution of 3 M sodium acetate pH 5.2<sup>36</sup>. For the transfection, 50  
186 µg of each plasmid was used for the precipitation. After precipitation, the DNA  
187 pellets were suspended and mixed in 100 µL of buffer P3 (Lonza) with 4 µL ATP  
188 (625 mM). Ring stage-iRBCs with a high parasitemia (approximately 10%) were  
189 centrifugated and 100 µL of packed iRBCs were resuspended in cold sterile  
190 cytomix (120 mM KCl, 0.2 mM CaCl<sub>2</sub>, 2 mM EGTA, 10 mM MgCl<sub>2</sub>, 25 mM HEPES,  
191 5 mM K<sub>2</sub>HPO<sub>4</sub>, 5 mM KH<sub>2</sub>PO<sub>4</sub>, pH 7.6) and added to DNA plasmids. The final  
192 mixture were split into two nucleocuvettes and immediately electroporated with  
193 Lonza Nucleofector 4D using the programme P3/CM-150<sup>37</sup>. After the  
194 electroporation the cells were immediately transferred to the T25 flasks previously  
195 prepared containing 10 mL of pre-warmed complete RPMI medium containing  
196 0.5% AlbuMAX™ II Lipid-Rich BSA (Gibco™). Conversely, the fresh RBCs were  
197 washed with homemade cold sterile cytomix and 100 µL of packed RBCs were  
198 used to complete the haematocrit of 2%. Forty eight hours (48h) post-transfection  
199 the parasites were submitted to the drug pressure using 1.25 nM of WR99210  
200 (Jacobus Pharmaceuticals Company, Inc.\*) for pCC1 selection and 1.5 µM of  
201 DSM-1 (Merck, Calbiochem®) for pDC2 selection<sup>37</sup>. After 3 weeks, the first  
202 parasites were seen through blood smears routinely made. The parasites were  
203 cultured into a parasitemia ≥5% and the DNA extraction were performed using

204 QIAamp DNA Blood Mini Kit (QIAGEN), and the cassette integration into the  
205 specific loci of the genomic DNA were assessed by 1% agarose gel using  
206 designed primers obtained by OligoCalc  
207 (<http://biotools.nubic.northwestern.edu/OligoCalc.html>).

208

### 209 **Biotinylation assay**

210

211 Parasites were routinely synchronized in a large 20 h-window by treatment  
212 with 5% (w/v) of D-sorbitol (Sigma-Aldrich). Before the assay, around 1 mL of  
213 iRBCs containing 5% of parasitemia with late stages corresponding to  $5 \times 10^8$   
214 cells were enriched by centrifugation over 63% (v/v) isotonic Percoll cushion  
215 (Percoll Plus 17-5445-01, GE Healthcare). The assays were performed by using  
216 complete RPMI medium without phenol red supplemented with or without 250  $\mu$ M  
217 of biotin-phenol (Iris Biotech, CDX-B0270) for 30 min at 37 °C, 5% CO<sub>2</sub> for both  
218 mutant and wild type (WT) strains. After the incubation period, both control and  
219 treated parasite cells were submitted to the addition of 1 mM of H<sub>2</sub>O<sub>2</sub> (final  
220 concentration; GE Healthcare) during 1 min. Immediately after the reaction the  
221 reactions were quenched twice washes with an antioxidant solution containing 10  
222 mM sodium azide (Sigma-Aldrich), 10 mM sodium ascorbate (Sigma-Aldrich) and  
223 5 mM of Trolox (Sigma-Aldrich) in PBS. Treated and non-treated biotin-phenol  
224 cells were spin down to obtain the transgenic or WT parasite pellets in order to  
225 make the blood smears used for immunofluorescence assay. The remaining  
226 iRBCs were lysed with 0.1% (w/v) saponin (Sigma-Aldrich) in PBS containing  
227 EDTA-free protease inhibitor cocktail (cOmplete™, Roche) and frozen for  
228 immunodetection by western blotting and pull-down of biotinylated proteins<sup>28–30</sup>.

229

### 230 **Protein extraction and pull-down of biotinylated proteins**

231

232 Erythrocyte-free parasites were lysed by using 4-5 volumes of the parasite  
233 pellet of RIPA buffer containing 50 mM Tris-HCl pH 7.0 (Invitrogen™), 150 mM  
234 NaCl (Sigma-Aldrich), 0.1% (w/v) SDS (Invitrogen™), 0.5% (w/v) sodium  
235 deoxycholate (Sigma-Aldrich), 1% (v/v) Triton X-100 (Sigma-Aldrich), EDTA-free  
236 protease inhibitor cocktail (cOmplete™, Roche), 10 mM sodium azide (Sigma-  
237 Aldrich), 10 mM sodium ascorbate (Sigma-Aldrich) and 5 mM of Trolox (Sigma-

238 Aldrich) in PBS <sup>28–30</sup>. The lysates were incubated for 30 min, 4 °C, followed by a  
239 centrifugation at 15.000 x g, for 20 min, 4 °C <sup>27</sup>. The supernatants were  
240 immediately transferred to new 1.5 mL tubes.

241 The protein extract from all samples were submitted to the enrichment of  
242 biotinylated proteins using Pierce™ streptavidin magnetic beads (Thermo  
243 Scientific). The beads were initially washed twice with the RIPA buffer and  
244 separated from supernatant with MagJET separation rack (Thermo Scientific).  
245 Thus, the RIPA-soluble protein fraction from all conditions were incubated with  
246 the streptavidin magnetic beads accordingly with its capacity, during 1 hour in a  
247 mild agitation, at room temperature. By using the magnetic rack, the biotinylated  
248 proteins loaded beads were separated from the flowthrough and washed as  
249 follow: (i) 2 x 1.4 mL with RIPA buffer; (ii) 1 x 1.4 mL with RIPA buffer with 1 M of  
250 urea and (iii) 2 x 1.4 mL with RIPA buffer. The elution was performed by using  
251 100 µL of a solution containing 20 mM DTT (GE Healthcare), 2 mM of biotin  
252 (Sigma-Aldrich) and NuPAGE™ LDS Sample Buffer supplemented with NuPAGE  
253 Sample Reducing Agent and NuPAGE™ Antioxidant (Invitrogen™), heated at 95  
254 °C, for 5 min <sup>28–30</sup>.

255

### 256 **NuPAGE™, Western-blot and streptavidin-blot**

257

258 NuPAGE™ Novex™ 4–12% Bis-Tris protein gels in MES buffer  
259 (Invitrogen) separated 20 µg of RIPA soluble fraction of erythrocyte-free  
260 parasites, before blotting onto nitrocellulose membrane (GE Healthcare). After  
261 transfer, the membranes were stained with 0.1% (w/v) Ponceau S (Sigma-  
262 Aldrich) in 5% (v/v) of acetic acid (Sigma-Aldrich). After blocking, nitrocellulose  
263 membranes were incubated with anti-FLAG coupled to horseradish peroxidase  
264 (HRP; Sigma-Aldrich; 1:800 dilution) or with streptavidin-HRP (Invitrogen™;  
265 1:10.000 dilution). Blots were developed with Amersham ECL Prime  
266 chemiluminescence substrate (GE Healthcare) and fluorograms were collected.

267

268

### 269 **Immunofluorescence assays**

270

271 Smears from late stages-enriched transgenic or WT parasites were  
272 prepared on glass slides and dried for at least 30 min. Next, they were fixed with  
273 4% (v/v) paraformaldehyde (Sigma-Aldrich) for 20 min and washed once with  
274 PBS. Cells were permeabilized with 0.1% (v/v) Triton X-100 (Sigma-Aldrich) in  
275 PBS and blocked for 3 hours at 8 °C by using 3% BSA in PBS. Then, parasites  
276 were co-probed with Alexa-Fluor 488-conjugated streptavidin (Invitrogen™,  
277 S11223; 1:800 dilution) and IgG rabbit antibodies directly raised against  
278 *PfMAHRP* or *PfERD2* (MRA; 1:200 dilution for both) for 1 hour at room  
279 temperature in blocking solution. After three washes in PBS, cells were incubated  
280 with Alexa-Fluor 546-conjugated anti-rabbit IgG donkey antibodies (Invitrogen™,  
281 A10040; 1:800 dilution). After a final wash, the slides were mounted with anti-  
282 fade mounting medium with 4',6-diamidino-2-phenylindole dihydrochloride  
283 (DAPI) (Molecular Probes). Confocal images were acquired with a LSM510 laser  
284 scanning confocal microscope (Zeiss).

285

## 286 **Proteomic analysis**

287

288 All enriched samples were precipitated with 4 volumes of cold acetone (-  
289 20 °C) to the sample in a proportion of 80:20, and the protein pellet was washed  
290 twice with cold (-20 °C) ethanol 70% (v/v) without disturbing it, followed with the  
291 air drying in the fume hood<sup>38-40</sup>. The protein pellet was resuspended in 25mM  
292 triethylammonium bicarbonate buffer (TEAB, Sigma-Aldrich), reduced with 5 mM  
293 dithiothreitol (GE Healthcare) for 30 minutes, at 55 °C, followed by alkylation of  
294 disulfide bonds with 14 mM iodoacetamide (Sigma-Aldrich) for 40 minutes in the  
295 dark, at room temperature. Next, the total protein extract of each sample was  
296 digested with trypsin gold (Promega) in the proportion of 1:50 (1µg of enzyme to  
297 50µg of substrate), at 37 °C, for 18 h. After tryptic digestion, the samples were  
298 desalted using a homemade desalting system of packed P-200 C18 columns  
299 (3M™ Empore™) and Poros OligoR3 resin (Applied Biosystems™). The pipeline  
300 for activation, peptide loading and washing were employed as it follows: 100 µL  
301 0.5% (v/v) methanol; twice 100 µL acetonitrile 80% (v/v) / acetic acid 0.5% (v/v);  
302 100 µL acetic acid 0.5% (v/v); loading peptides from samples; 100 µL acetic acid  
303 0.5% (v/v); elution with a gradient of 20 µL acetonitrile 25% (v/v) / acetic acid  
304 0.5% (v/v); 20 µL acetonitrile 50% (v/v) / acetic acid 0.5% (v/v); 20 µL acetonitrile

305 80% (v/v) / acetic acid 0.5% (v/v) and 20  $\mu$ L acetonitrile <sup>41</sup>. The eluted peptides  
306 were dried in SpeedVac centrifuge (Eppendorf™) using LoBind® tubes  
307 (Eppendorf™) and stocked at -20 °C until the day of usage.

308 LC was performed with an RSLCnano system (Ultimate 3000, Thermo  
309 Scientific) coupled online to an Orbitrap Exploris 480 mass spectrometer (Thermo  
310 Scientific). Peptides were trapped on a C18 column (75  $\mu$ m inner diameter  $\times$  2  
311 cm; nanoViper Acclaim PepMap™ 100, Thermo Scientific) with buffer A (2/98  
312 MeCN/H<sub>2</sub>O in 0.1% formic acid) at a flow rate of 3.0  $\mu$ L/min over 4 min. Separation  
313 was performed on a 50 cm  $\times$  75  $\mu$ m C18 column (nanoViper Acclaim PepMap™  
314 RSLC, 2  $\mu$ m, 100Å, Thermo Scientific) regulated to a temperature of 40°C with a  
315 linear gradient of 3% to 29% buffer B (B: 100% MeCN in 0.1% formic acid, A:  
316 100% H<sub>2</sub>O in 0.1% formic acid) at a flow rate of 300 nL/min over 91 min. MS full  
317 scans were performed in the ultrahigh-field Orbitrap mass analyzer in ranges m/z  
318 375–1500 with a resolution of 120 000 at m/z 200. The top 20 most intense ions  
319 were subjected to Orbitrap for further fragmentation via high energy collision  
320 dissociation (HCD) activation and a resolution of 15 000 with the auto gain control  
321 (AGC) target set to 100%. We selected ions with charge state from 2+ to 6+ for  
322 screening. Normalized collision energy (NCE) was set at 30 and the dynamic  
323 exclusion of 40s.

324 For identification, the data were searched against the *P. falciparum* strain  
325 3D7 proteome databank (Proteome UP000001450, from 02-16-2021) with 5456  
326 entries downloaded from Uniprot (<https://www.uniprot.org/>). To this file, it was  
327 manually included 438 entries corresponding to the matched “red blood cells” and  
328 “erythrocytes” associated key words searched against the proteome from *Homo*  
329 *sapiens* proteome databank (Proteome UP000005640, from 02-16-2021) and the  
330 KAHRP-Flag-APEX2 chimeric sequence. Enzyme specificity was set to trypsin  
331 and a maximum of two miss cleavages sites were allowed. As fixed modification  
332 was set carbamidomethylation of cysteine (+57.02). Oxidized methionine  
333 (+15.99), biotinyl-tyramide of tyrosine residues (+363.16) and N-terminal  
334 acetylation (+42.01) were set as variable modifications. Maximum allowed mass  
335 deviation was set to 10 ppm for monoisotopic precursor ions and 0.02 Da for  
336 MS/MS peaks. The resulting files were further processed using PEAKS Studio.  
337 FDR was set to 0.01 at the peptide level for the whole study.

338

## 339 **Bioinformatic analysis**

340

341 To construct Venn diagrams used for proteomic analysis, it was used the  
342 bioinformatics and evolutionary genomics web tool (available at:  
343 <http://bioinformatics.psb.ugent.be/webtools/Venn/>). The enrichment of post-  
344 translational modification (PTM) on the tyrosine residues by biotinyl-tyramide  
345 peptide motifs was done by using MoDL algorithm search ([https://meme-  
346 suite.org/meme/tools/momo](https://meme-suite.org/meme/tools/momo)) on the MoMo platform using the PSM list obtained  
347 from PEAKS analysis output files <sup>42</sup>. As the same manner, from proteins predicted  
348 to have the PEXEL motif (RxLx[EQD]) obtained from PlasmoDB  
349 (<https://plasmodb.org/plasmo/app>) databank, the enrichment was done by MEME  
350 Suite algorithm <sup>43</sup>. Overrepresented Gene Ontology (GO) terms were predicted  
351 by GO Cloud tool through PlasmoDB (<https://plasmodb.org/plasmo/app>)  
352 databank. The possibility to be secreted and/or exported to the extracellular  
353 environment of all proteins were assessed by SignalP <sup>44,45</sup> and SecretomeP  
354 WebServer <sup>46,47</sup>. For transmembrane protein prediction, TMHMM <sup>48</sup> and Phobius  
355 <sup>49</sup> were additionally employed.

356

## 357 **RESULTS**

358

### 359 **Construction and validation of KAHRP-Flag-APEX2 expressing** 360 **parasites for *in vivo* biotinylation assay**

361

362 The plasmids pCC1-KAHRP-Flag-APEX2 and pDC2-U6-Cas9-gRNA<sub>kahrp</sub>  
363 were co-transfected in *P. falciparum* 3D7 wild-type strain to generate a transgenic  
364 strain expressing the chimeric protein KAHRP-Flag-APEX2 (Figure 1A). After 21  
365 days of WR99210 drug pressure, the first transgenic parasites were observed. A  
366 diagnostic PCR was performed in order to assess the cassette integration to  
367 gDNA in agreement with the predicted length. As expected, the amplicons from  
368 the primers PS110/PS102 and PS103/PS114 were nearly 1.1 kb and 1.6 kb,  
369 respectively, confirming the cassette integration into gDNA. The amplicons from  
370 the primers PS105/PS102 and PS103/PS106 were nearly 1.8 kb and 1.5 kb,  
371 respectively, suggesting that there were episomal pCC1-KAHRP-Flag-APEX2  
372 plasmids not yet integrated to gDNA. No amplification was obtained from primers

373 PS110/PS114, probably because of the cassette large length, impossible to get  
374 resolved by conventional agarose gel (Figure 1B and C).

375 Four conditions with or without biotin-phenol (BP) substrate and hydrogen  
376 peroxide (H<sub>2</sub>O<sub>2</sub>) were employed to the transgenic parasites to assess the  
377 biotinylation pattern: (i) BP-/ H<sub>2</sub>O<sub>2</sub>-, (ii) BP-/ H<sub>2</sub>O<sub>2</sub>+, (iii) BP+/ H<sub>2</sub>O<sub>2</sub>- and (iv) BP+/  
378 H<sub>2</sub>O<sub>2</sub>+. After saponin treatment, the erythrocyte-free parasite soluble proteins  
379 were obtained by RIPA treatment (RIPA-soluble proteins) and separated by  
380 NuPAGE. In agreement with ExPASy prediction, the molecular weight of KAHRP  
381 (71.3 kDa) and Flag-APEX-2 (29.4 kDa) together add up to 100.7 kDa, as  
382 observed by Western blotting (Figure 2). The chimeric protein KAHRP-Flag-  
383 APEX2 is expressed in all conditions of treatment with or without BP/H<sub>2</sub>O<sub>2</sub> in  
384 RIPA-soluble proteins probed with anti-FLAG antibodies (Figure 2) from  
385 transgenic parasites. On the other hand, episome based Flag-APEX2 expressing  
386 mutant parasites were also obtained in order to contrast the expression of  
387 KAHRP-Flag-APEX2 chimeric protein, as a control together with *P. falciparum*  
388 3D7 wild-type strain total protein extract for further analysis (Figure S1A and B).

389 In order to assess whether the APEX2-based biotinylation assay was  
390 effective to promote the chemical post-translational modification (PTM) onto  
391 endogenous neighboring proteins of KAHRP-Flag-APEX2 in living cells, a  
392 streptavidin-HRP blot analysis was performed probing the biotinylated proteins  
393 from all conditions analyzed. Only the assay in presence of BP substrate, treated  
394 with an oxidant condition with H<sub>2</sub>O<sub>2</sub> showed a collection of bands of biotinylated  
395 endogenous proteins that spans a large molecular weight range (Figure 2). No  
396 signal was observed in the negative controls, in which APEX2, BP or H<sub>2</sub>O<sub>2</sub> are  
397 omitted (Figure 2 and S1B). In the episome-based Flag-APEX2 mutant parasites,  
398 the same pattern of biotinylated proteins was observed through streptavidin-HRP  
399 blot analysis only in the presence of BP and H<sub>2</sub>O<sub>2</sub> (Figure S1B).

400

401

402

### 403 **Imaging analysis by confocal immunofluorescence**

404

405 KAHRP-Flag-APEX2 expressing mutants from two conditions: BP+/  
406 H<sub>2</sub>O<sub>2</sub>- and BP+/ H<sub>2</sub>O<sub>2</sub>+, were analyzed by confocal fluorescence microscopy.

407 Immunofluorescence assays (IFAs) using streptavidin-AF488 further confirmed  
408 that endogenous neighboring proteins of KAHRP-Flag-APEX2 were biotinylated  
409 in live schizonts treated with BP+/H<sub>2</sub>O<sub>2</sub>+, revealing in addition numerous  
410 punctuated structures within the RBC cytoplasm (Figure 3). To further  
411 characterize the compartment by which endogenous neighboring proteins of  
412 KAHRP-Flag-APEX2 may be localized, we performed co-localization analysis  
413 using a specific marker of Maurer’s clefts (MC), by probing an antibody against  
414 membrane-associated histidine-rich protein (anti-MAHRP) known to colocalize  
415 with KAHRP, as previously established<sup>50–52</sup>. The MC are parasitophorous  
416 vacuole membrane (PVM) budding vesicles that are unequivocally known to  
417 support *P. falciparum* protein exportation<sup>11,53</sup>, among them KAHRP<sup>16</sup>. As  
418 observed in Figure 3B, a good localization was detected between MAHRP and  
419 the KAHRP-Flag-APEX2 partners in the punctuate MC of living schizonts in the  
420 presence of BP and H<sub>2</sub>O<sub>2</sub> (white arrows).

421 Conversely, IFAs using streptavidin-AF488 showed that endogenous  
422 neighboring proteins of episome-based Flag-APEX2 are localized in the cytosol  
423 of the parasites. The use of anti-MAHRP in late stages further confirmed that  
424 cytosolic Flag-APEX2 partners did not localized in the RBC cytoplasm nor in the  
425 MC probed with anti-MAHRP (Figure S2A). Similarly, it was also observed a  
426 partial co-localization between cytosolic biotinylated proteins and an antibody  
427 raised against *P. falciparum* cis-Golgi / endoplasmatic reticulum retention-  
428 defective protein (anti-ERD2), at perinuclear regions of *P. falciparum* segmented  
429 schizonts<sup>54–57</sup> (Figure S2B). At this point, APEX2 technology can be accurately  
430 used for living *P. falciparum* parasites in order to solve protein partners to a  
431 specific protein of interest or specific compartment.

432

### 433 **Proteomic and *in silico* analysis**

434

435 As long as we have produced a chemical PTM on tyrosine residues (Y) of  
436 KAHRP-Flag-APEX2 interacting-biotinylated protein partners, the next step was  
437 to enrich the KAHRP-Flag-APEX2-biotinylated proteins by using streptavidin-  
438 coated beads in denaturing conditions from all assay conditions. From the WT  
439 and mutant strains, only the conditions BP+/H<sub>2</sub>O<sub>2</sub>+ and BP-/H<sub>2</sub>O<sub>2</sub>+ were analyzed  
440 by mass spectrometry. A triplicate from these conditions of each strain was used



441 for further proteomic analysis. Thus, a total of (i) 2,663 proteins from 40,590  
442 peptides in the condition KAHRP-Flag-APEX2 BP+/H<sub>2</sub>O<sub>2</sub>+; (ii) 2,635 proteins  
443 from 36,068 peptides in the condition KAHRP-Flag-APEX2 BP-/H<sub>2</sub>O<sub>2</sub>+; (iii) 1,944  
444 proteins from 23,031 peptides in the condition 3D7 BP+/H<sub>2</sub>O<sub>2</sub>+ and (iv) 1,251  
445 proteins from 11,716 peptides in the condition 3D7 BP-/H<sub>2</sub>O<sub>2</sub>- were identified in  
446 our analysis (Tables S1).

447 From MS analysis, we initially performed a screening to select manually  
448 only identified proteins with 1 unique peptide and at least 2 peptides for each  
449 protein identification, with the variable biotin-phenol (+363.16) modification on Tyr  
450 residues. Intriguingly, we also identified biotinylated peptides in conditions whose  
451 experimentally no biotin-phenol tagging should have occurred, such as in the BP  
452 and/or APEX2 absence. We have reasoned that prediction of biotinylated  
453 peptides in these conditions could be due to fake interpretation of the spectrum  
454 by the software or indirect enrichment from correctly enriched biotinylated  
455 proteins<sup>28,30,58</sup>. A possible interpretation of these phenomenon could rely on the  
456 amounts of protein starting material and a disproportional amount of streptavidin-  
457 coated beads, once none of both can be accurately estimated, providing  
458 nonspecific binders<sup>58,59</sup>. For further analysis, we excluded biotinylated peptides  
459 shared between KAHRP-Flag-APEX2 BP+/H<sub>2</sub>O<sub>2</sub>+ (K BP+) condition with other  
460 negative conditions. Thus, a total of 240 exclusive non-redundant biotinylated  
461 peptides from K BP+ condition were considered for further analysis (Figure 4A).

462 Interestingly, no biotinylation was observed in the KAHRP-Flag-APEX2  
463 chimeric protein from BP-treated mutants (Tables S1). This maybe occurred due  
464 to a self-biotinylation inhibition possibly related to the structure of the protein  
465 fusion between KAHRP and APEX2. Moreover, no identification was also  
466 observed of the native version of KAHRP (PF3D7\_0202000). The 240 exclusive  
467 non-redundant biotinylated peptides from K BP+ condition corresponded to 208  
468 *P. falciparum* protein groups and 10 *H. sapiens* protein groups (Figure 4C and  
469 Table S2). Identified KAHRP-neighboring proteins were observed by IFA in  
470 punctuated structures within the RBC cytoplasm, together with MAHRP probed  
471 with antibodies, therefore, likely to be MC. KAHRP is already known to be  
472 exported through translocon PTEX localized at parasitophorous vacuole  
473 membrane (PVM)<sup>10,60,61</sup>. Most proteins exported by this mechanism must have  
474 a conserved motif (RxLxE/Q/D), termed as *Plasmodium* export element (PEXEL)

475 motif at its N-terminal end<sup>9,10,62</sup>. Once KAHRP reach host erythrocyte membrane,  
476 other proteins such as PfEMP1, are known to associate with it, supporting knob  
477 formation. This host membrane remodeling allows iRBCs to attach onto host  
478 endothelium forming rosettes<sup>16,63,64</sup>.

479 Thus, an *in silico* prediction analysis of exported proteins through PTEX  
480 machinery was performed to assess whether PEXEL-containing proteins are  
481 present in our dataset. In this sense, by using PlasmoDB Database  
482 (<https://plasmodb.org/plasmo/app>), we predicted from identified KAHRP-  
483 neighboring proteins, which protein group members possess PEXEL motif,  
484 followed by motif enrichment pattern obtained in MEME Suite algorithm. A total  
485 of 27 protein groups were predicted to have a PEXEL motif at its N-terminal end  
486 position (Figure 5A and Table 1) Among these proteins, we found PTP2  
487 (*PfEMP1*-trafficking protein, PF3D7\_0731100), GBP130 (glycophorin binding  
488 protein 130, PF3D7\_1016300), Pf332 (a megadalton antigen), PHISTb  
489 (*Plasmodium* helical interspaced subtelomeric b, PF3D7\_1401600 and  
490 PF3D7\_1476300), serine/threonine protein phosphatase UIS2, putative  
491 (PF3D7\_1464600) and RESA (ring-infected erythrocyte surface antigen).

492 Additional *in silico* predictions were performed to assess protein secretion  
493 by classical or non-classical pathways by SignalP and SecretomeP, respectively.  
494 To predict transmembrane protein domains, TMHMM and Phobius tools were  
495 both used, for a better description of transmembrane topology. Overall, a total of  
496 23 protein groups predicted by SignalP, 92 protein groups predicted by  
497 SecretomeP, 59 protein groups predicted by TMHMM and 89 protein groups  
498 predicted by Phobius were observed in our analyses (Figure 5B and Table S3).  
499 Moreover, it was notably remarked that only 40 of the 208 protein groups  
500 identified (about 19%), no sub-cellular location could be assessed by our *in silico*  
501 predictions (Table S4).

502 In our analysis, it was possible to observe that an intersection between  
503 these *in silico* analyses with a considerable shared sub-cellular prediction among  
504 these protein groups took place. For example, PTP2, GBP130 and a protein  
505 member of PHISTb family (PF3D7\_1401600) are predicted to have PEXEL-  
506 containing motif as previously reported<sup>9,10,60,62</sup>, including predictions for non-  
507 classical signal peptide and transmembrane domains, suggesting an evident  
508 exportation into host cell cytosol with potential extracellular roles associated to

509 the host erythrocyte membrane. Two soluble components of the translocon  
510 PTEX, PTEX88 and 150, also identified in our analysis were predicted to have  
511 classical signal peptide as previously observed <sup>61</sup>. Moreover, predicted  
512 transmembrane proteins were also observed in our dataset: UIS2 and  
513 components of RhopH/CLAG complex (RhopH1/CLAG3 and RhopH3), known to  
514 be associated with parasitophorous vacuole and host erythrocyte membranes  
515 <sup>23,25,66,67</sup>. Both UIS2 and these RhopH/CLAG complex members were also  
516 predicted to have PEXEL-containing motif and classical signal peptide,  
517 respectively (Table S4). Overall, these *in silico* predictions reinforce that most of  
518 identified KAHRP-neighboring proteins are exported mainly through non-classical  
519 or specie-specific pathways in agreement with the literature.

520 Next, the identified KAHRP-neighboring proteins were GO-categorized in  
521 PlasmoDB database (<https://plasmodb.org/plasmo/app>) to assess the “Cellular  
522 Compartment” ontology terms. A total of 35 GO terms were assumed for our data  
523 (Table S5). Interestingly, we observed an elevated protein count in the nucleus  
524 sub-cellular categorization (GO:0005634). This pattern could be associated to the  
525 difficulty of GO term accuracy annotation in *Plasmodium* species <sup>68,69</sup>.  
526 Nonetheless, this could also indicates that several nucleus proteins may also be  
527 exported. Unsurprisingly, a considerable protein count were found correctly  
528 predicted in their expected GO terms, such as PTEX88 and 150  
529 (GO:0032991~protein-containing complex, GO:0020026~merozoite dense  
530 granule, GO:0031982~vesicle and GO:0097619~PTEX complex) <sup>61,70</sup>, complex  
531 RhopH/CLAG: RhopH1/CLAG3.1, RhopH2 and RhopH3 (GO:0020008~rhoptry,  
532 GO:0045177~apical part of cell and GO:1903561~extracellular vesicle) <sup>66,67,71,72</sup>,  
533 serine/threonine protein phosphatase UIS2, putative (GO:0020005~symbiont-  
534 containing vacuole membrane) <sup>23,25</sup>, and ring-infected erythrocyte surface antigen  
535 (GO:0020026~merozoite dense granule) <sup>73,74</sup> (Figure 5C and D).

536 **Table 1. Predicted PEXEL-containing proteins from our subproteomic dataset.**

Gene ID <sup>1</sup>	Product Description	Match Locations	Motif <sup>2</sup>
PF3D7_0223100	rifin	(36-40)	MKDHYINILLFALPLNILVYNQRNYIYTRTPKATT<span class=\motif>RTLCE</span>CELYAPATYDDDPQMKEVMD...
PF3D7_0317500	kinesin-5	(23-27)	MLRNSYNNDKSSCVNIKVIVRC<span class=\motif>RPLNE</span>KEKNDINNEEVVRINNNEVI...
PF3D7_0320500	nicotinamidase, putative	(195-199)	... MCILTVDYHPAMHISFAETH<span class=\motif>RLLYE</span>KICNNLKCNNINNKSNMNC...
PF3D7_0515900	NLI interacting factor-like phosphatase, putative	(8-12)	MKKRKFE<span class=\motif>RCLYQ</span>ILKIVKFYMNWIKIKLIK...
PF3D7_0623100	nuclear polyadenylated RNA-binding protein NAB2, putative	(134-138)	... SKNRVSSAHNKKGGEDDFDK<span class=\motif>RNLS</span>TRRRSRSLASSKYSNEDMYF...
PF3D7_0628100	HECT domain-containing protein 1, putative	(77-81)	... GEFLLLQSSSRVISSYEHIL<span class=\motif>RLLHQ</span>AKVYLEFVRCLKLNCSVID...
PF3D7_0731100	EMP1-trafficking protein	(89-93)	... NIFSQEYAITKGSPINRYL<span class=\motif>RNLGE</span>KSEEGGINFMDLHNTFAPTK...
PF3D7_0814000	60S ribosomal protein L13-2, putative	(35-39)	MVAHNNVLPNVHLHKWWQRHVRVNFVSKNIKKKKR<span class=\motif>RLLRE</span>KRRKANGGTPIEKLHPIVHC...
PF3D7_1012900	autophagy-related protein 18	(43-47), (107-111)	... MANEKGFKIYNTNPFTQTYS<span class=\motif>RDLTD</span>RNKNGLYLAEMLYRCNILAI...
PF3D7_1016300	GBP130 protein	(84-88)	... NAYICGDKEYEKAVDYGFRES<span class=\motif>RILAE</span>GEDTCARKEKTLRKSQKT...
PF3D7_1121100	conserved protein, unknown function	(73-77)	... EEKISAPPKMNTLQANQGY<span class=\motif>RSLVQ</span>QNKMRSAFNIAETPLKTI...
PF3D7_1122500	protein KIC10	(36-40)	MQNFVDSYKRTSNNNETSERYINSIQNCDKDEK<span class=\motif>RILED</span>ENVQKNLSFINNENIYNKKL...
PF3D7_1126100	autophagy-related protein 7, putative	(69-73)	... LCSSTYVNKIKLGFYKLLN<span class=\motif>RYLIE</span>FAHPFIHVRTIEINKSFLK...
PF3D7_1138500	protein phosphatase PPM2	(86-90)	... GHGGPNVSKWISYNFRIFI<span class=\motif>RCLKE</span>ANEEMIKKNMKRSENYKLLK...
PF3D7_1149000	antigen 332, DBL-like protein	(78-82)	... GKKLREKHDESCDEFCDAWN<span class=\motif>RSLAD</span>YKDIFQGKDMWNDGKYGEAK...
PF3D7_1149400	Plasmodium exported protein, unknown function	(46-50)	... PKNVNLVKTDIYNGFVQENA<span class=\motif>RYLAE</span>QYINKKMDQTLQHRAQLRTA...
PF3D7_1241200	conserved Plasmodium protein, unknown function	(12-16), (65-69)	MEKQKLLNILQ<span class=\motif>RELKE</span>YGDEEMLSCFHRFYESIEAN...
PF3D7_1317100	DNA replication licensing factor MCM4	(6-10), (63-67)	MGTPR<span class=\motif>RRLGQ</span>QNNNNNSPFALSSSNIFGSN...
PF3D7_1349300	tyrosine kinase-like protein	(25-29)	MSEHSSGVSRLKFCNSDKLFYDNF<span class=\motif>RNLDD</span>RLNLNNNFNENRYEEIYNKK...
PF3D7_1361800	glideosome-associated connector	(36-40)	MPKIQVKRGGDPGVSTAVSSIMQHENFKRMLMFGL<span class=\motif>RSLSD</span>FCNPTSKAYKENASDALDRG...

537

PF3D7_1401600	Plasmodium exported protein (PHISTb), unknown function	(85-89)	... VCIYKVEGVSVHVTEPNSSSS <span style="font-family: monospace;">&lt;span class=\motif&gt;RSLYE&lt;/span&gt;NKGVTYESNVEVHDNFLNKL...</span>
PF3D7_1402300	26S proteasome regulatory subunit RPN6	(185-189)	... KIILYIIKQKYKTALSLID <span style="font-family: monospace;">&lt;span class=\motif&gt;RLLKE&lt;/span&gt;VKKVDDKTLLLELYIVQTKI...</span>
PF3D7_1407800	plasmepsin IV	(65-69)	... LFVLITGVFFFLLIGNFYSH <span style="font-family: monospace;">&lt;span class=\motif&gt;RKLYQ&lt;/span&gt;VIKNTKHTTIGFKIDRPHDK...</span>
PF3D7_1409000	WD repeat-containing protein, putative	(8-12)	MNKKGNK <span style="font-family: monospace;">&lt;span class=\motif&gt;RPLGE&lt;/span&gt;SLNVPLNSNILNEDNEDKKY...</span>
PF3D7_1464600	serine/threonine protein phosphatase UIS2, putative	(43-47)	... QYNYDCVVAINKKNSIIKNE <span style="font-family: monospace;">&lt;span class=\motif&gt;RILDE&lt;/span&gt;YENINNSENEEDEYEDYLDD...</span>
PF3D7_1476300	Plasmodium exported protein (PHISTb), unknown function	(56-60)	... VSLINEDNGFHIIIPFNKALG <span style="font-family: monospace;">&lt;span class=\motif&gt;RKLYE&lt;/span&gt;NNNVDKHLNFSVSLENVNDL...</span>
PF3D7_0102200*	ring-infected erythrocyte surface antigen	(86-90)	... GNLGYNGSSSSGVQFTDRCS <span style="font-family: monospace;">&lt;span class=\motif&gt;RNLYG&lt;/span&gt;ETLPVNPYADSENPIVVSQV...</span>

538

539 1 Gene ID obtained from PlasmoDB database (<https://plasmodb.org/plasmo/app/>).

540 2 Prediction performed in the web tool “identify genes based on protein motif pattern” from PlasmoDB database (<https://plasmodb.org/plasmo/app/>). The search was made by  
 541 using PEXEL motif (RxLx[E/Q/D]) previously established elsewhere <sup>10,62,65</sup>.

542 \* RESA (PF3D7\_0102200) is known to have an atypical PEXEL motif: RxLxG <sup>10</sup>.

543

544

545

546

547

548

549

550

551 **DISCUSSION**

552

553 **Proximity tagging approaches as feasible tools to decipher**  
554 **organelle proteomes and to unveil novel neighboring proteins of a**  
555 **target of interest**

556

557 Concerning *Plasmodium* species, to the best of our knowledge, no study  
558 is available using APEX2 technology to depict organelle proteome and/or protein  
559 neighbors of a given target. To date, only BioID (proximity-dependent Biotin-  
560 Identification), a similar technology based on *Escherichia coli* biotin-ligase  
561 modified (BirA\*) was used for this purpose in *Plasmodium* species. For instance,  
562 by using a leader sequence of the acyl-carrier protein (ACP) fused to BirA\*, the  
563 organelle mapping of the *P. falciparum* apicoplast of 346 proteins accurately  
564 identified was possible, still showing the essentiality of a protein until then, not  
565 associated with the apicoplast biogenesis, named ABCF-family protein (ABCF-1)  
566 <sup>22</sup>.

567 Other reports have showed that proteins from insoluble fractions, such as  
568 those found in the parasitophorous vacuole membrane (PVM), can be also  
569 assessed by this approach. In *P. berghei*, a total of 61 known and candidate PVM  
570 proteins were identified, by using exported protein 1 (EXP1) fused to BirA\*.  
571 Among these proteins, a serine/threonine protein phosphatase UIS2  
572 (PBANKA\_1328000) was reported <sup>25</sup>. By using a similar strategy, another report  
573 have showed that an ortholog of serine/threonine protein phosphatase UIS2 in *P.*  
574 *falciparum* (PF3D7\_1464600) was also reported in the PVM, showing a critical  
575 role in the parasite survival <sup>23</sup>. Interestingly, in this study we also observed that  
576 UIS2 interacts with KAHRP-Flag-APEX2. Considering its location at PVM, it  
577 seems reasonable to suppose that this interaction indeed occurs (see below). In  
578 this context, BirA\* based-BioID seems to be a very insightful and reliable tool to  
579 map different organelles in *Plasmodium* species, in the same manner APEX2 can  
580 do it for mammalian cells.

581 More recently, an enhanced version based in the BioID approach, known  
582 as DiQ-BioID (Dimerization-induced Quantification BioID) was employed in *P.*  
583 *falciparum*, in order to decipher kelch13-defined endocytosis mechanism related  
584 proteins, and its relevance to the artemisinin (ART)-resistant phenotype.

585 Remarkably, in this study a novel compartment associated to kelch-13 protein  
586 was appointed, named simply "kelch-13 compartment", since no co-localization  
587 of kelch-13 took place with other compartments. Moreover, an endocytic pathway  
588 associated to hemoglobin degradation upon kelch-13 mutations, followed by ART  
589 activation were also described. Many proteins were assessed to be involved with  
590 this endocytic pathway from cytosolic host content, among them UBP1 and KIC7,  
591 which are essential for parasite survival <sup>24</sup>.

592 To date, only few studies were published using APEX2 in other protozoan  
593 parasites. For example, in *T. gondii*, a total of 17 proteins belonging of secretory  
594 dense granule were assessed by both APEX2 and BirA\*-BioID strategies. Three  
595 of them, were confirmed to localize in this structure <sup>75</sup>. In another case, the  
596 mitochondrial matrix proteome mapping in *T. gondii* was possible by using BirA\*-  
597 BioID and APEX2. In this study, a total of 421 mitochondrial proteins were  
598 identified, whose 161 by both methodologies. From this organelle mapping, 22  
599 proteins without previous mitochondrial functional annotation were additionally  
600 assessed to be localized in the *T. gondii* mitochondrion, co-localizing with  
601 *TgTom40* probed with antibodies, a marker for this compartment widely used for  
602 these parasites. Moreover, ~75% of *T. gondii* mitochondrial proteome were  
603 categorized as important or critical for the parasite fitness based in phenotype  
604 analysis against other Apicomplexan. Among these proteins, *TgApiCox25*  
605 (*TGGT1\_264040*) was observed to be important for parasite growth and  
606 mitochondrial oxygen consumption upon genetic knockdown <sup>76</sup>.

607 More recently, a study that aimed investigate tip-specific proteins related  
608 with flagellum subdomains in *Trypanosoma brucei*, revealed 697 proteins from  
609 pellet fraction, which allowed protein enrichment from axonemal structures of  
610 these parasites. This enrichment was assessed through a subunit of the nexin-  
611 dynein regulatory complex (N-DRC) fused to APEX2. Additionally, 241 out 697 of  
612 these proteins had annotation to one or more flagellum structures <sup>77</sup>. In contrast,  
613 taking leverage of the known half-life of the phenoxy radicals provided by APEX2  
614 approach due to its spatial and temporal distribution <sup>28-30</sup>, a distinguishable  
615 pattern of identified proteins between subdomains of the distal and proximal end  
616 of the flagellum was observed and assessed <sup>77</sup>.

617 Overall, both BioID and APEX2 are technologies that appeared as a  
618 feasible tool to solve some gaps in our understanding of diverse models of study.

619 A great bottleneck, however, still being the elution of biotinylated  
620 peptides/proteins itself <sup>78</sup>. A remarkable protein count observed in this kind of  
621 analysis may lead to false positive protein identifications. Thus, a careful *in silico*  
622 and functional analysis are often required in order to confirm potential novel  
623 components of a structure or neighboring partners <sup>22,25,28,75–77</sup>. Therefore, novel  
624 strategies to enrich biotinylated peptides/proteins are highly required. Some  
625 reports have shed light into novel strategies that allow biotinylated  
626 peptides/proteins elution.

627 For example, BioSITE (Biotinylation Site Identification Technology)  
628 strategy allows biotinylated peptide enrichment by using immobilized anti-biotin  
629 antibodies with a remarkable sensitivity <sup>79</sup>, observed by their signature fragment  
630 ions from MS spectra <sup>80</sup>. Alternatively, a flexible method developed for direct MS  
631 detection of biotin-tagged proteins, named as DiDBiT (Direct Detection of Biotin-  
632 containing Tags), improves direct detection of biotinylated proteins about 200-  
633 fold <sup>58</sup>. More recently, a colorimetric competitive displacement assay, the  
634 streptavidin binding capacity (AVIDITY) assay was developed, in order to  
635 compare different binding capacity of streptavidin beads and ensure  
636 reproducibility and consistency of downstream applications <sup>81</sup>. In summary, a  
637 completely novel field of exploration concerning the use of APEX2 to study  
638 *Plasmodium* species is now open, in order to study unique compartments from  
639 this parasite or neighboring partners of a given protein target. Nonetheless, some  
640 limitations need to be outdone, in order to obtain a more accurate enrichment of  
641 biotinylated peptides allowing analytical reproducibility.

642

### 643 **KAHRP and its neighboring candidate proteins**

644

645 From a total of 208 biotinylated parasite protein groups identified, we have  
646 observed some proteins related to *P. falciparum* virulence, nutrient uptake and  
647 invasion. It is estimated that 5-8% of *P. falciparum* genome (about 200-400  
648 proteins) is exported to the host cell cytosolic environment <sup>10</sup>, and several of  
649 them were already described to be found in the Maurer's clefts (MC) <sup>9,50,51,82,83</sup>.  
650 MC are vesicular structures with intertwined tubular and disk-like forms that  
651 originates from one or more sites from the PVM. It extends across the host cell  
652 cytoplasm to the inner leaflet of the RBC membrane <sup>11,53</sup>. An important virulence



653 factor that is carried over these structures, together with KAHRP, is a protein  
654 member from *var* multigene family, named as *PfEMP1* (*P. falciparum* erythrocyte-  
655 membrane protein 1)<sup>84,85</sup>. Both KAHRP and *PfEMP1* are important for the knob  
656 formation and cytoadherence, nonetheless, *kahrp* gene would not be essential  
657 for *PfEMP1* transport, but it affects functional knob formation<sup>16,63,86</sup>.

658 To reach host cell membrane, many proteins exported through MC need  
659 to be processed by a translocation machinery, named as PTEX at PVM. These  
660 protein complex is composed by PTEX88 and 150, a hexameric chaperone  
661 HSP101, a thioredoxin TRX2 and pore-forming protein EXP2<sup>61,70</sup>. Proteins  
662 exported by this mechanism contain a PEXEL motif at N-terminal end<sup>10,65</sup>, which  
663 are recognized and cleaved by plasmepsin V (PMV)<sup>87,88</sup>. This process occurs  
664 co-translationally and independent of phosphatidylinositol-3-phosphate (PI(3)P)  
665 at ER membrane<sup>62</sup>. As such, KAHRP is one of these proteins processed by this  
666 mechanism<sup>10,62</sup>, and transiently carried over into MC throughout host cell  
667 environment<sup>16</sup>, since a co-localization between KAHRP and other proteins  
668 notoriously known to integrate MC, such as *PfMAHRP*, *PfSBP1* and *PfEMP1*  
669 were already reported<sup>16,50–52</sup>.

670 In this work, we have showed for the first time that APEX2 technology can  
671 be used for tagging a protein target in *P. falciparum*, coupled with using of  
672 additional approaches such as CRISPR-Cas9 and label-free shotgun proteomics.  
673 Through IFA, we also have showed a co-localization of endogenous neighboring  
674 proteins of KAHRP-Flag-APEX2 with MAHRP probed with antibodies in  
675 punctuate structures, likely MC in living schizonts<sup>16,50–52</sup> (Figure 3B). This result  
676 suggests that APEX2 can be used accurately to tag neighboring proteins of a  
677 given target with potential to tag compartments. This statement may be extended  
678 to the results of endogenous neighboring proteins of episome-based Flag-  
679 APEX2, since no co-localization with MAHRP probed with antibodies was  
680 observed (Figure S2A).

681 Unsurprisingly, two soluble proteins biotinylated of the translocon PTEX,  
682 PTEX88 and 150, were identified in our analysis. Proteins from this complex are  
683 proposed to integrate the apical region of merozoites, likely to be dense granules  
684<sup>61,70</sup>. For this reason and in agreement with our *in silico* predictions, both PTEX88  
685 and 150, have classical signal-peptide, suggesting their secretion from dense  
686 granules in order to form the translocon PTEX, possibly thereafter invasion (Table

687 S4). Since PTEX specifically interacts with exported proteins containing PEXEL  
688 motif, it is totally expected that KAHRP-Flag-APEX2 may be neighboring PTEX88  
689 and 150 during its own exportation, as much as others that we have also  
690 observed in our data of biotinylated proteins to have PEXEL motif, such as: PTP2,  
691 GBP130, PHISTb protein members, Pf332, UIS2 and RESA (Table 1). Therefore,  
692 it is still to be investigated whether these proteins were tagged by KAHRP-Flag-  
693 APEX2 before, during or after translocation through PTEX machinery, as much  
694 as others that have no PEXEL-containing motif, named as PNEPs (PEXEL-  
695 negative exported proteins)<sup>89,90</sup>.

696 Despite we were not able to detect a biotinylated version of KAHRP nor  
697 EMP1, we found PTP2 (PF3D7\_0731100, Previous ID: MAL7P1.172) which is a  
698 protein family member suggested to be essential for EMP1 trafficking mainly  
699 localized in the MC, showing PEXEL motif for protein exportation as previously  
700 described<sup>9</sup> (Tables 1 and S2; Figure 5). Although a wider understanding about  
701 the role of KAHRP on the host endothelium cytoadherence and its transport  
702 through MC<sup>16,63</sup>, there is no consensus about whether KAHRP might be  
703 transported by other types of membrane bound vesicles. PTP2 was described to  
704 play a key role in efficient cell-cell communication through exosome-like vesicles  
705 derived from MC. In the PTP2 absence, extracellular vesicles (EVs) are 16-fold  
706 fewer prone to be released into the extracellular space, implicating in the  
707 molecular machinery of communication<sup>91</sup>.

708 Later, it was revealed that EMP1 is only present in EVs from early ring-  
709 stage parasites. In addition, KAHRP was identified by proteomic approach from  
710 these EVs derived samples<sup>92</sup>, suggesting that an alternative route may be used  
711 for PEXEL-containing motif proteins other than through PTEX machinery.  
712 Overall, in the remaining EVs content, the presence of the proteins: (i) high  
713 molecular weight rhoptry protein 2 (RhopH2, PF3D7\_0929400); (ii) high  
714 molecular weight rhoptry protein 3 (RhopH3, PF3D7\_0905400), and; (iii)  
715 cytoadherence linked asexual protein 3.1 (RhopH1/CLAG3, PF3D7\_0302500)  
716 were also observed<sup>92</sup>. These proteins were also observed in our biotinylated  
717 subproteomic data (Table S2), and they are known rhoptry proteins released after  
718 invasion and associated to the nutrient uptake<sup>66,67,71,93</sup>. Together, these protein  
719 members are complexed to be part of the plasmodial surface anion channels

720 (PSAC) in the erythrocyte membrane to generate new permeability pathways  
721 (NPPs), allowing iRBCs a better permeability to a range of nutrients <sup>71,93,94</sup>.

722 In addition, RhopH2 interacts with RhopH1/CLAG3, RhopH3, components  
723 of the erythrocyte cytoskeleton and exported proteins involved in host cell  
724 remodeling <sup>71</sup>. Still, RhopH2 and RhopH1/CLAG3 are also known to be  
725 complexed and trafficked to the erythrocyte membrane remaining fully associated  
726 <sup>66</sup>. More recently, it was revealed that beyond RhopH1/CLAG3 and RhopH3,  
727 RhopH2 interacts with 5 exported proteins: RESA, members of the *Plasmodium*  
728 exported proteins group (PHISTb, PF3D7\_1201000, PF3D7\_0401800 and  
729 PF3D7\_1401200) and lysine-rich membrane-associated PHISTb protein (LyMP,  
730 PF3D7\_0532400) <sup>72</sup>. In our proteomic dataset, we were able to find RESA and  
731 members of the group of PHISTb proteins interacting with KAHRP-Flag-APEX2  
732 (Table S2). Moreover, it is still discussed that a new networking clusters of  
733 exported proteins interacting with cytoskeletal activity, transient trafficking hub  
734 connecting both MC and J-dots structures may occur supporting NPPs <sup>72</sup>.

735 As mentioned above, potential novel trafficking mechanisms integrating  
736 MC and J-dots, or even EVs, might support exportation for several proteins. Two  
737 other proteins that could be integrated into these new export pathways are  
738 GBP130 and Pf332. Both of them were found biotinylated as neighboring  
739 KAHRP-Flag-APEX2 partners. GBP130 was proposed to interact indirectly with  
740 both RhopH2 and RhopH1/CLAG3, due to its higher affinity to RhopH3 <sup>72</sup>.  
741 Moreover, GBP130 was previously reported to be exported <sup>9</sup>, possibly in a  
742 PEXEL-dependent manner <sup>10,60</sup>, supporting our *in silico* analysis (Figure 5 and  
743 Table 1). Alternatively, Pf332, a megadalton protein is also proposed to be  
744 exported via MC. It has been associated with iRBCs cytoadherence properties,  
745 still showing a diminished capacity to adhere to CD36 in mutant lineages due a  
746 decreased expression level of EMP1 affecting iRBCs membrane rigidity. In  
747 addition, Pf332 knockout parasites display abnormal morphology of MC <sup>95</sup>. Later,  
748 it was demonstrated that Pf332 is not only a resident peripheral membrane  
749 protein of MC <sup>96</sup>, but also, it interacts with host cell cytoskeleton <sup>97</sup>, compatible  
750 with previous observations <sup>98</sup>.

751 Another protein that might be involved in this iRBC membrane rigidity, and  
752 found in our biotinylated subproteomic data is RESA. RESA is a dense granule  
753 protein of merozoite released inside the RBC after invasion <sup>73</sup>, and despite its

754 interaction with RhopH/CLAG complex proteins <sup>72</sup>, it is also involved in the  
755 stabilization of the membrane host cell cytoskeleton <sup>99</sup>, playing a major role in  
756 reducing deformability of host cells at the early ring stages of parasite  
757 development <sup>100</sup>. The association of RESA to the host cytoskeletal proteins, such  
758 as Band 4.1 and  $\alpha/\beta$ -spectrin heterodimers was already reviewed <sup>8</sup>. It is also  
759 noteworthy to mention that we have also identified both host Band 4.1 and  $\alpha$ -  
760 spectrin biotinylated in our subproteomic data (Table S2). Therefore, whether  
761 KAHRP can be associated with all of biotinylated proteins found in this study is  
762 still to be defined by co-localization assays. Overall, our subproteomic dataset is  
763 mostly consistent with many published records regarding protein exportation in  
764 *Plasmodium* species, allowing that APEX2 technology can be used accurately for  
765 other applications in these species.

766

## 767 **CONCLUSIONS AND PERSPECTIVES**

768

769 The protein exportation in malaria parasites is undoubtedly complex. For  
770 this, *Plasmodium* species use different strategies to export those proteins with  
771 relevant importance into host cytosolic environment <sup>10,60</sup>. To support this  
772 transition parasite-to-host protein exportation, some mechanisms have been  
773 unveiled in the recent years. The PTEX machinery was probably the first  
774 mechanism detailed in order to support this process <sup>61</sup>. Thereafter, PEXEL motif  
775 (RxLxE/Q/D) was additionally assessed as a trafficking signal for protein  
776 exportation <sup>10,60</sup>. Most proteins transported into iRBC membrane have a PEXEL  
777 consensus motif at N-terminus end, which is cleaved by an aspartic acid protease  
778 in the endoplasmic reticulum (ER), called plasmepsin V (PMV) <sup>87,88</sup>. It was initially  
779 thought that this PEXEL motif processing requires an interaction with  
780 phosphatidylinositol-3-phosphate (PI(3)P) in the ER prior to and independent of  
781 PMV <sup>101</sup>, however, more recently this conclusion was refuted, suggesting that  
782 PEXEL does not bind PI(3)P and PEXEL is located at a conserved location to  
783 ensure co-translational processing by PMV <sup>62</sup>.

784 Protein exportation mechanisms in *Plasmodium* species are still a field of  
785 intense exploration and discoveries. MC have been widely studied and reviewed  
786 as a primary structure to be involved in protein exportation in malaria parasites  
787 <sup>10,11,50–52,102</sup>. Nonetheless, recent reports have shown that alternative

788 mechanisms regarding novel possibilities in the protein export in *Plasmodium*  
789 species exist<sup>72,91,92,103</sup>. In this context, it is noteworthy to mention that novel  
790 technologies have been used to solve bottlenecks in many fields of biology. A  
791 constant and unchangeable breakthrough concerning old and new paradigms are  
792 always being tested to provide the most accurate answer, in other words, no  
793 relevant biological question is totally set in stone.

794 An example of this breakthrough can be observed in APEX2 and BioID  
795 strategies, in order to solve proximity labeled proteins<sup>28-30</sup>. In this aspect, our  
796 study is the first one, which uses APEX2 technology to solve protein-partners of  
797 a given protein target in *P. falciparum*. From our findings, we observed many  
798 proteins already described as exported into host cell environment, possibly  
799 interacting with KAHRP. A functional validation of these protein-partners needs  
800 to be yet assessed, in order to verify their co-localization and potential interaction,  
801 as previously established elsewhere<sup>22-25</sup>. In addition, an important regard needs  
802 to be given into methodological challenges concerning biotinylated  
803 protein/peptide elution by using these proximity-tagging approaches<sup>58,79-81</sup>. In  
804 summary, these types of proteomic studies will be consistently increasing in the  
805 next few years, mostly because their powerfulness and resolution.

806

## 807 FIGURES AND SUPPLEMENTARY FIGURES

808

809 **Figure 1. Knock-in scheme of CRISPR-Cas9 system to tag *kahrp* gene in *P.***  
810 ***falciparum* with APEX2.** (A) A schematic figure of cassette integration from  
811 pCC1-KAHRP-Flag-APEX2 vector into parasite gDNA controlled by hDHFR  
812 selection marker. (B) PCR validation of cassette integration. (C) The pair of  
813 primers PS101/102 and PS103/104 showed expected size amplicons,  
814 suggesting a successful DNA integration.

815

816 **Figure 2. NuPAGE™, Western-blot and Streptavidin-blot of mutant**  
817 **parasites to confirm chimeric protein expression.** Ponceau S stained  
818 nitrocellulose membrane (left panel), Western-blot (middle panel, anti-FLAG-  
819 HRP dilution at 1:800) and Streptavidin-blot (right panel, streptavidin-HRP  
820 dilution at 1:10.000) of mutant parasites treated and/or not treated with BP and  
821 H<sub>2</sub>O<sub>2</sub>. From all treatment conditions, total protein extract were made by using

822 RIPA buffer (parasite and parasitophorous vacuole protein content). Legend for  
823 all assays: first slot (BP-/H<sub>2</sub>O<sub>2</sub>-, not treated with BP nor H<sub>2</sub>O<sub>2</sub>); second slot (BP-  
824 /H<sub>2</sub>O<sub>2</sub>+, not treated with BP and treated with H<sub>2</sub>O<sub>2</sub>); third slot (BP+/H<sub>2</sub>O<sub>2</sub>-, treated  
825 with BP but not treated with H<sub>2</sub>O<sub>2</sub>); fourth slot (BP+/H<sub>2</sub>O<sub>2</sub>+, both treated with BP  
826 and H<sub>2</sub>O<sub>2</sub>).

827

828 **Figure 3. Confocal immunofluorescence assay to validate biotinylated**  
829 **neighboring protein-partners of KAHRP.** (A) BP+/H<sub>2</sub>O<sub>2</sub>- and BP+/H<sub>2</sub>O<sub>2</sub>+  
830 treated mutant parasites were incubated with DAPI and streptavidin-AF488. As  
831 expected, fluorescence was observed only in the BP+/H<sub>2</sub>O<sub>2</sub>+ treated parasites.  
832 (B) By using anti-MAHRP (a Maurer's clefts marker, dilution 1:200), a notorious  
833 co-localization between KAHRP biotinylated protein-partners (in green) and  
834 MAHRP (in purple) was observed, suggesting that KAHRP (and its interacting  
835 partners) and MAHRP share the same vesicular compartment into host cell  
836 environment through Maurer's clefts (Merge, white arrows).

837

838 **Figure 4. Biotinylated peptides and proteins revealed through MS analysis.**  
839 (A) Venn Diagram of the peptides used for our proteomic analysis. Only the  
840 conditions: (i) KAHRP-Flag-APEX2 mutant treated with BP+/H<sub>2</sub>O<sub>2</sub>+ (K BP+  
841 group, in blue); (ii) KAHRP-Flag-APEX2 mutant treated with BP-/ H<sub>2</sub>O<sub>2</sub>+ (K BP-  
842 group, in red); (iii) *P. falciparum* 3D7 wild-type strain treated with BP+/ H<sub>2</sub>O<sub>2</sub>+  
843 (3D7 BP+ group, in green); and, (iv) *P. falciparum* 3D7 wild-type strain treated  
844 with BP-/ H<sub>2</sub>O<sub>2</sub>+ (3D7 BP+ group, in yellow) were considered. (B) From these  
845 peptides used for identification of protein groups, a total of 208 *P. falciparum*  
846 protein groups candidate to interact with KAHRP were further analyzed.

847

848 **Figure 5. Functional categorization of the candidate protein-partners of**  
849 **KAHRP.** (A) MEME enrichment motif from proteins predicted to have a PEXEL  
850 sequence at their N-terminus end, suggesting that part of these protein groups  
851 are exported into host cell environment, as previously observed elsewhere (refs.  
852 Marti et al., 2004; Maier et al., 2008; Boddey et al., 2016). (B) *In silico* predictions  
853 for (i) PEXEL motif (in blue), (ii) SignalP (in red); (iii) SecretomeP (in green); (iv)  
854 TMHMM (in yellow) and (v) Phobius (in brown). Overall, most protein groups  
855 supposedly interacting with KAHRP have one or more extracellular prediction.

856 (C) GO term enrichment predicted for "Cellular Compartment" from these protein  
857 groups, also represented by GOCloud (D), both obtained in the PlasmoDB  
858 Databank (<https://plasmodb.org/plasmo/app>).

859

860 **Figure S1. Episomal vector construction and cytosolic APEX2 expression.**

861 (A) Scheme of the plasmid pCC1-Flag-APEX2 used as positive control for APEX2  
862 expression. (B) Ponceau S stained nitrocellulose membrane (left panel),  
863 Western-blot (middle panel, anti-FLAG-HRP dilution at 1:800) and Streptavidin-  
864 blot (right panel, streptavidin-HRP dilution at 1:10.000) of mutant or *P. falciparum*  
865 3D7 wild-type strains treated and/or not treated with BP and H<sub>2</sub>O<sub>2</sub>. From all  
866 treatment conditions, total protein extract were made by using RIPA buffer  
867 (parasite and parasitophorous vacuole protein contents). Legend for all assays:  
868 first slot (BP-/H<sub>2</sub>O<sub>2</sub>-, not treated with BP nor H<sub>2</sub>O<sub>2</sub>); second slot (BP-/H<sub>2</sub>O<sub>2</sub>+, not  
869 treated with BP and treated with H<sub>2</sub>O<sub>2</sub>); third slot (BP+/H<sub>2</sub>O<sub>2</sub>-, treated with BP but  
870 not treated with H<sub>2</sub>O<sub>2</sub>); fourth slot (BP+/H<sub>2</sub>O<sub>2</sub>+, both treated with BP and H<sub>2</sub>O<sub>2</sub>).

871

872 **Figure S2. Confocal immunofluorescence assay to validate APEX2**  
873 **transiently expressing vector in the cytosol.** The images were obtained only

874 from only BP+/H<sub>2</sub>O<sub>2</sub>+ treated parasites. Both trophozoite (A) and schizont (B) are  
875 expressing APEX2 in the cytosol. As performed in the Figure 3, we used anti-  
876 MAHRP (a Maurer's clefts marker at dilution 1:200), to assess whether a non-  
877 specific biotinylation occurs in these mutants. An additional control were  
878 employed, by using anti-ERD2 (a *cis*-Golgi region marker at dilution 1:200). As  
879 expected, none or very little co-localization were assessed by both antibodies  
880 used in the assay, suggesting that no biotinylation occurs inappropriately in the  
881 compartments.

882

883 **SUPPLEMENTARY TABLES**

884

885 **Table S1. All proteomic data used in this study.** List of total proteins (A) and  
886 peptides (B) identified by MS from conditions: (i) mutant KAHRP-Flag-APEX2  
887 (BP+/H<sub>2</sub>O<sub>2</sub>+, both treated with BP and H<sub>2</sub>O<sub>2</sub>); (ii) mutant KAHRP-Flag-APEX2  
888 (BP-/H<sub>2</sub>O<sub>2</sub>+, not treated with BP and treated with H<sub>2</sub>O<sub>2</sub>); (iii) *P. falciparum* 3D7

889 wild-type (BP+/H<sub>2</sub>O<sub>2</sub>+, both treated with BP and H<sub>2</sub>O<sub>2</sub>); (iv) *P. falciparum* 3D7  
890 wild-type (BP-/H<sub>2</sub>O<sub>2</sub>+, not treated with BP and treated with H<sub>2</sub>O<sub>2</sub>).

891

892 **Table S2. Biotinylated proteins suggested as candidate protein-partner of**  
893 **KAHRP, based on their peptide exclusivity in the mutant KAHRP-Flag-**  
894 **APEX2 treated with BP+/H<sub>2</sub>O<sub>2</sub>+**.

895

896 **Table S3. List of proteins with extracellular location predicted by *in silico***  
897 **analysis by using SignalP (<http://www.cbs.dtu.dk/services/SignalP/>),**  
898 **SecretomeP (<http://www.cbs.dtu.dk/services/SecretomeP/>), TMHMM**  
899 **(<http://www.cbs.dtu.dk/services/TMHMM/>) and Phobius**  
900 **(<https://phobius.sbc.su.se/>).**

901

902 **Table S4. (See below)**

903

904 **Table S5. List of proteins with annotated GO term prediction accordingly to**  
905 **PlasmoDB Databank (<https://plasmodb.org/plasmo/app>).**

906

## 907 REFERENCES

908

- 909 (1) Global Malaria Programme: WHO Global. *World Malaria Report*; 2020.
- 910 (2) Partnership, S. C. T. Efficacy and Safety of RTS,S/AS01 Malaria Vaccine  
911 with or without a Booster Dose in Infants and Children in Africa: Final  
912 Results of a Phase 3, Individually Randomised, Controlled Trial. *Lancet*  
913 **2015**, 386 (9988), 31–45. [https://doi.org/10.1016/S0140-6736\(15\)60721-8](https://doi.org/10.1016/S0140-6736(15)60721-8).
- 914 (3) Olotu, A.; Fegan, G.; Wambua, J.; Nyangweso, G.; Leach, A.; Lievens, M.;  
915 Kaslow, D. C.; Njuguna, P.; Marsh, K.; Bejon, P. Seven-Year Efficacy of  
916 RTS,S/AS01 Malaria Vaccine among Young African Children. *N. Engl. J.*  
917 *Med.* **2016**, 374 (26), 2519–2529. <https://doi.org/10.1056/nejmoa1515257>.
- 918 (4) Dattoo, M. S.; Natama, H. M.; Somé, A.; Traoré, O.; Rouamba, T.; Bellamy,  
919 D.; Yameogo, P.; Valia, D.; Tegneri, M.; Ouedraogo, F.; Soma, R.;  
920 Sawadogo, S.; Sorgho, F.; Derra, K.; Rouamba, E.; Orindi, B.; Ramos-  
921 Lopez, F.; Flaxman, A.; Cappuccini, F.; Kailath, R.; Elias, S.;  
922 Mukhopadhyay, E.; Noe, A.; Cairns, M.; Lawrie, A.; Roberts, R.; Valéa, I.;



- 923 Sorgho, H.; Williams, N.; Glenn, G.; Fries, L.; Reimer, J.; Ewer, K. J.;  
924 Shaligram, U.; Hill, A. V. S.; Tinto, H. High Efficacy of a Low Dose  
925 Candidate Malaria Vaccine, R21 in Adjuvant Matrix-M, with Seasonal  
926 Administration to Children in Burkina Faso. *Lancet* **2021**, 397 (10287),  
927 1809–1818.
- 928 (5) Ippolito, M. M.; Moser, K. A.; Kabuya, J.-B. B.; Cunningham, C.; Juliano, J.  
929 J. Antimalarial Drug Resistance and Implications for the WHO Global  
930 Technical Strategy. *Curr. Epidemiol. Reports* **2021**.  
931 <https://doi.org/10.1007/s40471-021-00266-5>.
- 932 (6) Moxon, C. A.; Gibbins, M. P.; McGuinness, D.; Jr, D. A. M.; Marti, M. New  
933 Insights into Malaria Pathogenesis. *Annu. Rev. Pathol. Mech. Dis.* **2020**,  
934 15, 315–343.
- 935 (7) Wassmer, S. C.; Grau, G. E. R. Severe Malaria: What 's New on the  
936 Pathogenesis Front? *Int. J. Parasitol.* **2017**, 47, 145–152.  
937 <https://doi.org/10.1016/j.ijpara.2016.08.002>.
- 938 (8) Spillman, N. J.; Beck, J. R.; Goldberg, D. E. Protein Export into Malaria  
939 Parasite-Infected Erythrocytes: Mechanisms and Functional  
940 Consequences. *Annu. Rev. Biochem.* **2015**, 84 (January), 813–841.  
941 <https://doi.org/10.1146/annurev-biochem-060614-034157>.
- 942 (9) Maier, A. G.; Rug, M.; O'Neill, M. T.; Brown, M.; Chakravorty, S.; Szeszak,  
943 T.; Chesson, J.; Wu, Y.; Hughes, K.; Coppel, R. L.; Newbold, C.; Beeson,  
944 J. G.; Craig, A.; Crabb, B. S.; Cowman, A. F. Exported Proteins Required  
945 for Virulence and Rigidity of Plasmodium Falciparum-Infected Human  
946 Erythrocytes. *Cell* **2008**, 134 (1), 48–61.  
947 <https://doi.org/10.1016/j.cell.2008.04.051>.
- 948 (10) Marti, M.; Marti, M.; Good, R. T.; Rug, M.; Knuepfer, E.; Cowman, A. F.  
949 Targeting Malaria Virulence and Remodeling Proteins to the Host  
950 Erythrocyte. *Science* (80-. ). **2004**, 306 (2004), 1930–1934.  
951 <https://doi.org/10.1126/science.1102452>.
- 952 (11) Lanzer, M.; Wickert, H.; Krohne, G.; Vincensini, L.; Braun Breton, C.  
953 Maurer's Clefts: A Novel Multi-Functional Organelle in the Cytoplasm of  
954 Plasmodium Falciparum-Infected Erythrocytes. *Int. J. Parasitol.* **2006**, 36  
955 (1), 23–36. <https://doi.org/10.1016/j.ijpara.2005.10.001>.
- 956 (12) Stevenson, L.; Laursen, E.; Cowan, G. J.; Bandoh, B.; Barfod, L.;

- 957 Cavanagh, D. R.; Andersen, G. R.; Hviid, L. A2-Macroglobulin Can  
958 Crosslink Multiple Plasmodium Falciparum Erythrocyte Membrane Protein  
959 1 (PfEMP1) Molecules and May Facilitate Adhesion of Parasitized  
960 Erythrocytes. *PLoS Pathog.* **2015**, *11* (7), 1–19.  
961 <https://doi.org/10.1371/journal.ppat.1005022>.
- 962 (13) Subramani, R.; Barfod, L.; Petersen, J. E. V.; Hviid, L.; Hassenkam, T.;  
963 Hempel, C.; Quadt, K.; Jeppesen, A. E. Plasmodium Falciparum-Infected  
964 Erythrocyte Knob Density Is Linked to the PfEMP1 Variant Expressed.  
965 *MBio* **2015**, *6* (5), 1–7. <https://doi.org/10.1128/mbio.01456-15>.
- 966 (14) Looker, O.; Blanch, A. J.; Liu, B.; Nunez-Iglesias, J.; McMillan, P. J.; Tilley,  
967 L.; Dixon, M. W. A. The Knob Protein KAHRP Assembles into a Ring-  
968 Shaped Structure That Underpins Virulence Complex Assembly. *PLoS*  
969 *Pathog.* **2019**, *15* (5), 1–26. <https://doi.org/10.1371/journal.ppat.1007761>.
- 970 (15) Cutts, E. E.; Laasch, N.; Reiter, D. M.; Trenker, R.; Slater, L. M.; Stansfeld,  
971 P. J.; Vakonakis, I. Structural Analysis of P. Falciparum KAHRP and  
972 PfEMP1 Complexes with Host Erythrocyte Spectrin Suggests a Model for  
973 Cytoadherent Knob Protrusions. *PLoS Pathog.* **2017**, *13* (8), 1–28.  
974 <https://doi.org/10.1371/journal.ppat.1006552>.
- 975 (16) Wickham, M. E.; Rug, M.; Ralph, S. A.; Klonis, N.; Mcfadden, G. I.; Tilley,  
976 L.; Cowman, A. F. Trafficking and Assembly of the Cytoadherence  
977 Complex in Plasmodium Falciparum-Infected Human Erythrocytes. *EMBO*  
978 *J.* **2001**, *20* (20), 5636–5649. <https://doi.org/10.1093/emboj/20.20.5636>.
- 979 (17) Jinek, M.; Chylinski, K.; Fonfara, I.; Hauer, M.; Doudna, J. A.; Charpentier,  
980 E. A Programmable Dual-RNA-Guided DNA Endonuclease in Adaptive  
981 Bacterial Immunity. *Science* (80-. ). **2012**, *337* (6096), 816–821.  
982 <https://doi.org/10.1002/ajh.24462>.
- 983 (18) Wagner, J. C.; Platt, R. J.; Goldfless, S. J.; Zhang, F.; Nilis, J. C. Efficient  
984 CRISPR-Cas9–Mediated Genome Editing in Plasmodium Falciparum. *Nat.*  
985 *Methods* **2014**, *11* (9), 915–918. <https://doi.org/10.1038/nmeth.3063>.
- 986 (19) Ghorbal, M.; Gorman, M.; Macpherson, C. R.; Martins, R. M.; Scherf, A.;  
987 Lopez-Rubio, J.-J. Genome Editing in the Human Malaria Parasite  
988 Plasmodium Falciparum Using the CRISPR-Cas9 System. *Nat. Biotechnol.*  
989 **2014**, *32* (8), 819–821. <https://doi.org/10.1038/nbt.2925>.
- 990 (20) Gardner, M. J.; Hall, N.; Fung, E.; White, O.; Berriman, M.; Hyman, R. W.;

- 991 Carlton, J. M.; Pain, A.; Nelson, K. E.; Bowman, S.; Paulsen, I. T.; James,  
992 K.; Eisen, J. A.; Rutherford, K.; Salzberg, S. L.; Craig, A.; Kyes, S.; Chan,  
993 M.-S.; Nene, V.; Shallom, S. J.; Suh, B.; Peterson, J.; Angiuoli, S.; Perteza,  
994 M.; Allen, J.; Selengut, J.; Haft, D.; Mather, M. W.; Vaidya, A. B.; Martin, D.  
995 M. A.; Fairlamb, A. H.; Fraunholz, M. J.; Roos, D. S.; Ralph, S. A.;  
996 McFadden, G. I.; Cummings, L. M.; Subramanian, G. M.; Mungall, C.;  
997 Venter, J. C.; Carucci, D. J.; Hoffman, S. L.; Newbold, C.; Davis, R. W.;  
998 Fraser, C. M.; Barrell, B. Genome Sequence of the Human Malaria Parasite  
999 *Plasmodium Falciparum*. *Nature* **2002**, *419* (6906), 498–511.  
1000 <https://doi.org/10.1038/nature01097>.
- 1001 (21) Roux, K. J.; Kim, D. I.; Raida, M.; Burke, B. A Promiscuous Biotin Ligase  
1002 Fusion Protein Identifies Proximal and Interacting Proteins in Mammalian  
1003 Cells. *J. Cell Biol.* **2012**, *196* (6), 801–810.  
1004 <https://doi.org/10.1083/jcb.201112098>.
- 1005 (22) Boucher, M. J.; Ghosh, S.; Zhang, L.; Lal, A.; Jang, S. W.; Ju, A.; Zhang,  
1006 S.; Wang, X.; Ralph, S. A.; Zou, J.; Elias, J. E.; Yeh, E. Integrative  
1007 Proteomics and Bioinformatic Prediction Enable a High-Confidence  
1008 Apicoplast Proteome in Malaria Parasites. *PLoS Biol.* **2018**, *16* (9), 1–29.  
1009 <https://doi.org/10.1371/journal.pbio.2005895>.
- 1010 (23) Khosh-Naucke, M.; Becker, J.; Mesén-Ramírez, P.; Kiani, P.; Birnbaum, J.;  
1011 Fröhlke, U.; Jonscher, E.; Schlüter, H.; Spielmann, T. Identification of Novel  
1012 Parasitophorous Vacuole Proteins in *P. Falciparum* Parasites Using BioID.  
1013 *Int. J. Med. Microbiol.* **2018**, *308* (1), 13–24.  
1014 <https://doi.org/10.1016/j.ijmm.2017.07.007>.
- 1015 (24) Birnbaum, J.; Scharf, S.; Schmidt, S.; Jonscher, E.; Maria Hoeijmakers, W.  
1016 A.; Flemming, S.; Toenhake, C. G.; Schmitt, M.; Sabitzki, R.; Bergmann,  
1017 B.; Fröhlke, U.; Mesén-Ramírez, P.; Soares, A. B.; Herrmann, H.; Bártfai,  
1018 R.; Spielmann, T. A Kelch13-Defined Endocytosis Pathway Mediates  
1019 Artemisinin Resistance in Malaria Parasites. *Science (80-. )*. **2020**, *367*  
1020 (6473), 51–59. <https://doi.org/10.1126/science.aax4735>.
- 1021 (25) Schnider, C. B.; Bausch-Fluck, D.; Brühlmann, F.; Heussler, V. T.; Burda,  
1022 P.-C. BioID Reveals Novel Proteins of the *Plasmodium* Parasitophorous  
1023 Vacuole Membrane. *mSphere* **2018**, *3* (1), 1–13.  
1024 <https://doi.org/10.1128/msphere.00522-17>.

- 1025 (26) Chen, A. L.; Kim, E. W.; Toh, J. Y.; Vashisht, A. A.; Rashoff, A. Q.; Van, C.;  
1026 Huang, A. S.; Moon, A. S.; Bell, H. N.; Bentolila, L. A.; Wohlschlegel, J. A.;  
1027 Bradley, P. J. Novel Components of the Toxoplasma Inner Membrane  
1028 Complex Revealed by BioID. *MBio* **2015**, *6* (1), e02357-14.  
1029 <https://doi.org/10.1128/mBio.02357-14>.
- 1030 (27) Nadipuram, S. M.; Thind, A. C.; Rayatpisheh, S.; Wohlschlegel, J. A.;  
1031 Bradley, P. J. Proximity Biotinylation Reveals Novel Secreted Dense  
1032 Granule Proteins of Toxoplasma Gondii Bradyzoites. *PLoS One* **2020**, *15*  
1033 (5), 1–20. <https://doi.org/10.1371/journal.pone.0232552>.
- 1034 (28) Rhee, H.; Zou, P.; Udeshi, N. D.; Martell, J. D.; Mootha, V. K.; Carr, S. A.;  
1035 Ting, A. Y. Proteomic Mapping of Mitochondria in Living Cells via Spatially  
1036 Restricted Enzymatic Tagging. *Science (80-. )*. **2013**, *339* (March), 1328–  
1037 1331. <https://doi.org/10.1126/science.1230593>.
- 1038 (29) Lee, S. Y.; Kang, M. G.; Park, J. S.; Lee, G.; Ting, A. Y.; Rhee, H. W. APEX  
1039 Fingerprinting Reveals the Subcellular Localization of Proteins of Interest.  
1040 *Cell Rep.* **2016**, *15* (8), 1837–1847.  
1041 <https://doi.org/10.1016/j.celrep.2016.04.064>.
- 1042 (30) Lobingier, B. T.; Hüttenhain, R.; Eichel, K.; Miller, K. B.; Ting, A. Y.; von  
1043 Zastrow, M.; Krogan, N. J. An Approach to Spatiotemporally Resolve  
1044 Protein Interaction Networks in Living Cells. *Cell* **2017**, *169* (2), 350-  
1045 360.e12. <https://doi.org/10.1016/j.cell.2017.03.022>.
- 1046 (31) Trager, W.; Jensen, J. B. Human Malaria Parasites in Continuous Culture.  
1047 *Science (80-. )*. **1976**, *193*, 673–675.
- 1048 (32) Lim, M. Y. X.; LaMonte, G.; Lee, M. C. S.; Reimer, C.; Tan, B. H.; Corey,  
1049 V.; Tjahjadi, B. F.; Chua, A.; Nachon, M.; Wintjens, R.; Gedeck, P.;  
1050 Malleret, B.; Renia, L.; Bonamy, G. M. C.; Ho, P. C. L.; Yeung, B. K. S.;  
1051 Chow, E. D.; Lim, L.; Fidock, D. A.; Diagana, T. T.; Winzeler, E. A.; Bifani,  
1052 P. UDP-Galactose and Acetyl-CoA Transporters as Plasmodium Multidrug  
1053 Resistance Genes. *Nat. Microbiol.* **2016**, *1* (September).  
1054 <https://doi.org/10.1038/nmicrobiol.2016.166>.
- 1055 (33) Ganesan, S. M.; Morrisey, J. M.; Ke, H.; Painter, H. J.; Laroia, K.; Phillips,  
1056 M. A.; Rathod, P. K.; Mather, M. W.; Vaidya, A. B. Yeast Dihydroorotate  
1057 Dehydrogenase as a New Selectable Marker for Plasmodium Falciparum  
1058 Transfection. *Mol. Biochem. Parasitol.* **2011**, *177* (1), 29–34.

- 1059 <https://doi.org/10.1016/j.molbiopara.2011.01.004>.
- 1060 (34) Lam, S. S.; Martell, J. D.; Kamer, K. J.; Deerinck, T. J.; Ellisman, M. H.;  
1061 Mootha, V. K.; Ting, A. Y. Directed Evolution of APEX2 for Electron  
1062 Microscopy and Proximity Labeling. *Nat. Methods* **2014**, *12* (1), 51–54.  
1063 <https://doi.org/10.1038/nmeth.3179>.
- 1064 (35) Fidock, D. A.; Wellems, T. E. Transformation with Human Dihydrofolate  
1065 Reductase Renders Malaria Parasites Insensitive to WR99210 but Does  
1066 Not Affect the Intrinsic Activity of Proguanil. *Proc. Natl. Acad. Sci. U. S. A.*  
1067 **1997**, *94* (20), 10931–10936. <https://doi.org/10.1073/pnas.94.20.10931>.
- 1068 (36) Green, M. R.; Sambrook, J. Precipitation of DNA with Isopropanol. In *Cold*  
1069 *Spring Harbor Harbor Protocols*; 2017; pp 673–674.  
1070 <https://doi.org/10.1101/pdb.prot093385>.
- 1071 (37) Carrasquilla, M.; Adjalley, S.; Sanderson, T.; Marin-Menendez, A.; Coyle,  
1072 R.; Montandon, R.; Rayner, J. C.; Pance, A.; Lee, M. C. S. Defining  
1073 Multiplicity of Vector Uptake in Transfected Plasmodium Parasites. *Sci.*  
1074 *Rep.* **2020**, *10* (1), 1–11. <https://doi.org/10.1038/s41598-020-67791-z>.
- 1075 (38) Jiang, L.; He, L.; Fountoulakis, M. Comparison of Protein Precipitation  
1076 Methods for Sample Preparation Prior to Proteomic Analysis. *J.*  
1077 *Chromatogr. A* **2004**, *1023* (2), 317–320.  
1078 <https://doi.org/10.1016/j.chroma.2003.10.029>.
- 1079 (39) Fic, E.; Kedracka-Krok, S.; Jankowska, U.; Pirog, A.; Dziejzicka-  
1080 Wasylewska, M. Comparison of Protein Precipitation Methods for Various  
1081 Rat Brain Structures Prior to Proteomic Analysis. *Electrophoresis* **2010**, *31*  
1082 (21), 3573–3579. <https://doi.org/10.1002/elps.201000197>.
- 1083 (40) Puchades, M.; Westman, A.; Blennow, K.; Davidsson, P. Removal of  
1084 Sodium Dodecyl Sulfate from Protein Samples Prior to Matrix-Assisted  
1085 Laser Desorption/Ionization Mass Spectrometry. *Rapid Commun. Mass*  
1086 *Spectrom.* **1999**, *13* (5), 344–349. [https://doi.org/10.1002/\(sici\)1097-0231\(19990315\)13:5<344::aid-rcm489>3.0.co;2-v](https://doi.org/10.1002/(sici)1097-0231(19990315)13:5<344::aid-rcm489>3.0.co;2-v).
- 1088 (41) Rappsilber, J.; Mann, M.; Ishihama, Y. Protocol for Micro-Purification,  
1089 Enrichment, Pre-Fractionation and Storage of Peptides for Proteomics  
1090 Using StageTips. *Nat. Protoc.* **2007**, *2* (8), 1896–1906.  
1091 <https://doi.org/10.1038/nprot.2007.261>.
- 1092 (42) Ritz, A.; Shakhnarovich, G.; Salomon, A. R.; Raphael, B. J. Discovery of

- 1093 Phosphorylation Motif Mixtures in Phosphoproteomics Data. *Bioinformatics*  
1094 **2009**, 25 (1), 14–21. <https://doi.org/10.1093/bioinformatics/btn569>.
- 1095 (43) Bailey, T. L.; Johnson, J.; Grant, C. E.; Noble, W. S. The MEME Suite.  
1096 *Nucleic Acids Res.* **2015**, 43 (W1), W39–W49.  
1097 <https://doi.org/10.1093/nar/gkv416>.
- 1098 (44) Nielsen, H.; Tsirigos, K. D.; Brunak, S.; von Heijne, G. A Brief History of  
1099 Protein Sorting Prediction. *Protein J.* **2019**, 38 (3), 200–216.  
1100 <https://doi.org/10.1007/s10930-019-09838-3>.
- 1101 (45) Almagro Armenteros, J. J.; Tsirigos, K. D.; Sønderby, C. K.; Petersen, T.  
1102 N.; Winther, O.; Brunak, S.; von Heijne, G.; Nielsen, H. SignalP 5.0  
1103 Improves Signal Peptide Predictions Using Deep Neural Networks. *Nat.*  
1104 *Biotechnol.* **2019**, 37 (4), 420–423. [https://doi.org/10.1038/s41587-019-](https://doi.org/10.1038/s41587-019-0036-z)  
1105 [0036-z](https://doi.org/10.1038/s41587-019-0036-z).
- 1106 (46) Bendtsen, J. D.; Kiemer, L.; Fausbøll, A.; Brunak, S. Non-Classical Protein  
1107 Secretion in Bacteria. *BMC Microbiol.* **2005**, 5, 1–13.  
1108 <https://doi.org/10.1186/1471-2180-5-58>.
- 1109 (47) Bendtsen, J. D.; Jensen, L. J.; Blom, N.; Von Heijne, G.; Brunak, S.  
1110 Feature-Based Prediction of Non-Classical and Leaderless Protein  
1111 Secretion. *Protein Eng. Des. Sel.* **2004**, 17 (4), 349–356.  
1112 <https://doi.org/10.1093/protein/gzh037>.
- 1113 (48) Krogh, A.; Larsson, B.; Von Heijne, G.; Sonnhammer, E. L. L. Predicting  
1114 Transmembrane Protein Topology with a Hidden Markov Model:  
1115 Application to Complete Genomes. *J. Mol. Biol.* **2001**, 305 (3), 567–580.  
1116 <https://doi.org/10.1006/jmbi.2000.4315>.
- 1117 (49) Käll, L.; Krogh, A.; Sonnhammer, E. L. L. Advantages of Combined  
1118 Transmembrane Topology and Signal Peptide Prediction-the Phobius Web  
1119 Server. *Nucleic Acids Res.* **2007**, 35 (SUPPL.2), 429–432.  
1120 <https://doi.org/10.1093/nar/gkm256>.
- 1121 (50) Spycher, C.; Rug, M.; Pachlatko, E.; Hanssen, E.; Ferguson, D.; Cowman,  
1122 A. F.; Tilley, L.; Beck, H. P. The Maurer's Cleft Protein MAHRP1 Is  
1123 Essential for Trafficking of PfEMP1 to the Surface of Plasmodium  
1124 Falciparum-Infected Erythrocytes. *Mol. Microbiol.* **2008**, 68 (5), 1300–1314.  
1125 <https://doi.org/10.1111/j.1365-2958.2008.06235.x>.
- 1126 (51) Spycher, C.; Klonis, N.; Spielmann, T.; Kump, E.; Steiger, S.; Tilley, L.;

- 1127 Beck, H. P. MAHRP-1, a Novel Plasmodium Falciparum Histidine-Rich  
1128 Protein, Binds Ferriprotoporphyrin IX and Localizes to the Maurer's Clefts.  
1129 *J. Biol. Chem.* **2003**, 278 (37), 35373–35383.  
1130 <https://doi.org/10.1074/jbc.M305851200>.
- 1131 (52) Spycher, C.; Rug, M.; Klonis, N.; Ferguson, D. J. P.; Cowman, A. F.; Beck,  
1132 H.-P.; Tilley, L. Genesis of and Trafficking to the Maurer's Clefts of  
1133 Plasmodium Falciparum -Infected Erythrocytes . *Mol. Cell. Biol.* **2006**, 26  
1134 (11), 4074–4085. <https://doi.org/10.1128/mcb.00095-06>.
- 1135 (53) Wickert, H.; Göttler, W.; Krohne, G.; Lanzer, M. Maurer's Cleft Organization  
1136 in the Cytoplasm of Plasmodium Falciparum-Infected Erythrocytes: New  
1137 Insights from Three-Dimensional Reconstruction of Serial Ultrathin  
1138 Sections. *Eur. J. Cell Biol.* **2004**, 83 (10), 567–582.  
1139 <https://doi.org/10.1078/0171-9335-00432>.
- 1140 (54) Van Wye, J.; Ghori, N.; Webster, P.; Mitschler, R. R.; Elmendorf, H. G.;  
1141 Haldar, K. Identification and Localization of Rab6, Separation of Rab6 from  
1142 ERD2 and Implications for an "unstacked" Golgi, in Plasmodium  
1143 Falciparum. *Mol. Biochem. Parasitol.* **1996**, 83 (1), 107–120.  
1144 [https://doi.org/10.1016/S0166-6851\(96\)02759-4](https://doi.org/10.1016/S0166-6851(96)02759-4).
- 1145 (55) Krai, P.; Dalal, S.; Klemba, M. Evidence for a Golgi-to-Endosome Protein  
1146 Sorting Pathway in Plasmodium Falciparum. *PLoS One* **2014**, 9 (2).  
1147 <https://doi.org/10.1371/journal.pone.0089771>.
- 1148 (56) Hallée, S.; Boddey, J. A.; Cowman, A. F.; Richard, D. Evidence That the  
1149 Plasmodium Falciparum Protein Sortilin Potentially Acts as an Escorter for  
1150 the Trafficking of the Rhoptry-Associated Membrane Antigen to the  
1151 Rhoptries. *mSphere* **2018**, 3 (1). [https://doi.org/10.1128/msphere.00551-](https://doi.org/10.1128/msphere.00551-17)  
1152 17.
- 1153 (57) Elmendorf, H. G.; Haldar, K. Identification and Localization of ERD2 in the  
1154 Malaria Parasite Plasmodium Falciparum: Separation from Sites of  
1155 Sphingomyelin Synthesis and Implications for Organization of the Golgi.  
1156 *EMBO J.* **1993**, 12 (12), 4763–4773. [https://doi.org/10.1002/j.1460-](https://doi.org/10.1002/j.1460-2075.1993.tb06165.x)  
1157 2075.1993.tb06165.x.
- 1158 (58) Schiapparelli, L. M.; McClatchy, D. B.; Liu, H. H.; Sharma, P.; Yates, J. R.;  
1159 Cline, H. T. Direct Detection of Biotinylated Proteins by Mass Spectrometry.  
1160 *J. Proteome Res.* **2014**, 13 (9), 3966–3978.

- 1161 <https://doi.org/10.1021/pr5002862>.
- 1162 (59) Hung, V.; Udeshi, N. D.; Lam, S. S.; Loh, K. H.; Cox, K. J.; Pedram, K.;  
1163 Carr, S. A.; Ting, A. Y. Spatially Resolved Proteomic Mapping in Living  
1164 Cells with the Engineered Peroxidase APEX2. *Nat. Protoc.* **2016**, *11* (3),  
1165 456–475. <https://doi.org/10.1038/nprot.2016.018>.
- 1166 (60) Boddey, J. A.; Moritz, R. L.; Simpson, R. J.; Cowman, A. F. Role of the  
1167 Plasmodium Export Element in Trafficking Parasite Proteins to the Infected  
1168 Erythrocyte. *Traffic* **2009**, *10* (3), 285–299. [https://doi.org/10.1111/j.1600-](https://doi.org/10.1111/j.1600-0854.2008.00864.x)  
1169 [0854.2008.00864.x](https://doi.org/10.1111/j.1600-0854.2008.00864.x).
- 1170 (61) Koning-Ward, T. F.; Gilson, P. R.; Boddey, J. A.; Rug, M.; Smith, B. J.;  
1171 Papenfuss, A. T.; Sanders, P. R.; Lundie, R. J.; Maier, A. G.; Cowman, A.  
1172 F.; Crabb, B. S. A Newly Discovered Protein Export Machine in Malaria  
1173 Parasites. *Nature* **2009**, *459* (7249), 945–949.  
1174 <https://doi.org/10.1038/nature08104>.
- 1175 (62) Boddey, J. A.; O'Neill, M. T.; Lopaticki, S.; Carvalho, T. G.; Hodder, A. N.;  
1176 Nebl, T.; Wawra, S.; Van West, P.; Ebrahimzadeh, Z.; Richard, D.;  
1177 Flemming, S.; Spielmann, T.; Przyborski, J.; Babon, J. J.; Cowman, A. F.  
1178 Export of Malaria Proteins Requires Co-Translational Processing of the  
1179 PEXEL Motif Independent of Phosphatidylinositol-3-Phosphate Binding.  
1180 *Nat. Commun.* **2016**, *7* (May 2015). <https://doi.org/10.1038/ncomms10470>.
- 1181 (63) Crabb, B. S.; Cooke, B. M.; Reeder, J. C.; Waller, R. F.; Caruana, S. R.;  
1182 Davern, K. M.; Wickham, M. E.; Brown, G. V.; Coppel, R. L.; Cowman, A.  
1183 F. Targeted Gene Disruption Shows That Knobs Enable Malaria-Infected  
1184 Red Cells to Cytoadhere under Physiological Shear Stress. *Cell* **1997**, *89*  
1185 (2), 287–296. [https://doi.org/10.1016/S0092-8674\(00\)80207-X](https://doi.org/10.1016/S0092-8674(00)80207-X).
- 1186 (64) Wickert, H.; Wissing, F.; Andrews, K. T.; Stich, A.; Krohne, G.; Lanzer, M.  
1187 Evidence for Trafficking of PfEMP1 to the Surface of *P. falciparum*-Infected  
1188 Erythrocytes via a Complex Membrane Network. *Eur. J. Cell Biol.* **2003**, *82*  
1189 (6), 271–284. <https://doi.org/10.1078/0171-9335-00319>.
- 1190 (65) Hiller, N. L.; Bhattacharjee, S.; Ooij, C. Van; Liolios, K.; Harrison, T.; Lopez-  
1191 estran, C.; Haldar, K. A Host-Targeting Signal in Virulence Proteins  
1192 Reveals a Secretome in Malarial Infection. *Science* (80-. ). **2004**, *306*,  
1193 1934–1938. <https://doi.org/10.1126/science.1102737>.
- 1194 (66) Ahmad, M.; Manzella-Lapeira, J.; Saggi, G.; Ito, D.; Brzostowski, J. A.;



- 1195 Desai, S. A. Live-Cell FRET Reveals That Malaria Nutrient Channel  
1196 Proteins CLAG3 and RhopH2 Remain Associated throughout Their  
1197 Tortuous Trafficking. *MBio* **2020**, *11* (5), 1–14.
- 1198 (67) Sherling, E. S.; Knuepfer, E.; Brzostowski, J. A.; Miller, L. H.; Blackman, M.  
1199 J.; Van Ooij, C. The Plasmodium Falciparum Rhoptry Protein RhopH3  
1200 Plays Essential Roles in Host Cell Invasion and Nutrient Uptake. *Elife* **2017**,  
1201 *6*, 1–23. <https://doi.org/10.7554/eLife.23239>.
- 1202 (68) Martin, D. M. A.; Berriman, M.; Barton, G. J. GOTcha: A New Method for  
1203 Prediction of Protein Function Assessed by the Annotation of Seven  
1204 Genomes. *BMC Bioinformatics* **2004**, *5*, 1–17.  
1205 <https://doi.org/10.1186/1471-2105-5-178>.
- 1206 (69) Bernardes, J.; Vaquero, C.; Carbone, A. Plasmobase: A Comparative  
1207 Database of Predicted Domain Architectures for Plasmodium Genomes.  
1208 *Malar. J.* **2017**, *16* (1), 1–10. <https://doi.org/10.1186/s12936-017-1887-8>.
- 1209 (70) Bullen, H. E.; Charnaud, S. C.; Kalanon, M.; Riglar, D. T.; Dekiwadia, C.;  
1210 Kangwanransan, N.; Torii, M.; Tsuboi, T.; Baum, J.; Ralph, S. A.;  
1211 Cowman, A. F.; De Koning-Ward, T. F.; Crabb, B. S.; Gilson, P. R.  
1212 Biosynthesis, Localization, and Macromolecular Arrangement of the  
1213 Plasmodium Falciparum Translocon of Exported Proteins (PTEX). *J. Biol.*  
1214 *Chem.* **2012**, *287* (11), 7871–7884.  
1215 <https://doi.org/10.1074/jbc.M111.328591>.
- 1216 (71) Counihan, N. A.; Chisholm, S. A.; Bullen, H. E.; Srivastava, A.; Sanders, P.  
1217 R.; Jonsdottir, T. K.; Weiss, G. E.; Ghosh, S.; Crabb, B. S.; Creek, D. J.;  
1218 Gilson, P. R.; De Koning-Ward, T. F. Plasmodium Falciparum Parasites  
1219 Deploy RhopH2 into the Host Erythrocyte to Obtain Nutrients, Grow and  
1220 Replicate. *Elife* **2017**, *6*, 1–31. <https://doi.org/10.7554/eLife.23217>.
- 1221 (72) Jonsdottir, T. K.; Counihan, N. A.; Modak, J. K.; Kouskousis, B.; Sanders,  
1222 P. R.; Gabriela, M.; Bullen, H. E.; Crabb, B. S.; de Koning-Ward, T. F.;  
1223 Gilson, P. R. Characterisation of Complexes Formed by Parasite Proteins  
1224 Exported into the Host Cell Compartment of Plasmodium Falciparum  
1225 Infected Red Blood Cells. *Cell. Microbiol.* **2021**, No. January, 1–14.  
1226 <https://doi.org/10.1111/cmi.13332>.
- 1227 (73) Culvenor, J. G.; Day, K. P.; Anders, R. F. Plasmodium Falciparum Ring-  
1228 Infected Erythrocyte Surface Antigen Is Released from Merozoite Dense

- 1229 Granules after Erythrocyte Invasion. *Infect. Immun.* **1991**, *59* (3), 1183–  
1230 1187. <https://doi.org/10.1128/iai.59.3.1183-1187.1991>.
- 1231 (74) Aikawa, M.; Torii, M.; Sjölander, A.; Berzins, K.; Perlmann, P.; Miller, L. H.  
1232 Pf155/RESA Antigen Is Localized in Dense Granules of Plasmodium  
1233 Falciparum Merozoites. *Exp. Parasitol.* **1990**, *71* (3), 326–329.  
1234 [https://doi.org/10.1016/0014-4894\(90\)90037-D](https://doi.org/10.1016/0014-4894(90)90037-D).
- 1235 (75) Pan, M.; Li, M.; Li, L.; Song, Y.; Hou, L.; Zhao, J.; Shen, B. Identification of  
1236 Novel Dense-Granule Proteins in Toxoplasma Gondii by Two Proximity-  
1237 Based Biotinylation Approaches. *J. Proteome Res.* **2019**, *18* (1), 319–330.  
1238 <https://doi.org/10.1021/acs.jproteome.8b00626>.
- 1239 (76) Seidi, A.; Muellner-Wong, L. S.; Rajendran, E.; Tjhin, E. T.; Dagley, L. F.;  
1240 Aw, V. Y. T.; Faou, P.; Webb, A. I.; Tonkin, C. J.; van Dooren, G. G.  
1241 Elucidating the Mitochondrial Proteome of Toxoplasma Gondii Reveals the  
1242 Presence of a Divergent Cytochrome c Oxidase. *Elife* **2018**, *7*, 1–36.  
1243 <https://doi.org/10.7554/eLife.38131>.
- 1244 (77) Vélez-Ramírez, D. E.; Shimogawa, M. M.; Ray, S. S.; Lopez, A.;  
1245 Rayatpisheh, S.; Langousis, G.; Gallagher-Jones, M.; Dean, S.;  
1246 Wohlschlegel, J. A.; Hilla, K. L. APEX2 Proximity Proteomics Resolves  
1247 Flagellum Subdomains and Identifies Flagellum Tip-Specific Proteins in  
1248 *Trypanosoma Brucei*. *mSphere* **2021**, *6* (1), 1–19.  
1249 <https://doi.org/https://doi.org/10.1128/mSphere.01090-20>.
- 1250 (78) Chaiet, L.; Wolf, F. J. The Properties of Streptavidin, a Biotin-Binding  
1251 Protein Produced by Streptomyces. *Arch. Biochem. Biophys.* **1964**, *106*  
1252 (C), 1–5. [https://doi.org/10.1016/0003-9861\(64\)90150-X](https://doi.org/10.1016/0003-9861(64)90150-X).
- 1253 (79) Kim, D. I.; Cutler, J. A.; Na, C. H.; Reckel, S.; Renuse, S.; Madugundu, A.  
1254 K.; Tahir, R.; Goldschmidt, H. L.; Reddy, K. L.; Hugarir, R. L.; Wu, X.;  
1255 Zachara, N. E.; Hantschel, O.; Pandey, A. BioSITE: A Method for Direct  
1256 Detection and Quantitation of Site-Specific Biotinylation. *J. Proteome Res.*  
1257 **2018**, *17* (2), 759–769. <https://doi.org/10.1021/acs.jproteome.7b00775>.
- 1258 (80) Renuse, S.; Madugundu, A. K.; Jung, J. H.; Byeon, S. K.; Goldschmidt, H.  
1259 L.; Tahir, R.; Meyers, D.; Kim, D. I.; Cutler, J.; Kim, K. P.; Wu, X.; Hugarir,  
1260 R. L.; Pandey, A. Signature Fragment Ions of Biotinylated Peptides. *J. Am.*  
1261 *Soc. Mass Spectrom.* **2020**, *31* (2), 394–404.  
1262 <https://doi.org/10.1021/jasms.9b00024>.

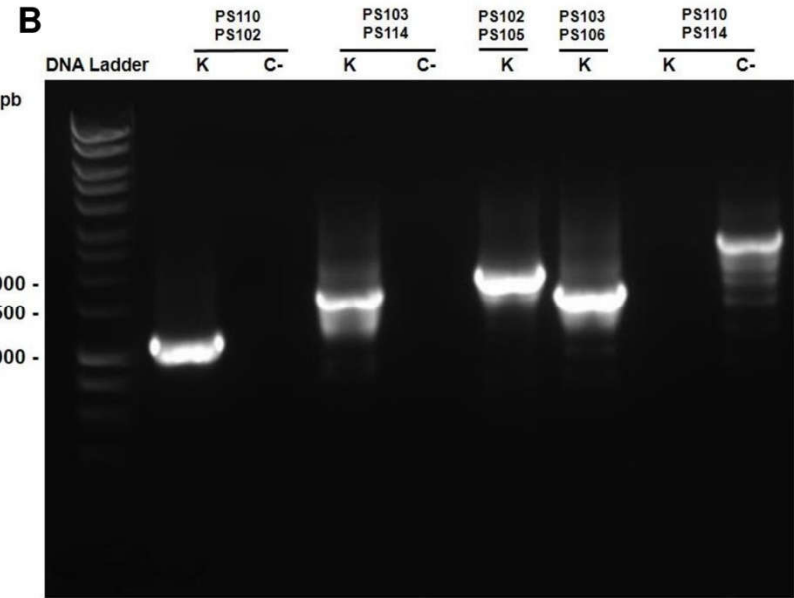
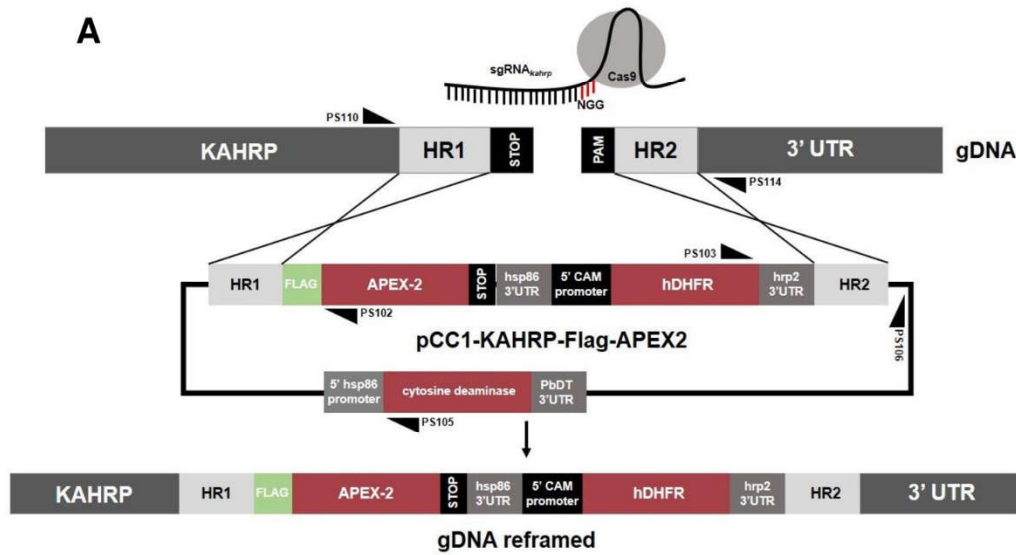
- 1263 (81) Berg Luecke, L.; Gundry, R. L. Assessment of Streptavidin Bead Binding  
1264 Capacity to Improve Quality of Streptavidin-Based Enrichment Studies. *J.*  
1265 *Proteome Res.* **2021**, *20* (2), 1153–1164.  
1266 <https://doi.org/10.1021/acs.jproteome.0c00772>.
- 1267 (82) Maier, A. G.; Rug, M.; O'Neill, M. T.; Beeson, J. G.; Marti, M.; Reeder, J.;  
1268 Cowman, A. F. Skeleton-Binding Protein 1 Functions at the  
1269 Parasitophorous Vacuole Membrane to Traffic PfEMP1 to the Plasmodium  
1270 Falciparum-Infected Erythrocyte Surface. *Blood* **2007**, *109* (3), 1289–1297.  
1271 <https://doi.org/10.1182/blood-2006-08-043364>.
- 1272 (83) Cooke, B. M.; Buckingham, D. W.; Glenister, F. K.; Fernandez, K. M.;  
1273 Bannister, L. H.; Marti, M.; Mohandas, N.; Coppel, R. L. A Maurer's Cleft-  
1274 Associated Protein Is Essential for Expression of the Major Malaria  
1275 Virulence Antigen on the Surface of Infected Red Blood Cells. *J. Cell Biol.*  
1276 **2006**, *172* (6), 899–908. <https://doi.org/10.1083/jcb.200509122>.
- 1277 (84) Oh, S. S.; Voigt, S.; Fisher, D.; Yi, S. J.; Leroy, P. J.; Derick, L. H.; Liu, S.  
1278 C.; Chishti, A. H. Plasmodium Falciparum Erythrocyte Membrane Protein 1  
1279 Is Anchored to the Actin-Spectrin Junction and Knob-Associated Histidine-  
1280 Rich Protein in the Erythrocyte Skeleton. *Mol. Biochem. Parasitol.* **2000**,  
1281 *108* (2), 237–247. [https://doi.org/10.1016/S0166-6851\(00\)00227-9](https://doi.org/10.1016/S0166-6851(00)00227-9).
- 1282 (85) Waller, K. L.; Nunomura, W.; Cooke, B. M.; Mohandas, N.; Coppel, R. L.  
1283 Mapping the Domains of the Cytoadherence Ligand Plasmodium  
1284 Falciparum Erythrocyte Membrane Protein 1 (PfEMP1) That Bind to the  
1285 Knob-Associated Histidine-Rich Protein (KAHRP). *Mol. Biochem. Parasitol.*  
1286 **2002**, *119* (1), 125–129. [https://doi.org/10.1016/s0166-6851\(01\)00395-4](https://doi.org/10.1016/s0166-6851(01)00395-4).
- 1287 (86) Rug, M.; Prescott, S. W.; Fernandez, K. M.; Cooke, B. M.; Cowman, A. F.  
1288 The Role of KAHRP Domains in Knob Formation and Cytoadherence of *P.*  
1289 *Falciparum* -Infected Human Erythrocytes. *Blood* **2006**, *108* (1), 370–378.  
1290 <https://doi.org/10.1182/blood-2005-11-4624>.Supported.
- 1291 (87) Boddey, J. A.; Hodder, A. N.; Günther, S.; Gilson, P. R.; Patsiouras, H.;  
1292 Kapp, E. A.; Pearce, J. A.; De Koning-Ward, T. F.; Simpson, R. J.; Crabb,  
1293 B. S.; Cowman, A. F. An Aspartyl Protease Directs Malaria Effector  
1294 Proteins to the Host Cell. *Nature* **2010**, *463* (7281), 627–631.  
1295 <https://doi.org/10.1038/nature08728>.
- 1296 (88) Russo, I.; Babbitt, S.; Muralidharan, V.; Butler, T.; Oksman, A.; Goldberg,

- 1297 D. E. Plasmepsin V Licenses Plasmodium Proteins for Export into the Host  
1298 Erythrocyte. *Nature* **2010**, 463 (7281), 632–636.  
1299 <https://doi.org/10.1038/nature08726>.
- 1300 (89) Spielmann, T.; Gilberger, T. W. Protein Export in Malaria Parasites: Do  
1301 Multiple Export Motifs Add up to Multiple Export Pathways? *Trends*  
1302 *Parasitol.* **2010**, 26 (1), 6–10. <https://doi.org/10.1016/j.pt.2009.10.001>.
- 1303 (90) Heiber, A.; Kruse, F.; Pick, C.; Grüning, C.; Flemming, S.; Oberli, A.;  
1304 Schoeler, H.; Retzlaff, S.; Mesén-Ramírez, P.; Hiss, J. A.; Kadekoppala,  
1305 M.; Hecht, L.; Holder, A. A.; Gilberger, T. W.; Spielmann, T. Identification  
1306 of New PNEPs Indicates a Substantial Non-PEXEL Exportome and  
1307 Underpins Common Features in Plasmodium Falciparum Protein Export.  
1308 *PLoS Pathog.* **2013**, 9 (8). <https://doi.org/10.1371/journal.ppat.1003546>.
- 1309 (91) Regev-Rudzki, N.; Wilson, D. W.; Carvalho, T. G.; Sisquella, X.; Coleman,  
1310 B. M.; Rug, M.; Bursac, D.; Angrisano, F.; Gee, M.; Hill, A. F.; Baum, J.;  
1311 Cowman, A. F. Cell-Cell Communication between Malaria-Infected Red  
1312 Blood Cells via Exosome-like Vesicles. *Cell* **2013**, 153 (5), 1120–1133.  
1313 <https://doi.org/10.1016/j.cell.2013.04.029>.
- 1314 (92) Sampaio, N. G.; Emery, S. J.; Garnham, A. L.; Tan, Q. Y.; Sisquella, X.;  
1315 Pimentel, M. A.; Jex, A. R.; Regev-Rudzki, N.; Schofield, L.; Eriksson, E.  
1316 M. Extracellular Vesicles from Early Stage Plasmodium Falciparum-  
1317 Infected Red Blood Cells Contain PfEMP1 and Induce Transcriptional  
1318 Changes in Human Monocytes. *Cell. Microbiol.* **2018**, 20 (5), 1–18.  
1319 <https://doi.org/10.1111/cmi.12822>.
- 1320 (93) Gupta, A.; Balabaskaran-nina, P.; Nguitragool, W.; Saggi, G. S.; Schureck,  
1321 M. A.; Desai, A. CLAG3 Self-Associates in Malaria Parasites and  
1322 Quantitatively Determines Nutrient Uptake Channels at the Host  
1323 Membrane. *MBio* **2018**, 9 (3), 1–18.
- 1324 (94) Nguitragool, W.; Bokhari, A. A. B.; Pillai, A. D.; Rayavara, K.; Sharma, P.;  
1325 Turpin, B.; Aravind, L.; Desai, S. A. Malaria Parasite Clag3 Genes  
1326 Determine Channel-Mediated Nutrient Uptake by Infected Red Blood Cells.  
1327 *Cell* **2011**, 145 (5), 665–677. <https://doi.org/10.1016/j.cell.2011.05.002>.
- 1328 (95) Glenister, F. K.; Fernandez, K. M.; Kats, L. M.; Hanssen, E.; Mohandas, N.;  
1329 Coppel, R. L.; Cooke, B. M. Functional Alteration of Red Blood Cells by a  
1330 Megadalton Protein of Plasmodium Falciparum. *Blood* **2009**, 113 (4), 919–

- 1331 928. <https://doi.org/10.1182/blood-2008-05-157735>.
- 1332 (96) Nilsson, S.; Angeletti, D.; Wahlgren, M.; Chen, Q.; Moll, K. Plasmodium  
1333 Falciparum Antigen 332 Is a Resident Peripheral Membrane Protein of  
1334 Maurer's Clefts. *PLoS One* **2012**, *7* (11).  
1335 <https://doi.org/10.1371/journal.pone.0046980>.
- 1336 (97) Waller, K. L.; Stubberfield, L. M.; Dubljevic, V.; Buckingham, D. W.;  
1337 Mohandas, N.; Coppel, R. L.; Cooke, B. M. Interaction of the Exported  
1338 Malaria Protein Pf332 with the Red Blood Cell Membrane Skeleton.  
1339 *Biochim. Biophys. Acta - Biomembr.* **2010**, *1798* (5), 861–871.  
1340 <https://doi.org/10.1016/j.bbamem.2010.01.018>.
- 1341 (98) Hodder, A. N.; Maier, A. G.; Rug, M.; Brown, M.; Hommel, M.; Pantic, I.;  
1342 Puig-De-Morales-Marinkovic, M.; Smith, B.; Triglia, T.; Beeson, J.;  
1343 Cowman, A. F. Analysis of Structure and Function of the Giant Protein  
1344 Pf332 in Plasmodium Falciparum. *Mol. Microbiol.* **2009**, *71* (1), 48–65.  
1345 <https://doi.org/10.1111/j.1365-2958.2008.06508.x>.
- 1346 (99) Pei, X.; Guo, X.; Coppel, R.; Bhattacharjee, S.; Haldar, K.; Gratzer, W.;  
1347 Mohandas, N.; An, X. The Ring-Infected Erythrocyte Surface Antigen  
1348 (RESA) of Plasmodium Falciparum Stabilizes Spectrin Tetramers and  
1349 Suppresses Further Invasion. *Blood* **2007**, *110* (3), 1036–1042.  
1350 <https://doi.org/10.1182/blood-2007-02-076919>.
- 1351 (100) Mills, J. P.; Diez-Silva, M.; Quinn, D. J.; Dao, M.; Lang, M. J.; Tan, K. S.  
1352 W.; Lim, C. T.; Milon, G.; David, P. H.; Mercereau-Puijalon, O.; Bonnefoy,  
1353 S.; Suresh, S. Effect of Plasmodial RESA Protein on Deformability of  
1354 Human Red Blood Cells Harboring Plasmodium Falciparum. *Proc. Natl.*  
1355 *Acad. Sci. U. S. A.* **2007**, *104* (22), 9213–9217.  
1356 <https://doi.org/10.1073/pnas.0703433104>.
- 1357 (101) Bhattacharjee, S.; Stahelin, R. V.; Speicher, K. D.; Speicher, D. W.; Haldar,  
1358 K. Endoplasmic Reticulum PI(3)P Lipid Binding Targets Malaria Proteins to  
1359 the Host Cell. *Cell* **2012**, *148* (1–2), 201–212.  
1360 <https://doi.org/10.1016/j.cell.2011.10.051>.
- 1361 (102) Maier, A. G.; Cooke, B. M.; Cowman, A. F.; Tilley, L. Malaria Parasite  
1362 Proteins That Remodel the Host Erythrocyte. *Nat. Rev. Microbiol.* **2009**, *7*  
1363 (5), 341–354. <https://doi.org/10.1038/nrmicro2110>.
- 1364 (103) Batinovic, S.; McHugh, E.; Chisholm, S. A.; Matthews, K.; Liu, B.; Dumont,

1365 L.; Charnaud, S. C.; Schneider, M. P.; Gilson, P. R.; De Koning-Ward, T.  
1366 F.; Dixon, M. W. A.; Tilley, L. An Exported Protein-Interacting Complex  
1367 Involved in the Trafficking of Virulence Determinants in Plasmodium-  
1368 Infected Erythrocytes. *Nat. Commun.* **2017**, *8* (May), 1–14.  
1369 <https://doi.org/10.1038/ncomms16044>.  
1370  
1371

1372 **Figure 1**

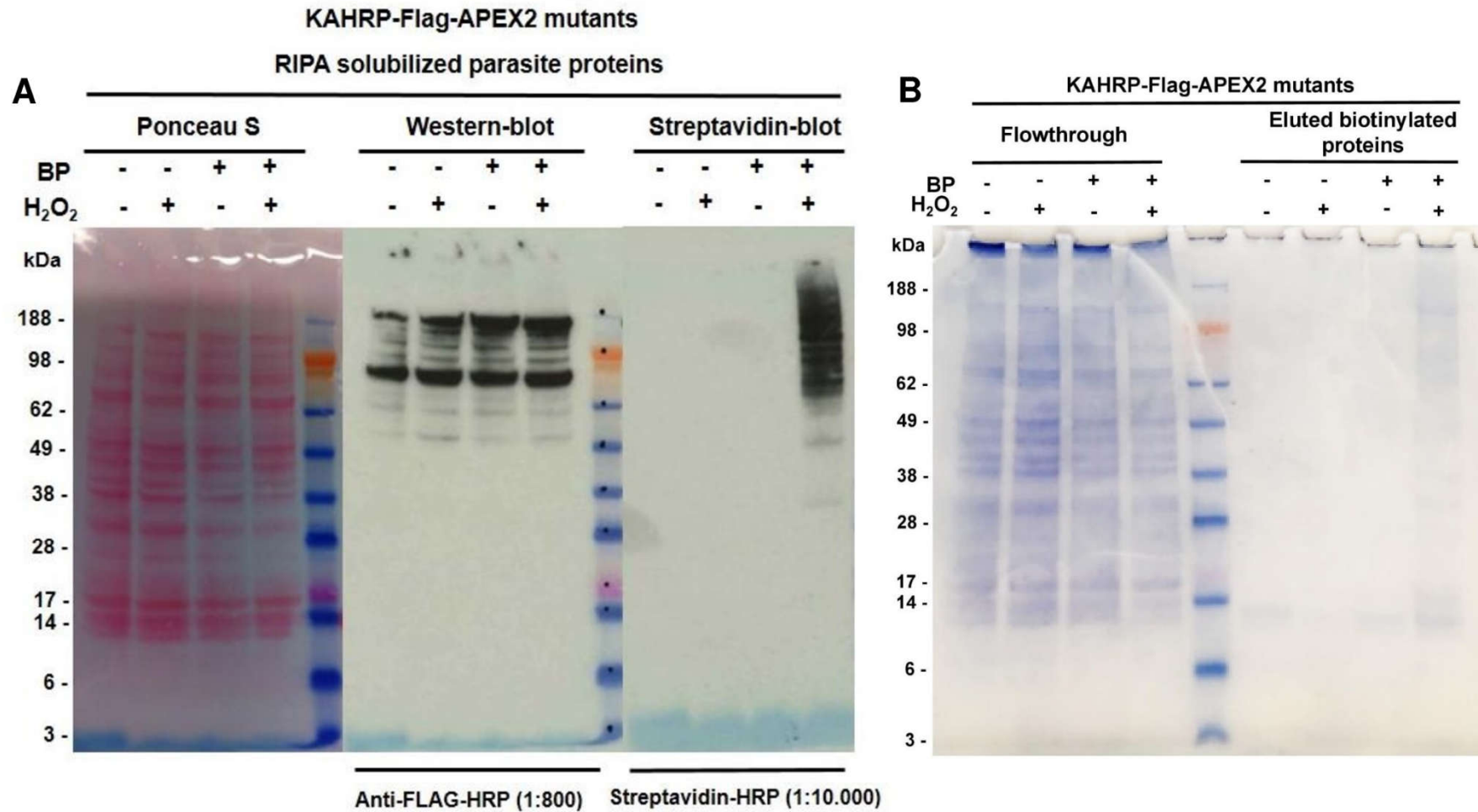


**C**

Region	Primers	DNA integration		Epissomal vector	
		Amplicon	Expected size	Amplicon	Expected size
HR1	FW: PS110	1134 pb	1,1 kb	1827 pb	1,8 kb
	RV: PS102				
HR2	FW: PS103	1641 pb	1,6 kb	1533 pb	1,5 kb
	RV: PS114				
pCC1 epissomal	FW: PS105	1827 pb	1,8 kb	~10800 pb	~11 kb
	RV: PS102				
pCC1 epissomal	FW: PS103	1533 pb	1,5 kb	~10800 pb	~11 kb
	RV: PS106				
Cassete integration	FW: PS110	~10800 pb	~11 kb	~10800 pb	~11 kb
	RV: PS114				

1373

1374 **Figure 2**

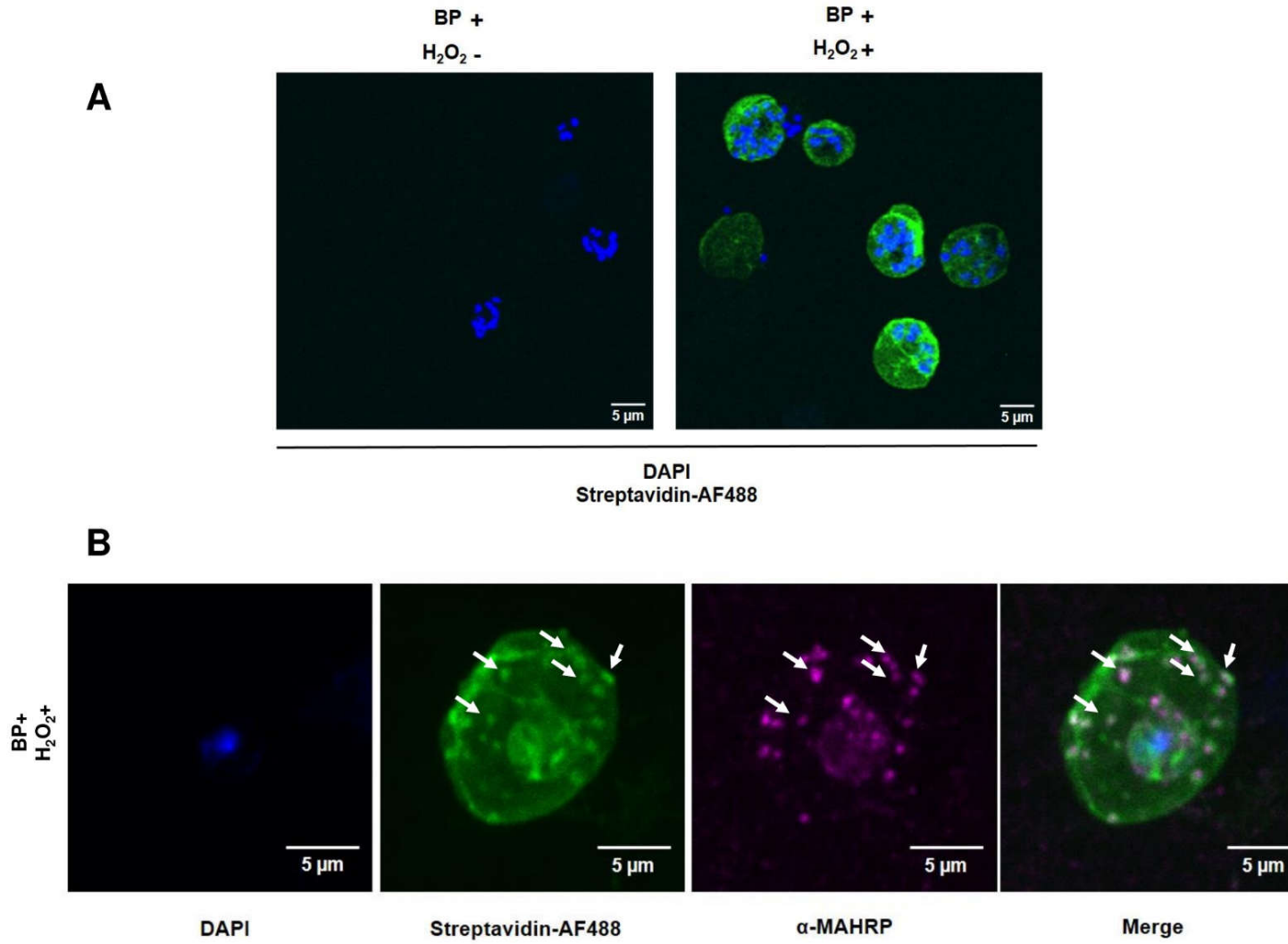


1375

1376

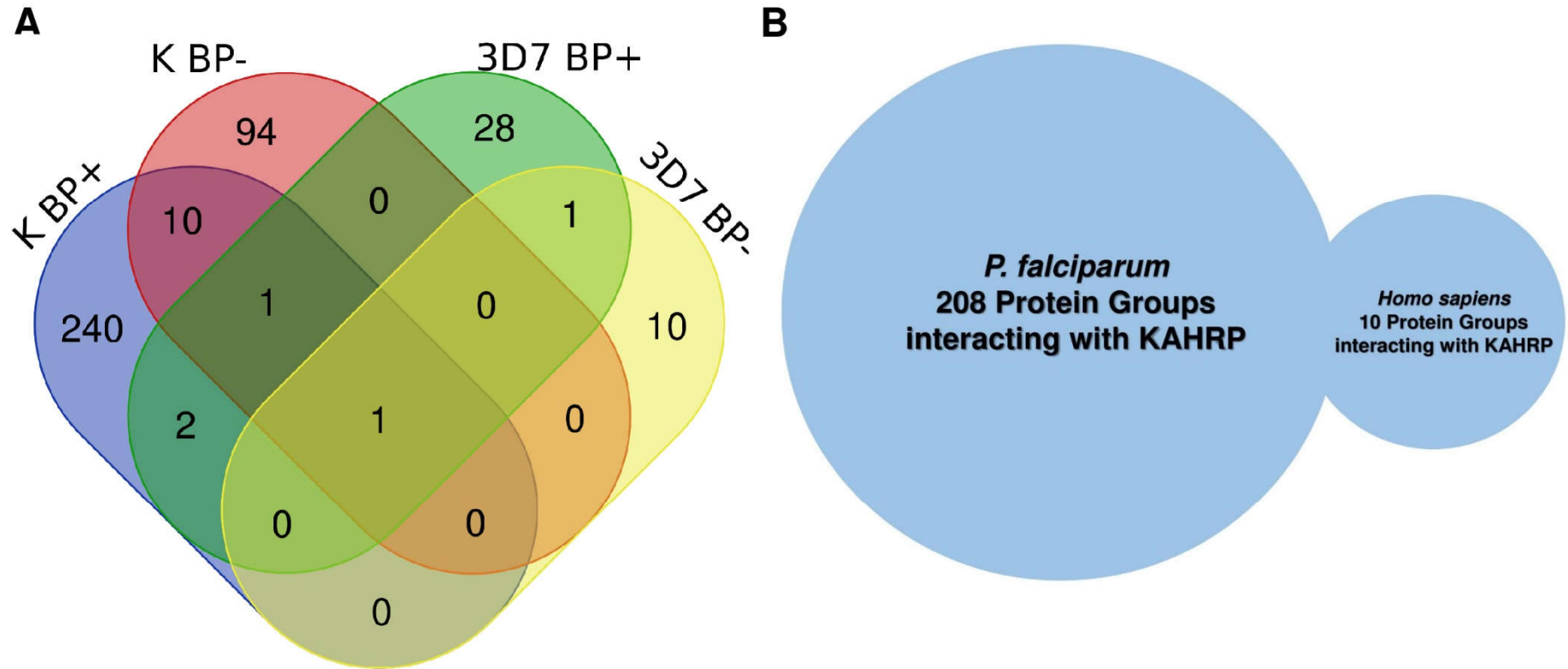


1377 **Figure 3**



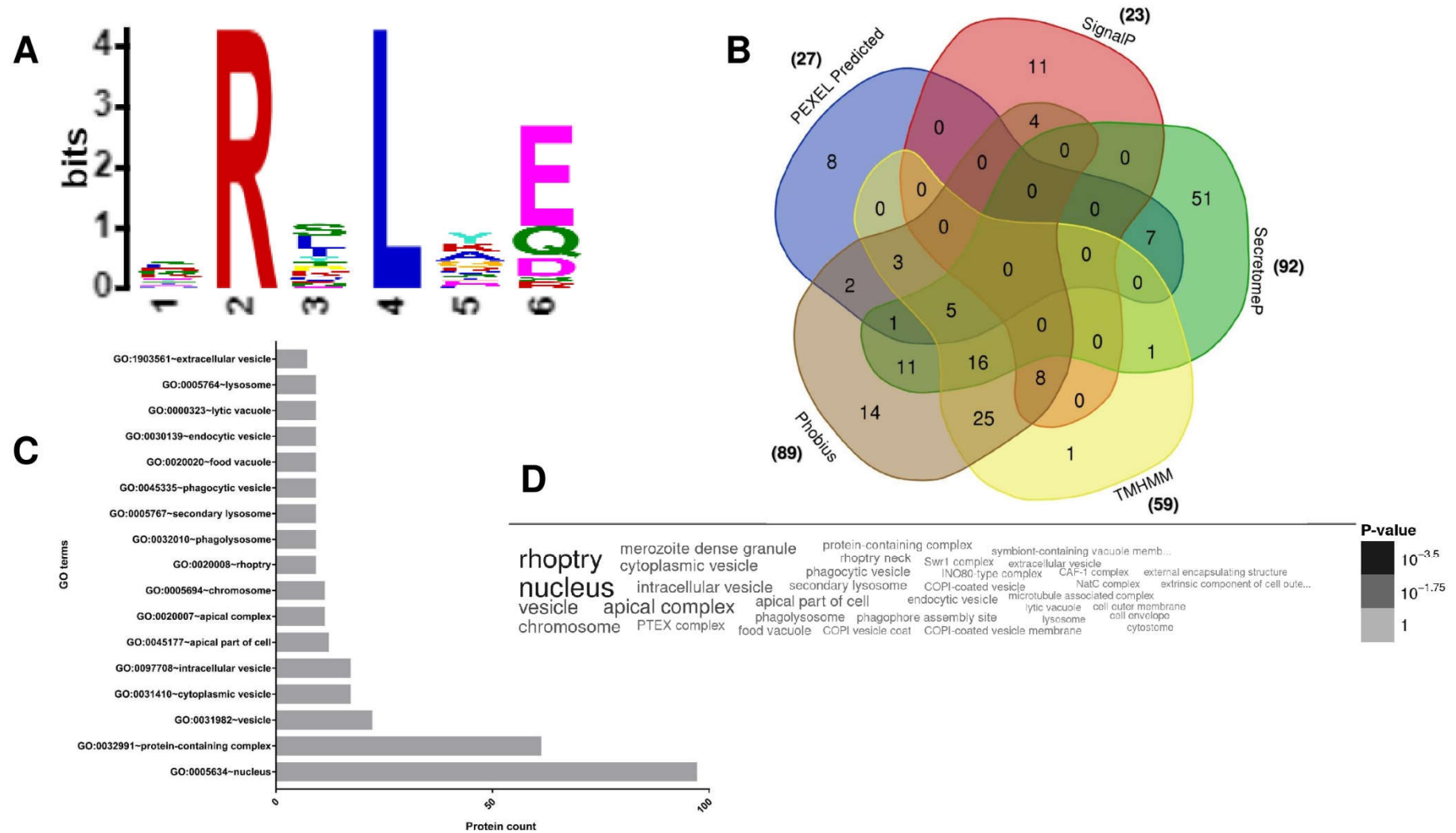
1378

1379 **Figure 4**



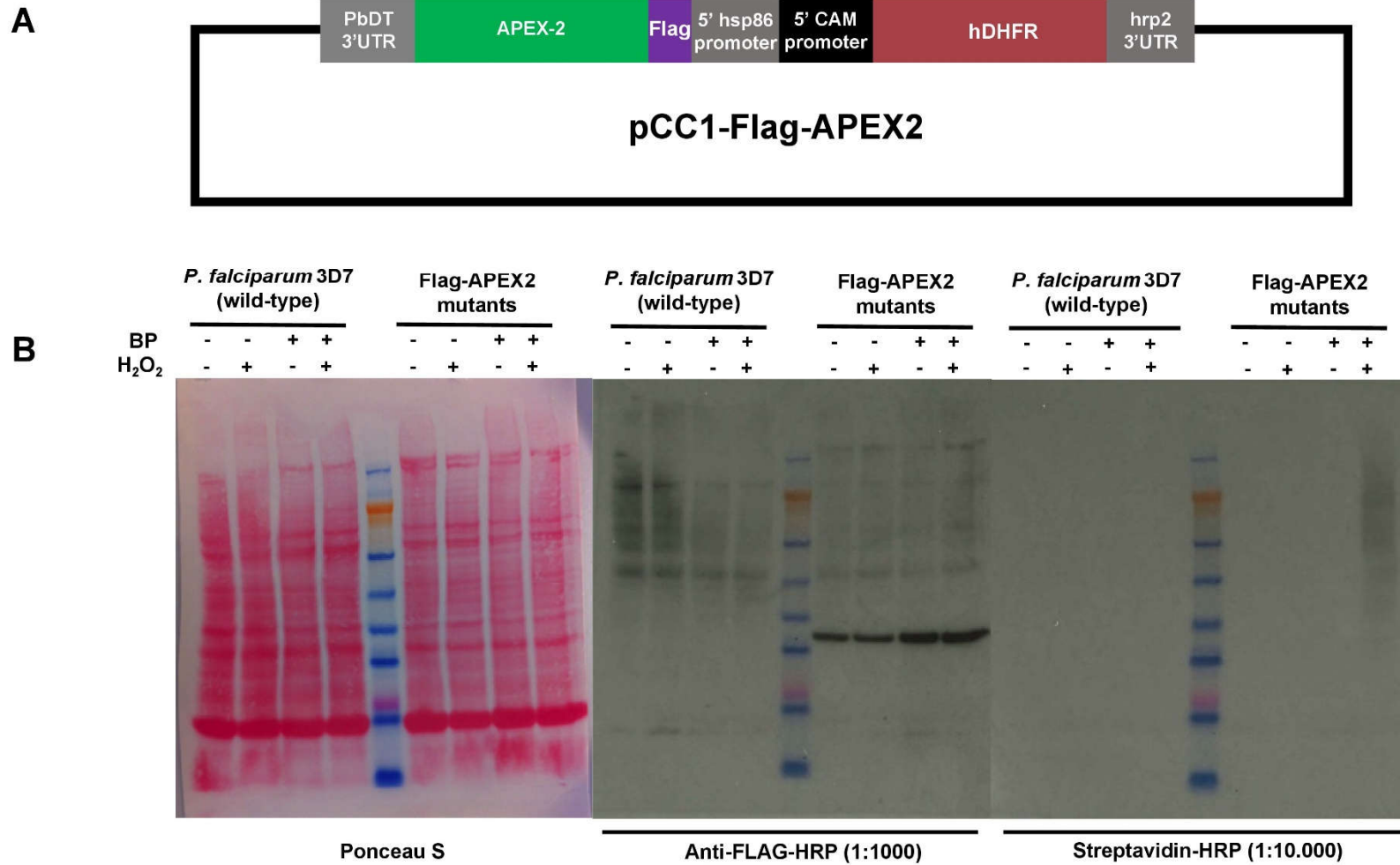
1380

1381 **Figure 5**



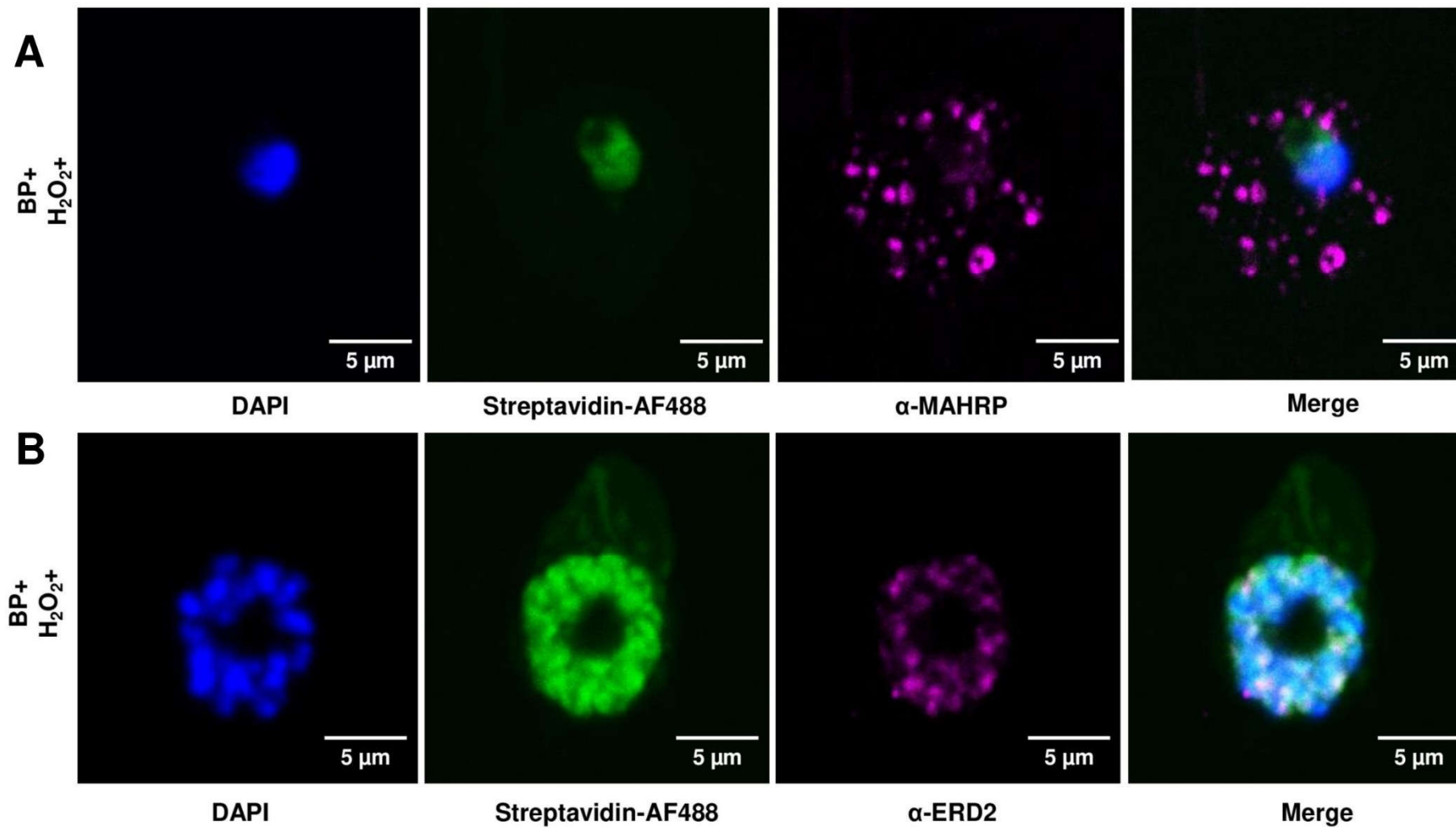
1382

1383 Figure Suppl. 01



1384

1385 Figure Suppl. 02



1386

**Table Suppl. 01**

(Too large to be attached)

Tables Suppl. 02, 03 and 05 are too large to be attached. Therefore, I choose to present only Table Suppl. 04, concerning *in silico* sub-cellular location shared among protein groups from our analysis (Table S4), to give you an overall impression of our data.

**Table S4. List of proteins with shared extracellular location predicted by *in silico* analysis by using PEXEL motif prediction tool available at PlasmoDB Databank (<https://plasmodb.org/plasmo/app>), SignalP (<http://www.cbs.dtu.dk/services/SignalP/>), SecretomeP (<http://www.cbs.dtu.dk/services/SecretomeP/>), TMHMM (<http://www.cbs.dtu.dk/services/TMHMM/>) and Phobius (<https://phobius.sbc.su.se/>).**

<b>PlasmoDB ID</b>	<b>Protein description</b>
<b>PEXEL Predicted, Phobius, SecretomeP and TMHMM (5)</b>	
PF3D7_0731100	EMP1-trafficking protein
PF3D7_1401600	Plasmodium exported protein (PHISTb), unknown function
PF3D7_1016300	GBP130 protein
PF3D7_1241200	conserved Plasmodium protein, unknown function
PF3D7_0628100	HECT domain-containing protein 1, putative
<b>PEXEL Predicted, Phobius and SecretomeP (1)</b>	
PF3D7_1149000	antigen 332, DBL-like protein
<b>PEXEL Predicted, Phobius and TMHMM (3)</b>	
PF3D7_0223100	rifin
PF3D7_1407800	plasmepsin IV
PF3D7_1476300	Plasmodium exported protein (PHISTb), unknown function
<b>Phobius, SignalP and TMHMM (8)</b>	
PF3D7_0828800	GPI-anchored micronemal antigen
PF3D7_0402300	reticulocyte binding protein homologue 1
PF3D7_1122300	conserved Plasmodium protein, unknown function
PF3D7_0505700	conserved Plasmodium membrane protein, unknown function
PF3D7_1122100	GPI transamidase component GPI16, putative
PF3D7_1452000	rhoptry neck protein 2

PF3D7_0616400	conserved Plasmodium protein, unknown function
PF3D7_1127500	protein disulfide-isomerase, putative
<b>Phobius, SecretomeP and TMHMM (16)</b>	
PF3D7_0618000	conserved Plasmodium membrane protein, unknown function
PF3D7_1303800	conserved Plasmodium protein, unknown function
PF3D7_0212500	conserved Plasmodium protein, unknown function
PF3D7_0724000	Rab GTPase activator and protein kinase, putative
PF3D7_1332600	DNA-(apurinic or apyrimidinic site) lyase 1
PF3D7_0922800	conserved Plasmodium protein, unknown function
PF3D7_1138400	guanylyl cyclase alpha
PF3D7_0820900	conserved Plasmodium protein, unknown function
PF3D7_1308400	conserved Plasmodium protein, unknown function
PF3D7_0704600	HECT-type E3 ubiquitin ligase UT
PF3D7_0721000	conserved Plasmodium membrane protein, unknown function
PF3D7_1351000	phosphatidylinositol transfer protein, putative
PF3D7_0612100	eukaryotic translation initiation factor 3 subunit L, putative
PF3D7_1228800	WD repeat-containing protein, putative
PF3D7_0418000	conserved Plasmodium protein, unknown function
PF3D7_0815500	conserved Plasmodium protein, unknown function
<b>PEXEL Predicted and SecretomeP (7)</b>	
PF3D7_1121100	conserved protein, unknown function
PF3D7_1138500	protein phosphatase PPM2
PF3D7_0623100	nuclear polyadenylated RNA-binding protein NAB2, putative
PF3D7_0317500	kinesin-5
PF3D7_1349300	tyrosine kinase-like protein
PF3D7_0814000	60S ribosomal protein L13-2, putative
PF3D7_1122500	protein KIC10
<b>PEXEL Predicted and Phobius (2)</b>	
PF3D7_1149400	Plasmodium exported protein, unknown function
PF3D7_1464600	serine/threonine protein phosphatase UIS2, putative
<b>Phobius and SignalP (4)</b>	
PF3D7_1234600	protein TOC75, putative
PF3D7_0905400	high molecular weight rhoptry protein 3
PF3D7_0302500	cytoadherence linked asexual protein 3.1
PF3D7_0220800	cytoadherence linked asexual protein 2

### **SecretomeP and TMHMM (1)**

PF3D7\_0615400 ribonuclease, putative

### **Phobius and SecretomeP (11)**

PF3D7\_0709300 Cg2 protein  
PF3D7\_0416400 histone acetyltransferase, putative  
PF3D7\_1233600 asparagine and aspartate rich protein 1  
PF3D7\_0609000 nucleoporin NUP637, putative  
PF3D7\_0724700 bromodomain protein 6, putative  
PF3D7\_0623800 tyrosine kinase-like protein, putative  
PF3D7\_1435300 glutamate synthase [NADH], putative  
PF3D7\_1203000 origin recognition complex subunit 1  
PF3D7\_0309000 dual specificity protein phosphatase  
PF3D7\_0219600 replication factor C subunit 1  
PF3D7\_0703500 erythrocyte membrane-associated antigen

### **Phobius and TMHMM (25)**

PF3D7\_0914700 major facilitator superfamily-related transporter, putative  
PF3D7\_0829000 conserved Plasmodium membrane protein, unknown function  
PF3D7\_1225100 isoleucine--tRNA ligase, putative  
PF3D7\_1470100 conserved Plasmodium protein, unknown function  
PF3D7\_1218200 symplekin domain-containing protein, putative  
PF3D7\_1214100 GPI ethanolamine phosphate transferase 3, putative  
PF3D7\_1429600 conserved Plasmodium protein, unknown function  
PF3D7\_1328300 conserved protein, unknown function  
PF3D7\_1433700 conserved Plasmodium protein, unknown function  
PF3D7\_1025500 conserved Plasmodium protein, unknown function  
PF3D7\_1119600 ATP-dependent zinc metalloprotease FTSH, putative  
PF3D7\_0523400 DnaJ protein, putative  
PF3D7\_0824400 nucleoside transporter 2  
PF3D7\_0811200 ER membrane protein complex subunit 1, putative  
PF3D7\_1452500 syntaxin-6, putative  
PF3D7\_1434500 dynein-related AAA-type ATPase, putative  
PF3D7\_1029400 LEM3/CDC50 family protein, putative  
PF3D7\_0523000 multidrug resistance protein 1  
PF3D7\_1313800 conserved Plasmodium membrane protein, unknown function  
PF3D7\_1358700 YOP1-like protein, putative



PF3D7\_1222100 conserved Plasmodium protein, unknown function  
PF3D7\_0921200 conserved Plasmodium membrane protein, unknown function  
PF3D7\_0703900 conserved Plasmodium membrane protein, unknown function  
PF3D7\_0304800 conserved Plasmodium membrane protein, unknown function  
PF3D7\_0505000 MMS19-like protein, putative

#### **PEXEL Predicted (8)**

PF3D7\_1402300 26S proteasome regulatory subunit RPN6  
PF3D7\_0515900 NLI interacting factor-like phosphatase, putative  
PF3D7\_0320500 nicotinamidase, putative  
PF3D7\_1012900 autophagy-related protein 18  
PF3D7\_1409000 WD repeat-containing protein, putative  
PF3D7\_1317100 DNA replication licensing factor MCM4  
PF3D7\_1126100 autophagy-related protein 7, putative  
PF3D7\_1361800 glideosome-associated connector

#### **SignalP (11)**

PF3D7\_1012200 rhoptry associated adhesin  
PF3D7\_0209000 6-cysteine protein P230  
PF3D7\_0214900 rhoptry neck protein 6  
PF3D7\_1344200 endoplasmic reticulum chaperone GRP170  
PF3D7\_0929400 high molecular weight rhoptry protein 2  
PF3D7\_0624400 conserved protein, unknown function  
PF3D7\_1436300 translocon component PTEX150  
PF3D7\_1037100 pyruvate kinase 2  
PF3D7\_1105600 translocon component PTEX88  
PF3D7\_1025300 conserved protein, unknown function  
PF3D7\_1035100 probable protein, unknown function

#### **SecretomeP (51)**

PF3D7\_0529400 conserved Plasmodium protein, unknown function  
PF3D7\_1217900 PPPDE peptidase domain-containing protein, putative  
PF3D7\_1344900 conserved Plasmodium protein, unknown function  
PF3D7\_0516700 ubiquitin carboxyl-terminal hydrolase 2, putative  
PF3D7\_0930600 peptidyl-prolyl cis-trans isomerase  
PF3D7\_0801700 sentrin-specific protease 2, putative

PF3D7_1235300	CCR4-NOT transcription complex subunit 4, putative
PF3D7_1441600	acid cluster protein 33 homologue, putative
PF3D7_0802000	glutamate dehydrogenase, putative
PF3D7_1203700	nucleosome assembly protein
PF3D7_0505400	conserved protein, unknown function
PF3D7_1326700	conserved Apicomplexan protein, unknown function
PF3D7_1128000	conserved Plasmodium protein, unknown function
PF3D7_1345800	conserved Plasmodium protein, unknown function
PF3D7_1317600	conserved Plasmodium protein, unknown function
PF3D7_1443000	serine/threonine protein kinase
PF3D7_0510500	topoisomerase I
PF3D7_1018900	conserved Plasmodium protein, unknown function
PF3D7_1446500	nucleoporin NUP313, putative
PF3D7_0321800	WD repeat-containing protein, putative
PF3D7_1428100	WW domain-binding protein 11, putative
PF3D7_0706500	conserved Plasmodium protein, unknown function
PF3D7_0729100	conserved Plasmodium protein, unknown function
PF3D7_1126500	WD repeat-containing protein, putative
PF3D7_1405900	RNA-binding protein, putative
PF3D7_1110400	RNA-binding protein, putative
PF3D7_0406500	NYN domain-containing protein, putative
PF3D7_0719300	actin-related protein ARP6
PF3D7_1227600	kinetochore protein SPC24, putative
PF3D7_0102200	ring-infected erythrocyte surface antigen
PF3D7_0804300	zinc finger protein, putative
PF3D7_0926000	protein kinase, putative
PF3D7_1107800	AP2 domain transcription factor, putative
PF3D7_0610200	RNA-binding protein 25, putative
PF3D7_1025900	conserved protein, unknown function
PF3D7_1251500	ATP-dependent RNA helicase DRS1, putative
PF3D7_0907600	translation initiation factor SUI1, putative
PF3D7_1221000	histone-lysine N-methyltransferase, H3 lysine-4 specific
PF3D7_1307900	tripartite motif protein, putative
PF3D7_0806500	DnaJ protein, putative
PF3D7_1417300	cysteine protease ATG4, putative

PF3D7\_1026600 conserved Plasmodium protein, unknown function  
PF3D7\_0621800 nascent polypeptide-associated complex subunit alpha, putative  
PF3D7\_1116100 serine esterase, putative  
PF3D7\_0107800 double-strand break repair protein MRE11  
PF3D7\_0913200 elongation factor 1-beta  
PF3D7\_0408500 flap endonuclease 1  
PF3D7\_0612200 leucine-rich repeat protein  
PF3D7\_0317300 conserved Plasmodium protein, unknown function  
PF3D7\_1409500 conserved Plasmodium protein, unknown function  
PF3D7\_1414500 atypical protein kinase, ABC-1 family, putative

#### **TMHMM (1)**

PF3D7\_0306400 FAD-dependent glycerol-3-phosphate dehydrogenase, putative

#### **Phobius (14)**


PF3D7\_1239800 conserved Plasmodium protein, unknown function  
PF3D7\_0508500 guanidine nucleotide exchange factor  
PF3D7\_1147500 protein farnesyltransferase subunit beta  
PF3D7\_1202300 dynein heavy chain, putative  
PF3D7\_0903400 ATP-dependent RNA helicase DDX60, putative  
PF3D7\_1149200 ring-infected erythrocyte surface antigen  
PF3D7\_0621000 conserved Plasmodium protein, unknown function  
PF3D7\_0911400 conserved Plasmodium protein, unknown function  
PF3D7\_0910100 exportin-7, putative  
PF3D7\_0926700 glutamine-dependent NAD(+) synthetase, putative  
PF3D7\_0502000 vacuolar protein sorting-associated protein 11, putative  
PF3D7\_0932800 importin alpha re-exporter, putative  
PF3D7\_1218900 WD repeat-containing protein, putative  
PF3D7\_0817700 rhoptry neck protein 5

#### **Non-predicted (40)**

PF3D7\_1414300 60S ribosomal protein L10, putative  
PF3D7\_0525100 acyl-CoA synthetase  
PF3D7\_0417200 bifunctional dihydrofolate reductase-thymidylate synthase  
PF3D7\_0905900 coatomer subunit beta, putative  
PF3D7\_1134800 coatomer subunit delta  
PF3D7\_0409000 conserved Plasmodium protein, unknown function  
PF3D7\_0410900 conserved Plasmodium protein, unknown function

PF3D7_0905000	conserved Plasmodium protein, unknown function
PF3D7_1344700	conserved Plasmodium protein, unknown function
PF3D7_1410200	CTP synthase
PF3D7_0811000	cullin-1, putative
PF3D7_0628600	DNA methyltransferase 1-associated protein 1, putative
PF3D7_1427500	DNA mismatch repair protein MSH2, putative
PF3D7_1206600	DNA-directed RNA polymerase III subunit RPC2, putative
PF3D7_1037500	dynamain-like protein
PF3D7_1122900	dynein heavy chain, putative
PF3D7_0418200	eukaryotic translation initiation factor 3 subunit M, putative
PF3D7_0110200	FAD-linked sulfhydryl oxidase ERV1, putative
PF3D7_0918900	gamma-glutamylcysteine synthetase
PF3D7_1453800	glucose-6-phosphate dehydrogenase-6-phosphogluconolactonase
PF3D7_0922600	glutamine synthetase, putative
PF3D7_1462800	glyceraldehyde-3-phosphate dehydrogenase
PF3D7_1012600	GMP synthase [glutamine-hydrolyzing]
PF3D7_0610400	histone H3
PF3D7_1012400	hypoxanthine-guanine phosphoribosyltransferase
PF3D7_0511300	MORN repeat protein, putative
PF3D7_1342600	myosin A
PF3D7_0303000	N-ethylmaleimide-sensitive fusion protein
PF3D7_1023200	orotidine 5'-phosphate decarboxylase
PF3D7_1128100	prefoldin subunit 5, putative
PF3D7_1328100	proteasome subunit beta type-7, putative
PF3D7_0621500	ribonuclease P/MRP protein subunit RPP1, putative
PF3D7_1015800	ribonucleoside-diphosphate reductase small chain, putative
PF3D7_1234800	splicing factor 3B subunit 3, putative
PF3D7_1237000	SUMO-activating enzyme subunit 2
PF3D7_0306800	T-complex protein 1 subunit beta
PF3D7_0921600	tetratricopeptide repeat protein, putative
PF3D7_1408900	tRNA-dihydrouridine synthase, putative
PF3D7_1015700	tubulin binding cofactor c, putative
PF3D7_1003800	U5 small nuclear ribonucleoprotein component, putative

## **CAPÍTULO 7**



**“Mapeamento de proteínas organelares de *P. falciparum* utilizando APEX2: resultados preliminares”**

## CAPÍTULO 7 - Mapeamento de proteínas organelares de *P. falciparum* utilizando APEX2: resultados preliminares

### 7.1. Construção dos vetores de expressão episossomal da proteína HA-APEX2 direcionada à diferentes organelas

A fim de realizar a expressão episossomal da proteína HA-APEX2 em compartimentos celulares de interesse de *P. falciparum*, elaboramos as construções em vetor pCC1, contendo o gene de seleção *hDHFR* (do inglês, *human dihydrofolate reductase*) regulado por um promotor CAM 5' e terminador *Hrp2* 3'UTR (**Figura 18, Painel A**). Após as sub-clonagens no pCC1 a partir do vetor comercial pMAT, das sequências sintetizadas da HA-APEX2 (Thermo Scientific), acrescentadas com os respectivos peptídeos de endereçamento (ou do inglês, *signal peptides* ou SP) do apicoplasto (ACP ou do inglês, *acyl-carrier protein*) (Waller et al., 2000), mitocôndria (TrxR ou do inglês, *thioredoxin reductase*) (Kehr et al., 2010), roptrias (RAP1 ou do inglês, *roptry-associated protein 1*) (Richard et al., 2009) e HA-APEX2 citosólica (sem peptídeo de endereçamento), as construções finais: HA<sub>(cito)</sub>-APEX2, SP<sub>(ACP)</sub>-HA-APEX2, SP<sub>(RAP1)</sub>-HA-APEX2 e SP<sub>(TrxR)</sub>-HA-APEX2, foram transformadas e amplificadas em bactérias competentes *E. coli* TOP10 (Invitrogen™). No âmbito de confirmar as construções, as sequências purificadas a partir das minipreparações



**Figura 18. Confirmação das construções episomais dos plasmídeos pCC1-HA<sub>(cito)</sub>-APEX2, pCC1-SP<sub>(ACP)</sub>-HA-APEX2, pCC1-SP<sub>(RAP1)</sub>-HA-APEX2 e pCC1-SP<sub>(TrxR)</sub>-HA-APEX2. (A)** Esquema do vetor pCC1 com os insertos da HA-APEX2 com seus respectivos peptídeos sinais de endereçamento ao apicoplasto (ACP), roptrias (RAP1) e mitocôndria (TrxR). **(B)** Padrão das digestões usando *Xho*I e *Sal*I, após as sub-clonagens em pCC1, analisado por gel de agarose 1%. Pannel à esquerda: (M) corresponde ao marcador 1kb Plus (Thermo Scientific); (1) corresponde ao vetor pCC1 vazio linearizado por *Xho*I e *Sal*I; (2) inserto, correspondendo ao tamanho aproximado esperado das sequências SP-HA-APEX2. Somente os clones do poço 4 (referente à construção HA-APEX2), poço 13 (referente à construção RAP-HA-APEX2) e, os poços 15 e 17 (referentes à construção TrxR-HA-APEX2), apresentaram uma ligação eficiente do inserto ao vetor pCC1 (representados em verde). **(C)** Devido ao fato de que a ligação da construção ACP-HA-APEX2 não ter ocorrido em (B), foi realizada uma nova ligação, com a obtenção dos clones nos poços 4 e 8, referentes à ligação eficiente da construção ACP-HA-APEX2. Todos os clones positivos foram utilizados para o procedimento de transfecção.

plasmidiais (minipreps) foram digeridas pelas enzimas de restrição *Xho*I e *Sal*I, que flanqueiam as sequências HA-APEX2. **(Figura 18, Pannel B e C).**

## 7.2. Confirmação da orientação dos insertos e da sequência dos plasmídeos

Com intuito de averiguar se a ligação dos insertos HA<sub>(cito)</sub>-APEX2, SP<sub>(ACP)</sub>-HA-APEX2, SP<sub>(RAP1)</sub>-HA-APEX2 e SP<sub>(TrxR)</sub>-HA-APEX2 estava na orientação correta (5' → 3'), foi realizado um teste simples, com uso da enzima de restrição *Hind*III, para averiguar o tamanho dos fragmentos, baseados na orientação do DNA plasmidial após a ligação. Caso a ligação, tivesse ocorrido de forma errada (3' → 5'), os fragmentos esperados seriam de aproximadamente de 4,7 kb e 2,5 kb. Caso a ligação, tivesse ocorrido de forma correta (5' → 3'), os fragmentos esperados seriam de aproximadamente de 3,9 kb e 3,4 kb. Através da análise por eletroforese em gel de agarose 1%, foi possível observar os fragmentos nas alturas esperadas de ~3,9 kb e ~3,4 kb, indicando a ligação correta dos insertos, ao vetor pCC1 **(Figura 19, Pannel A)**. As estimativas dos fragmentos foram obtidas através das simulações realizadas na plataforma *online* WebCutter 2.0 (<http://www.firstmarket.com/cutter/cut2.html>).

Para verificar se o processo de sub-clonagem ocorreu de forma eficiente, sem eventuais mutações que poderiam representar um problema para a expressão das proteínas exógenas, ou ainda, um *misleading* de endereçamento às organelas de interesse, foi realizado o sequenciamento das construções finais. Para tal, foi desenhado um par de oligonucleotídeos internamente da sequência da APEX2 (APEX2<sub>int</sub>), que sobrepusesse a sequência da APEX2 dos insertos ligados (*forward* ou *sense*: 5'-AGTTGGCTGGCGTTGTTGCC-3' e *reverse* ou *anti-sense*: 5'-CCAAACACATCTCTCAAATGGTC-3'). Essa estratégia foi necessária, pois as regiões que flanqueiam os insertos são altamente ricas em A+T, dificultando a escolha

dos oligonucleotídeos. Através da análise dos histogramas do sequenciamento utilizando a plataforma Chromas 2.6.6 (<https://technelysium.com.au/wp/chromas/>), foi possível inferir que a ligação dos insertos no vetor pCC1 ocorreu corretamente (**Figura 19, Painel B**).

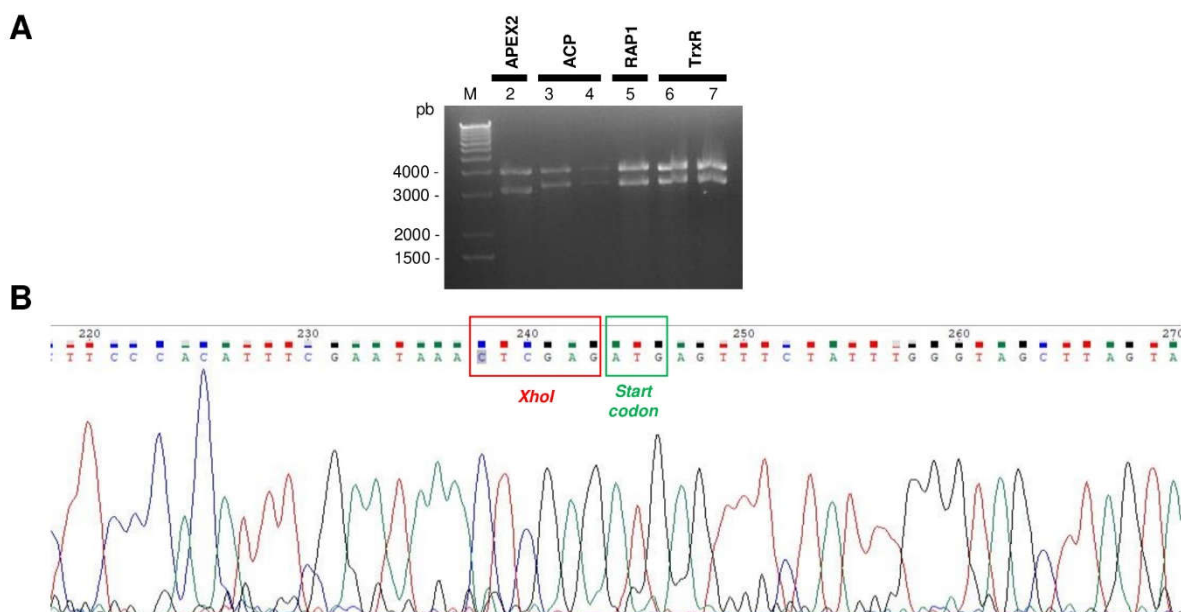


**Figura 19. Confirmação da orientação do inserto e sequenciamento dos plasmídeos. (A)** Gel de agarose mostrando os fragmentos obtidos com a digestão dos plasmídeos pCC1-SP<sub>(cito, acp, rap1, trx)</sub>-HA-APEX2 utilizando *Hind*III: (M) marcador 1kb Plus (Thermo Scientific); (2) digestão da construção HA-APEX2, com liberação de dois fragmentos com tamanhos de 3,2 kb e 3,9 kb; (3 e 4) digestão da construção ACP-HA-APEX2, com liberação de dois fragmentos com tamanhos de 3,4 kb e 3,9 kb; (5) digestão da construção RAP-HA-APEX2, com liberação de dois fragmentos com tamanhos de 3,35 kb e 3,9 kb; e, (6 e 7) digestão da construção TrxR-HA-APEX2, com liberação de dois fragmentos com tamanhos de 3,4 kb e 3,9 kb. **(B)** Histograma ilustrativo do sequenciamento das construções transientes HA<sub>(cito)</sub>-APEX2, SP<sub>(ACP)</sub>-HA-APEX2, SP<sub>(RAP1)</sub>-HA-APEX2 e SP<sub>(TrxR)</sub>-HA-APEX2. Note que no quadro vermelho e verde, constam o sítio de restrição *Xho*I e o *start* códon (ATG), respectivamente, sugerindo que todas as construções estão em *frame*.

Os sequenciamentos das regiões promotoras e terminadoras dos plasmídeos foram também realizados. Nesta rodada de sequenciamento, além dos vetores pCC1-HA<sub>(cito)</sub>-APEX2, pCC1- SP<sub>(ACP)</sub>-HA-APEX2, pCC1- SP<sub>(RAP1)</sub>-HA-APEX2 e pCC1- SP<sub>(TrxR)</sub>-HA-APEX2, o vetor pCC1-*empty* foi adicionalmente sequenciado para estas regiões. Deste modo, foi possível observar que o plasmídeo pCC1-*empty*, utilizado para realizar todas as construções, bem como os demais utilizados para o procedimento de sub-clonagem, apresentaram mutações nas regiões promotoras 5' UTR: (i) 5' *hsp86* para os insertos SP<sub>(cito, acp, rap1, trx)</sub>-HA-APEX2 e (ii) 5' *CAM* para a marca de seleção *hDHFR*; bem como, nas regiões terminadoras 3' UTR: (iii) 3' UTR *PbDT* para os insertos SP<sub>(cito, acp, rap1, trx)</sub>-HA-APEX2 e (iv) 3' UTR *hrp2* para a marca de seleção *hDHFR*. No entanto, a sequência da *hDHFR* que confere resistência a droga anti-folato WR99210, utilizado nas construções, apresentou apenas uma mutação silenciosa no códon 9 (**Figura 20 e Tabela 2**).



```

pCC1_hDHFR_Seq_FW -----
pCC1_hDHFR_Reverse_Seq_RVCP -----
pCC1_hDHFR -----
TATGTATATTTTAAACTAGAAAAGGAATAACTAATATTTATTTATTATC

pCC1_hDHFR_Seq_FW -----
pCC1_hDHFR_Reverse_Seq_RVCP -----
pCC1_hDHFR -----
ATTCAAGATTTATATTTTATAATAATAAATAOCTAATAGAAATATATCAG

pCC1_hDHFR_Seq_FW -----
pCC1_hDHFR_Reverse_Seq_RVCP -----
pCC1_hDHFR -----
----ATGCATGGTTCGCTAAACTGCATCGT SGTGTGTCCAGAACATG
----ATGCATGGTTCGCTAAACTGCATCGT SGTGTGTCCAGAACATG
GATCCATGCATGGTTCGCTAAACTGCATCGT SGTGTGTCCAGAACATG
*****

pCC1_hDHFR_Seq_FW -----
pCC1_hDHFR_Reverse_Seq_RVCP -----
pCC1_hDHFR -----
GGCATCGGCAAGAACGGGACTACCCCTGGCCAOCGCTCAGGAACGAATT
GGCATCGGCAAGAACGGGACTACCCCTGGCCAOCGCTCAGGAACGAATT
GGCATCGGCAAGAACGGGACTACCCCTGGCCAOCGCTCAGGAACGAATT
*****

pCC1_hDHFR_Seq_FW -----
pCC1_hDHFR_Reverse_Seq_RVCP -----
pCC1_hDHFR -----
TAGATATTTCCAGAGAAATGACCCAAOCTCTTCAGTAGAAGGTAAACAGA
TAGATATTTCCAGAGAAATGACCCAAOCTCTTCAGTAGAAGGTAAACAGA
TAGATATTTCCAGAGAAATGACCCAAOCTCTTCAGTAGAAGGTAAACAGA
*****

pCC1_hDHFR_Seq_FW -----
pCC1_hDHFR_Reverse_Seq_RVCP -----
pCC1_hDHFR -----
ATCTGGTGATTTATGGGTAAGAAGACCTGGTTCTCCATTCTGAGAAGAAT
ATCTGGTGATTTATGGGTAAGAAGACCTGGTTCTCCATTCTGAGAAGAAT
ATCTGGTGATTTATGGGTAAGAAGACCTGGTTCTCCATTCTGAGAAGAAT
*****

pCC1_hDHFR_Seq_FW -----
pCC1_hDHFR_Reverse_Seq_RVCP -----
pCC1_hDHFR -----
CGACCTTTAAAGGGTAGAATTAATTTAGTTCTCAGCAGAGAACTCAAGGA
CGACCTTTAAAGGGTAGAATTAATTTAGTTCTCAGCAGAGAACTCAAGGA
CGACCTTTAAAGGGTAGAATTAATTTAGTTCTCAGCAGAGAACTCAAGGA
*****

pCC1_hDHFR_Seq_FW -----
pCC1_hDHFR_Reverse_Seq_RVCP -----
pCC1_hDHFR -----
ACCTCCACAAGGAGCTCATTCTTTCCAGAAGTCTAGATGATGCTTAA
ACCTCCACAAGGAGCTCATTCTTTCCAGAAGTCTAGATGATGCTTAA
ACCTCCACAAGGAGCTCATTCTTTCCAGAAGTCTAGATGATGCTTAA
*****

pCC1_hDHFR_Seq_FW -----
pCC1_hDHFR_Reverse_Seq_RVCP -----
pCC1_hDHFR -----
AACTTACTGAACAACCCAGAAATTAGCAAATAAAGTAGACATGGTCTGGATA
AACTTACTGAACAACCCAGAAATTAGCAAATAAAGTAGACATGGTCTGGATA
AACTTACTGAACAACCCAGAAATTAGCAAATAAAGTAGACATGGTCTGGATA
*****

pCC1_hDHFR_Seq_FW -----
pCC1_hDHFR_Reverse_Seq_RVCP -----
pCC1_hDHFR -----
GTTGGTGGCAGTTCTGTTTATAAGGAAGCCATGAATCAOCCAGGCCATCT
GTTGGTGGCAGTTCTGTTTATAAGGAAGCCATGAATCAOCCAGGCCATCT
GTTGGTGGCAGTTCTGTTTATAAGGAAGCCATGAATCAOCCAGGCCATCT
*****

pCC1_hDHFR_Seq_FW -----
pCC1_hDHFR_Reverse_Seq_RVCP -----
pCC1_hDHFR -----
TAAACTATTTGTGACAAGGATCATGCAAGACTTTGAAAGTGACACGTTTT
TAAACTATTTGTGACAAGGATCATGCAAGACTTTGAAAGTGACACGTTTT
TAAACTATTTGTGACAAGGATCATGCAAGACTTTGAAAGTGACACGTTTT
*****

pCC1_hDHFR_Seq_FW -----
pCC1_hDHFR_Reverse_Seq_RVCP -----
pCC1_hDHFR -----
TTCCAGAAATTGATTTGGAGAAATATAAACTCTGCCAGAAATACCCAGGT
TTCCAGAAATTGATTTGGAGAAATATAAACTCTGCCAGAAATACCCAGGT
TTCCAGAAATTGATTTGGAGAAATATAAACTCTGCCAGAAATACCCAGGT
*****

pCC1_hDHFR_Seq_FW -----
pCC1_hDHFR_Reverse_Seq_RVCP -----
pCC1_hDHFR -----
GTTCTCTCTGATGTCCAGGAGGAGAAAGGCATTAAAGTACAAATTTGAAGT
GTTCTCTCTGATGTCCAGGAGGAGAAAGGCATTAAAGTACAAATTTGAAGT
GTTCTCTCTGATGTCCAGGAGGAGAAAGGCATTAAAGTACAAATTTGAAGT
*****

pCC1_hDHFR_Seq_FW -----
pCC1_hDHFR_Reverse_Seq_RVCP -----
pCC1_hDHFR -----
ATATGAGAGAATGATTA-----
ATATGAGAGAATGATTA-----
ATATGAGAGAATGATTAAGCTTATTTAATAATAGATTAAAAATATTATA
    
```

Figura 20. Alinhamento do gene *hDHFR* comparando os vetores pCC1-SP (*cito, acp, rap1, trxr*)-HA-APEX2 e vetor pCC1-empty. Trata-se do sequenciamento do gene de resistência *hDHFR* (*human dihydrofolate reductase*). Somente o códon 9 da sequência possui uma mutação silenciosa (destacado em vermelho), portanto, possivelmente não compromete a sua função.

Apesar disso, outras mutações nas regiões promotoras e terminadoras foram observadas (**Tabela 1**). Pelo fato de serem regiões repetitivas extremamente ricas em A e T (acima de 80%), essas mutações são comuns. As regiões UTR (do inglês, *untranslated region*) são por definição regiões não-codantes para uma molécula de mRNA, portanto, torna-se difícil avaliar se nessas regiões promotoras e terminadoras, essas mutações podem dificultar a seleção dos parasitas mutantes, sobretudo levando em consideração que é mais desafiador manter a seleção dos parasitas que possuem plasmídeos de expressão na forma episomal (Waterkeyn et al., 1999; Crabb et al., 2004).

**Tabela 2. Mutações detectadas por sequenciamento dos plasmídeos pCC1.**

Regiões	Mutações				
	pCC1-empty	pCC1-HA <sub>(cito)</sub> -APEX2	pCC1- SP <sub>(ACP)</sub> -HA-APEX2	pCC1- SP <sub>(RAP1)</sub> -HA-APEX2	pCC1-SP <sub>(TRXR)</sub> -HA-APEX2
<b>3'UTR <i>hrp2</i></b>	mismatches: posições 82 e 219	mismatches: posições 82 e 219	mismatches: posições 82 e 219	mismatches: posições 82 e 219	mismatches: posições 82 e 219
<b>3'UTR <i>PbDT</i></b>	mismatches: posições 284, 392 e 507-511	mismatches: posições 284, 392 e 507-511	mismatches: posições 284, 392 e 507-511	mismatches: posições 284, 392 e 507-511	mismatches: posições 284, 392 e 507-511
<b>5' <i>CAM</i></b>	Diversos mismatches*	Diversos mismatches*	Diversos mismatches*	Diversos mismatches*	Diversos mismatches*
<b><i>hDHFR</i></b>	mutação silenciosa no códon 9	mutação silenciosa no códon 9	mutação silenciosa no códon 9	mutação silenciosa no códon 9	mutação silenciosa no códon 9
<b>5' <i>hsp86</i></b>	mismatches: posições 463, 526,551, 590 e 686	mismatches: posições 251, 463, 526,551, 590 e 686	mismatches: posições 251, 463, 526,551, 590 e 686	mismatches: posições 251, 463, 526,551, 590 e 686	mismatches: posições 251, 463, 526,551, 590 e 686

\*Os histogramas dos sequenciamentos da região 5' *CAM* apresentou uma baixa qualidade por ser uma região rica em A+T. Desse modo, não foi possível apontar *mismatches* específicos.

### 7.3. Viabilidade de diferentes linhagens de *P. falciparum* na presença da WR99210 por ensaio de [<sup>3</sup>H] hipoxantina

O uso da droga anti-folato WR99210 das marcas Sigma-Aldrich e Jacobus Pharmaceuticals Incorporation foram utilizadas conforme descrito acima. A concentração mínima inibitória de 50% (IC<sub>50</sub>) foi determinada por uma regressão não-linear e analisados no software GraphPad Prism (GraphPad Software, CA). Como suspeitado, a droga proveniente da Sigma-Aldrich não inviabilizou o crescimento dos parasitas de *P. falciparum* das linhagens 3D7, NF54 e FcB1 na concentração esperada (**Figura 21**), portanto, não é viável para ser utilizar na seleção dos parasitas mutantes com a marca de seleção *hDHFR*.

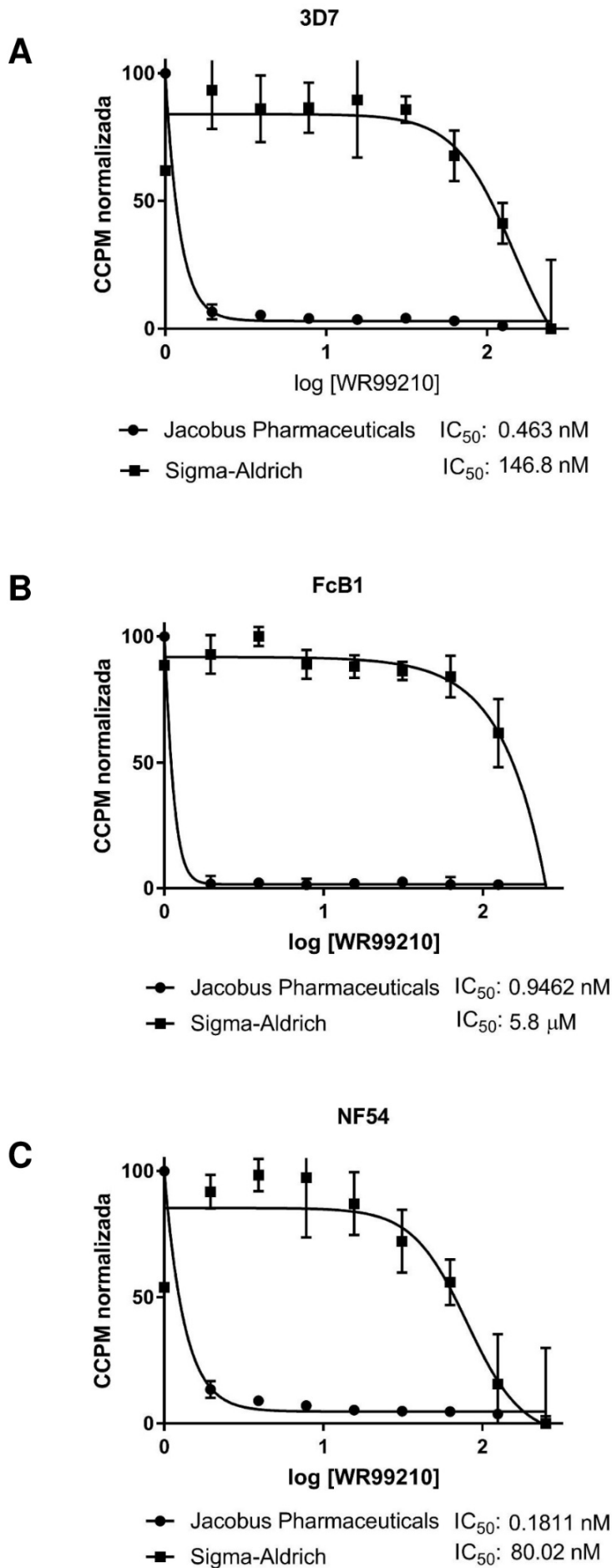


**Figura 21. Curvas-resposta de  $IC_{50}$  em diferentes linhagens de *P. falciparum* na presença da WR99210 das marcas Jacobus Pharmaceuticals Inc.\* e Sigma-Aldrich. (A) Curva de  $IC_{50}$  para *P. falciparum* linhagem 3D7. (B) Curva de  $IC_{50}$  para *P. falciparum* linhagem FcB1. (C) Curva de  $IC_{50}$  para *P. falciparum* linhagem NF54. As curvas de  $IC_{50}$  foram realizadas pelo método de [ $^3$ H] hipoxantina. Uma diluição seriada da droga anti-folato WR99210 (em escala nM: 250; 125; 62,5; 31,25; 15,63; 7,81; 3,90; 1,95; 0,98; 0,49; 0,24 e 0,12) das marcas Jacobus Pharmaceuticals Inc.\* (●) e Sigma-Aldrich (■) foi realizada para cada linhagem de *P. falciparum*. O controle negativo contendo apenas DMSO, para cada linhagem também foi realizado.**

## 7.4. Expressão heteróloga e purificação da proteína recombinante APEX2

A expressão da proteína recombinante, seguida da purificação utilizando a resina de níquel His-Select HF Nickel (Sigma-Aldrich) com um gradiente de imidazol (Sigma-Aldrich), foi realizada conforme descrito acima. Um SDS-PAGE foi realizado utilizando o *input* (extrato total), *flowthrough* (não-ligado a resina), as frações da eluição do gradiente de imidazol (5 mM, 20 mM, 50 mM, 100 mM, 200 mM e 500 mM), e, o gradiente do controle positivo, BSA (20 µg, 2 µg, 200 ng, 20 ng, 2 ng e 200 pg) (Figura 22). As frações da eluição da APEX2 recombinante eluída nas frações de 20mM foram utilizadas para a produção de anticorpos policlonais, por serem as frações com maior expressão da proteína recombinante, e com um baixo *background* de contaminantes.

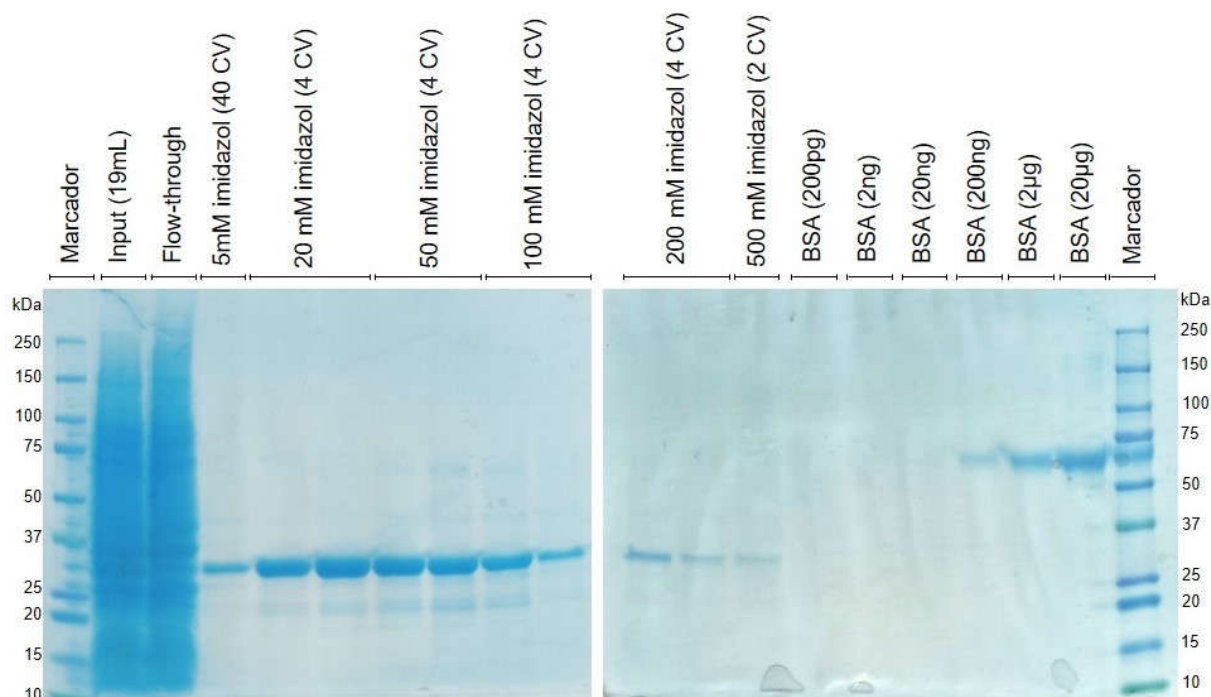


**Figura 22. Expressão e purificação da proteína recombinante APEX2.** O vetor pET100/D-TOPO®, contendo a sequência da 6xHis-APEX2 modificada foi transformado em bactérias competentes *E. coli* linhagem Rosetta™(DE3)pLyS. A lise se deu por BugBuster (Merck-Millipore) e sonicação. O extrato total foi aplicado como *input*, seguida das frações de eluição com imidazol (5-500mM). Como controle positivo do SDS-PAGE, um gradiente de BSA (variando entre 20 µg- 200 pg) também foi aplicado, bem como, o extrato não-ligado (*flowthrough*). As frações de 20mM de imidazol foram utilizadas para a produção de anticorpos policlonais anti-APEX2.

## 7.5. Validação dos soros anti-APEX2 por Western-blot

Os camundongos da linhagem BALB/c foram imunizados com injeções intraperitoneais utilizando adjuvante de Freund completo e incompleto (Sigma-Aldrich), conforme descrito acima. Os soros anti-APEX2 foram obtidos 60 dias após a

primeira imunização. Através do Western-blot foi possível observar que os soros anti-APEX2 de todos os animais utilizados, marcaram bem em todas as titulações utilizadas (1:200, 1:1.000 e 1:5.000) contra a proteína recombinante (**Figura 23**). Além disso, o soro pré-imune (controle negativo) não demonstrou nenhuma marcação inespecífica, sugerindo que os animais não foram expostos a nenhuma situação em que uma possível reação imune cruzada tenha acontecido.

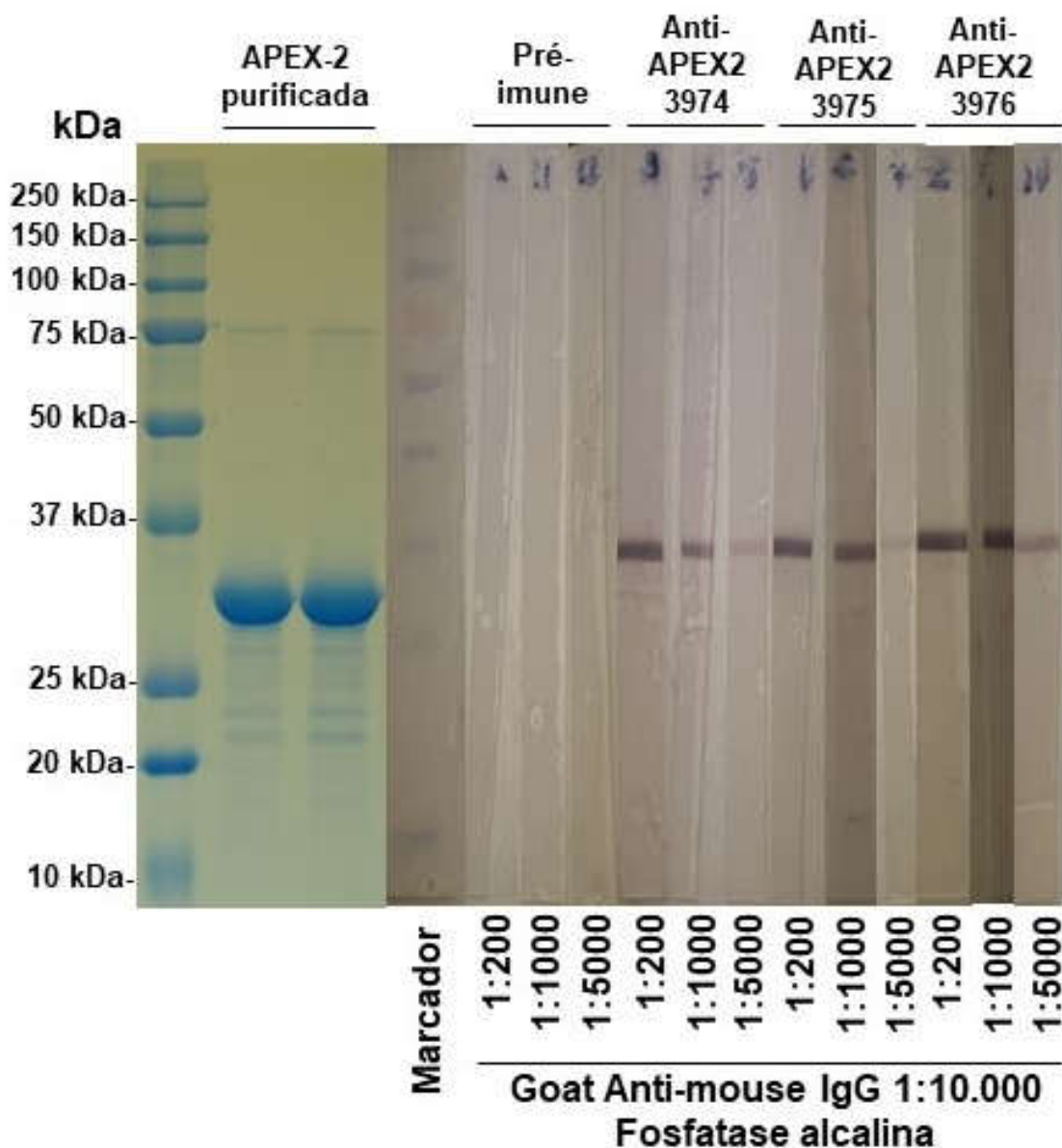


**Figura 23. Validação do soro anti-APEX2 por Western-blot.** Os camundongos da linhagem BALB/c foram imunizados conforme descrito. Os soros dos animais 3974, 3975 e 3976 foram obtidos após 60 dias da primeira imunização. Uma titulação de 1:200, 1:1.000 e 1:5.000 foi realizada para o soro de cada animal contra a proteína APEX2 recombinante. O controle pré-imune também seguiu a mesma titulação. O anticorpo secundário acoplado a fosfatase alcalina foi utilizado na titulação 1:10.000. O Western-blot foi revelado com o uso do substrato BCIP/NBT.

## 7.6. Obtenção dos mutantes de *P. falciparum* expressando pCC1-SP<sub>(cito, acp, rap1, trxr)</sub>-HA-APEX2

Os mutantes inicialmente obtidos não apresentavam nenhuma expressão da APEX2, pois estávamos utilizando a droga WR99210 proveniente da Sigma-Aldrich. Como demonstrado na **Figura 21**, a WR99210 desta marca não é adequada para selecionar *P. falciparum*, devido a sua baixíssima eficácia. Somente após a padronização da metodologia de transfecção com o uso da plataforma Amaxa II (Lonza) e com o uso da droga WR99210 proveniente da Jacobus Pharmaceuticals Inc.\* na quantidade de 1,25 nM, foi possível obter parasitas mutantes após 3-4 semanas pós-transfecção. Até o momento, obtivemos parasitas transfectados de forma epissomal apenas para as construções pCC1-HA<sub>(cito)</sub>-APEX2 (parasitas expressando APEX2 citosólica), pCC1- SP<sub>(RAP1)</sub>-HA-APEX2 (parasitas expressando APEX2 endereçada às roptrias) e pCC1-SP<sub>(TRXR)</sub>-HA-APEX2 (parasitas expressando APEX2 endereçada à mitocôndria) (**Figura 24**). As tentativas para obter parasitas que expressam APEX2 endereçada ao apicoplasto (construção pCC1-SP<sub>(ACP)</sub>-HA-APEX2) estão em andamento.

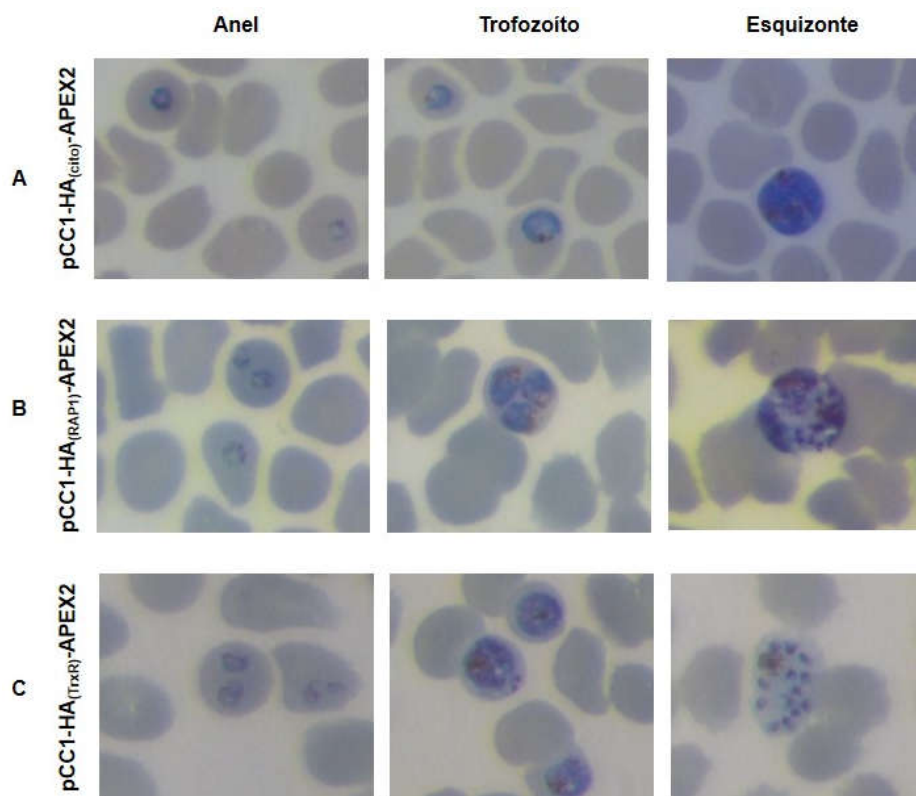


**Figura 24.** Micrografia das linhagens de *P. falciparum* transfectadas obtidas até o momento. **(A)** pCC1-HA<sub>(cito)</sub>-APEX2 (parasitas expressando APEX2 citosólica). **(B)** pCC1- SP<sub>(RAP1)</sub>-HA-APEX2 (parasitas expressando APEX2 endereçada às roptrias). **(C)** pCC1-SP<sub>(TRXR)</sub>-HA-APEX2 (parasitas expressando APEX2 endereçada à mitocôndria). As formas de anel (painéis à esquerda), trofozoíto (painéis do meio) e esquizonte (painéis à direita) também são mostrados.

A circular inset showing a microscopic view of numerous red blood cells (erythrocytes) against a dark background. The cells are biconcave and appear as reddish-orange discs. The text is overlaid on the right side of this circular area.

V - CONCLUSÕES  
E PERSPECTIVAS

## V. CONCLUSÕES E PERSPECTIVAS

A malária é certamente uma doença tropical que apresenta inúmeros desafios para a saúde pública mundial. A sua distribuição cosmopolita a torna um desafio para muitos países, onde o *P. falciparum*, a espécie mais virulenta é endêmica. Dentro deste contexto, a região da África Subsaariana é a que mais sofre com esta doença (Global Malaria Programme: WHO Global, 2020). As crianças abaixo de 5 anos e as mulheres grávidas são os grupos que mais sofrem, devido à inerente vulnerabilidade socioeconômica desta região (Tusting et al., 2013; Carrasco-Escobar et al., 2021). Além dos problemas socioeconômicos que afetam diretamente a população dessa região, a falta de instrução destas pessoas, decorrente deste problema, muitas vezes é um fator agravante quanto à busca por tratamento e prevenção contra a malária (Tusting et al., 2016; Degarege et al., 2019).

Outros fatores que agravam este cenário estão relacionados com o próprio agente etiológico endêmico desta região, o *P. falciparum*, bem como os vetores do gênero *Anopheles* spp. Ambos são totalmente adaptados ao hospedeiro humano, e as estratégias atualmente utilizadas com a finalidade de erradicá-los tem mostrado resistência. Por exemplo, o uso da combinação de derivados da artemisinina com outras drogas antimaláricas (ou ACTs), considerada a estratégia de linha de frente para os casos de malária não-complicada e severa (Global Malaria Programme: WHO Global, 2020), já vem apresentando alguns casos de resistência, sobretudo em países asiáticos, tais como Camboja (Noedl et al., 2008, 2010; Arieu et al., 2014; Straimer et al., 2015), Myanmar (Nyunt et al., 2017; He et al., 2019) e Vietnã (Thanh et al., 2017; Bui et al., 2020). Ainda mais agravante, alguns relatos de resistência às drogas parceiras utilizadas como coadjuvantes no tratamento baseado em ACTs tem sido observados (Blasco et al., 2017; Adebayo et al., 2020; Ippolito et al., 2021).

Nos países da América do Sul, como o Brasil, a espécie *P. vivax* é responsável pela maior parte dos casos reportados. Embora considerada uma forma mais leve da doença, alguns relatos de óbitos decorrentes da malária *vivax* já foram observados (Oliveira-Ferreira et al., 2010). A linha de frente para o tratamento deste tipo malária se dá pelo uso de ACTs, entretanto, relatos de resistência são igualmente observados (Chehuan et al., 2013; Marques et al., 2014). Em contrapartida, o controle vetorial também tem sido um desafio em muitos países acometidos pela malária. O sutil, porém, crescente número de mosquitos do gênero *Anopheles* spp. resistentes aos inseticidas utilizados nos mosquiteiros (ou ITN) e na pulverização residual interna (ou



IRS) tem sido igualmente reportados (Killeen et al., 2013; Global Malaria Programme: WHO Global, 2020). Desse modo, estudos que possibilitem um melhor entendimento tanto do agente etiológico quanto do vetor anofelino são absolutamente necessários.

A capacidade do parasita de remodelar os eritrócitos do hospedeiro, a fim de permitir a sua sobrevivência é uma característica singular dos parasitas do gênero *Plasmodium* spp. No momento da sua invasão, algumas proteínas do complexo apical, exercem papéis fundamentais na formação do *tight/moving junction*, tais como as proteínas do complexo RON-AMA1 e complexo Rh. Este contato inicial, permite os parasitas lançarem as proteínas presentes nas estruturas do complexo apical (roptrias, micronemas e grânulos densos), dentro do vacúolo parasitóforo em formação dentro da célula hospedeira (Proellocks et al., 2010; Besteiro et al., 2011; Counihan et al., 2013). Após a invasão, o parasita necessita ainda impor outras modificações para exportar proteínas sintetizadas *de novo* ou que formarão outros complexos de transporte (p. ex. translocon PTEX, *Maurer's clefts*, *J-dots*, complexo EPIC e complexo RhopH/CLAG), para conduzir muitas dessas proteínas até a membrana da célula hospedeira ou para meio extracelular, por meio de vesículas exosoma-*like* (Vincensini et al., 2008; Koning-Ward et al., 2009; Külzer et al., 2010; Regev-Rudzki et al., 2013; Batinovic et al., 2017).

O(s) processo(s) pelo(s) qual(is) as proteínas são exportadas até a membrana e/ou meio extracelular da célula hospedeira estão de longe, por ser(em) totalmente compreendidos. Muitas evidências tem mostrado que o translocon PTEX, inicialmente descrito por translocar proteínas contendo o motivo consenso PEXEL (RxLx[E/Q/D]) (Koning-Ward et al., 2009; Bullen et al., 2012; Boddey et al., 2016), não seja o único meio de utilizado para que as proteínas exportadas sejam translocadas. Mesmo algumas proteínas contendo PEXEL, já foram relatadas por serem encontradas em vesículas exosoma-*like* (Mantel et al., 2013; Regev-Rudzki et al., 2013; Sampaio et al., 2018), ou ainda, PNEPs, translocadas através do complexo EPIC (Batinovic et al., 2017). Dentro deste contexto, KAHRP juntamente com *PfEMP1*, ocupam um papel de grande relevância na virulência do *P. falciparum*.

Neste trabalho, estabelecemos pela primeira vez o uso conjunto de uma tríade de tecnologias: a edição genômica por CRISPR-Cas9, a abordagem de marcação por proximidade baseada em APEX2 e espectrometria de massas *shotgun label-free*. Com o uso do gene *kahrp*, amplamente conhecido por ser facilmente manipulado, (Ghorbal et al., 2014; Wagner et al., 2014), realizamos a inserção do gene da APEX2 na cauda 3' da KAHRP por CRISPR-Cas9, com a produção de uma proteína

quimérica, capaz de realizar a marcação das proteínas vizinhas parceiras de KAHRP por biotilação. Através dos ensaios de Western-blot, estreptavidina-blot e imunofluorescência, observamos uma evidente co-localização entre as proteínas biotiladas e a proteína MAHRP, marcada por anticorpos, conhecida por integrar as *Maurer's clefts* (MCs) de *P. falciparum* (Spycher et al., 2003, 2006, 2008), sugerindo que a proteína quimérica KAHRP segue um tráfego de exportação através das MCs, conforme previamente reportado (Wickham et al., 2001), potencialmente marcando as proteínas vizinhas que interajam com ela.

As análises proteômicas por espectrometria de massas *shotgun label-free* revelaram ainda que, a marcação dos resíduos de tirosina (Y) são abundantemente modificados pela biotina-fenol através das análises dos peptídeos utilizados para as identificações. A partir dos 240 peptídeos não-redundantes, um total de 208 grupos de proteínas provenientes da fração solúvel do parasita e 10 grupos de proteínas provenientes do humano foram identificadas. Dentre as proteínas do parasita identificadas, observamos a presença de algumas já conhecidas, por estarem envolvidas no processo de remodelamento da célula hospedeira, tais como GBP130, RESA, membros do grupo PHISTb e proteínas dos complexos: RhopH/CLAG (RhopH1/CLAG3.1, RhopH2 e RhopH3); e, translocon PTEX (PTEX88 e 150) (revisado em Boddey & Cowman, 2013; Spillman et al., 2015).

Em comparação a outra metodologia de marcação por proximidade, baseada no uso da biotina-ligase modificada de *E. coli* (BirA\*), a BioID, a vantagem do uso da APEX2 está baseada na sua rapidez e precisão na biotilação das proteínas (Rees et al., 2015). Alguns estudos que utilizaram ambas as metodologias, APEX2 e BioID, em *T. gondii*, ainda relataram que observaram uma superioridade da especificidade de marcação da APEX2 em relação a BioID (Seidi et al., 2018; Pan et al., 2019). Dentro deste contexto, ainda foi realizado neste trabalho a construção de plasmídeos de expressão episomal da APEX2, a fim de marcar alguns compartimentos pouco caracterizados a nível proteômico em *P. falciparum*. Duas organelas de origem endossimbiótica, o apicoplasto e a mitocôndria, que aparentam possuir uma inter-relação metabólica muito evidente (Ralph et al., 2004; Lim & McFadden, 2010), e, as roptrias, que como já apontado, possuem um papel crucial nos processos de invasão e pós-invasivos em *P. falciparum* (Proellocks et al., 2010; Besteiro et al., 2011; Counihan et al., 2013), foram utilizadas como alvos do estudo.

Os ensaios de transfecção inicialmente realizados, utilizando os vetores devidamente sequenciados: pCC1-HA<sub>(cito)</sub>-APEX2 (APEX2 de expressão citosólica),

pCC1-SP<sub>(ACP)</sub>-HA-APEX2 (APEX2 endereçada ao apicoplasto), pCC1-SP<sub>(RAP1)</sub>-HA-APEX2 (APEX2 endereçada às roptrias) e pCC1-SP<sub>(TIRX)</sub>-HA-APEX2 (APEX2 endereçada à mitocôndria), não foram promissores. Não foi possível observar a expressão da APEX2 em nenhuma das linhagens de parasitas transfectados. Além do fato de ser uma metodologia de baixíssimo rendimento, sobretudo em linhagens portando vetores episomais (Waterkeyn et al., 1999; Crabb et al., 2004), o uso da droga anti-folato amplamente utilizada, a WR99210, deve ser apenas utilizada da marca Jacobus Pharmaceuticals Inc\*. Através do ensaio de [<sup>3</sup>H] hipoxantina, observamos a total ineficácia da droga adquirida pela Sigma-Aldrich, inicialmente utilizada para selecionar os parasitas. Por esta razão, não foi possível validar nenhuma linhagem dos parasitas transfectados. Mais recentemente, um estudo estrutural comparando a WR99210 de ambas as marcas, demonstrou que, apesar de apresentar a mesma massa molecular, a isomeria da droga proveniente da Sigma-Aldrich é diferente daquela apresentada pela WR99210 da Jacobus Pharmaceuticals Inc.\*, portanto, sua ineficácia pode ser explicada por causa disso (Remcho et al., 2020).

Após a padronização do protocolo de transfecção utilizando PEMS (Fang et al., 2018; Hoeijmakers et al., 2019; Jonscher et al., 2019; Wilde et al., 2019; Birnbaum et al., 2020), utilizando a plataforma Amaxa II Nucleofector II AAD-1001N (Lonza), até então, não adequada para transfecções em *P. falciparum* (vide recomendação do *datasheet* do fabricante), obtivemos linhagens de parasitas transfectados, com o uso de 1,25 nM de WR99210 (Jacobus Pharmaceuticals Inc.\*). Possivelmente, o uso de uma quantidade inferior ao utilizado pelos trabalhos, deve-se ao fato de que mutações nas regiões promotoras e/ou terminadoras em nossos plasmídeos foram observados por sequenciamento, portanto, uma pressão seletiva superior poderá matar os parasitas antes de selecioná-los. Até o momento, obtivemos parasitas transfectados com pCC1-HA<sub>(cito)</sub>-APEX2, pCC1-SP<sub>(RAP1)</sub>-HA-APEX2 e pCC1-SP<sub>(TIRX)</sub>-HA-APEX2. Os ensaios para realizar uma próxima transfecção, a fim de obter parasitas transfectados com pCC1-SP<sub>(ACP)</sub>-HA-APEX2, além dos ensaios de validação por Western-blot, estreptavidina-blot e imunofluorescência estão em andamento.

Durante as análises do trabalho sobre as proteínas vizinhas parceiras de KAHRP, um evento curioso nos chamou muita atenção: uma contagem considerável de proteínas/peptídeos não-biotinilados identificados por nossas análises proteômicas. Este padrão de identificação em outros trabalhos utilizando como modelo, diferentes linhagens de células de mamífero (p. ex. HEK293T, U2OS e HeLa)

já foi observado (Rhee et al., 2013; Lee et al., 2016; Lobingier et al., 2017). Alguns trabalhos sugerem que, a quantidade desproporcional de material inicialmente utilizado juntamente com uma quantidade desproporcional das *beads* revestidas com estreptavidina, podem ocasionar em ligações não-específicas de proteínas não-biotiniladas (Schiapparelli et al., 2014; Hung et al., 2016). Além disso, ainda propõe-se que, as lavagens são etapas absolutamente essenciais para retirar ligantes não-específicos daquelas proteínas biotiniladas parcialmente enoveladas, mesmo que, em uma situação desnaturante (Hung et al., 2016).

Possivelmente, comparando-se as células de mamíferos e os protozoários, algumas considerações devem ser feitas antes de realizar o enriquecimento de proteínas biotiniladas pela APEX2. Primeiramente, deve-se entender que a quantidade de proteínas (biotiniladas ou não-biotiniladas) obtidas são proporcionais à biomassa de cada tipo de célula, portanto, a quantidade de proteínas biotiniladas proveniente dos protozoários será infinitamente menor comparando-se com àquelas das células de mamíferos. Ainda, dois pontos relevantes são: (i) o tempo de incubação das amostras de proteínas totais após o ensaio de biotinylation com as *beads* revestidas com estreptavidina, e; (ii) os tampões utilizados para as lavagens das proteínas biotiniladas. Alguns trabalhos que utilizaram APEX2 para marcar algumas estruturas em *T. gondii* e *T. brucei*, utilizaram tempos superiores de incubação com as *beads* revestidas com estreptavidina ou tampões contendo uma quantidade alta de agentes caotrópicos e detergentes, tais como ureia e SDS (Seidi et al., 2018; Pan et al., 2019; Vélez-Ramírez et al., 2021).

Um gargalo adicional que ainda necessita ser superado é a eluição dos peptídeos/proteínas biotiniladas. Atualmente, algumas ferramentas já se encontram disponíveis para este fim, tais como: BioSITE (*Biotinylation Site Identification Technology*), DiDBiT (*Direct Detection of Biotin-containing Tags*) e AVIDITY (*streptavidin binding capacity*) (Schiapparelli et al., 2014; Kim et al., 2018; Renuse et al., 2020; Berg Luecke & Gundry, 2021), entretanto, sua viabilidade para ser utilizada em protozoários necessita ser avaliada. Apesar de termos observado uma coerência dos nossos dados proteômicos das proteínas vizinhas parceiras de KAHRP, através das predições *in silico* e da literatura, ainda necessita ser avaliado se todas as proteínas identificadas de fato interagem com a KAHRP. Desse modo, muitas dúvidas ainda permanecem em aberto quanto ao envolvimento da KAHRP e estas proteínas potencialmente parceiras no exportoma de *P. falciparum*. De forma geral, possivelmente o uso da APEX2 poderá começar a ser empregada a partir de agora

como uma ferramenta mais acessível, para desvendar os mistérios inerentes da biologia de *P. falciparum*.

A circular inset showing a microscopic view of numerous red blood cells (erythrocytes) against a dark background. The cells are biconcave and appear as reddish-orange discs. The text is overlaid on this circular area.

## VI - REFERÊNCIAS BIBLIOGRÁFICAS

## vi. REFERÊNCIAS BIBLIOGRÁFICAS

- Accrombessi, M., Ouédraogo, S., Agbota, G. C., Gonzalez, R., Massougbodji, A., Menéndez, C., et al. (2015). Malaria in pregnancy is a predictor of infant haemoglobin concentrations during the first year of life in Benin, West Africa. *PLoS One* 10, 1–17. doi:10.1371/journal.pone.0129510.
- Adebayo, J. O., Tijjani, H., Adegunloye, A. P., Ishola, A. A., Balogun, E. A., and Malomo, S. O. (2020). Enhancing the antimalarial activity of artesunate. *Parasitol. Res.* 119, 2749–2764. doi:10.1007/s00436-020-06786-1.
- Ahmad, M., Manzella-Lapeira, J., Saggi, G., Ito, D., Brzostowski, J. A., and Desai, S. A. (2020). Live-Cell FRET Reveals that Malaria Nutrient Channel Proteins CLAG3 and RhoPH2 Remain Associated throughout Their Tortuous Trafficking. *MBio* 11, 1–14.
- Ahmadpour, E., Foroutan-Rad, M., Majidiani, H., Moghaddam, S. M., Hatam-Nahavandi, K., Hosseini, S. A., et al. (2019). Transfusion-transmitted malaria: A systematic review and meta-analysis. *Open Forum Infect. Dis.* 6, 1–8. doi:10.1093/ofid/ofz283.
- Alves, F. P., Durlacher, R. R., Menezes, M. J., Krieger, H., Pereira da Silva, L. H., and Camargo, E. P. (2002). High prevalence of asymptomatic *Plasmodium vivax* and *Plasmodium falciparum* infections in native Amazonian populations. *Am. J. Trop. Med. Hyg.* 66, 641–648. doi:10.4269/ajtmh.2002.66.641.
- Ariey, F., Witkowski, B., Amaratunga, C., Beghain, J., Langlois, A. C., Khim, N., et al. (2014). A molecular marker of artemisinin-resistant *Plasmodium falciparum* malaria. *Nature* 505, 50–55. doi:10.1038/nature12876.
- Arnold, M. S. J., Engel, J. A., Chua, M. J., Fisher, G. M., Skinner-Adams, T. S., and Andrews, K. T. (2016). Adaptation of the [3 H]Hypoxanthine Uptake Assay for In Vitro-Cultured *Plasmodium knowlesi* Malaria Parasites Megan. *Antimicrob. Agents Chemother.* 60, 4361–4363. doi:10.1128/AAC.02948-15.Address.
- Baker, D. A. (2010). Malaria gametocytogenesis. *Mol. Biochem. Parasitol.* 172, 57–65. doi:10.1016/j.molbiopara.2010.03.019.
- Baldi, D. L., Andrews, K. T., Waller, R. F., Roos, D. S., Howard, R. F., Crabb, B. S., et al. (2000). RAP1 controls rhopty targeting of RAP2 in the malaria parasite *Plasmodium falciparum*. *EMBO J.* 19, 2435–2443. doi:10.1093/emboj/19.11.2435.
- Baldi, D. L., Good, R., Duraisingh, M. T., Crabb, B. S., and Cowman, A. F. (2002).

- Identification and disruption of the gene encoding the third member of the low-molecular-mass rhoptry complex in *Plasmodium falciparum*. *Infect. Immun.* 70, 5236–5245. doi:10.1128/IAI.70.9.5236-5245.2002.
- Barbosa, S., Gozze, A. B., Lima, N. F., Batista, C. L., Bastos, M. da S., Nicolete, V. C., et al. (2014). Epidemiology of Disappearing *Plasmodium vivax* Malaria: A Case Study in Rural Amazonia. *PLoS Negl. Trop. Dis.* 8. doi:10.1371/journal.pntd.0003109.
- Barrangou, R., Fremaux, C., Deveau, H., Richards, M., Boyaval, P., Moineau, S., et al. (2007). CRISPR Provides Acquired Resistance Against Viruses in Prokaryotes. *Science (80-. )*. 315, 1709–1712. doi:10.1126/science.1138140.
- Batinovic, S., McHugh, E., Chisholm, S. A., Matthews, K., Liu, B., Dumont, L., et al. (2017). An exported protein-interacting complex involved in the trafficking of virulence determinants in *Plasmodium*-infected erythrocytes. *Nat. Commun.* 8, 1–14. doi:10.1038/ncomms16044.
- Baum, J., Chen, L., Healer, J., Lopaticki, S., Boyle, M., Triglia, T., et al. (2009). Reticulocyte-binding protein homologue 5 - An essential adhesin involved in invasion of human erythrocytes by *Plasmodium falciparum*. *Int. J. Parasitol.* 39, 371–380. doi:10.1016/j.ijpara.2008.10.006.
- Bengtsson, N. E., Hall, J. K., Odom, G. L., Phelps, M. P., Andrus, C. R., Hawkins, R. D., et al. (2017). Muscle-specific CRISPR/Cas9 dystrophin gene editing ameliorates pathophysiology in a mouse model for Duchenne muscular dystrophy. *Nat. Commun.* 8, 16007. doi:10.1038/ncomms16007.
- Berg Luecke, L., and Gundry, R. L. (2021). Assessment of Streptavidin Bead Binding Capacity to Improve Quality of Streptavidin-based Enrichment Studies. *J. Proteome Res.* 20, 1153–1164. doi:10.1021/acs.jproteome.0c00772.
- Besteiro, S., Dubremetz, J. F., and Lebrun, M. (2011). The moving junction of apicomplexan parasites: A key structure for invasion. *Cell. Microbiol.* 13, 797–805. doi:10.1111/j.1462-5822.2011.01597.x.
- Bezerra, J. M. T., Barbosa, D. S., Martins-Melo, F. R., Werneck, G. L., Braga, É. M., Tauil, P. L., et al. (2020). Changes in malaria patterns in Brazil over 28 years (1990-2017): Results from the Global Burden of Disease Study 2017. *Popul. Health Metr.* 18. doi:doi.org/10.21203/rs.3.rs-27809/v1.
- Bhagavathula, A. S., Elnour, A. A., and Shehab, A. (2016). Alternatives to currently used antimalarial drugs: In search of a magic bullet. *Infect. Dis. Poverty* 5, 1–12. doi:10.1186/s40249-016-0196-8.



- Bhattacharjee, S., Ooij, C. Van, Balu, B., Adams, J. H., and Haldar, K. (2008). Maurer's clefts of *Plasmodium falciparum* are secretory organelles that concentrate virulence protein reporters for delivery to the host erythrocyte. *Blood* 111, 2418–2427. doi:10.1182/blood-2007-09-115279.The.
- Bhattacharjee, S., Stahelin, R. V., Speicher, K. D., Speicher, D. W., and Haldar, K. (2012). Endoplasmic reticulum PI(3)P lipid binding targets malaria proteins to the host cell. *Cell* 148, 201–212. doi:10.1016/j.cell.2011.10.051.
- Birnbaum, J., Scharf, S., Schmidt, S., Jonscher, E., Maria Hoeijmakers, W. A., Flemming, S., et al. (2020). A Kelch13-defined endocytosis pathway mediates artemisinin resistance in malaria parasites. *Science* (80- ). 367, 51–59. doi:10.1126/science.aax4735.
- Blasco, B., Leroy, Di., and Fidock, D. A. (2017). Antimalarial drug resistance: Linking *Plasmodium falciparum* parasite biology to the clinic. *Nat. Med.* 23, 917–928. doi:10.1038/nm.4381.
- Boddey, J. A., and Cowman, A. F. (2013). *Plasmodium* Nesting: Remaking the Erythrocyte from the Inside Out. *Annu. Rev. Microbiol.* 67, 243–269. doi:10.1146/annurev-micro-092412-155730.
- Boddey, J. A., Hodder, A. N., Günther, S., Gilson, P. R., Patsiouras, H., Kapp, E. A., et al. (2010). An aspartyl protease directs malaria effector proteins to the host cell. *Nature* 463, 627–631. doi:10.1038/nature08728.
- Boddey, J. A., O'Neill, M. T., Lopaticki, S., Carvalho, T. G., Hodder, A. N., Nebl, T., et al. (2016). Export of malaria proteins requires co-translational processing of the PEXEL motif independent of phosphatidylinositol-3-phosphate binding. *Nat. Commun.* 7. doi:10.1038/ncomms10470.
- Bolotin, A., Quinquis, B., Sorokin, A., and Dusko Ehrlich, S. (2005). Clustered regularly interspaced short palindrome repeats (CRISPRs) have spacers of extrachromosomal origin. *Microbiology* 151, 2551–2561. doi:10.1099/mic.0.28048-0.
- Botté, C. Y., Dubar, F., McFadden, G. I., Maréchal, E., and Biot, C. (2012). *Plasmodium falciparum* Apicoplast Drugs: Targets or Off-Targets? *Chem. Rev.* 112, 1269–1283. doi:10.1021/cr200258w.
- Boucher, M. J., Ghosh, S., Zhang, L., Lal, A., Jang, S. W., Ju, A., et al. (2018). Integrative proteomics and bioinformatic prediction enable a high-confidence apicoplast proteome in malaria parasites. *PLoS Biol.* 16, 1–29. doi:10.1371/journal.pbio.2005895.

- Boyle, M. J., Wilson, D. W., Richards, J. S., Riglar, D. T., Tetteh, K. K. A., Conway, D. J., et al. (2010). Isolation of viable *Plasmodium falciparum* merozoites to define erythrocyte invasion events and advance vaccine and drug development. *Proc. Natl. Acad. Sci. U. S. A.* 107, 14378–14383. doi:10.1073/pnas.1009198107.
- Branon, T. C., Bosch, J. A., Sanchez, A. D., Udeshi, N. D., Svinkina, T., Carr, S. A., et al. (2018). Efficient proximity labeling in living cells and organisms with TurboID. *Nat. Biotechnol.* 36, 880–898. doi:10.1038/nbt.4201.
- Briand, V., Badaut, C., and Cot, M. (2009). Placental malaria, maternal HIV infection and infant morbidity. *Ann. Trop. Paediatr.* 29, 71–83. doi:10.1179/146532809X440699.
- Brickley, E. B., Spottiswoode, N., Kabyemela, E., Morrison, R., Kurtis, J. D., Wood, A. M., et al. (2016). Cord blood hepcidin: Cross-sectional correlates and associations with anemia, malaria, and mortality in a tanzanian birth cohort study. *Am. J. Trop. Med. Hyg.* 95, 817–826. doi:10.4269/ajtmh.16-0218.
- Brock, P. M., Fornace, K. M., Parmiter, M., Cox, J., Drakeley, C. J., Ferguson, H. M., et al. (2016). *Plasmodium knowlesi* transmission: Integrating quantitative approaches from epidemiology and ecology to understand malaria as a zoonosis. *Parasitology* 143, 389–400. doi:10.1017/S0031182015001821.
- Brouns, S. J. J., Jore, M. M., Lundgren, M., Westra, E. R., Slijkhuis, R. J. H., Snijders, A. P. L., et al. (2008). Small CRISPR RNAs Guide Antiviral Defense in Prokaryotes. *Science (80-. )*. 321, 960–964.
- Bui, P. Q., Huynh, Q. H., Tran, D. T., Le, D. T., Nguyen, T. Q., Truong, H. Van, et al. (2020). Pyronaridine-artesunate Efficacy and Safety in Uncomplicated *Plasmodium falciparum* Malaria in Areas of Artemisinin-resistant *Falciparum* in Viet Nam (2017-2018). *Clin. Infect. Dis.* 70, 2187–2195. doi:10.1093/cid/ciz580.
- Bullen, H. E., Charnaud, S. C., Kalanon, M., Riglar, D. T., Dekiwadia, C., Kangwanransan, N., et al. (2012). Biosynthesis, localization, and macromolecular arrangement of the *Plasmodium falciparum* translocon of exported proteins (PTEX). *J. Biol. Chem.* 287, 7871–7884. doi:10.1074/jbc.M111.328591.
- Cabral, P. H. O., Andrade, S. D., Alecrim, W. D., Alecrim, M. G. C., and Lacerda, M. V. G. (2006). Malaria and sickle cell anemia: Report of complications and clinical management of three patients in a highly endemic area FOR *Plasmodium vivax* malaria in the Brazilian Amazon. *Case Reports Clin. Pract. Rev.* 7, 220–223.
- Carlos, B. C., Rona, L. D. P., Christophides, G. K., and Souza-Neto, J. A. (2019). A

- comprehensive analysis of malaria transmission in Brazil. *Pathog. Glob. Health* 113, 1–13. doi:10.1080/20477724.2019.1581463.
- Carrasco-Escobar, G., Fornace, K., and Benmarhnia, T. (2021). Mapping socioeconomic inequalities in malaria in Sub-Saharan African countries. *Sci. Rep.* 11, 1–8. doi:10.1038/s41598-021-94601-x.
- Chang, H. H., Falick, A. M., Carlton, P. M., Sedat, J. W., DeRisi, J. L., and Marletta, M. A. (2008). N-terminal processing of proteins exported by malaria parasites. *Mol. Biochem. Parasitol.* 160, 107–115. doi:10.1016/j.molbiopara.2008.04.011.
- Charneau, S., Dourado Bastos, I. M., Mouray, E., Ribeiro, B. M., Santana, J. M., Grellier, P., et al. (2007). Characterization of PfDYN2, a dynamin-like protein of *Plasmodium falciparum* expressed in schizonts. *Microbes Infect.* 9, 797–805. doi:10.1016/j.micinf.2007.02.020.
- Chehuan, Y. F., Costa, M. R., Costa, J. S., Alecrim, M. G., Nogueira, F., Silveira, H., et al. (2013). In vitro chloroquine resistance for *Plasmodium vivax* isolates from the Western Brazilian Amazon. *Malar. J.* 12, 1–5. doi:10.1186/1475-2875-12-226.
- Chen, A. L., Kim, E. W., Toh, J. Y., Vashisht, A. A., Rashoff, A. Q., Van, C., et al. (2015). Novel components of the *Toxoplasma* inner membrane complex revealed by BioID. *MBio* 6, e02357-14. doi:10.1128/mBio.02357-14.
- Chen, Y., Murillo-Solano, C., Kirkpatrick, M. G., Antoshchenko, T., Park, H. W., and Pizarro, J. C. (2018). Repurposing drugs to target the malaria parasite unfolding protein response. *Sci. Rep.* 8, 1–12. doi:10.1038/s41598-018-28608-2.
- Collins, W. E., Wladuck, A., Sullivan, J. S., Andrews, K., Stowers, A., Morris, C. L., et al. (2000). Efficacy of vaccines containing rhoptry-associated proteins RAP1 and RAP2 of *Plasmodium falciparum* in *Saimiri boliviensis* monkeys. *Am. J. Trop. Med. Hyg.* 62, 466–479. doi:10.4269/ajtmh.2000.62.466.
- Cooke, B. M., Buckingham, D. W., Glenister, F. K., Fernandez, K. M., Bannister, L. H., Marti, M., et al. (2006). A Maurer’s cleft-associated protein is essential for expression of the major malaria virulence antigen on the surface of infected red blood cells. *J. Cell Biol.* 172, 899–908. doi:10.1083/jcb.200509122.
- Counihan, N. A., Chisholm, S. A., Bullen, H. E., Srivastava, A., Sanders, P. R., Jonsdottir, T. K., et al. (2017). *Plasmodium falciparum* parasites deploy RhopH2 into the host erythrocyte to obtain nutrients, grow and replicate. *Elife* 6, 1–31. doi:10.7554/eLife.23217.
- Counihan, N. A., Kalanon, M., Coppel, R. L., and De Koning-Ward, T. F. (2013). *Plasmodium* rhoptry proteins: Why order is important. *Trends Parasitol.* 29, 228–

236. doi:10.1016/j.pt.2013.03.003.
- Cowman, A. F., Healer, J., Marapana, D., and Marsh, K. (2016). Malaria: Biology and Disease. *Cell* 167, 610–624. doi:10.1016/j.cell.2016.07.055.
- Cox-Singh, J., Davis, T. M. E., Lee, K. S., Shamsul, S. S. G., Matusop, A., Ratnam, S., et al. (2008). Plasmodium knowlesi malaria in humans is widely distributed and potentially life threatening. *Clin. Infect. Dis.* 46, 165–171. doi:10.1086/524888.
- Cózar, C., Caballero, I., Colmenarejo, G., Sanz, L. M., Álvarez-Ruiz, E., Gamo, F. J., et al. (2016). Development of a novel high-density [3H]hypoxanthine scintillation proximity assay to assess Plasmodium falciparum growth. *Antimicrob. Agents Chemother.* 60, 5949–5956. doi:10.1128/AAC.00433-16.
- Crabb, B. S., Cooke, B. M., Reeder, J. C., Waller, R. F., Caruana, S. R., Davern, K. M., et al. (1997). Targeted gene disruption shows that knobs enable malaria-infected red cells to cytoadhere under physiological shear stress. *Cell* 89, 287–296. doi:10.1016/S0092-8674(00)80207-X.
- Crabb, B. S., Rug, M., Gilberger, T.-W., Thompson, J. K., Triglia, T., Maier, A. G., et al. (2004). “Transfection of the Human Malaria Parasite Plasmodium falciparum,” in *Methods in Molecular Biology*, 263–276. doi:10.1073/pnas.1112134108.
- Crawford, E. D., Quan, J., Horst, J. A., Ebert, D., Wu, W., and DeRisi, J. L. (2017). Plasmid-free CRISPR/Cas9 genome editing in Plasmodium falciparum confirms mutations conferring resistance to the dihydroisoquinolone clinical candidate SJ733. *PLoS One* 12, 1–13. doi:10.1371/journal.pone.0178163.
- Crosnier, C., Bustamante, L. Y., Bartholdson, S. J., Bei, A. K., Theron, M., Uchikawa, M., et al. (2011). Basigin is a receptor essential for erythrocyte invasion by Plasmodium falciparum. *Nature* 480, 534–537. doi:10.1038/nature10606.
- Crowell, A. M. J., Wall, M. J., and Doucette, A. A. (2013). Maximizing recovery of water-soluble proteins through acetone precipitation. *Anal. Chim. Acta* 796, 48–54. doi:10.1016/j.aca.2013.08.005.
- Dahl, E. L., and Rosenthal, P. J. (2007). Multiple antibiotics exert delayed effects against the Plasmodium falciparum apicoplast. *Antimicrob. Agents Chemother.* 51, 3485–3490. doi:10.1128/AAC.00527-07.
- Dahl, E. L., and Rosenthal, P. J. (2008). Apicoplast translation, transcription and genome replication: targets for antimalarial antibiotics. *Trends Parasitol.* 24, 279–284. doi:10.1016/j.pt.2008.03.007.
- Dahl, E. L., Shock, J. L., Shenai, B. R., Gut, J., DeRisi, J. L., and Rosenthal, P. J. (2006). Tetracyclines specifically target the apicoplast of the malaria parasite

- Plasmodium falciparum*. *Antimicrob. Agents Chemother.* 50, 3124–3131. doi:10.1128/AAC.00394-06.
- Datoo, M. S., Natama, M. H., Somé, A., Traoré, O., Rouamba, T., Bellamy, D., et al. (2021). Efficacy of a low-dose candidate malaria vaccine, R21 in adjuvant Matrix-M, with seasonal administration to children in Burkina Faso: a randomised controlled trial. *Lancet* 397, 1809–1818. doi:10.1016/S0140-6736(21)00943-0.
- Degarege, A., Fennie, K., Degarege, D., Chennupati, S., and Madhivanan, P. (2019). Improving socioeconomic status may reduce the burden of malaria in sub Saharan Africa: A systematic review and meta-analysis. *PLoS One* 14, 1–26. doi:10.1371/journal.pone.0211205.
- Djègbè, I., Agossa, F. R., Jones, C. M., Poupardin, R., Cornelie, S., Akogbéto, M., et al. (2014). Molecular characterization of DDT resistance in *Anopheles gambiae* from Benin. *Parasit. Vectors* 7, 1–9. doi:10.1186/1756-3305-7-409.
- Doudna, J. A., and Charpentier, E. (2014). The new frontier of genome engineering with CRISPR-Cas9. *Science (80- )*. 346. doi:10.1126/science.1258096.
- Douglas, N. M., Lampah, D. A., Kenangalem, E., Simpson, J. A., Poespoprodjo, J. R., Sugiarto, P., et al. (2013). Major Burden of Severe Anemia from Non-Falciparum Malaria Species in Southern Papua: A Hospital-Based Surveillance Study. *PLoS Med.* 10, 1–17. doi:10.1371/journal.pmed.1001575.
- Eastman, R. T., Dharia, N. V., Winzeler, E. A., and Fidock, D. A. (2011). Piperaquine resistance is associated with a copy number variation on chromosome 5 in drug-pressured *Plasmodium falciparum* parasites. *Antimicrob. Agents Chemother.* 55, 3908–3916. doi:10.1128/AAC.01793-10.
- Ehlgen, F., Pham, J. S., de Koning-Ward, T., Cowman, A. F., and Ralph, S. A. (2012). Investigation of the *Plasmodium falciparum* food vacuole through inducible expression of the chloroquine resistance transporter (PfCRT). *PLoS One* 7. doi:10.1371/journal.pone.0038781.
- Elguero, E., Délicat-Loembet, L. M., Rougeron, V., Arnathau, C., Roche, B., Becquart, P., et al. (2015). Malaria continues to select for sickle cell trait in Central Africa. *Proc. Natl. Acad. Sci. U. S. A.* 112, 7051–7054. doi:10.1073/pnas.1505665112.
- Elyazar, I. R. F., Sinka, M. E., Gething, P. W., Tarmidzi, S. N., Surya, A., Kusriastuti, R., et al. (2013). *The distribution and bionomics of Anopheles malaria vector mosquitoes in Indonesia*. 1st ed. Elsevier Ltd. doi:10.1016/B978-0-12-407705-8.00003-3.
- Fang, H., Gomes, A. R., Klages, N., Pino, P., Maco, B., Walker, E. M., et al. (2018).

- Epistasis studies reveal redundancy among calcium-dependent protein kinases in motility and invasion of malaria parasites. *Nat. Commun.* 9. doi:10.1038/s41467-018-06733-w.
- Ferreira, M. U., and Castro, M. C. (2016). Challenges for malaria elimination in Brazil. *Malar. J.* 15, 1–18. doi:10.1186/s12936-016-1335-1.
- Fichera, M. E., and Roos, D. S. (1997). A plastid organelle as a drug target in apicomplexan parasites. *Nature* 390, 407–409. doi:10.1038/37132.
- Fleige, T., Fischer, K., Ferguson, D. J. P., Gross, U., and Bohne, W. (2007). Carbohydrate metabolism in the *Toxoplasma gondii* apicoplast: Localization of three glycolytic isoenzymes, the single pyruvate dehydrogenase complex, and a plastid phosphate translocator. *Eukaryot. Cell* 6, 984–996. doi:10.1128/EC.00061-07.
- Formstecher, E., Aresta, S., Collura, V., Hamburger, A., Meil, A., Trehin, A., et al. (2005). Protein interaction mapping: A *Drosophila* case study. *Genome Res.* 15, 376–384. doi:10.1101/gr.2659105.
- Foth, B. J., Stimmler, L. M., Handman, E., Crabb, B. S., Hodder, A. N., and McFadden, G. I. (2005). The malaria parasite *Plasmodium falciparum* has only one pyruvate dehydrogenase complex, which is located in the apicoplast. *Mol. Microbiol.* 55, 39–53. doi:10.1111/j.1365-2958.2004.04407.x.
- Fried, M., and Duffy, P. E. (2017). Malaria during pregnancy. *Cold Spring Harb. Perspect. Med.* 7. doi:10.1101/cshperspect.a025551.
- Garavelli, P. L., and Corti, E. (1992). Chloroquine resistance in *Plasmodium vivax*: the first case in Brazil. *Trans. R. Soc. Trop. Med. Hyg.* 86, 128. doi:10.1016/0035-9203(92)90535-K.
- Gardiner, D. L., Spielmann, T., Dixon, M. W. A., Hawthorne, P. L., Ortega, M. R., Anderson, K. L., et al. (2004). CLAG 9 is located in the rhoptries of *Plasmodium falciparum*. *Parasitol. Res.* 93, 64–67. doi:10.1007/s00436-004-1098-4.
- Gardner, M. J., Hall, N., Fung, E., White, O., Berriman, M., Hyman, R. W., et al. (2002). Genome sequence of the human malaria parasite *Plasmodium falciparum*. *Nature* 419, 498–511. doi:10.1038/nature01097.
- Gasiunas, G., Barrangou, R., Horvath, P., and Siksnys, V. (2012). Cas9-crRNA ribonucleoprotein complex mediates specific DNA cleavage for adaptive immunity in bacteria. *Proc. Natl. Acad. Sci.* 109, E2579–E2586. doi:10.1073/pnas.1208507109.
- Ghorbal, M., Gorman, M., Macpherson, C. R., Martins, R. M., Scherf, A., and Lopez-

- Rubio, J.-J. (2014). Genome editing in the human malaria parasite *Plasmodium falciparum* using the CRISPR-Cas9 system. *Nat. Biotechnol.* 32, 819–821. doi:10.1038/nbt.2925.
- Gleave, K., Lissenden, N., Chaplin, M., Choi, L., and Ranson, H. (2021). Piperonyl butoxide (PBO) combined with pyrethroids in insecticide-treated nets to prevent malaria in Africa. *Cochrane Database Syst. Rev.* 2021. doi:10.1002/14651858.CD012776.pub3.
- Global Malaria Programme: WHO Global (2020). World Malaria Report. Available at: <https://www.who.int/publications/i/item/9789240015791>.
- Goel, S., Valiyaveetil, M., Achur, R. N., Goyal, A., Mattei, D., Salanti, A., et al. (2010). Dual stage synthesis and crucial role of cytoadherence-linked asexual gene 9 in the surface expression of malaria parasite var proteins. *Proc. Natl. Acad. Sci. U. S. A.* 107, 16643–16648. doi:10.1073/pnas.1002568107.
- Gomes, E. C. de S., Cruz, D. L. da, Santos, M. A. V. M., Souza, R. M. C., Oliveira, C. M. F. de, Ayres, C. F. J., et al. (2020). Outbreak of autochthonous cases of malaria in coastal regions of Northeast Brazil: the diversity and spatial distribution of species of *Anopheles*. *Parasit. Vectors* 13, 1–11. doi:10.1186/s13071-020-04502-7.
- Goodman, C. D., Pasaje, C. F. A., Kennedy, K., McFadden, G. I., and Ralph, S. A. (2016). Targeting Protein Translation in Organelles of the Apicomplexa. *Trends Parasitol.* 32, 953–965. doi:10.1016/j.pt.2016.09.011.
- Goodman, C. D., Su, V., and McFadden, G. I. (2007). The effects of anti-bacterials on the malaria parasite *Plasmodium falciparum*. *Mol. Biochem. Parasitol.* 152, 181–191. doi:10.1016/j.molbiopara.2007.01.005.
- Green, M. R., and Sambrook, J. (2017). “Precipitation of DNA with isopropanol,” in *Cold Spring Harbor Protocols*, 673–674. doi:10.1101/pdb.prot093385.
- Gupta, A., Thiruvengadam, G., and Desai, S. A. (2015). The conserved clag multigene family of malaria parasites: essential roles in host-pathogen interaction. *Drug Resist. Updat.* 18, 47–54. doi:10.1038/jid.2014.371.
- Haase, S., Herrmann, S., Grüning, C., Heiber, A., Jansen, P. W., Langer, C., et al. (2009). Sequence requirements for the export of the *Plasmodium falciparum* Maurer’s clefts protein REX2. *Mol. Microbiol.* 71, 1003–1017. doi:10.1111/j.1365-2958.2008.06582.x.
- Haft, D. H., Selengut, J., Mongodin, E. F., and Nelson, K. E. (2005). A guild of 45 CRISPR-associated (Cas) protein families and multiple CRISPR/cas subtypes

- exist in prokaryotic genomes. *PLoS Comput. Biol.* 1, 0474–0483. doi:10.1371/journal.pcbi.0010060.
- Hall, N., Pain, A., Berriman, M., Churcher, C., Harris, B., Harris, D., et al. (2002). Sequence of *Plasmodium falciparum* chromosomes 1, 3–9 and 13. *Nature* 419, 527–531. doi:10.1038/nature01095.
- Han, S., Udeshi, N. D., Deerinck, T. J., Svinkina, T., Ellisman, M. H., Carr, S. A., et al. (2017). Proximity Biotinylation as a Method for Mapping Proteins Associated with mtDNA in Living Cells. *Cell Chem. Biol.* 24, 404–414. doi:10.1016/j.chembiol.2017.02.002.
- Harvey, K. L., Gilson, P. R., and Crabb, B. S. (2012). A model for the progression of receptor-ligand interactions during erythrocyte invasion by *Plasmodium falciparum*. *Int. J. Parasitol.* 42, 567–573. doi:10.1016/j.ijpara.2012.02.011.
- Hawthorne, P. L., Trenholme, K. R., Skinner-Adams, T. S., Spielmann, T., Fischer, K., Dixon, M. W. A., et al. (2004). A novel *Plasmodium falciparum* ring stage protein, REX, is located in Maurer’s clefts. *Mol. Biochem. Parasitol.* 136, 181–189. doi:10.1016/j.molbiopara.2004.03.013.
- He, Y., Campino, S., Benavente, E. D., Warhurst, D. C., Beshir, K. B., Lubis, I., et al. (2019). Artemisinin resistance-associated markers in *Plasmodium falciparum* parasites from the China-Myanmar border: Predicted structural stability of K13 propeller variants detected in a low-prevalence area. *PLoS One* 14, 1–13. doi:10.1371/journal.pone.0213686.
- Heiber, A., Kruse, F., Pick, C., Grüring, C., Flemming, S., Oberli, A., et al. (2013). Identification of New PNEPs Indicates a Substantial Non-PEXEL Exportome and Underpins Common Features in *Plasmodium falciparum* Protein Export. *PLoS Pathog.* 9. doi:10.1371/journal.ppat.1003546.
- Hiller, N. L., Bhattacharjee, S., Ooij, C. Van, Liolios, K., Harrison, T., Lopez-estran, C., et al. (2004). A Host-Targeting Signal in Virulence Proteins Reveals a Secretome in Malarial Infection. *Science* (80- ). 306, 1934–1938. doi:10.1126/science.1102737.
- Hoeijmakers, W. A. M., Miao, J., Schmidt, S., Toenhake, C. G., Shrestha, S., Venhuizen, J., et al. (2019). Epigenetic reader complexes of the human malaria parasite, *Plasmodium falciparum*. *Nucleic Acids Res.* 47, 11574–11588. doi:10.1093/nar/gkz1044.
- Horrocks, P., Pinches, R. A., Chakravorty, S. J., Papakrivos, J., Christodoulou, Z., Kyes, S. A., et al. (2005). PfEMP1 expression is reduced on the surface of



- knobless *Plasmodium falciparum* infected erythrocytes. *J. Cell Sci.* 118, 2507–2518. doi:10.1242/jcs.02381.
- Howes, R. E., Piel, F. B., Patil, A. P., Nyangiri, O. A., Gething, P. W., Dewi, M., et al. (2012). G6PD Deficiency Prevalence and Estimates of Affected Populations in Malaria Endemic Countries: A Geostatistical Model-Based Map. *PLoS Med.* 9. doi:10.1371/journal.pmed.1001339.
- Hu, H., Zhou, Q., and Li, Z. (2015). SAS-4 protein in *Trypanosoma brucei* controls life cycle transitions by modulating the length of the flagellum attachment zone filament. *J. Biol. Chem.* 290, 30453–30463. doi:10.1074/jbc.M115.694109.
- Hung, V., Udeshi, N. D., Lam, S. S., Loh, K. H., Cox, K. J., Pedram, K., et al. (2016). Spatially resolved proteomic mapping in living cells with the engineered peroxidase APEX2. *Nat. Protoc.* 11, 456–75. doi:10.1038/nprot.2016.018.
- Imwong, M., Madmanee, W., Suwannasin, K., Kunasol, C., Peto, T. J., Tripura, R., et al. (2019). Asymptomatic natural human infections with the simian malaria parasites *Plasmodium cynomolgi* and *Plasmodium knowlesi*. *J. Infect. Dis.* 219, 695–702. doi:10.1093/infdis/jiy519.
- Ippolito, M. M., Moser, K. A., Kabuya, J.-B. B., Cunningham, C., and Juliano, J. J. (2021). Antimalarial Drug Resistance and Implications for the WHO Global Technical Strategy. *Curr. Epidemiol. Reports.* doi:10.1007/s40471-021-00266-5.
- Irving, H., and Wondji, C. S. (2017). Investigating knockdown resistance (kdr) mechanism against pyrethroids/DDT in the malaria vector *Anopheles funestus* across Africa. *BMC Genet.* 18, 1–11. doi:10.1186/s12863-017-0539-x.
- Ishino, Y., Krupovic, M., and Forterre, P. (2018). History of CRISPR-Cas from Encounter with a Mysterious Repeated Sequence to Genome Editing Technology. *J. Bacteriol.* 200, e00580-17.
- Ishino, Y., Shinagawa, H., Makino, K., Amemura, M., and Nakata, A. (1987). Nucleotide sequence of the *iap* gene, responsible for alkaline phosphatase isozyme conversion in *Escherichia coli*, and identification of the gene product. *J. Bacteriol.* 169, 5429–5433. doi:10.1128/jb.169.12.5429-5433.1987.
- Ito, D., Chen, J. H., Takashima, E., Hasegawa, T., Otsuki, H., Takeo, S., et al. (2021). Identification of a Novel RAMA/RON3 Rhopty Protein Complex in *Plasmodium falciparum* Merozoites. *Front. Cell. Infect. Microbiol.* 10, 1–11. doi:10.3389/fcimb.2020.605367.
- Jaffer, A., Protopopoff, N., Mosha, F. W., Malone, D., Rowland, M. W., and Oxborough, R. M. (2015). Evaluating the sterilizing effect of pyriproxyfen treated mosquito nets

- against *Anopheles gambiae* at different blood-feeding intervals. *Acta Trop.* 150, 131–135. doi:10.1016/j.actatropica.2015.07.011.
- Jain, A., Zode, G., Kasetti, R. B., Ran, F. A., Yan, W., Sharma, T. P., et al. (2017). CRISPR-Cas9–based treatment of myocilin- associated. *Proc. Natl. Acad. Sci.* doi:10.1073/pnas.1706193114.
- Jansen, R., Embden, J. D. A. Van, Gastra, W., and Schouls, L. M. (2002). Identification of genes that are associated with DNA repeats in prokaryotes. *Mol. Microbiol.* 43, 1565–1575.
- Jinek, M., Chylinski, K., Fonfara, I., Hauer, M., Doudna, J. A., and Charpentier, E. (2012). A Programmable Dual-RNA-Guided DNA Endonuclease in Adaptive Bacterial Immunity. *Science (80-. )*. 337, 816–821. doi:10.1002/ajh.24462.
- Jomaa, H., Jomaa, H., Wiesner, J., Sanderbrand, S., Eberl, M., Zeidler, J., et al. (1999). Inhibitors of the Nonmevalonate Pathway of Isoprenoid Biosynthesis as Antimalarial Drugs. *Science (80-. )*. 285, 1573–1576.
- Jonscher, E., Flemming, S., Schmitt, M., Sabitzki, R., Reichard, N., Birnbaum, J., et al. (2019). PfVPS45 Is Required for Host Cell Cytosol Uptake by Malaria Blood Stage Parasites. *Cell Host Microbe* 25, 166-173.e5. doi:10.1016/j.chom.2018.11.010.
- Jonsdottir, T. K., Counihan, N. A., Modak, J. K., Kouskousis, B., Sanders, P. R., Gabriela, M., et al. (2021). Characterisation of complexes formed by parasite proteins exported into the host cell compartment of *Plasmodium falciparum* infected red blood cells. *Cell. Microbiol.*, 1–14. doi:10.1111/cmi.13332.
- Kaewsapsak, P., Shechner, D. M., Mallard, W., Rinn, J. L., and Ting, A. Y. (2017). Live-cell mapping of organelle-associated RNAs via proximity biotinylation combined with protein-RNA crosslinking. *Elife* 6, 1–31. doi:10.7554/elife.29224.
- Kaneko, O., Lim, B. Y. S. Y., Iriko, H., Ling, I. T., Otsuki, H., Grainger, M., et al. (2005). Apical expression of three RhopH1/Clag proteins as components of the *Plasmodium falciparum* RhopH complex. *Mol. Biochem. Parasitol.* 143, 20–28. doi:10.1016/j.molbiopara.2005.05.003.
- Kaneko, O., Tsuboi, T., Ling, I. T., Howell, S., Shirano, M., Tachibana, M., et al. (2001). The high molecular mass rhoptry protein, RhopH1, is encoded by members of the clag multigene family in *Plasmodium falciparum* and *Plasmodium yoelii*. *Mol. Biochem. Parasitol.* 118, 223–231. doi:10.1016/S0166-6851(01)00391-7.
- Karunaweera, N. D., Grau, G. E., Gamage, P., Carter, R., and Mendis, K. N. (1992). Dynamics of fever and serum levels of tumor necrosis factor are closely associated during clinical paroxysms in *Plasmodium vivax* malaria. *Proc. Natl.*

- Acad. Sci.* 89, 3200–3203. doi:10.1073/pnas.89.8.3200.
- Kats, L. M., Black, C. G., Proellocks, N. I., and Coppel, R. L. (2006). Plasmodium rhoptries: how things went pear-shaped. *Trends Parasitol.* 22, 269–276. doi:10.1016/j.pt.2006.04.001.
- Kehr, S., Sturm, N., Rahlfs, S., Przyborski, J. M., and Becker, K. (2010). Compartmentation of redox metabolism in malaria parasites. *PLoS Pathog.* 6. doi:10.1371/journal.ppat.1001242.
- Khosh-Naucke, M., Becker, J., Mesén-Ramírez, P., Kiani, P., Birnbaum, J., Fröhlke, U., et al. (2018). Identification of novel parasitophorous vacuole proteins in *P. falciparum* parasites using BioID. *Int. J. Med. Microbiol.* 308, 13–24. doi:10.1016/j.ijmm.2017.07.007.
- Killeen, G. F., Seyoum, A., Sikaala, C., Zomboko, A. S., Gimnig, J. E., Govella, N. J., et al. (2013). Eliminating malaria vectors. *Parasit. Vectors* 6, 1–10. doi:10.1186/1756-3305-6-172.
- Kim, D. I., Cutler, J. A., Na, C. H., Reckel, S., Renuse, S., Madugundu, A. K., et al. (2018). BioSITE: A Method for Direct Detection and Quantitation of Site-Specific Biotinylation. *J. Proteome Res.* 17, 759–769. doi:10.1021/acs.jproteome.7b00775.
- King, C. H., Dickman, K., and Tisch, D. J. (2005). Reassessment of the cost of chronic helminthic infection: A meta-analysis of disability-related outcomes in endemic schistosomiasis. *Lancet* 365, 1561–1569. doi:10.1016/S0140-6736(05)66457-4.
- Koama, B., Namountougou, M., Sanou, R., Ndo, S., Ouattara, A., Dabiré, R. K., et al. (2015). The sterilizing effect of pyriproxyfen on the malaria vector *Anopheles gambiae*: Physiological impact on ovaries development. *Malar. J.* 14, 1–8. doi:10.1186/s12936-015-0609-3.
- Kobayashi, T., Sato, S., Takamiya, S., Komaki-Yasuda, K., Yano, K., Hirata, A., et al. (2007). Mitochondria and apicoplast of *Plasmodium falciparum*: Behaviour on subcellular fractionation and the implication. *Mitochondrion* 7, 125–132. doi:10.1016/j.mito.2006.11.021.
- Koning-Ward, T. F., Gilson, P. R., Boddey, J. A., Rug, M., Smith, B. J., Papenfuss, A. T., et al. (2009). A newly discovered protein export machine in malaria parasites. *Nature* 459, 945–949. doi:10.1038/nature08104.
- Kramer, K. J., Kan, S. C., and Siddiqui, W. A. (1982). Concentration of *Plasmodium falciparum*-infected erythrocytes by density gradient centrifugation in Percoll. *J. Parasitol.* 68, 336–7. Available at: <http://www.ncbi.nlm.nih.gov/pubmed/6281409>.

- Külzer, S., Rug, M., Brinkmann, K., Cannon, P., Cowman, A., Lingelbach, K., et al. (2010). Parasite-encoded Hsp40 proteins define novel mobile structures in the cytosol of the *P. falciparum*-infected erythrocyte. *Cell. Microbiol.* 12, 1398–1420. doi:10.1111/j.1462-5822.2010.01477.x.
- Kupka, R. (2015). The role of folate in malaria - implications for home fortification programmes among children aged 6-59 months. *Matern. Child Nutr.* 11, 1–15. doi:10.1111/mcn.12102.
- Lalremruata, A., Magris, M., Vivas-Martínez, S., Koehler, M., Esen, M., Kempaiah, P., et al. (2015). Natural infection of *Plasmodium brasilianum* in humans: Man and monkey share quartan malaria parasites in the Venezuelan Amazon. *EBioMedicine* 2, 1186–1192. doi:10.1016/j.ebiom.2015.07.033.
- Lambros, C., and Vanderberg, J. P. (1979). Synchronization of *Plasmodium falciparum* erythrocytic stages in culture. *J. Parasitol.* 65, 418–20. Available at: <http://www.ncbi.nlm.nih.gov/pubmed/383936>.
- Lander, N., Chiurillo, M. A., Storey, M., Vercesi, A. E., and Docampo, R. (2016). CRISPR/Cas9-mediated endogenous C-terminal tagging of *Trypanosoma cruzi* genes reveals the acidocalcisome localization of the inositol 1,4,5-trisphosphate receptor. *J. Biol. Chem.* 291, 25505–25515. doi:10.1074/jbc.M116.749655.
- Lanzer, M., Wickert, H., Krohne, G., Vincensini, L., and Braun Breton, C. (2006). Maurer’s clefts: A novel multi-functional organelle in the cytoplasm of *Plasmodium falciparum*-infected erythrocytes. *Int. J. Parasitol.* 36, 23–36. doi:10.1016/j.ijpara.2005.10.001.
- Lee, A. H., Dhingra, S. K., Lewis, I. A., Singh, M. K., Siriwardana, A., Dalal, S., et al. (2018). Evidence for Regulation of Hemoglobin Metabolism and Intracellular Ionic Flux by the *Plasmodium falciparum* Chloroquine Resistance Transporter. *Sci. Rep.* 8, 1–13. doi:10.1038/s41598-018-31715-9.
- Lee, S. Y., Kang, M. G., Park, J. S., Lee, G., Ting, A. Y., and Rhee, H. W. (2016). APEX Fingerprinting Reveals the Subcellular Localization of Proteins of Interest. *Cell Rep.* 15, 1837–1847. doi:10.1016/j.celrep.2016.04.064.
- Li, P., Li, J., Wang, L., and Di, L. J. (2017). Proximity Labeling of Interacting Proteins: Application of BioID as a Discovery Tool. *Proteomics* 17, 1–10. doi:10.1002/pmic.201700002.
- Lim, L., and McFadden, G. I. (2010). The evolution, metabolism and functions of the apicoplast. *Philos. Trans. R. Soc. B Biol. Sci.* 365, 749–763. doi:10.1098/rstb.2009.0273.

- Ling, I. T., Florens, L., Dluzewski, A. R., Kaneko, O., Grainger, M., Yim Lim, B. Y. S., et al. (2004). The *Plasmodium falciparum* clag9 gene encodes a rhoptry protein that is transferred to the host erythrocyte upon invasion. *Mol. Microbiol.* 52, 107–118. doi:10.1111/j.1365-2958.2003.03969.x.
- Ling, I. T., Kaneko, O., Narum, D. L., Tsuboi, T., Howell, S., Taylor, H. M., et al. (2003). Characterisation of the rhoph2 gene of *Plasmodium falciparum* and *Plasmodium yoelii*. *Mol. Biochem. Parasitol.* 127, 47–57. doi:10.1016/S0166-6851(02)00302-X.
- Lobingier, B. T., Hüttenhain, R., Eichel, K., Miller, K. B., Ting, A. Y., von Zastrow, M., et al. (2017). An Approach to Spatiotemporally Resolve Protein Interaction Networks in Living Cells. *Cell* 169, 350-360.e12. doi:10.1016/j.cell.2017.03.022.
- Long, S., Brown, K. M., Drewry, L. L., Anthony, B., Phan, I. Q. H., and Sibley, L. D. (2017). Calmodulin-like proteins localized to the conoid regulate motility and cell invasion by *Toxoplasma gondii*. *PLoS Pathog.* 13, 1–28. doi:10.1371/journal.ppat.1006379.
- Lu, J., Tong, Y., Pan, J., Yang, Y., Liu, Q., Tan, X., et al. (2016). A redesigned CRISPR/Cas9 system for marker-free genome editing in *Plasmodium falciparum*. *Parasit. Vectors* 9, 198. doi:10.1186/s13071-016-1487-4.
- Ludin, P., Woodcroft, B., Ralph, S. A., and Mäser, P. (2012). In silico prediction of antimalarial drug target candidates. *Int. J. Parasitol. Drugs Drug Resist.* 2, 191–199. doi:10.1016/j.ijpddr.2012.07.002.
- Maeda, T., Saito, T., Harb, O. S., Roos, D. S., Takeo, S., Suzuki, H., et al. (2009). Pyruvate kinase type-II isozyme in *Plasmodium falciparum* localizes to the apicoplast. *Parasitol. Int.* 58, 101–105. doi:10.1016/j.parint.2008.10.005.
- Maier, A. G., Rug, M., O’Neill, M. T., Brown, M., Chakravorty, S., Szeszak, T., et al. (2008). Exported Proteins Required for Virulence and Rigidity of *Plasmodium falciparum*-Infected Human Erythrocytes. *Cell* 134, 48–61. doi:10.1016/j.cell.2008.04.051.
- Maitland, K. (2016). Severe Malaria in African Children — The Need for Continuing Investment. *N. Engl. J. Med.* 375, 2416–2417. doi:10.1056/nejmp1613528.
- Mantel, P. Y., Hoang, A. N., Goldowitz, I., Potashnikova, D., Hamza, B., Vorobjev, I., et al. (2013). Malaria-infected erythrocyte-derived microvesicles mediate cellular communication within the parasite population and with the host immune system. *Cell Host Microbe* 13, 521–534. doi:10.1016/j.chom.2013.04.009.
- Marchadier, E., Carballido-López, R., Brinster, S., Fabret, C., Mervelet, P., Bessières,

- P., et al. (2011). An expanded protein-protein interaction network in *Bacillus subtilis* reveals a group of hubs: Exploration by an integrative approach. *Proteomics* 11, 2981–2991. doi:10.1002/pmic.201000791.
- Marques, M. M., Costa, M. R. F., Santana Filho, F. S., Vieira, J. L. F., Nascimento, M. T. S., Brasil, L. W., et al. (2014). Plasmodium vivax chloroquine resistance and anemia in the western brazilian amazon. *Antimicrob. Agents Chemother.* 58, 342–347. doi:10.1128/AAC.02279-12.
- Martell, J. D., Deerinck, T. J., Sancak, Y., Poulos, T. L., Mootha, V. K., Sosinsky, G. E., et al. (2012). Engineered ascorbate peroxidase as a genetically encoded reporter for electron microscopy. *Nat. Biotechnol.* 30, 1143–1148. doi:10.1038/nbt.2375.
- Marti, M., Marti, M., Good, R. T., Rug, M., Knuepfer, E., and Cowman, A. F. (2004). Targeting Malaria Virulence and Remodeling Proteins to the Host Erythrocyte. *Science (80-. )*. 306, 1930–1934. doi:10.1126/science.1102452.
- Mavoko, H. M., Nabasumba, C., da Luz, R. I., Tinto, H., D’Alessandro, U., Kambugu, A., et al. (2017). Efficacy and safety of re-treatment with the same artemisinin-based combination treatment (ACT) compared with an alternative ACT and quinine plus clindamycin after failure of first-line recommended ACT (QUINACT): a bicentre, open-label, phase 3, randomise. *Lancet Glob. Heal.* 5, e60–e68. doi:10.1016/S2214-109X(16)30236-4.
- McAllaster, M. R., Ikeda, K. N., Lozano-Núñez, A., Anrather, D., Unterwurzacher, V., Gossenreiter, T., et al. (2015). Proteomic identification of novel cytoskeletal proteins associated with TbPLK, an essential regulator of cell morphogenesis in *Trypanosoma brucei*. *Mol. Biol. Cell* 26, 3013–3029. doi:10.1091/mbc.e15-04-0219.
- McHugh, E., Batinovic, S., Hanssen, E., Mcmillan, P. J., Kenny, S., Griffin, M. D. W., et al. (2015). A repeat sequence domain of the ring-exported protein-1 of *Plasmodium falciparum* controls export machinery architecture and virulence protein trafficking. *Mol. Microbiol.* 98, 1101–1114. doi:10.1111/mmi.13201.
- Mills, J. P., Diez-Silva, M., Quinn, D. J., Dao, M., Lang, M. J., Tan, K. S. W., et al. (2007). Effect of plasmodial RESA protein on deformability of human red blood cells harboring *Plasmodium falciparum*. *Proc. Natl. Acad. Sci. U. S. A.* 104, 9213–9217. doi:10.1073/pnas.0703433104.
- Mogollon, C. M., Van Pul, F. J. A., Imai, T., Ramesar, J., Chevalley-Maurel, S., De Roo, G. M., et al. (2016). Rapid generation of marker-free *P. falciparum*

- fluorescent reporter lines using modified CRISPR/Cas9 constructs and selection protocol. *PLoS One* 11. doi:10.1371/journal.pone.0168362.
- Mojica, F. J. M., Díez-Villaseñor, C., García-Martínez, J., and Soria, E. (2005). Intervening sequences of regularly spaced prokaryotic repeats derive from foreign genetic elements. *J. Mol. Evol.* 60, 174–182. doi:10.1007/s00239-004-0046-3.
- Molina-Cruz, A., Zilversmit, M. M., Neafsey, D. E., Hartl, D. L., and Barillas-Mury, C. (2016). Mosquito Vectors and the Globalization of *Plasmodium falciparum* Malaria. *Annu. Rev. Genet.* 50, 447–465. doi:10.1146/annurev-genet-120215-035211.
- Morriswood, B., Havlicek, K., Demmel, L., Yavuz, S., Sealey-Cardona, M., Vidilaseris, K., et al. (2013). Novel Bilobe Components in *Trypanosoma brucei* Identified Using Proximity-Dependent Biotinylation. *Eukaryot. Cell* 12, 356–367. doi:10.1128/ec.00326-12.
- Moxon, C. A., Gibbins, M. P., McGuinness, D., Jr, D. A. M., and Marti, M. (2020). New Insights into Malaria Pathogenesis. *Annu. Rev. Pathol. Mech. Dis.* 15, 315–343.
- Mremi, A., Yahaya, J. J., Nyindo, M., and Mollel, E. (2021). Transfusion-Transmitted Infections and associated risk factors at the Northern Zone Blood Transfusion Center in Tanzania: A study of blood donors between 2017 and 2019. *PLoS One* 16, 1–12. doi:10.1371/journal.pone.0249061.
- Muhammad, A., Ibrahim, S. S., Mukhtar, M. M., Irving, H., Abajue, M. C., Edith, N. M. A., et al. (2021). High pyrethroid/DDT resistance in major malaria vector *Anopheles coluzzii* from Niger-Delta of Nigeria is probably driven by metabolic resistance mechanisms. *PLoS One* 16, 1–16. doi:10.1371/journal.pone.0247944.
- Mullin, K. A., Lim, L., Ralph, S. A., Spurck, T. P., Handman, E., and McFadden, G. I. (2006). Membrane transporters in the relict plastid of malaria parasites. *Proc. Natl. Acad. Sci.* 103, 9572–9577. doi:10.1073/pnas.0602293103.
- Nacer, A., Roux, E., Pomel, S., Scheidig-Benatar, C., Sakamoto, H., Lafont, F., et al. (2011). *clag9* is not essential for PfEMP1 surface expression in non-cytoadherent *Plasmodium falciparum* parasites with a chromosome 9 deletion. *PLoS One* 6, 1–11. doi:10.1371/journal.pone.0029039.
- Nagaraj, V. A., Arumugam, R., Gopalakrishnan, B., Jyothsna, Y. S., Rangarajan, P. N., and Padmanaban, G. (2008). Unique properties of *Plasmodium falciparum* porphobilinogen deaminase. *J. Biol. Chem.* 283, 437–444. doi:10.1074/jbc.M706861200.
- Neuhaus, H. E., and Emes, M. J. (2000). Nonphotosynthetic metabolism in plastids.

- Annu. Rev. Plant Biol.* 51, 111–140. doi:10.1146/annurev.arplant.51.1.111.
- Ngufor, C., Fongnikin, A., Rowland, M., and N’Guessan, R. (2017). Indoor residual spraying with a mixture of clothianidin (a neonicotinoid insecticide) and deltamethrin provides improved control and long residual activity against pyrethroid resistant *Anopheles gambiae* sl in Southern Benin. *PLoS One* 12, 1–14. doi:10.1371/journal.pone.0189575.
- Nguitragool, W., Bokhari, A. A. B., Pillai, A. D., Rayavara, K., Sharma, P., Turpin, B., et al. (2011). Malaria parasite clag3 genes determine channel-mediated nutrient uptake by infected red blood cells. *Cell* 145, 665–677. doi:10.1016/j.cell.2011.05.002.
- Niu, Y., Shen, B., Cui, Y., Chen, Y., Wang, J., Wang, L., et al. (2014). Generation of gene-modified cynomolgus monkey via Cas9/RNA-mediated gene targeting in one-cell embryos. *Cell* 156, 836–843. doi:10.1016/j.cell.2014.01.027.
- Noedl, H., Se, Y., Sriwichai, S., Schaecher, K., Teja-Isavadharm, P., Smith, B., et al. (2010). Artemisinin resistance in Cambodia: A clinical trial designed to address an emerging problem in Southeast Asia. *Clin. Infect. Dis.* 51. doi:10.1086/657120.
- Noedl, H., Youry, S., Kurt, S., Bryan, L. S., Duong, S., and Mark, M. F. (2008). Evidence of Artemisinin-Resistant Malaria in Western Cambodia. *N. Engl. J. Med.* 359, 2619–2620.
- Nyunt, M. H., Soe, M. T., Myint, H. W., Oo, H. W., Aye, M. M., Han, S. S., et al. (2017). Clinical and molecular surveillance of artemisinin resistant falciparum malaria in Myanmar (2009-2013) NCT02792816 NCT. *Malar. J.* 16, 1–11. doi:10.1186/s12936-017-1983-9.
- Oh, S. S., Voigt, S., Fisher, D., Yi, S. J., Leroy, P. J., Derick, L. H., et al. (2000). Plasmodium falciparum erythrocyte membrane protein 1 is anchored to the actin-spectrin junction and knob-associated histidine-rich protein in the erythrocyte skeleton. *Mol. Biochem. Parasitol.* 108, 237–247. doi:10.1016/S0166-6851(00)00227-9.
- Oliveira-Ferreira, J., Lacerda, M. V. G., Brasil, P., Ladislau, J. L. B., Tauil, P. L., and Daniel-Ribeiro, C. T. (2010). Malaria in Brazil: An overview. *Malar. J.* 9, 1–15. doi:10.1186/1475-2875-9-115.
- Oliveira, A. S. de, Rosa, I. I. R., Novaes, E., Oliveira, L. S. de, Baeza, L. C., Borges, C. L., et al. (2018). The exoproteome profiles of three *Staphylococcus saprophyticus* strains reveal diversity in protein secretion contents. *Microbiol. Res.* 216, 85–96. doi:10.1016/j.micres.2018.08.008.



- Olotu, A., Fegan, G., Wambua, J., Nyangweso, G., Leach, A., Lievens, M., et al. (2016). Seven-Year Efficacy of RTS,S/AS01 Malaria Vaccine among Young African Children. *N. Engl. J. Med.* 374, 2519–2529. doi:10.1056/nejmoa1515257.
- Otienoburu, S. D., Maïga-Ascofaré, O., Schramm, B., Jullien, V., Jones, J. J., Zolia, Y. M., et al. (2016). Selection of *Plasmodium falciparum* pfcr1 and pfmdr1 polymorphisms after treatment with artesunate-amodiaquine fixed dose combination or artemether-lumefantrine in Liberia. *Malar. J.* 15, 1–6. doi:10.1186/s12936-016-1503-3.
- Oxborough, R. M., Seyoum, A., Yihdego, Y., Dabire, R., Gnanguenon, V., Wat’Senga, F., et al. (2019). Susceptibility testing of *Anopheles* malaria vectors with the neonicotinoid insecticide clothianidin; Results from 16 African countries, in preparation for indoor residual spraying with new insecticide formulations. *Malar. J.* 18, 1–11. doi:10.1186/s12936-019-2888-6.
- Pan, M., Li, M., Li, L., Song, Y., Hou, L., Zhao, J., et al. (2019). Identification of Novel Dense-Granule Proteins in *Toxoplasma gondii* by Two Proximity-Based Biotinylation Approaches. *J. Proteome Res.* 18, 319–330. doi:10.1021/acs.jproteome.8b00626.
- Parroche, P., Lauw, F. N., Goutagny, N., Latz, E., Monks, B. G., Visintin, A., et al. (2007). Malaria hemozoin is immunologically inert but radically enhances innate responses by presenting malaria DNA to Toll-like receptor 9. *Proc. Natl. Acad. Sci.* 104, 1919–1924. doi:10.1073/pnas.0608745104.
- Partnership, S. C. T. (2015). Efficacy and safety of RTS,S/AS01 malaria vaccine with or without a booster dose in infants and children in Africa: Final results of a phase 3, individually randomised, controlled trial. *Lancet* 386, 31–45. doi:10.1016/S0140-6736(15)60721-8.
- Payne, D. (1987). Spread of chloroquine resistance in *Plasmodium falciparum*. *Parasitol. Today* 3, 241–246. doi:10.1016/0169-4758(87)90147-5.
- Pei, X., Guo, X., Coppel, R., Bhattacharjee, S., Haldar, K., Gratzer, W., et al. (2007). The ring-infected erythrocyte surface antigen (RESA) of *Plasmodium falciparum* stabilizes spectrin tetramers and suppresses further invasion. *Blood* 110, 1036–1042. doi:10.1182/blood-2007-02-076919.
- Peña-Rosas, J. P., De-Regil, L. M., Malave, H. G., Flores-Urrutia, M. C., and Dowswell, T. (2015). Intermittent oral iron supplementation during pregnancy. *Cochrane Database Syst. Rev.* 2015. doi:10.1002/14651858.CD009997.pub2.
- Petersen, W., Külzer, S., Engels, S., Zhang, Q., Ingmundson, A., Rug, M., et al. (2016).

- J-dot targeting of an exported HSP40 in *Plasmodium falciparum*-infected erythrocytes. *Int. J. Parasitol.* 46, 519–525. doi:10.1016/j.ijpara.2016.03.005.
- Pham, T. B., Phong, C. H., Bennett, J. B., Hwang, K., Jasinskiene, N., Parker, K., et al. (2019). Experimental population modification of the malaria vector mosquito, *Anopheles stephensi*. *PLoS Genet.* 15, 1–32. doi:10.1371/journal.pgen.1008440.
- Phillips, M. A., Burrows, J. N., Manyando, C., Huijsduijnen, R. H. van, Voorhis, W. C. Van, and Wells, T. N. C. (2017). Malaria. *Nat. Rev. Dis. Prim.* 3, 1–24. doi:10.1016/S0140-6736(18)30324-6.
- Pina-Costa, A., Brasil, P., di Santi, S. M., de Araujo, M. P., Suárez-Mutis, M. C., Santelli, A. C. F. e. S., et al. (2014). Malaria in Brazil: What happens outside the Amazonian endemic region. *Mem. Inst. Oswaldo Cruz* 109, 618–633. doi:10.1590/0074-0276140228.
- Pourcel, C., Salvignol, G., and Vergnaud, G. (2005). CRISPR elements in *Yersinia pestis* acquire new repeats by preferential uptake of bacteriophage DNA, and provide additional tools for evolutionary studies. *Microbiology* 151, 653–663. doi:10.1099/mic.0.27437-0.
- Pradel, G., and Schlitzer, M. (2010). Antibiotics in Malaria Therapy and their Effect on the Parasite Apicoplast. *Curr. Mol. Med.* 10, 335–349. doi:10.2174/156652410791065273.
- Price, R. N., Uhlemann, A. C., Brockman, A., McGready, R., Ashley, E., Phaipun, L., et al. (2004). Mefloquine resistance in *Plasmodium falciparum* and increased *pfmdr1* gene copy number. *Lancet* 364, 438–447. doi:10.1016/S0140-6736(04)16767-6.
- Price, R. N., von Seidlein, L., Valecha, N., Nosten, F., Baird, J. K., and White, N. J. (2014). Global extent of chloroquine-resistant *Plasmodium vivax*: A systematic review and meta-analysis. *Lancet Infect. Dis.* 14, 982–991. doi:10.1016/S1473-3099(14)70855-2.
- Proellocks, N. I., Coppel, R. L., and Waller, K. L. (2010). Dissecting the apicomplexan rhoptry neck proteins. *Trends Parasitol.* 26, 297–304. doi:10.1016/j.pt.2010.02.012.
- Pule, G. D., Chimusa, E. R., Mnika, K., Mhandire, K., Kampira, E., Dandara, C., et al. (2017). Beta-globin gene haplotypes and selected Malaria-associated variants among black Southern African populations. *Glob. Heal. Epidemiol. genomics* 2, e17. doi:10.1017/ghg.2017.14.
- Qiu, P., Jiang, J., Liu, Z., Cai, Y., Huang, T., Wang, Y., et al. (2019). BMAL1 knockout

- macaque monkeys display reduced sleep and psychiatric disorders. *Natl. Sci. Rev.* 6, 87–100. doi:10.1093/nsr/nwz002.
- Ralph, S. A., D’Ombrain, M. C., and McFadden, G. I. (2001). The apicoplast as an antimalarial drug target. *Drug Resist. Updat.* 4, 145–151. doi:10.1054/drup.2001.0205.
- Ralph, S. A., van Dooren, G. G., Waller, R. F., Crawford, M. J., Fraunholz, M. J., Foth, B. J., et al. (2004). Metabolic maps and functions of the *Plasmodium falciparum* apicoplast. *Nat. Rev. Microbiol.* 2, 203–216. doi:10.1038/nrmicro843.
- Rappsilber, J., Mann, M., and Ishihama, Y. (2007). Protocol for micro-purification, enrichment, pre-fractionation and storage of peptides for proteomics using StageTips. *Nat. Protoc.* 2, 1896–1906. doi:10.1038/nprot.2007.261.
- Rawsthorne, S. (2002). Carbon flux and fatty acid synthesis in plants. *Prog. Lipid Res.* 41, 182–196. doi:10.1016/S0163-7827(01)00023-6.
- Rees, J. S., Li, X.-W., Perrett, S., Lilley, K. S., and Jackson, A. P. (2015). Protein Neighbors and Proximity Proteomics. *Mol. Cell. Proteomics* 14, 2848–2856. doi:10.1074/mcp.R115.052902.
- Regev-Rudzki, N., Wilson, D. W., Carvalho, T. G., Sisquella, X., Coleman, B. M., Rug, M., et al. (2013). Cell-cell communication between malaria-infected red blood cells via exosome-like vesicles. *Cell* 153, 1120–1133. doi:10.1016/j.cell.2013.04.029.
- Remcho, T. P., Guggilapu, S. D., Cruz, P., Nardone, G. A., Heffernan, G., O’Connor, R. D., et al. (2020). Regioisomerization of antimalarial drug WR99210 explains the inactivity of a commercial stock. *Antimicrob. Agents Chemother.* 65. doi:10.1128/AAC.01385-20.
- Renuse, S., Madugundu, A. K., Jung, J. H., Byeon, S. K., Goldschmidt, H. L., Tahir, R., et al. (2020). Signature Fragment Ions of Biotinylated Peptides. *J. Am. Soc. Mass Spectrom.* 31, 394–404. doi:10.1021/jasms.9b00024.
- Rhee, H., Zou, P., Udeshi, N. D., Martell, J. D., Mootha, V. K., Carr, S. A., et al. (2013). Proteomic Mapping of Mitochondria in Living Cells via Spatially Restricted Enzymatic Tagging. *Science (80- )*. 339, 1328–31. doi:10.1126/science.1230593.
- Richard, D., Kats, L. M., Langer, C., Black, C. G., Mitri, K., Boddey, J. A., et al. (2009). Identification of rhoptry trafficking determinants and evidence for a novel sorting mechanism in the malaria parasite *Plasmodium falciparum*. *PLoS Pathog.* 5. doi:10.1371/journal.ppat.1000328.
- Richard, D., MacRaild, C. A., Riglar, D. T., Chan, J. A., Foley, M., Baum, J., et al. (2010). Interaction between *Plasmodium falciparum* apical membrane antigen 1

- and the rhoptry neck protein complex defines a key step in the erythrocyte invasion process of malaria parasites. *J. Biol. Chem.* 285, 14815–14822. doi:10.1074/jbc.M109.080770.
- Ridley, R. G. (2002). Medical need, scientific opportunity and the drive for antimalarial drugs. *Nature* 415, 686–693.
- Riglar, D. T., Richard, D., Wilson, D. W., Boyle, M. J., Dekiwadia, C., Turnbull, L., et al. (2011). Super-resolution dissection of coordinated events during malaria parasite invasion of the human erythrocyte. *Cell Host Microbe* 9, 9–20. doi:10.1016/j.chom.2010.12.003.
- Rogerson, S. J., Desai, M., Mayor, A., Sicuri, E., Taylor, S. M., and van Eijk, A. M. (2018). Burden, pathology, and costs of malaria in pregnancy: new developments for an old problem. *Lancet Infect. Dis.* 18, e107–e118. doi:10.1016/S1473-3099(18)30066-5.
- Rønn, A. M., Msangeni, H. A., Mhina, J., Wernsdorfer, W. H., and Bygbjerg, I. C. (1996). High level of resistance of *Plasmodium falciparum* to sulfadoxine-pyrimethamine in children in Tanzania. *Trans. R. Soc. Trop. Med. Hyg.* 90, 179–181. doi:10.1016/S0035-9203(96)90129-7.
- Roper, C., Pearce, R., Nair, S., Sharp, B., Nosten, F., and Anderson, T. (2004). Intercontinental spread of pyrimethamine-resistant malaria. *Science* (80-. ). 305, 1124. doi:10.1126/science.1098876.
- Rug, M., Prescott, S. W., Fernandez, K. M., Cooke, B. M., and Cowman, A. F. (2006). The role of KAHRP domains in knob formation and cytoadherence of *P. falciparum*-infected human erythrocytes. *Blood* 108, 370–378. doi:10.1182/blood-2005-11-4624.Supported.
- Russo, I., Babbitt, S., Muralidharan, V., Butler, T., Oksman, A., and Goldberg, D. E. (2010). Plasmepsin V licenses *Plasmodium* proteins for export into the host erythrocyte. *Nature* 463, 632–636. doi:10.1038/nature08726.
- Saito, T., Nishi, M., Lim, M. I., Wu, B., Maeda, T., Hashimoto, H., et al. (2008). A novel GDP-dependent pyruvate kinase isozyme from *Toxoplasma gondii* localizes to both the apicoplast and the mitochondrion. *J. Biol. Chem.* 283, 14041–14052. doi:10.1074/jbc.M709015200.
- Sam-Yellowe, T. Y., Perkins, M. E., and Interaction, M. E. (1991). Interaction of the 140 / 130 / 110 kDa Rhoptry Protein Complex *Plasmodium falciparum* with the Erythrocyte Membrane and Liposomes Erythrocyte invasion by the malarial parasite is a multistep process involving sequential events : surface attachment , m.

- Exp. Parasitol.* 171, 161–171.
- Sambrook, J., and Russell, D. W. (2001). *Molecular Cloning: A Laboratory Manual*. 3rd ed. New York: Cold Spring Harbor Laboratory Press.
- Sampaio, N. G., Emery, S. J., Garnham, A. L., Tan, Q. Y., Sisquella, X., Pimentel, M. A., et al. (2018). Extracellular vesicles from early stage *Plasmodium falciparum*-infected red blood cells contain PfEMP1 and induce transcriptional changes in human monocytes. *Cell. Microbiol.* 20, 1–18. doi:10.1111/cmi.12822.
- Santana-Filho, F. S., Arcanjo, A. R. D. L., Chehuan, Y. M., Costa, M. R., Martinez-Espinosa, F. E., Vieira, J. L., et al. (2007). Chloroquine-resistant *Plasmodium vivax*, Brazilian Amazon. *Emerg. Infect. Dis.* 13, 1125–1126. doi:10.3201/eid1307.061386.
- Santana, M. S., de Lacerda, M. V. G., Barbosa, M. D. G. V., Duarte Alecrim, W., and Costa Alecrim, M. D. G. (2009). Glucose-6-phosphate dehydrogenase deficiency in an endemic area for malaria in Manaus: A cross-sectional survey in the Brazilian Amazon. *PLoS One* 4, 4–7. doi:10.1371/journal.pone.0005259.
- Sato, S., Clough, B., Coates, L., and Wilson, R. J. M. (2004). Enzymes for heme biosynthesis are found in both the mitochondrion and plastid of the malaria parasite *Plasmodium falciparum*. *Protist* 155, 117–125. doi:10.1078/1434461000169.
- Sato, S., and Wilson, R. J. M. (2002). The genome of *Plasmodium falciparum* encodes an active  $\delta$ -aminolevulinic acid dehydratase. *Curr. Genet.* 40, 391–398. doi:10.1007/s00294-002-0273-3.
- Scherf, A., Lopez-Rubio, J. J., and Riviere, L. (2008). Antigenic variation in *Plasmodium falciparum*. *Annu. Rev. Microbiol.* 62, 445–470. doi:10.1146/annurev.micro.61.080706.093134.
- Schiapparelli, L. M., McClatchy, D. B., Liu, H. H., Sharma, P., Yates, J. R., and Cline, H. T. (2014). Direct detection of biotinylated proteins by mass spectrometry. *J. Proteome Res.* 13, 3966–3978. doi:10.1021/pr5002862.
- Schnider, C. B., Bausch-Fluck, D., Brühlmann, F., Heussler, V. T., and Burda, P.-C. (2018). BioID Reveals Novel Proteins of the *Plasmodium* Parasitophorous Vacuole Membrane. *mSphere* 3, 1–13. doi:10.1128/msphere.00522-17.
- Seidi, A., Muellner-Wong, L. S., Rajendran, E., Tjhin, E. T., Dagley, L. F., Aw, V. Y. T., et al. (2018). Elucidating the mitochondrial proteome of *Toxoplasma gondii* reveals the presence of a divergent cytochrome c oxidase. *Elife* 7, 1–36. doi:10.7554/eLife.38131.

- Sherling, E. S., Knuepfer, E., Brzostowski, J. A., Miller, L. H., Blackman, M. J., and Van Ooij, C. (2017). The *Plasmodium falciparum* rhoptry protein RhopH3 plays essential roles in host cell invasion and nutrient uptake. *Elife* 6, 1–23. doi:10.7554/eLife.23239.
- Singh, B., and Daneshvar, C. (2013). Human infections and detection of *Plasmodium knowlesi*. *Clin. Microbiol. Rev.* 26, 165–184. doi:10.1128/CMR.00079-12.
- Singh, B., Sung, L. K., Matusop, A., Radhakrishnan, A., Shamsul, S. S. G., Cox-Singh, J., et al. (2004). A large focus of naturally acquired *Plasmodium knowlesi* infections in human beings. *Lancet* 363, 1017–1024. doi:10.1016/S0140-6736(04)15836-4.
- Sinka, M. E., Bangs, M. J., Manguin, S., Rubio-Palis, Y., Chareonviriyaphap, T., Coetzee, M., et al. (2012). A global map of dominant malaria vectors. *Parasit. Vectors* 5, 69. doi:10.1186/1756-3305-5-69.
- Smith, J. L., and Brooker, S. (2010). Impact of hookworm infection and deworming on anaemia in non-pregnant populations: A systematic review: Systematic Review. *Trop. Med. Int. Heal.* 15, 776–795. doi:10.1111/j.1365-3156.2010.02542.x.
- Souza, P. F., Xavier, D. R., Mutis, M. C. S., da Mota, J. C., Peiter, P. C., de Matos, V. P., et al. (2019). Spatial spread of malaria and economic frontier expansion in the Brazilian Amazon. *PLoS One* 14, 1–25. doi:10.1371/journal.pone.0217615.
- Spielmann, T., and Gilberger, T. W. (2010). Protein export in malaria parasites: do multiple export motifs add up to multiple export pathways? *Trends Parasitol.* 26, 6–10. doi:10.1016/j.pt.2009.10.001.
- Spielmann, T., Hawthorne, P. L., Dixon, M. W. A., Hannemann, M., Klotz, K., Kemp, D. J., et al. (2006). A Cluster of Ring Stage-specific Genes Linked to a Locus Implicated in Cytoadherence in *Plasmodium falciparum* Codes for PEXEL-negative and PEXEL-positive Proteins Exported into the Host Cell. *Mol. Biol. Cell* 17, 3613–3624. doi:10.1091/mbc.e06-04-0291.
- Spillman, N. J., Beck, J. R., and Goldberg, D. E. (2015). Protein export into malaria parasite-infected erythrocytes: Mechanisms and functional consequences. *Annu. Rev. Biochem.* 84, 813–841. doi:10.1146/annurev-biochem-060614-034157.
- Spycher, C., Klonis, N., Spielmann, T., Kump, E., Steiger, S., Tilley, L., et al. (2003). MAHRP-1, a novel *Plasmodium falciparum* histidine-rich protein, binds ferriprotoporphyrin IX and localizes to the Maurer’s clefts. *J. Biol. Chem.* 278, 35373–35383. doi:10.1074/jbc.M305851200.
- Spycher, C., Rug, M., Klonis, N., Ferguson, D. J. P., Cowman, A. F., Beck, H.-P., et al.

- (2006). Genesis of and Trafficking to the Maurer's Clefts of *Plasmodium falciparum* -Infected Erythrocytes . *Mol. Cell. Biol.* 26, 4074–4085. doi:10.1128/mcb.00095-06.
- Spycher, C., Rug, M., Pachlatko, E., Hanssen, E., Ferguson, D., Cowman, A. F., et al. (2008). The Maurer's cleft protein MAHRP1 is essential for trafficking of PfEMP1 to the surface of *Plasmodium falciparum*-infected erythrocytes. *Mol. Microbiol.* 68, 1300–1314. doi:10.1111/j.1365-2958.2008.06235.x.
- Ssentongo, P., Ba, D. M., Ssentongo, A. E., Ericson, J. E., Wang, M., Liao, D., et al. (2020). Associations of malaria, HIV, and coinfection, with anemia in pregnancy in sub-Saharan Africa: A population-based cross-sectional study. *BMC Pregnancy Childbirth* 20, 1–11. doi:10.1186/s12884-020-03064-x.
- Staines, H. M., Burrow, R., Teo, B. H. Y., Ster, I. C., Kremsner, P. G., and Krishna, S. (2018). Clinical implications of *Plasmodium* resistance to atovaquone/proguanil: A systematic review and meta-analysis. *J. Antimicrob. Chemother.* 73, 581–595. doi:10.1093/jac/dkx431.
- Straimer, J., Gnädig, N. F., Witkowski, B., Amaratunga, C., Duru, V., Ramadani, A. P., et al. (2015). K13-propeller mutations confer artemisinin resistance in *Plasmodium falciparum* clinical isolates. *Science* (80- ). 347, 428–431. doi:10.1126/science.1260867.
- Subramani, R., Barfod, L., Petersen, J. E. V., Hviid, L., Hassenkam, T., Hempel, C., et al. (2015). *Plasmodium falciparum*-Infected Erythrocyte Knob Density Is Linked to the PfEMP1 Variant Expressed. *MBio* 6, 1–7. doi:10.1128/mbio.01456-15.
- Suresh, N., and Haldar, K. (2018). Mechanisms of artemisinin resistance in *Plasmodium falciparum* malaria. *Curr. Opin. Pharmacol.* 42, 46–54. doi:10.1016/j.coph.2018.06.003.
- Tchigossou, G., Djouaka, R., Akoton, R., Riveron, J. M., Irving, H., Atoyebi, S., et al. (2018). Molecular basis of permethrin and DDT resistance in an *Anopheles funestus* population from Benin. *Parasit. Vectors* 11, 1–13. doi:10.1186/s13071-018-3115-y.
- Thanh, N. V., Nhien, N. T., Thi, N., Tuyen, K., Tong, N. T., Thuy, N., et al. (2017). Rapid decline in the susceptibility of *Plasmodium falciparum* to dihydroartemisinin – piperazine in the south of Vietnam. *Malar. J.*, 1–10. doi:10.1186/s12936-017-1680-8.
- Tilley, L., Straimer, J., Gnädig, N. F., Ralph, S. A., and Fidock, D. A. (2016). Artemisinin Action and Resistance in *Plasmodium falciparum*. *Trends Parasitol.* 32, 682–696.

doi:10.1016/j.pt.2016.05.010.

- Trager, W., and Jensen, J. B. (1976). Human Malaria Parasites in Continuous Culture. *Science* (80- ). 193, 673–675.
- Trenholme, K. R., Gardiner, D. L., Holt, D. C., Thomas, E. A., Cowman, A. F., and Kemp, D. J. (2000). clag9: A cytoadherence gene in *Plasmodium falciparum* essential for binding of parasitized erythrocytes to CD36. *Proc. Natl. Acad. Sci.* 97, 4029–4033. doi:10.1073/pnas.040561197.
- Tu, Z., Zhao, H., Li, B., Yan, S., Wang, L., Tang, Y., et al. (2019). CRISPR/Cas9-mediated disruption of SHANK3 in monkey leads to drug-treatable autism-like symptoms. *Hum. Mol. Genet.* 28, 561–571. doi:10.1093/hmg/ddy367.
- Tusting, L. S., Rek, J., Arinaitwe, E., Staedke, S. G., Kanya, M. R., Cano, J., et al. (2016). Why is malaria associated with poverty? Findings from a cohort study in rural Uganda. *Infect. Dis. Poverty* 5, 1–11. doi:10.1186/s40249-016-0164-3.
- Tusting, L. S., Willey, B., Lucas, H., Thompson, J., Kafy, H. T., Smith, R., et al. (2013). Socioeconomic development as an intervention against malaria: A systematic review and meta-analysis. *Lancet* 382, 963–972. doi:10.1016/S0140-6736(13)60851-X.
- van den Berg, H., Manuweera, G., and Konradsen, F. (2017). Global trends in the production and use of DDT for control of malaria and other vector-borne diseases. *Malar. J.* 16, 1–8. doi:10.1186/s12936-017-2050-2.
- van Dooren, G. G., Stimmler, L. M., and McFadden, G. I. (2006). Metabolic maps and functions of the *Plasmodium* mitochondrion. *FEMS Microbiol. Rev.* 30, 596–630. doi:10.1111/j.1574-6976.2006.00027.x.
- Varadharajan, S., Dhanasekaran, S., Bonday, Z. Q., Rangarajan, P. N., and Padmanaban, G. (2002). Involvement of  $\delta$ -aminolaevulinic acid synthase encoded by the parasite gene in de novo haem synthesis by *Plasmodium falciparum*. *Biochem. J.* 367, 321–327.
- Varnaité, R., and MacNeill, S. A. (2016). Meet the neighbors: Mapping local protein interactomes by proximity-dependent labeling with BioID. *Proteomics* 16, 2503–2518. doi:10.1002/pmic.201600123.
- Vélez-Ramírez, D. E., Shimogawa, M. M., Ray, S. S., Lopez, A., Rayatpisheh, S., Langousis, G., et al. (2021). APEX2 Proximity Proteomics Resolves Flagellum Subdomains and Identifies Flagellum Tip-Specific Proteins in *Trypanosoma brucei*. *mSphere* 6, 1–19. doi:https://doi.org/10.1128/mSphere.01090-20.
- Venkatesan, M., Gadalla, N. B., Stepniewska, K., Dahal, P., Nsanzabana, C., Moriera,



- C., et al. (2014). Polymorphisms in *Plasmodium falciparum* chloroquine resistance transporter and multidrug resistance 1 genes: Parasite risk factors that affect treatment outcomes for *P. falciparum* malaria after artemether-lumefantrine and artesunate-amodiaquine. *Am. J. Trop. Med. Hyg.* 91, 833–843. doi:10.4269/ajtmh.14-0031.
- Vermeulen, M., Lelie, N., Coleman, C., Sykes, W., Jacobs, G., Swanevelder, R., et al. (2019). Assessment of HIV transfusion transmission risk in South Africa: a 10-year analysis following implementation of individual donation nucleic acid amplification technology testing and donor demographics eligibility changes. *Transfusion* 59, 267–276. doi:10.1111/trf.14959.
- Vijaykumar, M., Naik, R. S., and Gowda, D. C. (2001). *Plasmodium falciparum* Glycosylphosphatidylinositol-induced TNF- $\alpha$  Secretion by Macrophages is Mediated without Membrane Insertion or Endocytosis. *J. Biol. Chem.* 276, 6909–6912. doi:10.1074/jbc.C100007200.
- Vincensini, L., Fall, G., Berry, L., Blisnick, T., and Braun Breton, C. (2008). The RhopH complex is transferred to the host cell cytoplasm following red blood cell invasion by *Plasmodium falciparum*. *Mol. Biochem. Parasitol.* 160, 81–89. doi:10.1016/j.molbiopara.2008.04.002.
- Wagner, J. C., Platt, R. J., Goldfless, S. J., Zhang, F., and Niles, J. C. (2014). Efficient CRISPR-Cas9-mediated genome editing in *Plasmodium falciparum*. *Nat. Methods* 11, 915–8. doi:10.1038/nmeth.3063.
- Waller, K. L., Nunomura, W., Cooke, B. M., Mohandas, N., and Coppel, R. L. (2002). Mapping the domains of the cytoadherence ligand *Plasmodium falciparum* erythrocyte membrane protein 1 (PfEMP1) that bind to the knob-associated histidine-rich protein (KAHRP). *Mol. Biochem. Parasitol.* 119, 125–129. doi:10.1016/s0166-6851(01)00395-4.
- Waller, R. F., Keeling, P. J., Donald, R. G. K., Striepen, B., Handman, E., Lang-Unnasch, N., et al. (1998). Nuclear-encoded proteins target to the plastid in *Toxoplasma gondii* and *Plasmodium falciparum*. *Proc. Natl. Acad. Sci. U. S. A.* 95, 12352–12357. doi:10.1073/pnas.95.21.12352.
- Waller, R. F., Ralph, S. A., Reed, M. B., Su, V., Douglas, J. D., Minnikin, D. E., et al. (2003). A type II pathway for fatty acid biosynthesis presents drug targets in *Plasmodium falciparum*. *Antimicrob. Agents Chemother.* 47, 297–301. doi:10.1128/AAC.47.1.297-301.2003.
- Waller, R. F., Reed, M. B., Cowman, A. F., and Mcfadden, G. I. (2000). Protein

- trafficking to the plastid of *Plasmodium falciparum* is via the secretory pathway. *EMBO J.* 19, 1794–1802.
- Wang, H., La Russa, M., and Qi, L. S. (2016). CRISPR/Cas9 in Genome Editing and Beyond. *Annu. Rev. Biochem.* 85, 227–264. doi:10.1146/annurev-biochem-060815-014607.
- Wassmer, S. C., and Grau, G. E. R. (2017). Severe malaria: what 's new on the pathogenesis front? *Int. J. Parasitol.* 47, 145–152. doi:10.1016/j.ijpara.2016.08.002.
- Waterkeyn, J. G., Crabb, B. S., and Cowman, A. F. (1999). Transfection of the human malaria parasite *Plasmodium falciparum*. *Int. J. Parasitol.* 29, 945–955. doi:10.1385/1-59259-793-9:263.
- White, N. J. (2018). Anaemia and malaria. *Malar. J.* 17, 1–17. doi:10.1186/s12936-018-2509-9.
- Wickert, H., Wissing, F., Andrews, K. T., Stich, A., Krohne, G., and Lanzer, M. (2003). Evidence for trafficking of PfEMP1 to the surface of *P. falciparum*-infected erythrocytes via a complex membrane network. *Eur. J. Cell Biol.* 82, 271–284. doi:10.1078/0171-9335-00319.
- Wickham, M. E., Rug, M., Ralph, S. A., Klonis, N., Mcfadden, G. I., Tilley, L., et al. (2001). Trafficking and assembly of the cytoadherence complex in *Plasmodium falciparum*-infected human erythrocytes. *EMBO J.* 20, 5636–5649. doi:10.1093/emboj/20.20.5636.
- Wijesekera, S. K., Carter, R., Rathnayaka, L., and Mendis, K. N. (1996). A malaria parasite toxin associated with *Plasmodium vivax* paroxysms. *Clin. Exp. Immunol.* 104, 221–227. doi:10.1046/j.1365-2249.1996.07699.x.
- Wilde, M. L., Triglia, T., Marapana, D., Thompson, J. K., Kouzmitchev, A. A., Bullen, H. E., et al. (2019). Protein kinase A is essential for invasion of *Plasmodium falciparum* into human erythrocytes. *MBio* 10, 1–15. doi:10.1128/mBio.01972-19.
- Winter, R. W., Kelly, J. X., Smilkstein, M. J., Dodean, R., Hinrichs, D., and Riscoe, M. K. (2008). Antimalarial quinolones: Synthesis, potency, and mechanistic studies. *Exp. Parasitol.* 118, 487–497. doi:10.1016/j.exppara.2007.10.016.
- Wright, G. J., and Rayner, J. C. (2014). *Plasmodium falciparum* Erythrocyte Invasion: Combining Function with Immune Evasion. *PLoS Pathog.* 10, 1–7. doi:10.1371/journal.ppat.1003943.
- Wu, J., Platero-Luengo, A., Martinez, E. A., Ross, P. J., Carlos, J., Correspondence, I. B., et al. (2017). Interspecies Chimerism with Mammalian Pluripotent Stem Cells.

- Cell* 168, 473–486. doi:10.1016/j.cell.2016.12.036.
- Wu, Y., Liang, D., Wang, Y., Bai, M., Tang, W., Bao, S., et al. (2013). Brief Report Correction of a Genetic Disease in Mouse via Use of CRISPR-Cas9. *Stem Cell* 13, 659–662. doi:10.1016/j.stem.2013.10.016.
- Xiao, B., Yin, S., Hu, Y., Sun, M., Wei, J., Huang, Z., et al. (2019). Epigenetic editing by CRISPR/dCas9 in *Plasmodium falciparum*. *Proc. Natl. Acad. Sci.* 116, 255–260. doi:10.1073/pnas.1813542116.
- Yeh, E., and DeRisi, J. L. (2011). Chemical rescue of malaria parasites lacking an apicoplast defines organelle function in blood-stage *Plasmodium falciparum*. *PLoS Biol.* 9. doi:10.1371/journal.pbio.1001138.
- Young, C. S., Hicks, M. R., Ermolova, N. V., Nakano, H., Jan, M., Younesi, S., et al. (2016). A Single CRISPR-Cas9 Deletion Strategy that Targets the Majority of DMD Patients Restores Dystrophin Function in hiPSC-Derived Muscle Cells. *Cell Stem Cell* 18, 533–540. doi:10.1016/j.stem.2016.01.021.
- Yu, H., Tardivo, L., Tam, S., Weiner, E., Gebreab, F., Fan, C., et al. (2011). Next-generation sequencing to generate interactome datasets. *Nat. Methods* 8, 478–480. doi:10.1038/nmeth.1597.
- Zhang, W. W., and Matlashewski, G. (2015). CRISPR-Cas9-mediated genome editing in *Leishmania donovani*. *MBio* 6, 1–14. doi:10.1128/mBio.00861-15.
- Zheng, J., Jia, H., and Zheng, Y. (2015). Knockout of leucine aminopeptidase in *Toxoplasma gondii* using CRISPR/Cas9. *Int. J. Parasitol.* 45, 141–148. doi:10.1016/j.ijpara.2014.09.003.

A circular inset showing a microscopic view of numerous red blood cells (erythrocytes) against a dark background. The cells are biconcave and appear as bright red discs. The text "VII - ANEXOS" is overlaid on the right side of the circle.

VII - ANEXOS

## vii. ANEXOS

- **PARTICIPAÇÃO EM EVENTOS CIENTÍFICOS:**

**Participante:** São Paulo School of Advanced Science of Mass spectrometry (SPSAS-MS) (2018). Apresentação de pôster: “***In vivo* protein interaction of KAHRP in *Plasmodium falciparum* erythrocyte cycle stage by APEX2-based proximity tagging mediated by CRISPR- Cas9**”, Centro Nacional de Pesquisa em Energia e Materiais (CNPEM), Campinas, SP.

**Participante:** São Paulo School of Advanced Science of Cell Biology (SPCell) (2018). Apresentação de pôster: “***In vivo* protein interaction of KAHRP in *Plasmodium falciparum* erythrocyte cycle stage by APEX2-based proximity tagging mediated by CRISPR-Cas9**”, Universidade de São Paulo (USP), SP.

**Participante:** 55º Congresso Brasileiro da Sociedade Brasileira de Medicina Tropical / XXVI Congresso Brasileiro de Parasitologia (2019). Apresentação de pôster: “***In vivo* protein interaction of KAHRP in *Plasmodium falciparum* erythrocyte cycle stage by APEX2-based proximity tagging mediated by CRISPR-Cas9**”, Universidade Federal de Minas Gerais (UFMG), Belo Horizonte, MG.

**Palestrante:** I Congresso Internacional de Estudantes e Profissionais da Saúde (2017). Palestra: “O sistema de edição genômica CRISPR-Cas9 no estudo de doenças genéticas, tropicais e negligenciadas: uma nova perspectiva na ciência” / Mini-curso: “Introdução à bioinformática aplicada na análise de genomas”.

**Organização:** II Congresso Nacional Multidisciplinar da Saúde (CoNMSaúde) (2017).

**Organização:** III Congresso Nacional Multidisciplinar da Saúde (CoNMSaúde) (2018).

**Organização:** III Simpósio do Programa de Pós-Graduação em Patologia Molecular (2018).

- **ARTIGOS PUBLICADOS EM PERIÓDICOS INTERNACIONAIS (2017-2021)**

**Oliveira LS**, Alborghetti MR, Carneiro RG, Bastos IMD, Amino R, Grellier P, Charneau S. Calcium in the Backstage of Malaria Parasite Biology. *Front Cell Infect Microbiol.* 2021 Jul 28;11:708834. doi: 10.3389/fcimb.2021.708834. PMID: 34395314; PMCID: PMC8355824.

Mandacaru SC, Queiroz RML, Alborghetti MR, **Oliveira LS**, de Lima CMR, Bastos IMD, Santana JM, Roepstorff P, Ricart CAO, Charneau S. Exoproteome profiling of *Trypanosoma cruzi* during amastigogenesis early stages. *PLoS One.* 2019 Nov 22;14(11):e0225386. doi: 10.1371/journal.pone.0225386. PMID: 31756194; PMCID: PMC6874342.

Oliveira AS, Rosa IIR, Novaes E, **Oliveira LS**, Baeza LC, Borges CL, Marlinghaus L, Soares CMA, Giambiagi-deMarval M, Parente-Rocha JA. The exoproteome profiles of three *Staphylococcus saprophyticus* strains reveal diversity in protein secretion contents. *Microbiol Res.* 2018 Nov;216:85-96. doi: 10.1016/j.micres.2018.08.008. Epub 2018 Aug 23. PMID: 30269860.

Oliveira AS, Rosa IIR, Novaes E, **Oliveira LS**, Baeza LC, Borges CL, Marlinghaus L, de Almeida Soares CM, Giambiagi-deMarval M, Parente-Rocha JA. A proteomic dataset of secreted proteins by three *Staphylococcus saprophyticus* strains. *Data Brief.* 2018 Oct 27;21:1472-1476. doi: 10.1016/j.dib.2018.10.122. PMID: 30456272; PMCID: PMC6234272.



# Calcium in the Backstage of Malaria Parasite Biology

Lucas Silva de Oliveira<sup>1,2†</sup>, Marcos Rodrigo Alborghetti<sup>1,3†</sup>, Renata Garcia Carneiro<sup>1</sup>, Izabela Marques Dourado Bastos<sup>4</sup>, Rogerio Amino<sup>5</sup>, Philippe Grellier<sup>2</sup> and Sébastien Charneau<sup>1\*</sup>

<sup>1</sup> Laboratory of Biochemistry and Protein Chemistry, Department of Cell Biology, Institute of Biology, University of Brasilia, Brasilia, Brazil, <sup>2</sup> UMR 7245 MCAM, Molécules de Communication et Adaptation des Micro-organismes, Muséum National d'Histoire Naturelle, CNRS, Équipe Parasites et Protistes Libres, Paris, France, <sup>3</sup> Brazilian Biosciences National Laboratory, Brazilian Center for Research in Energy and Materials, Campinas, Brazil, <sup>4</sup> Laboratory of Host-Pathogen Interaction, Department of Cell Biology, Institute of Biology, University of Brasilia, Brasilia, Brazil, <sup>5</sup> Unité Infection et Immunité Paludéennes, Institut Pasteur, Paris, France

## OPEN ACCESS

### Edited by:

Nobuko Yoshida,  
Federal University of São Paulo, Brazil

### Reviewed by:

Celia R. S. Garcia,  
University of São Paulo, Brazil  
Paul R. Gilson,  
Burnet Institute, Australia  
Sanjay A. Desai,  
National Institutes of Health (NIH),  
United States

### \*Correspondence:

Sébastien Charneau  
charneau@unb.br

<sup>†</sup>These authors have contributed  
equally to this work

### Specialty section:

This article was submitted to  
Parasite and Host,  
a section of the journal  
Frontiers in Cellular and  
Infection Microbiology

**Received:** 12 May 2021

**Accepted:** 14 July 2021

**Published:** 28 July 2021

### Citation:

de Oliveira LS, Alborghetti MR,  
Carneiro RG, Bastos IMD, Amino R,  
Grellier P and Charneau S (2021)  
Calcium in the Backstage of  
Malaria Parasite Biology.  
Front. Cell. Infect. Microbiol. 11:708834.  
doi: 10.3389/fcimb.2021.708834

The calcium ion (Ca<sup>2+</sup>) is a ubiquitous second messenger involved in key biological processes in prokaryotes and eukaryotes. In *Plasmodium* species, Ca<sup>2+</sup> signaling plays a central role in the parasite life cycle. It has been associated with parasite development, fertilization, locomotion, and host cell infection. Despite the lack of a canonical inositol-1,4,5-triphosphate receptor gene in the *Plasmodium* genome, pharmacological evidence indicates that inositol-1,4,5-triphosphate triggers Ca<sup>2+</sup> mobilization from the endoplasmic reticulum. Other structures such as acidocalcisomes, food vacuole and mitochondria are proposed to act as supplementary intracellular Ca<sup>2+</sup> reservoirs. Several Ca<sup>2+</sup>-binding proteins (CaBPs) trigger downstream signaling. Other proteins with no EF-hand motifs, but apparently involved with CaBPs, are depicted as playing an important role in the erythrocyte invasion and egress. It is also proposed that a cross-talk among kinases, which are not members of the family of Ca<sup>2+</sup>-dependent protein kinases, such as protein kinases G, A and B, play additional roles mediated indirectly by Ca<sup>2+</sup> regulation. This statement may be extended for proteins directly related to invasion or egress, such as SUB1, ERC, IMC11, IMC1g, GAP45 and EBA175. In this review, we update our understanding of aspects of Ca<sup>2+</sup>-mediated signaling correlated to the developmental stages of the malaria parasite life cycle.

**Keywords:** Ca<sup>2+</sup> signaling, *Plasmodium*, intracellular messenger, homeostasis, invasion, egress

## INTRODUCTION

A plethora of cell types employ the calcium ion (Ca<sup>2+</sup>), mobilized from extracellular and/or intracellular environments, to coordinate different Ca<sup>2+</sup>-dependent processes. The control of intracellular Ca<sup>2+</sup> signals is dynamic. Overall, fluctuations in Ca<sup>2+</sup> concentrations are modulated by an influx and/or efflux promoted by membrane channels, such as store-operated calcium channels (SOCEs), plasma membrane Ca<sup>2+</sup>-ATPase (PMCA) and sarco(endo)plasmic reticulum Ca<sup>2+</sup>-ATPase (SERCA) pumps. Generally, this orchestration in the Ca<sup>2+</sup> concentration follows a signaling pathway that obeys the order: stimuli, G-protein coupled receptor, phospholipase C (PLC)

activation, mobilization of phosphatidylinositol 4,5-bisphosphate (PI(4,5)P<sub>2</sub>), production of inositol 1,4,5-phosphate (IP<sub>3</sub>), IP<sub>3</sub> recognition by IP<sub>3</sub>-sensitive receptor channels (IP<sub>3</sub>Rs) in the endoplasmic reticulum (ER) and downstream Ca<sup>2+</sup> cascade (Berridge et al., 2003; Clapham, 2007).

In the group of apicomplexan parasites, the protozoan parasites *Toxoplasma gondii* and *Plasmodium* spp. are the most well-established study models. In *T. gondii*, Ca<sup>2+</sup> signaling is involved in specific parasite processes: motility, conoid extrusion, attachment, invasion and egress from the host cell (Borges-Pereira et al., 2015; Hortua-Triana et al., 2018). Similarly, Ca<sup>2+</sup> homeostasis and signaling have been extensively studied in *Plasmodium* species. Malaria is still the most life-threatening vector-borne disease globally, with an estimated 409,000 deaths and 229 million cases reported in 2019 (Global Malaria Programme: WHO Global, 2020). The increase and dissemination of antimalarial resistance (Cowman et al., 2016; Phillips et al., 2017; Global Malaria Programme: WHO Global, 2020), together with the augmentation of malaria cases since 2015, point to an urgent need for the discovery of new antimalarial drugs. The *Plasmodium* life cycle is strongly regulated by fluctuations in Ca<sup>2+</sup> cellular levels, with deficiency causing impairment in parasite growth and invasion rate (Wasserman et al., 1982). This ion also acts as a messenger regulating critical *Plasmodium* biological processes. As such, proteins involved in Ca<sup>2+</sup> homeostasis and signaling are strong candidates as new antimalarial targets (Gazarini et al., 2007; Vidadala et al., 2014; Mossaad et al., 2015; Bansal et al., 2016; Fang et al., 2017; Iyer et al., 2018). In this review, we present an overview of the mechanisms related to the Ca<sup>2+</sup> homeostasis in *Plasmodium* species and an update of the main downstream Ca<sup>2+</sup> signaling pathways and effectors involved in the parasite motility, invasion, development, and egress.

## Ca<sup>2+</sup> HOMEOSTASIS IN MALARIA PARASITES

Ca<sup>2+</sup> signaling is widely conserved in Eukaryotes, with reliance on this ion as a secondary messenger to switch on or off diverse biological process. Given their evolutionary distance from other Eukaryotes, malaria parasites represent a challenging task for the study of Ca<sup>2+</sup>-mediated mechanisms, with Ca<sup>2+</sup> uptake by this microorganism presenting several peculiar features. Since *Plasmodium* asexual developmental stages are predominantly intracellular in red blood cells (RBCs), Ca<sup>2+</sup> has to cross several barriers to reach the parasite, which include the red blood cell membrane (RBCM) and parasitophorous vacuole membrane (PVM) (Kirk, 2001; Kirk, 2004; Kirk and Lehane, 2014).

Ca<sup>2+</sup> fluctuations in *Plasmodium* species are very complex and demand the support of intracellular Ca<sup>2+</sup> storage. For example, gametocytes or schizont fractions from *Plasmodium chabaudi* infected RBCs (iRBCs) present 10-20 times more Ca<sup>2+</sup> than uninfected RBCs. Moreover, it has been observed that this ion concentrates in parasite storage compartments (Tanabe et al., 1982). This pattern of Ca<sup>2+</sup> concentration was also observed in

*Plasmodium falciparum* (Adovelande et al., 1993). To overcome these barriers and promote the observed intracellular Ca<sup>2+</sup> increase, malaria parasites facilitate RBCM permeability, causing increased Ca<sup>2+</sup> influx and decreased Ca<sup>2+</sup> efflux (Tanabe et al., 1982; Desai et al., 1996). A nonselective cation conductance at RBCM, induced by *P. falciparum* growth, has been proposed as a mechanism involved in Ca<sup>2+</sup> permeability (Brand et al., 2003; Duranton et al., 2003). Furthermore, Na<sup>+</sup> associated to Ca<sup>2+</sup> influx is also involved in intracellular parasite growth by this mechanism, potentially involving an ethylisopropyl-amiloride (EIPA)-sensitive channel (Brand et al., 2003).

In addition to the RBCM, PVM is another barrier to Ca<sup>2+</sup> reaching the *Plasmodium* parasite. Using a cell-attached path clamp method, a 140-pS channel that is permeable to Ca<sup>2+</sup>, other ions and nutrients was identified and proposed to mediate this transport through the PVM (Desai et al., 1993). Despite such advances, mechanisms involving Ca<sup>2+</sup> transport into malaria parasites remain poorly understood, with considerable attention now given to this area with regard to potential therapeutic intervention. Blocking the *Plasmodium* translocon for exported proteins machinery (PTEX)-mediated protein export across the PV and out into the RBC cytosol by conditional knockdown approach, significantly reduced Ca<sup>2+</sup> permeability in iRBCs (Kushwaha et al., 2018), revealing that exported parasite proteins are potentially involved in Ca<sup>2+</sup> uptake and transport.

Determination of the concentration of intracellular Ca<sup>2+</sup> in apicomplexan parasites is still controversial, primarily because of the technical limitations due to inhibitors, ionophores and fluorometric measurement assay sensitivities. It is widely accepted that the intracellular concentration of Ca<sup>2+</sup> is around 0.09-0.1 μM in physiological conditions, similar to those found in other Eukaryotes (Alleva and Kirk, 2001; Moreno et al., 2011; Lourido and Moreno, 2015). Nonetheless, an increase of up to a hundred-fold in Ca<sup>2+</sup> concentrations was noted in the late stage of the intraerythrocytic cycle forms, ranging from 1-10 μM (Glushakova et al., 2013). Also, a high Ca<sup>2+</sup> concentration (40 μM) was reported in the parasitophorous vacuole (PV) required for proper parasite development (Gazarini et al., 2003). More recently, by using the Ca<sup>2+</sup> sensor yellow cameleon (YC)-Nano, dynamic measurement of intracellular Ca<sup>2+</sup> in different life stages of *P. falciparum* shows significant fluctuations throughout the parasite development: ring (~370 nM), trophozoite (~30 nM), schizont (~310 nM), merozoite (~950 nM), and gametocyte (stage III, ~130 nM, stage IV-V, ~520 nM) stages (Pandey et al., 2016).

Actors modulating such Ca<sup>2+</sup> fluctuations have now begun to be identified, although it is still a subject under debate. For example, cytoplasmic Ca<sup>2+</sup> increase may be related to potassium (K<sup>+</sup>) availability, especially when parasites are faced with an abrupt change from high to low K<sup>+</sup> concentration. Exposition of *P. falciparum* merozoites to an ionic environment with a low K<sup>+</sup> concentration (which is the environment usually found by parasites after egress from RBCs) increases the levels of cytosolic Ca<sup>2+</sup> (Singh et al., 2010). This leads to the production of cyclic-adenosine monophosphate (cAMP) by PfACβ



(adenylyl-cyclase  $\beta$ ) upon  $\text{HCO}_3^-$  (bicarbonate ions) stimulation, followed by activation of protein kinase A (PKA) and microneme secretion (Dawn et al., 2014; Kumar et al., 2017). However, exactly how  $\text{K}^+$  acts on signaling for merozoite maturation and invasion is controversial, in contrast to intracellular cationic remodeling in iRBC (Pillai et al., 2013).

In addition, it was also demonstrated that a putative and conserved protein member from the Epac (exchange protein directly activated by cAMP, PF3D7\_1417400) pathway in *P. falciparum* is potentially involved in the rise of cytosolic  $\text{Ca}^{2+}$  levels, facilitating *P. falciparum* merozoite invasion by triggering microneme secretion (Dawn et al., 2014). Nonetheless, this pathway is apparently not required for parasite growth and egress (Patel et al., 2019). Moreover, key elements in this  $\text{Ca}^{2+}$  mobilization were shown to involve the serpentine GPCR-like receptor *PfSR25*, a monovalent cation sensor coupled to PLC in triggering the cytoplasmic  $\text{Ca}^{2+}$  increase. Data also support the involvement of *PfSR25* in parasite stress survival (Moraes et al., 2017).

Host molecules can also modulate parasite  $\text{Ca}^{2+}$  levels. For example, melatonin, which appears as a critical signal controlling

synchronous maturation of *Plasmodium in vivo*, triggers an increase in  $\text{Ca}^{2+}$  cytoplasmic concentration through  $\text{Ca}^{2+}$  release from intracellular stores by an  $\text{IP}_3$ -dependent pathway activation (Gazarini et al., 2003; Beraldo et al., 2005; Beraldo et al., 2007; Alves et al., 2011; Pecenin et al., 2018). Under melatonin stimulation,  $\text{Ca}^{2+}$  mobilization is affected by the melatonin receptor antagonist luzindole, the PLC inhibitor U73122 (Hotta et al., 2000) and  $\text{IP}_3$  receptor blockers (2-APB, 2-aminoethyl diphenylborinate derivatives) (Beraldo et al., 2007; Pecenin et al., 2018). Together, these data support a complex  $\text{Ca}^{2+}$ -signalling network in high demand for intraerythrocytic parasite development (Figure 1).

## $\text{Ca}^{2+}$ STORAGE ORGANELLES

### Endoplasmic Reticulum (ER)

The ER is the central organelle for  $\text{Ca}^{2+}$  storage, with a specific pathway to control calcium influx and efflux in the cell of apicomplexan parasites (Moreno et al., 2011; Lourido and

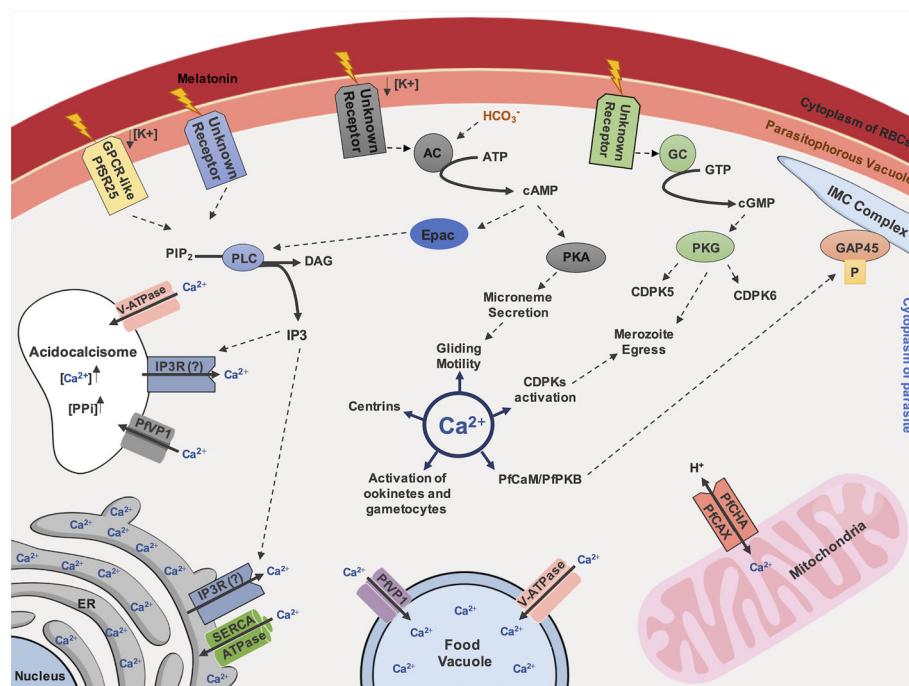


**FIGURE 1** |  $\text{Ca}^{2+}$ -dependent signaling pathway in *Plasmodium* species.  $\text{Ca}^{2+}$  inside the cytoplasm of parasite controls important processes for parasite survival, such as gliding motility, mediated by activation of PfCaM/PfPKB complex and following phosphorylation of the IMC member protein, GAP45. Additionally, centrins, CDPKs activation, activation of ookinetes and gametocytes are described as  $\text{Ca}^{2+}$ -regulated. A GPCR-like protein, named as PfSR25, has been described as potential regulator in  $\text{Ca}^{2+}$  homeostasis in malaria parasites, depending on availability of potassium ( $\text{K}^+$ ) and mediated by  $\text{IP}_3$  signaling. Melatonin was also described as a trigger for  $\text{IP}_3$  dependent pathways. Endoplasmic Reticulum (ER) is reported as the major storage of  $\text{Ca}^{2+}$  and the uptake of this ion possibly depends on SERCA-type  $\text{Ca}^{2+}$ -ATPases.  $\text{Ca}^{2+}$  discharge depends on receptors activated by  $\text{IP}_3$ , nonetheless, an  $\text{IP}_3$ R remains to be discovered in *Plasmodium* species. The presence of V-ATPase and VP1 on the food vacuole and acidocalcisome membranes are related to the  $\text{Ca}^{2+}$  uptake upon an acidic environment maintenance. Acidocalcisome could also have an  $\text{IP}_3$ R that allows exit of  $\text{Ca}^{2+}$ . Calcium can also enter in mitochondria through  $\text{Ca}^{2+}/\text{H}^+$  antiporter called PfCHA/PfCAX. Activation of PKA and PKG, by cAMP and cGMP, respectively, generated by adenylyl-cyclase (AC) and guanylyl-cyclase (GC), respectively, could also participate in  $\text{Ca}^{2+}$  homeostasis, however the membrane receptors that stimulate these pathways remains to be elucidated. Still, upon  $\text{HCO}_3^-$  activation, AC can also stimulate Epac activation by cAMP, triggering  $\text{IP}_3$  signaling through PLC activation. Additionally, a cross-talk among kinases are also proposed to be associated to the merozoite egress mediated by proteolytic cascade events.

Moreno, 2015). Both *P. falciparum* and *T. gondii* have  $\text{Ca}^{2+}$  pumps in the ER membrane, known as SERCA-type  $\text{Ca}^{2+}$ -ATPases, that provide  $\text{Ca}^{2+}$  transport activity (Eckstein-Ludwig et al., 2003; Nagamune et al., 2007; Nagamune et al., 2008). *Pf*ATP6 is the only SERCA-type  $\text{Ca}^{2+}$ -ATPase found in the *P. falciparum* genome (Gardner et al., 2002). Due to structural similarities to a SERCA inhibitor, known as thapsigargin (Thg), the antimalarial drug, artemisinin, was thought to act against *Pf*ATP6, occasionally inhibiting  $\text{Ca}^{2+}$  mobilization into ER. Initial evidence for this hypothesis were observed in *Xenopus* oocysts expressing different *P. falciparum* transporters, including *Pf*ATP6 (Eckstein-Ludwig et al., 2003). However, molecular docking and experimental validation assays showed that the interaction between *P. falciparum* SERCA (*Pf*SERCA) and dihydroartemisinin (dART) was ~2.3-fold weaker than those observed between human SERCA and dART, indicating that dART do not inhibit *Pf*SERCA pump activity, refuting the initial conclusion (Pandey et al., 2016).

Generally,  $\text{Ca}^{2+}$  mobilization from ER storage requires IP3 activation. The production of this molecular signal is provided by PLC (Singh and Chitnis, 2012; Brochet and Billker, 2016). Although IP3-mediated  $\text{Ca}^{2+}$  release from intracellular stores have been widely reported (Lovett et al., 2002; Alves et al., 2011; Glushakova et al., 2013; Pecenin et al., 2018; Borges-Pereira et al., 2020), no genetic information is known about the presence of IP3R in apicomplexan (Lourido and Moreno, 2015; Garcia et al., 2017). It has been widely accepted that a different IP3-dependent mechanism may exist in apicomplexan to mobilize  $\text{Ca}^{2+}$  from intracellular stores (Moreno et al., 2011; Lourido and Moreno, 2015). This statement is based on many reports, which have shown that upstream inhibition of the IP3 pathway by using PLC inhibitor (Hotta et al., 2000; Beraldo et al., 2005; Beraldo et al., 2007), and downstream inhibition by using IP3 receptor blocker (Beraldo et al., 2007; Pecenin et al., 2018) and SERCA inhibitor (Alves et al., 2011; Glushakova et al., 2013; Pecenin et al., 2018; Borges-Pereira et al., 2020), all lead to the blockage of  $\text{Ca}^{2+}$  mobilization in- or outward from the cytosolic environment or IP3-sensitive stores. Since there is no clear evidence that an IP3R exists at the ER in *Plasmodium* species, how  $\text{Ca}^{2+}$  mobilization occurs into this compartment and how the ER may contribute to  $\text{Ca}^{2+}$  homeostasis through an IP3-sensible mechanism are still unresolved.

## Acidic Organelles

Other  $\text{Ca}^{2+}$ -storage organelles are described in Apicomplexans, such as acidocalcisomes and food vacuole (FV), which stock  $\text{Ca}^{2+}$  in an acidic environment (Lourido and Moreno, 2015). The acidocalcisome is a lysosomal-like compartment, rich in pyrophosphate (PPi), polyphosphate (PolyP) complexed with  $\text{Ca}^{2+}$  and other cations (Moreno and Docampo, 2009; Docampo and Huang, 2016). This organelle was observed in *P. falciparum* by Ruiz et al. (2004) after being described in other parasites, such as *Trypanosoma brucei* (Vercesi et al., 1994), *Trypanosoma cruzi* (Docampo et al., 1995) and *T. gondii* (Moreno and Zhong, 1996).

Two enzymes found in the *P. falciparum* genome, described as vacuolar- $\text{H}^+$ -pyrophosphatase (VP1) and vacuolar- $\text{H}^+$ -

ATPase (V-ATPase), can use PPi and ATP, respectively, to pump protons toward the lumen of acidocalcisomes, providing acidification of the structures, supporting  $\text{Ca}^{2+}$ -storage maintenance in these organelles (Docampo et al., 2005). VP1 and V-ATPase are also localized in the FV in *Plasmodium* species, suggesting this acidic compartment may also have a role in regulating  $\text{Ca}^{2+}$ -storage (Saliba et al., 2003). The potential role of these acidic organelles in  $\text{Ca}^{2+}$  storage is supported by the V-ATPase and VP1 blockage in malaria parasites by their respective inhibitors, bafilomycin  $\text{A}_1$  and amino-methylene-diphosphonate (AMDP), causing an increase in cytosolic  $\text{Ca}^{2+}$  levels (Luo et al., 1999; Biagini et al., 2003).

While the FV in malaria parasites can store around 300-400 nM of  $\text{Ca}^{2+}$ , this compartment is not considered a major intracellular  $\text{Ca}^{2+}$  store organelle (Biagini et al., 2003; Rohrbach et al., 2005). Despite the pH-dependency for  $\text{Ca}^{2+}$  maintenance in the FV, measurement of this ion is challenging, considering the different pH of cellular compartments (Rohrbach et al., 2005). Moreover, the role of FV is associated with hemoglobin degradation (Moura et al., 2009; Tong et al., 2018), chloroquine (CQ) action and CQ-resistance in malaria parasites (Ehlgen et al., 2012; Tong et al., 2018). *P. falciparum* chloroquine resistance transporter (*Pf*CRT), present in the food vacuole membrane (FVM), is apparently very important to balance these processes (Ehlgen et al., 2012; Lee et al., 2018), including its participation in the release of  $\text{Ca}^{2+}$  from FV (Lee et al., 2018).

The involvement of  $\text{Ca}^{2+}$  in the functions of FV was initially suggested in *P. chabaudi* by using CQ, where the balance between concentration of intracellular  $\text{Ca}^{2+}$  and  $\text{Ca}^{2+}$  in acidic organelles were affected (Gazarini et al., 2007). This could be explained by the parasite's FV permeability to low-micromolar levels of CQ, leading to  $\text{Ca}^{2+}$  efflux (Ch'ng et al., 2011). Despite FV potentially playing a role in dynamic intracellular  $\text{Ca}^{2+}$  storage during asexual intraerythrocytic development (Biagini et al., 2003; Lee et al., 2018), the peculiar metabolic features of this organelle shed light on the possibilities for rational drug design against *Plasmodium* species. For example, a recent report showed that from the 400 Pathogen Box compounds, 10 displayed disruption of FV  $\text{Ca}^{2+}$  levels comparable to those with CQ, suggesting a compromised FV membrane integrity leading to programmed cell death (PCD) in the parasite (Tong et al., 2018).

A number of reports have discussed new perspectives on acidocalcisomes in parasites. In *T. gondii*, the  $\text{Ca}^{2+}/\text{H}^+$ -ATPase (TgA1) and a vacuolar-type  $\text{H}^+$ -pyrophosphatase (TgVP1) are localized in these organelles (Luo et al., 2001; Drozdowicz et al., 2003). Gene disruption revealed that TgA1 is required for polyphosphate storage, intracellular  $\text{Ca}^{2+}$  homeostasis, microneme secretion, invasion and virulence (Luo et al., 2005). Moreover,  $\text{Ca}^{2+}$  uptake occurs in these structures by proton pumping activity (Rohloff et al., 2011). In *Trypanosoma brucei*, an IP3R was found in the acidocalcisomes, suggesting that, besides the usual pathway for ER  $\text{Ca}^{2+}$  release, IP3 can also provide additional regulation for  $\text{Ca}^{2+}$  mobilization from acidocalcisomes (Huang et al., 2013). Proteomic analysis of this

structure in *T. brucei* confirmed the presence of IP3R. The presence of VP1, V-ATPase and vacuolar- $\text{Ca}^{2+}$ -ATPase (TbPMC1) was also revealed, highlighting evidence of an acidic environment for  $\text{Ca}^{2+}$  maintenance (Huang et al., 2014). Given the evolutionary evidence of the acidocalcisome (Docampo et al., 2010), it should be not surprising that similar mechanisms may be found in *Plasmodium* species, supporting  $\text{Ca}^{2+}$  homeostasis in these parasites (**Figure 1**).

## Mitochondrion

Besides the primary role of mitochondria in cellular energy metabolism, they can store  $\text{Ca}^{2+}$  in both human and murine malaria species (Uyemura et al., 2000). Parasite mitochondria can accumulate part of the  $\text{Ca}^{2+}$  released in the cytoplasm by pharmacological agents, suggesting a role in maintaining  $\text{Ca}^{2+}$  homeostasis (Gazarini and Garcia, 2004). Interestingly, melatonin modulates transcript levels of three genes potentially related to mitochondria fusion/fission in *P. falciparum*: FIS1, DYN1 and DYN2 (Scarpelli et al., 2018). Considering that melatonin has already been associated with  $\text{Ca}^{2+}$  mobilization (Gazarini et al., 2003; Beraldo et al., 2005; Beraldo et al., 2007; Alves et al., 2011; Pecenin et al., 2018), *Plasmodium* mitochondrion fusion/fission could potentially be controlled by  $\text{Ca}^{2+}$  signaling during the asexual life cycle.

In addition, the expression of the mitochondrial  $\text{Ca}^{2+}/\text{H}^{+}$  antiporter gene *pfcha* (or  $\text{Ca}^{2+}/\text{H}^{+}$  exchanger, PfCAX) from *P. falciparum* in the *Xenopus laevis* oocysts has been shown to cause  $\text{Ca}^{2+}$  uptake after the alkalization of the intracellular environment, suggesting that the out- or inward-directed  $\text{Ca}^{2+}$  proton movement is pH-dependent (Rotmann et al., 2010). Regarding this feature in  $\text{Ca}^{2+}$  transport in *P. berghei*, PbcAX expression has been observed in certain sexual stages (gametocytes, zygotes and ookinetes), essential to ookinete forms and parasite transmission to the mosquito *in vivo*, but not essential to the erythrocytic stages of *P. berghei*. A *pbcax* disrupted strain revealed a stage-specific role of this transporter for *Plasmodium* survival (Guttery et al., 2013).

$\text{Ca}^{2+}$  disturbance of the *Plasmodium* FV caused by CQ-treatment directly affects the mitochondrial transmembrane potential (Ch'ng et al., 2011; Tong et al., 2018) and triggers a PCD-like phenotype (Tong et al., 2018), providing evidence for  $\text{Ca}^{2+}$ -regulating a functional interplay between *Plasmodium* FV and mitochondria. Additional studies are required to understand the roles of the malaria parasite mitochondrion in  $\text{Ca}^{2+}$  fluctuation and how CQ affects mitochondrial membrane potential in a  $\text{Ca}^{2+}$ -dependent manner in the FV (**Figure 1**).

## $\text{Ca}^{2+}$ BINDING PROTEINS (CaBPs)

CaBPs are conserved among species and present a helix-loop-helix structural motif, known as an EF-hand motif. This motif is generally pair-structured and exposes its calcium-binding domain where two  $\text{Ca}^{2+}$  ions connect to it. Analysis of the *P. falciparum* genome databank (PlasmoDB) identified 103 potential proteins with EF-hand motifs. Nonetheless, this

number is undoubtedly overestimated due to the divergence of the EF-hand motif and some rifins. Without rifins, 43 proteins containing EF-hands were recorded in *P. falciparum* (Lourido and Moreno, 2015). Some reports have proposed that this number is even lower, with about only 30 putative CaBPs (Brochet and Billker, 2016). Three main families of CaBPs are categorized in the Apicomplexa: the calmodulin (CaM) family (including centrins or caltractrins), the calcineurin B-like (CBL) family and the  $\text{Ca}^{2+}$ -dependent protein kinases (CDPK) family (Moreno et al., 2011; Lourido and Moreno, 2015; Brochet and Billker, 2016).

Calmodulin in *P. falciparum* (PfCaM) is localized diffusely in the cytoplasm during mature stages of the intraerythrocytic cycle and at the apical pole end of merozoites within the ductule of rhoptries (Scheibel et al., 1987). Furthermore, a protein kinase B (PfPKB) interacts with PfCaM, which is not a member of the CDPK family, in the schizont/merozoite stages of *P. falciparum*. PfPKB is regulated by PfCaM in a  $\text{Ca}^{2+}$ -dependent manner when the generation of IP3 by PLC mediates  $\text{Ca}^{2+}$  release. Consequently, PLC is an upstream modulator of PfPKB activity, regulating  $\text{Ca}^{2+}$  levels inside the parasite and allowing PfCaM-PfPKB interaction (Vaid and Sharma, 2006; Vaid et al., 2008). This protein complex phosphorylates PfGAP45, an anchoring protein of the actin-myosin motor complex from the IMC (inner membrane complex) (Vaid et al., 2008).

Current understanding is limited regarding a group of four *P. falciparum* centrins (PfcENs 1 to 4: PF3D7\_0107000, PF3D7\_1446600, PF3D7\_1027700 and PF3D7\_1105500, respectively), that contain four EF-hand motifs. This group of proteins are involved in parasite cell division at centrosome-like structures, probably in a  $\text{Ca}^{2+}$ -dependent manner (Mahajan et al., 2008). A recent report showed that during mitosis, PbcEN-4 is localized at distinct perinuclear foci, suggesting an association to the putative centrosomal structure, known as the microtubule-organizing center (MTOC) in *P. berghei*. Moreover, *cen-4* gene does not seem to be compensated by increased transcription levels of other centrins and it is dispensable for malaria proliferation (Roques et al., 2019). In contrast, large-scale functional screening of *P. berghei* showed that *cen-1* and *cen-2* genes are essential for parasite survival (Bushell et al., 2017) (**Figure 1**). Other CaBPs and their participation in diverse cellular processes in malaria parasites will be discussed in the next sections (**Figure 2**).

## $\text{Ca}^{2+}$ -DEPENDENT PROTEIN KINASES (CDPKs)

Protein phosphorylation is one of the most studied post-translational modifications in eukaryotic cellular processes. Regarding the importance of  $\text{Ca}^{2+}/\text{CaM}$  in kinase activation, many classes of  $\text{Ca}^{2+}/\text{CaM}$ -dependent kinases (CaMKs) are known in mammals. *P. falciparum* protein kinase 2 (PfPK2) is the unique homolog of human functional CaMK that phosphorylates its substrate in a  $\text{Ca}^{2+}$ - and CaM-dependent manner, and it is expressed during invasion (Kato et al., 2008).

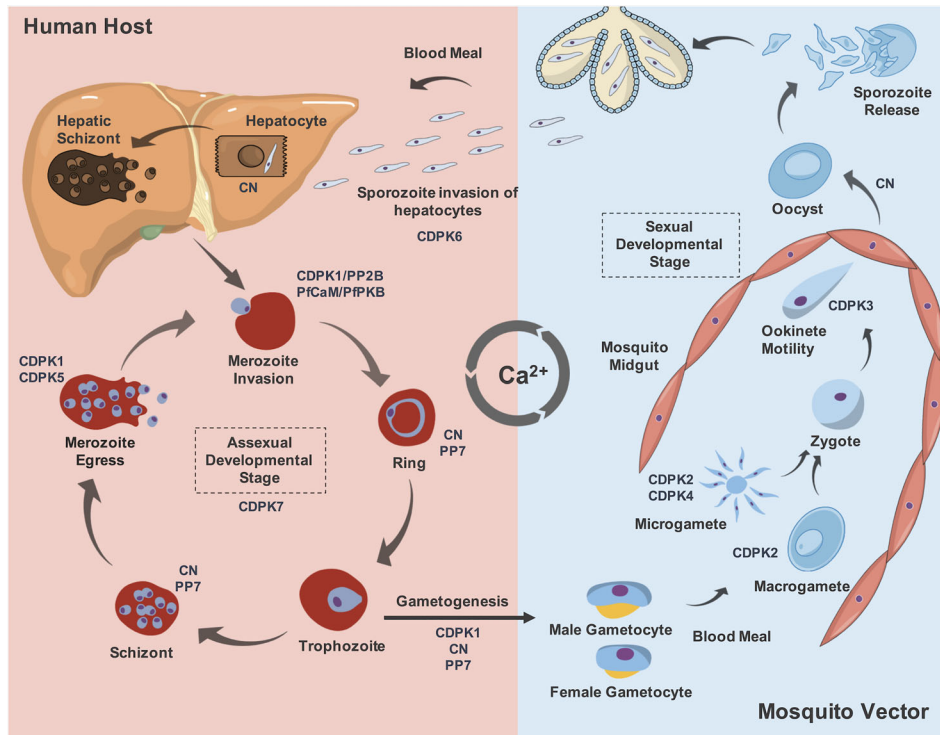


**FIGURE 2** | The role of some described  $\text{Ca}^{2+}$ -binding proteins involved in the development stage differentiation and their expression throughout *Plasmodium* life cycle. During the blood meal, the mosquito vector from genus *Anopheles*, inoculate sporozoites released from its salivary glands that will invade hepatocytes. This process is described to be CDPK6-dependent. Moreover, CN allows sporozoite-to-liver stages development inside hepatocytes. Following formation of merozoites in the liver cells, they are released in the bloodstream to continue asexual development stages, invading new RBCs. This process is mediated by CDPK1, CN and Pfcam/PfPKB complex. The role of CDPK7 to maintain the asexual developmental stages is also reported. In addition, the presence of the phosphatases CN and PP7 are implicated in the ring and schizont stages. After schizont maturation, the merozoites are released into the bloodstream to invade new RBCs, which mechanism that requires the action of CDPK1 and CDPK5. Some parasites pass through a morphological transition to form gametocytes, and this process depends on CDPK1, CN and PP7. After a blood meal of the mosquito vector, these forms mature into male exflagellated and female gametocytes, named as microgametes and macrogametes, respectively. For this transition, CDPK2 and CDPK4 are required. These forms are fused into a zygote, which matures to a motile ookinete. The ookinete motility is regulated by CDPK3. The ookinete exits from the lumen of mosquito midgut as an oocyst and this transition is mediated by CN. The maturation of the oocyst will release new sporozoites which will migrate into the salivary glands of the mosquito vector. Thus, in an eventual blood meal, these new sporozoites will infect a new host and complete the parasite life cycle in order to propagate malaria disease.

However, apicomplexan parasites use a group of  $\text{Ca}^{2+}$ -dependent protein kinases (CDPKs), which are not present in humans. Canonical CDPKs have four EF-hand  $\text{Ca}^{2+}$ -binding domains attached to the C-terminus of a catalytic kinase domain that shows high homology with CaMK. While CaMKs can self-inhibit through a C-terminal helix, CDPKs are regulated by their  $\text{Ca}^{2+}$ -binding domains. In these cases, CDPKs undergo structural and conformational changes, promoting the regulation of other proteins by phosphorylation (Wernimont et al., 2010). *P. falciparum* possesses seven CDPKs (PfCDPK1 to PfCDPK7), with correspondent orthologs in plants, but not in animals or fungi (Kadian et al., 2017; Ghartey-Kwansah et al., 2020). It has been proposed that CDPKs could be a novel field for exploration of new antimalarial drugs (Hui et al., 2015).

For instance, transcriptomic data analysis has suggested that PfCDPK1 is primarily expressed in the late schizont stage (Bozdech et al., 2003; Le Roch et al., 2003). In agreement with this, PfCDPK1 is found in the PV and merozoite membrane throughout

schizogony and merozoite egress, and performs crucial roles in the invasion process (Azevedo et al., 2013; Bansal et al., 2013). PfCDPK1 is known to phosphorylate both the myosin light chain and an IMC member, PfGAP45, in mature schizonts *in vitro*, when merozoites are formed (Green et al., 2008). As previously reported, PfGAP45 is also phosphorylated by PfPKB (Vaid et al., 2008), but it is proposed that this IMC member is phosphorylated on CDPK1 non-dependent phosphosites (Green et al., 2008). PfCDPK1 knockout mutants showed that this kinase is required for normal growth of *P. falciparum* during asexual proliferation, with critical involvement in gametogenesis, making its transmission to the mosquito unfeasible (Bansal et al., 2018). In contrast, CDPK1 deletion in *P. berghei* showed no difference for the asexual development and host cell invasion, suggesting different functions of the homologs in both species (Jebiwott et al., 2013).

PfCDPK1 mutant parasites on the bulky gatekeeper residue T145M (gatekeeper residue in the wild-type is a Thr, modified to a Met at the position 145 in the mutants) showed prominently

reduced activity compared to wild-type parasites. This lower activity seems to be compensated by PKG, influencing the up-regulation of transcription levels of CDPK5 and CDPK6 in the CDPK1 T145M mutant parasites (Bansal et al., 2016), suggesting that a  $Ca^{2+}$ -based signaling may modulate a very collaborative role in the CDPK family and other kinases in malaria parasites (Green et al., 2008; Brochet et al., 2014). Some reports have highlighted the importance of PfCDPK1 in the phosphorylation of members of IMC, such as GAP45 and IMC1g (Green et al., 2008; Kumar et al., 2017). PfCDPK1 knock-down mutants using the FKBP destabilization domain (DD) showed different patterns of phosphorylation in the protein-partners, revealed by iTRAQ-based phosphoproteomic analysis, including the phosphorylation pattern on S149 of PfPKA, which is a kinase also involved in  $Ca^{2+}$ -signaling mediated by cAMP (Kumar et al., 2017). Additionally, PfCDPK1 can phosphorylate PfSERA5 (*P. falciparum* serine repeat antigen 5). The PfCDPK1 inhibitor, purfalcamine, blocked SERA5 phosphorylation, leading to the blockage of merozoite egress (Iyer et al., 2018). Despite this evidence on PfCDPK1 as a promising target for therapeutic intervention, a recent chemical genetics approach casts doubt on this suitability for blood stages (Green et al., 2016). Nevertheless, PfCDPK1 continues to represent a good target for a mosquito transmission-blocking strategy, as previously mentioned (Bansal et al., 2018).

In contrast to PfCDPK1, PfCDPK2 function is poorly understood in *Plasmodium*. In all rodent and some other malaria species, the *cdpk2* gene is lacking (Tewari et al., 2010). Initially thought as an essential gene in *P. falciparum*, a recent report has pointed out that in PfCDPK2 knockout mutants obtained by CRISPR-Cas9, it is dispensable in asexual proliferation in *P. falciparum*. Still, CDPK2 seems to play an essential role in male gametocyte exflagellation and possibly in female gametocytes, compromising parasite transmission to mosquitoes (Bansal et al., 2017). Likewise, CDPK4 has been demonstrated to play crucial roles in gametocyte exflagellation (Billker et al., 2004; Ojo et al., 2012). The bumped-kinase inhibitor 1 (BKI-1), which is more than 20-fold more selective for PfCDPK4 over PfCDPK1, inhibited the microgamete exflagellation of *P. falciparum*, but did not block asexual parasite proliferation. A strong correlation between PfCDPK4 activity inhibition and blockage of exflagellation by a series of closely related BKI analogues was observed, supporting that the exflagellation blockage was due to the inhibition of PfCDPK4 rather than other kinases. Furthermore, BKI-1 blocks *P. berghei* transmission to mosquitoes (Ojo et al., 2012).

The apparent role of CDPK4 in the onset of axoneme motility, DNA condensation and cytokinesis during the first 10 min of exflagellation induction has been reported (Fang et al., 2017). An increased interest in the CDPK4 as a new antimalarial target for pyrazolopyrimidine-based inhibitors has also been reported, which could result in new therapeutic strategies for malaria treatment in the near future (Vidadala et al., 2014). Regarding the sexual stages of development, CDPK3 is intimately implicated in regulating the motility of the ookinete in the mosquito vector midgut (Ishino et al., 2006; Siden-Kiamos

et al., 2006). *In vitro* migration assays also suggested that this motility is stimulated by  $Ca^{2+}$  mobilization from intracellular stores (Ishino et al., 2006).

PfCDPK5 is an important regulator of parasite egress, a highly coordinated event requiring PfSERA5 (Dvorin et al., 2010; Absalon et al., 2018). The egress in CDPK5-deficient merozoites is impaired. PfCDPK5 is localized within micronemes and plays a central role in the microneme protein discharge, correlating a defect in this process to the impaired egress observed in PfCDPK5-deficient parasites. In addition, PKG has been identified as an important protein that cooperates in the egress signaling pathway together with PfCDPK5 (Absalon et al., 2018). This could explain the increased transcriptional expression levels of PKG and PfCDPK5 in the PfCDPK1 mutants as mentioned above, suggesting an integrated cross-talk among kinases in malaria parasites (Bansal et al., 2016), including their role in  $Ca^{2+}$  mobilization in gametocyte activation of *P. berghei* and egress of merozoites in *P. falciparum* (Brochet et al., 2014).

Functional studies to understand the roles of CDPK6 and CDPK7 are still lacking. PbCDPK6 has been demonstrated to play a critical role in sporozoite invasion of cells with high expression of heparan sulphate proteoglycans (HSPGs), such as hepatocytes, involving the induction of the circumsporozoite protein (CSP) cleavage upon contact with hepatocytes (Coppi et al., 2007). As previously highlighted, PfCDPK6 could be playing a compensatory role in the asexual blood stages of *P. falciparum* in the absence of a functional PfCDPK1 (Bansal et al., 2016). Still, additional studies need to be performed to address this question adequately. On the other hand, PfCDPK7 is an atypical member of the CDPK family, containing a pleckstrin homology domain adjacent to the kinase domain and two  $Ca^{2+}$ -binding EF-hands, present at its N-terminus. PfCDPK7 interacts with  $PIP_2$  through its pleckstrin domain, suggesting that this feature may determine its subcellular localization, possibly at ER exit sites. Moreover, knockout mutants of PfCDPK7 have also shown its importance for the growth of asexual stages of development, presenting abnormal morphology (Kumar et al., 2014). Despite this evidence on the roles of CDPK6 and CDPK7, their downstream signals, which may be implicated in other biological processes, are still largely unknown (Figure 2).

## CA<sup>2+</sup>-RELATED PHOSPHATASES

Sixty-seven candidate phosphatases were identified in the *P. falciparum* genome by *in silico* analysis (Pandey et al., 2014). At least three serine/threonine protein phosphatases (STPP) are involved in  $Ca^{2+}$  signaling: STPP 2B catalytic subunit A (Wilkes and Doerig, 2008; Singh et al., 2014), STPP 7 (PP7) (Kumar et al., 2004; Wilkes and Doerig, 2008; Singh et al., 2014) and a putative STPP 8 (PPP8), which is inferred as containing a  $Ca^{2+}$  binding site EF-hand (Yang and Arrizabalaga, 2017; Mitchell et al., 2019).

Calcineurin (CN), also known as STPP 2B or PP3, is a heterodimeric complex containing a catalytic subunit (CNA) and a regulatory subunit (CNB) (Steinbach et al., 2007). CN is

conserved from yeast to humans (Yang and Arrizabalaga, 2017) and involved in several cellular processes. It has been extensively studied and reviewed (Crabtree, 2001; Wilkins and Molkentin, 2004; Liu et al., 2015; Park et al., 2019). High  $\text{Ca}^{2+}$  concentration induces the formation of a  $\text{Ca}^{2+}$ -CaM complex, leading to CN activation, the release of its autoinhibitory domain and exposition of the active site to dephosphorylate its target (Rusnak and Mertz, 2000; Park et al., 2019).

CN in *Plasmodium* spp. is required for host cell attachment and invasion in a receptor-dependent pathway distinct from the AMA1-RON2 (apical membrane antigen-1/rhoptry neck protein 2) system but with some degree of functional overlap (Paul et al., 2015). CN knockdown demonstrated an increase of sensibility to an invasion-inhibitory antibody directed against basigin, an important receptor for RBC invasion, suggesting that CN regulates this process (Duraisingh et al., 2008; Otto et al., 2014; Paul et al., 2015). This might occur regardless of apical organelle proteins involved in invasion (Paul et al., 2015). However, CN has also been described as essential to  $\text{Ca}^{2+}$ -dependent microneme secretion, and its activity is increased after the exposure of merozoites to a low  $\text{K}^+$  environment. The mechanism involving CN and microneme secretion includes regulating apical actin depolymerization (Singh et al., 2014).

Stage-specific conditional degradation of CN in *P. berghei* further demonstrates its role in gametocyte development, fertilization and ookinete-to-oocyst and sporozoite-to-liver stage transitions (Philip and Waters, 2015). CN protein expression and/or activity regulation might provide a regulatory hub during the parasite cell cycle. The protein has been detected at the schizont, ring, sporozoite, merozoite and gametocyte stages, but not in the trophozoite stage (Wilkes and Doerig, 2008; Pandey et al., 2014). Activity inhibition by cyclosporin and FK506 resulted in increased levels of phosphorylated HSP90, phosphoglycerate kinase, actin-1, adenosine deaminase and glyceraldehyde-3-phosphate dehydrogenase. Moreover, actin-1 is potentially a direct substrate of CN in *P. falciparum* (Singh et al., 2014).

Similar to CN, protein phosphatase 7 (PP7) contains EF-hands and IQ (the first two amino acids of the motif: Ile and Gln) calmodulin-binding motifs but, in contrast, is monomeric. The CaM-binding motif was found to inhibit phosphatase activity in *Arabidopsis* PP7 (Dobson et al., 2001; Kutuzov et al., 2001; Yang and Arrizabalaga, 2017). PP7 is not detected at the trophozoite stage but at the schizont, ring, merozoite and gametocyte stages (Dobson et al., 2001; Pandey et al., 2014). These observations indicate that PfPP7 is regulated across all parasite stages and could constitute a potential target to control the parasite cell cycle. PP8 or EFPP is a putative STPP with a long N-terminal domain with EF-hand motifs and is specific to apicomplexans. Mutations were observed in their catalytic domain which put into question their phosphatase activity. Their functions have not yet been investigated (Kutuzov and Andreeva, 2008; Yang and Arrizabalaga, 2017).

Most studies involving the roles of  $\text{Ca}^{2+}$  signaling and phosphatases are focused on calcineurin. However, other phosphatases without  $\text{Ca}^{2+}$ -binding motifs could be affected by

$\text{Ca}^{2+}$  signaling through their protein partners possessing these motifs. According to STRING prediction and Gene Ontology analyses, amongst the 67 candidate phosphatases identified in *P. falciparum*, ten potentially interact with proteins involved in  $\text{Ca}^{2+}$  signaling: putative acid phosphatase (PF3D7\_0918000), putative protein phosphatase 2C (PF3D7\_0829100), putative 4-nitrophenylphosphatase (PF3D7\_0715000), putative protein phosphatase (PF3D7\_0802800), putative RNA lariat debranching enzyme (PF3D7\_1340600), putative acid phosphatase (PF3D7\_1403900), hypothetical protein (PF3D7\_1464600), hypothetical protein (PF3D7\_1469200), protein phosphatase 2C (PF3D7\_0410300) and putative phosphoesterase (PF3D7\_1206000) (Pandey et al., 2014). However, the effects of  $\text{Ca}^{2+}$  on the phosphatase protein-interaction network remain poorly understood in *Plasmodium* species. Therefore, biochemical assays and phosphatase protein partner screenings are a reasonable approach for discovery of new antimalarials (Khalife and Pierrot, 2016).

## OTHER EFFECTORS INVOLVED IN $\text{Ca}^{2+}$ SIGNALING

*P. falciparum* reticulocyte binding-like protein 1 (PfRh1) performs a role in initial sensing of  $\text{Ca}^{2+}$  followed by signal transduction, causing erythrocyte binding antigen-175 (EBA-175) release from microneme and allowing tight junction formation (Gao et al., 2013). The biochemical pathways regarding  $\text{Ca}^{2+}$  modulation that led to microneme secretion are largely unknown, highlighting the need for further studies in *Plasmodium* species. As previously mentioned, components of the motor complex involved in merozoite invasion are phosphorylated by PfCDPK1 (Green et al., 2008; Vaid et al., 2008). In *P. berghei* sporozoites, this complex is involved in gliding motility and host cell invasion. Living-cell imaging studies demonstrate that while cytoplasmic elevated  $\text{Ca}^{2+}$  levels are required for gliding, alone this is insufficient, since artificial increases using an ionophore allowed adhesin translocation to the surface but no gliding motion (Carey et al., 2014). Moreover, the *P. falciparum* inner membrane complex 11 (PfIMC11) has been proposed as a protein to potentially connect this motor complex to the IMC membrane. It is also involved in gliding and invasion processes in a  $\text{Ca}^{2+}$ -dependent manner. PfIMC11 interacts directly with  $\text{Ca}^{2+}$  and its interaction with actin is enhanced in the presence of this ion (Kumar et al., 2019). The gliding motility used by ookinete and merozoite invasion is also supported by CDPK4, in a compensatory manner to CDPK1 (and vice versa). Both  $\text{Ca}^{2+}$ -dependent kinases are involved in IMC stability, phosphorylating the glideosome-associated protein 40 (GAP40) and the CDPK4 substrate SOC6 (PBANKA\_070770), involved in IMC biogenesis (Fang et al., 2018).

Following microneme secretion, the interaction of PfEBA-175 and the RBCs receptor glycoporphin A (glyA) results in a cytoplasmic lowering of  $\text{Ca}^{2+}$  levels, which, in turn, stimulates the release of rhoptry proteins such as cytoadherence-linked

asexual protein gene 3.1 (CLAG3.1/RhopH1) and *P. falciparum* reticulocyte binding-like protein 2b (PfRh2b) (Singh et al., 2010). Rhoptry discharge in RBCs contributes to the tight-junction and PV formation, modifying the host cell environment (Boothroyd and Dubremetz, 2008; Santos and Soldati-Favre, 2011). The repression of *P. berghei* rhoptry neck protein 11 (PbRON11) in sporozoites reduced attachment and motility, leading to the impairment of the infection in the mosquito salivary gland and hepatocyte cells. This protein contains putative EF-hand domains and might act by controlling rhoptry protein secretion in a  $\text{Ca}^{2+}$ -dependent manner (Bantuchai et al., 2019).

Merozoite egress from RBCs is triggered by elevation of cyclic guanosine monophosphate (cGMP) and PKG activation, essential for the protein discharge of secretory organelles, known to support this process (Collins et al., 2013; Alam et al., 2015). Correlation of  $\text{Ca}^{2+}$  with parasite egress was previously reported (Collins et al., 2013; Glushakova et al., 2013). Events documented in the final hour of the cell cycle include  $\text{Ca}^{2+}$  release from ER of the schizonts, activation of PfCDPK5 and, in the last 10-20 minutes of the cell cycle, vacuole swelling and red blood cell cytoskeleton destabilization by calpain, a host enzyme activated by  $\text{Ca}^{2+}$  (Glushakova et al., 2013). More recently, PKG was found to interact with and phosphorylate a multipass membrane protein, termed as important for  $\text{Ca}^{2+}$  mobilization 1 (ICM1). Conditional knockdown of ICM1 revealed an essential role in  $\text{Ca}^{2+}$  mobilization to initiate both *Plasmodium* gametogenesis and merozoite egress (Balestra et al., 2021). Additionally, guanylyl-cyclase alpha ( $\text{GC}\alpha$ )-null mutant parasites were unable to synthesize cGMP for PKG activation in schizonts, leading to a reduction in  $\text{Ca}^{2+}$  release from internal stores (Nofal et al., 2021).

Conditional gene disruption of the *P. falciparum* phosphodiesterase  $\beta$  (PfPDE $\beta$ ) leads to a dramatic reduction in schizont cAMP and cGMP hydrolytic activity, resulting in elevated cAMP levels and inappropriate cAMP-induced increased phosphorylation of PKA substrates. In addition, PKA seem to assume a compensatory role with PKG, in order to phosphorylate *P. falciparum* myosin A (PfMyoA), an important component of the so-called glideosome, a parasite complex involved in host cell invasion, in PfPDE $\beta$  mutants, bypassing the need for PKG activity by elevated cAMP levels upon  $\text{Ca}^{2+}$  signaling, possibly by PKA action (Flueck et al., 2019). Together, these findings point towards PfPDE $\beta$  regulating cAMP and cGMP production, followed by PKA and PKG activation. Nonetheless, the molecular dynamics of  $\text{Ca}^{2+}$  signaling associated with these events are still poorly understood.

A family of proteins containing multiple EF-hand motifs, named as the CREC family (calumenin, reticulocalbin 1 and 3, ERC-55, Cab-45), has been remarkably underexplored, considering that proteins from this family are widely found from protozoans to mammals (Honoré and Vorum, 2000). A member of this family is found in the ER of *P. falciparum*, known as PfERC (endoplasmic reticulum-resident calcium-binding protein) (La Greca et al., 1997). This protein is a key regulator of the egress proteolytic cascade of *P. falciparum* merozoites. The use of SERCA inhibitor cyclopiazonic acid (CPA) and an ionophore, ionomycin, did not change the amounts of

cytosolic  $\text{Ca}^{2+}$  in knockdown parasites bearing a glucosamine-inducible ribozyme gene (PfERC-*glsS*) from ER or neutral  $\text{Ca}^{2+}$  storages, suggesting that the availability of  $\text{Ca}^{2+}$  from different sources does not change upon knockdown of PfERC. Moreover, PfERC is required for the complete maturation of the aspartic protease plasmepsin X (PMX) in a  $\text{Ca}^{2+}$ -dependent manner, which is required to cleave the subtilisin-like protease (SUB1) (Fierro et al., 2020).

Additional evidence for  $\text{Ca}^{2+}$  importance for SUB1 discharge and proteolytic cascade events have been reported. Chelation of intracellular  $\text{Ca}^{2+}$  in *P. falciparum* schizonts blocks the SUB1 discharge from merozoite exoemes into PV, resulting in a decrease of SERA5 proteolytic cleavage and harming PVM rupture and merozoite egress (Agarwal et al., 2013). Mature SUB1 discharge into PV results in the proteolytic cleavage of protein family members involved in merozoite egress and RBC invasion, such as SERA5 and MSP1 (merozoite surface protein 1) (Nasamu et al., 2017; Pino et al., 2017). Additionally to SERA5, SERA6 has been associated to the parasite egress from RBCs upon SUB1 catalytic processing into the PV (Ruecker et al., 2012). In the absence of SERA6, the rupture of RBCM does not occur, suggesting that SERA6 could be associated to an additional proteolytic cascade event related to the  $\beta$ -spectrin cleavage of host cell cytoskeleton (Thomas et al., 2018). Moreover, autocatalytic maturation of SERA6 needs a PV-located protein cofactor, named merozoite surface antigen 180, which is also a SUB1 substrate. This multi-step proteolytic process is required for dismantling the host RBC cytoskeleton facilitating the parasite egress (Tan et al., 2021). Therefore, it remains to be further described how  $\text{Ca}^{2+}$  may modulate actors in these proteolytic cascade events.

$\text{Ca}^{2+}$  signaling has also been shown to be involved in pre-erythrocytic cycle stages. After hepatocyte invasion, elongated sporozoites transform into a spherical form (exo-erythrocytic form, EEF) in a temperature-dependent process (Shortt and Garnham, 1948; Meis et al., 1983; Kaiser et al., 2003). It has been proposed that the  $\text{Ca}^{2+}$  signal regulates this morphological transition, with intracellular  $\text{Ca}^{2+}$  increased at the center of a bulbous structure in *P. berghei*, reinforcing that  $\text{Ca}^{2+}$  plays central roles in diverse life-cycle stages (Doi et al., 2011). Sporozoite salivary gland proteome analyses revealed several components that could be involved in the  $\text{Ca}^{2+}$  signaling pathway at this stage, such as G-protein-coupled receptors, adenylyl and guanylyl cyclases and a carbonic anhydrase. Host proteins are also involved in EEF transformations and  $\text{Ca}^{2+}$  signaling. Protein kinase C-mediated NF- $\kappa$ B activation induces expression of CXCR4 (C-X-C chemokine receptor type 4) in hepatocytes and intracellular  $\text{Ca}^{2+}$  elevation, essential to EEF development (Bando et al., 2019). The interplay between host and parasite proteins, however, remains highly elusive.

## CONCLUDING REMARKS

*Plasmodium* species contain distinctive features when compared to other eukaryotes. Such characteristics define its phylum or

genus, in which attachment to the host cell, motility, invasion and egress are essential for survival and dissemination. Since  $\text{Ca}^{2+}$  signaling regulates important and specific *Plasmodium* cellular processes such as microneme secretion, attachment, gliding motility, invasion and egress, actors involved in these pathways, which are regulated by this ion, could be considered potential drug targets. Striking progress to achieve a broader understanding of  $\text{Ca}^{2+}$  signaling in *Plasmodium* has been made, including the potential involvement of host compounds in  $\text{Ca}^{2+}$  uptake, such as  $\text{K}^+$ ,  $\text{Na}^+$ , ionic strength and melatonin (Brand et al., 2003; Gazarini et al., 2003; Singh et al., 2010; Pillai et al., 2013; Pecenin et al., 2018).

However, several gaps in understanding remain in these organisms, covering mechanisms involved in increased  $\text{Ca}^{2+}$  uptake by iRBCs, together with transport through PVM and the parasite cellular membrane. Moreover, IP3R or alternative functional protein identification in *Plasmodium* would be an important breakthrough to explore  $\text{Ca}^{2+}$  mobilization and storage, as well as backstage actors which support those processes as promising therapeutic targets. Actually, a plethora of *Plasmodium* proteins with standard and unusual  $\text{Ca}^{2+}$  binding motifs, which are known or suspected to be involved in  $\text{Ca}^{2+}$  signaling, could be explored to this end. This also includes proteins without  $\text{Ca}^{2+}$ -binding motifs acting as indirect effectors.

The association of classical techniques employed to study permeability, protein channels and pumps, together with more recent high-throughput approaches is a promise to fulfill these gaps. Mass spectrometry-based proteomics (Garcia et al., 2018;

Blomqvist et al., 2020; Garcia et al., 2021), including novel proteomic approaches to understand *in vivo* protein-partners, such as BioID and APEX-2 proximity-labelling techniques (Rhee et al., 2013; Kehrer et al., 2016; Boucher et al., 2018; Birnbaum et al., 2020), metabolomics (Beri et al., 2019) and new  $\text{Ca}^{2+}$  ratiometric techniques coupled to imaging reporters (Brochet et al., 2014; Carey et al., 2014; Pandey et al., 2016; Absalon et al., 2018; Borges-Pereira et al., 2020) are examples of such technologies required for improved understanding of the role of  $\text{Ca}^{2+}$  in the backstage of malaria parasite biology and drug screening assay design.

## AUTHOR CONTRIBUTIONS

All authors contributed to the article and approved the submitted version.

## ACKNOWLEDGMENTS

We would like to thank the CAPES/COFECUB programme [923/18], CAPES-PROEX, INCT-MCTI/CNPq/FAPs [16/2014], CNPq Universal [430610/2016-5], and FAPDF [Demanda Espontânea 193.001.723/2017]. We also thank Pr. Concepta McManus Pimentel and Pr. Robert Neil Gerard Miller at University of Brasilia for orthographic correction.

## REFERENCES

- Absalon, S., Blomqvist, K., Rudloff, R. M., DeLano, T. J., Pollastri, M. P., and Dvorin, J. D. (2018). Calcium-Dependent Protein Kinase 5 Is Required for Release of Egress-Specific Organelles in *Plasmodium Falciparum*. *MBio* 9, 1–16. doi: 10.1128/mBio.00130-18
- Adovelande, J., Bastide, B., Deleze, J., and Schrevel, J. (1993). Cytosolic Free Calcium in *Plasmodium Falciparum*-Infected Erythrocytes and the Effect of Verapamil: A Cytofluorometric Study. *Exp. Parasitol.* 76, 247–258. doi: 10.1006/expr.1993.1030
- Agarwal, S., Singh, M. K., Garg, S., Chitnis, C. E., and Singh, S. (2013).  $\text{Ca}^{2+}$ -Mediated Exocytosis of Subtilisin-Like Protease 1: A Key Step in Egress of *Plasmodium Falciparum* Merozoites. *Cell. Microbiol.* 15, 910–921. doi: 10.1111/cmi.12086
- Alam, M. M., Solyakov, L., Bottrill, A. R., Flueck, C., Siddiqui, F. A., Singh, S., et al. (2015). Phosphoproteomics Reveals Malaria Parasite Protein Kinase G as a Signalling Hub Regulating Egress and Invasion. *Nat. Commun.* 6, 7285. doi: 10.1038/ncomms8285
- Alleva, L. M., and Kirk, K. (2001). Calcium Regulation in the Intraerythrocytic Malaria Parasite *Plasmodium Falciparum*. *Mol. Biochem. Parasitol.* 117, 121–128. doi: 10.1016/S0166-6851(01)00338-3
- Alves, E., Bartlett, P. J., Garcia, C. R. S., and Thomas, A. P. (2011). Melatonin and IP(3)-Induced  $\text{Ca}^{2+}$  Release From Intracellular Stores in the Malaria Parasite *Plasmodium Falciparum* Within Infected Red Blood Cells. *J. Biol. Chem.* 286, 5905–5912. doi: 10.1074/jbc.M110.188474
- Azevedo, M. F., Sanders, P. R., Krejany, E., Nie, C. Q., Fu, P., Bach, L. A., et al. (2013). Inhibition of *Plasmodium Falciparum* CDPK1 by Conditional Expression of Its J-Domain Demonstrates a Key Role in Schizont Development. *Biochem. J.* 452, 433–441. doi: 10.1042/BJ20130124
- Balestra, A. C., Koussis, K., Klages, N., Howell, S. A., Flynn, H. R., Bantscheff, M., et al. (2021).  $\text{Ca}^{2+}$  Signals Critical for Egress and Gametogenesis in Malaria Parasites Depend on a Multipass Membrane Protein That Interacts With PKG. *Sci. Adv.* 7 (13), 1–17. doi: 10.1126/sciadv.abe5396
- Bando, H., Pradipta, A., Iwanaga, S., Okamoto, T., Okuzaki, D., Tanaka, S., et al. (2019). CXCR4 Regulates *Plasmodium* Development in Mouse and Human Hepatocytes. *J. Exp. Med.* 216, 1733–1748. doi: 10.1084/jem.20182227
- Bansal, A., Molina-Cruz, A., Brzostowski, J., Liu, P., Luo, Y., Gunalan, K., et al. (2018). PfCDPK1 Is Critical for Malaria Parasite Gametogenesis and Mosquito Infection. *Proc. Natl. Acad. Sci. U. S. A.* 115, 774–779. doi: 10.1073/pnas.1715443115
- Bansal, A., Molina-Cruz, A., Brzostowski, J., Mu, J., and Miller, L. H. (2017). *Plasmodium Falciparum* Calcium-Dependent Protein Kinase 2 Is Critical for Male Gametocyte Exflagellation But Not Essential for Asexual Proliferation. *MBio* 8, 1–17. doi: 10.1128/mBio.01656-17
- Bansal, A., Ojo, K. K., Mu, J., Maly, D. J., van Voorhis, W. C., and Miller, L. H. (2016). Reduced Activity of Mutant Calcium-Dependent Protein Kinase 1 Is Compensated in *Plasmodium Falciparum* Through the Action of Protein Kinase G. *MBio* 7, 1–12. doi: 10.1128/mBio.02011-16
- Bansal, A., Singh, S., More, K. R., Hans, D., Nangalia, K., Yogavel, M., et al. (2013). Characterization of *Plasmodium Falciparum* Calcium-Dependent Protein Kinase 1 (PfCDPK1) and Its Role in Microneme Secretion During Erythrocyte Invasion. *J. Biol. Chem.* 288, 1590–1602. doi: 10.1074/jbc.M112.411934
- Bantuchai, S., Nozaki, M., Thongkukiatkul, A., Lorsuwannarat, N., Tachibana, M., Baba, M., et al. (2019). Rhoptry Neck Protein 11 has Crucial Roles During Malaria Parasite Sporozoite Invasion of Salivary Glands and Hepatocytes. *Int. J. Parasitol.* 49, (9):725–735. doi: 10.1016/j.ijpara.2019.05.001
- Beraldo, F. H., Almeida, F. M., Da Silva, A. M., and Garcia, C. R. S. (2005). Cyclic AMP and Calcium Interplay as Second Messengers in Melatonin-Dependent Regulation of *Plasmodium Falciparum* Cell Cycle. *J. Cell Biol.* 170, 551–557. doi: 10.1083/jcb.200505117
- Beraldo, F. H., Mikoshiba, K., and Garcia, C. R. S. (2007). Human Malarial Parasite, *Plasmodium Falciparum*, Displays Capacitative Calcium Entry: 2-Aminoethyl Diphenylborinate Blocks the Signal Transduction Pathway of Melatonin Action on the P. *Falciparum* Cell Cycle. *J. Pineal Res.* 43, 360–364. doi: 10.1111/j.1600-079X.2007.00486.x



- Beri, D., Ramdani, G., Balan, B., Gadara, D., Poojary, M., Momeux, L., et al. (2019). Insights Into Physiological Roles of Unique Metabolites Released From Plasmodium-Infected RBCs and Their Potential as Clinical Biomarkers for Malaria. *Sci. Rep.* 9, 1–11. doi: 10.1038/s41598-018-37816-9
- Berridge, M. J., Bootman, M. D., and Roderick, H. L. (2003). Calcium Signalling: Dynamics, Homeostasis and Remodelling. *Nat. Rev. Mol. Cell Biol.* 4, 517–529. doi: 10.1038/nrm1155
- Biagini, G. A., Bray, P. G., Spiller, D. G., White, M. R. H., and Ward, S. A. (2003). The Digestive Food Vacuole of the Malaria Parasite Is a Dynamic Intracellular Ca<sup>2+</sup> Store. *J. Biol. Chem.* 278, 27910–27915. doi: 10.1074/jbc.M304193200
- Billker, O., Dechamps, S., Tewari, R., Wenig, G., Franke-Fayard, B., and Brinkmann, V. (2004). Calcium and a Calcium-Dependent Protein Kinase Regulate Gamete Formation and Mosquito Transmission in a Malaria Parasite. *Cell* 117, 503–514. doi: 10.1016/S0092-8674(04)00449-0
- Birnbaum, J., Scharf, S., Schmidt, S., Jonscher, E., Maria Hoeijmakers, W. A., Flemming, S., et al. (2020). A Kelch13-Defined Endocytosis Pathway Mediates Artemisinin Resistance in Malaria Parasites. *Science (80-)* 367, 51–59. doi: 10.1126/science.aax4735
- Blomqvist, K., Helmel, M., Wang, C., Absalon, S., Labunska, T., Rudlaff, R. M., et al. (2020). Influence of Plasmodium Falciparum Calcium-Dependent Protein Kinase 5 (PfCDPK5) on the Late Schizont Stage Phosphoproteome. *mSphere* 5, 1–10. doi: 10.1128/mSphere.00921-19
- Boothroyd, J. C., and Dubremetz, J. F. (2008). Kiss and Spit: The Dual Roles of Toxoplasma Rhoptries. *Nat. Rev. Microbiol.* 6, 79–88. doi: 10.1038/nrmicro1800
- Borges-Pereira, L., Budu, A., McKnight, C. A., Moore, C. A., Vella, S. A., Triana, M. A. H., et al. (2015). Calcium Signaling Throughout the Toxoplasma Gondii Lytic Cycle a Study Using Genetically Encoded Calcium Indicators. *J. Biol. Chem.* 290, 26914–26926. doi: 10.1074/jbc.M115.652511
- Borges-Pereira, L., Thomas, S. J., dos Anjos e Silva, A. L., Bartlett, P. J., Thomas, A. P., and Garcia, C. R. S. (2020). The Genetic Ca<sup>2+</sup> Sensor GCaMP3 Reveals Multiple Ca<sup>2+</sup> Stores Differentially Coupled to Ca<sup>2+</sup> Entry in the Human Malaria Parasite Plasmodium Falciparum. *J. Biol. Chem.* 295, 14998–15012. doi: 10.1074/jbc.RA120.014906
- Boucher, M. J., Ghosh, S., Zhang, L., Lal, A., Jang, S. W., Ju, A., et al. (2018). Integrative Proteomics and Bioinformatic Prediction Enable a High-Confidence Apicoplast Proteome in Malaria Parasites. *PLoS Biol.* 16, 1–29. doi: 10.1371/journal.pbio.2005895
- Bozdech, Z., Llinás, M., Pulliam, B. L., Wong, E. D., Zhu, J., and DeRisi, J. L. (2003). The Transcriptome of the Intraerythrocytic Developmental Cycle of Plasmodium Falciparum. *PLoS Biol.* 1, 85–100. doi: 10.1371/journal.pbio.0000005
- Brand, V. B., Sandu, C. D., Duranton, C., Lang, K. S., Huber, S. M., and Lang, F. (2003). Growth on the Cation Permeability of the Human Host Erythrocyte. *Cell. Physiol. Biochem.* 13, 347–356. doi: 10.1159/000075122
- Brochet, M., and Billker, O. (2016). Calcium Signalling in Malaria Parasites. *Mol. Microbiol.* 100, 397–408. doi: 10.1111/mmi.13324
- Brochet, M., Collins, M. O., Smith, T. K., Thompson, E., Sebastian, S., Volkman, K., et al. (2014). Phosphoinositide Metabolism Links cGMP-Dependent Protein Kinase G to Essential Ca<sup>2+</sup> Signals at Key Decision Points in the Life Cycle of Malaria Parasites. *PLoS Biol.* 12 (13), 1–15. doi: 10.1371/journal.pbio.1001806
- Bushell, E., Gomes, A. R., Sanderson, T., Anar, B., Girling, G., Herd, C., et al. (2017). Functional Profiling of a Plasmodium Genome Reveals an Abundance of Essential Genes. *Cell* 170, 260–272.e8. doi: 10.1016/j.cell.2017.06.030
- Carey, A. F., Singer, M., Bargieri, D., Thiberge, S., Frischknecht, F., Ménard, R., et al. (2014). Calcium Dynamics of Plasmodium Berghei Sporozoite Motility. *Cell. Microbiol.* 16, 768–783. doi: 10.1111/cmi.12289
- Ch'ng, J. H., Liew, K., Goh, A. S. P., Sidhartha, E., and Tan, K. S. W. (2011). Drug-Induced Permeabilization of Parasite's Digestive Vacuole Is a Key Trigger of Programmed Cell Death in Plasmodium Falciparum. *Cell Death Dis.* 2, 1–11. doi: 10.1038/cddis.2011.97
- Clapham, D. E. (2007). Calcium Signaling. *Cell* 131, 1047–1058. doi: 10.1016/j.cell.2007.11.028
- Collins, C. R., Hackett, F., Strath, M., Penzo, M., Withers-Martinez, C., Baker, D. A., et al. (2013). Malaria Parasite cGMP-Dependent Protein Kinase Regulates Blood Stage Merozoite Secretory Organelle Discharge and Egress. *PLoS Pathog.* 9 (5), 1–13. doi: 10.1371/journal.ppat.1003344
- Coppi, A., Tewari, R., Bishop, J. R., Bennett, B. L., Lawrence, R., Esko, J. D., et al. (2007). Heparan Sulfate Proteoglycans Provide a Signal to Plasmodium Sporozoites to Stop Migrating and Productively Invade Host Cells. *Cell Host Microbe* 2, 316–327. doi: 10.1016/j.chom.2007.10.002
- Cowman, A. F., Healer, J., Marapana, D., and Marsh, K. (2016). Malaria: Biology and Disease. *Cell* 167, 610–624. doi: 10.1016/j.cell.2016.07.055
- Crabtree, G. R. (2001). Calcium, Calcineurin, and the Control of Transcription. *J. Biol. Chem.* 276 (4), 2313–2316. doi: 10.1074/jbc.R000024200
- Dawn, A., Singh, S., More, K. R., Siddiqui, F. A., Pachikara, N., Ramdani, G., et al. (2014). The Central Role of cAMP in Regulating Plasmodium Falciparum Merozoite Invasion of Human Erythrocytes. *PLoS Pathog.* 10 (12), 1–14. doi: 10.1371/journal.ppat.1004520
- Desai, S. A., Krogstad, D. J., and McCleskey, E. W. (1993). A Nutrient-Permeable Channel on the Intraerythrocytic Malaria Parasite. *Nature* 362, 643–646. doi: 10.1038/362643a0
- Desai, S. A., McCleskey, E. W., Schlesinger, P. H., and Krogstad, D. J. (1996). A Novel Pathway for Ca<sup>2+</sup> Entry Into Plasmodium Falciparum-Infected Blood Cells. *Am. J. Trop. Med. Hyg.* 54, 464–470. doi: 10.4269/ajtmh.1996.54.464
- Dobson, S., Bracchi, V., Chakrabarti, D., and Barik, S. (2001). Characterization of a Novel Serine/Threonine Protein Phosphatase (PfPPJ) From the Malaria Parasite, Plasmodium Falciparum. *Mol. Biochem. Parasitol.* 115, 29–39. doi: 10.1016/S0166-6851(01)00260-2
- Docampo, R., de Souza, W., Miranda, K., Rohloff, P., and Moreno, S. N. J. (2005). Acidocalcisomes - Conserved From Bacteria to Man. *Nat. Rev. Microbiol.* 3, 251–261. doi: 10.1038/nrmicro1097
- Docampo, R., and Huang, G. (2016). Acidocalcisomes of Eukaryotes. *Curr. Opin. Cell Biol.* 41, 66–72. doi: 10.1016/j.cob.2016.04.007
- Docampo, R., Scott, D. A., Vercesi, A. E., and Moreno, S. N. J. (1995). Intracellular Ca<sup>2+</sup> Storage in Acidocalcisomes of Trypanosoma Cruzi. *Biochem. J.* 310, 1005–1012. doi: 10.1042/bj3101005
- Docampo, R., Ulrich, P., and Moreno, S. N. J. (2010). Evolution of Acidocalcisomes and Their Role in Polyphosphate Storage and Osmoregulation in Eukaryotic Microbes. *Philos. Trans. R. Soc B Biol. Sci.* 365, 775–784. doi: 10.1098/rstb.2009.0179
- Doi, Y., Shinzawa, N., Fukumoto, S., Okano, H., and Kanuka, H. (2011). Calcium Signal Regulates Temperature-Dependent Transformation of Sporozoites in Malaria Parasite Development. *Exp. Parasitol.* 128 (2), 176–180. doi: 10.1016/j.exppara.2011.02.011
- Drozdowicz, Y. M., Shaw, M., Nishi, M., Striepen, B., Liwinski, H. A., Roos, D. S., et al. (2003). Isolation and Characterization of TgVPI, a Type I Vacuolar H<sup>+</sup>-Translocating Pyrophosphatase From Toxoplasma Gondii: The Dynamics of Its Subcellular Localization and the Cellular Effects of a Diphosphonate Inhibitor. *J. Biol. Chem.* 278, 1075–1085. doi: 10.1074/jbc.M209436200
- Duraisingh, M. T., DeSimone, T., Jennings, C., Refour, P., and Wu, C. (2008). Erythrocyte Invasion by Plasmodium Falciparum: Multiple Ligand-Receptor Interactions and Phenotypic Switching. *Subcell. Biochem.* 46–57. doi: 10.1007/978-0-387-78267-6\_3
- Duranton, C., Huber, S. M., Karl, S., Brand, V. B., Sandu, C. D., and Lang, F. (2003). Cellular Physiology Biochemistry and Biochemistry Y Electrophysiological Properties of the Plasmodium Falciparum-Induced Cation Conductance of Human Erythrocytes. *Cell. Physiol. Biochem.* 49, 189–198. doi: 10.1159/000072421
- Dvorin, J. D., Martyn, D. C., Patel, S. D., Grimley, J. S., Collins, R., Hopp, C. S., et al. (2010). A Plant-Like Kinase in Plasmodium Falciparum Regulates Parasite Egress From Erythrocytes. *Science (80-)* 328, 910–912. doi: 10.1126/science.1188191.A
- Eckstein-Ludwig, U., Webb, R. J., Van Goethem, I. D. A., East, J. M., Lee, A. G., Kimura, M., et al. (2003). Artemisinins Target the SERCA of Plasmodium Falciparum. *Nature* 424, 957–961. doi: 10.1038/nature01813
- Ehlgen, F., Pham, J. S., de Koning-Ward, T., Cowman, A. F., and Ralph, S. A. (2012). Investigation of the Plasmodium Falciparum Food Vacuole Through Inducible Expression of the Chloroquine Resistance Transporter (PfCRT). *PLoS One* 7 (6), 1–12. doi: 10.1371/journal.pone.0038781
- Fang, H., Gomes, A. R., Klages, N., Pino, P., Maco, B., Walker, E. M., et al. (2018). Epistasis Studies Reveal Redundancy Among Calcium-Dependent Protein Kinases in Motility and Invasion of Malaria Parasites. *Nat. Commun.* 9 (4248), 1–14. doi: 10.1038/s41467-018-06733-w
- Fang, H., Klages, N., Baechler, B., Hillner, E., Yu, L., Pardo, M., et al. (2017). Multiple Short Windows of Calcium-Dependent Protein Kinase 4 Activity Coordinate Distinct Cell Cycle Events During Plasmodium Gametogenesis. *Elife* 6, 1–23. doi: 10.7554/eLife.26524

- Fierro, M. A., Asady, B., Brooks, C. F., Cobb, D. W., Villegas, A., Moreno, S. N. J., et al. (2020). An Endoplasmic Reticulum CREC Family Protein Regulates the Egress Proteolytic Cascade in Malaria Parasites. *MBio* 11, 1–21. doi: 10.1128/mBio.03078-19
- Flueck, C., Drought, L. G., Jones, A., Patel, A., Perrin, A. J., Walker, E. M., et al. (2019). Phosphodiesterase Beta Is the Master Regulator of cAMP Signalling During Malaria Parasite Invasion. *PLoS Biol.* 17, 1–32. doi: 10.1371/journal.pbio.3000154
- Gao, X., Gunalan, K., Yap, S. S. L., and Preiser, P. R. (2013). Triggers of Key Calcium Signals During Erythrocyte Invasion by Plasmodium Falciparum. *Nat. Commun.* 4 (2862), 1–11. doi: 10.1038/ncomms3862
- Garcia, C. R. S., Alves, E., Pereira, P. H. S., Bartlett, P. J., Thomas, A. P., Mikoshiba, K., et al. (2017). InsP3 Signaling in Apicomplexan Parasites. *Curr. Top. Med. Chem.* 17, 2158–2165. doi: 10.2174/1568026617666170130121042
- Garcia, C. H. S., Depoix, D., Carvalho, P. C., Bastos, I. M. D., Ricart, C. A. O., de Sousa, M. V., et al. (2021). Comparative Proteomic Analysis of Kinesin-8B Deficient Plasmodium Berghei During Gametogenesis. *J. Proteomics* 236, 104118. doi: 10.1016/j.jprot.2021.104118
- Garcia, C. H. S., Depoix, D., Queiroz, R. M. L., Souza, J. M. F., Fontes, W., de Sousa, M. V., et al. (2018). Dynamic Molecular Events Associated to Plasmodium Berghei Gametogenesis Through Proteomic Approach. *J. Proteomics* 180, 88–98. doi: 10.1016/j.jprot.2017.11.009
- Gardner, M. J., Hall, N., Fung, E., White, O., Berriman, M., Hyman, R. W., et al. (2002). Genome Sequence of the Human Malaria Parasite Plasmodium Falciparum. *Nature* 419, 498–511. doi: 10.1038/nature01097
- Gazarini, M. L., and Garcia, C. R. S. (2004). The Malaria Parasite Mitochondrion Senses Cytosolic Ca<sup>2+</sup> Fluctuations. *Biochem. Biophys. Res. Commun.* 321, 138–144. doi: 10.1016/j.bbrc.2004.06.141
- Gazarini, M. L., Sigolo, C. A. O., Markus, R. P., Thomas, A. P., and Garcia, C. R. S. (2007). Antimalarial Drugs Disrupt Ion Homeostasis in Malarial Parasites. *Mem. Inst. Oswaldo Cruz* 102, 329–334. doi: 10.1590/S0074-02762007000300012
- Gazarini, M. L., Thomas, A. P., Pozzan, T., and Garcia, C. R. S. (2003). Calcium Signaling in a Low Calcium Environment: How the Intracellular Malaria Parasite Solves the Problem. *J. Cell Biol.* 161, 103–110. doi: 10.1083/jcb.200212130
- Ghartey-Kwansah, G., Yin, Q., Li, Z., Gumpfer, K., Sun, Y., Yang, R., et al. (2020). Calcium-Dependent Protein Kinases in Malaria Parasite Development and Infection. *Cell Transplant.* 29, 1–12. doi: 10.1177/0963689719884888
- Global Malaria Programme: WHO Global (2020). *World Malaria Report*. Available at: <https://www.who.int/publications/i/item/9789240015791>.
- Glushakova, S., Lizunov, V., Blank, P. S., Melikov, K., Humphrey, G., and Zimmerberg, J. (2013). Cytoplasmic Free Ca<sup>2+</sup> Is Essential for Multiple Steps in Malaria Parasite Egress From Infected Erythrocytes. *Malar. J.* 12, 1–12. doi: 10.1186/1475-2875-12-41
- Green, J. L., Moon, R. W., Whalley, D., Bowyer, P. W., Wallace, C., Rochani, A., et al. (2016). Imidazopyridazine Inhibitors of Plasmodium Falciparum Calcium-Dependent Protein Kinase 1 Also Target Cyclic GMP-Dependent Protein Kinase and Heat Shock Protein 90 to Kill the Parasite at Different Stages of Intracellular Development. *Antimicrob. Agents Chemother.* 60, 1464–1475. doi: 10.1128/AAC.01748-15
- Green, J. L., Rees-Channer, R. R., Howell, S. A., Martin, S. R., Knuepfer, E., Taylor, H. M., et al. (2008). The Motor Complex of Plasmodium Falciparum: Phosphorylation by a Calcium-Dependent Protein Kinase. *J. Biol. Chem.* 283, 30980–30989. doi: 10.1074/jbc.M803129200
- Guttery, D. S., Pittman, J. K., Frénel, K., Poulin, B., McFarlane, L. R., Slavic, K., et al. (2013). The Plasmodium Berghei Ca<sup>2+</sup>/H<sup>+</sup> Exchange, PbCAX, Is Essential for Tolerance to Environmental Ca<sup>2+</sup> During Sexual Development. *PLoS Pathog.* 9 (2), 1–17. doi: 10.1371/journal.ppat.1003191
- Honoré, B., and Vorum, H. (2000). The CREC Family, a Novel Family of Multiple EF-Hand, Low-Affinity Ca<sup>2+</sup>-Binding Proteins Localised to the Secretory Pathway of Mammalian Cells. *FEBS Lett.* 466, 11–18. doi: 10.1016/S0014-5793(99)01780-9
- Hortua-Triana, M. A., Márquez-Nogueras, K. M., Vella, S. A., and Moreno, S. N. J. (2018). Calcium Signaling and the Lytic Cycle of the Apicomplexan Parasite Toxoplasma Gondii. *Biochim. Biophys. Acta Mol. Cell Res.* 1865, 1846–1856. doi: 10.1016/j.bbamcr.2018.08.004
- Hotta, C. T., Gazarini, M. L., Beraldo, F. H., Varotti, F. P., Lopes, C., Markus, R. P., et al. (2000). Calcium-Dependent Modulation by Melatonin of the Circadian Rhythm in Malarial Parasites. *Nat. Cell Biol.* 2, 466–468. doi: 10.1038/35017112
- Huang, G., Bartlett, P. J., Thomas, A. P., Moreno, S. N. J., and Docampo, R. (2013). Acidocalcisomes of Trypanosoma Brucei Have an Inositol 1,4,5-Trisphosphate Receptor That Is Required for Growth and Infectivity. *PNAS* 110 (12), 1887–1892. doi: 10.1371/journal.ppat.1004555
- Huang, G., Ulrich, P. N., Storey, M., Johnson, D., Tischer, J., Tovar, J. A., et al. (2014). Proteomic Analysis of the Acidocalcisome, an Organelle Conserved From Bacteria to Human Cells. *PLoS Pathog.* 10 (12), 1–17. doi: 10.1371/journal.ppat.1004555
- Hui, R., El Bakkouri, M., and Sibley, L. D. (2015). Designing Selective Inhibitors for Calcium-Dependent Protein Kinases in Apicomplexans. *Trends Pharmacol. Sci.* 36, 452–460. doi: 10.1016/j.tips.2015.04.011
- Ishino, T., Orito, Y., Chinzei, Y., and Yuda, M. (2006). A Calcium-Dependent Protein Kinase Regulates Plasmodium Ookinete Access to the Midgut Epithelial Cell. *Mol. Microbiol.* 59, 1175–1184. doi: 10.1111/j.1365-2958.2005.05014.x
- Iyer, G. R., Singh, S., Kaur, I., Agarwal, S., Siddiqui, M. A., Bansal, A., et al. (2018). Calcium-Dependent Phosphorylation of Plasmodium Falciparum Serine Repeat Antigen 5 Triggers Merozoite Egress. *J. Biol. Chem.* 293, 9736–9746. doi: 10.1074/jbc.RA117.001540
- Jebiwott, S., Govindaswamy, K., Mbugua, A., and Bhanot, P. (2013). Plasmodium Berghei Calcium Dependent Protein Kinase 1 Is Not Required for Host Cell Invasion. *PLoS One* 8, 1–5. doi: 10.1371/journal.pone.0079171
- Kadian, K., Gupta, Y., Kempaiah, P., Gupta, N., and Rawat, M. (2017). Calcium Dependent Protein Kinases (CDPKs): Key to Malaria Eradication. *Curr. Top. Med. Chem.* 17, (19):1–6. doi: 10.2174/1568026617666170130112714
- Kaiser, K., Camargo, N., and Kappe, S. H. I. (2003). Transformation of Sporozoites Into Early Exoerythrocytic Malaria Parasites Does Not Require Host Cells. *J. Exp. Med.* 197, 1045–1050. doi: 10.1084/jem.20022100
- Kato, K., Sudo, A., Kobayashi, K., Tohya, Y., and Akashi, H. (2008). Characterization of Plasmodium Falciparum Protein Kinase 2. *Mol. Biochem. Parasitol.* 162, 87–95. doi: 10.1016/j.molbiopara.2008.07.007
- Kehrer, J., Frischknecht, F., and Mair, G. R. (2016). Proteomic Analysis of the Plasmodium Berghei Gametocyte Egressome and Vesicular BioID of Osmiophilic Body Proteins Identifies Merozoite TRAP-Like Protein (MTRAP) as an Essential Factor for Parasite Transmission. *Mol. Cell. Proteomics* 15, 2852–2862. doi: 10.1074/mcp.m116.058263
- Khalife, J., and Pierrot, C. (2016). Phosphatases are Emerging as Novel Druggable Targets in Plasmodium. *Future Microbiol.* 11, 603–606. doi: 10.2217/fmb-2016-0029
- Kirk, K. (2001). Membrane Transport in the Malaria-Infected Erythrocyte. *Physiol. Rev.* 81, 495–537. doi: 10.1152/physrev.2001.81.2.495
- Kirk, K. (2004). Channels and Transporters as Drug Targets in the Plasmodium-Infected Erythrocyte. *Acta Trop.* 89, 285–298. doi: 10.1016/j.actatropica.2003.10.002
- Kirk, K., and Lehane, A. M. (2014). Membrane Transport in the Malaria Parasite and its Host Erythrocyte. *Biochem. J.* 457, 1–18. doi: 10.1042/BJ20131007
- Kumar, V., Behl, A., Kapoor, P., Nayak, B., Singh, G., Singh, A. P., et al. (2019). Inner Membrane Complex 11 Protein of Plasmodium Falciparum Links Membrane Lipids With Cytoskeletal Element ‘Actin’ and Its Associated Motor ‘Myosin.’ *Int. J. Biol. Macromol.* 126 (1), 673–684. doi: 10.1016/j.jbiomac.2018.12.239
- Kumar, S., Kumar, M., Ekka, R., Dvorin, J. D., Paul, A. S., Madugundu, A. K., et al. (2017). PfCDPK1 Mediated Signaling in Erythrocytic Stages of Plasmodium Falciparum. *Nat. Commun.* 8, 1–12. doi: 10.1038/s41467-017-00053-1
- Kumar, R., Musiyenko, A., Oldenburg, A., Adams, B., and Barik, S. (2004). Post-Translational Generation of Constitutively Active Cores From Larger Phosphatases in the Malaria Parasite, Plasmodium Falciparum: Implications for Proteomics. *BMC Mol. Biol.* 5, 1–15. doi: 10.1186/1471-2199-5-6
- Kumar, P., Tripathi, A., Ranjan, R., Halbert, J., Gilberger, T., Doerig, C., et al. (2014). Regulation of Plasmodium Falciparum Development by Calcium-Dependent Protein Kinase 7 (PfCDPK7). *J. Biol. Chem.* 289, 20386–20395. doi: 10.1074/jbc.M114.561670
- Kushwaha, A. K., Apolis, L., Ito, D., and Desai, S. A. (2018). Increased Ca<sup>2+</sup> Uptake by Erythrocytes Infected With Malaria Parasites: Evidence for Exported Proteins and Novel Inhibitors. *Cell. Microbiol.* 20, 1–12. doi: 10.1111/cmi.12853
- Kutuzov, M. A., and Andreeva, A. V. (2008). Protein Ser/Thr Phosphatases of Parasitic Protozoa. *Mol. Biochem. Parasitol.* 161, 81–90. doi: 10.1016/j.molbiopara.2008.06.008

- Kutuzov, M. A., Bennett, N., and Andreeva, A. V. (2001). Interaction of Plant Protein Ser/Thr Phosphatase PP7 With Calmodulin. *Biochem. Biophys. Res. Commun.* 289, 634–640. doi: 10.1006/bbrc.2001.6020
- La Greca, N., Hibbs, A. R., Rifkin, C., Foley, M., and Tilley, L. (1997). Identification of an Endoplasmic Reticulum-Resident Calcium-Binding Protein With Multiple EF-Hand Motifs in Asexual Stages of *Plasmodium Falciparum*. *Mol. Biochem. Parasitol.* 89, 283–293. doi: 10.1016/S0166-6851(97)00134-5
- Lee, A. H., Dhingra, S. K., Lewis, I. A., Singh, M. K., Siriwardana, A., Dalal, S., et al. (2018). Evidence for Regulation of Hemoglobin Metabolism and Intracellular Ionic Flux by the *Plasmodium Falciparum* Chloroquine Resistance Transporter. *Sci. Rep.* 8, 1–13. doi: 10.1038/s41598-018-31715-9
- Le Roch, K. G., Zhou, Y., Blair, P. L., Grainger, M., Moch, J. K., Haynes, J. D., et al. (2003). Discovery of Gene Function by Expression Profiling of the Malaria Parasite Life Cycle. *Science (80-)* 301, 1503–1508. doi: 10.1126/science.1087025
- Liu, S., Hou, Y., Liu, W., Lu, C., Wang, W., and Sun, S. (2015). Components of the Calcium-Calcineurin Signaling Pathway in Fungal Cells and Their Potential as Antifungal Targets. *Eukaryot. Cell* 14 (4), 324–334. doi: 10.1128/EC.00271-14
- Lourido, S., and Moreno, S. N. J. (2015). The Calcium Signaling Toolkit of the Apicomplexan Parasites *Toxoplasma Gondii* and *Plasmodium Spp.* *Cell Calcium* 57, 186–193. doi: 10.1016/j.ceca.2014.12.010
- Lovett, J. L., Marchesini, N., Moreno, S. N. J., and David Sibley, L. (2002). *Toxoplasma Gondii* Microneme Secretion Involves Intracellular Ca<sup>2+</sup> Release From Inositol 1,4,5-Triphosphate (IP<sub>3</sub>)/ryanodine-Sensitive Stores. *J. Biol. Chem.* 277, 25870–25876. doi: 10.1074/jbc.M202553200
- Luo, S., Marchesini, N., Moreno, S. N. J., and Docampo, R. (1999). A Plant-Like Vacuolar H<sup>+</sup>-Pyrophosphatase in *Plasmodium Falciparum*. *FEBS Lett.* 460, 217–220. doi: 10.1016/S0014-5793(99)01353-8
- Luo, S., Ruiz, F. A., and Moreno, S. N. J. (2005). The Acidocalcisome Ca<sup>2+</sup>-ATPase (TgA1) of *Toxoplasma Gondii* is Required for Polyphosphate Storage, Intracellular Calcium Homeostasis and Virulence. *Mol. Microbiol.* 55, 1034–1045. doi: 10.1111/j.1365-2958.2004.04464.x
- Luo, S., Vieira, M., Graves, J., Zhong, L., and Moreno, S. N. J. (2001). A Plasma Membrane-Type Ca<sup>2+</sup>-ATPase Co-Localizes With a Vacuolar H<sup>+</sup>-Pyrophosphatase to Acidocalcisomes of *Toxoplasma Gondii*. *EMBO J.* 20, 55–64. doi: 10.1093/emboj/20.1.55
- Mahajan, B., Selvapandian, A., Gerald, N. J., Majam, V., Zheng, H., Wickramarachchi, T., et al. (2008). Centrin, Cell Cycle Regulation Proteins in Human Malaria Parasite *Plasmodium Falciparum*. *J. Biol. Chem.* 283, 31871–31883. doi: 10.1074/jbc.M800028200
- Meis, J. F. G. M., Verhave, J. P., Jap, P. H. K., Sinden, R. E., and Meuwissen, J. H. E. T. (1983). Malaria Parasites - Discovery of the Early Liver Form. *Nature* 302, 424–426. doi: 10.1038/302424a0
- Mitchell, A. L., Attwood, T. K., Babbitt, P. C., Blum, M., Bork, P., Bridge, A., et al. (2019). InterPro in 2019: Improving Coverage, Classification and Access to Protein Sequence Annotations. *Nucleic Acids Res* 47 (D1), 351–360. doi: 10.1093/nar/gky1100
- Moraes, M. S., Budu, A., Singh, M. K., Borges-Pereira, L., Levano-Garcia, J., Currà, C., et al. (2017). *Plasmodium Falciparum* GPCR-Like Receptor SR25 Mediates Extracellular K<sup>+</sup> Sensing Coupled to Ca<sup>2+</sup> Signaling and Stress Survival. *Sci. Rep.* 7, 1–13. doi: 10.1038/s41598-017-09959-8
- Moreno, S. N. J., Ayong, L., and Pace, D. A. (2011). Calcium Storage and Function in Apicomplexan Parasites. *Essays Biochem.* 51, 97–110. doi: 10.1042/bse0510097.Calcium
- Moreno, S. N. J., and Docampo, R. (2009). The Role of Acidocalcisomes in Parasitic Protists. *J. Eukaryot. Microbiol.* 56, 208–213. doi: 10.1111/j.1550-7408.2009.00404.x
- Moreno, S. N. J., and Zhong, L. (1996). Acidocalcisomes in *Toxoplasma Gondii* Tachyzoites. *Biochem. J.* 313, 655–659. doi: 10.1042/bj3130655
- Mossaad, E., Furuyama, W., Enomoto, M., Kawai, S., Mikoshiba, K., and Kawazu, S. I. (2015). Simultaneous Administration of 2-Aminoethyl Diphenylborinate and Chloroquine Reverses Chloroquine Resistance in Malaria Parasites. *Antimicrob. Agents Chemother.* 59, 2890–2892. doi: 10.1128/AAC.04805-14
- Moura, P. A., Dame, J. B., and Fidock, D. A. (2009). Role of *Plasmodium Falciparum* Digestive Vacuole Plasmepsins in the Specificity and Antimalarial Mode of Action of Cysteine and Aspartic Protease Inhibitors. *Antimicrob. Agents Chemother.* 53, 4968–4978. doi: 10.1128/AAC.00882-09
- Nagamune, K., Beatty, W. L., and Sibley, L. D. (2007). Artemisinin Induces Calcium-Dependent Protein Secretion in the Protozoan Parasite *Toxoplasma Gondii*. *Eukaryot. Cell* 6, 2147–2156. doi: 10.1128/EC.00262-07
- Nagamune, K., Moreno, S. N., Chini, E. N., and Sibley, L. D. (2008). Calcium Regulation and Signaling in Apicomplexan Parasites. *Mol. Mech. Parasite Invasion* 47, 70–81. doi: 10.1007/978-0-387-78267-6\_5
- Nasamu, A. S., Glushakova, S., Russo, I., Vaupel, B., Kim, A. S., Fremont, D. H., et al. (2017). Plasmepsins IX and X are Essential and Druggable Mediators of Malaria Parasite Egress and Invasion. *Science (80-)* 518, 518–522. doi: 10.1126/science.aan1478
- Nofal, S. D., Patel, A., Blackman, M. J., Flueck, C., and Baker, D. A. (2021). *Plasmodium Falciparum* Guanylyl Cyclase-Alpha and the Activity of its Appended P4-ATPase Domain are Essential for cGMP Synthesis and Blood-Stage Egress. *MBio* 12, 1–19. doi: 10.1128/mBio.02694-20
- Ojo, K. K., Billker, O., Van Voorhis, W. C., Ojo, K. K., Pfander, C., Mueller, N. R., et al. (2012). Transmission of Malaria to Mosquitoes Blocked by Bumped Kinase Inhibitors. *J. Clin. Invest.* 122, 2301–2305. doi: 10.1172/JCI61822.powers
- Otto, T. D., Rayner, J. C., Böhme, U., Pain, A., Spottiswoode, N., Sanders, M., et al. (2014). Genome Sequencing of Chimpanzee Malaria Parasites Reveals Possible Pathways of Adaptation to Human Hosts. *Nat. Commun.* 5 (4754), 1–9. doi: 10.1038/ncomms5754
- Pandey, K., Ferreira, P. E., Ishikawa, T., Nagai, T., Kaneko, O., and Yahata, K. (2016). Ca<sup>2+</sup> Monitoring in *Plasmodium Falciparum* Using the Yellow Cameleon-Nano Biosensor. *Sci. Rep.* 6, 1–13. doi: 10.1038/srep23454
- Pandey, R., Mohammed, A., Pierrot, C., Khalife, J., Malhotra, P., and Gupta, D. (2014). Genome Wide in Silico Analysis of *Plasmodium Falciparum* Phosphatome. *BMC Genomics* 15 (1024), 1–22. doi: 10.1186/1471-2164-15-1024
- Park, H. S., Lee, S. C., Cardenas, M. E., and Heitman, J. (2019). Calcium-Calmodulin-Calcineurin Signaling: A Globally Conserved Virulence Cascade in Eukaryotic Microbial Pathogens. *Cell Host Microbe* 26 (4), 453–462. doi: 10.1016/j.chom.2019.08.004
- Patel, A., Perrin, A. J., Flynn, H. R., Bisson, C., Withers-Martinez, C., Treeck, M., et al. (2019). Cyclic AMP Signalling Controls Key Components of Malaria Parasite Host Cell Invasion Machinery. *PLoS Biol* 17 (5), 1–33. doi: 10.1371/journal.pbio.3000264
- Paul, A. S., Saha, S., Engelberg, K., Jiang, R. H. Y., Coleman, B. I., Kosber, A. L., et al. (2015). Parasite Calcineurin Regulates Host Cell Recognition and Attachment by Apicomplexans. *Cell Host Microbe* 18, 49–60. doi: 10.1016/j.chom.2015.06.003
- Pecenin, M. F., Borges-Pereira, L., Levano-Garcia, J., Budu, A., Alves, E., Mikoshiba, K., et al. (2018). Blocking IP<sub>3</sub> Signal Transduction Pathways Inhibits Melatonin-Induced Ca<sup>2+</sup> Signals and Impairs *P. Falciparum* Development and Proliferation in Erythrocytes. *Cell Calcium* 72, 81–90. doi: 10.1016/j.ceca.2018.02.004
- Philip, N., and Waters, A. P. (2015). Conditional Degradation of *Plasmodium* Calcineurin Reveals Functions in Parasite Colonization of Both Host and Vector. *Cell Host Microbe* 18, 122–131. doi: 10.1016/j.chom.2015.05.018
- Phillips, M. A., Burrows, J. N., Manyando, C., van Huijsduijnen, R. H., Van Voorhis, W. C., and Wells, T. N. C. (2017). Malaria. *Nat. Rev. Dis. Primers* 3, 1–24. doi: 10.1016/S0140-6736(18)30324-6
- Pillai, A. D., Addo, R., Sharma, P., Nguiragool, W., Srinivasan, P., and Desai, S. A. (2013). Malaria Parasites Tolerate a Broad Range of Ionic Environments and do Not Require Host Cation Remodelling. *Mol. Microbiol.* 88, 20–34. doi: 10.1111/mmi.12159
- Pino, P., Caldelari, R., Mukherjee, B., Vahokoski, J., Klages, N., Maco, B., et al. (2017). A Multistage Antimalarial Targets the Plasmepsins IX and X Essential for Invasion and Egress. *Science (80-)* 528, 522–528. doi: 10.1126/science.aaf8675
- Rhee, H., Zou, P., Udeshi, N. D., Martell, J. D., Mootha, V. K., Carr, S. A., et al. (2013). Proteomic Mapping of Mitochondria in Living Cells Via Spatially Restricted Enzymatic Tagging. *Science* 339, 1328–1331. doi: 10.1126/science.1230593
- Rohloff, P., Miranda, K., Rodrigues, J. C. F., Fang, J., Galizzi, M., Plattner, H., et al. (2011). Calcium Uptake and Proton Transport by Acidocalcisomes of *Toxoplasma Gondii*. *PLoS One* 6 (4), 1–9. doi: 10.1371/journal.pone.0018390
- Rohrbach, P., Friedrich, O., Hentschel, J., Plattner, H., Fink, R. H. A., and Lanzer, M. (2005). Quantitative Calcium Measurements in Subcellular Compartments of *Plasmodium Falciparum*-Infected Erythrocytes. *J. Biol. Chem.* 280, 27960–27969. doi: 10.1074/jbc.M500777200

- Roques, M., Stanway, R. R., Rea, E. I., Markus, R., Brady, D., Holder, A. A., et al. (2019). Plasmodium Centrin PbCEN-4 Localizes to the Putative MTOC and is Dispensable for Malaria Parasite Proliferation. *Biol. Open* 8, bio036822. doi: 10.1242/bio.036822
- Rotmann, A., Sanchez, C., Guiguemde, A., Rohrbach, P., Dave, A., Bakouh, N., et al. (2010). PfCHA Is a Mitochondrial Divalent Cation/H<sup>+</sup> Antiporter in Plasmodium Falciparum. *Mol. Microbiol.* 76, 1591–1606. doi: 10.1111/j.1365-2958.2010.07187.x
- Ruecker, A., Shea, M., Hackett, F., Suarez, C., Hirst, E. M. A., Milutinovic, K., et al. (2012). Proteolytic Activation of the Essential Parasitophorous Vacuole Cysteine Protease SERA6 Accompanies Malaria Parasite Egress From Its Host Erythrocyte. *J. Biol. Chem.* 287, 37949–37963. doi: 10.1074/jbc.M112.400820
- Ruiz, F. A., Luo, S., Moreno, S. N. J., and Docampo, R. (2004). Polyphosphate Content and Fine Structure of Acidocalcisomes of Plasmodium Falciparum. *Microsc. Microanal.* 10, 563–567. doi: 10.1017/S1431927604040875
- Rusnak, F., and Mertz, P. (2000). Calcineurin: Form and Function. *Physiol. Rev.* 80, 1483–1521. doi: 10.1152/physrev.2000.80.4.1483
- Saliba, K. J., Allen, R. J. W., Zissis, S., Bray, P. G., Ward, S. A., and Kirk, K. (2003). Acidification of the Malaria Parasite's Digestive Vacuole by a H<sup>+</sup>-ATPase and a H<sup>+</sup>-Pyrophosphatase. *J. Biol. Chem.* 278, 5605–5612. doi: 10.1074/jbc.M208648200
- Santos, J. M., and Soldati-Favre, D. (2011). Invasion Factors Are Coupled to Key Signalling Events Leading to the Establishment of Infection in Apicomplexan Parasites. *Cell. Microbiol.* 13 (6), 787–796. doi: 10.1111/j.1462-5822.2011.01585.x
- Scarpelli, P. H., Tessarin-Almeida, G., Viçoso, K. L., Lima, W. R., Borges-Pereira, L., Meissner, K. A., et al. (2018). Melatonin Activates FIS1, DYN1, and DYN2 Plasmodium Falciparum Related-Genes for Mitochondria Fission: Mitomeald-GFP as a Tool to Visualize Mitochondria Structure. *J. Pineal Res.* 66, 1–12. doi: 10.1111/jpi.12484
- Scheibel, L. W., Colombani, P. M., Hess, A. D., Aikawa, M., Atkinson, C. T., and Milhous, W. K. (1987). Calcium and Calmodulin Antagonists Inhibit Human Malaria Parasites (Plasmodium Falciparum): Implications for Drug Design. *Proc. Natl. Acad. Sci. U. S. A.* 84, 7310–7314. doi: 10.1073/pnas.84.20.7310
- Shortt, H. E., and Garnham, P. C. (1948). Pre-Erythrocytic Stage of Mammalian Malaria Parasites. *Nature* 161, 126–127. doi: 10.1038/161126b0
- Siden-Kiamos, I., Ecker, A., Nybäck, S., Louis, C., Sinden, R. E., and Billker, O. (2006). Plasmodium Berghei Calcium-Dependent Protein Kinase 3 Is Required for Ookinete Gliding Motility and Mosquito Midgut Invasion. *Mol. Microbiol.* 60, 1355–1363. doi: 10.1111/j.1365-2958.2006.05189.x
- Singh, S., Alam, M. M., Pal-Bhowmick, I., Brzostowski, J. A., and Chitnis, C. E. (2010). Distinct External Signals Trigger Sequential Release of Apical Organelles During Erythrocyte Invasion by Malaria Parasites. *PLoS Pathog* 6 (2), 1–14. doi: 10.1371/journal.ppat.1000746
- Singh, S., and Chitnis, C. E. (2012). Signalling Mechanisms Involved in Apical Organelle Discharge During Host Cell Invasion by Apicomplexan Parasites. *Microbes Infect.* 14, 820–824. doi: 10.1016/j.micinf.2012.05.007
- Singh, S., More, K. R., and Chitnis, C. E. (2014). Role of Calcineurin and Actin Dynamics in Regulated Secretion of Microneme Proteins in Plasmodium Falciparum Merozoites During Erythrocyte Invasion. *Cell. Microbiol.* 16 (1), 50–63. doi: 10.1111/cmi.12177
- Steinbach, W. J., Reedy, J. L., Cramer, R. A., Perfect, J. R., and Heitman, J. (2007). Harnessing Calcineurin as a Novel Anti-Infective Agent Against Invasive Fungal Infections. *Nat. Rev. Microbiol.* 5 (6), 418–430. doi: 10.1038/nrmicro1680
- Tanabe, K., Mikkelsen, R. B., and Wallach, D. F. H. (1982). Calcium Transport of Plasmodium Chabaudi-Infected Erythrocytes. *J. Cell Biol.* 93, 680–684. doi: 10.1083/jcb.93.3.680
- Tan, M. S. Y., Koussis, K., Withers-Martinez, C., Howell, S. A., Thomas, J. A., Hackett, F., et al. (2021). Autocatalytic Activation of a Malarial Egress Protease is Druggable and Requires a Protein Cofactor. *EMBO J.* 40, 1–18. doi: 10.15252/embj.2020107226
- Tewari, R., Straschil, U., Bateman, A., Böhme, U., Cherevach, I., Gong, P., et al. (2010). The Systematic Functional Analysis of Plasmodium Protein Kinases Identifies Essential Regulators of Mosquito Transmission. *Cell Host Microbe* 8, 377–387. doi: 10.1016/j.chom.2010.09.006
- Thomas, J. A., Tan, M. S. Y., Bisson, C., Borg, A., Umrekar, T. R., Hackett, F., et al. (2018). A Protease Cascade Regulates Release of the Human Malaria Parasite Plasmodium Falciparum From Host Red Blood Cells. *Nat. Microbiol.* 3, 447–455. doi: 10.1038/s41564-018-0111-0
- Tong, J. X., Chandramohanadas, R., and Tan, K. S.-W. (2018). High-Content Screening of the Medicines for Malaria Venture Pathogen Box for Plasmodium Falciparum Digestive Vacuole-. *Antimicrob. Agents Chemother.* 62, 1–17. doi: 10.1128/AAC.02031-17
- Uyemura, S. A., Luo, S., Moreno, S. N. J., and Docampo, R. (2000). Oxidative Phosphorylation, Ca<sup>2+</sup> Transport, and Fatty Acid-Induced Uncoupling in Malaria Parasites Mitochondria. *J. Biol. Chem.* 275, 9709–9715. doi: 10.1074/jbc.275.13.9709
- Vaid, A., and Sharma, P. (2006). PfPKB, a Protein Kinase B-Like Enzyme From Plasmodium Falciparum: II. Identification of Calcium/Calmodulin as Its Upstream Activator and Dissection of a Novel Signaling Pathway. *J. Biol. Chem.* 281, 27126–27133. doi: 10.1074/jbc.M601914200
- Vaid, A., Thomas, D. C., and Sharma, P. (2008). Role of Ca<sup>2+</sup>/calmodulin-PfPKB Signaling Pathway in Erythrocyte Invasion by Plasmodium Falciparum. *J. Biol. Chem.* 283, 5589–5597. doi: 10.1074/jbc.M708465200
- Vercesi, A. E., Moreno, S. N. J., and Docampo, R. (1994). Ca<sup>2+</sup>/H<sup>+</sup> Exchange in Acidic Vacuoles of Trypanosoma Brucei. *Biochem. J.* 304, 227–233. doi: 10.1042/bj3040227
- Vidadala, R. S. R., Ojo, K. K., Johnson, S. M., Zhang, Z., Leonard, S. E., Mitra, A., et al. (2014). Development of Potent and Selective Plasmodium Falciparum Calcium-Dependent Protein Kinase 4 (PfCDPK4) Inhibitors That Block the Transmission of Malaria to Mosquitoes. *Eur. J. Med. Chem.* 74, 562–573. doi: 10.1016/j.ejmech.2013.12.048
- Wasserman, M., Alarcon, C., and Mendoza, P. M. (1982). Effects of Ca<sup>2+</sup> Depletion on the Asexual Cell Cycle of Plasmodium Falciparum. *Am. J. Trop. Med. Hyg.* 31, 711–717. doi: 10.4269/ajtmh.1982.31.711
- Wernimont, A. K., Artz, J. D., Finerty, J. R. P., Lin, Y., Amani, M., Allali-hassani, A., et al. (2010). Structures of Apicomplexan Calcium-Dependent Protein Kinases Reveal Mechanism of Activation by Calcium. *Nat. Struct. Mol. Biol.* 17, 596–601. doi: 10.1038/nsmb.1795.Structures
- Wilkes, J. M., and Doerig, C. (2008). The Protein-Phosphatome of the Human Malaria Parasite Plasmodium Falciparum. *BMC Genomics* 9 (412), 1–19. doi: 10.1186/1471-2164-9-412
- Wilkins, B. J., and Molkenin, J. D. (2004). Calcium-Calcineurin Signaling in the Regulation of Cardiac Hypertrophy. *Biochem. Biophys. Res. Commun.* 322 (4), 1178–1191. doi: 10.1016/j.bbrc.2004.07.12'1
- Yang, C., and Arrizabalaga, G. (2017). The Serine/Threonine Phosphatases of Apicomplexan Parasites. *Mol. Microbiol.* 106, 1–21. doi: 10.1111/mmi.13715

**Conflict of Interest:** The authors declare that the research was conducted in the absence of any commercial or financial relationships that could be construed as a potential conflict of interest.

**Publisher's Note:** All claims expressed in this article are solely those of the authors and do not necessarily represent those of their affiliated organizations, or those of the publisher, the editors and the reviewers. Any product that may be evaluated in this article, or claim that may be made by its manufacturer, is not guaranteed or endorsed by the publisher.

Copyright © 2021 de Oliveira, Alborghetti, Carneiro, Bastos, Amino, Grellier and Charneau. This is an open-access article distributed under the terms of the Creative Commons Attribution License (CC BY). The use, distribution or reproduction in other forums is permitted, provided the original author(s) and the copyright owner(s) are credited and that the original publication in this journal is cited, in accordance with accepted academic practice. No use, distribution or reproduction is permitted which does not comply with these terms.

## GLOSSARY

IP3R	inositol-1,4,5-triphosphate receptor
IP3	inositol-1,4,5-triphosphate
ER	endoplasmic reticulum
SOCEs	store-operated calcium channels
PMCA	plasma membrane Ca <sup>2+</sup> -ATPase
SERCA	sarco(endo)plasmic reticulum Ca <sup>2+</sup> -ATPase
PLC	phospholipase C
PI(4,5)P <sub>2</sub>	phosphatidylinositol 4,5-bisphosphate
RBCs	red blood cells
RBCM	red blood cell membrane
PVM	parasitophorous vacuole membrane
iRBCs	infected red blood cells
uRBCs	uninfected red blood cells
EIPA	ethylisopropyl-amiloride
PTEX	<i>Plasmodium</i> translocon of exported proteins
PV	parasitophorous vacuole
cAMP	cyclic-adenosine monophosphate
PfACβ	<i>P. falciparum</i> adenyllyl-cyclase β
HCO <sub>3</sub> <sup>-</sup>	bicarbonate ion
Epac	exchange protein directly activated by cAMP
Rap1	Ras-related protein 1
PfSR25	G-protein-coupled receptor-like
U73122	inhibitor of PLC
2-APB	2-aminoethyl diphenylborinate, inhibitor of IP3 signaling
PfATP6	a <i>P. falciparum</i> SERCA-type Ca <sup>2+</sup> -ATPase
Thg	thapsigargin
FV	food vacuole
PPi	pyrophosphate
PolyP	polyphosphate
VP1	vacuolar-H <sup>+</sup> -pyrophosphatase
V-ATPase	vacuolar-H <sup>+</sup> -ATPase
CQ	chloroquine
PfCRT	<i>P. falciparum</i> chloroquine resistance transporter
FVM	food vacuole membrane
TgA1	<i>T. gondii</i> Ca <sup>2+</sup> /H <sup>+</sup> -ATPase
TgVP1	<i>T. gondii</i> vacuolar-type H <sup>+</sup> -pyrophosphatase
AMDP	amino-methylene-diphosphonate
TbPMC1	<i>T. brucei</i> vacuolar-Ca <sup>2+</sup> -ATPase
PfCHA or PfCAX	<i>P. falciparum</i> Ca <sup>2+</sup> /H <sup>+</sup> antiporter or <i>P. falciparum</i> Ca <sup>2+</sup> /H <sup>+</sup> exchanger
CaBPs	Ca <sup>2+</sup> binding proteins
EF-hand motif	motif for Ca <sup>2+</sup> binding
CaM	calmodulin
CBL	calcineurin B-like family
CDPKs	Ca <sup>2+</sup> -dependent protein kinases family (1-7)
PfPKB	<i>P. falciparum</i> protein kinase B
PfGAP45	<i>P. falciparum</i> gliideosome-associated protein 45

(Continued)

Continued

IMC	inner membrane complex
PfCENs	<i>P. falciparum</i> centrins (1-4)
MTOC	microtubule-organizing center
CaMKs	Ca <sup>2+</sup> /CaM-dependent kinases
PfPK2	<i>P. falciparum</i> protein kinase 2
PKG	cGMP-dependent protein kinase
PKA	cAMP-dependent protein kinase
IMC1g	inner membrane complex protein 1g
ITRAQ	isobaric tag for relative and absolute quantification
PfSERA5	<i>P. falciparum</i> serine repeat antigen 5
HSP90	heat-shock protein
HSPGs	heparan sulphate proteoglycans
CSP	circumsporozoite protein
STPPs	serine/threonine protein phosphatases
CN	calcineurin
CNA	catalytic subunit of the calcineurin
CNB	regulatory subunit of the calcineurin
AMA1-RON2	apical membrane antigen-1/hoptry neck protein 2
PP7	protein phosphatase 7
IQ	the first two amino acids of the calmodulin binding motif: Ile and Gln
PPP8	serine/threonine protein phosphatase 8
EBA-175	175 kDa erythrocyte binding antigen
PfRh1	<i>P. falciparum</i> reticulocyte binding-like protein 1
PfIMC11	<i>P. falciparum</i> inner membrane complex 11
GAP40	gliideosome-associated protein 40
SOC6	substrate of CDPK4 6
glyA	glycophorin A
CLAG3.1/	cytoadherence-linked asexual protein gene 3.1
RhopH1	<i>P. falciparum</i> reticulocyte binding-like protein 2b
PfRh2b	<i>P. berghei</i> rhoptry neck protein 11
PbRON11	<i>P. berghei</i> rhoptry neck protein 11
cGMP	cyclic guanosine monophosphate
ICM-1	important for calcium mobilization-1 protein
cKO	conditional knockout
GCα	guanylyl cyclase alpha
PfPDEβ	<i>P. falciparum</i> phosphodiesterase beta
PfMyoA	<i>P. falciparum</i> myosin A
CREC family	Calumenin, Reticulocalbin 1 and 3, ERC-55, Cab-45
PfERC	<i>P. falciparum</i> endoplasmic reticulum-resident calcium-binding protein
GPA	cyclopiazonic acid
SUB1	subtilisin-like protease
PMX	plasmepsin X
MSP1	merozoite surface protein 1
EEF	exo-erythrocytic form
NF-κB	nuclear factor κB
CXCR4	C-X-C chemokine receptor type 4
BioID	proximity-dependent biotin identification
APEX-2	ascorbate peroxidase-2

RESEARCH ARTICLE

# Exoproteome profiling of *Trypanosoma cruzi* during amastigogenesis early stages

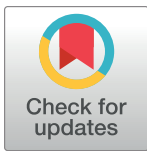
Samuel C. Mandacaru<sup>1</sup>, Rayner M. L. Queiroz<sup>1,2</sup>, Marcos R. Alborghetti<sup>1</sup>, Lucas S. de Oliveira<sup>1</sup>, Consuelo M. R. de Lima<sup>1</sup>, Izabela M. D. Bastos<sup>3</sup>, Jaime M. Santana<sup>3</sup>, Peter Roepstorff<sup>2</sup>, Carlos André O. Ricart<sup>1</sup>, Sébastien Charneau<sup>1\*</sup>

**1** Laboratory of Protein Chemistry and Biochemistry, Department of Cell Biology, Institute of Biology, University of Brasilia, Brasilia, Brazil, **2** Department of Biochemistry and Molecular Biology, University of Southern Denmark, Odense, Denmark, **3** Pathogen-Host Interface Laboratory, Department of Cell Biology, Institute of Biology, University of Brasilia, Brasilia, Brazil

☞ These authors contributed equally to this work.

✉ Current address: Cambridge Centre for Proteomics, Department of Biochemistry, University of Cambridge, Cambridge, United Kingdom

\* [charneau@unb.br](mailto:charneau@unb.br)



**OPEN ACCESS**

**Citation:** Mandacaru SC, Queiroz RML, Alborghetti MR, de Oliveira LS, de Lima CMR, Bastos IMD, et al. (2019) Exoproteome profiling of *Trypanosoma cruzi* during amastigogenesis early stages. PLoS ONE 14(11): e0225386. <https://doi.org/10.1371/journal.pone.0225386>

**Editor:** Martin E. Rottenberg, Karolinska Institutet, SWEDEN

**Received:** June 13, 2019

**Accepted:** November 4, 2019

**Published:** November 22, 2019

**Copyright:** © 2019 Mandacaru et al. This is an open access article distributed under the terms of the [Creative Commons Attribution License](https://creativecommons.org/licenses/by/4.0/), which permits unrestricted use, distribution, and reproduction in any medium, provided the original author and source are credited.

**Data Availability Statement:** All Mass spectrometer output files (Raw data) are available from the MassIVE database (accession number MSV000083878, doi:[10.25345/C5KK92](https://doi.org/10.25345/C5KK92), <https://massive.ucsd.edu/ProteoSAFe/dataset.jsp?task=246ae8d5bffd4f9fa3830063e84a58f3>).

**Funding:** This work was supported by MCTI/CNPq/FNDCT/PRO-CENTRO-OESTE, FAPDF, INCT-CNPq-FAPEG (465771/2014-9), CAPES-COFECUB grant 923/18, CNPq grant 433208/2016-3, FAPDF (fellowship to SCM), CAPES (PNPD fellowship to

## Abstract

Chagas disease is caused by the protozoan *Trypanosoma cruzi*, affecting around 8 million people worldwide. After host cell invasion, the infective trypomastigote form remains 2–4 hours inside acidic phagolysosomes to differentiate into replicative amastigote form. *In vitro* acidic-pH-induced axenic amastigogenesis was used here to study this step of the parasite life cycle. After three hours of trypomastigote incubation in amastigogenesis promoting acidic medium (pH 5.0) or control physiological pH (7.4) medium samples were subjected to three rounds of centrifugation followed by ultrafiltration of the supernatants. The resulting exoproteome samples were trypsin digested and analysed by nano flow liquid chromatography coupled to tandem mass spectrometry. Computational protein identification searches yielded 271 and 483 protein groups in the exoproteome at pH 7.4 and pH 5.0, respectively, with 180 common proteins between both conditions. The total amount and diversity of proteins released by parasites almost doubled upon acidic incubation compared to control. Overall, 76.5% of proteins were predicted to be secreted by classical or non-classical pathways and 35.1% of these proteins have predicted transmembrane domains. Classical secretory pathway analysis showed an increased number of mucins and mucin-associated surface proteins after acidic incubation. However, the number of released trans-sialidases and surface GP63 peptidases was higher at pH 7.4. Trans-sialidases and mucins are anchored to the membrane and exhibit an enzyme-substrate relationship. In general, mucins are glycoproteins with immunomodulatory functions in Chagas disease, present mainly in the epimastigote and trypomastigote surfaces and could be enzymatically cleaved and released in the phagolysosome during amastigogenesis. Moreover, evidence for flagella discard during amastigogenesis are addressed. This study provides the first comparative analysis of the exoproteome during amastigogenesis, and the presented data evidence the dynamism of its profile in response to acidic pH-induced differentiation.

MRA and fellowship to LSO). The funders had no role in study design, data collection and analysis, decision to publish, or preparation of the manuscript.

**Competing interests:** The authors have declared that no competing interests exist.

## Introduction

*Trypanosoma cruzi* is the etiologic agent of Chagas disease in Central and South America, with more than 10,000 deaths annually worldwide [1]. An increasing number of cases are being reported in non-endemic regions including the United States and Europe due to intense migration of individuals from endemic areas of Latin America [2–6]. In humans, *T. cruzi* infection usually develops from an acute phase characterized by high parasitemia and a robust immune response, into a clinically variable chronic phase. In the absence of treatment during the chronic phase, parasite proliferation is highly contained by a humoral and cellular immune response. However the infection remains persistent, particularly in the myocardium and smooth muscle, which may lead to the development of cardiac and digestive complications [7,8]. The treatment of Chagas disease is currently based around chemotherapy, since no effective vaccine is available. Only two drugs are available: nifurtimox and benznidazole. Benznidazole is considered the first-line treatment in most countries due to its effectiveness for the treatment of acute, congenital, reactive and early chronic infections. In many cases, this drug is able to reduce disease progression, but the high toxicity has the potential to cause serious side effects, leading to interruption of patient treatment. Additionally, the low efficacy of the current drugs is low in adult patients with the chronic disease [9,10].

In order to carry out its lifecycle, infective *T. cruzi* trypomastigotes invade nucleated mammalian host cells and differentiate intracellularly into replicative amastigote forms (amastigogenesis). After internalization, trypomastigotes remain 2–4 h inside acidic phagolysosomes [11], escaping into the host cell cytoplasm to complete its differentiation. To facilitate the escape process, the parasite recruits trans-sialidase proteins and release pore-forming molecules called Tc-TOX [12,13]. It has also been recently reported that *T. cruzi* infection blocks the expression of host cell immunoproteasome subunits, proteasome activator protein PA28b, TAP1 and MHC class I molecule by an unknown posttranscriptional control [14]. This indicates that trypomastigotes release proteins and/or other molecules in response to processes caused by or following the differentiation induction.

The secreted/excreted protein repertoire (here generically referred as exoproteome) plays important roles in homeostasis, immune response, development, proteolysis, adhesion, cell proliferation, cell differentiation, morphogenesis and cellular communication [15]. Furthermore, secreted/excreted proteins account for approximately 10% of the proteins encoded by a genome [15–18]. Trypomastigotes are able to release membranous vesicles filled with virulent factors such as trans-sialidases [19,20]. It is these extracellular vesicles that have been shown to be involved in the pathogenesis of Chagas disease by increasing heart parasitism and inflammation [20].

Classically secreted proteins can be identified by the presence of an N-terminal cleavable signal peptide (SP) that is typically 15–30 amino acids long. Furthermore, a class of secretory proteins, known as leaderless proteins, is exported from the cell without signal sequences through non-classical secretion pathways. For example cell surface shedding and inclusion into exosomes and other secretory vesicles [21], or even release from the plasma membrane through the enzymatic cleavage of their lipid anchor [22].

The acidic milieu is a key step in triggering amastigogenesis and parasite molecular response during this process and has been studied through high-throughput quantitative proteomic and phosphoproteomic approaches [23]. Queiroz and colleagues, analysing intracellular proteins 2 hours after induction, reported the overexpression of several proteins predicted to be secreted, indicating an increase in vesicular traffic. This observation leads us to hypothesize a change in parasite exoproteome repertoire after acidic-pH induction. To address this hypothesis, we evaluate the exoproteome changes of *T. cruzi* trypomastigote upon the first

three hours of acidic-pH-induced axenic amastigogenesis compared to the exoproteome of trypomastigote incubated at physiological pH for the same period.

## Materials and methods

### Trypomastigote cell culture

Trypomastigotes, Y strain [24], were maintained in monolayers of HeLa cells grown in DMEM supplemented with 5% fetal bovine serum, at pH 7.4, according to [25,26]. The parasites of the outbreak from the 4th to 5th day after infection were carefully collected from the supernatant, consisting of over 98% trypomastigotes [26].

### Exoproteome samples

Trypomastigote cells were washed 3 times with DMEM, pH 7.4, without serum, by centrifugation at  $2,500 \times g$  for 10 min. Then,  $1.0 \times 10^9$  washed parasites were resuspended in 5 mL DMEM without serum at pH 7.4 or pH 5.0, ( $2.0 \times 10^8$  cells/mL final concentration) and incubated in a 25 cm<sup>2</sup> culture flasks at 37°C for 3 h with gently shaking every 20 min. After incubation, the parasites motility was microscopically monitored and the samples were collected only if ~ 95% of the cells remained mobile [27]. For pH 7.4 we obtained samples in duplicate and for pH 5.0 in triplicate. In order to remove cells following incubation, the medium was centrifuged for 5 min at room temperature in 3 rounds to ensure complete removal of cells and avoid mechanical cell lysis: firstly, at  $2,000 \times g$ , then at  $4,000 \times g$  and the last at  $6,000 \times g$ , with the supernatants transferred to new tubes after each centrifugation. After cell removal, the supernatants containing the exoproteomes were concentrated and buffer exchanged to 20 mM triethylammonium bicarbonate using Amicon<sup>TM</sup> filter units with 3 kDa cut-off membrane (Millipore, Billerica, MA, USA), dried and stored at -20°C.

### Sample preparation for LC-MS/MS

The exoproteome samples were resuspended in 20 mM triethylammonium bicarbonate, reduced with 20 mM dithiothreitol at 56°C for 45 min, alkylated with 40 mM iodoacetamide in the dark at room temperature for 60 min and digested overnight at 37°C with 1 µg modified trypsin (Promega, Madison, USA). After digestion, the sample was acidified to 0.1% trifluoroacetic acid (TFA), final concentration, and desalted with homemade microcolumns of Poros Oligo R3 resin (PerSeptive Biosystems, Framingham, USA) packed (1 cm long) in p200 tips (adapted from [28]). Prior to lyophilization, a Biochrom 30 amino acid analyzer (Biochrom, Cambridge, U.K.) was employed to determine peptide concentration according to the manufacturers protocol [29].

### LC-MS/MS and data analysis

Samples were analysed by an EASY-nano LC system (Proxeon Biosystems, Odense, Denmark) coupled online to an LTQ-Orbitrap Velos mass spectrometer (Thermo Scientific, Waltham, USA). The exoproteomes at physiological pH and acidic pH were analysed in duplicate and in triplicate, respectively. Two µg of peptides from each fraction were loaded onto an 18 cm fused silica emitter (75 µm inner diameter) manually packed with reverse phase capillary column ReproSil-Pur C18-AQ 3 µm resin (Dr. Maisch GmbH, Germany) and eluted using a gradient from 100% phase A (0.1% formic acid) to 35% phase B (0.1% formic acid, 95% acetonitrile) for 210 min for each sample, 35% to 100% phase B for 5 min and 100% phase B for 8 min in (a total of 223 min at 250 nL/min) [29]. After each run, the column was washed with 90% phase B and re-equilibrated with phase A. Mass spectra were acquired in positive ion mode applying



data-dependent automatic survey MS scan and tandem mass spectra (MS/MS) acquisition. Each MS scan in the orbitrap (mass range of  $m/z$  of 400–1800 and resolution 60,000) was followed by MS/MS of the seven most intense ions in the LTQ. Fragmentation in the LTQ was performed by HCD and selected sequenced ions were dynamically excluded for 30 s. Raw data were viewed in Xcalibur v.2.1 (Thermo Scientific, Waltham, USA). Data processing was performed using Proteome Discoverer v.1.3 (Thermo Scientific, Waltham, USA). Raw files were generated, and these were searched using Proteome Discoverer with SequestHT algorithm against *Trypanosoma cruzi* database containing the proteins of the parasite reference proteome database downloaded from UniProt (early 2017). Contaminant proteins (several types of human keratins, BSA and porcine trypsin) were also added to the database and all contaminant proteins identified were manually removed from the result lists. The searches were performed with the following parameters: MS accuracy 10 ppm, MS/MS accuracy 0.5 Da, trypsin digestion with up to 2 missed cleavage allowed, fixed carbamidomethyl modification of cysteine and variable modification of oxidized methionine. The number of proteins, protein groups and number of peptides were filtered for a false discovery rate (FDR) less than 1%; peptides with rank 1 and proteins with at least 3 peptides using Proteome Discoverer. ProteinCenter™ software (Thermo Scientific, Waltham, USA) was used to generate FASTA formatted files of groups of proteins of interest, GO annotation and statistical analysis between conditions (Fisher's exact test). Improved annotation of the identified proteins was acquired using Blast2GO software (<http://www.blast2go.com/b2ghome>) using default parameters. SignalP v.4.1 (<http://www.cbs.dtu.dk/services/SignalP/>) and SecretomeP v.2.0 (<http://www.cbs.dtu.dk/services/SecretomeP/>) were used to predict proteins secreted by classical and non-classical pathways, respectively. The parameters, eukaryotes/mammal, gram positive and gram negative were set to predict the secretion pathways. The TMHMM algorithm (<http://www.cbs.dtu.dk/services/TMHMM/>) was used to predict the number of transmembrane helices in the protein sequences.

## Results and discussion

In order to identify proteins secreted by *T. cruzi* during amastigogenesis, we performed a qualitative exoproteome analysis of trypomastigote in two different conditions. Thus, samples from parasites incubated for 3 hours at pH 7.4 (control) or at pH 5.0 (amastigogenesis) were investigated by shotgun/bottom-up proteomics (Fig 1). The computational analysis of LC-MS/MS data identified 271 and 483 protein groups at pH 7.4 and pH 5.0 respectively, with 180 common protein groups being present in both conditions (Fig 2A; S1 Table).

The acidic pH-induced differentiation causes drastic metabolic and morphologic changes in *T. cruzi* trypomastigotes [23], preparing the parasite for a replicative stage. As demonstrated by Engel et al. (1985), the amastigote pre-replicative lag period spans from 18.2 to 34.2 hours, depending on the cloned stock analyzed. In 1995, Tomlinson *et al.* showed that, 2 hours after pH induction, almost no trypomastigotes were observed in culture and 4h after pH induction, more than 90% of trypomastigotes were transformed into amastigotes. Focusing on the transformation phase of this parasite, the exoproteome was analyzed at a time point of 3 hours after pH-induced differentiation. After this time, the exoproteome reflects changes in the trypomastigote transformation to amastigote and not the amastigote exoproteome "*per se*". In fact, amastigogenesis dynamics after pH lowering was also evaluated by Hernández-Osorio [30] and they found that, after 3 hours, intermediate forms were predominant (over 80%). Therefore, the exoproteome analysed here can be related to early trypomastigote morphological changes, microenvironment modulation to the next replicative phase and host cell metabolism modulation to parasite survival and replication. In 2013, Caradonna et al. [31], demonstrated

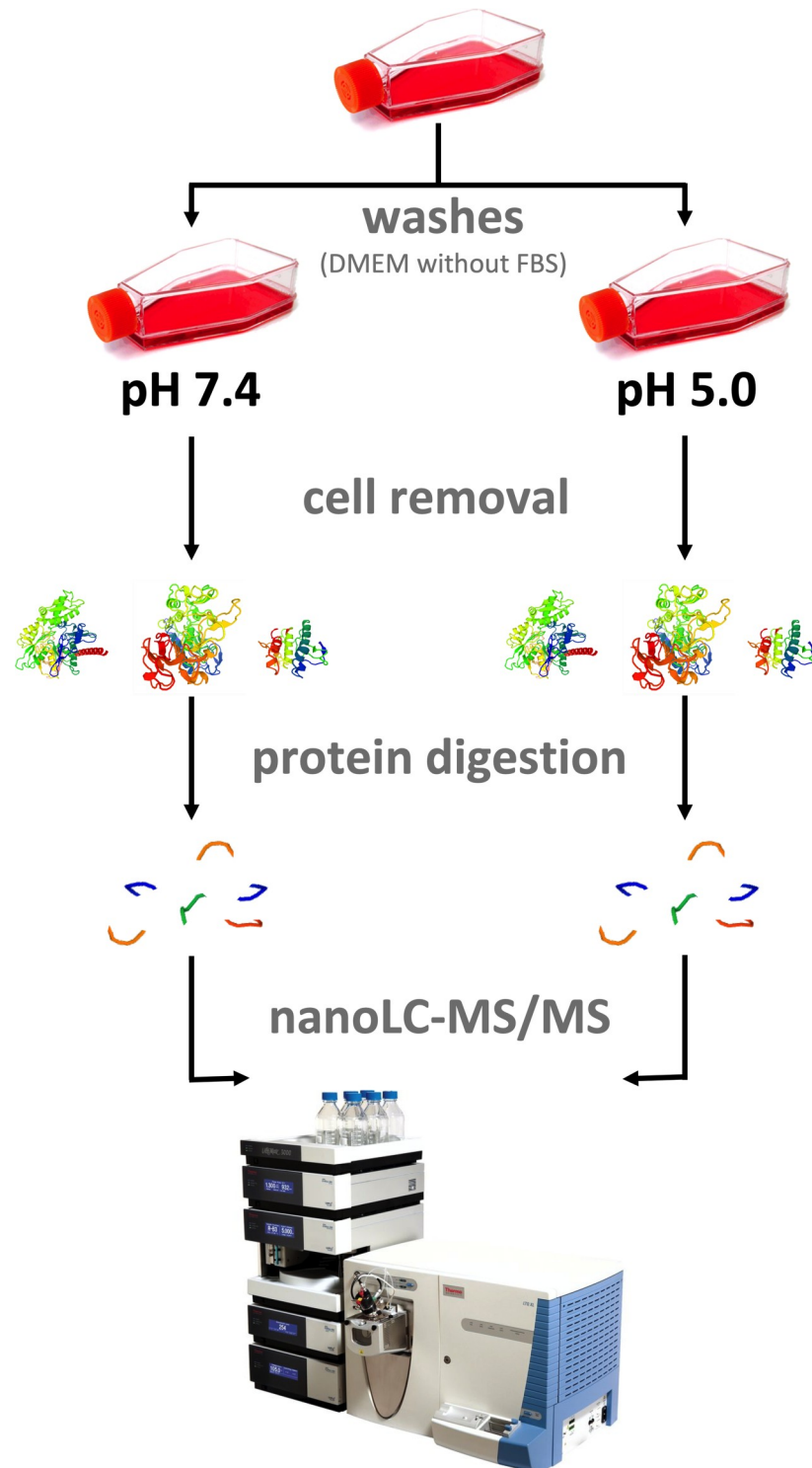


**Fig 1. Experimental setup.** Tissue culture-derived trypomastigotes were harvested and washed before incubation in DMEM without FBS at pH 7.4 or pH 5.0 for 3 h. After incubation, the parasites were removed by three cycles of centrifugation and the proteins presented in the supernatant were TCA/acetone precipitated. Following protein digestion, peptides were subjected to nanoLC-MS/MS analysis.

<https://doi.org/10.1371/journal.pone.0225386.g001>

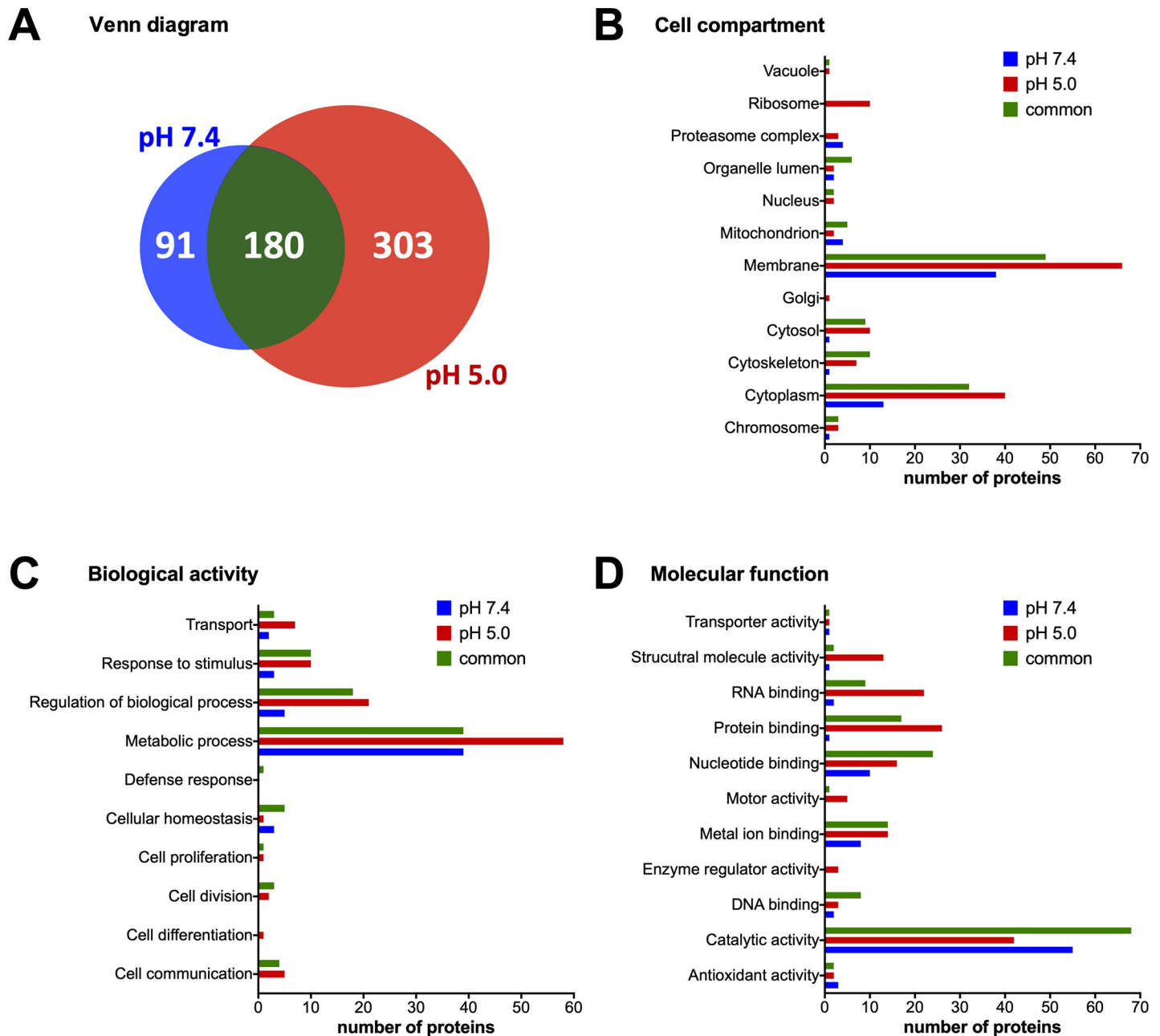


**Fig 2. Comparison of *T. cruzi* trypomastigote exoproteome at pH 7.4 and pH 5.0.** Venn diagram of protein groups identified in each condition (A). Protein categorization by GO annotation for cell compartment (B), molecular function (C) and biological activity (D). Y-axis represents the number of proteins present in each GO term.

<https://doi.org/10.1371/journal.pone.0225386.g002>

that several host metabolism and cytoskeleton modulations which support parasite intracellular growth. Energy production, nucleotide metabolism, pteridine metabolism and fat acid oxidation were shown as interconnected pathways between host and parasite, regulated by host Akt signaling. The capability of adaptation would be especially relevant in the context of a natural dynamic infection in the mammalian host as observed during amastigogenesis. Plasticity within the same population could reflect the ability to change the environment in order to control growth rates. Some specific microenvironments can be a critical issue underlying tissue

tropism and persistent infection [31]. An example of this can be observed during *T. cruzi* infection in adipose tissue and muscle. The fatty acid rich environment and high metabolism of energy production of these cells, provide a space against immune system [31]. The total amount and diversity of proteins released by the parasites almost doubled upon acidic induction within the three hours of incubation (Fig 2A). While hundreds of proteins were identified in both conditions, a significant number of identified proteins were specific for each one (Fig 2A). While 33.6% (91/271) of proteins were specific of pH 7.4 exoproteome, 62.7% (303/483) were specific of pH 5.0 condition (S1 Table). It suggests that there is an increase in protein diversity in exoproteome during amastigogenesis.

Overall, at pH 5.0 all GO categories increased except for proteasome complex and mitochondrion (cell compartment), cellular homeostasis (biological activity) and catalytic activity and antioxidant activity (molecular function) (Fig 2B–2D). Fisher’s exact test between conditions also showed proteins with catalytic activity and hydrolase activity (a subcategory of catalytic activity) under-represented at pH 5.0 (Table 1). Fig 2B highlights the common membrane components in exoproteome, particularly at pH 5.0—indicating potential parasite surface remodeling. Metabolic process, regulation of biological process, response to stimulus and transport (Fig 2C) are the most represented term of the biological activity category. In terms of molecular function, the high number of proteins with catalytic activity corroborate the myriad of metabolic processes in the exoproteome (Fig 2D). Altogether, it is likely that the parasite renews its metabolism during the first hours of amastigogenesis.

Secretome analysis of *T. cruzi* epimastigotes and metacyclic trypomastigotes reported a considerable amount of microvesicles and exosomes [32]. The parasite has different strategies to mediate intercellular communication [33,34], and these vesicles can be used to interact directly with host cells by transferring several small molecules such as proteins, mRNAs, microRNAs and small molecules [33]. Vesicles can transport proteins in soluble form, associated or as integral components of membranes. Transmembrane domains were predicted in 27% of proteins (155/574), with 33 proteins exclusively detected at pH 7.4, 70 at pH 5.0 and 52 in both conditions. These proteins presented up to four predicted transmembrane helices (Fig 3A). Based on this analysis, our results indicate that cell-derived trypomastigotes in both pH conditions could also release vesicles. Moreover, the increased proportion of transmembrane proteins in the exoproteome at pH 5.0, compared to pH 7.4 condition, indicates that transition of trypomastigotes to the early stage of amastigotes may trigger other types of secretion/excretion besides vesicles. However, further experiments to confirm this hypothesis are necessary. All 155 proteins with predicted transmembrane domains were also predicted to be secreted (Fig 3B), suggesting that these proteins could be present in vesicles or being secreted/excreted.

*In silico* screening of excreted/secreted proteins based on genomic information cannot be considered self-sustaining evidence for its secretion as the prediction accuracy is highly dependent on the tool performance and quality of the genomic annotations. Furthermore, predicted secretory proteins may not be expressed in the particular cell/condition under examination or

**Table 1. Under-represented GO terms in parasites incubated at pH 5.0 compared to pH 7.4.**

	Description	Count <sup>a</sup>	Ref. Count <sup>b</sup>	Raw p-value <sup>c</sup>	FDR p-value <sup>d</sup>
Molecular Function	catalytic activity	113	125	4.10E-07	2.75E-04
	hydrolase activity	63	78	6.23E-05	2.09E-02

<sup>a</sup> number of times this feature occurs in the analysis data set.

<sup>b</sup> number of times this feature occurs in the reference data set.

<sup>c</sup> raw p-value indicating the significance of this difference in feature occurrence between the data sets.

<sup>d</sup> FDR corrected version of the raw p-value.

<https://doi.org/10.1371/journal.pone.0225386.t001>

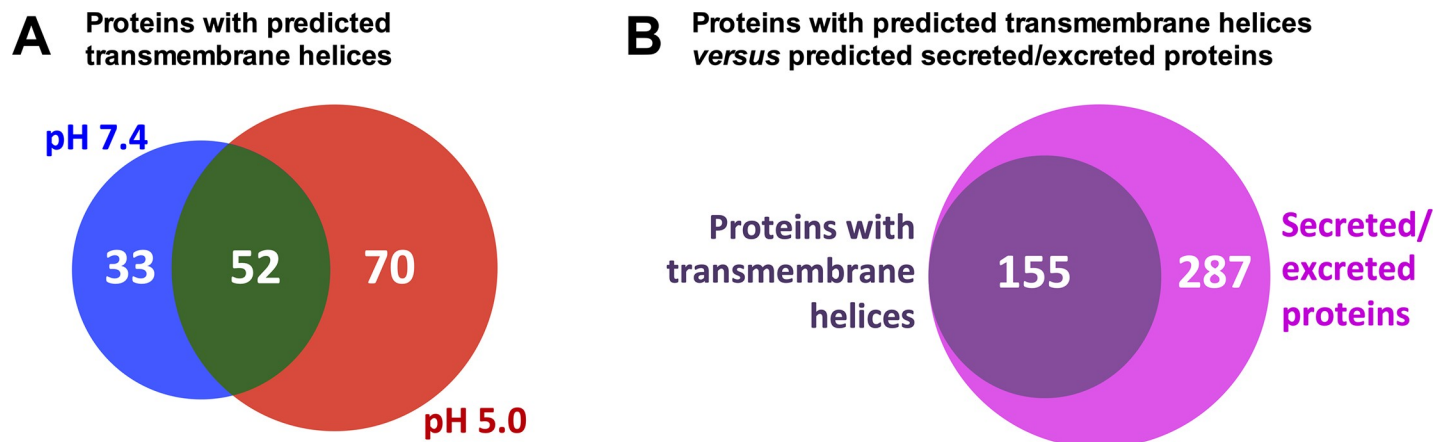


**Fig 3. TMHMM analysis.** Increased number of proteins predicted to possess transmembrane domain in pH 5.0 related to pH 7.4 (A) and all proteins with predicted transmembrane domains are also predicted to be secreted/excreted (B).

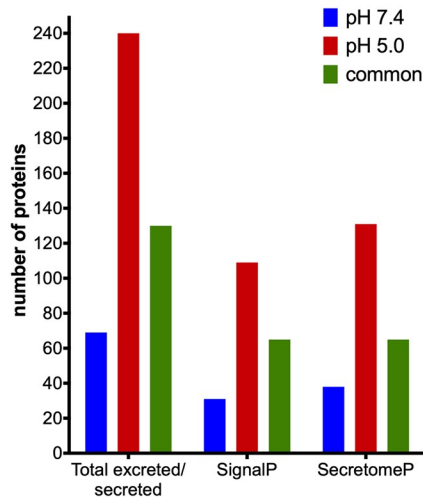
<https://doi.org/10.1371/journal.pone.0225386.g003>

have a retention signal that prevents their secretion [15]. Integrating bioinformatic analysis to predict secreted proteins with proteomic data reinforce the excreted/secreted status of a particular protein and provides validation for the subproteome enrichment and its quality. Herein, *in silico* prediction of secretion through classical (SignalP) and non-classical pathways (SecretomeP) of trypanomastigote exoproteomes at pH 7.4 and pH 5.0 showed remarkably that 76.5% (439/574) of all detected proteins are predicted to be secreted in both algorithms (Fig 4A). Almost twice the number of proteins predicted to be secreted was identified in the acidic condition (199 proteins at pH 7.4 versus 370 proteins at pH 5.0, Fig 4A). This corroborates the hypothesis raised from previously published findings on over expression of several proteins (e.g. some Rab proteins and ADP-ribosylation factors), within 2 hours of acidic induction, indicating an increase in vesicular traffic [23]. In addition, most proteins were predicted to be released through non-classical pathways at pH 5.0 (131 versus 109). While a modest difference, it is in accordance with other findings for members of the kinetoplastidae order [35–37]. Despite computational prediction presents some issues (e.g. none of the algorithms were designed specifically for Trypanosomatids), a very high percentage of predicted proteins together with the GO annotation profiles are concordant synergic and ratify our sampling and results.

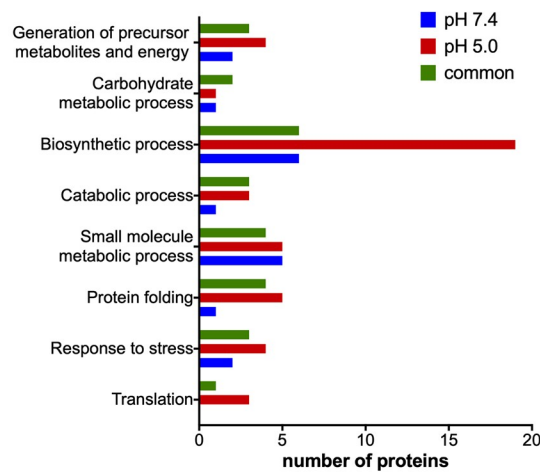
Kinetoplastids database was explored with *Blast2GO* software in order to characterize the total of proteins predicted to be secreted/excreted. The biological processes: translation, response to stress, protein folding, biosynthetic process, generation of precursor metabolites and energy displayed higher number of proteins at pH 5.0 (Fig 4B). DNA binding, ion binding, structural constituent of ribosome and unfolded protein binding were molecular functions predominantly represented at pH 5.0 and hydrolase activity acting on glycosyl bonds and peptidase activity were under represented in this condition (Fig 4C). As expected, the most assigned term was *hydrolase activity on glycosyl bonds* due to the extent of trans-sialidases family members.

The most abundant proteins identified on classical secretory pathway analysis are shown on Fig 5. Trans-sialidases (TS) are enzymes that transfer sialic acid to mucins and both macromolecules are anchored to the plasma membrane by glycosylphosphatidylinositol [38,39]. This enzymatic reaction promotes protection to the parasite against the host immune system and promotes cell invasion. TS function is also important for parasitic escape from parasitophorous vacuole. The number of trans-sialidases identified in acidic conditions was lower than at

**A Pathways of secretion**



**B Biological process (Total excreted/secreted)**



**C Molecular function (Total excreted/secreted)**

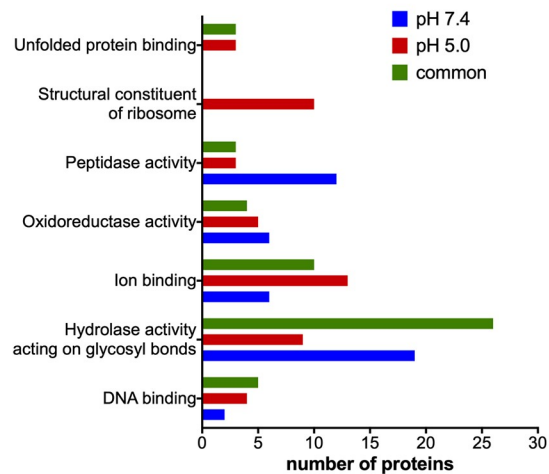


**Fig 4. Secretory pathway prediction.** Total number of predicted proteins secreted and by classical (SignalP) and non-classical pathways (SecretomeP) (A). Blast2GO annotation of *T. cruzi* trypomastigote exoproteome at pH 7.4 and pH 5.0 and comparison of most abundant biological activity (B) and molecular function GO terms (C) of annotated secrete/excreted proteins.

<https://doi.org/10.1371/journal.pone.0225386.g004>

pH 7.4 (35 and 44, respectively) (Fig 5). Furthermore, specific trans-sialidases were identified in each condition, as previously reported [40]. Specific trans-sialidases, at pH 5.0, could be involved in parasitophorous escape and, at pH 7.4, could be involved in immune system escape and cell invasion (Fig 5).

Mucins repertory changes along parasite cell cycle [22] and, as expected, striking identification differences between both conditions for mucin and mucin-like proteins were observed.

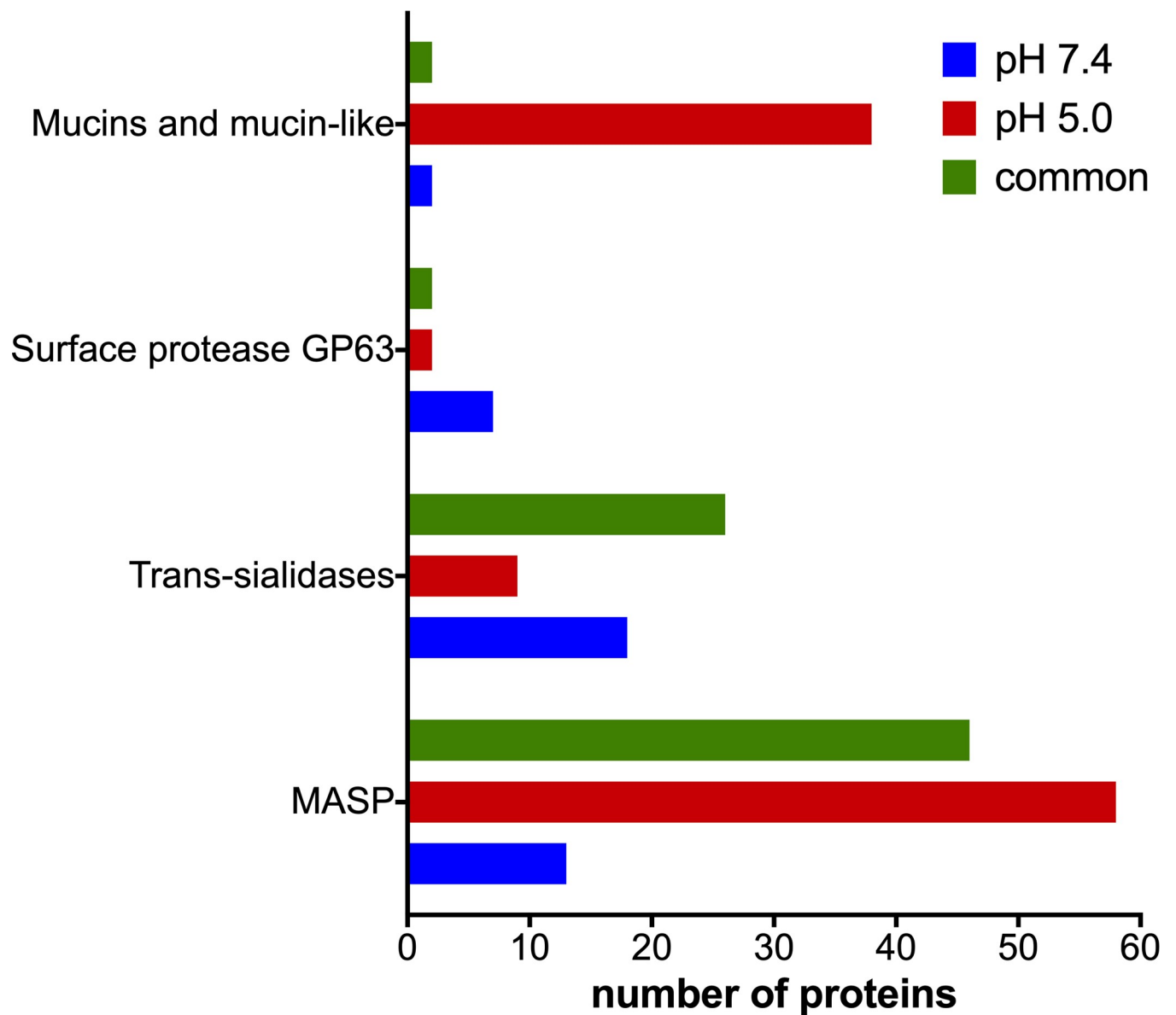


**Fig 5. Representative proteins from classical secretory pathway in *T. cruzi*.** Most abundant proteins released through classical pathway within *T. cruzi* trypomastigote exoproteome at pH 7.4 and pH 5.0.

<https://doi.org/10.1371/journal.pone.0225386.g005>

These families jumped from 2 representatives in the exoproteome at pH 7.4 to 38 different proteins at pH 5.0. Interestingly, a transcriptomic analysis showed a decrease in mRNA for mucins during amastigogenesis and an increase of transcripts for membrane-bound/secreted phospholipase A1 [41] and for surface-localized phosphatidylinositol-phospholipase C (PI-PLC) [42]. This increase in phospholipase transcripts may explain the increase of mucins in this secretome analysis [43]. Similarly, a study performed an analysis of glycoconjugate mucin secretion in cultured rat conjunctival goblet cells, and observed an increase of mucin secretion directly related to the phospholipase C and phospholipase A2 dependent- $\text{Ca}^{2+}$  performance under physiological conditions [43]. This mechanism may be employed as the same manner in *T. cruzi* parasites, considering that many cellular processes are conserved among eukaryotes. This data provides evidence that the parasite remodels the cell coat releasing surface proteins during amastigogenesis.

Mucin-associated surface proteins (MASP) exhibited the same pattern of mucins with a considerable increase in acidic pH, from 13 proteins identified specifically at pH 7.4 to 58 specifically at pH 5.0 and 56 in both conditions. The *T. cruzi* genome has approximately 1,300 clustered genes coding for MASPs and these proteins can be shed by circulating and infective parasites [44,45]. Using anti-MASP antibodies, Bartholomeu et al., (2009), detected MASP in the supernatant of PI-PLC treated trypomastigotes [44]. In this scenario, increased MASP levels after acidification condition could be explained by increasing action of phospholipases, in the same fashion for mucins, even with downregulation of MASP transcripts during early amastigote development [46]. In addition, few members of these families (trans-sialidases, mucins and MASP) were also predicted to be secreted through non-classical pathway.

In addition, some heat shock proteins (HSPs) and HSP-associated proteins, such as chaperonins, co-chaperones, prefoldins, calreticulin and cyclophilins or peptidyl prolyl isomerases were found in both exoproteome conditions. In the acidic environment, 13 HSPs and HSP-associated proteins were detected, and some of them playing important roles in the macrophage activity. For example, Hsp10 inhibits classical LPS-induced activation of macrophages due to pro-inflammatory cytokine synthesis [47,48]. *T. cruzi* parasites also infect macrophages, and require an ideal environment to replicate, nonetheless, this mechanism needs to be experimentally demonstrated in this organism. Moreover (change), Hsp10 is considered a circulating anti-inflammatory factor that possibly acts to contain macrophage activation [49].

Conversely, in both conditions, cyclophilins or peptidyl prolyl isomerases, Hsp70 and clusterin are involved in the classically activation of macrophages [50]. In *Toxoplasma gondii*, cyclophilin-18 induced IL-12 production by dendritic cells and triggered cell signalling through CCR5. This mechanism may provide a strong protective response to the parasite allowing its transmission, avoiding host's intermediates [51]. Interestingly, Hsp70 of *Mycobacterium tuberculosis* inhibits the infection of CD4+ T cells by HIV-1, blocking the CCR5 co-receptor [52] in other words, despite its role as a chaperone in the activation of macrophages [50] and protein folding, this protein may help the parasite in its survival and proliferation, inhibiting invasion of competitive microorganisms. Further, clusterin is known as a secreted extracellular chaperone capable to bind unfolded proteins, which could promote receptor-mediated endocytosis and intracellular lysosomal degradation [53]. Likewise, prefoldin, only found at pH 5.0, seems to act as a co-chaperone mediating chaperone-substrate interactions [54]. These observations seem to be feasible to occur *in vivo*, considering the high acidic environment of phagolysosome and the whole arsenal of *T. cruzi* HSP and HSP-associated proteins.

Since proteases are involved in crucial steps of the biological life cycle of *T. cruzi* including aspects of host-parasite interaction, these enzymes are subjects of special attention [55–57]. The most studied zinc-dependent metalloproteases, also termed as GP63 family in



trypanosomatids, are described as major surface glycoproteins with acid protease activity and virulence factors [58,59]. GP63 genes are present at high-copy-number [60] and encode proteins involved in parasite-host interaction. After 3 hours of incubation, the number of specific identifications at pH 5.0 and pH 7.4 was 2 and 7, respectively and 2 were present in both conditions. GP63, MASP, mucin-like proteins are surface membrane proteins that compose extracellular vesicles of trypomastigote [61] and of the early stages of amastigote differentiation accordingly to our data. Besides its ability to interact with the host extracellular matrix, GP63 is also able to inhibit NK cellular function. In trypanosomatids, this promotes resistance to antimicrobial peptides, intracellular amastigote survival in macrophages and degradation of cytosolic proteins of host cells. Altogether it demonstrates the versatility of GP63 in parasite survival in conditions of stress [62–64].

Calpain-like proteins is another family of proteins with a large number of different genes present in trypanosomatid genomes [65]. Calpains are found as microtubule-interacting proteins in *T. cruzi* and *T. brucei* [56]. Two calpain-like cysteine peptidases were only released at pH 7.4 as well as at pH 5.0, respectively, and 2 more in both conditions. One calpain peptidase and the calpain-like CAP5.5 (cytoskeleton-associated protein 5.5) were recently described as immunoreactive proteins recognized by serum immunoglobulin from chagasic patients with early cardiomyopathy [66]. Moreover, CAP5.5 was shown to be secreted/excreted by metacyclic trypomastigotes [32]. According to our data, calpain cysteine peptidases and CAP5.5 are released (associated or not to vesicles) during the trypomastigote differentiation into amastigote.

Several proteins related to ubiquitin signaling were identified from the exoproteome at pH 5.0 and pH 7.4 (S2 Table). None of them were classified as secreted through classical pathway. For the parasites, ubiquitination and ubiquitin-proteasome pathway are crucial in key steps in host colonization (proliferation and cell differentiation) [67] and for the host cells to modify immunoregulatory functions [68]. Bacteria and viruses secrete ubiquitin signaling related proteins into host cell. In *T. cruzi*, a protein related to ubiquitin signaling was shown to be secreted into the host cell and to localize in the nucleus [69]. Our data suggests that such proteins may function in the host cell nuclei orchestrating host regulatory elements towards parasite survival inside the host cell.

Intraflagellar vesicle transport occurs via microtubules driven by motors such as proteins belonging to the kinesin and the dynein family [70]. SNF-7 is a protein related to cargo transport through cytoskeleton and vesicle coating, which was secreted at pH 5.0 conditions only. Secretion profiles of transport and vesicle structures may indicate a dynamic parasite behaviour including an actively remodelling intracellular expression pattern related to the exportation of molecules during early stages of amastigogenesis. It fits with the idea that after cell invasion, trypomastigote disassemble and discard their flagella into host cell cytoplasm where it is degraded. This process releases flagellar proteins that enter the MHC-I processing pathway and presentation to CD8+ T cells as demonstrated for paraflagellar rod protein PAR4. Additionally, it was demonstrated that TcPAR4 immunization in mice enhanced resistance to *T. cruzi* [71]. Our results corroborate previous observations that TcPAR4 is released after parasite cell invasion. Paraflagellar rod component Par4 putative (Q4CUM0) was found exclusively in the parasite exoproteome at pH 5.0 (Table 2). This work provides 22 flagellar proteins exclusively identified at pH 5.0 and 12 proteins shared at pH 5.0 and pH 7.4. Among these proteins, kinesins and dyneins (or associated proteins) were found only at pH 5.0 or shared in both conditions. Strikingly, no flagellar proteins were identified as being released exclusively at pH 7.4. As demonstrated to TcPAR4, these proteins can be candidates for vaccines or good protein targets for new chemotherapy strategies.

**Table 2. Flagellar and flagellar-associated proteins in the *T. cruzi* exoproteome.**

UniProt	Description	pH 7.4	pH 5.0
<i>Secreted proteins only detected from amastigogenesis early stages</i>			
Q4D2I4	putative ADP ribosylation factor 3		X
Q4DS99	paraflagellar rod component, putative		X
Q4D0Q5	flagella associated protein		X
Q4CQP1	putative STOP axonemal protein		X
Q4DG71	putative Flagellar attachment zone protein 1		X
Q4D1B7	putative paraflagellar rod component		X
Q4CUM0	paraflagellar rod component Par4, putative		X
Q4DRP5	flagellar pocket cytoskeletal protein bilbo1		X
Q4DWL5	paraflagellar rod component		X
Q4D113	flagellar member 7		X
Q4D8M9	putative paraflagellar rod proteome component 9		X
Q4DHQ3	flagellar radial spoke protein-like, putative		X
Q4DSB9	<i>T. brucei</i> spp.-specific protein		X
Q4CR32	hypothetical protein		X
Q4CUF2	flagellar protofilament ribbon protein, putative		X
Q4DRF1	putative paraflagellar rod component		X
Q4DZQ3	putative flagellar antigen		X
Q4DG38	putative dynein-associated protein		X
Q4DFG6	kinesin-like protein		X
Q4E1M8	kinesin, putative		X
Q4DYM0	kinesin, putative		X
Q4DWH2	dynein, putative		X
Q4DCS6	outer dynein arm docking complex protein		X
<i>Secreted proteins detected from trypomastigote and amastigogenesis early stages</i>			
Q4DQ49	centrin, putative	X	X
Q4CTX0	flagellar calcium-binding 24 kDa protein	X	X
Q4DQS9	Flagellar attachment zone protein 10	X	X
Q4D7Y4	kinetoplastid membrane protein 11	X	X
Q4D634	paraflagellar rod protein 2	X	X
Q4DGZ9	flagellar member 3	X	X
Q4DUG1	flagellar member 3	X	X
Q4DIP8	flagellar associated protein	X	X
Q4CP97	putative mitochondrial paraflagellar rod component (PFC16)	X	X
Q4DIF6	paraflagellar rod protein 2	X	X
Q4D4E6	dynein intermediate chain, putative	X	X
Q4E2Q5	putative OSM3-like kinesin	X	X

<https://doi.org/10.1371/journal.pone.0225386.t002>

## Conclusion

Acidic-pH-induced axenic amastigogenesis creates a lysosome-like environment, mimicking conditions when the parasite enters into the host cell. Exploiting this model, exoproteome analyses of early stages of amastigogenesis allowed the identification of several exclusive proteins at pH 5.0 related to cell communication, response to stimulus, regulation of biological process and cell division. In this scenario, exclusive proteins identified at pH 5.0 have the potential to modulate host cellular metabolism, allowing parasite survival, differentiation and proliferation. *T. cruzi* exoproteome changes during its life stage may provide advantages to

parasites over host. Regarding trypomastigotes maintained in pH 7.4 or pH 5.0 for 3 hours, this is the first study to investigate the *T. cruzi* exoproteome change during the amastigogenesis. Our data provide evidence and direction for further studies to explore exoproteome changes during the first hours of amastigogenesis; highlighting the increase in number and diversity of proteins in acidic condition. This corroborates previous studies on the increase in vesicular trafficking during amastigogenesis. Furthermore, this work provides a list of vesicular and flagellar proteins released after acidic induction that could be explored as potential candidates to multitarget vaccines.

## Supporting information

**S1 Table. Proteins identified exclusively at pH7.4, at pH 5.0 and in both conditions.**

(XLSX)

**S2 Table. *Trypanosoma cruzi* proteins related to ubiquitin signaling and ubiquitin-proteasome pathway from exoproteome at pH 5.0 and pH 7.4.**

(PDF)

## Acknowledgments

We wish to thank Owen Vennard, Cambridge Centre for Proteomics, for helpful English corrections on the manuscript.

## Author Contributions

**Conceptualization:** Rayner M. L. Queiroz, Izabela M. D. Bastos, Carlos André O. Ricart, Sébastien Charneau.

**Formal analysis:** Samuel C. Mandacaru, Rayner M. L. Queiroz, Marcos R. Alborghetti, Consuelo M. R. de Lima, Izabela M. D. Bastos, Jaime M. Santana, Carlos André O. Ricart, Sébastien Charneau.

**Investigation:** Samuel C. Mandacaru, Rayner M. L. Queiroz.

**Methodology:** Samuel C. Mandacaru, Rayner M. L. Queiroz, Lucas S. de Oliveira.

**Project administration:** Jaime M. Santana, Sébastien Charneau.

**Resources:** Izabela M. D. Bastos, Jaime M. Santana, Peter Roepstorff, Carlos André O. Ricart, Sébastien Charneau.

**Supervision:** Peter Roepstorff, Carlos André O. Ricart, Sébastien Charneau.

**Writing – original draft:** Samuel C. Mandacaru, Rayner M. L. Queiroz, Marcos R. Alborghetti, Lucas S. de Oliveira, Consuelo M. R. de Lima, Izabela M. D. Bastos, Jaime M. Santana, Peter Roepstorff, Carlos André O. Ricart, Sébastien Charneau.

**Writing – review & editing:** Samuel C. Mandacaru, Rayner M. L. Queiroz, Marcos R. Alborghetti, Lucas S. de Oliveira, Consuelo M. R. de Lima, Izabela M. D. Bastos, Jaime M. Santana, Peter Roepstorff, Carlos André O. Ricart, Sébastien Charneau.

## References

1. WHO (2010) First WHO report on neglected tropical diseases.
2. Albajar-Vinas P, Jannin J (2011) The hidden Chagas disease burden in Europe. *Euro Surveill* 16.

3. Rassi A Jr., Rassi A, Marin-Neto JA (2010) Chagas disease. *Lancet* 375: 1388–1402. [https://doi.org/10.1016/S0140-6736\(10\)60061-X](https://doi.org/10.1016/S0140-6736(10)60061-X) PMID: 20399979
4. Roca C, Pinazo MJ, Lopez-Chejade P, Bayo J, Posada E, López-Solana J, et al. (2011) Chagas disease among the Latin American adult population attending in a primary care center in Barcelona, Spain. *PLoS Negl Trop Dis* 5: e1135. <https://doi.org/10.1371/journal.pntd.0001135> PMID: 21572511
5. Coura JR, Vinas PA (2010) Chagas disease: a new worldwide challenge. *Nature* 465: S6–7. <https://doi.org/10.1038/nature09221> PMID: 20571554
6. Bern C, Montgomery SP (2009) An estimate of the burden of Chagas disease in the United States. *Clin Infect Dis* 49: e52–54. <https://doi.org/10.1086/605091> PMID: 19640226
7. Basso B (2013) Modulation of immune response in experimental Chagas disease. *World J Exp Med* 3: 1–10. <https://doi.org/10.5493/wjem.v3.i1.1> PMID: 24520540
8. Cardillo F, de Pinho RT, Antas PR, Mengel J (2015) Immunity and immune modulation in *Trypanosoma cruzi* infection. *Pathog Dis* 73: ftv082. <https://doi.org/10.1093/femspd/ftv082> PMID: 26438729
9. Hasslocher-Moreno AM, do Brasil PE, de Sousa AS, Xavier SS, Chambela MC, Sperandio da Silva GM (2012) Safety of benznidazole use in the treatment of chronic Chagas' disease. *J Antimicrob Chemother* 67: 1261–1266. <https://doi.org/10.1093/jac/dks027> PMID: 22331592
10. Bern C (2011) Antitrypanosomal therapy for chronic Chagas' disease. *N Engl J Med* 364: 2527–2534. <https://doi.org/10.1056/NEJMct1014204> PMID: 21714649
11. Burleigh BA, Andrews NW (1995) The mechanisms of *Trypanosoma cruzi* invasion of mammalian cells. *Annu Rev Microbiol* 49: 175–200. <https://doi.org/10.1146/annurev.mi.49.100195.001135> PMID: 8561458
12. Rubin-de-Celis SS, Uemura H, Yoshida N, Schenkman S (2006) Expression of trypomastigote trans-sialidase in metacyclic forms of *Trypanosoma cruzi* increases parasite escape from its parasitophorous vacuole. *Cell Microbiol* 8: 1888–1898. <https://doi.org/10.1111/j.1462-5822.2006.00755.x> PMID: 16824037
13. Andrews NW (1993) Living dangerously: how *Trypanosoma cruzi* uses lysosomes to get inside host cells, and then escapes into the cytoplasm. *Biol Res* 26: 65–67. PMID: 7670547
14. Camargo R, Faria LO, Kloss A, Favali CB, Kuckelkorn U, Kloetzel PM, et al. (2014) *Trypanosoma cruzi* infection down-modulates the immunoproteasome biosynthesis and the MHC class I cell surface expression in HeLa cells. *PLoS One* 9: e95977. <https://doi.org/10.1371/journal.pone.0095977> PMID: 24752321
15. Caccia D, Dugo M, Callari M, Bongarzone I (2013) Bioinformatics tools for secretome analysis. *Biochim Biophys Acta* 1834: 2442–2453. <https://doi.org/10.1016/j.bbapap.2013.01.039> PMID: 23395702
16. Clamp M, Fry B, Kamal M, Xie X, Cuff J, Lin MF, et al. (2007) Distinguishing protein-coding and noncoding genes in the human genome. *Proc Natl Acad Sci U S A* 104: 19428–19433. <https://doi.org/10.1073/pnas.0709013104> PMID: 18040051
17. Skalnikova H, Motlik J, Gadhur SJ, Kovarova H (2011) Mapping of the secretome of primary isolates of mammalian cells, stem cells and derived cell lines. *Proteomics* 11: 691–708. <https://doi.org/10.1002/pmic.201000402> PMID: 21241017
18. Pavlou MP, Diamandis EP (2010) The cancer cell secretome: a good source for discovering biomarkers? *J Proteomics* 73: 1896–1906. <https://doi.org/10.1016/j.jprot.2010.04.003> PMID: 20394844
19. Affranchino JL, Ibanez CF, Luquetti AO, Rassi A, Reyes MB, Macina RA, et al. (1989) Identification of a *Trypanosoma cruzi* antigen that is shed during the acute phase of Chagas' disease. *Mol Biochem Parasitol* 34: 221–228. [https://doi.org/10.1016/0166-6851\(89\)90050-9](https://doi.org/10.1016/0166-6851(89)90050-9) PMID: 2499788
20. Buschiazzi A, Muia R, Larrieux N, Pitcovsky T, Mucci J, Campetella O (2012) *Trypanosoma cruzi* trans-sialidase in complex with a neutralizing antibody: structure/function studies towards the rational design of inhibitors. *PLoS Pathog* 8: e1002474. <https://doi.org/10.1371/journal.ppat.1002474> PMID: 22241998
21. Raimondo F, Morosi L, Chinello C, Magni F, Pitto M (2011) Advances in membranous vesicle and exosome proteomics improving biological understanding and biomarker discovery. *Proteomics* 11: 709–720. <https://doi.org/10.1002/pmic.201000422> PMID: 21241021
22. Buscaglia CA, Campo VA, Frasch AC, Di Noia JM (2006) *Trypanosoma cruzi* surface mucins: host-dependent coat diversity. *Nat Rev Microbiol* 4: 229–236. <https://doi.org/10.1038/nrmicro1351> PMID: 16489349
23. Queiroz RM, Charneau S, Mandacaru SC, Schwammle V, Lima BD, Roepstorff P, et al. (2014) Quantitative proteomic and phosphoproteomic analysis of *Trypanosoma cruzi* amastigogenesis. *Mol Cell Proteomics* 13: 3457–3472. <https://doi.org/10.1074/mcp.M114.040329> PMID: 25225356
24. Ld Silva (1953) Sobre uma cepa de *Trypanosoma cruzi* altamente virulenta para o camundongo branco. *Fol Clin Biol* 20: 191–207.

25. Andrews NW, Colli W (1982) Adhesion and interiorization of *Trypanosoma cruzi* in mammalian cells. *J Protozool* 29: 264–269. <https://doi.org/10.1111/j.1550-7408.1982.tb04024.x> PMID: 7047731
26. Queiroz RM, Ricart CA, Machado MO, Bastos IM, de Santana JM, de Sousa MV, et al. (2016) Insight into the Exoproteome of the Tissue-Derived Trypomastigote form of *Trypanosoma cruzi*. *Front Chem* 4: 42. <https://doi.org/10.3389/fchem.2016.00042> PMID: 27872839
27. Tomlinson S, Vandekerckhove F, Frevert U, Nussenzweig V (1995) The induction of *Trypanosoma cruzi* trypomastigote to amastigote transformation by low pH. *Parasitology* 110 (Pt 5): 547–554.
28. Gobom J, Nordhoff E, Mirgorodskaya E, Ekman R, Roepstorff P (1999) Sample purification and preparation technique based on nano-scale reversed-phase columns for the sensitive analysis of complex peptide mixtures by matrix-assisted laser desorption/ionization mass spectrometry. *J Mass Spectrom* 34: 105–116. [https://doi.org/10.1002/\(SICI\)1096-9888\(199902\)34:2<105::AID-JMS768>3.0.CO;2-4](https://doi.org/10.1002/(SICI)1096-9888(199902)34:2<105::AID-JMS768>3.0.CO;2-4) PMID: 10093212
29. Queiroz RM, Charneau S, Bastos IM, Santana JM, Sousa MV, Roepstorff P, et al. (2014) Cell surface proteome analysis of human-hosted *Trypanosoma cruzi* life stages. *J Proteome Res* 13: 3530–3541. <https://doi.org/10.1021/pr401120y> PMID: 24978697
30. Hernandez-Osorio LA, Marquez-Duenas C, Florencio-Martinez LE, Ballesteros-Rodea G, Martinez-Calvillo S, Manning-Cela RG (2010) Improved method for in vitro secondary amastigogenesis of *Trypanosoma cruzi*: morphometrical and molecular analysis of intermediate developmental forms. *J Biomed Biotechnol* 2010: 283842. <https://doi.org/10.1155/2010/283842> PMID: 20037731
31. Caradonna KL, Engel JC, Jacobi D, Lee CH, Burleigh BA (2013) Host metabolism regulates intracellular growth of *Trypanosoma cruzi*. *Cell Host Microbe* 13: 108–117. <https://doi.org/10.1016/j.chom.2012.11.011> PMID: 23332160
32. Bayer-Santos E, Aguilar-Bonavides C, Rodrigues SP, Cordero EM, Marques AF, Varela-Ramirez A, et al. (2012) Proteomic analysis of *Trypanosoma cruzi* secretome: characterization of two populations of extracellular vesicles and soluble proteins. *J Proteome Res*.
33. Freire-de-Lima L, da Fonseca LM, da Silva VA, da Costa KM, Morrot A, Freire-de-Lima CG, et al. (2016) Modulation of Cell Sialoglycophenotype: A Stylish Mechanism Adopted by *Trypanosoma cruzi* to Ensure Its Persistence in the Infected Host. *Front Microbiol* 7: 698. <https://doi.org/10.3389/fmicb.2016.00698> PMID: 27242722
34. Cestari I, Ansa-Addo E, Deolindo P, Inal JM, Ramirez MI (2012) *Trypanosoma cruzi* immune evasion mediated by host cell-derived microvesicles. *J Immunol* 188: 1942–1952. <https://doi.org/10.4049/jimmunol.1102053> PMID: 22262654
35. Cuervo P, De Jesus JB, Saboia-Vahia L, Mendonca-Lima L, Domont GB, Cupolillo E (2009) Proteomic characterization of the released/secreted proteins of *Leishmania (Viannia) braziliensis* promastigotes. *J Proteomics* 73: 79–92. <https://doi.org/10.1016/j.jprot.2009.08.006> PMID: 19703603
36. Grebaut P, Chuchana P, Brizard JP, Demetree E, Seveno M, Bossard G, et al. (2009) Identification of total and differentially expressed excreted-secreted proteins from *Trypanosoma congolense* strains exhibiting different virulence and pathogenicity. *Int J Parasitol* 39: 1137–1150. <https://doi.org/10.1016/j.ijpara.2009.02.018> PMID: 19285981
37. Geiger A, Hirtz C, Becue T, Bellard E, Centeno D, Gargani D, et al. (2010) Exocytosis and protein secretion in *Trypanosoma*. *BMC Microbiol* 10: 20. <https://doi.org/10.1186/1471-2180-10-20> PMID: 20102621
38. Dc-Rubin SS, Schenkman S (2012) *Trypanosoma cruzi* trans-sialidase as a multifunctional enzyme in Chagas' disease. *Cell Microbiol* 14: 1522–1530. <https://doi.org/10.1111/j.1462-5822.2012.01831.x> PMID: 22747789
39. Freire-de-Lima L, Oliveira IA, Neves JL, Penha LL, Alisson-Silva F, Dias WB, et al. (2012) Sialic acid: a sweet swing between mammalian host and *Trypanosoma cruzi*. *Front Immunol* 3: 356. <https://doi.org/10.3389/fimmu.2012.00356> PMID: 23230438
40. Atwood JA, 3rd, Weatherly DB, Minning TA, Bundy B, Cavola C, Opperdoes FR, et al. (2005) The *Trypanosoma cruzi* proteome. *Science* 309: 473–476. <https://doi.org/10.1126/science.1110289> PMID: 16020736
41. Belaunzaran ML, Wilkowsky SE, Lammel EM, Gimenez G, Bott E, Barbieri MA, et al. (2013) Phospholipase A1: a novel virulence factor in *Trypanosoma cruzi*. *Mol Biochem Parasitol* 187: 77–86. <https://doi.org/10.1016/j.molbiopara.2012.12.004> PMID: 23275096
42. de Paulo Martins V, Okura M, Maric D, Engman DM, Vieira M, Docampo R, et al. (2010) Acylation-dependent export of *Trypanosoma cruzi* phosphoinositide-specific phospholipase C to the outer surface of amastigotes. *J Biol Chem* 285: 30906–30917. <https://doi.org/10.1074/jbc.M110.142190> PMID: 20647312
43. Lippestad M, Hodges RR, Utheim TP, Serhan CN, Dartt DA (2018) Signaling pathways activated by resolvin E1 to stimulate mucin secretion and increase intracellular Ca(2+) in cultured rat conjunctival goblet cells. *Exp Eye Res* 173: 64–72. <https://doi.org/10.1016/j.exer.2018.04.015> PMID: 29702100

44. Bartholomeu DC, Cerqueira GC, Leao AC, daRocha WD, Pais FS, Macedo C, et al. (2009) Genomic organization and expression profile of the mucin-associated surface protein (masp) family of the human pathogen *Trypanosoma cruzi*. *Nucleic Acids Res* 37: 3407–3417. <https://doi.org/10.1093/nar/gkp172> PMID: 19336417
45. dos Santos SL, Freitas LM, Lobo FP, Rodrigues-Luiz GF, Mendes TA, Oliveira AC, et al. (2012) The MASP family of *Trypanosoma cruzi*: changes in gene expression and antigenic profile during the acute phase of experimental infection. *PLoS Negl Trop Dis* 6: e1779. <https://doi.org/10.1371/journal.pntd.0001779> PMID: 22905275
46. Li Y, Shah-Simpson S, Okrah K, Belew AT, Choi J, Caradonna KL, et al. (2016) Transcriptome Remodeling in *Trypanosoma cruzi* and Human Cells during Intracellular Infection. *PLoS Pathog* 12: e1005511. <https://doi.org/10.1371/journal.ppat.1005511> PMID: 27046031
47. Vanags D, Williams B, Johnson B, Hall S, Nash P, Taylor A, et al. (2006) Therapeutic efficacy and safety of chaperonin 10 in patients with rheumatoid arthritis: a double-blind randomised trial. *Lancet* 368: 855–863. [https://doi.org/10.1016/S0140-6736\(06\)69210-6](https://doi.org/10.1016/S0140-6736(06)69210-6) PMID: 16950363
48. Johnson BJ, Le TT, Dobbin CA, Banovic T, Howard CB, Flores Fde M, et al. (2005) Heat shock protein 10 inhibits lipopolysaccharide-induced inflammatory mediator production. *J Biol Chem* 280: 4037–4047. <https://doi.org/10.1074/jbc.M411569200> PMID: 15546885
49. Shamaei-Tousi A, D’Aiuto F, Nibali L, Steptoe A, Coates AR, Parkar M, et al. (2007) Differential regulation of circulating levels of molecular chaperones in patients undergoing treatment for periodontal disease. *PloS one* 2: e1198. <https://doi.org/10.1371/journal.pone.0001198> PMID: 18030332
50. Henderson B, Henderson S (2009) Unfolding the relationship between secreted molecular chaperones and macrophage activation states. *Cell Stress and Chaperones* 14: 329–341. <https://doi.org/10.1007/s12192-008-0087-4> PMID: 18958583
51. Aliberti J, Valenzuela JG, Carruthers VB, Hieny S, Andersen J, Charest H, et al. (2003) Molecular mimicry of a CCR5 binding-domain in the microbial activation of dendritic cells. *Nature immunology* 4: 485. <https://doi.org/10.1038/ni915> PMID: 12665855
52. Babaahmady K, Oehlmann W, Singh M, Lehner T (2007) Inhibition of human immunodeficiency virus type 1 infection of human CD4+ T cells by microbial HSP70 and the peptide epitope 407–426. *J Virol* 81: 3354–3360. <https://doi.org/10.1128/JVI.02320-06> PMID: 17251296
53. Wilson MR, Easterbrook-Smith SB (2000) Clusterin is a secreted mammalian chaperone. *Trends in biochemical sciences* 25: 95–98. [https://doi.org/10.1016/s0968-0004\(99\)01534-0](https://doi.org/10.1016/s0968-0004(99)01534-0) PMID: 10694874
54. Vainberg IE, Lewis SA, Rommelaere H, Ampe C, Vandekerckhove J, Klein HL, et al. (1998) Prefoldin, a chaperone that delivers unfolded proteins to cytosolic chaperonin. *Cell* 93: 863–873. [https://doi.org/10.1016/s0092-8674\(00\)81446-4](https://doi.org/10.1016/s0092-8674(00)81446-4) PMID: 9630229
55. Alvarez VE, Niemirowicz GT, Cazzulo JJ (2012) The peptidases of *Trypanosoma cruzi*: digestive enzymes, virulence factors, and mediators of autophagy and programmed cell death. *Biochim Biophys Acta* 1824: 195–206. <https://doi.org/10.1016/j.bbapap.2011.05.011> PMID: 21621652
56. Branquinho MH, Marinho FA, Sengenito LS, Oliveira SS, Goncalves KC, Ennes-Vidal V, et al. (2013) Calpains: potential targets for alternative chemotherapeutic intervention against human pathogenic trypanosomatids. *Curr Med Chem* 20: 3174–3185. <https://doi.org/10.2174/0929867311320250010> PMID: 23899207
57. Bastos IM, Motta FN, Grellier P, Santana JM (2013) Parasite prolyl oligopeptidases and the challenge of designing chemotherapeutics for Chagas disease, leishmaniasis and African trypanosomiasis. *Curr Med Chem* 20: 3103–3115. <https://doi.org/10.2174/0929867311320250006> PMID: 23514419
58. Kulkarni MM, Olson CL, Engman DM, McGwire BS (2009) *Trypanosoma cruzi* GP63 proteins undergo stage-specific differential posttranslational modification and are important for host cell infection. *Infect Immun* 77: 2193–2200. <https://doi.org/10.1128/IAI.01542-08> PMID: 19273559
59. Pech-Canul AC, Monteon V, Solis-Oviedo RL (2017) A Brief View of the Surface Membrane Proteins from *Trypanosoma cruzi*. *J Parasitol Res* 2017: 3751403. <https://doi.org/10.1155/2017/3751403> PMID: 28656101
60. Ma L, Chen K, Meng Q, Liu Q, Tang P, Hu S, et al. (2011) An evolutionary analysis of trypanosomatid GP63 proteases. *Parasitol Res* 109: 1075–1084. <https://doi.org/10.1007/s00436-011-2348-x> PMID: 21503641
61. Bernabo G, Levy G, Ziliani M, Caeiro LD, Sanchez DO, Tekiel V (2013) TcTASV-C, a protein family in *Trypanosoma cruzi* that is predominantly trypomastigote-stage specific and secreted to the medium. *PLoS One* 8: e71192. <https://doi.org/10.1371/journal.pone.0071192> PMID: 23923058
62. Yao C (2010) Major surface protease of trypanosomatids: one size fits all? *Infection and immunity* 78: 22–31. <https://doi.org/10.1128/IAI.00776-09> PMID: 19858295

63. Olivier M, Atayde VD, Isnard A, Hassani K, Shio MT (2012) Leishmania virulence factors: focus on the metalloprotease GP63. *Microbes and infection* 14: 1377–1389. <https://doi.org/10.1016/j.micinf.2012.05.014> PMID: 22683718
64. d'Avila-Levy CM, Altoé EC, Uehara LA, Branquinha MH, Santos AL (2014) GP63 function in the interaction of trypanosomatids with the invertebrate host: facts and prospects. *Proteins and Proteomics of Leishmania and Trypanosoma*: Springer. pp. 253–270.
65. Ersfeld K, Barraclough H, Gull K (2005) Evolutionary relationships and protein domain architecture in an expanded calpain superfamily in kinetoplastid parasites. *J Mol Evol* 61: 742–757. <https://doi.org/10.1007/s00239-004-0272-8> PMID: 16315106
66. Caminha MA, de Lorena VMB, de Oliveira Junior W, Perales J, Carvalho PC, Lima DB, et al. (2019) Trypanosoma cruzi immunoproteome: Calpain-like CAP5.5 differentially detected throughout distinct stages of human Chagas disease cardiomyopathy. *J Proteomics* 194: 179–190. <https://doi.org/10.1016/j.jprot.2018.11.019> PMID: 30503829
67. Munoz C, San Francisco J, Gutierrez B, Gonzalez J (2015) Role of the Ubiquitin-Proteasome Systems in the Biology and Virulence of Protozoan Parasites. *Biomed Res Int* 2015: 141526. <https://doi.org/10.1155/2015/141526> PMID: 26090380
68. Hu H, Sun SC (2016) Ubiquitin signaling in immune responses. *Cell Res* 26: 457–483. <https://doi.org/10.1038/cr.2016.40> PMID: 27012466
69. Hashimoto M, Murata E, Aoki T (2010) Secretory protein with RING finger domain (SPRING) specific to Trypanosoma cruzi is directed, as a ubiquitin ligase related protein, to the nucleus of host cells. *Cell Microbiol* 12: 19–30. <https://doi.org/10.1111/j.1462-5822.2009.01375.x> PMID: 19702650
70. Wren KN, Craft JM, Tritschler D, Schauer A, Patel DK, Smith EF, et al. (2013) A differential cargo-loading model of ciliary length regulation by IFT. *Curr Biol* 23: 2463–2471. <https://doi.org/10.1016/j.cub.2013.10.044> PMID: 24316207
71. Kurup SP, Tarleton RL (2014) The Trypanosoma cruzi flagellum is discarded via asymmetric cell division following invasion and provides early targets for protective CD8(+) T cells. *Cell Host Microbe* 16: 439–449. <https://doi.org/10.1016/j.chom.2014.09.003> PMID: 25299330



Contents lists available at ScienceDirect

## Data in Brief

journal homepage: [www.elsevier.com/locate/dib](http://www.elsevier.com/locate/dib)



### Data Article

# A proteomic dataset of secreted proteins by three *Staphylococcus saprophyticus* strains



Andrea Santana de Oliveira <sup>a</sup>, Isabella Inês Rodrigues Rosa <sup>a</sup>,  
Evandro Novaes <sup>b</sup>, Lucas Silva de Oliveira <sup>a</sup>,  
Lilian Cristiane Baeza <sup>c</sup>, Clayton Luiz Borges <sup>a</sup>,  
Lennart Marlinghaus <sup>d</sup>, Célia Maria de Almeida Soares <sup>a</sup>,  
Marcia Giambiagi-deMarval <sup>e</sup>, Juliana Alves Parente-Rocha <sup>a,\*</sup>

<sup>a</sup> Laboratório de Biologia Molecular, Instituto de Ciências Biológicas, Universidade Federal de Goiás, Goiânia, Goiás, Brazil

<sup>b</sup> Escola de Agronomia, Universidade Federal de Goiás, Goiânia, Goiás, Brazil

<sup>c</sup> Centro de Ciências Médicas e Farmacêuticas, Universidade Estadual do Oeste do Paraná, Cascavel, Brazil

<sup>d</sup> Department of Medical Microbiology, Ruhr-University, Bochum, Germany

<sup>e</sup> Laboratório de Microbiologia Molecular, Instituto de Microbiologia Prof. Paulo de Góes, Universidade Federal do Rio de Janeiro, Rio de Janeiro, Brazil

### ARTICLE INFO

#### Article history:

Received 26 August 2018

Received in revised form

19 October 2018

Accepted 23 October 2018

Available online 27 October 2018

### ABSTRACT

This article presents a proteomic dataset generated from a comparative analysis of the exoproteome of *Staphylococcus saprophyticus*, ATCC 15305, 7108 and 9325 strains. The extract of secreted proteins were obtained after incubation of stationary phase cells in BHI medium. All samples were submitted to nano-ESI-UPLC-MS<sup>E</sup>, and the spectrum obtained was processed and analyzed by ProteinLynx Global Server (PLGS), Uniprot and Pedant databases, for identification, annotation and functional classification of proteins. Fold changes and protein relative abundances were properly reported. This report is related to the research article entitled “The exoproteome profiles of three *Staphylococcus saprophyticus* strains

DOI of original article: <https://doi.org/10.1016/j.micres.2018.08.008>

\* Corresponding author.

E-mail address: [juliana.alves.parente@cnpq.br](mailto:juliana.alves.parente@cnpq.br) (J.A. Parente-Rocha).

<https://doi.org/10.1016/j.dib.2018.10.122>

2352-3409/© 2018 The Authors. Published by Elsevier Inc. This is an open access article under the CC BY license (<http://creativecommons.org/licenses/by/4.0/>).



reveal diversity in protein secretion contents” (Oliveira et al., 2018). The proteomic data generated have been deposited to the ProteomeXchange Consortium, via the PRIDE partner repository, with a project number PXD008643, <https://www.ebi.ac.uk/pride/archive/projects/PXD008643>.

© 2018 The Authors. Published by Elsevier Inc. This is an open access article under the CC BY license (<http://creativecommons.org/licenses/by/4.0/>).

## Specifications table

Subject area	Molecular Microbiology
More specific subject area	Proteomic
Type of data	Table; figure
How data was acquired	Nanoscale LC separation of tryptic peptides was performed using a ACQUITY UPLC <sup>®</sup> M-Class system (Waters Corporation, USA), and mass spectrometry analysis was performed on a Synapt G1 MS <sup>TM</sup> (Waters, USA)
Data format	Filtered and Analyzed
Experimental factors	The secreted protein extract were obtained by TCA precipitation of culture supernatant obtained after incubation of <i>S.saprophyticus</i> cells in BHI medium. For protein identification, the samples were trypsin digested.
Experimental features	The secreted proteins were identified by nano-ESI-UPLC-MS <sup>E</sup> ; the proteomic data was processed and analyzed by ProteinLynx Global Server (PLGS), Uniprot and Pedant databases. Statistical analysis were performed using R software.
Data source location	Goiânia, Goiás, Brazil.
Data accessibility	The analyzed data in excel format are available in this article, and raw data are accessible in <i>ProteomeXchange Consortium</i> [1], via the PRIDE partner repository, under Project number PXD008643 [ <a href="https://www.ebi.ac.uk/pride/archive/projects/PXD008643">https://www.ebi.ac.uk/pride/archive/projects/PXD008643</a> ]
Related research article	Oliveira AS, Rosa IIR, Novaes E, Oliveira LS, Baeza LC, Borges CL, Marlinghaus L, Soares CMA, Giambiagi-deMarval M, A. P-RJ. The exoproteome profiles of three <i>Staphylococcus saprophyticus</i> strains reveal diversity in protein secretion contents. <i>Microbiol Res.</i> 2018 216: 85–96 [2]

## Value of the data

- This dataset is an important step towards understanding the variability in *S. saprophyticus* exoproteome profiles. The data presented from *S.saprophyticus* exoproteomes pointed that the protein repertoire can be different among the strains showing metabolic flexibility can be involved in the ability to survive.
- The proteomic data present in this article might be significant in explaining differences among *S. saprophyticus* strains, since it will contribute in the identification of strain-specific virulence factors of *S. saprophyticus*.
- These comparative proteomic data will also contribute to support analysis to elucidate if differences in protein secretion can be related to *S. saprophyticus*'s ability to cause infection.

## 1. Data

This article presents a dataset generated from a comparative analysis of the exoproteome of three phenotypical different *Staphylococcus saprophyticus* strains (ATCC 15305, 7108 and 9325). The list of all proteins identified are provided in [Supplementary Table 1](#), which the fold change of each protein's expression and protein relative abundance are shown. In this table, the amount of each protein quantified is shown in ngram. Detection dynamic range, mass error and proteomic quality data are shown in [Fig. 1](#). This report presents data from the research article entitled “The exoproteome profiles of three *S. saprophyticus* strains reveal diversity in protein secretion contents”, where the differences encountered in the exoproteomes are described and validated [2].

## 2. Experimental design, materials and methods

The exoproteomes obtained from the three *S. saprophyticus* strains were submitted to nano-ESI-UPLC-MS<sup>E</sup> for total protein identification, as described below. The data showed in this article were generated by a comparative proteomic analysis performed using statistical tools from R software.

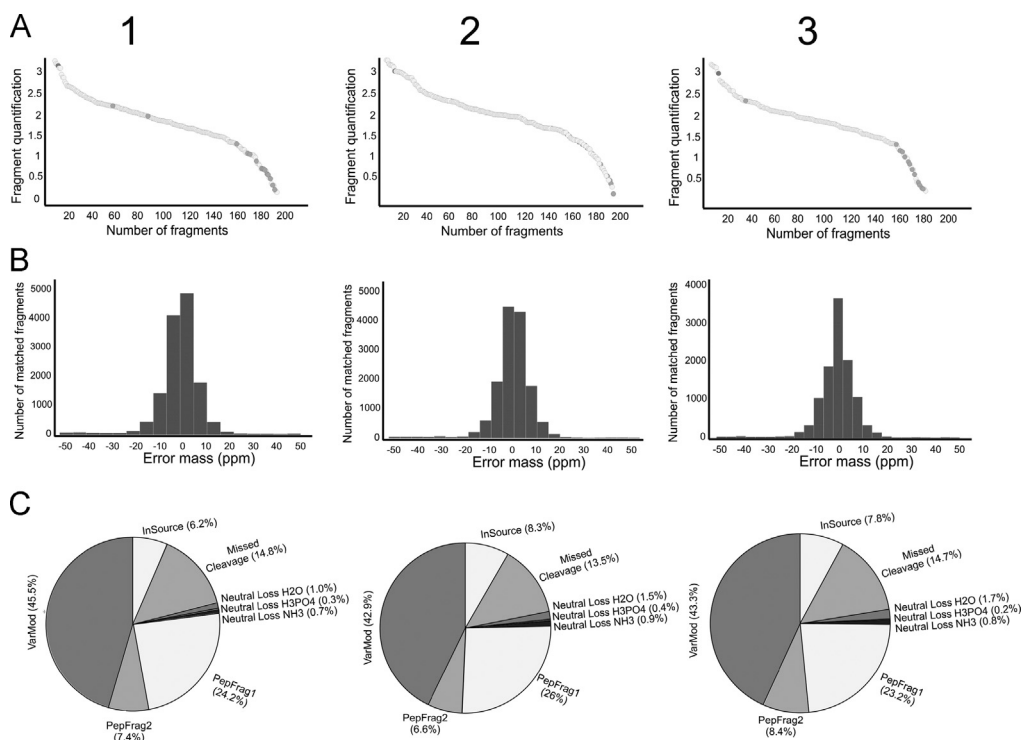


**Fig. 1.** Data from mass spectrometry analysis. Columns 1 to 3 refers to data obtained from the samples ATCC 15305, 7108 and 9325, respectively. A: Detection dynamic range. Quantified fragments were sorted according to the fragment amount (Fmol) and plotted in the graphics. Standard protein was indicated by black circle. A protein with a low coefficient of variance between samples was used to normalize the expression data and allow comparisons. B: Mass error of the identified fragments. The number of identified fragments according to the error range (x-axis). C: Nano-ESI-UPLC-MS<sup>E</sup> data quality analysis. PepFrag1 and PepFrag2 correspond to the peptides matches compared to the database by PLGS, VarMod corresponds to variable modifications, In Source corresponds to fragmentation that occurred in the ionization source, Missed Cleavage indicates the missed cleavage performed by trypsin and Neutral loss H<sub>2</sub>O and NH<sub>3</sub> correspond to water and ammonia precursor losses.

### 3. Protein identification by nano-ESI-UPLC-MS<sup>E</sup>

The extract of secreted proteins from three *S. saprophyticus* strains were obtained from the culture supernatant in the stationary phase. The protein precipitation was performed by addition of Trichloroacetic acid (TCA) (Sigma-Aldrich, St. Louis, MO, USA) at a final concentration of 10% (w/v). After obtainment of a secreted protein extract of the three *S. saprophyticus* strains, a total of 500 µg of each protein sample was used for enzymatic digestion by trypsin, that were processed according as described [2]. ACQUITY UPLC<sup>®</sup> M-Class system (Waters Corporation, USA) was used for nanoscale LC separation of digested peptides, and Synapt G1 MS<sup>TM</sup> (Waters, USA) used for analysis of mass spectrometry, as previous described [3]. All samples were analyzed from three experimental replicates. The mass error tolerance for each peptide identified was under 50 ppm. The protein identification criteria also included the detection of at least 2 fragment ions per peptide, 5 fragments per protein and the determination of at least 1 peptide per protein, as showed in spectrometry data analysis in Fig. 1.

### 4. Processing and proteomic data analysis

The data from mass spectrometry were processed by ProteinLynx Global Server (PLGS) version 3.0.2 (Waters, Manchester, UK), and Uniprot Database (<http://www.uniprot.org/>), by searching proteins sequences from *S. saprophyticus*. The annotation and functional classification of proteins identified was made by Uniprot (<http://www.uniprot.org/>), and Pedant in the MIPS (<http://mips.helmholtz-muenchen.de/funecatDB/>) database. The NCBI database (<https://www.ncbi.nlm.nih.gov>) was used for annotation of proteins that were not characterized.

In order to measure of protein expression, the *n*-gram of each protein identified in *S. saprophyticus* was used. R software was used to combine the generated data into a matrix, where rows indicated the proteins, and columns the samples (strains × replicates). Proteins were described as differentially expressed using a threshold of 0.05 false discovery. The fold change of each protein's expression was showed in logarithm scale and was calculated by comparison of the quantification in strains 7108 and 9325 with the level in the ATCC 15305 strain. The protein abundance was calculated by analyzing the protein data from the technical replicate of the strains (Supplementary Table 1).

### Acknowledgments

This work was supported by Conselho Nacional de Desenvolvimento Científico e Tecnológico (CNPq, Brazil process number 444662/2014-6) and Fundação de Amparo à Pesquisa do Estado de Goiás (FAPEG, Brazil Pronex). ASO, IIRR and LSO were supported by scholarship from Coordenação de Aperfeiçoamento de Pessoal de Nível Superior (CAPES, Brazil).

### Transparency document. Supporting information

Transparency data associated with this article can be found in the online version at <https://doi.org/10.1016/j.dib.2018.10.122>.

### Appendix A. Supplementary material

Supplementary data associated with this article can be found in the online version at <https://doi.org/10.1016/j.dib.2018.10.122>.

## References

- [1] J.A. Vizcaino, A. Csordas, N. del-Toro, J.A. Dianes, J. Griss, I. Lavidas, G. Mayer, Y. Perez-Riverol, F. Reisinger, T. Ternent, Q. W. Xu, R. Wang, H. Hermjakob, Update of the PRIDE database and its related tools, *Nucleic Acids Res.* 44 (2016) D447–D456.
- [2] A.S. Oliveira, I.I.R. Rosa, E. Novaes, L.S. Oliveira, L.C. Baeza, C.L. Borges, L. Marlinghaus, C.M.A. Soares, M. Giambiagi-deMarval, Juliana Alves Parente-Rocha, The exoproteome profiles of three *Staphylococcus saprophyticus* strains reveal diversity in protein secretion contents, *Microbiol. Res.* 216 (2018) 85–96.
- [3] A.R. de Oliveira, L.N. Oliveira, E.G.A. Chaves, S.S. Weber, A.M. Bailao, J.A. Parente-Rocha, L.C. Baeza, C.M.A. Soares, C.L. Borges, Characterization of extracellular proteins in members of the *Paracoccidioides* complex, *Fungal Biol.* 122 (2018) 738–751.



## The exoproteome profiles of three *Staphylococcus saprophyticus* strains reveal diversity in protein secretion contents



Andrea Santana de Oliveira<sup>a</sup>, Isabella Inês Rodrigues Rosa<sup>a</sup>, Evandro Novaes<sup>b</sup>,  
Lucas Silva de Oliveira<sup>a</sup>, Lilian Cristiane Baeza<sup>c</sup>, Clayton Luiz Borges<sup>a</sup>, Lennart Marlinghaus<sup>d</sup>,  
Célia Maria de Almeida Soares<sup>a</sup>, Marcia Giambiagi-deMarval<sup>e</sup>, Juliana Alves Parente-Rocha<sup>a,\*</sup>

<sup>a</sup> Laboratório de Biologia Molecular, Instituto de Ciências Biológicas, Universidade Federal de Goiás, Goiânia, Goiás, Brazil

<sup>b</sup> Escola de Agronomia, Universidade Federal de Goiás, Goiânia, Goiás, Brazil

<sup>c</sup> Centro de Ciências Médicas e Farmacêuticas, Universidade Estadual do Oeste do Paraná, Cascavel, Brazil

<sup>d</sup> Department of Medical Microbiology, Ruhr-University, Bochum, Germany

<sup>e</sup> Laboratório de Microbiologia Molecular, Instituto de Microbiologia Prof. Paulo de Góes, Universidade Federal do Rio de Janeiro – Rio de Janeiro, Rio de Janeiro, Brazil

### ARTICLE INFO

#### Keywords:

*Staphylococcus saprophyticus*

Exoproteome

Diversity

SsaA secretion

Proteases

Antigenic proteins

### ABSTRACT

*Staphylococcus saprophyticus* is a gram-positive microorganism responsible for urinary tract infections (UTIs). Although some virulence factors are characterized, such as urease, autolysins, adhesins and hemagglutinins, large-scale proteomic studies have not been performed within this species. We performed the characterization of the exoproteome from three *S. saprophyticus* strains: the reference strain ATCC 15,305, a non-capsular strain 7108 and the 9325 strain containing a thick capsule which were cultured in BHI medium and culture supernatants were analysed by using mass spectrometry approach. We observed a core of 72 secreted proteins. In addition, it was possible to detect diversity in the protein profiles of the exoproteomes. Interestingly, strain 7108 presented no secretion of three antigenic proteins, including the classical SsaA antigen. In addition, the level of antigenic proteins secreted by strain 9325 was higher than in ATCC 15,305. This result was confirmed by Western blot analysis using anti-SsaA polyclonal antibodies, and no production/ secretion of SsaA was detected in strain 7108. Transcriptional data shows that 7108 strain produces transcripts encoding SsaA, suggesting post-transcriptional regulation occurs in this strain. Moreover, when compared with the other strains that were analyzed, it was possible to detect higher levels of proteases secreted by strain 7108 and higher levels of antigenic proteins and transglycosylases secreted by 9325 strain. The results reveal diversity in protein secretion among strains. This research is an important first step towards understanding the variability in *S. saprophyticus* exoproteome profile and could be significant in explaining differences among strains.

### 1. Introduction

*Staphylococcus saprophyticus* is a gram-positive bacterium that causes urinary tract infections (UTIs) (Gatermann et al., 1988). This species is the causative agent of 40% of UTIs in young women (Raz et al., 2005). The pathogenicity of *S. saprophyticus* is not completely known, but some virulence factors have been described. Surface proteins, such as Ssp protein and hemagglutinin, are described as being active in the bacteria attachment in the bladder (Gatermann et al., 1993). Urease has been known as a virulence factor in *S. saprophyticus*, contributing to uropathogenicity in rats (Gatermann et al., 1989). The inhibition of urease activity can delay *S. saprophyticus* growth in artificial urine medium (Loes et al., 2014). Another important virulence

factor of *S. saprophyticus* is D-serine-deaminase protein (DSDA), since D-serine is encountered in urine where it acts as a bacteriostatic. A mutant for *dsda* gene, when exposed to the murine model, has presented attenuated virulence (Korte-Berwanger et al., 2013). Despite the prognosis in the majority of infections caused by *S. saprophyticus*, this bacterium can be seen to spread in the environment without difficulty. Furthermore, *S. saprophyticus* presents temporal persistence and can carry cassette resistance to other species, as the presence of erythromycin cassette resistances to *ermC*, *msrA*, *msrB*, *mphC*, and *linA* were found in 93% of the strains isolated in Brazil (Sousa et al., 2017).

In *Staphylococcus aureus*, the pathogenicity results from the synthesis of cell surface-associated proteins and extracellular proteins influencing a highly variable set of virulence factors (Kusch and Engelmann,

\* Corresponding author.

E-mail address: [juliana.parente@pq.cnpq.br](mailto:juliana.parente@pq.cnpq.br) (J.A. Parente-Rocha).

<https://doi.org/10.1016/j.micres.2018.08.008>

Received 4 May 2018; Received in revised form 7 August 2018; Accepted 21 August 2018

Available online 23 August 2018

0944-5013/ © 2018 Elsevier GmbH. All rights reserved.

2014). Proteins that are targeted for secretion by the classical pathway generally possess a signal peptide at the N-terminal extremity. There are seven known secretory systems in bacteria. They are known individually as a “Type Secretion System” (TSS), and each one secretes particular toxins and other important proteins for pathogens (Tseng et al., 2009). Non-classical pathways with unclear mechanisms also occurs in bacteria (Wang et al., 2016).

One aspect that can influence the ability of *S. aureus* to cause infection is the presence of capsular polysaccharide (CP). Strains containing CP presents enhance virulence and survival *in vivo* in mice model compared to non-capsular strain (Watts et al., 2005). *S. saprophyticus* strains can present CP but is not required to cause infection since capsular (such as ATCC 15,303 and 9325 strains) and non-capsular (such as 7108 strain) strains were isolated from patients and can be internalized into human bladder cells at similar rates (Szabados et al., 2008). One study performed using 236 *S. saprophyticus* strains isolated from patients demonstrated that capsule was presented in 1.3% of the strains. The absence of capsule is related to a hydrophobic profile and can confer adherence properties since surface adherent proteins, such as SdrI and UafA, are more exposed. The capsule confers a hydrophilic profile and absence of hemagglutination ability. The degradation of the capsule of 9325 strain turned the cells hydrophobic, suggesting the capsule is responsible for masking hydrophobic profile (Kleine et al., 2010). In counterpart, the capsule is associated to a resistant mechanism to shield its surface from recognition by the host immune system (O’Riordan and Lee, 2004). In the same way, the capsule can contribute inhibiting UafA-mediated adherence of *S. saprophyticus* to the T24 cell line (Kuroda et al., 2005) and can increase the resistant to complement-mediated opsonophagocytic killing by human neutrophils (Park et al., 2010).

Other important aspect that can contribute to the ability to establishment of infection in the human host in the presence of genes encoding virulence factors. Several known virulence factors have been tracked in *S. saprophyticus* strains, such as: *ure* (encoding urease), *sdrI* (encoding collagen-binding protein), *ssp* (encoding surface associated lipase), *dsd* (encoding D-serine deaminase), *capD* (encoding UDP-GlcNAc 4,6-dehydratase), *aas* and *uafA* (encoding surface proteins) and the regulatory genes *agr*, *sarA* and *rot*. Interestingly, studies performed with 236 *S. saprophyticus* strains (including ATCC 15,305, 7108 and 9325 strains) demonstrated that 100% of the strains possess genes encoding urease, UafA, DsdA, Aas and regulatory genes *agr*, *sarA* and *rot*, suggesting these genes are required to survival and/or infection. On the other hand, gene encoding SdrI is detected in 10% of strains isolated from patients and gene encoding Ssp in detected in around 87% of the these strains (7108 possess both genes and ATCC 15,305 and 9325 are negative for both genes) (Kleine et al., 2010).

Although a large amount of proteomic data from the *Staphylococcus* species is available (Atshan et al., 2015; Carvalhais et al., 2015; Bonar et al., 2016), no large-scale proteomic study has been performed with *S. saprophyticus*. Added to this, the virulence factors described for *S. saprophyticus* are mostly associated with cell wall and just urease protein is a secreted protein characterized in this specie as virulence factor. In this study, we performed identification and differential expression analyses of secreted proteins profiles from three *S. saprophyticus* strains presenting phenotypic differences in the capsule: ATCC 15,305, 7108 and 9325. The 9325 strain possess a thick capsule while ATCC 15,305 possess a lower capsule and 7108 is non-capsular strain. It was possible to identify proteins secreted in all isolates, as well as specifically-secreted proteins. In order to validate the proteomic analyses, we selected the SsaA protein, an antigenic protein whose homologous protein in *S. epidermidis* was detected in high levels in patients presenting endocarditis (Lang et al., 2000). Western blot analysis was performed and the results corroborate the proteomic data. The comparative analysis between the *S. saprophyticus* exoproteomes will contribute to the elucidation of the mechanisms that can be used by different strains to promote pathogenesis in the genitourinary tract.

## 2. Material and methods

### 2.1. Ethics statement

This study was approved by the Ethics in Research Committee of the “Universidade Federal de Goiás” (protocol N°047/13). The animal experiments were conducted in accordance with legislation for the protection of animals used for scientific purposes (EU Directive 2010/63).

### 2.2. *S. saprophyticus* strains and culture conditions

*Staphylococcus saprophyticus* strains ATCC 15,305, 7108 and 9325 were used in this study. These strains were previously phenotypically characterized and they differ in the presence of capsule (ATCC 15,305 possess capsule, 7108 is non-capsular and 9325 possess a thick capsule) and in the presence of virulence factors (Kleine et al., 2010; Park et al., 2010). *S. saprophyticus* cells were cultured in BHI medium (Sigma-Aldrich, St. Louis, MO, USA) and stored at -80 °C in 50% (v/v) glycerol. In order to obtain the exoproteome from the isolates, a single *S. saprophyticus* colony of each strain was pre-incubated separately in BHI medium until the stationary phase (after 18 h) with shaking at 36 °C. The *S. saprophyticus* cells were harvested by centrifugation at 4000 g for 10 min, washed with PBS and transferred to the same volume of a fresh BHI medium for 1, 3 and 6 h at 100 g and 36 °C to establish the best time point for proteomic analysis. The supernatant was collected after this period of incubation. Proteomic analyses were performed following 3 h of incubation in BHI medium after the stationary phase was obtained.

### 2.3. Obtaining the secreted proteins by *S. saprophyticus*

The cultures were centrifuged at 4000 g for 10 min, and the supernatant was filtered through 0.45- $\mu$ m and 0.22- $\mu$ m filters (Millipore®, Bedford, MA, USA). Trichloroacetic acid (TCA) (Sigma-Aldrich, St. Louis, MO, USA) at a final concentration of 10% (w/v) was added to the supernatant, and protein precipitation was performed for 16 h at 4 °C. A protein pellet was obtained by centrifuging the supernatant for 1 h at 5000 g and 4 °C. The pellet was washed 3 times with cold acetone (Sigma-Aldrich, St. Louis, MO, USA), resuspended in 50 mM ammonium bicarbonate buffer (Sigma-Aldrich, St. Louis, MO, USA), pH 8.5 and concentrated in a 3-kDa disposable Amicon ultrafilter (Millipore®, Bedford, MA, USA).

### 2.4. Analysis of *S. saprophyticus* cell growth and viability

The *S. saprophyticus* cell growth was monitored by spectrophotometry SpectraMax Paradigm (Molecular Devices, Lagerhausstrasse, Austria) in 660 nm wavelength. The experiment was performed with the three selected strains in duplicate. Standard error of the mean was obtained. Cells presenting optical density (OD) higher than 1.0 were diluted prior measuring of OD. The cells viability experiment was performed by using flow cytometry with propidium iodide to label dead cells, as previously described (Grossklau et al., 2013). Control dead cells were obtained by boiling the samples during 10 min. A total of 1 mL of the culture in the same condition used for proteomic analysis and control dead cells were incubated with 1  $\mu$ g of propidium iodide during 10 minutos before flow cytometry analysis. A minimum of 5000 cells per sample was acquired and the instrument used was Guava® easyCyte (Merck Millipore, Darmstadt, Germany).

### 2.5. Analysis of culture supernatant by polymerase chain reaction (PCR)

The PCR analysis of the culture supernatant was performed using genomic DNA as control. Genomic DNA was extracted after cell lysis in Bead Beater equipment (Biospec, Bartlesville, OK, USA) with glass beads (Sigma-Aldrich, St. Louis, MO, USA) using a standard method (Sambrook and Russel, 2001). The PCR reaction was performed using

Green Taq Master Mix (Promega, Madison, WI, USA), with 2 µL of concentrated supernatant culture or genomic DNA and oligonucleotides to amplify a 189-bp fragment of the *rpsa* gene (accession number [BAE18415.1](#)) encoding the 30S ribosomal protein S1. The oligonucleotides used were 30S sense: 5' GTCGTAAGCAGTAGAGGCATT 3' and 30S antisense: 5' AAACGTGAACAAGTCCATCAAC 3'. The reaction was performed with 40 cycles at 94 °C for 30 s, 50 °C for 30 s and 72 °C for 30 s. The PCR amplicons were visualized in a 1% agarose gel stained with Gel Red (Biotium, Hayward, CA, USA). The PCR sensitivity was evaluated using genomic DNA as a template at concentrations of 50 ng to 1 pg.

## 2.6. Digestion of protein extracts for nano-ESI-UPLC-MS<sup>E</sup> acquisition

Enzymatic digestion of proteins was processed according as described (Murad et al., 2011; Murad and Rech, 2012) with some modifications. In brief, a total of 500 µg of protein extract was used for trypsin digestion. The samples were treated with RapiGEST™ SF Surfactant (0.2% v/v) (Waters, Milford, MA, USA) in a dry bath at 80 °C for 15 min. The reduction of disulfide bonds was performed with 100 mM dithiothreitol (DTT) (GE Healthcare, Piscataway, NJ, USA) at 60 °C for 30 min, and alkylation of cysteine with 300 mM iodoacetamide (GE Healthcare, Piscataway, NJ, USA) for 30 min at room temperature. The proteins were subsequently digested with 5 U of trypsin (Promega, Madison, WI, USA) at 37 °C in a dry bath for 16 h. Afterwards, the samples were treated with 5% trifluoroacetic acid solution (Sigma-Aldrich, St. Louis, MO, USA) incubated for 90 min at 37 °C in a dry bath, and centrifuged at 18,000 g at 4 °C for 30 min. The supernatants were dried in a speed vacuum (Eppendorf, Hamburg, Germany). All obtained peptides were suspended in 80 µL of a solution containing 20 mM of ammonium formate and 150 fmol/µL of PHB (Rabbit Phosphorylase B) (Waters Corporation, Manchester, UK) as internal standard.

Nanoscale LC separation of tryptic peptides was performed using a ACQUITY UPLC® M-Class system (Waters Corporation, USA), as described (de Oliveira et al., 2018). The lock mass was used for calibration of the apparatus, using GFP ([Glu1]-Fibrinopeptide B human (Sigma-Aldrich, St. Louis, MO, USA)). Mass spectrometry analysis was performed on a Synapt G1 MS™ (Waters, USA). Samples were analyzed from three replicates.

## 2.7. Data processing and protein identification

The mass spectrometer data obtained were processed using the ProteinLynx Global Server version 3.0.2 (Waters, Manchester, UK). The data were subjected to automatic background subtraction, deisotoping and charge state deconvolution. The processed spectra were searched against protein sequences from *S. saprophyticus* (<http://www.uniprot.org/organisms/Saprophyticus>) and against a databank from reverse sequences. This predicted database from reversed proteins is used to calculate false positive rate. The mass error tolerance for peptide identification was under 50 ppm. The identification of protein was allowed with a maximum 4% false discovery rate in at least three technical replicate injections. The mass spectrometry proteomics data have been deposited to the ProteomeXchange Consortium (Vizcaino et al., 2016) via the PRIDE partner repository (Project number PXD008643).

## 2.8. Statistical analysis of proteomic data

The n-gram of each protein, from each *S. saprophyticus* strain and replicate, was used as a measure of protein expression. The n-gram data were put into the R software and combined into a matrix, where rows indicated the proteins, and columns the samples (strains x replicates). Expression data were log<sub>2</sub> transformed and quantile normalized with the limma package (Ritchie et al., 2015) using the normalizeBetweenArrays function. Proteins with excessive missing data (more than six of the nine total samples) were subtracted from the analyses.

Differential expression analyses between the three *S. saprophyticus* strains were performed with an empirical Bayes method implemented in the limma package (Phipson et al., 2016). Proteins were declared differentially expressed using a threshold of 0.05 false discovery.

Uniprot (<http://www.uniprot.org>), as well as Pedant in the MIPS (<http://mips.helmholtz-muenchen.de/funecatDB/>) database, were used for functional classification. The NCBI database was employed for annotation of uncharacterized proteins and for re-annotation of proteins that presented annotation errors (<https://www.ncbi.nlm.nih.gov/>).

## 2.9. Cloning and heterologous expression of SsaA from *S. saprophyticus*

The complete gene sequence encoding the SsaA protein (*ssaA*) was obtained in the NCBI database (accession number [BAE17758.1](#)) and used to design oligonucleotides for the In-Fusion HD Cloning Kit (Clontech) in the online Tool ([http://www.clontech.com/US/Support/xxclt\\_onlineToolsLoad.jsp?citemId=https://www.takara-bio.co.jp/infusion\\_primer/infusion\\_primer\\_form.php&section=16260&xxheight=1800](http://www.clontech.com/US/Support/xxclt_onlineToolsLoad.jsp?citemId=https://www.takara-bio.co.jp/infusion_primer/infusion_primer_form.php&section=16260&xxheight=1800)). The restriction site for *EcoRI* was used to clone the gene *ssaA* in the pGEX-4T-3 expression vector. The oligonucleotides were synthesized (IDT-Integrated DNA Technology) and are shown in the Supplementary Table 1. PCR amplification of the *ssaA* gene was performed as follows: 94 °C for 5 min, followed by 40 cycles of 94 °C for 30 s, 50 °C for 30 s, and 72 °C for 2 min. A final extension of 5 min at 72 °C was also done. The cloning procedure was performed by using the In-Fusion HD Cloning Kit (Clontech) according to the manufacturer's instructions. The pGEX-*ssaA* vector was used to transform *Escherichia coli* BL21 (DE3) cells. The production of heterologous protein was performed in *E. coli* cells cultured in LB medium until optical density of 0.4–0.45 at 660 nm was achieved by adding 0.5 M of Isopropyl β-D-1-thiogalactopyranoside (IPTG) for 1 h. The heterologous expression was evaluated in SDS-PAGE polyacrylamide gel stained with Coomassie blue (Sigma Aldrich).

## 2.10. Generation of polyclonal antibodies against SsaA protein

Polyclonal antibodies were obtained through inoculation of the fusion protein removed from SDS-PAGE in Balb/c mice, as previously described (Brito et al., 2011). A total of three immunizations was performed over an interval of 15 days. We used 100 µg of the SsaA fusion protein for each inoculation. The experiment was performed in triplicate, and pre-immune serum from each animal was obtained and stored at -20 °C in 50% glycerol. After the immunizations, the animals were euthanized in a CO<sub>2</sub> chamber and the sera containing polyclonal antibodies against SsaA (anti-SsaA) were obtained.

## 2.11. Western blot analysis

For Western blot experiments we used a total of 40 µg of the total protein extracts and of the exoproteomes from the isolates. The proteins were applied in SDS-PAGE and transferred to a nitrocellulose membrane. The membrane was blocked with blocking solution (Phosphate buffer containing 5% (w/v) skimmed milk, 0.01% (v/v) Tween 20) for 2 h. The membrane was washed with a phosphate buffer and incubated with anti-SsaA at 1:1000 ratio, followed by incubation with anti-Mouse IgG coupled with alkaline phosphatase at 1:5000 ratio for 1 h. The reaction was revealed by Fast BCIP/NBT (5-bromo-4-chloro-3-indolylphosphate/nitroblue tetrazolium - Sigma-Aldrich), as previously described (Brito et al., 2011).

## 2.12. Amplification of ORF encoding SsaA from the *S. saprophyticus* isolates and DNA sequencing

The *ssaA* ORFs from the three *S. saprophyticus* isolates were amplified by PCR, as described above, and purified using the QIAquick PCR Purification (Qiagen). The PCR products were quantified by using

NanoDrop 2000 (ThermoScientific), and 300 ng of each PCR product was used for sequencing. DNA sequencing was performed with the BigDye Terminator v3.1 Cycle Sequencing Kit (Thermo Fisher Scientific) according to the manufacturer's instructions. The samples were sequenced using a 3500 XL platform (Thermo Fisher Scientific). The reactions were performed in triplicate for each primer. The results were analyzed in the Phred/Phrad/Consed package with a phred20 quality threshold.

### 2.13. Real time PCR for quantification of *SsaA* transcripts (RT-PCRq)

The *S. saprophyticus* cells were cultured in the same condition used for proteomic analysis before RNA extraction. The RNA extractions were performed using TRIzol reagent (Invitrogen, Carlsbad, CA, USA) according to the manufacturer's protocol. The RNAs were treated with DNase I (Thermo Scientific, Foster City, CA, USA) prior the cDNA synthesis. The reverse transcription was performed using the RETROscript first strand synthesis kit (Thermo Scientific, Foster City, CA, USA) following the manufacturer's instructions. The cDNA target specificity of each primer pair was confirmed by melting curve analysis. The endogenous control of RT-PCRq reaction was performed using oligonucleotides that amplify a fragment of 30S ribosomal ORF sequence (accession number in NCBI database: gi|73661309, GeneID:3,615,961). The choice of the normalizing gene was evaluated by NormFinder Visual Basic application for Microsoft Excel (Andersen et al., 2004). The oligonucleotides used in this experiment are described in the Supplementary Table 1. The RT-PCRq reactions were performed in triplicate using a PowerUp SYBR Green Master Mix (Thermo Scientific, Foster City, CA, USA). Standard curves were generated by a 1:5 cDNA dilution. The standard curve method was used for relative gene quantification (Bookout et al., 2006).

## 3. Results

### 3.1. Evaluation of cell growth and viability

The cell growth was evaluated by monitoring optical density in spectrophotometry. The Supplementary Fig. 1 shows that *S. saprophyticus* cells remain in lag phase in the first 3 h and exponential phase occurs until around 9 h. After this point the cells remains in stationary phase until the 18 h analyzed. *S. saprophyticus* cells after incubation in BHI medium for 18 h were collected and incubated in fresh BHI medium and OD was monitored for 1, 3 and 6 h. The cell growth occurs in the first 3 h and after 6 h a reduction in OD occurs in the strain 9325, probably due to cell lysis (Supplementary Fig. 1). The time of 3 h was chosen for proteomic analysis. In order to check cell viability, these cells were evaluated by using flow cytometry. The *S. saprophyticus* cells were incubated in BHI medium for 18 h and then were transferred to a fresh BHI medium and cell viability was evaluated by flow cytometry after 3 h. Fig. 1 shows that culturing conditions used for proteomic analysis allow to obtain cells with high cell viability.

### 3.2. Overview of proteins secreted by *S. saprophyticus*

The exoproteome of the three isolates listed above were obtained. The protein samples were trypsin digested and peptides identified, as described above. A total of 119 proteins were identified in the ATCC 15,305 strain, 118 proteins in the 7108 strain, and 105 proteins in the 9325 strain. The protein abundance was evaluated analyzing the protein data from the experimental triplicate of the three strains. The dataset of the exoproteomes is available and shows the proteins identified by spectrometry analysis and the amount of protein quantified in ngram, as well as the quality analysis of the data (Oliveira et al., 2018).

Analysis of the three exoproteomes identified a total of 72 proteins secreted by all the three *S. saprophyticus* strains. Moreover, we identified proteins secreted by two isolates and other proteins secreted by

only one of them. The number of proteins identified in each strain is shown in Fig. 2, Panel A. Fig. 2, Panel B shows a schematic representation of the proteins identified in the strains. The core of proteins identified in the analyzed strains includes proteins related to glycolysis and the pentose phosphate pathway (shown as moonlighting proteins), as well as proteins related to cell wall, iron capture and stress response. It is worth noting that the characterized Uro-adherence factor A (UroA) was not detected in the exoproteome of strain 9325 and the antigenic protein SsaA was not detected as a secreted protein in strain 7108. In addition, 7108 secretes proteases that were not detected in the other strains that were analyzed, and 9325 secretes proteins related to stress response that were also not detected in the other strains.

The fold change (in logarithm scale) of each protein's expression was calculated comparing its quantification in strains 7108 and 9325 with its level in the ATCC 15,305 strain. The list of proteins identified in the three *S. saprophyticus* isolates is laid out in Table 1. It was possible to detect 7 proteins related to glycolysis in the exoproteomes of the three *S. saprophyticus* isolates: enolase, glucose 6 phosphate isomerase, triosephosphate isomerase (TPI), glyceraldehyde 3 phosphate dehydrogenase (GAPDH), phosphoglycerate kinase and two fructose biphosphate aldolases (FBA), which were probably acting as moonlighting proteins in the exoproteome. Furthermore, we detected proteins related to the pentose phosphate pathway, such as transaldolase, transketolase and 6-phosphogluconate dehydrogenase decarboxylating protein.

Interestingly, we detected 7 proteins related to stress response in the exoproteome from the isolate analyzed, such as alkyl hydroperoxide reductase subunit C, catalase, thiol peroxidase, superoxide dismutase (SOD) [Mn/Fe] and thioredoxins. This demonstrates that *S. saprophyticus* presents a conserved machinery that is able to respond to stresses, including the response to oxidative damage in the host.

Three transglycosylases (IsaA and SceD1-2) were detected in the exoproteomes of the three *S. saprophyticus* strains. These proteins are related to cell wall synthesis and remodeling. IsaA is an immunodominant antigen related to methicillin resistance (Cordwell et al., 2002) and to the biofilm stabilization (Islam et al., 2015) in *S. aureus*.

It is important to mention that although we identified several proteins related to protein synthesis (33 ribosomal proteins and 7 other proteins) they do not seem to be related to cell lysis, since we monitored the cell viability (Fig. 1). Also, we calculated the percentage of proteins related to protein synthesis and the values were 4.9%, 7.8% and 5.7% in ATCC 15,305, 7108 and 9325, respectively (Oliveira et al., 2018). Secretion of ribosomal proteins are described in *S. aureus* and. These proteins do not possess signal peptides and they are probably secreted by a non-classical pathway (Sibbald et al., 2006).

The secretion of the classical virulence factor urease was detected in two strains in this proteomic analysis (ATCC 15,305 and 7108). It was not expected since all *S. saprophyticus* strains exhibit urease activity (Gatermann et al., 1989). However, since the *S. saprophyticus* cells were cultured in rich medium before our proteomic analysis, it explain the lower detection of this enzyme in the exoproteomes (0.25% of the ATCC 15,305 exoproteome and 0.77% of the 7108 exoproteome). In addition, the secretion of urease is stimulated by urea and our analysis were performed in BHI medium without this molecule and, for this reason, urease was not the focus of this work.

### 3.3. Most secreted proteins identified in *S. saprophyticus* strains

In order to identify the most abundant proteins secreted by *S. saprophyticus* strains, we evaluated the average amount (in nanograms) of each of them within the three exoproteomes. We obtained the percentages of the proteins that were secreted in the highest quantities, and the results are listed in Table 2. The 15 most plentiful proteins in the exoproteome of each strain corresponded to around 60–70% of the total of protein secretion. There were six proteins with the highest rates of



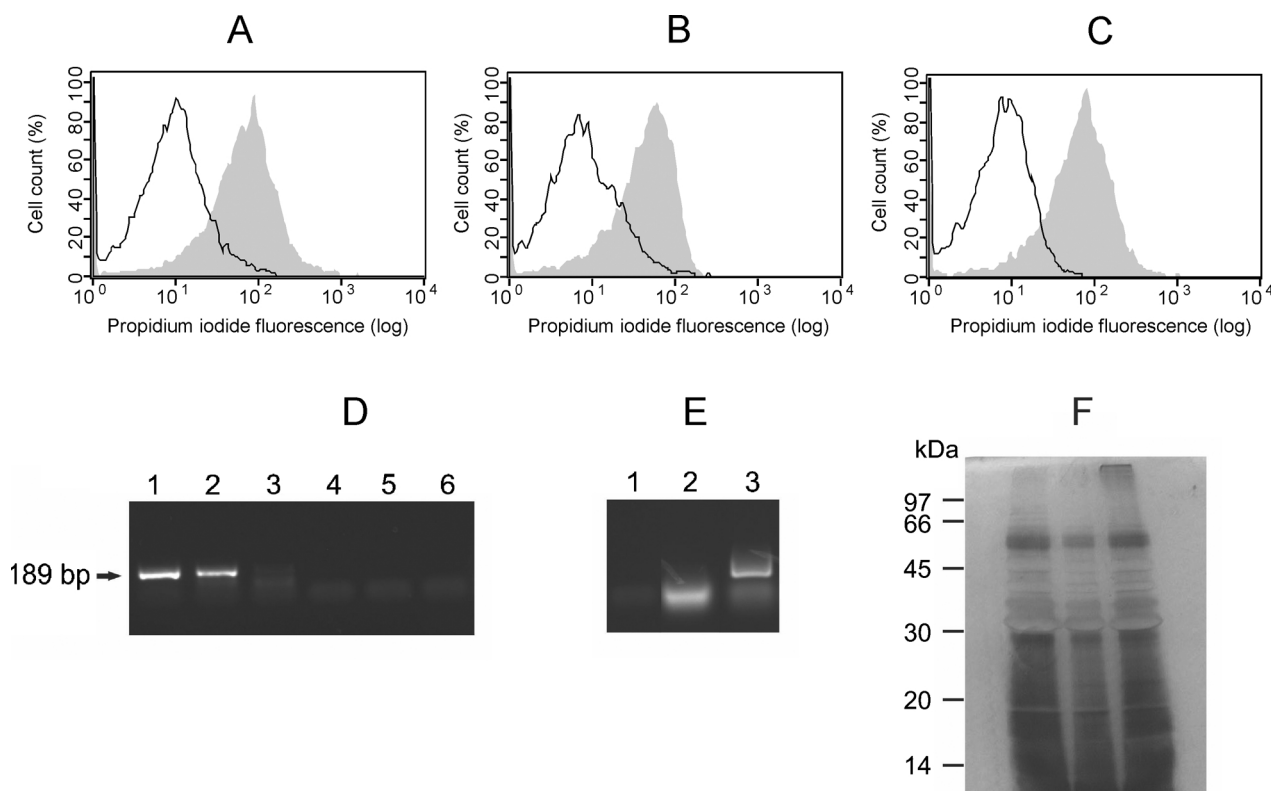


**Fig. 1.** Evaluation of *S. saprophyticus* cell viability, analysis of cell lysis and protein secretion profile of *S. saprophyticus*. The cell viability was evaluated to show the majority of cells used for proteomic analysis was not dead, using propidium iodide as dead cell marker, as described above. A: Cell viability of ATCC 15,305 cells. B: Cell viability of 7108 cells. C: Cell viability of 9325 cells. The grey peaks correspond to control dead cells and the clear peaks corresponds to the cells cultured in the same conditions used for proteomic analysis. D: PCR sensitivity for the *rpsa* gene was assessed using *S. saprophyticus* genomic DNA from ATCC strain 15,305 as a template (50 ng to 1 pg). PCR was performed with 5 concentrations of genomic DNA: 50 ng (lane 1), 5 ng (lane 2), 50 pg (lane 3), 5 pg (lane 4) and 1 pg (lane 5). A negative control without genomic DNA was also performed (lane 6). E: PCR performed with the culture supernatant (2 µL) of *S. saprophyticus* concentrated by a 3-kDa filter obtained after 1 h (lane 1), 3 h (Lane 2) and 6 h (lane 3) of incubation in BHI medium. F: Exoproteome profile of *S. saprophyticus* after 1 h (lane 1), 3 h (lane 2) and 6 h (lane 3).

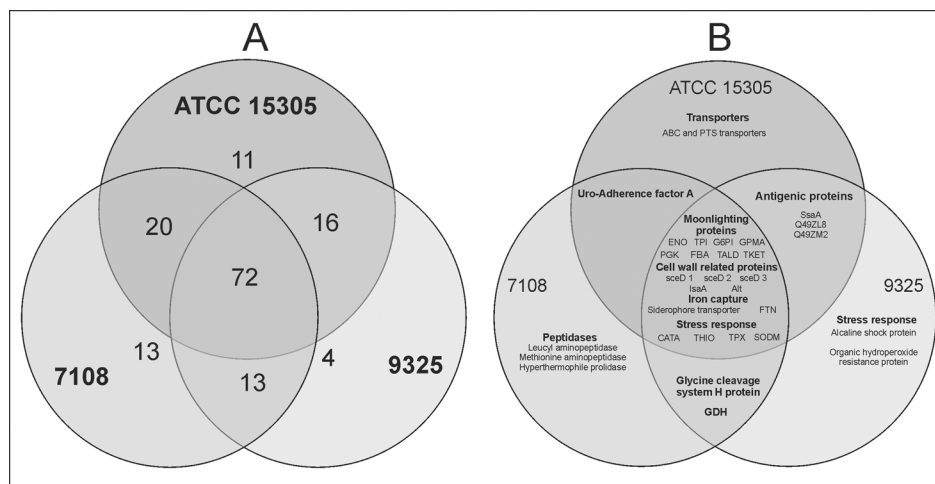


**Fig. 2.** Venn diagrams containing the number of proteins identified in the *S. saprophyticus* strains ATCC 15,305, 7108 and 9325 and schematic representation of the proteins identified in the exoproteomes. A: A total of 72 proteins were secreted by all the *S. saprophyticus* strains that were analyzed, 20 proteins were identified in strains ATCC 15,305 and 7108, 16 proteins were identified in strains ATCC 15,305 and 9325, and 13 proteins were identified in strains 7108 and 9325. A total of 28 proteins were identified in just one strain (13 proteins in 7108, 11 proteins in ATCC 15,305 and 4 proteins in 9325). B: ENO: enolase; TPI: triose phosphate dehydrogenase; G6PI: glucose 6 phosphate isomerase; TALD: transaldolases; TAKET: transketolases; GPMA: 2,3-bisphosphoglycerate-dependent phosphoglycerate mutase; PGK: phosphoglycerate kinase FBA: fructose biphosphate aldolases; sceD 1: transglycosylase sceD 1; sceD2: transglycosylase sceD 2;

sceD3: transglycosylase sceD 3; IsaA: Immunogenic protein IsaA; ALT: autolysin; FTN: ferritin; CATA: catalase A; THIO: thioredoxin; TPX: thiol peroxidase; SODM: superoxide dismutase (Mn/Fe); GDH: glucose-1-dehydrogenase.

secretion in all of the analyzed strains: bifunctional autolysin, a 60 kDa chaperonin, transglycosylases Isa and sceD 2, and two uncharacterized proteins (accession numbers Q49VF9 and Q49VV4). Autolysin is the most secreted protein in the ATCC 15,305 and 9325 strains, corresponding to around 30% of the protein species secreted by them. Autolysin is also abundant in the exoproteome of strain 7108, corresponding to around 10% of all the protein species secreted by this

isolate. In *S. aureus* the secretion of bifunctional autolysin is higher in virulent strains (Bonar et al., 2016). The role of autolysin in *S. saprophyticus* has been associated with cell wall remodeling during separation, and in *S. epidermidis* this protein is also described as acting as a binding protein (Heilmann et al., 1997; Hell et al., 1998).

The most abundant protein secreted by strain 7108 is uro-adherence factor A, corresponding to around 23% of the proteins secreted by this

**Table 1**  
Proteins identified in all analyzed *S. saprophyticus* strains.

Accession number <sup>1</sup>	Protein description	Log FC <sup>2</sup>		t-statistic <sup>3</sup>		p-value <sup>4</sup>	
		7108	9325	7108	9325	7108	9325
Glycolysis							
ENO_STAS1	Enolase	0.64	0.54	3.07	2.59	0.03	0.09
G6PI_STAS1	Glucose-6-phosphate isomerase	-1.28	-0.24	-9.5	-1.77	≤ 0.01	0.25
TPIS_STAS1	Triosephosphate isomerase	0.37	-0.41	2.42	-2.67	0.07	0.09
Q49VZ9_STAS1	Glyceraldehyde-3-phosphate dehydrogenase	1.26	-0.69	8.69	-4.75	≤ 0.01	0.01
PGK_STAS1	Phosphoglycerate kinase	1.08	-0.14	5.72	-0.72	≤ 0.01	0.63
Q4A0Q6_STAS1	Fructose-bisphosphate aldolase class I	0.19	0.34	0.9	1.62	0.48	0.29
Q49Z72_STAS1	Fructose-bisphosphate aldolase class I	-0.12	0.34	-0.57	1.63	0.67	0.29
Pyruvate dehydrogenase complex							
Q49WM1_STAS1	Dihydrolipoyl dehydrogenase	-2.02	-0.13	-7.39	-0.46	≤ 0.01	0.80
Lactic fermentation							
LDH_STAS1	L-lactate dehydrogenase	2.15	0.00	13.86	0.03	≤ 0.01	1.00
Pentose phosphate pathway							
Q49YL0_STAS1	Transaldolase	-0.98	-0.15	-8.27	-1.29	≤ 0.01	0.42
Q49XD6_STAS1	Transketolase	0.54	0.05	3.69	0.37	0.01	0.87
Q49XV6_STAS1	6-phosphogluconate dehydrogenase decarboxylating	-0.66	0.62	-5.16	4.83	≤ 0.01	0.01
C-compounds metabolism							
GPMA_STAS1	2,3-bisphosphoglycerate-dependent phosphoglycerate mutase	-1.70	-0.11	-9.59	-0.64	≤ 0.01	0.68
Q49ZH5_STAS1	Glucose-1-dehydrogenase	0.06	-0.84	0.13	-1.76	0.95	0.26
Fatty acid metabolism							
ACP_STAS1	Acyl carrier protein	-1.53	-0.05	-4.97	-0.16	≤ 0.01	1.00
Q49WB7_STAS1	3-oxoacyl-[acyl-carrier-protein] synthase	-1.38	-0.92	-4.29	-2.85	0.01	0.07
Isoprenoid metabolism							
ISPD_STAS1	2-c-methyl-d-erythritol 4-phosphate cytidylyltransferase	-1.66	-1.37	-4.35	-3.6	≤ 0.01	0.03
ATP synthesis							
ATPA_STAS1	ATP synthase subunit alpha	-0.81	-0.29	-5.68	-2.02	≤ 0.01	0.18
ATPB_STAS1	ATP synthase subunit beta	-1.46	0.43	-2.33	0.69	0.08	0.66
Nucleotide and nucleoside metabolism							
Q49Z85_STAS1	Purine nucleoside phosphorylase DeoD	-1.68	-0.19	-5.96	-0.66	≤ 0.01	0.66
Q49XS7_STAS1	Bacterial nucleoid DNA-binding protein	-1.66	-0.40	-14.07	-3.39	≤ 0.01	0.04
Amino acids metabolism							
GCSH_STAS1	Glycine cleavage system H protein	-1.04	0.10	-4.4	0.42	0.01	0.83
Q49V22_STAS1	Cysteine synthase	-0.42	0.15	-0.88	0.32	0.49	0.90
Transcription							
Q49WH6_STAS1	Putative transcriptional regulator	1.58	2.09	3.76	4.98	0.01	0.01
Cell signaling							
Q49ZE7_STAS1	Adenylate kinase	-1.29	0.08	-4.21	0.26	0.01	0.94
Cell wall synthesis							
ISAA_STAS1	Probable transglycosylase IsaA	0.11	-0.36	0.23	-0.75	0.87	0.62
SCED1_STAS1	Probable transglycosylase sceD 1	1.40	-0.34	10.32	-2.5	≤ 0.01	0.10
SCED2_STAS1	Probable transglycosylase sceD 2	0.49	-0.97	1.52	-3	0.23	0.06
Q49WH3_STAS1	Bifunctional autolysin	1.35	0.00	14.55	0	≤ 0.01	1.00
Protein synthesis							
RS10_STAS1	30S ribosomal protein S10	1.25	0.05	2.58	0.1	0.06	1.00
RS16_STAS1	30S ribosomal protein S16	-0.79	0.32	-3.09	1.23	0.03	0.43
RL2_STAS1	50S ribosomal protein L2	-0.70	-1.06	-1.44	-2.2	0.25	0.15
RL6_STAS1	50S ribosomal protein L6	0.10	0.53	0.35	1.8	0.81	0.25
RL7_STAS1	50S ribosomal protein L7/L12	-1.30	0.16	-11.18	1.41	≤ 0.01	0.37
RL11_STAS1	50S ribosomal protein L11	-0.80	0.04	-5.26	0.27	≤ 0.01	0.93
RL15_STAS1	50S ribosomal protein L15	-0.58	0.38	-1.17	0.78	0.35	0.62
RL25_STAS1	50S ribosomal protein L25	-0.34	0.73	-1.87	4.07	0.15	0.02
RL29_STAS1	50S ribosomal protein L29	-0.98	-0.25	-3.81	-0.96	0.01	0.53
EFTS_STAS1	Elongation factor Ts	-0.55	0.65	-2.36	2.77	0.08	0.07
EFTU_STAS1	Elongation factor Tu	1.37	0.30	7.42	1.63	≤ 0.01	0.29
SYE_STAS1	Glutamate-tRNA ligase	-1.50	-1.32	-3.32	-2.91	0.02	0.06
RRF_STAS1	Ribosome-recycling factor	-1.22	0.15	-9.1	1.12	≤ 0.01	0.46
TIG_STAS1	Trigger factor	-0.51	0.12	-3.2	0.77	0.03	0.62
Protein folding, degradation and modification							
Q4A0H6_STAS1	Glutamyl endopeptidase	1.05	-0.64	7.65	-4.7	≤ 0.01	0.01
CLPP_STAS1	ATP-dependent Clp protease proteolytic subunit	-0.85	0.09	-8.23	0.9	≤ 0.01	0.55
Q49WC9_STAS1	Oligopeptidase F	-2.39	-1.09	-3.17	-1.45	0.03	0.36
CH10_STAS1	10 kDa chaperonin	-1.89	0.82	-7.07	3.06	≤ 0.01	0.06
CH60_STAS1	60 kDa chaperonin	0.48	1.27	2.72	7.12	0.05	≤ 0.01
GRPE_STAS1	Protein grpE	-1.12	0.84	-4.93	3.7	≤ 0.01	0.03
DNAK_STAS1	Chaperone protein DnaK	0.22	3.15	0.3	4.33	0.83	0.01

(continued on next page)

Table 1 (continued)

Accession number <sup>1</sup>	Protein description	Log FC <sup>2</sup>		t-statistic <sup>3</sup>		p-value <sup>4</sup>	
		7108	9325	7108	9325	7108	9325
<b>Iron metabolism</b>							
FTN_STAS1	Ferritin	-1.45	0.52	-10.31	3.68	≤ 0.01	0.03
HEM3_STAS1	Porphobilinogen deaminase	0.00	0.34	0	1.13	1.00	0.46
HEMH_STAS1	Ferrochelatase	-0.64	-0.62	-4.8	-4.64	≤ 0.01	0.01
<b>Transport</b>							
Q49ZK8_STAS1	ABC-type cobalamin Fe3 + siderophore transport system	-0.80	-0.75	-2.78	-2.6	0.05	0.09
<b>Stress response</b>							
AHPC_STAS1	Alkyl hydroperoxide reductase subunit C	-1.88	-0.94	-15.42	-7.71	≤ 0.01	≤ 0.01
CATA_STAS1	Catalase	0.24	1.02	2.3	9.8	0.08	≤ 0.01
TPX_STAS1	Probable thiol peroxidase	-0.32	0.14	-1.59	0.68	0.21	0.66
Q49Z86_STAS1	Starvation-inducible DNA-binding protein	-0.03	0.63	-0.33	6.48	0.82	≤ 0.01
SODM_STAS1	Superoxide dismutase [Mn/Fe]	-1.51	0.09	-15.24	0.88	≤ 0.01	0.55
THIO_STAS1	Thioredoxin	-1.51	-0.28	-6.9	-1.3	≤ 0.01	0.42
Q49V79_STAS1	Beta lactamase	1.29	0.90	3.65	2.57	0.01	0.09
<b>Virulence factor</b>							
Q49ZM2_STAS1	Putative secretory antigen	0.99	-1.44	1.24	-1.81	0.33	0.25
Q4A0W2_STAS1	Immunodominant antigen	0.12	1.08	0.61	5.5	0.65	≤ 0.01
<b>Uncharacterized proteins</b>							
Q49ZY4_STAS1	Uncharacterized protein	-1.00	-1.10	-3.61	-3.98	0.02	0.02
Q49VC9_STAS1	Uncharacterized protein	0.62	-0.66	4.04	-4.26	0.01	0.01
Q49ZZ3_STAS1	Uncharacterized protein	0.48	-0.43	2.19	-1.94	0.10	0.21
Q49VV4_STAS1	Uncharacterized protein	-0.85	-0.21	-6.07	-1.49	≤ 0.01	0.34
Q49VF9_STAS1	Uncharacterized protein	0.19	-0.24	0.78	-0.98	0.55	0.53
Q49WI5_STAS1	Uncharacterized protein	0.41	0.55	0.72	0.95	0.58	0.53
Y954_STAS1	Uncharacterized protein	-1.45	-0.52	-11.75	-4.26	≤ 0.01	0.01
UP355_STAS1	Uncharacterized protein	-0.11	1.04	-0.34	3.34	0.81	0.04
Y2125_STAS1	Uncharacterized protein	-0.54	0.35	-2.12	1.38	0.11	0.38

<sup>1</sup> Accession number provided by Uniprot Database (<http://www.uniprot.org/>).

<sup>2</sup> Obtained from limma's topTable by subtracting the average expression in log2 scale against that of ATCC 15,305 strain.

<sup>3</sup> Estimate of the Student's t statistic comparing expression against that of the ATCC 15,305 strain.

<sup>4</sup> p-value from the Student's t distribution. Proteins with p-value ≤ 0.05 were considered regulated among the strains.

Table 2

Most secreted proteins secreted by *S. saprophyticus* strains (ATCC 15,305, 7108 and 9325).

Accession number	Protein description	ATCC 15,305 strain		7108 strain		9325 strain	
		ng	% in the exoproteome	ng	% in the exoproteome	ng	% in the exoproteome
Q49WH3_STAS1	Bifunctional autolysin	315.99	27.79	114.24	9.92	220.15	30.10
UAFA_STAS1	Uro-adherence factor A	114.91	10.11	259.04	22.49	-	-
LTAS_STAS1	Lipoteichoic acid synthase	45.50	4.00	-	-	17.77	2.43
CH60_STAS1	60 kDa chaperonin	45.33	3.99	30.29	2.63	15.89	2.17
ISAA_STAS1	Probable transglycosylase IsaA	41.50	3.65	29.66	2.58	42.22	5.77
SCED2_STAS1	Probable transglycosylase sceD 2	33.89	2.98	16.98	1.47	40.78	5.58
Q49UH9_STAS1	Mannosyl-glycoprotein endo-beta-N-acetylglucosamidase-like domain	32.49	2.86	-	-	-	-
Q49VF9_STAS1	Uncharacterized protein	30.95	2.72	23.10	2.01	26.16	3.58
Q49VV4_STAS1	Uncharacterized protein	26.88	2.36	34.85	3.03	22.67	3.10
Q49VC9_STAS1	Uncharacterized protein	24.65	2.17	*	*	27.10	3.71
DNAK_STAS1	Chaperone protein DnaK	21.10	1.86	14.27	1.24	-	-
LDH_STAS1	L-lactate dehydrogenase	19.02	1.67	*	*	15.24	2.08
Q49XD6_STAS1	Transketolase	18.19	1.60	*	*	13.31	1.82
Q49VZ9_STAS1	Glyceraldehyde-3-phosphate dehydrogenase	16.23	1.43	*	*	21.16	2.89
Q49XC4_STAS1	Uncharacterized protein	16.04	1.41	-	-	-	-
Q49WC9_STAS1	Oligopeptidase F	*	*	55.98	4.86	10.67	1.46
Q49WM1_STAS1	Dihydropolyl dehydrogenase	*	*	33.47	2.91	*	*
AHPC_STAS1	Alkyl hydroperoxide reductase subunit C	*	*	18.93	1.64	*	*
Q49ZZ3_STAS1	Uncharacterized protein	*	*	*	*	14.10	1.93
EFTS_STAS1	Elongation factor Ts	*	*	16.56	1.44	*	*
Q49YL0_STAS1	Transaldolase	*	*	15.35	1.33	*	*
SCED1_STAS1	Probable transglycosylase sceD 1	*	*	*	*	12.79	1.75
Q49VK7_STAS1	Secretory antigen SsaA-like protein	*	*	-	-	10.78	1.47
DNAK_STAS1	Chaperone protein DnaK	*	*	14.27	1.24	-	-
SODM_STAS1	Superoxide dismutase [Mn/Fe]	*	*	14.17	1.23	*	*
Total		802.67	70.59	691.16	60.01	510.78	69.85

\* Detected but not included in the list of the 15 most abundant proteins in this strain.

Not detected in this strain.

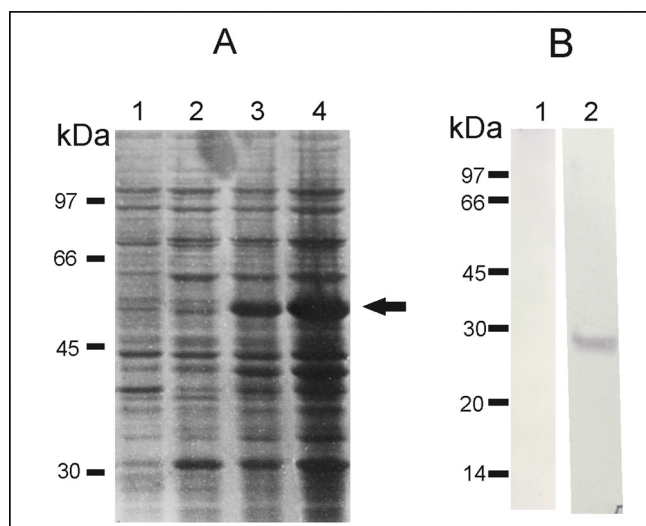


**Fig. 3.** Heterologous expression of SsaA protein from *S. saprophyticus* and polyclonal antibodies obtainment. A: Heterologous expression of SsaA fused to GST protein in the *E. coli* system. The protein extracts were obtained without IPTG (lane 1), and then again later, after the addition of IPTG 0.5 mM (lanes 2–4). Extracts were taken after 30 min (lane 2), 1 h (lane 3) and 2 h (lane 4) of incubation with IPTG. The black arrow indicates the band corresponding to recombinant SsaA fused to GST protein used for polyclonal antibodies obtainment. B: Western blot to test specificity of polyclonal antibodies. Anti-SsaA were obtained after inoculation of recombinant protein in mice, as described. Negative control performed with pre-immune sera was performed (lanes 1). The specificity of the polyclonal antibodies was shown performing Western blot with protein extract from *S. saprophyticus* ATCC 15,305 strain, showing reaction with one protein specie with molecular weight compatible with the predicted molecular size of SsaA (lane 2).

isolate. Uro-adherence factor A is also secreted by strain ATCC 15,305, being the second most secreted protein in this strain (10.11% of the exoproteome). However, uro-adherence factor A was not detected in the exoproteome of strain 9325. Among all the proteins secreted in abundance by each strain (15 proteins of each isolate), three were only secreted by two isolates: uro-adherence factor A (not secreted by the 9325 strain), lipoteichoic acid synthase (not secreted in the 7108 strain) and a chaperone DNA K protein (not secreted by the 9325 strain). These results show that the secreted proteins vary in abundance, and, in some cases, proteins are not secreted by all the isolates.

### 3.4. Validation of proteomic results – western blot to evaluate SsaA secretion

In order to validate the proteomic results, we selected the SsaA protein, which was detected in the exoproteome of two isolates (ATCC 15,305 and 9325) and was not detected in the exoproteome of the 7108 strain. The gene encoding the SsaA protein was obtained in GeneBank, cloned and then the protein was expressed in a heterologous system. The expressed protein was used to inoculate Balb/C mice to obtain polyclonal antibodies (anti-SsaA). Fig. 3 shows the heterologous expression and the obtainment of anti-SsaA polyclonal antibodies. The production of anti-SsaA polyclonal antibodies was performed in triplicate. Three animals were used to obtain polyclonal antibodies anti-SsaA and the sera were tested independently in three concentrations: 1:500 (lanes 2), 1:750 (lanes 3) and 1:1000 (lanes 4), showing similar results (Supplementary Fig. 3).

Afterwards, we used the anti-SsaA antibodies to evaluate the production and secretion of SsaA by the *S. saprophyticus* strains. Fig. 4 shows that SsaA is detected in strains ATCC 15,305 and 9325, both in the cytoplasm (Panel C) and in the exoproteome (Panel D), but not in the 7108 strain (neither in the cytoplasm nor in the exoproteome).

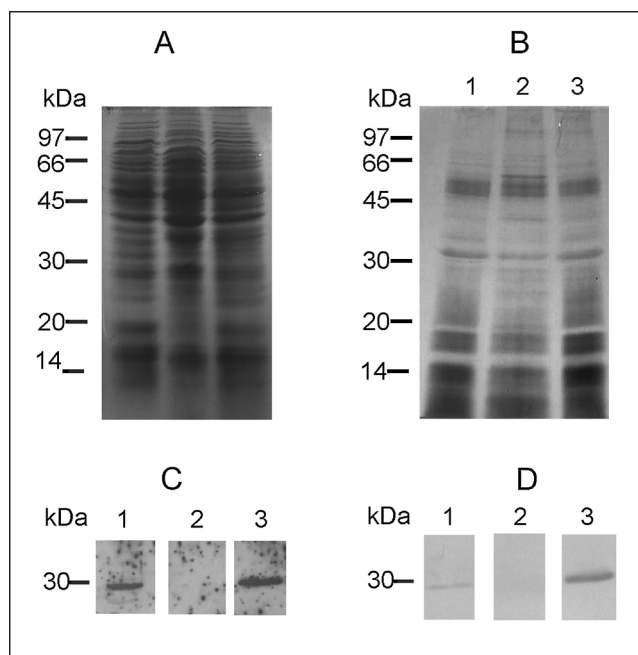


**Fig. 4.** Western blot using anti-SsaA with exoproteome of *S. saprophyticus* strains ATCC 15,305, 7108 and 9325. A: Total protein extract from *S. saprophyticus* strains ATCC 15,305 (lane 1), 7108 (lane 2) and 9325 (lane 3). B: Protein extract from culture supernatant obtained from the *S. saprophyticus* strains ATCC 15,305 (lane 1), 7108 (lane 2) and 9325 (lane 3). C: Western blot made by using anti-SsaA in total protein extract from *S. saprophyticus* strains ATCC 15,305 (lane 1), 7108 (lane 2) and 9325 (lane 3). D: Western blot culture supernatant obtained from the *S. saprophyticus* strains ATCC 15,305 (lane 1), 7108 (lane 2) and 9325 (lane 3).

These results corroborate the proteomic data. In addition, as evaluated by the proteomic approach, strain 9325 was found to secrete higher levels of SsaA compared with ATCC 15,305.

In order to evaluate if strain 7108 possess the ORF encoding SsaA protein, we performed a PCR reaction to amplify this ORF. The amplified fragment was sequenced and the results show that all *S. saprophyticus* strains analyzed (ATCC 15,305, 7108 and 9325) present amplification of the ORF encoding SsaA protein. The amplicons were sequenced and no alteration in the nucleotide sequences were detected among the strains (Supplementary Fig. 2). The NCBI database also contains a previous draft from the 7108 genome and the gene encoding SsaA is sequenced without mutation in this data (accession number NZ\_LMYQ00000000, Locus tag ASS79\_RS03200). These data suggest that the inability of the 7108 strain to produce and secrete SsaA protein is not related to a coding sequence alteration, but is more likely related to transcriptional and/or post-transcriptional events.

Since the gene encoding SsaA was encountered in the three *S. saprophyticus* strains, we performed RT-PCRq experiment to evaluate the production of transcripts encoding SsaA protein in the strains analyzed. The result is shown in the Fig. 5. The *S. saprophyticus* ATCC15305 produces lower amounts of the transcript encoding SsaA protein. On the other hand, the strain 9325 produces higher amounts of the transcripts (30-fold compared to ATCC 15,305). This result corroborates proteomic analysis suggesting that the high secretion of SsaA in the strain 9325 is a function of increased mRNA production or higher stability of this molecule in this strain. The *S. saprophyticus* 7108 strain also produces transcripts encoding SsaA at high level (20-fold compared to ATCC 15,305 strain). The result suggests post-transcriptional events regulates the production and secretion of SsaA protein in the 7108 strain.

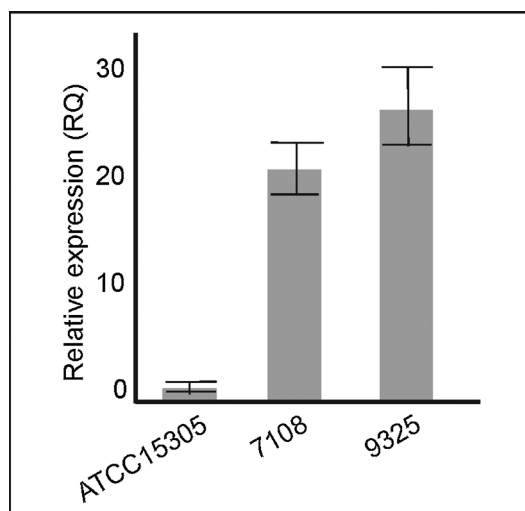


**Fig. 5.** Quantitative real time PCR (RT-PCRq) to quantify transcripts encoding SsaA in the *S. saprophyticus* strains. The RT-PCRq reactions were performed with cDNAs from three *S. saprophyticus* strains. The values were normalized using transcripts encoding 30S ribosomal protein. The reactions were performed in triplicate and standard deviation are shown.

### 3.5. Abundance of some proteins in the *S. saprophyticus* exoproteomes

We detected that strain 7108 secreted higher amounts of proteases when compared with the other strains. In order to quantify the percentage of proteases secreted by each *S. saprophyticus* strain, we calculated the percentage of proteases secreted by all three strains (identified in at least two replicates), as demonstrated in Fig. 6, Panel A. The percentage values were obtained from the amount of proteins (in ngram) identified in each strain. From the total number of proteins secreted by ATCC 15,305, 1.25% are proteins classified as proteases and peptidases; in strain 9325 we identified that 2.35% of the exoproteome is composed of proteases and peptidases. On the other hand, strain 7108 secreted a higher content of proteins identified as proteases and peptidases, with a percentage of 7.24.

In the same way, we also evaluated the percentage of proteins that were classified as antigenic. These proteins were detected in higher amounts in strain 9325, as shown in Fig. 6, Panel B. From the total number of proteins secreted by strain 9325, 4.46% correspond to four proteins described as antigenic (an immunodominant antigen Q4A0W2, two secretory antigens Q49ZM2 and Q49ZL8 and the staphylococcal secretory antigen SsaA). These same proteins were identified in strain

ATCC 15,305, but only amounted to 1.89% of the total number of proteins secreted by this strain. The amount of antigenic proteins secreted by strain 7108 is lower (0.26%), and this strain does not secrete the SsaA protein in a detectable level, as is demonstrated by the Western blot analysis (Fig. 4). The secretion of the antigenic proteins Q49ZM2 and Q49ZL8 was also not detected by proteomic approach in strain 7108.

The secretion of transglycosylases was also evaluated by comparing the three *S. saprophyticus* strains. Three transglycosylases were detected in the three isolates (IsaA and sceD1-2). However, IsaA, sceD 1 and sceD2 were secreted in higher amounts in strain 9325. The analysis of percentage of secretion is shown in Fig. 6, Panel C, and reveals that from the total number of proteins secreted by the 9325 strain, 13.1% corresponds to transglycosylases. In strains ATCC 15,305 and 7108 the percentage of secretion of transglycosylases is 7.68 and 4.36, respectively. The transglycosylase secretion content probably reflects the polysaccharide content outside the cell, since strain 9325 possess the highest polysaccharide capsule, followed by ATCC 15,305 and 7108, respectively. It is important to point out that the presence of capsules in different sizes is reported in *S. saprophyticus* strains, and that more than one capsular serotype exists (Park et al., 2010).

## 4. Discussion

The heterogeneity of *S. saprophyticus* strains has been described in terms of genotypic and phenotypic variations among strains isolated from humans and animals. Analysis of animal and human *S. saprophyticus* strains reveals that strains from both animal and clinical sources presents classical virulence and adherence factors. However, the ability to adhere to collagen I was higher in clinical strains (Kleine et al., 2010). The genotypic variation among coagulase negative *Staphylococcus* species strains isolated from inpatients and outpatients was also reported by using pulsed-field gel electrophoresis typing (Talebi et al., 2016).

The presence of capsule in *S. saprophyticus* strains have been reported and it is attributed to the capsule gene cluster *cap<sub>Ssp</sub>*. However, non-capsular clinical strains are also reported. Since clinical non-capsular strains have been reported, the capsule is not essential for infection in human host and it is presented only in 1.3% of clinical *S. saprophyticus* strains, suggesting other aspects can be involved during pathogenesis. In order to enlarge the characterization of *S. saprophyticus* strains, our study presents, for the first time, large-scale identification of proteins secreted by three *S. saprophyticus* strains. In addition, we compared the exoproteome profiles of the three strains and detected diversity in them. Our study identified proteins secreted in the

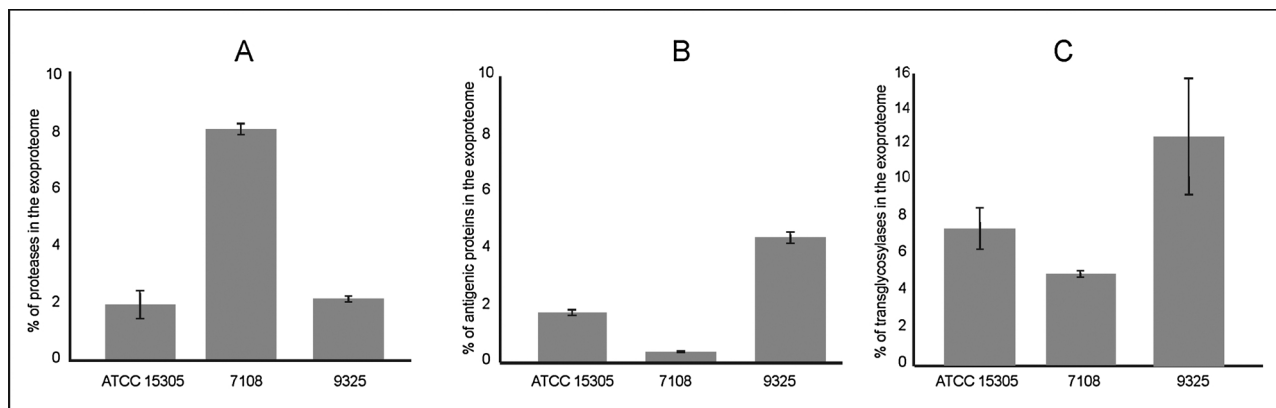


**Fig. 6.** Abundance of proteases, classical antigenic proteins and transglycosylases in the exoproteomes from *S. saprophyticus* strains ATCC 15,305, 7108 and 9325. The total number of proteins identified (in nanogram) was calculated, and the amount of proteins corresponding to proteases, antigenic proteins and transglycosylases was obtained. The error bars corresponds to standard error of mean. A: Percentage of proteins identified as proteases in the exoproteomes analyzed. B: Percentage of proteins described and antigenic proteins in the exoproteomes analyzed. C: Percentage of transglycosylases in the exoproteomes analyzed.

stationary phase of growth, and proteins related to several biological functions were detected.

A core of secreted proteins was detected. These proteins have been found in various studies on the *S. aureus* exoproteome (Burlak et al., 2007; Muthukrishnan et al., 2011). These proteins can play different roles extracellularly as moonlighting proteins and includes glycolytic enzymes (GAPDH, TPI, ENO, FBA and phosphoglycerate kinase), proteins related to pyruvate dehydrogenase complex and other enzymes related to energy metabolism, such as glucose 1 dehydrogenase, from Entner-Doudoroff pathway. For example, enolase is related to plasmid binding in several streptococcal species such as *Streptococcus oralis* (Kinnby et al., 2008). GAPDH is also encountered on the cell surface and outside the cell in several bacterial species, including *Streptococcus pneumoniae* and *Lactobacillus crispatus* (Bergmann et al., 2004; Antikainen et al., 2007). Recently, studies comparing *S. aureus* community-associated (CA) and hospital-associated (HA) strains identified that HA strains secrete moonlighting proteins at higher levels when compared to CA strains, suggesting the secretion of moonlighting proteins increases the virulence and survival ability (Mekonnen et al., 2017).

Other proteins were detected in two or one of the strains, suggesting heterogeneity in the content of the exoproteome occur among the strains (Fig. 2, Panel A). Differences in proteomic profiles in *S. epidermidis* were also detected in cells cultured during biofilm formation and in glucose-enriched medium (Carvalho et al., 2015). Comparative analysis using several *S. aureus* strains depicted a core of secreted proteins and several proteins are secreted only by one or a few isolates, showing that heterogeneity exists among isolates (Sibbald et al., 2006).

Other virulence factor detected in our analysis is the UafA protein, associated to adherence event in the host. This protein was not detected in the exoproteome from 9325 strain, but is included in the list of the most secreted protein in the strains ATCC 15,305 and 7108 (Table 2). Previous work shown that the strains ATCC 15,305, 7108 and 9325 possess the gene *uafA* (Kleine et al., 2010). We speculate that the capsule can inhibit the secretion of UafA and it is supported by the fact that the adherence mediated by UafA is inhibited by capsule (Kuroda et al., 2005). Special note must be made of the fact that we identified that the antigenic protein SsaA was secreted by the isolated strains ATCC 15,305 and 9325, but not by 7108. This data was confirmed by Western blot analysis (Fig. 4), and we also evaluated the presence of the ORF encoding SsaA protein without mutation in the three strains (Supplementary Fig. 2). Surprisingly 7108 produces transcripts encoding SsaA at high level (Fig. 5) suggesting the absence of production of the SsaA protein occurs due post-transcriptional events. The post-transcriptional regulation occurs in bacteria and can be regulated by small RNAs (sRNA). *Pseudomonas aeruginosa* possess post-transcriptional regulation mediated by one sRNA named RgsA and requires the RNA chaperone Hfq to regulate some target, such as the alternative sigma factor RposS (Lu et al., 2018). The function of SsaA is not completely clear. Transcripts encoding SsaA protein are overexpressed in *S. aureus* and *S. epidermidis* during infection in *Caenorhabditis elegans* (JebaMercy et al., 2015). Furthermore, the secretion of SsaA protein is higher in planktonic *S. aureus* cells in comparison with cells recovered from biofilm (Resch et al., 2006). In *S. epidermidis*, higher amounts of anti-SsaA IgG are present in patients' sera during endocarditis, but not with other *S. epidermidis* infections (Lang et al., 2000). The evaluation of SsaA secretion by other *S. saprophyticus* strains, and the comparison with data obtained from experimental infection in animal models, are necessary to contribute to the elucidation of the role of this protein during the infective process in *S. saprophyticus*. The elucidation of post-transcriptional regulation in *S. saprophyticus* is also needed and can contribute to understand the metabolic flexibility in this model.

In order to evaluate the major differences occurring in the exoproteome profile we screened the most regulated proteins among the three strains. We detected that they differs in the secretion of proteases, antigenic proteins and transglycosylases (Fig. 6). The strain 7108 secretes

higher content of proteases compared to the other two strains. Proteases are specially important during infection and secreted proteases from *S. aureus* are associated with degradation of host immune system proteins (Stapels et al., 2017) and can be used during degradation of epithelial cells (Murphy et al., 2018). The strain 9325 secretes higher level of antigenic proteins and transglycosylases (followed by ATC 15,305 and 7108). The function of the antigenic proteins is not completely known but the absence of these antigenic proteins can act as an immune system evader while the presence of these antigenic proteins can enhance phagocytosis by the host (that is especially important for intracellular pathogens). Proteomic analysis comparing two *Mycobacterium tuberculosis* strains also detected differences in the secretion of antigenic protein. These proteins may play a role in evasion of host immune responses (antigenic variation) and the ability of secretion of antigenic protein can reflect that different strains can use different mechanism to interact with host immune system (Cornejo-Granados et al., 2017). In addition, strain 9325 secretes higher level of transglycosylases. These proteins besides act in the cell wall synthesis, and are crucial in the complement activation mediated by IgG in *S. aureus* (Lee et al., 2015). Together, these results show *S. saprophyticus* present variation in the relative abundance of proteins related to host-interaction process and suggest that strains can use more than one strategy during interaction with human cells.

Heterogeneity in the exoproteome content described in this study for *S. saprophyticus* uropathogenic strains is also reported in other species such as *S. aureus* and *S. epidermidis*, and is associated with genomic plasticity and variant gene regulation (Ziebandt et al., 2010). Proteomic studies, using two-dimensional gel electrophoresis (2-DGE) with *S. aureus* strains isolated from different sites of infection, identified 12 proteins detected only in isolates from bacteremia, suggesting that the ability to secrete some proteins can be related to the ability to cause infection in the host (Liew et al., 2015). The comparative exoproteome was also performed using three *S. epidermidis* and several proteins predicted to be secreted by classical and non-classical pathways were detected. In addition, several strain-specific proteins were detected (Siljamaki et al., 2014).

This study presents for the first time the proteomic approach to investigate the exoproteome profile of *S. saprophyticus*. Furthermore, we validate the proteomic data by using anti-SsaA polyclonal antibodies. Differences detected among the proteins secreted by these strains were discussed and these data will contribute towards enlarging the knowledge of *S. saprophyticus* biology, as well as in the identification of strain-specific factors that are able to contribute to virulence and adaptation. Further analysis is required in order to elucidate if the secretion process used by these *S. saprophyticus* strains can explain differences in the exoproteome profiles and whether secretion can be related to *S. saprophyticus*'s ability to cause infection in its host.

## 5. Conclusions

The *S. saprophyticus* strains analyzed in this work presented a core of secreted proteins, common in the strains. Otherwise, some proteins related with adhesion (for example, Uro-adherence factor A), and virulence factors, such as proteases and antigenic proteins, are not secreted by all the *S. saprophyticus* strains analyzed, demonstrating that these strains possess versatility in the exoproteome profile.

## Conflict of interest

The authors declare no conflict of interest.

## Acknowledgments

We thank Juliano Domiraci Pაცე for his helpful suggestions. We thank Alex Jesus de Carvalho (*in memoriam*) for his helpful contribution and kind relationship in the research group. This work was supported

by Conselho Nacional de Desenvolvimento Científico e Tecnológico (CNPq, process number 444662/2014-6) and Fundação de Amparo à Pesquisa do Estado de Goiás (FAPEG, Pronex). ASO, IIRR and LSO were supported by scholarship from Coordenação de Aperfeiçoamento de Pessoal de Nível Superior (CAPES).

## Appendix A. Supplementary data

Supplementary material related to this article can be found, in the online version, at doi:<https://doi.org/10.1016/j.micres.2018.08.008>.

## References

- Andersen, C.L., Jensen, J.L., Orntoft, T.F., 2004. Normalization of real-time quantitative reverse transcription-PCR data: a model-based variance estimation approach to identify genes suited for normalization, applied to bladder and colon cancer data sets. *Cancer Res.* 64 (15), 5245–5250.
- Antikainen, J., Kuparinen, V., Lahteenmaki, K., Korhonen, T.K., 2007. pH-dependent association of enolase and glyceraldehyde-3-phosphate dehydrogenase of *Lactobacillus crispatus* with the cell wall and lipoteichoic acids. *J. Bacteriol.* 189 (12), 4539–4543.
- Atshan, S.S., Shamsudin, M.N., Sekawi, Z., Thian Lung, L.T., Barantalab, F., Liew, Y.K., Alreshidi, M.A., Abduljaleel, S.A., Hamat, R.A., 2015. Comparative proteomic analysis of extracellular proteins expressed by various clonal types of *Staphylococcus aureus* and during planktonic growth and biofilm development. *Front. Microbiol.* 6, 524.
- Bergmann, S., Rohde, M., Hammerschmidt, S., 2004. Glyceraldehyde-3-phosphate dehydrogenase of *Streptococcus pneumoniae* is a surface-displayed plasminogen-binding protein. *Infect. Immun.* 72 (4), 2416–2419.
- Bonar, E., Wojcik, I., Jankowska, U., Kedracka-Krok, S., Bukowski, M., Polakowska, K., Lis, M.W., Kosecka-Strojek, M., Sabat, A.J., Dubin, G., Friedrich, A.W., Miedzobrodzki, J., Dubin, A., Wladyka, B., 2016. Identification of secreted exoproteome fingerprints of highly-virulent and non-virulent *Staphylococcus aureus* strains. *Front. Cell. Infect. Microbiol.* 6, 51.
- Bookout, A.L., Cummins, C.L., Mangelsdorf, D.J., Pesola, J.M., Kramer, M.F., 2006. In: In: Frederick, M., Ausubel (Eds.), *High-Throughput Real-Time Quantitative Reverse Transcription PCR. Current Protocols in Molecular Biology* 15. pp. 8 Chapter 15:Unit.
- Brito, W.A., Rezende, T.C., Parente, A.F., Ricart, C.A., Sousa, M.V., Bao, S.N., Soares, C.M.A., 2011. Identification, characterization and regulation studies of the aconitase of *Paracoccidioides brasiliensis*. *Fungal Biol.* 115 (8), 697–707.
- Burlak, C., Hammer, C.H., Robinson, M.A., Whitney, A.R., McGavin, M.J., Kreiswirth, B.N., Deleo, F.R., 2007. Global analysis of community-associated methicillin-resistant *Staphylococcus aureus* exoproteins reveals molecules produced *in vitro* and during infection. *Cell. Microbiol.* 9 (5), 1172–1190.
- Carvalho, V., Franca, A., Pier, G.B., Vilanova, M., Cerca, N., Vitorino, R., 2015. Comparative proteomic and transcriptomic profile of *Staphylococcus epidermidis* biofilms grown in glucose-enriched medium. *Talanta* 132, 705–712.
- Cordwell, S.J., Larsen, M.R., Cole, R.T., Walsh, B.J., 2002. Comparative proteomics of *Staphylococcus aureus* and the response of methicillin-resistant and methicillin-sensitive strains to Triton X-100. *Microbiology (Reading, Engl.)* 148 (Pt 9), 2765–2781.
- Cornejo-Granados, F., Zatarain-Barron, Z.L., Cantu-Robles, V.A., Mendoza-Vargas, A., Molina-Romero, C., Sanchez, F., Del Pozo-Yauner, L., Hernandez-Pando, R., Ochoa-Leyva, A., 2017. Secretome prediction of two *M. tuberculosis* clinical isolates reveals their high antigenic density and potential drug targets. *Front. Microbiol.* 8, 128.
- de Oliveira, A.R., Oliveira, L.N., Chaves, E.G.A., Weber, S.S., Bailao, A.M., Parente-Rocha, J.A., Baeza, L.C., de Almeida, Soares, C.M., Borges, C.L., 2018. Characterization of extracellular proteins in members of the *Paracoccidioides* complex. *Fungal Biol.* 122 (8), 738–751.
- Gatermann, S., Marre, R., Heesemann, J., Henkel, W., 1988. Hemagglutinating and adherence properties of *Staphylococcus saprophyticus*: epidemiology and virulence in experimental urinary tract infection of rats. *FEMS Microbiol. Immunol.* 1 (3), 179–185.
- Gatermann, S., John, J., Marre, R., 1989. *Staphylococcus saprophyticus* urease: characterization and contribution to uropathogenicity in unobstructed urinary tract infection of rats. *Infect. Immun.* 57 (1), 110–116.
- Gatermann, S., Meyer, H.G., Marre, R., Wanner, G., 1993. Identification and characterization of surface proteins from *Staphylococcus saprophyticus*. *Zentralbl. Bakteriol.* 278 (2-3), 258–274.
- Grossklau, D.A., Bailao, A.M., Vieira Rezende, T.C., Borges, C.L., de Oliveira, M.A., Parente, J.A., Soares, C.M.A., 2013. Response to oxidative stress in *Paracoccidioides* yeast cells as determined by proteomic analysis. *Microb. Infect. Institut Pasteur* 15 (5), 347–364.
- Heilmann, C., Hussain, M., Peters, G., Gotz, F., 1997. Evidence for autolysin-mediated primary attachment of *Staphylococcus epidermidis* to a polystyrene surface. *Mol. Microbiol.* 24 (5), 1013–1024.
- Hell, W., Meyer, H.G., Gatermann, S.G., 1998. Cloning of aas, a gene encoding a *Staphylococcus saprophyticus* surface protein with adhesive and autolytic properties. *Mol. Microbiol.* 29 (3), 871–881.
- Islam, N., Ross, J.M., Marten, M.R., 2015. Proteome analyses of *Staphylococcus aureus* biofilm at elevated levels of NaCl. *Clin. Microbiol.* 4 (5).
- Jeba-Mercy, G., Prithika, U., Lavanya, N., Sekar, C., Balamurugan, K., 2015. Changes in *Caenorhabditis elegans* immunity and *Staphylococcal* virulence factors during their interactions. *Gene* 558 (1), 159–172.
- Kinby, B., Booth, N.A., Svensater, G., 2008. Plasminogen binding by oral streptococci from dental plaque and inflammatory lesions. *Microbiology (Reading, Engl.)* 154 (Pt 3), 924–931.
- Kleine, B., Gatermann, S., Sakinc, T., 2010. Genotypic and phenotypic variation among *Staphylococcus saprophyticus* from human and animal isolates. *BMC Res. Notes* 3, 163.
- Korte-Berwanger, M., Sakinc, T., Kline, K., Nielsen, H.V., Hultgren, S., Gatermann, S.G., 2013. Significance of the D-serine-deaminase and D-serine metabolism of *Staphylococcus saprophyticus* for virulence. *Infect. Immun.* 81 (12), 4525–4533.
- Kuroda, M., Yamashita, A., Hirakawa, H., Kumano, M., Morikawa, K., Higashide, M., Maruyama, A., Inose, Y., Matoba, K., Toh, H., Kuhara, S., Hattori, M., Ohta, T., 2005. Whole genome sequence of *Staphylococcus saprophyticus* reveals the pathogenesis of uncomplicated urinary tract infection. *Proc. Natl. Acad. Sci. U. S. A.* 102 (37), 13272–13277.
- Kusch, H., Engelmann, S., 2014. Secrets of the secretome in *Staphylococcus aureus*. *Int. J. Med. Microbiol.* 304 (2), 133–141.
- Lang, S., Livesley, M.A., Lambert, P.A., Littler, W.A., Elliott, T.S., 2000. Identification of a novel antigen from *Staphylococcus epidermidis*. *FEMS Immunol. Med. Microbiol.* 29 (3), 213–220.
- Lee, J.H., Kim, N.H., Winstel, V., Kurokawa, K., Larsen, J., An, J.H., Khan, A., Seong, M.Y., Lee, M.J., Andersen, P.S., Peschel, A., Lee, B.L., 2015. Surface glycoproteins are crucial for *in vitro* anti-wall teichoic acid IgG-mediated complement activation and Opsonophagocytosis of *Staphylococcus aureus*. *Infect. Immun.* 83 (11), 4247–4255.
- Liew, Y.K., Awang Hamat, R., van Belkum, A., Chong, P.P., Neela, V., 2015. Comparative exoproteomics and host inflammatory response in *Staphylococcus aureus* skin and soft tissue infections, bacteremia, and subclinical colonization. *Clin. Vaccine Immunol.* 22 (5), 593–603.
- Loes, A.N., Ruyle, L., Arvizu, M., Gresko, K.E., Wilson, A.L., Deutch, C.E., 2014. Inhibition of urease activity in the urinary tract pathogen *Staphylococcus saprophyticus*. *Lett. Appl. Microbiol.* 58 (1), 31–41.
- Lu, P., Wang, Y., Hu, Y., Chen, S., 2018. RgsA, an RpoS-dependent sRNA, negatively regulates rpoS expression in *Pseudomonas aeruginosa*. *Microbiology (Reading, Engl.)*.
- Mekonnen, S.A., Palma Medina, L.M., Glasner, C., Tsompanidou, E., de Jong, A., Grasso, S., Schaffer, M., Mader, U., Larsen, A.R., Gumpert, H., Westh, H., Volker, U., Otto, A., Becher, D., van Dijk, J.M., 2017. Signatures of cytoplasmic proteins in the exoproteome distinguish community- and hospital-associated methicillin-resistant *Staphylococcus aureus* USA300 lineages. *Virulence* 8 (6), 891–907.
- Murad, A.M., Rech, E.L., 2012. NanoUPLC-MSE proteomic data assessment of soybean seeds using the Uniprot database. *BMC Biotechnol.* 12, 82.
- Murad, A.M., Souza, G.H., Garcia, J.S., Rech, E.L., 2011. Detection and expression analysis of recombinant proteins in plant-derived complex mixtures using nanoUPLC-MS (E). *J. Sep. Sci.* 34 (19), 2618–2630.
- Murphy, J., Ramezanzpour, M., Stach, N., Dubin, G., Psaltis, A.J., Wormald, P.J., Vreugde, S., 2018. *Staphylococcus aureus* V8 protease disrupts the integrity of the airway epithelial barrier and impairs IL-6 production *in vitro*. *Laryngoscope* 128 (1), E8–E15.
- Muthukrishnan, G., Quinn, G.A., Lamers, R.P., Diaz, C., Cole, A.L., Chen, S., Cole, A.M., 2011. Exoproteome of *Staphylococcus aureus* reveals putative determinants of nasal carriage. *J. Proteome Res.* 10 (4), 2064–2078.
- O’Riordan, K., Lee, J.C., 2004. *Staphylococcus aureus* capsular polysaccharides. *Clin. Microbiol. Rev.* 17 (1), 218–234.
- Oliveira, A.S., Rosa, I.I.R., Novaes, E., Oliveira, L.S., Baeza, L.C., Borges, C.L., Marlinghaus, L., Soares, C.M.A., Giambiagi-deMarval, M., P-RJ, A., 2018. A Proteomic Dataset of Secreted Proteins by Three *Staphylococcus saprophyticus* Strains. Data in Brief submitted.
- Park, S., Kelley, K.A., Vinogradov, E., Solinga, R., Weidenmaier, C., Misawa, Y., Lee, J.C., 2010. Characterization of the structure and biological functions of a capsular polysaccharide produced by *Staphylococcus saprophyticus*. *J. Bacteriol.* 192 (18), 4618–4626.
- Phipson, B., Lee, S., Majewski, I.J., Alexander, W.S., Smyth, G.K., 2016. Robust hyperparameter estimation procedure against hypervariable genes and improves power to detect differential expression. *Ann. Appl. Stat.* 10 (2), 946–963.
- Raz, R., Colodner, R., Kunin, C.M., 2005. Who are you—*Staphylococcus saprophyticus*? *Clin. Infect. Dis.* 40 (6), 896–898.
- Resch, A., Leicht, S., Saric, M., Pasztor, L., Jakob, A., Gotz, F., Nordheim, A., 2006. Comparative proteome analysis of *Staphylococcus aureus* biofilm and planktonic cells and correlation with transcriptome profiling. *Proteomics* 6 (6), 1867–1877.
- Ritchie, M.E., Phipson, B., Wu, D., Hu, Y., Law, C.W., Shi, W., Smyth, G.K., 2015. Limma powers differential expression analyses for RNA-seq and microarray studies. *Nucleic Acids Res.* 43 (7), e47.
- Sambrook, J., Russell, D.W., 2001. *Molecular Cloning. A Laboratory Manual*. Cold Spring Harbor Laboratory Press, New York.
- Sibald, M.J., Ziebandt, A.K., Engelmann, S., Hecker, M., de Jong, A., Harmsen, H.J., Raangs, G.C., Stokroos, I., Arends, J.P., Dubois, J.Y., van Dijk, J.M., 2006. Mapping the pathways to staphylococcal pathogenesis by comparative secretomics. *Microbiol. Mol. Biol. Rev.* 70 (3), 755–788.
- Siljamaki, P., Varmanen, P., Kankainen, M., Sukura, A., Savijoki, K., Nyman, T.A., 2014. Comparative exoprotein profiling of different *Staphylococcus epidermidis* strains reveals potential link between nonclassical protein export and virulence. *J. Proteome Res.* 13 (7), 3249–3261.
- Sousa, V.S., da-Silva, A.P.S., Sorenson, L., Paschoal, R.P., Rabello, R.F., Campana, E.H., Pinheiro, M.S., Dos Santos, L.O.F., Martins, N., Botelho, A.C.N., Picao, R.C., Fracalanza, S.E.L., Riley, L.W., Sensabaugh, G., Moreira, B.M., 2017. *Staphylococcus saprophyticus* recovered from humans, food, and recreational waters in Rio De Janeiro, Brazil. *Int. J. Microbiol.*, 4287547 2017.

- Stapels, D.A.C., Woehl, J.L., Milder, F.J., Tromp, A.T., van Batenburg, A.A., de Graaf, W.C., Broll, S.C., White, N.M., Rooijackers, S.H.M., Geisbrecht, B.V., 2017. Evidence for multiple modes of neutrophil serine protease recognition by the EAP family of Staphylococcal innate immune evasion proteins. *Protein Sci.* 164 (4), 716–724.
- Szabados, F., Kleine, B., Anders, A., Kaase, M., Sakinc, T., Schmitz, I., Gatermann, S., 2008. *Staphylococcus saprophyticus* ATCC 15305 is internalized into human urinary bladder carcinoma cell line 5637. *FEMS Microbiol. Lett.* 285 (2), 163–169.
- Talebi, M., Shafiee, M., Sadeghi, J., Moghadam, N.A., Saifi, M., Pourshafie, M.R., 2016. Genotypic diversity of methicillin-resistant coagulase-negative staphylococci isolated from inpatients and outpatients. *Microb. Drug Resist.* 22 (2), 147–154.
- Tseng, T.T., Tyler, B.M., Setubal, J.C., 2009. Protein secretion systems in bacterial-host associations, and their description in the gene ontology. *BMC Microbiol.* 9 (Suppl 1), S2.
- Vizcaino, J.A., Csordas, A., del-Toro, N., Dianes, J.A., Griss, J., Lavidas, I., Mayer, G., Perez-Riverol, Y., Reisinger, F., Ternent, T., Xu, Q.W., Wang, R., Hermjakob, H., 2016. Update of the PRIDE database and its related tools. *Nucleic Acids Res.* 44 (D1), D447–D456 2016.
- Wang, G., Xia, Y., Song, X., Ai, L., 2016. Common non-classically secreted bacterial proteins with experimental evidence. *Curr. Microbiol.* 72 (1), 102–111.
- Watts, A., Ke, D., Wang, Q., Pillay, A., Nicholson-Weller, A., Lee, J.C., 2005. *Staphylococcus aureus* strains that express serotype 5 or serotype 8 capsular polysaccharides differ in virulence. *Infect. Immun.* 73 (6), 3502–3511.
- Ziebandt, A.K., Kusch, H., Degner, M., Jaglitz, S., Sibbald, M.J., Arends, J.P., Chlebowicz, M.A., Albrecht, D., Pantucek, R., Doskar, J., Ziebuhr, W., Broker, B.M., Hecker, M., van Dijl, J.M., Engelmann, S., 2010. Proteomics uncovers extreme heterogeneity in the *Staphylococcus aureus* exoproteome due to genomic plasticity and variant gene regulation. *Proteomics* 10 (8), 1634–1644.